THESE DE DOCTORAT

Présentée devant

L'UNIVERSITE DE LILLE

UFR CHIMIE

DOCTEUR DE L'UNIVERSITE DE LILLE

Mention ≪ Molécules et Matière Condensée ≫

Par

Obaid Hasan HASHMI

Ecole Doctorale Sciences de la Matière, du Rayonnement et de L'Environnement

Unité de Catalyse et de Chimie du Solide, UMR CNRS 8181

Equipe Méthodologie Organométallique en Catalyse Homogène

Engineering of iron-based polymerization catalysts: towards the design of original multi-structured thermoplastic (co) polymers

---

Soutenue le 24 Juin 2021 à Villeneuve d'Ascq

Thèse Dirigée par

Marc VISSEAUX, Professeur des Universités, Université de Lille, directeur de thèse

Yohan CHAMPOURET, Chargé de Recherche CNRS, Université de Lille, co-directeur de thèse

Président du jury :

Francine AGBOSSOU-NIEDERCORN, Directrice de Recherche CNRS, Université de Lille

Rapporteurs :

Blanca MARTIN-VACA, Professeur des Universités, Université Paul Sabatier, Toulouse

Gregory A. SOLAN, Associate Professor, University of Leicester, Royaume-Uni.

Examinateurs :

Lionel MAGNA, Ingénieur de Recherche, IFP Energies Nouvelles, Lyon

Jean RAYNAUD, Chargé de Recherche CNRS, C2P2-LCPP, Lyon

Mathieu SAUTHIER, Professeur des Universités, Université de Lille

Engineering of iron-based polymerization catalysts: towards the design of original multi-structured thermoplastic (co) polymers

Abstract: A series of iminopyridine-/iminoquinoline-based ligands **L1-L11** of type [(Ar)N=C(R)]-R' (Ar = 2,6-Me$_2$-C$_6$H$_3$ or 2,6-^{i}Pr$_2$-C$_6$H$_3$ or 3,5-(CF$_3$)$_2$-C$_6$H$_3$ or C$_6$F$_5$, R = H or Me and R' = 2-C$_5$H$_4$N or 2-C$_5$H$_3$N-5-Me or 2-C$_9$H$_6$N or 8-C$_9$H$_6$N) and their corresponding iron (II) complexes **(1-11)** were developed. The complexes were fully characterized including by X-ray for new complexes (**6-11**) and their catalytic applications were investigated for the controlled coordinative polymerization of isoprene. The modulation of steric and electronic properties within this family of ligands/complexes has shown to influence the stereo-selectivity and activity of the polymerization of isoprene after activation with various cocatalysts. The resulting catalysts produced polyisoprenes with an excellent conversion, high activity and a variety of stereo-/regio-regularities. Some of these catalysts were also assessed for the coordinative polymerization of styrene and displayed good activity for the formation of syndiotactic enriched polystyrenes. Another organometallic methodology has been utilized for the synthesis of aminopyridine ligands (*rac-*L^{1}H and *rac-*L^{2}H) and their corresponding iron amide complexes **12, 13Py** and **14Py** for their application in the Ring-Opening (Co)polymerizaion of *L*-lactide and ε-caprolactone where the homoleptic complexes **13Py** and **14Py** proved to be effective.

    Keywords: Iron, Homogeneous Catalysis, Coordinative Polymerization, Iminopyridine, Iminoquinoline, Isoprene, Styrene, Lactide, ε-caprolactone

---

Ingénierie des catalyseurs de polymérisation à base de fer : vers la conception de (co)polymères thermoplastiques multi-structurés originaux

Résumé: Une série de ligands **L1-L11** à base d'iminopyridine/iminoquinoline du type [(Ar)N=C(R)]-R' (Ar = 2,6-Me$_2$-C$_6$H$_3$ ou 2,6-^{i}Pr$_2$-C$_6$H$_3$ ou 3,5-(CF$_3$)$_2$-C$_6$H$_3$ ou C$_6$F$_5$, R = H ou Me et R' = 2-C$_6$H$_5$N ou 2-C$_6$H$_4$N-5-Me ou 2-C$_9$H$_7$N or 8-C$_9$H$_7$N) et leurs complexes de fer (II) correspondants **(1-11)** ont été développés. Les complexes ont été entièrement caractérisés, y compris par rayons X pour les nouveaux complexes **(6-11)**, et leurs applications catalytiques ont été étudiées pour la polymérisation coordonnée contrôlée de l'isoprène. La modulation des propriétés stériques et électroniques au sein de cette famille de ligands/complexes s'est avérée influencer la stéréo-sélectivité et l'activité de la polymérisation de l'isoprène après activation avec divers cocatalyseurs. Les catalyseurs obtenus ont produit des polyisoprènes avec une excellente conversion, une activité élevée et une variété de stéréo-/régio-régularités. Certains de ces catalyseurs ont également été évalués pour la polymérisation coordinative du styrène et ont montré une bonne activité pour la formation de polystyrènes syndiotactiques enrichis. Une autre méthodologie organométallique a été utilisée pour la synthèse de ligands aminopyridine (*rac-*L^{1}H and *rac-*L^{2}H) et de leurs complexes amides de fer correspondants **12, 13Py** et **14Py** pour leur application dans la (Co)polymérisation par ouverture de cycle de *L*-lactide et ε-caprolactone où les complexes homoleptiques **13Py** et **14Py** se sont avérés efficaces.

Mot Clés: Fer, Catalyse Homogène, Polymérisation coordonnée, Iminopyridine, Iminoquinoléine, Isoprène, Styrène, Lactide, ε-caprolactone

ACKNOWLEDGEMENTS

I would like to sincerely thank my directors of thesis Prof. Marc Visseaux and Dr. Yohan Champouret for providing me such a great opportunity to learn under their guidance at the UCCS laboratory in the University of Lille.

Prof., I would not have been able to do any of this without your constant guidance and encouragement. Your enthusiasm always inspired me to give my hundred percent in research. From you, I learned how to be always optimistic and remain calm in this field where the outcomes are not only governed by hard work but also by luck. I couldn't have asked for more in an advisor, and I'm so glad to have been part of your team MOCAH. Thank you so much for trusting me from the very beginning.

Yohan, I came to you as an average student with minimal bench skills and little confidence, and you had the compassion, patience, and enthusiasm to develop me into a good chemist. You were always there to clear my doubts, to help me out in some very difficult situations I encountered during the past 3 years. I am so glad that I was able to learn every single day from you. Thank you so much.

I am very grateful to Prof. Blanca Martin-Vaca and Dr. Gregory A. Solan for accepting to be the rapporteurs of my thesis. I would also like to equally thank Dr. Lionel Magna, Dr. Jean Raynaud, Dr. Francine Agbossou-Niedercorn and Prof. Mathieu Sautheir for accepting to be the examiners of my Ph.D.

I am thankful to all the members of the UCCS specially, Prof. Franck Dumeignil and Prof. Jean-François Paul for their help in administrative procedures. The members of the MOCAH team, Prof. André Mortreux, Dr. Thomas Chenal, Maxime Beauvois and Yassir Zohri are acknowledge for their help during this period. My deepest thanks to Dr Frédéric Capet who helped me till the end to obtain all my crystal structures. Céline Delabre and Patrick Doubias are also acknowledged for their continuous support in characterization techniques.

I would also like to thank my friends Elodie Louisy, Abdel Kader, Bouchaibe Mouhsine and Yasmeena Homrani for their support and gags that kept me entertained during the work. My good friend Silvia, you have been one of the nicest persons I came across during this whole time. A big thanks to my Indian friends in Lille who never made me feel like I am away from my roots.

Sami, though you left when I came here but you have helped me a lot during this phase. To me you are no less than an elder brother who always gave the best advice.

Last, but not the least, I would like to thank my mother, for always remembering me in her prayers. My brother Junaid Hashmi, who motivated me from the very beginning to pursue this domain. You are the best brother one could ever ask for. To the love of my life, Ghazala, I could have never ever done this without you. Thank you for being such a good listener and my problem solver. During the last couple of months, you have always been my pillar of strength who motivated me every single day to go that extra mile and never give up at any cost.

TABLE OF CONTENTS

GLOSSARY OF ABBREVIATIONS

B

BD	butadiene
BEM	n-butylethylmagnesuim, $(^n\text{Bu})(\text{Et})\text{Mg}$
BHT	butylated hydroxytoluene
Bn	benzyl
br	broad

C

CTA	chain transfer agent
CCTP	coordinative chain transfer polymerization
CSP	chain shuttling polymerization
[C]	Concentration

D

D	deuterated
d	doublet
dd	doublet of doublets
ddd	doublet of doublets of doublets
DSC	differential scanning calorimetry
Đ	Dispersity
δ	chemical shift
$\Delta v_{1/2}$	Half peak width
DCM	dichloromethane

E

Et	ethyl
Et$_2$O	diethylether
EtOH	ethanol
ε-CL	ε-caprolactone

I

^{i}Pr	isopropyl
IP	isoprene

L

Lactide	LA

M

M	metal
m	meta
m	multiplet
MAO	methylaluminoxane, [AlMeO]$_n$
MALDI-ToF-MS	matrix assisted laser desorption ionisation-time of flight-mass spectrometry
Me	methyl
MeOH	methanol
M_n	number-average molecular weight
$M_{n(th)}$	theoretical number average molecular weight
M_w	weight-average molecular weight

N

NMR	nuclear magnetic resonance

O

o	ortho
ORTEP	oak ridge thermal ellipsoid program

P

p	para
PBD	polybutadiene
PCL	poly(ε-caprolactone)
PI	polyisoprene
PLLA	poly(*L*-lactide)
Ph	phenyl, -C_6H_5
ppm	part(s) per million
PS	polystyrene

Q

q	quartet

R

R	alkyl or aryl
rac-	racemic mixture
ROP	ring opening polymerization
RT	room temperature

S

s	singlet
SEC	size exclusion chromatography

T

T	temperature
t	triplet
T_m	melting temperature
T_g	glass transition temperature
TMS	trimethylsilyl, $-SiMe_3$
TOF	turn over frequency

X

XRD	x-ray diffraction

GENERAL INTRODUCTION

Metal complexes are one of the most essential instruments for organic chemists. In the past few decades, the rapid development of organometallic chemistry and catalysis has changed the face of modern chemical science by making numerous breakthrough contributions to organic synthesis, pharmaceutical applications, chemical industry, materials science, energy research, and several other areas.[1] Nevertheless, such extensive use of metal compounds has highlighted the significance of environmental and toxicity issues.[2]

Modern catalysis has been dominated by noble transition metals, such as palladium, platinum, ruthenium and iridium, and these metals have been used in a wide range of reactions.[3] The main advantage they possess over their first-row transition metal counterparts is their preference for undergoing two-electron processes. Despite their prevalence in catalysis, there are several problems associated with their continued use in catalytic processes. For one, the fact that precious metals are by definition scarce indicates that they i) lack abundance, ii) are very expensive, and iii) are susceptible to supply fluctuations, which fuels growing concerns about their continued availability. Nearly a decade ago, the British Geological Society released a list of metals at risk of supply disruption.[4] Antimony, the platinum-group metals (ruthenium, rhodium, palladium, osmium, iridium, and platinum), mercury, and tungsten are estimated to be at the highest risk. These factors may not directly influence the research in academia, but have profound implications for industry and for the future of sustainable chemistry.

As a result, the current requirements for clean, fast, efficient, and selective processes have increased the demand for such metal-based reaction promoters, especially the ones that can be applied in catalytic amounts and/or that are recyclable. In this context, iron catalysis has experienced a very strong growth over the last decade, driven by the need to develop a chemistry that is increasingly in line with environmental concerns, such as the optimization of the planet's resources and the management of the waste from any industrial transformation.[5]

On a historical point of view, heterogenous iron catalysis has undoubtedly transformed the world.[6] At the dawn of the twentieth century, the development of catalytic systems based on iron for the production of ammonia in the Haber-Bosch process has contributed to the development of intensive agriculture and, consequently, to the support of the global population growth.[7] Similar in terms of economic relevance, though arguably less vital, is the Fischer−Tropsch process that allows basically any carbonaceous material to be converted into liquid fuel. Originally designed for coal processing, natural gas is the dominant feedstock in the current economic and political

context, but renewable (waste) carbon sources are expected to gain importance in the future. In contrast, homogeneous iron catalysis has become a focal research area only recently as evident from the exponential rise in the number of publications after the turn of the millennium.[8] A variety of attractive reasons speak in favor of homogeneous iron catalysis:

- Iron, its oxides and many of its salts are readily available, cheap with negligible environmental impact and of low toxicity.[9]

- This metal is an essential element of life since its presence in specific proteins that helps to bind and transport oxygen through the circulatory system of all living organisms (Figure 1).[10]
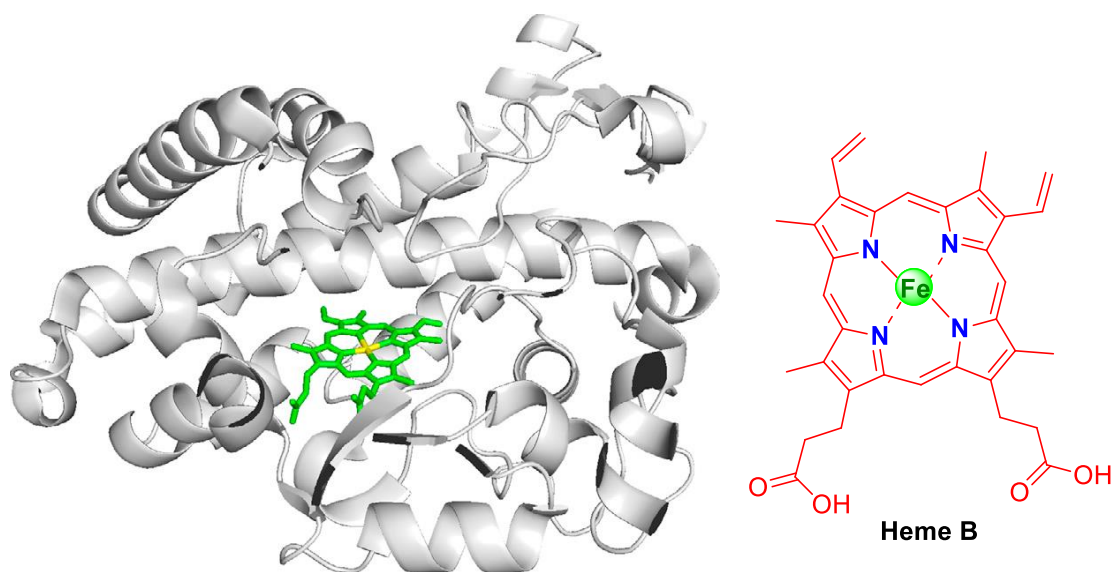
Figure 1. Iron-containing enzymes found in nature: Mycobacterium tuberculosis CYP121 containing a heme-iron center (PDB: 3G5H) (left)[11] and structure of heme B unit (right)

- Due to iron's central position in the periodic table, just above ruthenium, which is arguably one of the most versatile central metals in contemporary catalysis research, it can have the property of both an "early" and "late" transition metal and, thanks to its ability to exhibit multiple oxidation states, any type of reaction is, in principle, within reach.[8]

- Iron cations also bind strongly to many N- and O-based ligands, and these ligands can replace phosphine ligands and related ligands in iron chemistry, which require additional cost and labor.

- The organometallic and coordination chemistry of iron, suitable for homogeneous catalysis, remains a wide-open field of research with enormous opportunities for discovery and innovation.

Due to all these reasons, it is most likely that homogeneous iron catalysis will eventually gain importance in organic chemistry, polymerization, small molecule activation, electrocatalysis etc.[8c,12] and replace the frequent use of noble metals in this field.[3] A variety of comprehensive reviews focusing on the development of iron catalysis in organic synthesis and transformations including those in hydrogenation, hydrosilylation, hydroboration, addition, C-H activation, C-C coupling etc. are available in literature that can be redirected to for further information.[1i,5] On the other hand, apart from applications of iron in organic catalysis, there have also been outstanding developments regarding the use of iron in polymerization catalysis, in particular, the coordination-insertion polymerization (Scheme 1).[13]
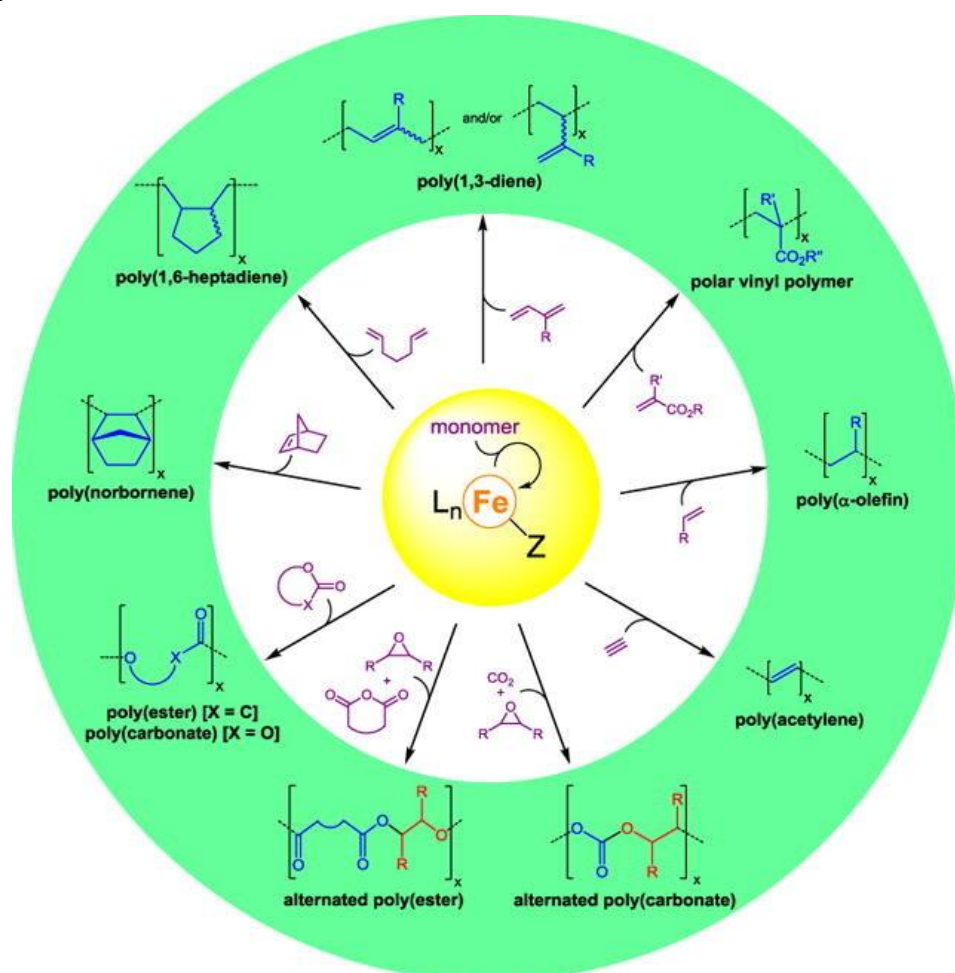
Scheme 1. Coordination-insertion polymerization catalysis using iron-based complexes

After the pioneering work of Gibson and Brookhart related to the polymerization of ethylene,[14] which will be briefly recalled in this thesis, many advances have been made in the field of iron-catalyzed ethylene polymerization,[15,16] in particular by the group of Sun that has developed thermally stable systems by improving the rigidity of the catalysts as well as introducing highly hindered *N*-aryl moieties on the bisiminopyridine ligand.[14j,17] In parallel, there have also been an increasing number of studies on the coordination-insertion polymerization of a large variety of organic monomers ranging from non-polar to polar.[13] In particular, the field of iron-catalyzed polymerization of 1,3-dienes has seen a considerable surge of interest since the pioneering work of Ritter *et al*. in 2012,[18] however, this competitive research domain still lacks the potential to replace the dominating industrial catalytic systems that are mainly based on other transition metals (e.g. Ti, Co, Ni) or rare earths (Nd).[19] In addition, the stereo-/regio-selectivity of these systems remains an issue that needs to be further improved. From this point of view, much remains to be done for understanding the structure-properties relationships of iron-catalyzed 1,3-dienes polymerization. Lastly, with respect to the Ring-Opening polymerization (ROP) of cyclic esters, various iron catalytic systems have been reported in the literature but most of them still lack high activity and control over the stereoselectivity of polymerization.

Therefore, in this context, the primary objective of this thesis work was to develop a new family of iron-based catalysts comprising an iminopyridine skeleton, that can be used to synthesize polyisoprene with controlled microstructures. The secondary aim is to develop new iron amide complexes for their potential application in the controlled Ring-Opening polymerization (ROP) of cyclic esters.

Chapter 1 presents an introduction to the field of iron-catalyzed coordination-insertion polymerization through a bibliographic survey covering the recent advancements in this field regarding 1,3-dienes and Ring-Opening Polymerization of polar monomers, which has progressed steadily over the last decade.

Chapter 2 describes the synthesis and development of alkylated *N*-aryl substituted iminopyridine iron complexes and their catalytic applications in the controlled coordinative polymerization of isoprene and styrene.

Chapter 3 focuses on the development of a new family of iminopyridine iron complexes bearing electron withdrawing fluorinated groups on the *N*-aryl moiety, their structural features and characterization as well as their reactivity towards isoprene and styrene polymerization. The catalytic activities and selectivity of these newly developed systems are compared to the ones described in *Chapter 2*.

Chapter 4 explores and establishes the first reversible coordinative chain transfer polymerization (CCTP) of isoprene with iron-based catalytic systems described in *Chapters 2* and *3*. It also demonstrates the implementation of chain shuttling polymerization (CSP), which is one of the remarkable extensions of CCTP.

Finally, *Chapter 5* deals with the synthesis and characterization of newly developed homoleptic/heteroleptic amidopyridine iron amide complexes and their catalytic applications in the Ring-Opening (co)Polymerization (ROcOP) of *L*-LA and ε-CL.

References

(1)   (a) Muci, A. R.; Buchwald, S. L., Cross-Coupling Reactions. In *Practical Palladium Catalysts for C-N and C-O Bond Formation*; Miyaura, N., Ed.; Springer: Berlin, Heidelberg, New York, 2002.
(b) *Metal Catalyzed Cross-Coupling Reactions and More*; de Meijere, A., Brase, S., Oestreich, M., Eds.; Wiley-VCH: Weinheim, Germany, 2014.
(c) *Organotransition Metal Chemistry: From Bonding to Catalysis*; Hartwig, J. F., Ed. University Science Books: Sausalito, CA, 2010.
(d) Correa, A.; Garcia Mancheno, O.; Bolm, C. *Chem. Soc. Rev.* **2008**, *37* (6), 1108−1117.
(e) Gorin, D. J.; Sherry, B. D.; Toste, F. D. *Chem. Rev.* **2008**, *108* (8), 3351−3378.
(f) Vougioukalakis, G. C.; Grubbs, R. H. *Chem. Rev.* **2010**, *110* (3), 1746−1787.
(g) Molnar, A. *Chem. Rev.* **2011**, *111* (3), 2251−2320.
(h) Johansson Seechurn, C. C.; Kitching, M. O.; Colacot, T. J.; Snieckus, V. *Angew. Chem., Int. Ed.* **2012**, *51* (21), 5062−5085.
(i) Furstner, A. *ACS Cent. Sci.* **2016**, *2* (11), 778−789.

(2)   Egorova, K. S.; Ananikov, V. P. Toxicity of Metal Compounds: Knowledge and Myths. 2017, 20.

(3)   Ludwig, J. R.; Schindler, C. S. *Chem* **2017**, *2* (3), 313–316.

(4)   Umile, T.P., Catalysis for Sustainability: Goals, Challenges, and Impacts (CRC Press) 2015.

(5)   (a) Wei, D.; Darcel, C. *Chem. Rev.* **2019**, *119* (4), 2550–2610.
(b) Bolm, C.; Legros, J.; Le Paih, J.; Zani, L. *Chem. Rev.* **2004**, *104* (12), 6217–6254.
(c) Bauer, I.; Knölker, H. J. *Chem. Rev.* **2015**, *115* (9), 3170– 3387.

(6)   Ertl, G.; Knözinger, H.; Schüth, F.; Weitkamp, J., Eds. *Handbook of Heterogeneous Catalysis*, 2nd ed.; Wiley-VCH: Weinheim, 2008; Vol. 1−8.

(7)   World Fertilizer Trends and Outlook to 2020. 38

(8)   (a) Plietker, B., Ed. *Iron Catalysis. Fundamentals and Applications*; Springer: Heidelberg, 2011; Top. Organomet. Chem.,Vol. 33.
(b) Bauer, E. B., Ed. *Iron Catalysis II*; Springer International Publishing: Cham, CH, 2015; Top. Organomet. Chem.,Vol. 50.
(c) Bullock, R. M., Ed. *Catalysis without Precious Metals*. Wiley-VCH: Weinheim, 2010.
(d) Marek, I., Rappoport, Z., Eds. *The Chemistry of Organoiron Compounds*; Wiley: Chichester, 2014.

(9)   (a) Egorova, K.S.; Ananikov, V.P. *Organometallics* **2017**, *36*, 4071;
(b) Egorova, K.S.; Ananikov, V.P. *Angew. Chem. Int. Ed.* **2016**, *55*, 12150;
(c) Bauer, E.B. *Top. Organomet. Chem.* **2015**, 50, 1.

(10)   Bertini, I.; Gray, H. B.; Lippard, S. J.; Valentine, J. S., Eds. *Bioinorganic Chemistry*; University Science Books: Mill Valley, CA,1994.

(11)   Belin, P.; Le Du, M. H.; Fielding, A.; Lequin, O.; Jacquet, M.; Charbonnier, J.-B.; Lecoq, A.; Thai, R.; Courcon, M.; Masson, C.; Dugave, C.; Genet, R.; Pernodet, J.-L.; Gondry, M. *Proceedings of the National Academy of Sciences* **2009**, *106* (18), 7426–7431.

(12)   (a) Okamura, M.; Kondo, M.; Kuga, R.; Kurashige, Y.; Yanai, T.; Hayami, S.; Praneeth, V. K. K.; Yoshida, M.; Yoneda, K.; Kawata, S.; Masaoka, S. *Nature* **2016**, *530*, 465−468.
(b) Lee, Y.; Mankad, N. P.; Peters, J. C. *Nat. Chem.* **2010**, *2*, 558−565.
(c) Gärtner, F.; Sundararaju, B.; Surkus, A.-E.; Boddien, A.; Loges, B.; Junge, H.; Dixneuf, P. H.; Beller, M. *Angew. Chem., Int. Ed.* **2009**, *48*, 9962−9965.

(13)   Champouret, Y.; Hashmi, O. H.; Visseaux, M. *Coord. Chem. Rev.* **2019**, *390*, 127–170.

(14)   (a) Britovsek, G.J.P.; Gibson, V.C.; McTavish, S.J.; Solan, G.A.; White, A.J.P.; Williams, D.J.; Kimberley, B.S.; Maddox, P.J. *Chem. Commun.* **1998**, 849;
(b) Bennet A.M.A.(DuPont), WO 98/27124, 1998.;
(c) Small, B.L.; Brookhart, M.; Bennett, A.M.A. *J. Am. Chem. Soc.* **1998**, *120*, 4049;
(d) Britovsek, G.J.; Dorer, B.; Gibson, V.C.; Kimberley, B.S.; Solan, G.A. (BP Chemicals). WO 9912981, A1 19990318, 1999

(15)   (a) Bianchini, C.; Giambastiani, G.; Rios, I.G.; Mantovani, G.; Meli, A.; Segarra, A.M. *Coord. Chem. Rev.* **2006**, *250*, 1391;

(b) Gibson, V.C.; Redshaw, C.; Solan, G.A. *Chem. Rev.* **2007**, *107*, 1745;

(c) Sun, W.-H.; Zhang, S.; Zuo, W. *C. R. Chimie* **2008**, *11*, 307;

(d) Xiao, T.; Zhang, W. ; Lai, J. ; Sun, W.-H. *C. R. Chimie* **2011**, *14*, 851;

(e) Zhang, W.; Sun, W.-H.; Redshaw, C. *Dalton Trans.* **2013**, *42*, 8988;

(f) Ma, J.; Feng, C.; Wang, S.; Zhao, K.-Q.; Sun, W.-H.; Redshaw, C.; Solan*, G.A. *Inorg. Chem. Front.* **2014**, *1*, 14;

(g) Boudier, A.; Breuil, P.-A.R.; Magna, L.; Olivier-Bourbigou, H.; Braunstein, P. *Chem. Commun.* **2014**, *50*, 1398;

(h) Small, B.L. *Acc. Chem. Res.* **2015**, *48*, 2599;

(i) Flisak, Z.; Sun, W.-H. *ACS Catal.* **2015**, *5*, 4713;

(j) Wang, Z.; Solan, G.A.; Zhang, W.; Sun, W.-H. *Coord. Chem. Rev.* **2018**, *363*, 92;

(k) Suo, H.; Solan, G.A.; Ma, Y.; Sun, W.-H. *Coord. Chem. Rev.* **2018**, *372*, 101;

(l) Chen, W.; Zhang, G.A.; Solan, R.; Zhang, L.; Hao Guo, X.; Sun, W.-H. *Organometallics* **2018**, *37*, 4002.

(16)   (a) Gibson, V.C.; Solan, G.A. *Top. Organomet. Chem.* **2009**, *26*, 107;

(b) Li, L.; Gomes, P.T. in: Bianchini, C.; Cole-Hamilton, D.J. ; van Leeuwen (Ed.), P.W.N.M. Olefin Upgrading Catalysis by Nitrogen-based Metal Complexes II, vol. 36, Catalysis by metal complexes. Springer, Dordrecht, 2012 pp. 77;

(c) Burcher, B.; Breuil, P.-A.R.; Magna, L.; Olivier-Bourbigou, H. *Top. Organomet. Chem.* **2015**, *50*, 217;

(d) Gibson, V.C.; Solan, G.A. in: Bullock (Ed.), R.M. *Catalysis without Precious Metals*, Wiley-VCH, Weinheim, 2010, p. 111.

(17)   Yang, W.; Ma, Z.; Yi, J.; Sun, W.-H. *Catalysts* **2017**, *7*, 120.

(18)   Raynaud, J.; Wu, J. Y.; Ritter, T. *Angew. Chem. Int. Ed.* **2012**, *51* (47), 11805–11808.

(19)   Srivastava, V.K.; Maiti, M.; Basak, G.C.; Jasra, R.V. *J. Chem. Sci.* **2014**, *126*, 415–427.

CHAPTER 1. BIBLIOGRAPHY

Reproduced in part with permission from:

1.1. Coordination-insertion polymerization by means of Iron catalysts

1.1.1. Principles of Coordination-insertion polymerization

Since the initial discovery more than sixty years ago of Karl Ziegler and Giulio Natta,[1] coordination-insertion catalysis has emerged as a preferred choice for controlling the polymerization of a wide range of unsaturated hydrocarbon monomers and many others.[2] Indeed, compared with other polymerization methodologies such as anionic or radical polymerization, the resulting microstructure of the growing chain has in this case the advantage of being dictated by the catalyst environment.[3]

Conventional Ziegler-Natta (Z-N) systems are based on heterogeneous and, to a lesser extent, homogeneous catalysts, which predominantly consist in an early transition or rare earth metal-based compound (pre-catalyst) in combination with a main group alkyl or a borane (or borate) co-reagent (cocatalyst).[4] Heterogeneous Z-N catalysts dominate the industrial manufacturing of polyolefins and related polymers; however, these systems possess several active sites that make them difficult to characterize and generally lead to polymers whose microstructure may be less controlled with broad dispersity (molecular weight distribution). On the other hand, homogeneous catalysts, which are represented by single-site catalysts with well-defined structures, are capable of producing polymers with a narrower dispersity and, to some extent, controlling the stereo-, regio- and chemo-selectivity according to the steric and electronic properties of the ancillary ligand(s).[5] After the discovery of methylaluminoxane (MAO) as a cocatalyst in the late 1970s, most of the research works on homogeneous Z-N catalysts have been focused on the preparation of well-defined early transition metal-based systems, initially with Group IV metallocenes and their derivatives, followed by the development of post-metallocene catalysts.[6] Advances in this area have enabled to prepare metal-based complexes capable of polymerizing, in some cases, various monomers in a living fashion, along with efficient control over selectivity,[7] dispersity and the preparation of end-functionalized polymers as well as block copolymers.[8] More recently, well-defined late-transition metal complexes have also shown considerable potential as catalysts for the polymerization of unsaturated hydrocarbon monomers, allowing, *inter alia*, the preparation of polymers that display unprecedented architectures.[9] Furthermore, one of the advantages of late-transition metal-based is that they have demonstrated, in some cases, to be more tolerant toward functional groups in comparison with the more oxophilic counterparts based on early metals.[10]

With regard to Z-N catalytic systems, the well-accepted mechanism for the coordination-insertion polymerization of α-olefins was proposed at the beginning of the 1960s' by Cossee and Arlman.[11] In this respect, the coordination-insertion polymerization of α-olefins (and corresponding unsaturated hydrocarbon monomers) refers to a polymerization process involving the prior coordination of the double bond of the incoming monomer on the metal (M) active center to generate a π complex intermediate. The coordination of the monomer is then followed by its insertion into the active metal-Z bond (or metal-polymer) of the initiating (propagating) species, the growing chain remaining attached to the metal center (Scheme 1.1a).
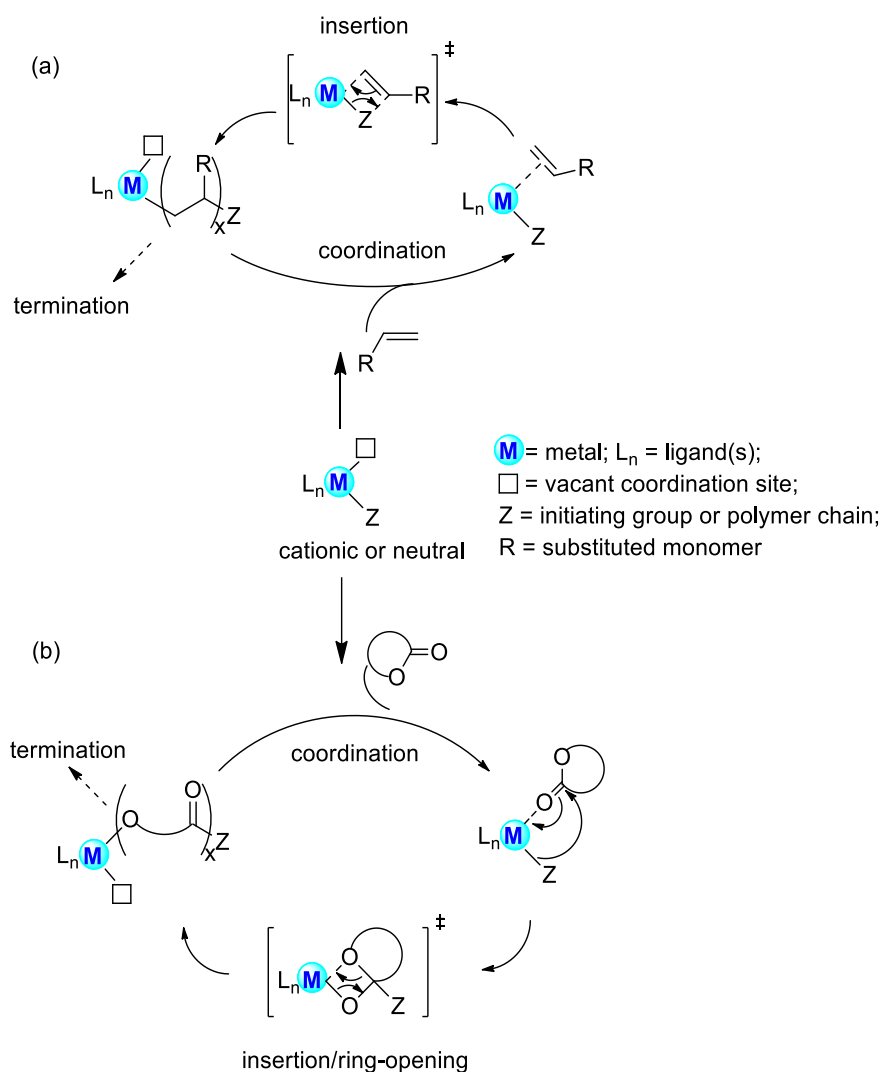
Scheme 1.1. Mechanism of metal-catalyzed coordination-insertion polymerization of (a) unsaturated hydrocarbon monomers and (b) polar cyclic monomers.

Not only unsaturated hydrocarbon monomers can be polymerized by a coordination-insertion mechanism, but also, in a lower degree, several families of polar cyclic monomers such

as cyclic esters or carbonates and others.[12] The coordination proceeds via σ donation of the heteroatom of the polar cyclic monomer on the metal center, which subsequently inserts into the metal-Z bond (or metal-polymer) by addition of the Z group on the carbon of the carbonyl group. This step is then followed by the ring opening of the heterocycle through the cleavage of the carbon-acyl bond (Scheme 1.1b); this polymerization process is commonly designated as coordination-insertion Ring-Opening Polymerization (ROP).[13]

The simultaneous investigation conducted independently by the groups of V. Gibson, M. Brookhart and A. Bennett (DuPont) in the late 1990s demonstrated a very high efficiency and selectivity of the first-generation iron-based complexes for the polymerization and/or oligomerization of ethylene upon activation with an excess of MAO, producing exclusively linear oligomers or polymers (Chart 1.1).[14]
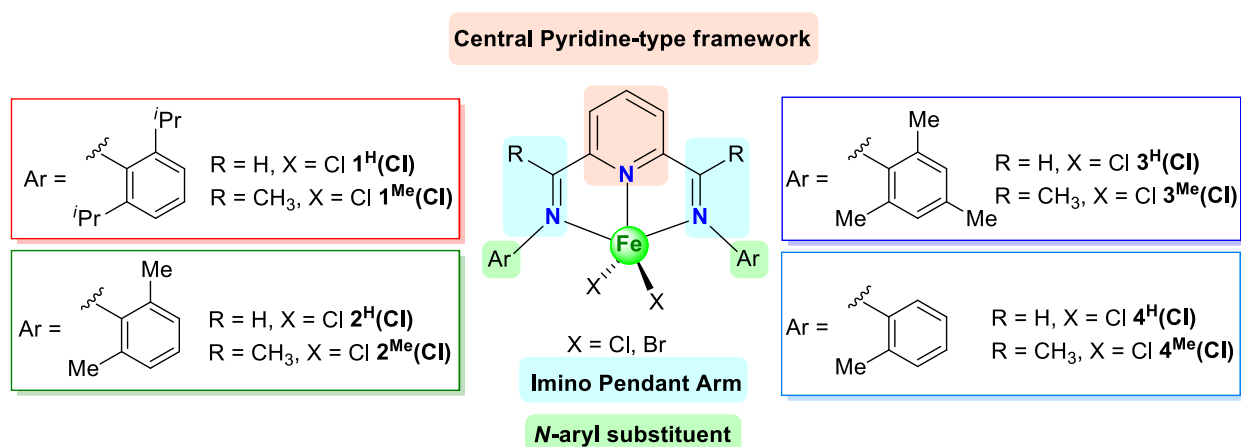
Chart 1.1. Selected iron-BIP complexes used for the polymerization/oligomerization of ethylene.

Briefly, the key feature of these pre-catalysts, with respect to their reactivity with ethylene, is the presence of a bis(imino)pyridyl (BIP) tridentate pincer ligand that can produce, according to the steric hindrance of the *N*-aryl substituents, either short chain oligomers or high molecular weight polyethylene.[15,16] Over the past two decades, a considerable amount of efforts has been devoted to the modification of the BIP ligand framework and the development of related architecture, with the aim to improve the activity, the selectivity and the thermal stability of the original iron-based catalyst system.[17,18] Apart from inspiring several research groups to exploit the potential of BIP ligand, the revolutionary work of Gibson and co-workers has also proven to be the basis for the polymerization of other monomers.[19]

Herein, the purpose of this bibliographic survey is to provide an overview of well-defined single-site iron-based catalysts specifically involved in homogeneous coordination-insertion polymerization of some selective monomers. Over the past decade, research groups working on coordination-insertion olefin polymerization using iron-based pre-catalysts have contributed to the publication of several exhaustive reviews in this field, either by focusing on a single type of monomer (mainly ethylene), or based on a family of structurally well-defined iron complexes (*vide supra*). However, to our knowledge, there are still numerous studies focusing on the advances in iron-based catalysts for the coordination-insertion polymerization of various monomers such as 1,3-dienes and in particular, cyclic esters which was only briefly reported ten years ago.[20] Hence, this chapter will cover advances in iron-based catalysts for the coordination-insertion (co)polymerization of monomers   specifically 1,3-dienes and polar cyclic esters. Particular emphasis will be made on the recent developments of the polymerization of isoprene, lactide and ε-caprolactone monomers, which have been in particular studied experimentally in this thesis work.

The catalyst performances have been converted in turnover frequencies (TOF, turnover number per time unit in h^{-1}) either from the reported activities [TOF = activity ($g_{polymer}.mol_{cat.}^{-1}.h^{-1}$)/$M_{monomer}$ ($g.mol^{-1}$)] or the isolated polymer yields {TOF = [$n_{polymer}$ (mol)/$n_{cat.}$ (mol)]/time (h)]} or the conversion of monomer {TOF = [conv. (%) * monomer/cat. (ratio)]/time (h)}. However, it should be noted that the performance of the catalytic systems is often strongly dependent on the experimental conditions, such as, for example, the nature of the monomer, the catalyst concentration, the type of solvent, the reaction time, the stirring rate and many other parameters, thus, the comparison of the different systems for a given transformation must be taken with precaution.[7f] The activities are classified into different categories as shown below:

Low [TOF (h^{-1}) < 100], Moderate [100 < TOF (h^{-1}) < 1 000], High [1 000 < TOF (h^{-1}) < 10 000], Very high [10 000 < TOF (h^{-1}) < 100 000] and Extremely high [TOF (h^{-1}) > 100 000]. In a similar way, we have classified the stereoselectivities as fair (50 – 65%), moderate (65 – 85%) and high (>85%).

1.1.2. Iron-catalyzed polymerization of 1,3-diene monomers

1.1.2.1. General overview

The polymerization of 1,3-dienes has seen a considerable surge of interest over the past two decades, due to the wide range of industrial applications of the resultant polymers that can display different thermal, mechanical and physical properties depending on its chain microstructures (*e.g.* 1,4-*cis*, 1,4-*trans*, iso-, syndio-, atactic-3,4 and/or -1,2 vinyl arrangements, Scheme 1.2).[21] Over the different polymerization methodologies such as radical,[22] cationic,[23] or anionic processes,[24] the fine control of the stereo/regio-regularity of the chain microstructure can be reached, to some extent, only through coordination-insertion polymerization using Ziegler-Natta type catalysts.

Butadiene: R = H

Isoprene: R = Me

β-Myrcene: R =

1,4-*cis*   1,4-*trans*   3,4   1,2

iso-, syndio- or atactic
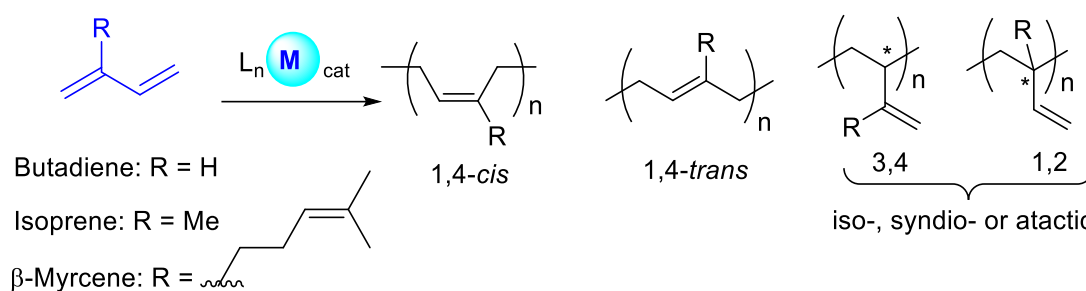
Scheme 1.2. Polymer microstructures from the polymerization of 1,3-dienes

The most commonly used 1,3-diene monomers for the coordination-insertion polymerization include butadiene (BD), isoprene (IP) and β-myrcene (*vide supra*). Though, butadiene and isoprene are petro-sourced, polyisoprene (PI) can be found in nature [*Gutta-percha* (1,4-*trans*) or *Hevea bransiliensis* (1,4-*cis*)] in contrast to polybutadiene (PB) which is only synthetically produced. Likewise, the 3,4 and 1,2 motifs (very scarce) can only be produced synthetically. With regards to unsustainable renewable nature of petroleum resources and the energy crisis, research groups have also started to focus on the replacement of petro-sourced monomers by bio-sourced monomers such as myrcene, ocimene and β-farnesene for the development of biobased green rubber materials.[25,26]

For many years, most of the research works have been focusing on the synthesis of 1,4-*cis* polydienes, which is one of the major components used in the tire manufacturing and elastomer industry due to its natural rubber-like characteristics.[27,28] In particular, 1,4-*cis*-polybutadiene rubber (PB) is the second-largest group of synthetic elastomers used worldwide after styrene-

butadiene rubber (SB) and the total world production capacity of 1,4-*cis*-PB is ~2.2 MT/year with a trend to increase further.[28] On a commercialized scale, 1,4-*cis*-PB was being produced using solution polymerization with Z–N type catalysts.[29] On the other hand, 1,4-*cis* polyisoprene (PI) also displays characteristics similar to that of natural rubber, which can also be produced by Z–N-type catalytic system. However, due to difficulty of synthesis of isoprene monomer, synthetic 1,4-*cis*-PI cannot compete economically with natural rubber.[27,28]

More recently, 1,4-*trans* polydienes have shown to display excellent anti-fatigue properties, among others, that can be used in long durability "green" tires. On the other hand, the selective crosslinking of the pendant vinyl-groups in 1,2- (or 3,4-) polydiene can improve the performance of the material with wet-skid and low rolling resistance tread.[30]

The coordinative polymerization of conjugated dienes (specifically butadiene) was first discovered in 1954,[31] soon after the low-pressure polymerization of ethylene that was published by Ziegler and co-workers.[29] Thereafter, researchers from the academia and industries have continuously focused to improve the performances of the catalytic systems (activity/productivity, selectivity, efficiency in metal catalyst), with the aim of optimizing the preparation of synthetic polymers such as 1,4-*cis* PB. Several single-site metal-based systems of rare earth[32] and transition[33] metals have shown to be highly active for the polymerization of 1,3-dienes, affording simultaneously high molar masses and control over the microstructure, but to date, industrial concerns in the recent period are mainly dominated by four metallic elements—namely neodymium, nickel, cobalt, and titanium.[34] For the synthesis of 1,4-*cis* PB, the industry catalysts are generally based on ternary systems, with a pre-catalyst associated to an activator and an aluminum chain transfer agent as depicted below in Table 1.1.

Table 1.1. Different catalytic systems used for the production of 1,4-*cis*-PB

Catalytic system	Metal (mg/L)	1,4-*cis*-PB (kg/gM)	1,4-*cis* (%)
$TiCl_4/I_2/Al(^iBu)_3$	50	4-10	93
$Co(O_2CR)_2/H_2O/AlEt_2Cl$	1-2	40-160	96
$Ni(O_2CR)_2/BF_3.OEt_2/AlEt_3$	5	30-90	97
$Nd(O_2CR)_2/Et_3Al_2Cl_3/Al(^iBu)_2H$	10	7-15	98

With the advancement in industrial technology neodymium catalyst, in aliphatic solvents, was discovered in the early 1980s and dominates the industrial production of 1,4-*cis* PB since

then.[35] On the other hand, 1,4-*trans* polydienes are rather synthesized either by means of binary catalytic systems often comprising an alkylmagnesium cocatalyst,[36] or by combination with an aluminum derivative in the case of transition metal systems.[37]

It is generally accepted that the stereo- and regio-selectivity of 1,3-dienes polymerization depend on the mode of coordination of the incoming diene monomer (*s-η^2-trans*, *s-η^4-trans* or *s-η^4-cis*) and the conformation of the terminal η^3-allyl unit of the growing polymer chain that is bound to the metal center in *anti* or *syn* fashion, which are exchangeable (Scheme 1.3).[38] In that context, it was shown that stereo- and regio-control can be attained providing that suitable ligand design (steric and electronic) and/or appropriate alkylating agent are combined.

In the case of iron-based catalysts, coordinative polymerization of 1,3-dienes has not been intensively investigated when compared to the field of ethylene polymerization. A majority of the works related to this topic has been reviewed in 2010 by Ricci *et al*.[39, 40] and in a book chapter by Olivier-Bourbigou and coworkers in 2015.[18c] Several research works focusing on well-defined iron-based catalysts have been published since these last bibliographic surveys; therefore, we will present (as far as possible) a comprehensive coverage of the literature in this field. The first section will briefly present studies on the use and impact of various (in particular phosphorous) additives as ligands to the catalytic behavior of iron inorganic FeZ_3 precatalysts, the second part will be devoted to iron-based counterparts bearing tridentate ligands and, finally, the last section will deal with iron complexes supported by bidentate ligands, which is one of the main focus of this thesis work.

The first report on the use of an iron complex for the polymerization of 1,3-dienes was described in 1964 by Noguchi *et al*.[41] Polymerizations of BD and IP were performed at 30 °C for 20 hours using a combination of $Fe(dmg)_2$ (dmg = dimethylglyoximate) and $AlEt_3$ (Al/Fe = 4). PB with content mixture of 1,2/1,4-*trans*/1,4-*cis* units = 63/13/24 and polyisoprene with a quasi-equal amount of 3,4-/1,4-*cis* units = 45/54 along with a very small portion of 1,2 content (1%) were obtained.
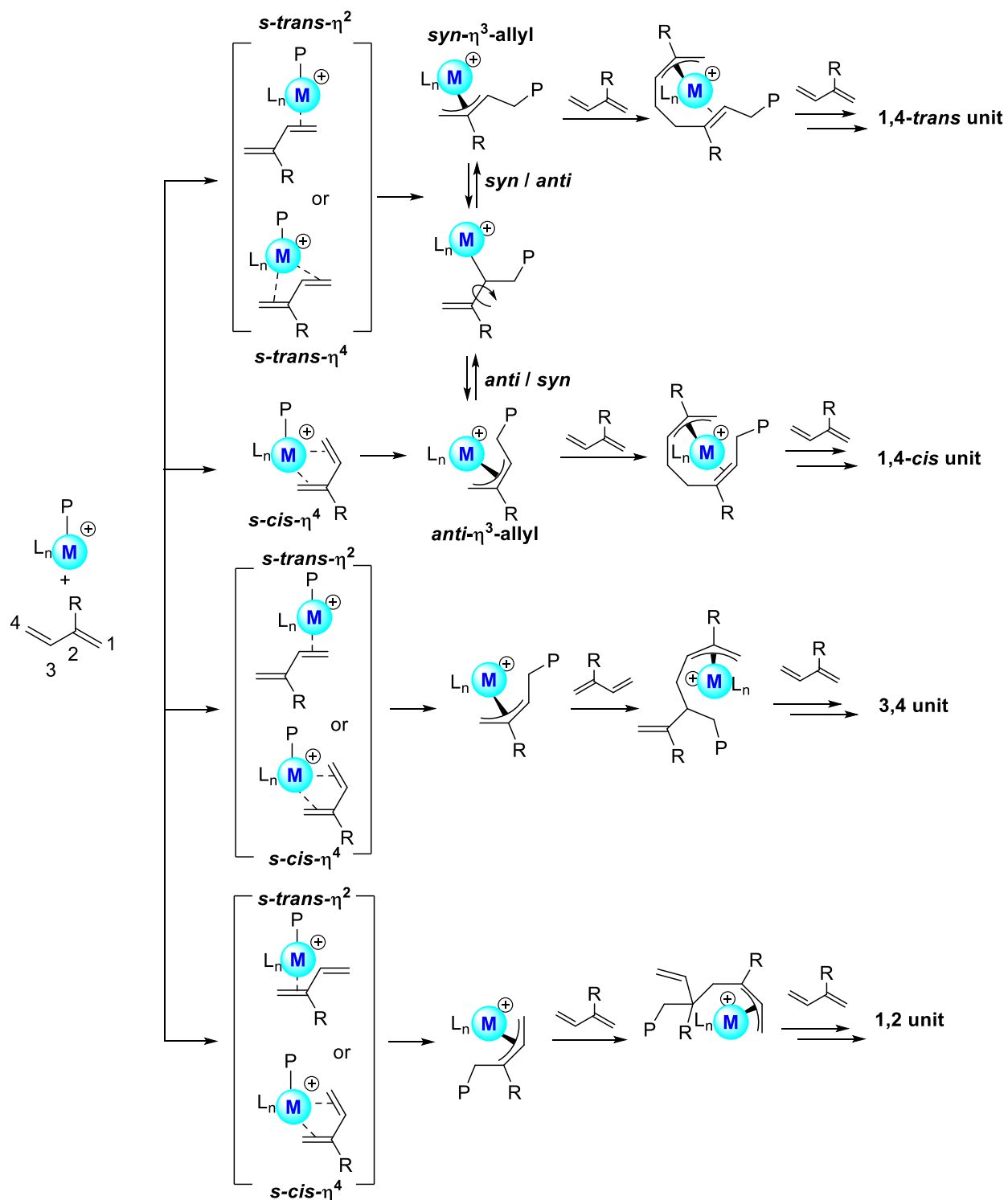
Scheme 1.3. Proposed mechanism of coordinative 1,3-diene polymerization, relevant step for the formation of 1,2/1,4/3,4 microstructure[38]

In 1970, Swift *et al.* studied various cyano-substituted pyridine ligands in combination with Fe(acac)$_3$/AlEt$_3$ (or Al^{i}Bu$_3$) (acac = acetylacetonate) for the polymerization of IP and BD, most of them exhibiting very low activity or none.[42] The best result was obtained with Fe(acac)$_3$/phenyl-2-pyridylacetonitrile/AlEt$_3$ (1/1/3) system, with a TOF of 21 h^{-1} at 25 °C, affording polyisoprene of composition 1,4-*cis*/3,4/1,2 units ≈ 48/50/2. In parallel, BD polymerization was carried out using Fe(acac)$_3$/2-cyanopyridine/AlEt$_3$ (1/1/3) producing PB (TOF = 17 h^{-1}) with an equal fraction of 1,4-*cis* and 1,2 structures (Chart 1.2).
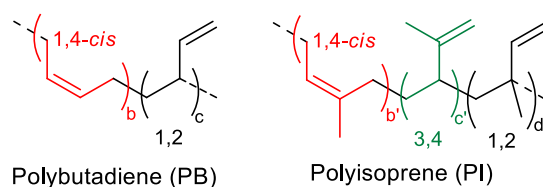
Chart 1.2. Linked microstructures of 1,3-dienes

1.1.2.2. Iron precursors with phosphorous additives for the polymerization of butadiene

In parallel with the development of well-defined iron-based pre-catalysts for the polymerization of butadiene (which will be discussed later in section 2.1.2.2), the group of Zhang and Dong investigated the effect of electron donor phosphorous additives in combination with Fe(acac)$_3$/AlR$_3$ or Fe(2-ethylhexanoate)$_3$/AlR$_3$ [Fe(2-EHA)$_3$]. These catalysts are systematically generated by mixing all the reagents *in situ*, which implies that the mechanism of formation of the active species and its structure remain, until now, unclear. Nevertheless, it has been found that some of these systems display a high tolerance to the polymerization temperature and produce highly regular syndiotactic 1,2-PB under appropriate conditions. For a detailed comparison of various additives and their effect on polymerization, readers are advised to refer to this comprehensive review written by our group in reference.[19] Herein, we will discuss the combination of one of these additives with a catalytic system (Chart 1.3).

Diethyl phosphite
(DEP)
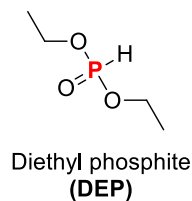
Chart 1.3. Diethyl phosphite (**DEP**) used in combination with Fe(2- EHA)$_3$ for the polymerization of BD

The use of diethyl phosphite (**DEP**)[43] as additive in a ratio of [**DEP**]/[Fe] = 2 – 6, when combined with Fe(2-EHA)$_3$/Al^{i}Bu$_3$, exhibited living character and afforded PB with a prominent content of 1,2-units (> 85%) under appropriate conditions.[44] By applying the ternary Fe(2-EHA)$_3$/Al^{i}Bu$_3$/**DEP** catalytic system, the regio-regularity of the resulting polymer was found to be strongly influenced by the amount of aluminum cocatalyst. When the [Al]/[Fe] ratio was less than ten, amorphous polybutadiene consisting of a mixture of 1,2- and 1,4-*cis* units with a very small portion of 1,4-*trans* was produced, while increasing the ratio above ten, PB with both high content of 1,2-units (> 85%) and syndiotacticity (*rrrr* > 81%) was obtained.[45] The preparation of butadiene-based block copolymers has been further investigated by taking advantage of the living character of this ternary catalytic system.[43] Butadiene was first completely polymerized at 40 °C for 24 hours with Fe(2-EHA)$_3$/**DEP**/Al^{i}Bu$_3$ (BD/Fe/**DEP**/Al = 1 000/1/3/6), which was then followed by the *in situ* addition of 860 eqs. of isoprene to yield a block copolymer of poly(butadiene-*b*-isoprene). In a similar manner, stereoblock copolymer with an amorphous polybutadiene block segment comprised of a mixture of 1,4-*cis*/1,2 content and a crystalline syndiotactic segment was prepared by sequential polymerization using Fe(2-EHA)$_3$/**DEP** in presence of different amounts of cocatalyst. The first stage of the copolymerization was performed using 5 eqs. of Al^{i}Bu$_3$, producing the first amorphous polybutadiene block with 52% of 1,2 content. Subsequently, *in situ* addition of an excess of Al^{i}Bu$_3$ (30 eqs.) and butadiene resulted in a change of selectivity of the catalytic system, providing a second crystalline polybutadiene block.[44]

1.1.2.3. Iron-based catalysts bearing tridentate ligand for the polymerization of 1,3-dienes

The discovery of highly active ethylene polymerization catalysts, (BIP)FeCl$_2$/MAO, prompted some research groups to study their catalytic potential in the polymerization of 1,3-diene monomers (Chart 1.4). An early report claimed that this catalytic system was inactive toward the polymerization of 1,3-dienes, presumably due to the presence of bulky substituents on the *N*-aryl ring of the BIP ligand that could be detrimental to the coordination of the 1,3-diene monomer on the metal center, as compared to the less congested ethylene monomer.[46] The group of Zhang re-examined the use of the iron-based complex supported by the BIP ligand for the 1,3-dienes polymerization, but this time using a BIP ligand that did not incorporate a substituent on the *N*-aryl moiety in order to facilitate the coordination of the monomer.[47] Complexes (BIP)FeCl$_2$ [**7(Cl)**] and (BIP)FeCl$_3$ [**7Cl)'**] were evaluated in butadiene polymerization in presence of 100 eqs. of

MAO. Complex **7(Cl)'** quantitatively produced polymers (TOF = 250 h^{-1} at 20 °C) with high content of 1,4-*trans* units (> 94%), whereas the FeCl$_2$ counterpart **7(Cl)** was less active with mixture of microstructure consisting of 1,4- *cis*/1,4-*trans*/3,4 units ≈ 35/55/10. The high 1,4-*trans* selectivity using **7(Cl)'**/MAO was attributed to the preferential *single*-η^2 coordination mode of butadiene on the metal center due to the tridentate BIP ligand, which could generate a metal-alkyl active species with one less coordination site than that of the corresponding metal with bidentate nitrogen ligand (*vide infra*). The relatively higher activity of complex **7(Cl)'** in comparison with **7(Cl)** was ascribed, by the authors, to a higher electrophilicity of the Fe (III) center than its Fe (II) counterpart. Though, the divergence in activity (and selectivity) of both complexes may also stem from the distinct nature of the pre-catalysts, with the solid-state structure of **11(Cl)** being isolated[48] as an ion pair [(BIP)$_2$Fe][FeCl$_4$] while complex **11(Cl)'** is under monomeric form [(BIP)FeCl$_3$].

FeCl$_2$; R$_1$ = R$_2$ = H [**7(Cl)**]

R$_1$ = R$_2$ = H [**7(Cl)'**]   R$_1$ = H, R$_2$ = Me (**10'**)
R$_1$ = Me, R$_2$ = H (**4Me'**)   R$_1$ = H, R$_2$ = ^{i}Pr (**11'**)
FeCl$_3$ ⎰ R$_1$ = Et, R$_2$ = H (**8'**)   R$_1$ = H, R$_2$ = F (**12'**)
R$_1$ = ^{i}Pr, R$_2$ = H (**9'**)   R$_1$ = H, R$_2$ = CF$_3$ (**13'**)

Low to moderate activities
7(Cl)' and **10'-13'**- Highly 1,4-*trans* selective
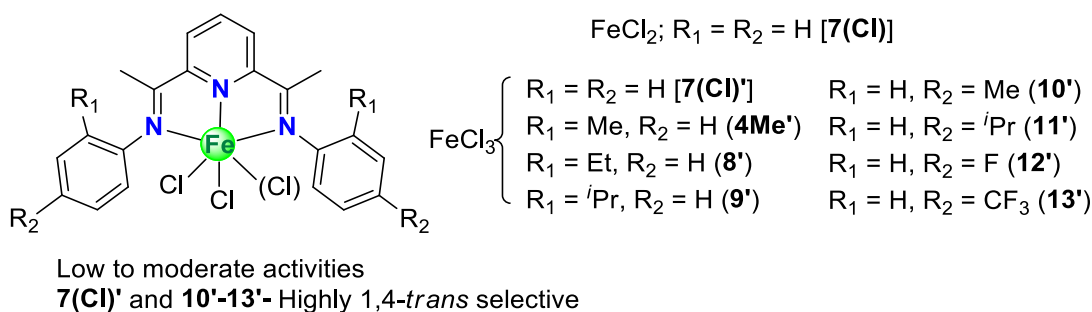
Chart 1.4. (BIP)FeCl$_2$/FeCl$_3$ complexes for butadiene polymerization[47,49]

The same research group carried out further investigations in the field by varying the steric and electronic effect of the BIP ligand.[49] Seven iron (III)-based complexes (**4^{Me}'**, **8'**, **9'** and **10'**–**13'**) supported by different BIP ligands have been evaluated toward the polymerization of butadiene in presence of 40 eqs. of Al^{i}Bu$_3$ and compared with the former complex **7(Cl)'**. Activation of pre-catalyst **7(Cl)'** with an excess of Al^{i}Bu$_3$ showed similar activity and afforded polybutadiene having identical M_n and microstructure content to that using excess MAO. However, the activity and selectivity of the polymerization were greatly influenced by the substituent on the aryl ring of the BIP ligand. It was noticed that an increase of the steric bulkiness at the 2-position of each *N*-aryl group decreases both the activity and the 1.4-*trans* selectivity, with the activity of the catalysts being in the order **7(Cl)'** > **4^{Me}'** > **8'** > **9'** and the composition of the 1.4-*trans* units varying as **7(Cl)'** (95%) > **4^{Me}'** (43%) > **8'** (30%) > **9'** (10%). In contrast, a significant increase of M_n of the resulting polymer was observed for complexes **4^{Me}'**, **8'** and **9'** (M_n > 250 kg/mol) compared to complex **7(Cl)'** (M_n = 29 kg/mol). The authors suggested that the

decrease of activity could be attributed to the difficulty of the incoming monomer to coordinate to the iron center, due to the presence of sterically hindered substituent at the 2-position of each *N*-aryl group for **4^{Me}'**, **8'** and **9'**. Conversely, the presence of a congested iron center is able to delay the appearance of chain transfer with respect to chain propagation, resulting in higher M_n for the polymers produced with complexes **4^{Me}'**, **8'** and **9'**. At this stage, the reason for the decrease in 1,4-*trans* selectivity observed for **7(Cl)'**, **4^{Me}'**, **8'** and **9'** could not be explained. It is noteworthy that the authors prepared an iron complex bearing a BIP ligand with cyclohexyl-substituent instead of aryl-substituent on the imino group, which proved to display very low activity after activation with Al^{i}Bu$_3$ (TOF = 12.5 h^{-1} at 20 °C). Regarding the modification at the 4-position of each *N*-aryl group of the BIP structure, it was found that the presence of an electron-donating alkyl substituent in **10'** (Me) and **11'** (*^{i}*Pr) had essentially no effect on the activity and the 1,4-*trans* selectivity of the catalyst. However, an electron-withdrawing group, F in **12'** and CF$_3$ in **13'**, disrupts the active species by increasing the Lewis acidity of the iron metal center, which, in contrast to bidentate pyridine-imine ligand, reduces the catalytic activity that followed the order **7(Cl)'** > **12'** > **13'**, while keeping the same 1,4-*trans* selectivity. Overall, the authors concluded that modification at the 2-position of the *N*-aryl group of the BIP ligand influences both the activity and the selectivity, whereas the 4-positions altered only the catalytic performance.
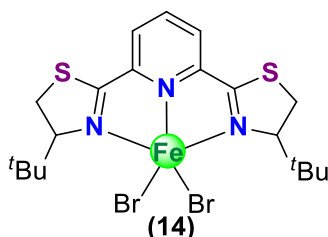
Very highly active and moderately 1,4-*cis* selective

Chart 1.5. [Bis(thiazolinyl)phenyl]FeBr$_2$ complex (**14**) for butadiene polymerization[50]

Britovsek and his collaborators have studied other variants of BIP ligand architecture by introducing a thiazoline moiety on the imino carbon atom. After activation by 500 eqs. of MAO, the iron complex (**14**, Chart 1.5) showed high activity towards the polymerization of butadiene (TOF = 16 266 h^{-1}), producing polymer of high M_n (110 000 g/mol) and narrow dispersity (1.77) with a microstructure consisting of moderate 1,4-*cis* content (74%) as well as a mixture of 1,4-*trans* (17%) and 1,2 units (10%).[50]

Apart from the complexes described above, a variety of iron-based precatalysts supported by tridentate ligands have been reported in literature. These include well defined iron systems bearing *N,N,N*-terpyridine-type and *N,N,O*-pyridyloxy-benzaldimine ligands,[46] 2,6-bis(2-benzimidazolyl)pyridyl and 2,6-bis(pyrazol)pyridine ligands,[51,52] bis(imino)aryl NCN pincer ligand,[53] 2-(methyl-2-benzimidazolyl)-6-(1-arylimino)-ethyl)-pyridine ligand[54] and 2,6-bis(oxazolin-2-yl)pyridine ligand[55] reported by various research groups as shown in Chart 1.6. Overall, it appears that the activity of catalytic systems derived from these precatalysts for the polymerization of butadiene/isoprene is relatively low when compared to highly active system described by Britovsek (Chart 1.5). A brief comparison of these systems can be found in our review.[19]
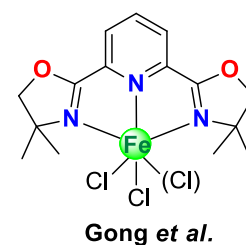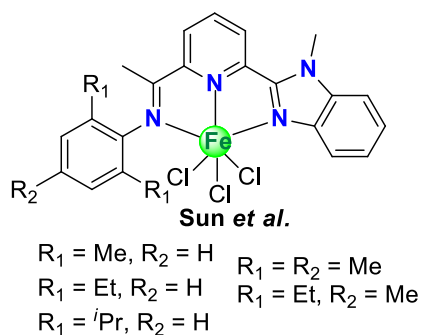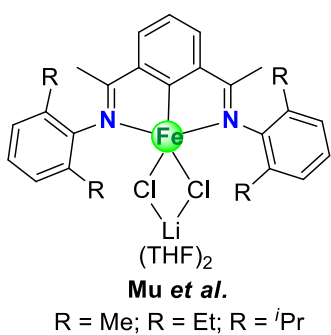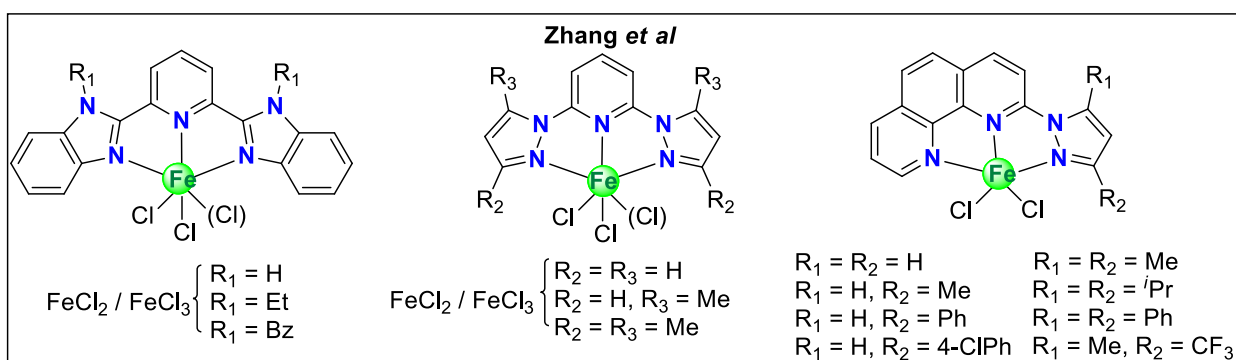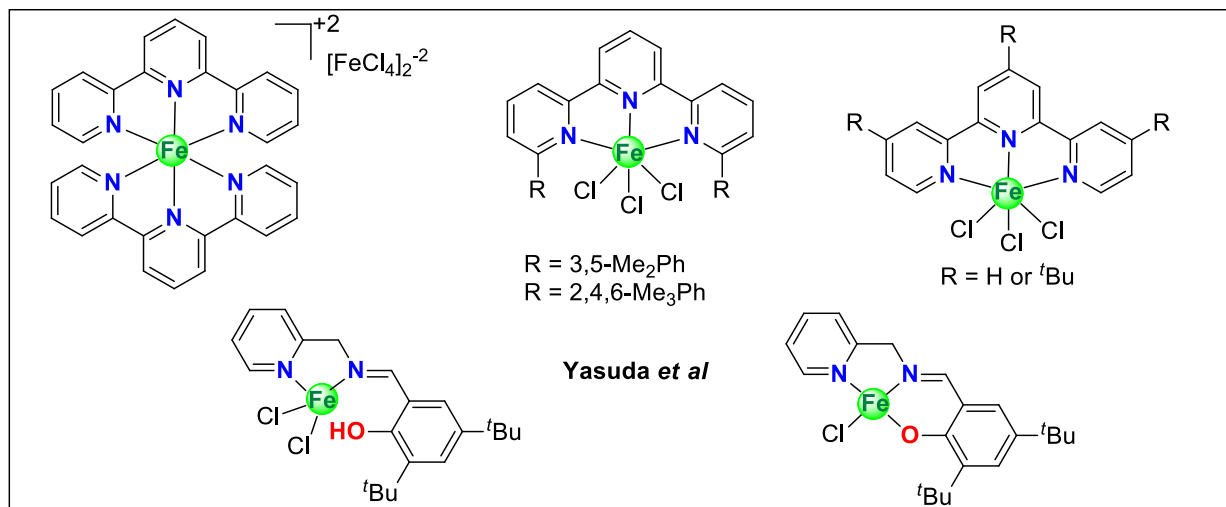
Chart 1.6. Iron-based complexes bearing tridentate ligands used for the polymerization of 1,3-dienes

1.1.2.4. Iron-based catalysts bearing bidentate ligand for the polymerization of 1,3-dienes

The molecular structures of the iron complexes bearing bidentate ligand discussed in this section are depicted in Chart 1.7 below.
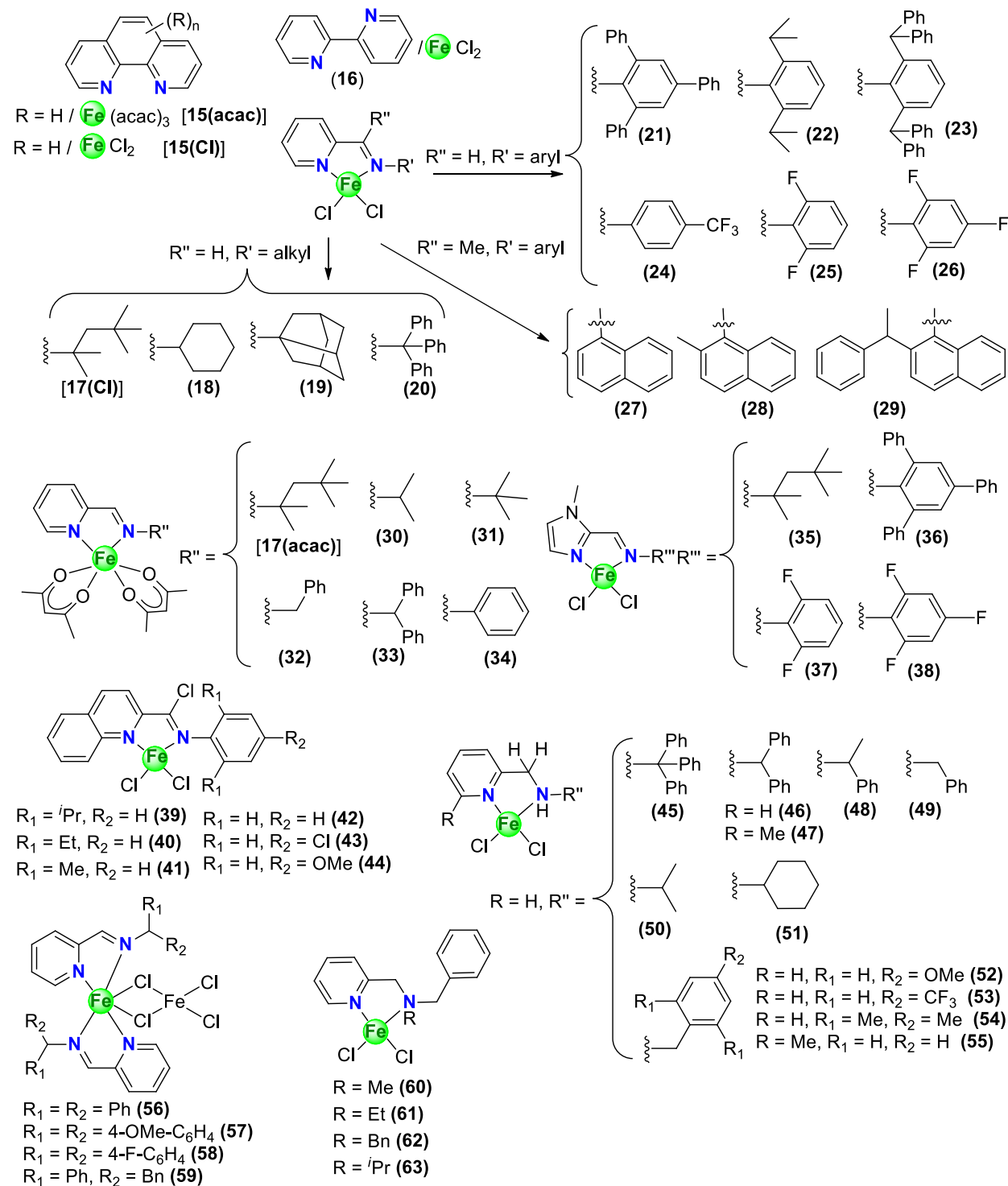
Chart 1.7. Iron-based complexes bearing bidentate ligands for the polymerization of 1,3-dienes.

The group of Wu described in 1982 the polymerization of butadiene using a catalytic system based on Fe(acac)$_3$/Al^{i}Bu$_3$ (1/50) in presence of 1 eq. of 1,10-phenanthroline ligand [**15(acac),** Chart 1.8].[56] Butadiene was found to be converted in high yield at 18 °C in toluene (TOF = 1 668 h^{-1}), with a 1,4-*cis*/1,2/1,4-*trans* = 50/46/4 microstructure of the resulting polybutadiene. In addition, the authors suggested that Fe (III)(acac)$_3$ was probably reduced to Fe (II) after reacting with Al^{i}Bu$_3$ and in presence of 1,10-phenanthroline, producing a putative Fe(1,10-phenanthroline)(^{i}Bu)$_2$ complex.

15(acac)/Al^{i}Bu$_3$ for BD
Moderately active
Fairly 1,4-*cis* selective

R = H / Fe (acac)$_3$ [**15(acac)**]
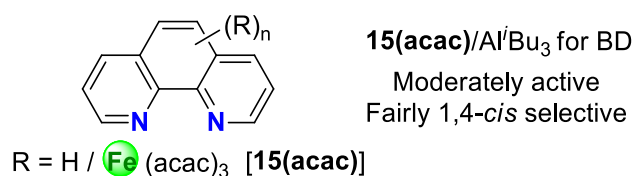
Chart 1.8. [1,10-phenanthroline]Fe(acac)$_3$ complex for butadiene polymerization[56,57,58]

Using the same catalytic system (Chart 1.8), Xie *et al.* showed that the polymerization of isoprene in toluene was able to provide polymer in high conversion, with microstructure consisting of 3,4/1,4-*cis* units of *ca* 30/70, while in apolar hexane solvent, much lower yield was observed.[57] Independently, Hsu *et al.* showed that an additional amount of water (H$_2$O/Al^{i}Bu$_3$ = 0.064) was needed to afford polyisoprene with excellent yield at 10 °C in hexane. The resulting microstructure of the polymer revealed a content mixture of 3,4/1,4-*cis* units of 81/19 with no trace of 1,2 and 1,4-*trans* fractions.[58] The author suggested that the generation of "*a more electron accepting bridged alkyl aluminoxane*" could be accountable for this high activity.

After these initial reports, it was only at the beginning of the 21st century that Ricci and coworkers revitalized the field of coordinative 1,3-dienes polymerization with iron-based catalysts. Several catalytic systems have been studied by combining FeCl$_2$ with various aromatic and aliphatic nitrogen ligands, as well as phosphine bidentate ligands, in presence of alkyl aluminum cocatalysts (Al^{i}Bu$_3$, AlEt$_3$ and MAO).[59] The authors found that most of the active Fe-based catalysts consist of complexes bearing bidentate aromatic nitrogen ligands when activated with an excess of MAO, whereas the use of Al^{i}Bu$_3$ or AlEt$_3$ as cocatalysts was less effective in term of activity and control over the selectivity. Conversely, the use of aliphatic nitrogen bidentate ancillary ligands displays very low activities and regio-/stereo-selectivities, while iron complexes bearing bidentate phosphine ligands were essentially inactive. In this study, FeCl$_2$/MAO system with 1,10-phenanthroline [**15(Cl)**] or 2,2'-bipyridine (**16**) have shown to exhibit very high catalytic

activities for the polymerization of 1,3-dienes at 20 °C when activated with 1000 eqs./Fe of MAO (Chart 1.9). For example, the system **15(Cl)**/MAO enabled the polymerization of butadiene with a TOF of *ca* 2.73 x 10^6 h^{-1}, affording polymer with a mixed structure of 1,4-*cis*/1,2 content = 30/70.

15(Cl)/MAO for BD
Extremely active
Moderately 1,2 selective
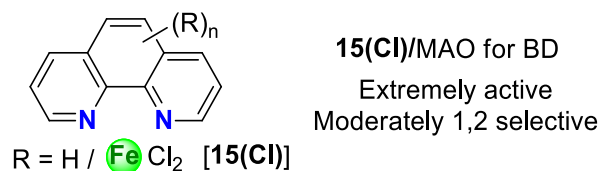
R = H / Fe Cl$_2$ [**15(Cl)**]

Chart 1.9. [1,10-phenanthroline]FeCl$_2$ [**15(Cl)**]complex for butadiene polymerization[59]

Moreover, the resulting polymer had a high molecular weight (M_w = 1 517 kg/mol) with narrow molecular weight distribution (M_w/M_n = 1.2), which indicated the presence of a single-site active species. Various substituted-1,10-phenanthroline ligands combined with FeCl$_2$ were also screened for the polymerization of butadiene, after activation with MAO, and proved to be less active when compared to the system bearing unsubstituted 1,10-phenanthroline ligand. In particular, the use of 2,9-dimethyl-1,10-phenanthroline ligand showed lower catalytic activity with respect to the polymerization of butadiene (TOF = 340 h^{-1} at 20 °C), probably because of an increase of the steric hindrance around the coordination sphere of the metal catalyst that could disrupt the coordination of the incoming monomer.

Using **16**/MAO catalytic system at 20 °C, polybutadiene (TOF = 2.73 x 10^6 h^{-1}) with 1,4-*cis*/1,2 structures (33/67) and syndiotactic sequence (*rrrr* = 36.9%) was obtained (Chart 1.10). As noted above, the use of **16**/Al^{i}Bu$_3$ or AlEt$_3$ exhibited lower catalytic activity (TOF ≈ 49 x 10^3 and 25 x 10^3 h^{-1}, respectively) as well as a slight decrease of 1,2 selectivity, emphasizing the role of the cocatalyst toward the selectivity of the polymerization.[59] In addition, it was shown that the selectivity was dependent on the reaction temperature, with low temperature leading to a high increase content of 1,2 units at – 78 °C (content of 1,2 fraction = 91% and *rrrr* = 52.5%), while the activity of the catalysts decreased drastically (TOF = 18 h^{-1}). Similar results were obtained using (2,2'-bipyridine)$_2$FeEt$_2$ complex when activated with MAO.[60]

In the case of isoprene, high activity was observed using **16**/MAO (TOF ≈ 800 x 10^3 h^{-1}),[59] affording polyisoprene with a microstructure containing 1,4-*cis*/3,4 units = 33/67. As in butadiene polymerization, a significant increase of 3,4-selectivity was noticed at – 78 °C (1,4-*cis*/3,4 units = 7/93), likely corresponding to syndiotactic polyisoprene sequence, although in this case the yield was poor (TOF = 14 h^{-1}). Since the binary **16**/MAO produces stereo-regular 3,4-polyisoprene,

Rosa *et al.* used this recipe at – 30 °C to prepare a syndiotactic-rich polyisoprene with 1,4-*cis*/3,4 contents of 15/85 and *rrrr* = 53%, which, after hydrogenation, gave for the first time a syndiotactic-rich poly(3-methyl-1-butene).[61]
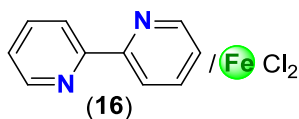
(16)/MAO
Extremely active for BD, IP, PD and DMB
Poor activity for BD and 3-MP at low temperature
Moderately 1,2 selective for BD and PD
Highly 1,2 selective for BD and 3-MP at low temperature

(16)/AlR$_3$
Highly active for BD and IP
Fairly 1,4-*cis* selective for BD and IP

Chart 1.10. [2,2'-bipyridine]FeCl$_2$ **(16)** complex for 1,3-dienes polymerization[59,61,62,63]

Polymerization of 1,3-pentadiene (PD) and 2,3-dimethyl-1,3-butadiene (DMB) was also undertaken with **16**/MAO catalytic system at 20 °C, yielding quantitatively poly(1,3-pentadiene) (TOF = 79 x 10^3 h^{-1}) with structure content of 1,4-*cis*/1,2 units (30/60) and highly stereo-regular poly(2,3-dimethyl-1,3-butadiene) (TOF = 703 x 10^3 h^{-1}) with 1,4-*cis* units > 99%, respectively.

Later, the same group reported the polymerization of 3-methyl-1,3-pentadiene (3-MP) using **16**/MAO at – 30 °C affording, for the first time, highly crystalline poly(3-methyl-1,3-pentadiene) with syndiotactic 1,2 sequence (1,2 content of 99% and *rrrr* ≥ 99%).[62] However, the activity of the catalyst was found to be very low under these conditions (TOF = 3 h^{-1}).

The origin of the regio-selectivity of the **16**/MAO catalytic system toward the polymerization of isoprene and 3-methyl-1,3-pentadiene (3-MP) has been recently investigated by DFT calculation by the group of Luo.[63] The authors started their studies by representing the active species in the form of the cationic complex [(2,2'-bipyridine)$_2$FeMe]$^+$. The calculation revealed that in this active species, the 2,2'-bipyridine is a redox-inert ligand that contrasts with that observed in related redox-active iminopyridine and bis(imino)pyridine ligands.[64] More importantly, calculation of the insertion pathway suggested that the 3,4-regio-selectivity of isoprene was favored over the 1,4-insertion, similarly, it appears that the steric factor also governs the 1,2-regio-regularity of the polymerization of 3-MP with the (2,2'-bipryidine)$_2$FeCl$_2$/MAO.

Subsequently, Ritter and coworkers have described the selective polymerization of isoprene with high catalytic activity using well-defined substituted iminopyridyl iron-based complexes [**17(Cl)** and **21**], upon activation with AlEt$_3$ or Al^{i}Bu$_3$ and [Ph$_3$C][B(C$_6$F$_5$)$_4$] (Chart 1.11).[25] In this study, the authors found that an inversion of selectivity of the polymerization could

be reached depending on the nature of the substituent attached to the imino group. Using an octyl-substituted iminopyridyl iron complex **17(Cl)** with Fe/Al^{i}Bu$_3$/[Ph$_3$C][B(C$_6$F$_5$)$_4$] = 1/3/1, polyisoprene with microstructure containing 1,4-*trans*/1,4-*cis*/3,4 units = 91/1/8 was quantitatively achieved at 23 °C (TOF = 500 h^{-1}).

17(Cl)   **(21)**
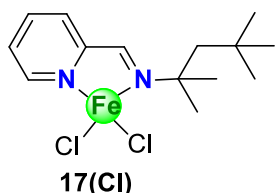
17(Cl)/Al^{i}Bu$_3$/[Ph$_3$C][B(C$_6$F$_5$)$_4$]
Low activity for IP, My and highly active for Fa
Highly 1,4-*trans* selective for IP and My
Fairly 1,4-*cis* selective for Fa
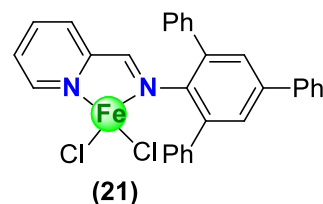
21/AlR$_3$/[Ph$_3$C][B(C$_6$F$_5$)$_4$]
Moderate to low activity for IP,My and Fa
Moderate to Highly 1,4-*cis* selective for all

Chart 1.11. [Iminopyridine]FeCl$_2$ **17(Cl)** and **21** complexes for 1,3-dienes polymerization[25]

On the other hand, 1,4-*cis* polyisoprene with 1,4-*trans*/1,4-*cis*/3,4 content = 1/66/33 was obtained, to some extent, after 1 hour at 23 °C (TOF = 1 x 10^3 h^{-1}) with supermesityl-substituted iron complex **21** using Fe/AlEt$_3$/[Ph$_3$C][B(C$_6$F$_5$)$_4$] = 1/3/1. Moreover, the % of 1,4-*cis* polyisoprene could be improved up to 85% at lower temperature with content of 3,4 decreasing to 14% (TOF = 246 h^{-1} at – 78 °C). With these catalytic systems, the M_n were as expected for one polymer chain per Fe metal, with relatively narrow molecular weight distributions (Đ = 1.7 – 2.0, M_w = 62.5 – 75 kg/mol). It should be noted that the replacement of the alkyl group of the aluminum agent (^{i}Bu *vs* Et) has little influence on the selectivity of the polymerization. In addition, the authors conducted the polymerization of bio-sourced 1,3-diene monomers, β-myrcene (My) and farnesene (Fa) isomers (mixture of α and β isomers), and they have shown that only the β isomers could be polymerized with pre-catalyst **17(Cl)** and **21**. As for isoprene, the selectivity of the polymerization of both monomers, after activation with AlR$_3$/[Ph$_3$C][B(C$_6$F$_5$)$_4$] (R = ^{i}Bu for **17(Cl)** and R = Et for **21**), strongly depends on the nature of the imino group, with complex **17(Cl)** producing poly-β-myrcene or poly-β-farnesene with high content of 1,4-*trans* units (88 and 87%, respectively), while complex **21** yields polymers consisting of large amount of 1,4-*cis* units (76 and 71%, respectively).

In 2016, Chen and coworkers expanded this work by using iron-based complexes supported by various alkyl- (**17(Cl)** – **20**) and aryl- (**21** – **23**) substituted-iminopyridyl for the polymerization

of isoprene (Chart 1.12).[65] Different alkylaluminum reagents were assessed in presence of pre-catalyst **18**. Only an excess of MAO (500 eqs./Fe) was capable of producing polyisoprene in high yield (TOF = 804 h^{-1} at 25 °C) and high M_n (> 60 kg/mol), while the use of 150 eqs. of AlEt$_2$Cl gave polymer in high yield but with low molar masses, and Al^{i}Bu$_3$ or AlEtCl$_2$ were not efficient. After 2 hours at 25 °C in presence of 500 eqs. of MAO, the aryl-substituted-iminopyridine iron based complexes **21** – **23** afforded polymers with higher M_n = 103 – 182 kg/mol and TOF = 1 038 – 1 224 h^{-1} than the related alkyl-substituted Fe pre-catalysts **17(Cl)** – **20** (M_n = 61 - 79 kg/mol and TOF = 726 – 1 038 h^{-1}). The authors suggested that the electron-withdrawing aryl group could enhance the electrophilicity at the metal center, which in turn lead to stronger monomer coordination and faster chain propagation. In addition, the steric hindrance around the metal center, conferred by the presence of bulky aryl group, could reduce the appearance of chain transfer, thereby producing a polyisoprene with a higher M_n. However, in contrast to the work of Ritter and coworkers, the *trans*/*cis* ratio was scarcely affected by the nature of the substituent on the imino group (alkyl *vs* aryl) when an excess of MAO was used as the alkylating agent. In fact, polyisoprenes with moderate 1,4-*cis* content (*ca* 63 – 78%) and low 1,4-*trans* (*ca* 3 – 9%) units were produced with all pre-catalyst **17(Cl)** – **23**, emphasizing that the alkylating agent/cocatalyst couple plays an important role in controlling the stereo-selectivity. It is noteworthy that the nature of the imino substituent slightly influence the regio-selectivity with a larger amount of 3,4 content, at the expense of mainly 1,4-*cis* units, for the alkyl-substituted Fe complexes **17(Cl)** – **20** with 1.4-*cis*/3,4 content ≈ 77.5/15, when compared to the aryl-substituted pre-catalysts **21** – **23** that displayed a microstructure consisting of 1.4-*cis*/3,4 units ≈ 66/30. As previously seen in Ritter's work, the activity of the pre-catalysts **17(Cl)** and **21** decreases at – 25 °C and the resulting polymers display higher M_n when compared to the polymerization conducted at room temperature, most likely due to a decrease of chain transfer at lower temperature. Interestingly, the resulting polyisoprene microstructure was not affected by the reaction temperature.

Recently, further investigations have been described by the group of Wang regarding the nature of the imino substituent using fluorinated-aryl iminopyridine ligands (**24** – **26**) as well as complexes **17(Cl)** and **21** (Chart 1.12).[66] These complexes have been employed for the polymerization of isoprene, in combination with an excess of MAO and in absence or presence of 1 eq. of [Ph$_3$C][B(C$_6$F$_5$)$_4$]. The authors showed that under the same experimental condition, the incorporation of fluorinated aryl moiety on the imino group of the iron complexes **24** – **26** provided

polyisoprene in higher yield than complexes **17(Cl)** and **21**. Using an excess of MAO, the activities were in the order **24 > 25 >> 26 > 21 > 17(Cl)**, which followed the trend observed previously with electron-withdrawing substituents leading to higher activity of the catalyst due to an increase of Lewis acid character at the iron metal center.
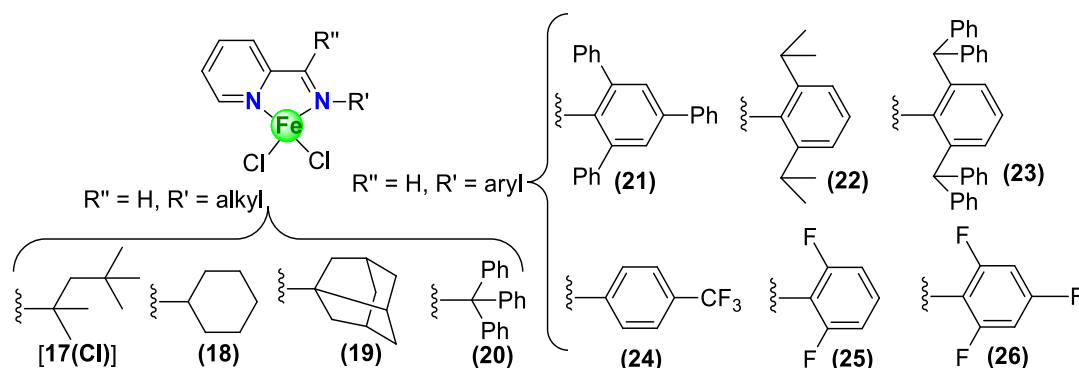
17(Cl)-21/MAO Moderate (Activity and 1,4-*cis* selectivity)
22-25/MAO Moderate to low (Activity and 1,4-*cis* selectivity)
17(Cl), 21, 24-26/MAO Low activity and high 1,4-*trans* selectivity

Chart 1.12. [Iminopyridine]FeCl$_2$ **17(Cl) – 26** complexes for isoprene polymerization[65,66]

In presence of 500 eqs. of MAO, complexes **24** and **25** produced polyisoprene with relatively low M_n (*ca* 90 kg/mol) and broad Đ (3.5 – 4.3), while complex **26** afforded polymers with high M_n (190 kg/mol) and narrow molecular weight distribution (Đ = 2.1); these differences are, to date, not completely rationalized. The microstructures of the polymers resulting from the polymerization of isoprene with catalysts **24 – 26** were not impacted by the nature of the fluorinated substituent, with a quasi-equal content of 1,4-*cis* and 3,4 units. However, when the polymerization of isoprene was conducted with complexes **17(Cl), 24 – 26** in presence of 5 eqs. of MAO and 1 eq. of [Ph$_3$C][B(C$_6$F$_5$)$_4$], preferential 1,4-*trans* selectivity (up to 95%) was observed with total absence of 1,4-*cis* units, again indicating that the cocatalyst plays a significant part in the control of stereo-selectivity. In contrast to the binary **24 – 26**/MAO system, the resulting polyisoprenes displayed narrow molecular weight distribution and low M_n (M_n = 1.4 – 1.6 kg/mol and Đ = 1.7 – 2.2), probably due to an increase of chain transfer when the ternary **24 – 26**/MAO/[Ph$_3$C][B(C$_6$F$_5$)$_4$] system was used. Surprisingly, the polymerization of isoprene using the binary **17(Cl)** or **21**/MAO (MAO/Fe = 500) catalyst behaved very differently in comparison with the study of Chen *et al*. Firstly, the activity of the catalysts proved to be very low at 25 °C and, secondly, the polymers did not exhibit the same microstructure as previously described. The authors have shown that preferential 1,4-*trans* stereo-selective polymerization of isoprene was

achieved using **17(Cl)**/MAO (1,4-*trans*/3,4 units = 90/10, with TOF = 138 h^{-1}), with polymer displaying bimodal molecular weight distribution. This is very different from the work of Chen *et al.* who showed that the same system produced polyisoprene in high yield featuring a narrow molecular weight distribution with a slight preference for 1,4-*cis* units (1,4-*cis* = 77.5%). When compared to the work of Chen *et al.* using **21**/MAO, a fairly similar microstructure content of the resulting polyisoprene was obtained (1,4-*cis*/3,4 with ratio = 65/35 *vs* 63/34), but the polymer was produced in lower yield (TOF = 264 *vs* 1 224 h^{-1}) with lower M_n. The introduction of dealkylating agent [Ph$_3$C][B(C$_6$F$_5$)$_4$] in presence of 5 eqs. of MAO and complex **17(Cl)** enhanced the 1,4-*trans* stereo-selectivity of isoprene polymerization (98%), despite the production of polymer in low yield and low M_n, in contrast to the work of Ritter and coworkers. Conversely, the combination of **21**/MAO/[Ph$_3$C][B(C$_6$F$_5$)$_4$] has proved ineffective with respect to the polymerization of isoprene.

In mid-2020, the group of Luo and Wang attempted to rationalize the stereoselectivities observed with the Ritter's catalytic system comprising the iminopyridine complexes **17(Cl)** and **21** (Chart 1.11).[67] In this study, the electronic structures and mechanism behind the catalytic performances of **17(Cl)**/Al^{i}Bu$_3$/[Ph$_3$C][B(C$_6$F$_5$)$_4$] and **21**/AlEt$_3$/[Ph$_3$C][B(C$_6$F$_5$)$_4$] systems were probed through DFT computations. Firstly, the electronic structures and the spin state were investigated on the basis of calculated Mössbauer spectroscopic parameters and single point energy using the crystal structure. The ground state of expected active species [(iminopyridine)Fe(Me)]$^+$ was found to be in quintet state, indicating that the active species **A1** (for **17(Cl)**) and **A2** (for **21**) are high spin species with relatively similar electron densities, thus revealing the limited effect of electron density on the selectivity (Figure 1.1).
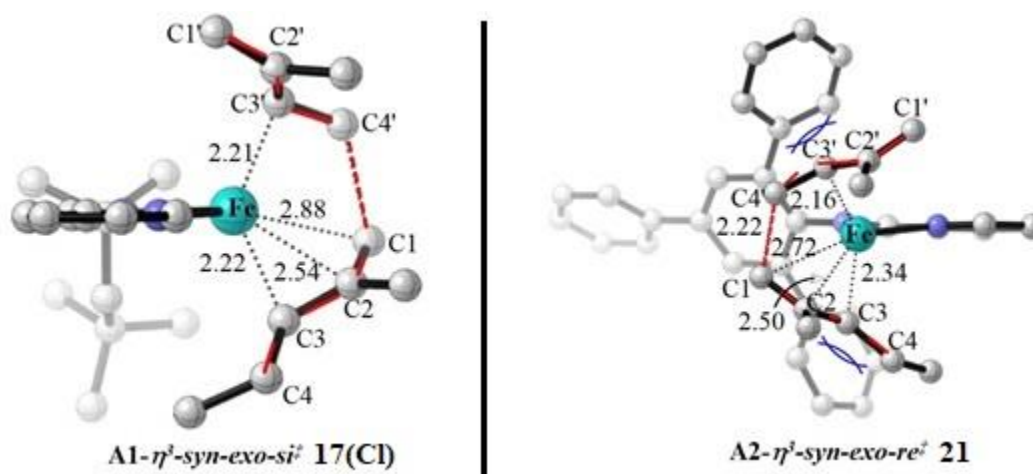
Figure 1.1. Optimized transition state structures with selected structural parameter (Å) [67]

For the isoprene polymerization with cationic **17Me⁺**, it was observed that the formation of 1,4-*trans* units was due to the higher coordination energy as well as the higher insertion energy possessed by the *cis* monomer, leading to the negligible number of 1,4-*cis* units in the polymer chain. This meant that the *syn* allyl conformer combines more tightly with the Fe center than *anti* allyl, which results in the electronic stabilization of **A1-η³-syn-exo-si** transition state.

On the contrary, for the cationic [(supermesityl-iminopyridine)Fe(Me)⁺, the energy of favored transition state for the *cis*-insertion was found to be lower than that for the *trans*-insertion which rationalizes the 1,4-*cis* preferential polymerization in this case. The relative instability of **A2-η³-syn-exo-re** transition state could be ascribed to the repulsive interaction between the terminal C=C bond, polymer chain and the phenyl of supermesityl substituent. Therefore, the absence of 1,4-*trans* selectivity in the polymerization of isoprene was attributed to the steric hindrance between the supermesityl group and polymer chain.

The same year, Sun *et al.* targeted the iminopyridine skeleton to obtain a new series of bis-chelated ketiminopyridine complexes **27 – 29**, bearing different *N*-aryl substituents as various naphthyl derivatives (Chart 1.13).[68] These complexes were deployed as precatalysts for isoprene polymerization. Initially, the authors studied the effect of cocatalyst on the activity and the selectivity of various catalytic systems derived from the complex **28** and a series of cocatalysts including MAO, MMAO, EASC and AlMe₂Cl, from which it was observed that good catalytic activity was only achieved when the precatalyst was activated with MAO or MMAO (TOF = 6 400 – 6 600 h⁻¹).

27 and **28**/MAO - Moderately active and fairly 1,4-*cis* selective
29/MAO - Moderately active and 1,4-*trans* selective
27 and **28**/EASC - Moderately active and 1,4-*trans* selective
29/EASC - Low activity and high 1,4-*trans* selectivity
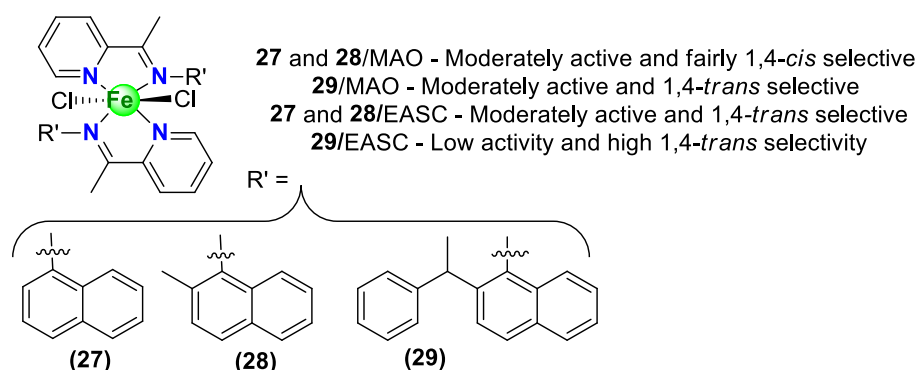
Chart 1.13. [ketiminopyridine]FeCl₂ **27 – 29** complexes for isoprene polymerization[68]

The polymerizations of isoprene catalyzed by **28**/MAO or **28**/MMAO systems at room temperature were very similar in terms of activity (TOF = 6 600 *vs* 6 400 h⁻¹) and molecular weights (M_n = 70.7 *vs* 65.5 kg/mol, *Đ* = 2.0 *vs* 3.2) whereas they were different in terms of

selectivity (1,4-*cis*/1,4-*trans*/3,4 = 51/27/22 *vs* 30/51/19). In contrast to **28**/MAO or **28**/MMAO systems, the catalytic system **28**/EASC proved to be less active (TOF = 2 640 h^{-1}) but moderately 1,4-*trans* selective (1,4-*cis*/1,4-*trans* = 19/81), producing polyisoprene with low molecular weights and narrow dispersity (M_n = 1.9 kg/mol and Đ = 1.3) because of low yield (33%). Increasing the temperature from 20 °C to 70 °C during the polymerization increased the catalytic activity of **28**/MAO system (TOF = 3 800 *vs* 6 800 h^{-1}), however, the molecular weights of the resulting polyisoprenes decreased from 148 kg/mol to 55 kg/mol owing to the increased chain transfer reactions at higher temperatures. Lastly, the substituent's steric effect on the catalytic activity and selectivity of **27 – 29**/MAO system was also briefly mentioned, where the activity was decreased in the order **27** > **28** > **29** due to the increased steric bulk around the iron center hindering the monomer coordination and, subsequently, its insertion. On the other hand, the introduction of steric substituents on the ortho-position of amine moiety increased the 1,4-*trans* content (1,4-*trans* = 27 **(28)** *vs* 32 **(27)** *vs* 64 **(29)**).

Independently, Liu *et al.* have modified the iminopyridine skeleton by replacing the pyridine ring with a quinoline moiety and by introducing an additional chloride substituent on the carbon of the imino group (Chart 1.14).[69]

38-43/MAO
Poor activity and selectivity

R$_1$ = ^{i}Pr, R$_2$ = H **(38)**   R$_1$ = H, R$_2$ = H **(41)**
R$_1$ = Et, R$_2$ = H **(39)**   R$_1$ = H, R$_2$ = Cl **(42)**
R$_1$ = Me, R$_2$ = H **(40)**   R$_1$ = H, R$_2$ = OMe **(43)**
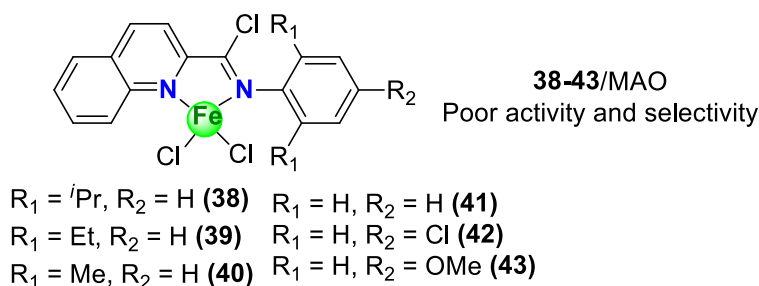
Chart 1.14. [*N*-arylcarboximidoylchloride-quinoline]FeCl$_2$ **38-43** complexes for butadiene polymerization[69]

Thus, several iron-based complexes supported by 2-(*N*-arylcarboximidoylchloride)-quinoline ligands, bearing different substituents on the aryl group (**38 – 43**), were used for the polymerization of butadiene after activation with 100 eqs. of MAO. In contrast to the related highly active (1,10-phenanthroline)FeCl$_2$ [**17(Cl)**] and (2,2'-bipyridine)FeCl$_2$ (**16**) pre-catalysts, complexes **38 – 43** associated to MAO display low activities in butadiene polymerization (TOF < 60 h^{-1} at 20 °C) and poor selectivity (63–78/8–20/13–17 for 1,4-*cis*/1,4-*trans*/1,2 units, respectively).

The group of Wang has further investigated the effect of the auxiliary ligands in the iron-based iminopyridyl complexes [*e.g.* **17(Cl)** – **26**], for the polymerization of isoprene by replacing both chloride anions with two acetylacetonato groups [**17(acac)**, **30** – **34**] (Chart 1.15).[70] Upon treatment with 500 eqs. of MAO, complexes **17(acac)** and **30** – **34** displayed good activities, the binary **34**/MAO, **33**/MAO, **32**/MAO and **30**/MAO systems being the most effective catalysts (TOF up to 12 000 h^{-1}) that also afforded polyisoprene with the highest M_n (43 000 – 67 000 g/mol). The authors suggested that the catalytic performances were related to the electronic effect of the substituent on the imino group, with complexes bearing electron-withdrawing group exhibiting the highest activity. The microstructure of the resulting polyisoprene, produced with the pre-catalysts **30** and **32** – **34**, showed poor selectivity with an almost equal content in 1,4-*cis* and 3,4 units (1,4-*cis* = 36 – 55% *vs* 3,4 = 42 – 54 %).
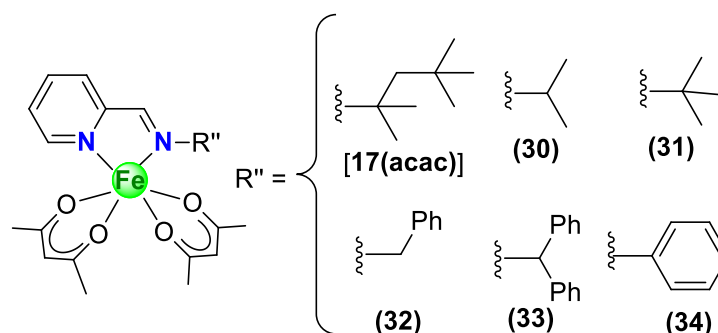
17(acac)/MAO - Low activity and moderate 1.4-*trans* selectivity at room temperature
Low activity and low selectivity at low temperature
30,32-34/MAO - Highly active but not selective at room temperature
31/MAO - Moderately active and 1,4-*trans* selective at room temperature

Chart 1.15. [Iminopyridine]Fe(acac)$_2$ complexes **17(acaac), 30-34** for isoprene polymerization[70]

In contrast, the binary **17(acac)**/MAO and **31**/MAO catalytic systems generated polymers with high 1,4-*trans* content (> 74 %). When compared to the related iron-based iminopyridyl **17(Cl)** complex the polymer produced in this study afforded similar microstructure than the previous investigation performed by the same group[66] but, in this case, with an activity 5 times higher (TOF = 590 h^{-1} vs 138 h^{-1}, respectively). However, the resulting selectivity found with the binary **17(acac)**/MAO catalytic system (1,4-*trans* content = 87 %) or **17(Cl)**/MAO (1,4-*trans* content = 90 %)[66] is in sharp contrast with the result reported by the group of Chen using **17(Cl)**/MAO (1,4-*cis* content = 78 %),[65] under the same experimental conditions. The origin of the selectivity is still unclear but, as suggested by the authors, this behavior may be related to the

nature of the counter anion (acac$^-$ vs Cl$^-$). Increasing the temperature of the polymerization from –30 °C to 50 °C using complexes **17(acac)** or **32**, combined with MAO, resulted in a significant increase of 1,4-*trans* contents (1,4-*trans* = 36% *vs* 86% for **17(acac)** and 0% *vs* 13% for **32**), suggesting that higher temperature favor the 1,4-*trans* selectivity.

In parallel, the same group described the polymerization of isoprene using the akin iron-based iminoimidazole pre-catalysts **35 – 38** (replacement of the pyridyl moiety in complexes **17**, **21**, **25** and **26** by an imidazole group).[71] Studies of various cocatalyst systems have shown that only the combination of 10 eqs. of AlEtCl$_2$ and 1 eq. of [CPh$_3$][B(C$_6$F$_5$)$_4$] allowed the formation of polymers (Chart 1.16). In all case, high 1,4-*trans* polyisoprenes were obtained with complexes **35 – 38** (1,4-*trans* units > 96%), but, no correlation between the nature of the substituent on the imino group and the catalytic activity (TOF ≈ 500 h^{-1}) and selectivity of each complex as well as the molecular characteristic of the resulting polymers (M_n ≈ 1 800 g/mol) could be drawn.
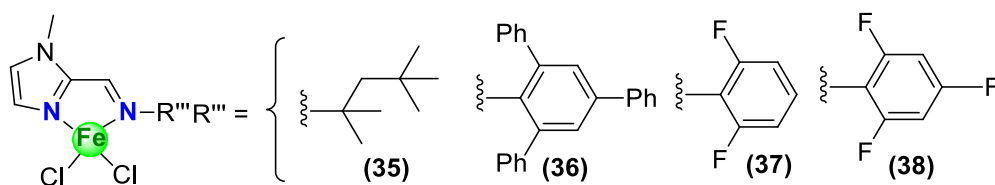
35-38/AlEtCl$_2$/Al^{i}Bu$_3$/[Ph$_3$C][B(C$_6$F$_5$)$_4$] - High 1,4-*trans* selectivity with low activity

Chart 1.16. [Iminoimidazole]FeCl$_2$ complexes **35-38** for isoprene polymerization[71]

Independently, the polymerization of isoprene has been successfully achieved in a hybrid material constituted of carbon nanotubes (CNTs) and iron nanoparticules (NPs). Specifically, the system consists of an iron-based pre-catalyst supported by a bidentate 2-[1-(1-naphthalenylimino)ethyl]-pyridyl ligand immobilized on the iron NPs through π interactions, themselves confined in CNTs.[72] Upon activation with a combination of Al(^{i}Pr)$_3$/[CPh$_3$][B(C$_6$F$_5$)$_4$], this hybrid system was able to produce a CNT-confined Fe NPs covered with a polyisoprene (stereoregularity not specified) air barrier.

Recently, Wang *et al*. reported a series of aminopyridine iron (II) chloride complexes **45 – 55** for their catalytic application in isoprene polymerization (Chart 1.17).[73] Upon activation with MAO, the catalytic activities of complexes varied as of the steric and electronic influences of substituents. The observed catalytic activities of these catalysts appended with different substituents varied in the order **49 = 50 = 51 > 48 > 46 > 45 > 47**, which suggests that more bulky

groups occupying the space around the metal center in the active species slow down the rate of coordination and insertion of the monomer.
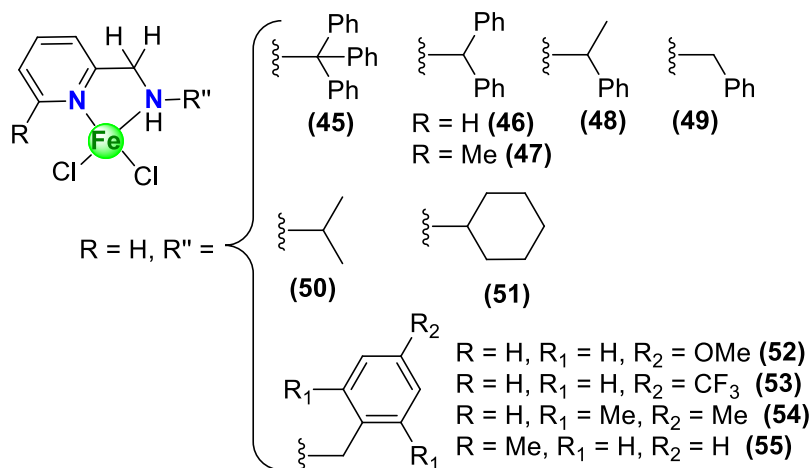
49-51/MAO - Highly active and fairly 1,4-*cis* or 3,4 selective for isoprene
46 and **47**/MAO - Low activity and moderate 1,4-*trans* selectivity (**46**) or 1,4-*cis* selectivity (**47**)
53/MAO - Highly active and fairly 3,4 selective

Chart 1.17. [Aminopyridine]FeCl$_2$ complexes **45-55** for isoprene polymerization[73]

This was also proved from the lowest activity (TOF = 130 h^{-1}) exhibited by the complex **47** where the addition of methyl group on the ortho position of pyridine imparted more steric bulk at the iron center leading to poor conversions (13%). However, the increased steric hindrance at the iron center produced high molecular weight polyisoprenes as observed for complexes **47** (M_n = 123 kg/mol) and **45** (M_n = 112 kg/mol), which speaks in favor of the promotion of chain propagation compared to transfer with aluminum species. Regarding the selectivity, in general, all the complexes produced polyisoprenes with nearly equal 1,4-*cis* and 3,4 contents whereas exceptionally for the complexes **46** and **47**, an inversion of selectivity was observed indicating the effect of ligand tuning on the microstructure (1,4-*trans*/1,4-*cis*/3,4 = 69/9/22 *vs* 4/69/27).

For the remaining set of complexes **52 – 55**, the activity was found in the order **53** > **54** > **52** > **55** for which the authors suggested that the activity gradually increases with respect to the electron withdrawing nature of the *para* substituents. The highest activity (TOF = 10 920 h^{-1}) in this series was exhibited by **53** with CF$_3$ substituent on the *para* position whereas **49** proved to be the most active precatalyst (TOF = 28 000 h^{-1}). Besides, comparatively more sterically hindered complexes favored 1,4-*cis* enchainment rather than 1,4-*trans,* which was suggested on the basis of microstructure obtained with **55** (1,4-*trans*/1,4-*cis*/3,4 = 15/44/41). Overall, these complexes reflect the absence of a high stereo-selectivity for the formation of any microstructure. Lastly, the

authors also proposed the possible active species which could be cation-pyridine-amine or cation-pyridine amide resulting from the deprotonation of catalyst by free AlMe$_3$.

Later, the same group reported a series of unsymmetrical binuclear iminopyridine iron (II) complexes **56 – 59** for isoprene polymerization (Chart 1.18).[74] These complexes displayed an abnormal binuclear structure with seemingly Fe(II)/Fe(II) species. Later, the authors noticed two quadrupole doublets in the Mössbauer spectrum of **56**, on the basis of which, they suggested that the complex **56** consists of high-spin iron (II) and low-spin iron (II) centers. Upon activation with MAO (500 eqs.), the complex **56** exhibited very high activity (TOF = 15 000 h^{-1}) and produced high molecular weight polyisoprene ($M_n = 270$ kg/mol) with broad dispersity ($Ð = 2.7$). Decreasing the Al/Fe ratio to 10 could not produce polyisoprene, indicating that such amount of cocatalyst was insufficient to generate the active species. The authors also noticed the negligible effect of temperature on the activity of **56** where the temperature was increased from 0 to 50 °C. Further, increasing the electron density on the iron center decreased the conversion (88%) and increased the molecular weights ($M_n = 480$ kg/mol) as observed with **57**, which was attributed to the reduced Lewis acidity of the Fe center and the ability of monomer coordination. This was also supported by the result with complex **58** bearing electron-withdrawing aryl group where full conversion was obtained. Regarding the microstructure content, most of all complexes exhibit fair 1,4-*cis* selectivity (>50 %) with the remaining percentage being of 3,4 motifs. However, a slight change from Ph substituent to benzyl (Bn) in **59**, resulted in some contribution of 1,4-*trans* units in the polymer chain.

R$_1$ = R$_2$ = Ph **(56)**
R$_1$ = R$_2$ = 4-OMe-C$_6$H$_4$ **(57)**
R$_1$ = R$_2$ = 4-F-C$_6$H$_4$ **(58)**
R$_1$ = Ph, R$_2$ = Bn **(59)**

56/MAO - Very highly active and fairly 1,4-*cis* selective
57-59/MAO - Highly active and similar 1,4-*cis* selectivity
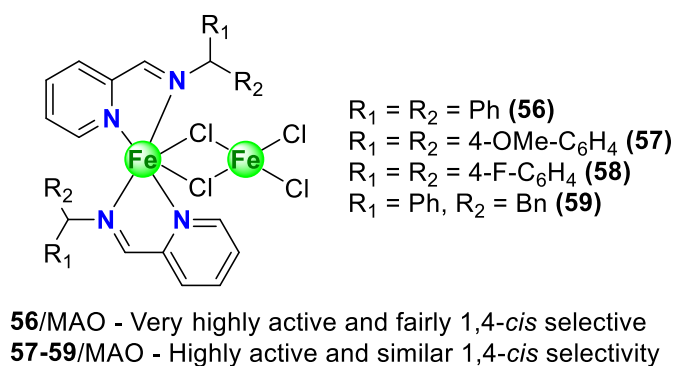
Chart 1.18. Unsymmetrical binuclear [iminopyridine]FeCl$_2$ complexes **56-59** for isoprene polymerization[74]

In addition, the monomer to Fe ratio was increased gradually from 2 500 to 20 000 which increased the catalytic activity (TOF = 99 400 h^{-1}) of **56** nearly by 7 times. The authors also

investigated the long lifetime of active species, which is essential for the synthesis of ultra-high molecular weight polyisoprenes. They observed that the catalytic system **56**/MAO could maintain high catalytic activity after 12 h before adding the monomer indicating that the lifetime of active species is long enough.

The group of Wang revitalized the domain of aminopyridine iron (II) systems by reporting a new series of complexes **60 – 63** for isoprene polymerization (Chart 1.19).[26] Upon activation with MAO, the resulting catalysts displayed good activity in order of increasing steric hindrance **63 > 62 > 61**. The lowest activity was observed for the complex **61** (TOF = 550 h^{-1}) substituted with Et whereas the highest activity was displayed by complex **63** (TOF = 34 800 h^{-1}), which possess the most sterically hindered ^{i}Pr group.

R = Me **(60)**
R = Et **(61)**
R = Bn **(62)**
R = ^{i}Pr **(63)**
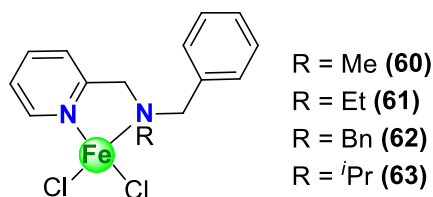
63/MAO ‒ Very highly active and fairly 3,4 selective for isoprene
Low activity for farnesene and myrcene, inactive for ocimene
61/MAO ‒ Low activity and fair 3,4 selectivity for isoprene

Chart 1.19. [Aminopyridine]FeCl$_2$ complexes **60-63** for dienes polymerization[26]

In general, the authors proposed that the catalytic activity is significantly dependent on the steric bulk imparted by the ligand and the Lewis acidity of the metal center. Increasing the steric hindrance of the ligand inhibits the coordination of the monomer with the metal, leading to a decrease in catalytic activity. However, the iron center of complex **63** showed Lewis acidity stronger than that of **61**, thus facilitating the coordination as well as the insertion of isoprene, thereby increasing the overall activity. Additionally, it was observed that the molecular weight of polyisoprenes was highly dependent on the steric hindrance of the catalyst, in which the M_n decreased with the increase in steric bulk (M_n = 430 kg/mol for **60** *vs* 270 kg/mol for **63**), which could be associated with strong repulsion between the ligand and the polymer chains, thus facilitating the transfer of chain from Fe to Al. Overall, the complexes favored the preferential formation of 3,4 motifs in fair to moderate amounts (55 – 63%) along with the contribution of 1,4-*cis* units (45 – 37 %). Interestingly, complex **63** possess a good level thermal tolerance (90% yield of polyisoprene at 100 °C), which likely derives from the protection provided by the bulky ^{i}Pr

substituent of the amine moiety. It is also worthy to notice that changing the cocatalyst to MMAO and DMAO had no obvious influence on the activity, selectivity and molecular weight.

Apart from isoprene, the polymerization of bio-sourced dienes (Ocimene, myrcene and β-farnesene) was also assessed with the catalyst **63**/MAO where it failed to promote the ocimene polymerization, whereas myrcene and β-farnesene were successfully polymerized with less activities (TOF = 445 h^{-1} and 680 h^{-1} respectively) when compared to isoprene. The unsuccessful polymerization of ocimene with **63**/MAO was attributed to the possible steric hindrance between the long chain group from ocimene and the iron active species.

For a better comparison, the selected data for the polymerization of isoprene with iron catalysts bearing bidentate ligands is displayed below in Table 1.2.

Table 1.2. Selected data for the polymerization of 1,3-dienes with iron complexes bearing bidentate ligands.

Complex	IP/Fe	Activation/Fe	T (°C)	Time (min)	Conv. (%)	TOF (h^{-1})	1,4-*cis* (%)	1,4-*trans* (%)	3,4 (%)	M_n (kg/mol)	Đ
16	6 665	MAO (1 000)	20	0.5	100	800 000	33	-	67	-	-
17(Cl)	1 000	Al^{i}Bu$_3$/Trityl Borate (3/1)	23	120	>99	498	1	91	8	62.5*	2.0
17(Cl)	2 500	MAO (500)	25	120	83.1	1 038	78	8	14	61	1.6
17(Cl)	2 500	MAO (500)	25	120	10.9	138	-	90	10	627/4	2.1/1.7
17(Cl)	1 250	MAO/Trityl Borate (5/1)	25	120	30.2	192	-	98	2	15	1.8
17(acac)	2 000	MAO (500)	25	120	55	590	3	87	10	12	2.0
17(acac)	2 000	MAO (50)	25	300	92	440	5	86	9	19	1.9
17(acac)	2 000	MAO (50)	- 30	120	2.5	30	32	36	32	6	1.4
17(acac)	2 000	MAO (50)	50	120	20	150	7	80	13	7	1.9
18	2 500	MAO (500)	25	120	64.1	804	77	9	14	60	2.1
19	2 500	MAO (500)	25	120	58.2	726	77	8	15	70	1.8
20	2 500	MAO (500)	25	120	61.3	768	78	8	14	61	2.1
21	1 000	Al^{i}Bu$_3$/Trityl Borate (3/1)	23	60	>99	1 002	66	1	33	75*	1.9
21	1 000	Al^{i}Bu$_3$/ Trityl Borate (3/1)	– 78	240	>99	246	85	1	14	70*	1.7
21	2 500	MAO (500)	25	120	98.1	1 224	63	3	34	103	2.1
21	2 500	MAO (500)	25	120	21.1	264	65	-	35	61	1.5
21	1 250	MAO/Trityl Borate (5/1)	25	120	<1	-	-	-	-	-	-
22	2 500	MAO (500)	25	120	83.2	1 038	70	5	25	180	1.8

*Calculated from $M_n = M_w/Đ$, Trityl Borate = [Ph$_3$C][B(C$_6$F$_5$)$_4$]

Complex	IP/Fe	Activation/Fe	T (°C)	Time (min)	Conv. (%)	TOF (h⁻¹)	1,4-cis (%)	1,4-trans (%)	3,4 (%)	M_n (kg/mol)	Đ
23	2 500	MAO (500)	25	120	85.7	1 074	71	5	24	182	1.6
24	2 500	MAO (500)	25	120	>99	1 236	54	-	46	91	4.3
24	1 250	MAO/Trityl Borate (5/1)	25	120	52.8	330	-	95	5	14	1.7
25	2 500	MAO (500)	25	120	85.3	1 068	54	-	46	97	3.5
25	1 250	MAO/Trityl Borate (5/1)	25	120	76.3	474	-	98	2	15	2.1
26	2 500	MAO (500)	25	120	32.7	408	56	-	44	190	2.1
26	1 250	MAO/Trityl Borate (5/1)	25	120	64.8	408	0	96	4	16	2.2
27	4 000	MAO (1 000)	60	30	>99	7920	50	32	18	191	3.6
28	4 000	MAO (1 000)	60	30	98	7840	51	14	35	61.6	1.9
28	4 000	MAO (1 000)	40	30	83	6 640	51	27	22	70.7	2.0
28	4 000	MAO (1 000)	70	30	85	6 800	-	-	-	55.2	2.1
28	4 000	MMAO (1 000)	40	30	80	6 400	30	51	19	65.5	3.3
28	4 000	EASC (100)	40	30	33	2640	19	81	-	1.9	1.3
29	4 000	MAO (1 000)	60	30	23	1840	24	64	12	21.1	1.8
30	2 000	MAO (500)	25	10	>99	12 000	39	16	45	58	2.7
31	2 000	MAO (500)	25	120	>99	1 000	12	74	14	17	3.0
32	2 000	MAO (500)	25	10	>99	12 000	36	10	54	67	2.2
32	2 000	MAO (50)	25	10	>99	12 000	39	9	52	115	1.9
32	2 000	MAO (50)	- 30	10	>99	12 000	45	0	55	107	2.3
32	2 000	MAO (50)	50	10	>99	12 000	38	13	49	86	2.1

Complex	IP/Fe	Activation/Fe	T (°C)	Time (min)	Conv. (%)	TOF (h⁻¹)	*1,4-cis* (%)	*1,4-trans* (%)	3,4 (%)	M_n (kg/mol)	Đ
33	2 000	MAO (50)	25	10	>99	12 000	55	3	42	65	2.7
34	2 000	MAO (500)	25	10	>99	12 000	51	-	49	43	3.3
35	1 250	AlEtCl₂/Trityl Borate (10/1)	25	120	81	500	-	98	2	1.6	2.8
36	1 250	AlEtCl₂/Trityl Borate (10/1)	25	120	88	540	-	96	4	1.8	4.4
37	1 250	AlEtCl₂/Trityl Borate (10/1)	25	120	76	470	-	97	3	2.0	3.3
38	1 250	AlEtCl₂/Trityl Borate (10/1)	25	120	80	500	-	97	3	1.5	3.1
45	2 000	MAO (500)	25	120	33	330	53	-	47	112	1.7
46	2 000	MAO (500)	25	120	68	680	9	69	22	20	3.7
47	2 000	MAO (500)	25	120	13	130	69	4	27	123	1.6
48	2 000	MAO (500)	25	120	70	700	46	8	46	26	4.7
49	2 000	MAO (500)	25	120	>99	990	29	22	49	39	3.9
49	10 000	MAO (500)	25	10	47	28 200	29	17	54	60	2.4
49	2 000	MAO (200)	25	10	77	9240	28	25	47	45	4.0
50	2 000	MAO (500)	25	120	>99	990	41	10	49	81	2.1
51	2 000	MAO (500)	25	120	>99	990	44	4	52	111	1.7
52	2 000	MAO (200)	25	10	65	7 800	18	38	44	41	3.2
53	2 000	MAO (200)	25	10	91	10 920	32	19	49	52	4.1
54	2 000	MAO (200)	25	10	70	8 400	36	17	47	37	5.2
55	2 000	MAO (200)	25	10	11	1 320	44	15	41	63	3.2

Complex	IP/Fe	Activation/Fe	T (°C)	Time (min)	Conv. (%)	TOF (h^{-1})	*1,4-cis* (%)	*1,4-trans* (%)	3,4 (%)	M_n (kg/mol)	Đ
56	2 500	MAO (500)	25	-	>99	15 000	53	3	44	270	2.6
56	2 500	MAO (500)	25	-	<1	-	-	-	-	-	-
56	2 500	MAO (500)	0	-	>99	15 000	54	-	46	700	2.4
56	2 500	MAO (500)	50	-	95	14 240	50	8	42	300	2.7
56	20 000	MAO (500)	25	-	83	99 380	54	-	46	850	1.9
57	2 500	MAO (500)	25	-	88	13 200	54	2	44	480	2.4
58	2 500	MAO (500)	25	-	>99	15 000	54	3	43	500	2.2
59	2 500	MAO (500)	25	-	>99	15 000	44	13	43	470	2.3
60	2 000	MAO (500)	25	120	>99	990	37	-	63	430	1.8
61	2 000	MAO (500)	25	120	55	550	39	-	61	440	1.9
62	2 000	MAO (500)	25	120	77	770	42	-	58	310	2.0
63	2 000	MAO (500)	25	120	>99	990	44	-	56	270	1.9
63	2 000	MAO (500)	100	10	90	10 800	40	13	47	160	1.8
63	10 000	MAO (500)	25	10	58	34 800	45	-	55	380	1.9

1.1.3. Iron-catalyzed Ring Opening Polymerization of cyclic esters

1.1.3.1. General overview

   The ROP of cyclic esters and related monomers by means of iron catalysts takes place by activation of the monomer by the metal, similarly as it proceeds with many elements of the periodic table.[75] This will obviously be dependent on the Lewis acid character of the cation, itself being related to the set of ligands in a given complex and also to the formal oxidation state of the metal (generally +II or +III for iron). In absence of any active ligand bound to the metal and in the presence of an additional (generally protic) nucleophile, the mechanism of the reaction is expected to be of Activated Monomer Mechanism (AMM) type (Scheme 1.4a). Such polymerization process is operating with most inorganic salts, the nucleophile being in most cases an alcohol that was added intentionally, or impurities present in the mixture like typically residual water. When the complex comprises an active ligand, typically alkoxide (phenoxide) or amido and in some cases alkyl (generally poor initiator) in a well-defined purposely synthesized compound or resulting from the reaction of any alkyl/amido precursor with an alcohol molecule, the polymerization reaction is expected to undergo through a Coordination-insertion Mechanism (CM) process (Scheme 1.4b).
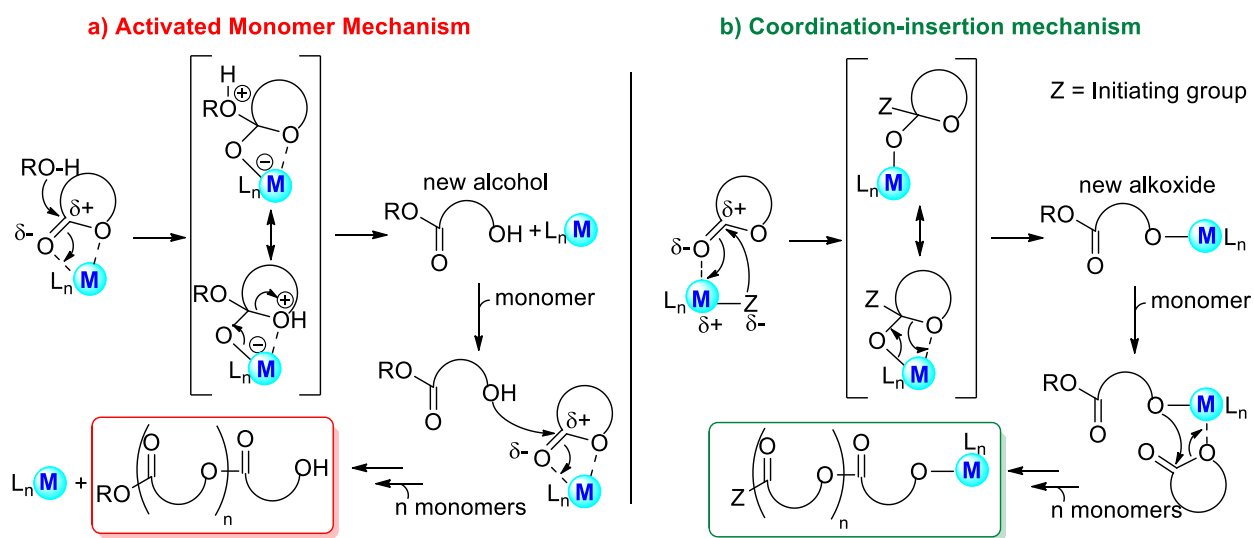
Scheme 1.4. ROP by (a) Activated Monomer Mechanism[76], (b) Coordination-insertion mechanism[77]

1.1.3.2. Selective iron-based catalysts for the ROP of lactide and ε-caprolactone

A various plethora of iron complexes has been developed for the ROP of cyclic esters, which is described in our comprehensive review. Herein, we will only discuss some of the best known iron catalytic systems for the ROP of cyclic esters, especially lactide (LA) which is bio-sourced and ε-caprolactone (ε-CL) which is mainly a petro-sourced monomer. The ROP of LA and CL produces polylactide (PLA) and poly(ε-caprolactone) (PCL) respectively, a type of biodegradable polymers becoming more popular due to both environmental and strategic reasons.[78] Furthermore, they are really important materials in the biomedical field,[79] and the birth of these polymers has significantly influenced the development and rapid growth of various technologies in modern medicine.[80] PLA belongs to the family of polymers derived from α-hydroxy acid such as lactic acid (2-hydroxypropionic acid). The monomer lactide has two chiral centers due to which it exists in the form of three stereoisomer namely *D*-lactide (two *R*-lactic acids), *L*-lactide (two *S*-lactic acid) and meso-lactide (*R*- and *S*-lactic acid). The racemic mixture of *D*- and *L*-lactide is called *rac*-lactide (Chart 1.20).

meso-lactide   *D*-lactide   *L*-lactide

rac-lactide (1:1)
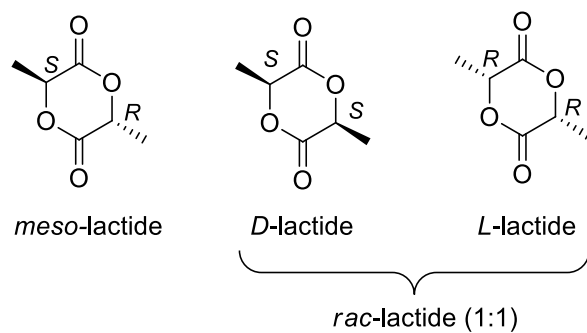
Chart 1.20. Stereoisomers of lactide

There are three main routes used to synthesize PLA depending on the molecular weight of the resulting aliphatic polymer, namely, i) a direct condensation polymerization, ii) a combined melt polycondensation with a Solid-State Process (SSP) starting from oligomers in the presence of tin, titanium or zinc-based catalysts,[81] and the last is the iii) ROP[82] in the presence of organic or metal complex catalysts, starting from a purified lactide structure.[83] Metal complexes are one of the most efficient catalysts for the ROP of bio-sourced monomers[84] due to which PLA is mainly produced through metal-mediated ROP of *L*-lactide, derived from fermentation of starch consisting of two stereoisomers *S*- and *R*-lactic acid (Scheme 1.5).[85]
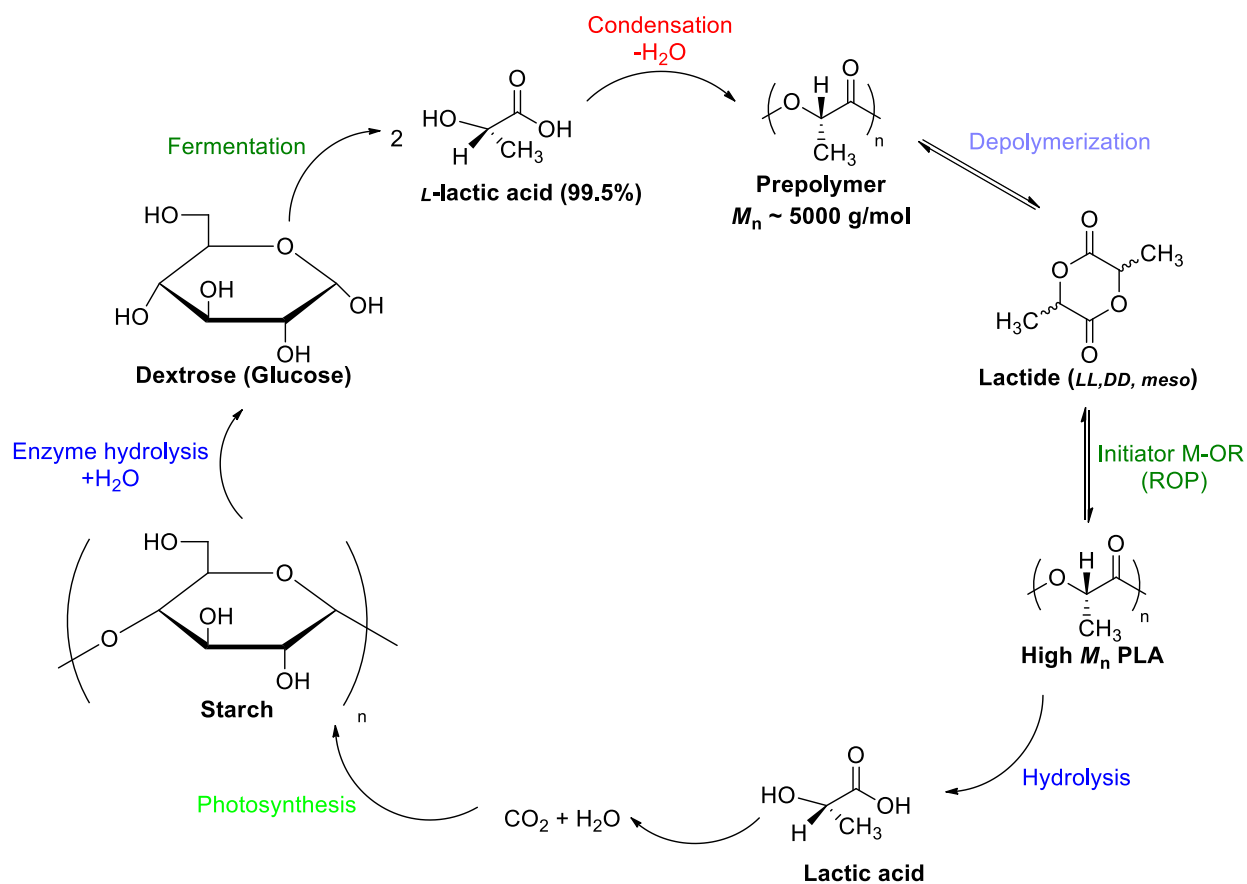
Scheme 1.5. PLA manufacturing overview[85]

Former studies that are relevant for the ROP of LA and ε-CL have been based on FeX_2 or FeX_3 (X = Cl, Br, ClO_4),[86] Fe powder,[87] carboxylates[88] homo- or hetero-metallic alkoxides/phenoxides,[89] salen-iron based systems[90] and β-diketonate complexes,[91] which are in the form of a discrete compound or in situ generated from metal/reagent combination and amido derivatives. We have narrowed our study to well-defined, most active and stereoselective systems, including iron-based coordination catalysts, complexes bearing neutral ligands or anionic ligands, some of which are shown below in Chart 1.21.

Fe(acac)$_3$
(64)

R = *p*-methoxyphenyl [**2^{Me}(OR$_a$)**]
R = neopentyl [**2^{Me}(OR$_b$)**]
R = 4-*tert*-butylphenyl [**2^{Me}(OR$_c$)**]

R = *p*-methoxyphenyl [**2^{Me}(OR$_a$)'**]
R = neopentyl [**2^{Me}(OR$_b$)'**]

(65)

Fe(μ-O)$_5$(OEt)$_{13}$
(66)

Fe(OCMe$_2$Ph)$_6$
(67)

(68)

(69)

R$_1$ = R$_2$ = Me [**2^{Me}(TMS)**]
R$_1$ = H, R$_2$ = ^{t}Bu [**5(TMS)**]

(70) CHPh$_2$

(71)

(72)

(73)

🔵 =

(rac)	(R,R)						
R = ^{t}Bu	^{t}Bu	^{t}Bu	H	^{t}Bu	^{t}Bu	Cl	Cl
(a)	**(b)**	**(c)**	**(d)**	**(e)**	**(f)**	**(g)**	**(h)**

X$_1$ = N(SiMe$_3$)$_2$, X$_2$ = N, R$_1$ = C(Ph)$_3$, R$_2$ = Me **(74)**
X$_1$ = N(SiMe$_3$)$_2$, X$_2$ = N, R$_1$ = OMe, R$_2$ = Me **(75)**
X$_1$ = N(SiMe$_3$)$_2$, X$_2$ = N, R$_1$ = CH(Me)$_2$, R$_2$ = H **(76)**
X$_1$ = N(SiMe$_3$)$_2$, X$_2$ = N, R$_1$ = CH(Me)(Et), R$_2$ = H **(77)**
X$_1$ = N(SiMe$_3$)$_2$, X$_2$ = C, R$_1$ = C(Ph)$_3$, R$_2$ = Me **(78)**
X$_1$ = Cl, X$_2$ = N, R$_1$ = C(Ph)$_3$, R$_2$ = Me **(79)**

Chart 1.21. Selective iron-based complexes for the ROP of LA and ε-CL

Following the studies of Dobrzynski *et al.* and Carpentier *et al.* who assessed Fe(acac)₃ **(67)** for the bulk polymerization of 2,2-dimethyltrimethylene carbonate (DMC) and trimethylene carbonate (TMC),[92] the homoleptic Fe(acac)₃ derivative **(64)** was assessed for the ROP of *L*-LA by the group of Park, Lee and Kim where the initiator **(64)** showed low activity (TOF = 63 h⁻¹) at 130 °C in toluene as single component catalyst (Chart 1.22).[93] Concerning the reaction mechanism, the authors advanced cautiously by proposing the formation of an active cationic species by loss of an acetylacetonate ligand or by splitting into two ionic mononuclear entities. The same compound had been previously shown to be much more active (TOF = 684 h⁻¹) with additional BnOH (3 eqs.) *vs. rac*-LA polymerization at 130 °C in bulk.[94] The ROP process was well controlled in this case (narrow *Đ*, M_n close to theoretical value). This catalyst behavior compared well with that of complex Fe(dbmOH)₃ (dbm = dibenzoylmethane) **(65)** under the same experimental conditions, which was found even more active (TOF = 891 h⁻¹).
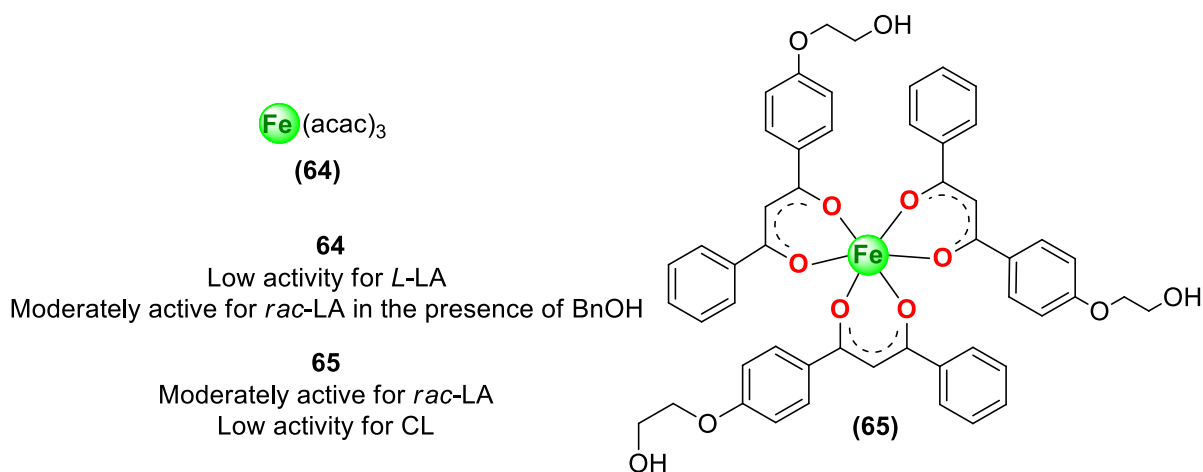
Chart 1.22. Acetylacetonate and β-diketonate iron-based complexes for ROP of LA and CL[92,93,94,95]

In this homoleptic tris(β-diketonate) derivative, the ligand bears an additional hydroxyl function so as to include within the same molecule the catalyst and the initiator. The ROP reaction afforded an iron-star Fe(dbmPLA)₃ which was further easily demetalated into dbmPLA macroligand. Noteworthy, chain extension was noted with additional *rac*-lactide in the presence of Fe(dbmPLA)₃. Ligand exchange between the β-diketonate ligand in the iron catalyst and the alcohol as CTA was proposed to take place, on the basis of kinetic studies.[95] Complex **65** also enabled, in a similar way, the ROP of ε-CL (in bulk at 110 °C) and of sequentially added CL and *rac*-LA to afford Fe(dbmPLA)₃ and Fe(dbmPCL-*b*-PLA)₃, respectively, which were further

demetalated into functionalized dbmPLA and dbmPCL-*b*-PLA.[96] ^{1}H NMR spectroscopic and kinetic studies established a slight tendency to transesterification (exchange of copolymer chains with PCL chain attached to the active catalyst resulting to even or odd number of triads) for such polymerizations conducted under harsh conditions, especially at high monomer conversions (conv. > 70%).

The first study with structurally characterized iron complexes used as catalysts for the ROP of lactide have been based on iron (III) alkoxides $Fe_5(\mu\text{-}O)(OEt)_{13}$ (**66**) and $Fe_2(OCMe_2Ph)_6$ (**67**) (Chart 1.23).[97] Complex **66** (under the form of a cluster) was found to be very active (TOF = 1 250 h^{-1}). The authors established the living character of the polymerization and two chains growing per metal, with possibly little transesterification. A coordination-insertion mechanism was proposed with the absence of epimerization of the monomer which could have led to the formation of *meso*-lactide Catalyst **67** (as a dimer) had similar behavior, although slightly less active (TOF = 950 h^{-1}). The iron (III) alkoxide of formula $[Fe(OR)_3]_2$ (**68**) (R = $CHPh_2$) was synthesized by the same group and characterized by X-ray diffraction studies.[98]
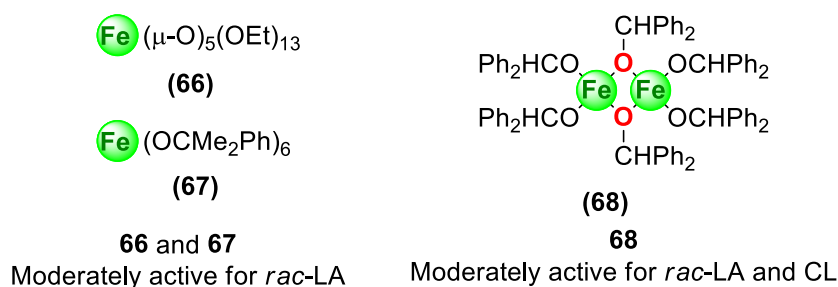
Chart 1.23. Iron alkoxides complexes for ROP of LA and CL[97,98]

This homoleptic alkoxide, which was found dimeric in the solid state, was ten times more active than the monoalkoxide **70** (see further in this section) for the ROP of CL, and enabled more controlled polymerization with initiation efficiency evaluated at 100%. This difference in reactivity was less pronounced for the ROP of *rac*-LA but the process was again in favor of **68**. This latter complex is a rare example of compounds displaying higher activity toward LA than CL. Sequential CL/LA copolymerization could then *de facto* be obtained successfully with complex **68**. In terms of activity/control of the ROP of LA, complex **68** compares well with the behavior of very active catalysts **66** and **67**. However, a certain lack of reproducibility due to high sensitivity to impurities was noticed.

In 2013, the group of Byers investigated a series of iron (II)-BIP alkoxide/aryloxide complexes as initiators in the ROP of *rac*-LA at room temperature in dichloromethane (Chart 1.24).[99] The complex **2^Me(OR_a)**, which was isolated by reacting the alkyl precursor **2^Me(TMS)** with two eqs. of 4-methoxy-phenol, exhibited poor activity (TOF = *ca* 15 h^-1). The analogs complexes **2^Me(OR_b)** and **2^Me(OR_c)** were *in situ* formed in the same way (but not isolated) and have shown to exhibit similar reactivity and results for the ROP of *rac*-LA, whereas complex **2^Me(TMS)** was sluggishly active on its own. The performances of these catalysts were optimized a few years later[100] with TOF values up to 2 820 h^-1 in toluene at room temperature, which competes with the best metal-based catalysts towards the ROP of lactide.[101,75] With such complexes [**2^Me(OR_a-c)**], the process was found living and operating according to a coordination-insertion mechanism, the number of growing chain per metal being dependent on the aryloxide (one chain)/alkyloxide (two chains) nature of the initiating group. The use of a chiral alcohol did not allow the control of the stereo-selectivity of the transformation.

R = *p*-methoxyphenyl [**2^Me(OR_a)**]
R = neopentyl [**2^Me(OR_b)**]
R = 4-*tert*-butylphenyl [**2^Me(OR_c)**]

2^Me(OR_a) - Low activity for *rac*-LA
2^Me(OR_b) - Moderately active for *rac*-LA

R_1 = R_2 = Me [**2^Me(TMS)**]
R_1 = H, R_2 = ^tBu [**5(TMS)**]

2^Me(TMS) and 5(TMS)
Highly stereoselective for *rac*-LA and *meso*-LA
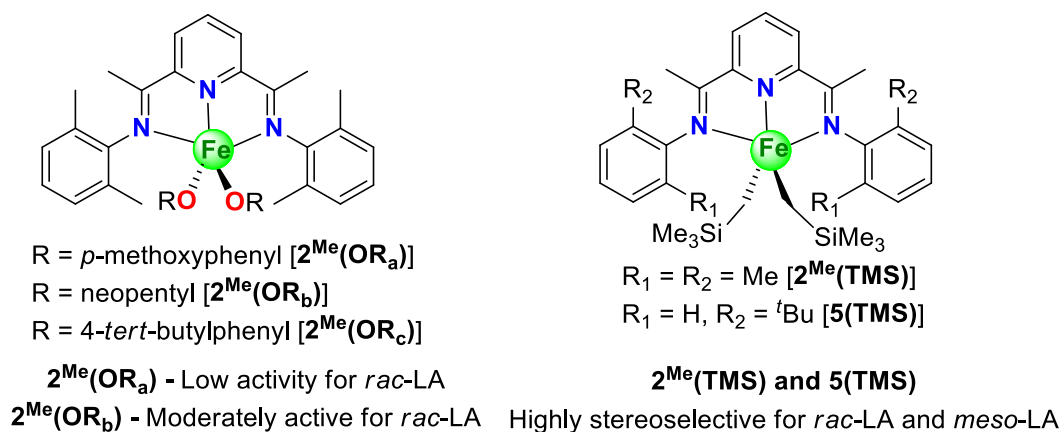
Chart 1.24. Bisiminopyridine Iron complexes for ROP of LA[99,100,101,105]

In the same study, the iron (III) complex **2^Me(OR_a)^+**, which resulted from the oxidation of its iron(II) congener **2^Me(OR_a)**, was found to be inactive for the ROP of LA. This difference in behavior was exploited to produce a redox-controlled catalytic system with switch on/off of the polymerization ability, depending on the oxidation state of the iron metal center (a recent study including theoretical support was published by the same group with CL.[102] Subsequently, the authors found that the iron (III) complex **2^Me(OR_a)^+** was able to polymerize cyclohexene oxide, whereas the iron (II) counterpart [**2^Me(OR_a)**] was inactive. The distinct monomer selectivity of this iron-based catalyst, as a function of its oxidation state, allowed the authors to elegantly prepare a PLA-*b*-PCHO block copolymer by *in situ* switching from one species to another, using an

appropriate oxidizing or reducing agent.[103] Another paper from the same authors exploited the same features to propose a way of elaborating innovative redox crosslinking of PLA from intentionally synthesized epoxy-grafted lactide monomer.[104]

The first stereo-selective ROP of LA with an iron-based catalyst was achieved in a smart study by the same group, using *in situ* generated chiral iron (II) catalysts based on BIP complexes **2^Me(TMS)** and **5(TMS)** in the presence of silanols (Chart 1.24).[105] With *rac*-LA at room temperature in THF solution, the polymerization exhibited a living character and heterotactic PLA with P_r up to 75% was obtained (P_r probability of racemic linkages). However, deviations from the theoretical M_n values were observed, due to slow initiation. Syndiotactic PLA with P_r up to 92% was achieved from the polymerization of *meso*-LA with **5(TMS)** combined with selected silanols (Chart 1.25).

Heterotactic PLA (-*SS*-*RR*-)$_n$ Syndiotactic PLA (-*SR*-*SR*-)$_n$
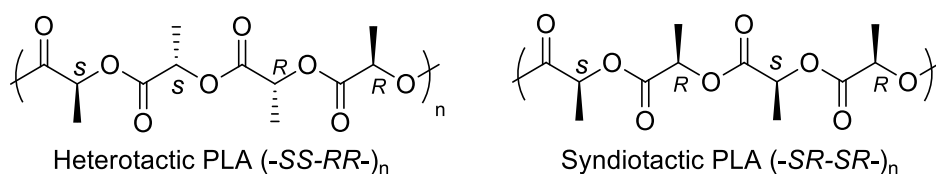
Chart 1.25. Tacticity in PLA arising from stereoselective polymerization of LA

The iron bis(siloxide) complex **69** containing a bidentate iminopyridine ligand was then intentionally prepared (and characterized by X-ray diffraction studies) as a model for the η^2 coordination mode of BIP (Chart 1.26). This complex behaved similarly as the binary **5(TMS)**/silanol catalytic system, affording slightly lower stereo-selectivity. Enantiomorphic-site control was advanced to explain these results, with DFT calculations as support. According to the authors, these iron-catalyzed reactions benefit from synergistic effect involving silanol and BIP ligands bound to the metal.

R = *p*-methoxyphenyl [**2^Me(OR_a)'**]
R = neopentyl [**2^Me(OR_b)'**]

(69)

69/Ph$_3$SiOH - Highly stereoselective for *rac*-LA
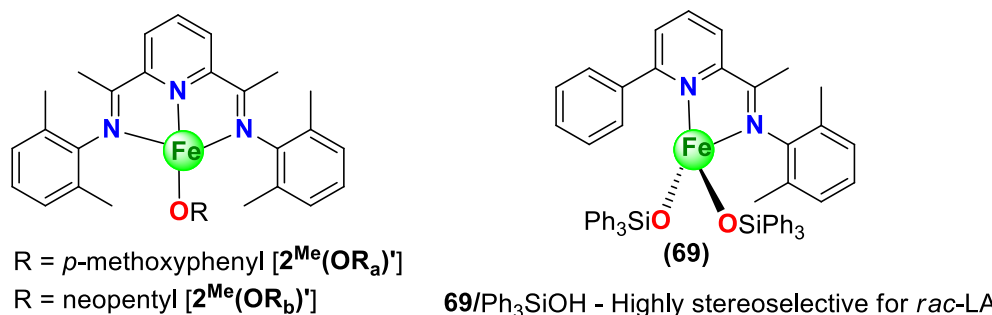
[**2^Me(OR_a)'** - Moderate activity for *rac*-LA and very poor activity for CL
2^Me(OR_b)' - Moderate activity for *rac*-LA and highly active for CL

Chart 1.26. BIP Iron alkoxide/aryloxide and iron bis(siloxide) complexes for ROP of LA[100,105]

With the aim to focus on the impact of the oxidation state of the metal, Byers and coworkers prepared a family of formally iron(I)-(BIP) alkoxide complexes that have been involved in the ROP of a variety of cyclic polar molecules: LA, CL, VL, γ-butyrolactone (GBL), BBL, TMC, ethylene carbonate (EC) and cyclohexene oxide (Chart 1.26).[100] Complex **2^{Me}(OR$_a$)'** (Iron (II)) exhibited similar activity as the iron (II) **2^{Me}(OR$_a$)** in ROP of *rac*-LA, but slow initiation rates were advanced to explain the higher than expected molecular weights. Faster polymerization resulted from the use of the neopentyl alkoxide complexes **2^{Me}(OR$_b$)'** and **2^{Me}(OR$_b$)**, as already observed,[99] the process being additionally living. Surprisingly, complex **2^{Me}(OR$_a$)** was found inactive toward the ROP of CL at room temperature, whereas complex **2^{Me}(OR$_a$)'** was found fairly active. With complex **2^{Me}(OR$_b$)'** as catalyst, very high activity was obtained (TOF = 11 880 h^{-1}, the best one up to now for an iron catalyst) and the process was better controlled than with **2^{Me}(OR$_a$)'**. The complex **2^{Me}(OR$_b$)'** exhibited the best ROP catalyst performances among the studied series of catalysts with other monomers like BBL (but with uncompleted conversion), VL and TMC. Remarkably, the alkoxide catalyst **2^{Me}(OR$_b$)'** displayed much higher reactivity and control of the polymerization process than its phenoxide analog **2^{Me}(OR$_a$)'**. However, GBL was not homo-polymerized by **2^{Me}(OR$_b$)'** but it could be incorporated into polymers of CL (up to 33 mol%). Poly(CL*co*VL) were also prepared by means of **2^{Me}(OR$_b$)'**. However, the combination of *rac*-LA and CL did not produce statistical copolymers, but only PLA. This trend, *a priori* surprising, considering that the homoROP of CL is much faster than that of LA, follows in fact a general behavior that is well documented.[106] Block copolymers could however be prepared. On the basis of a set of specific analyses (X-ray, Mössbauer, SQUID magnetometry) completed with theoretical (DFT) investigations, the authors concluded that the bis(imino)pyridine Fe(I) complexes **2^{Me}(OR)'** can rather be seen as iron (II) derivatives surrounded by a one-electron reduced ligand. The iron (III) cationic analogues were found inactive toward the same ROP processes, but they were capable of performing the ROP of epoxides.

The iron (III) alkoxide of formula L$_2$FeOR (R = CHPh$_2$, **70**, L = *N,N'*-bis(trimethylsilyl)benzamidinate) was synthesized and characterized by X-ray diffraction studies (Chart 1.27).[107] This monoalkoxide, which exists as a monomer in the solid state, was found less active for the ROP of CL than the homoleptic alkoxide complex **68** and operating in a less controlled manner (broader dispersity values and initiation efficiency limited to 50% with **70**). The same trend of higher activity of **68** *vs.* **70**, although less pronounced, was observed toward LA

polymerization under comparable conditions. In contrast to what is generally reported, complex **70** displays higher activity toward LA than CL, in a similar manner to that found with complex **68**. It is however worth mentioning that a lack of reproducibility was noticed, due, according to the authors, to too high sensitivity to impurities.

(70)
Moderate activity for *rac*-LA
Poorly active for CL

(71)
Moderate activity for *rac*-LA
Highly active for CL

(72)
Poorly active for LA
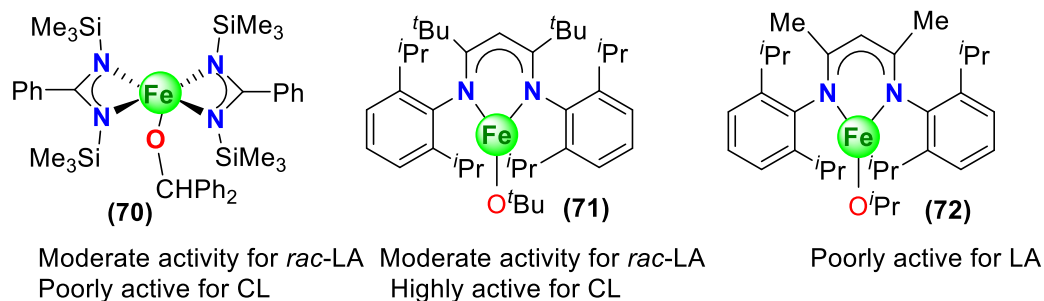
Chart 1.27. Bis(trimethylsilyl)benzamidinate Iron alkoxide and diketiminate iron alkoxide complexes for ROP of LA and CL[107,108,109]

The discrete diketiminate iron (II) monoalkoxide **71**, which was prepared by Gibson and coworkers from the chloro diketiminate precursor,[108] adopts a monomeric structure in the solid state (Chart 1.27).[109] The authors showed that this compound behaves efficiently as initiator toward the ROP of LA and CL. Under mild experimental conditions (room temperature, toluene solution), TOF values reach 282 h^{-1} (1 140 h^{-1} for CL) and the process is well-controlled in term of kinetics. However, transesterification was observed at high conversion and M_n values (not corrected, based on PS standards) were higher than theoretically expected for one polymer chain per metal (M_{nexp} = 37.5 kg/mol *vs*. $M_{n(th)}$ = 13.5 kg/mol), which argues for uncomplete catalyst efficiency. A decade later, Li *et al.* synthesized the less sterically congested diketiminate monoalkoxide Fe (II) complex **72** (Chart 1.27). The ROP of *rac*-lactide was performed with this complex in toluene solution at 70 °C, which exhibited moderate activity and poor control with respect to molecular weights.[110] Lower activities than the similar iron complex **71** reported by Gibson were noted,[109] suggesting that the steric hindrance of the diketiminate iron (II) monoalkoxides has an impact over their polymerization activity. No stereo-selectivity was observed.

More recently, the group of Pang achieved the ROP of lactide (*rac*-, *L*- and *meso*- were studied) and CL in bulk with a series of new Salen-iron (III) complexes **73a-h** (Chart 1.28).[111] The initiation was promoted by activating the air-stable (Salen)FeCl precursors with propylene oxide (PO), which also served as solvent. Varying the substituents and ligand backbone made stereo-selective polymerization of *rac*-LA possible, for the first time with an Fe (III) catalyst and little

later to the studies of Byers (*vide supra*), to yield either predominantly isotactic (P_m up to 0.78) or heterotactic (P_r up to 0.63) polylactides. The stereo-selectivity was shown to proceed *via* a chain end control mechanism.

Poor activity for *rac*-LA and CL but moderate stereoselectivity
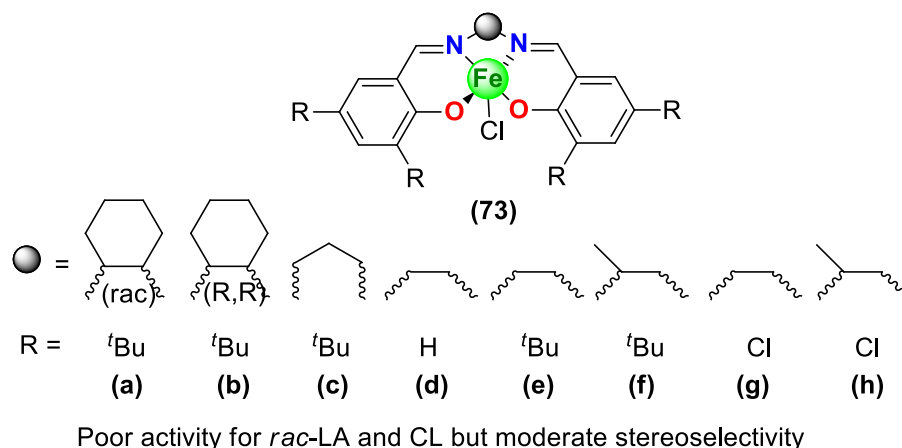
Chart 1.28. Salen Iron (III) complexes for ROP of LA and CL[111]

The activity of these catalysts, which was related to the flexibility of the bridging moiety as well as to the substitutions on the phenolic rings, was found significantly higher than their Al-based Salen counterparts. Complexes **73a-h** were also found active toward the ROP of CL, under similar conditions as for lactide but at room temperature. Similar structure-reactivity relationships were noted regarding the impact of the phenyl substituents, but the presence of the methyl on the amine bridge severely decreased the activity. The control over molecular weights was average with both types of monomers. The mechanism (Scheme 1.6) was demonstrated to proceed by coordination-insertion into the metal-alkoxide moiety resulting firstly from the insertion of epoxide (as co-initiation reagent) into the Fe-Cl bond.
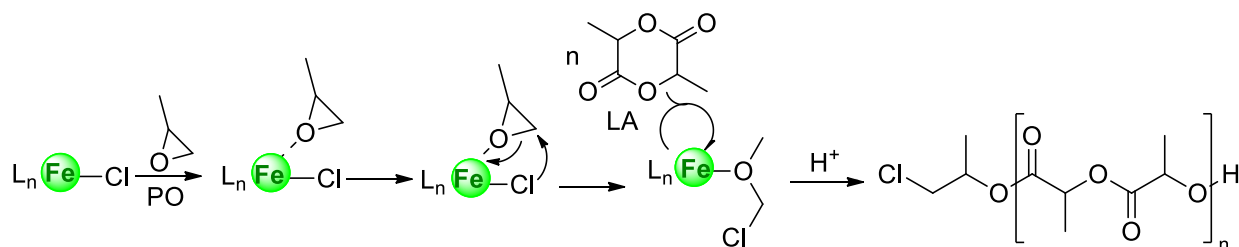
Scheme 1.6. Proposed mechanism of iron-catalyzed ROP activated by epoxide[111]

Very recently, Thomas et al. reported a series of achiral iron amide complexes **74 – 79** bearing mono(phenolate) ligands for the stereoselective ROP of *rac*-LA (Chart 1.29).[112] In this study, all the complexes were found active under mild reaction conditions, producing highly

isotactic PLA (up to 92% isotacticity). The complex **79** was characterized by X-ray diffraction studies and further investigated *via* DFT studies, which revealed that a stable five-coordinated iron species is able to ring-open LA. On the other hand, the complex **74** proved to be an efficient initiator for the ROP of *rac*-LA, producing high molecular weight (M_n = 112 500 g/mol) isotactic PLA (P_m = 0.84) with low activity (TOF (h^{-1}) = 221). Changing the amido initiator by an alkoxy initiator ($-O^iPr$) for **74** did not significantly influenced the stereoselectivity. However, the addition of ^iPrOH to **76**, enhanced the initiation and drastically increased the catalytic activity (TOF (h^{-1}) = 32 160), although maintained the high stereoselectivity (P_m = 0.82).

X_1 = N(SiMe$_3$)$_2$, X_2 = N, R_1 = C(Ph)$_3$, R_2 = Me **(74)**
X_1 = N(SiMe$_3$)$_2$, X_2 = N, R_1 = OMe, R_2 = Me **(75)**
X_1 = N(SiMe$_3$)$_2$, X_2 = N, R_1 = ^iPr, R_2 = H **(76)**
X_1 = N(SiMe$_3$)$_2$, X_2 = N, R_1 = CH(Me)(Et), R_2 = H **(77)**
X_1 = N(SiMe$_3$)$_2$, X_2 = C, R_1 = C(Ph)$_3$, R_2 = Me **(78)**
X_1 = Cl, X_2 = N, R_1 = C(Ph)$_3$, R_2 = Me **(79)**

(74) Low activity at room temperature and low temperature
(76)/^iPrOH High activity
Moderate to high selectivity obserevd for all
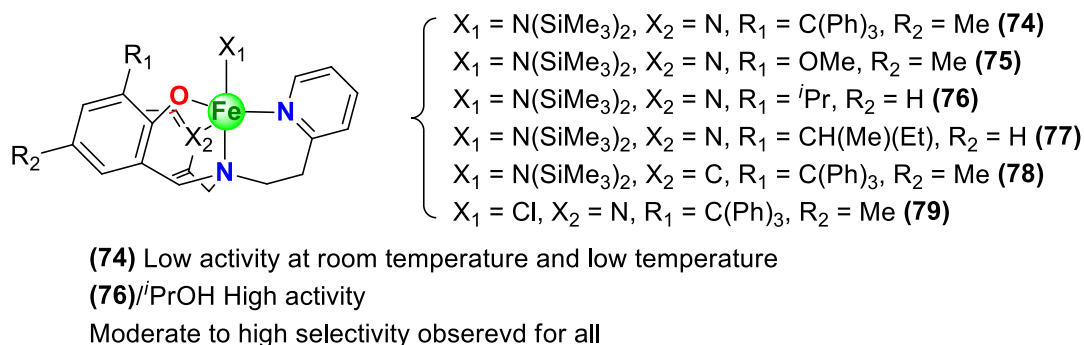
Chart 1.29. Iron amide complexes bearing tripodal phenolate ligands for ROP of LA[112]

Later, the influence of ligand substituents on the microstructures of PLAs was examined where it was observed that the complexes **75** and **76,** bearing *ortho*-methoxy or *ortho*-isopropyl groups, respectively, gave relatively low selectivity for isotactic PLA (P_m = 0.79). But when the steric hindrance was sufficient, the *ortho*-substituents on the ligand did not significantly affect the stereoselectivity as observed with **74** and **77**. Nevertheless, substituting the initiator by tetracoordinated complex **78**, decreased the polymerization stereoselectivity (P_m = 0.68) due to the vacant coordination site, leading to an additional monomer addition site and consequently affected the catalyst selectivity. In addition, the tacticity of PLA produced by **74**, increased by decreasing the temperature of the reaction up to – 10°C (P_m = 0.92). Lastly, for the first time, the authors also observed a linear dependence between T_g and the degree of stere-regularity of PLAs.

To compare and summarized the results discussed above, the selected data corresponding to the polymerization of LA and CL with iron-based catalysts is depicted below in Table 1.3.

Table 1.3. Selected polymerization data for the ROP of LA and CL with iron-based complexes.

Complex (ox. state)	Monomer	[M]/[Fe]	Initiator or CTA/[Fe]	T (°C)	Time (h)	Conv. (%)	TOF (h⁻¹)	M_n (kg/mol)	Đ	Solvent
64 (III)	*L*-LA	100	-	130	1	63	63	10.0	1.10	toluene
64 (III)	*rac*-LA	225	BnOH (3)	130	15 min	76	684	9.2	1.23	bulk
65 (III)	*rac* -LA	225	OH (3)[b]	130	10 min	66	891	8.1	1.16	bulk
65 (III)	CL	225	OH (3)[b]	110	4	56	14	5.9	1.38	bulk
66 (III)	*rac*-LA	450	-	70	21min	97	1 250	32.0	1.17	toluene
67 (III)	*rac*-LA	450	-	70	35 min	98	756	34.0	1.60	toluene
68 (III)[a]	*rac*-LA	1 000	-	70	37 min	94	1 524	54.4	1.25	toluene
68 (III)[a]	CL	200	-	25	26 min	100	462	20.9	1.20	toluene
2^{Me}(OR$_a$) (II)	*rac*-LA	50	-	RT	3	93	15.5	6.8	1.16	DCM
2^{Me}(TMS) (II)	*rac*-LA	50	4-MeO-C$_6$H$_4$OH (2)	RT	3	88	14.7	6.2	1.18	DCM
2^{Me}(TMS) (II)	*rac*-LA	50	NpOH (2)	RT	2	96	24	4.1	1.27	DCM
2^{Me}(OR$_a$) (II)	*rac*-LA	50	-	RT	20 min	94	141	16.1	1.15	CB
2^{Me}(OR$_b$) (II)	*rac*-LA	500	-	RT	10 min	94	2 820	94.8	1.37	toluene
2^{Me}(TMS) (II)[c]	*rac*-LA	50	Ph$_3$SiOH (2)	RT	9	-	-	42.9	1.31	THF
5(TMS) (II)[c]	*rac*-LA	50	MePh$_2$SiOH (2)	RT	9	-	-	15.7	1.38	THF
5(TMS) (II)[c]	*meso*-LA	50	Et$_3$SiOH (2)	RT	3	-	-	11.5	1.62	THF
69 (II)[c]	*rac*-LA	50	Ph$_3$SiOH (2)	RT	9	-	-	43.1	1.40	THF
2^{Me}(OR$_a$)' (I)	*rac*-LA	100	-	RT	20 min	86	258	25.7	1.16	CB

[a]Lack of reproducibility due to high sensitivity to impurities; [b]Alcohol comprised in the catalyst; [c]Tacticty (P_r) = 0.66 with **2^{Me}(TMS),** 0.75 with **5(TMS)** for *rac*-LA, 0.92 with **5(TMS)** for *meso*-LA, 0.85 with **69**.

Complex (ox. state)	Monomer	[M]/[Fe]	Initiator or CTA/[Fe]	T (°C)	Time (h)	Conv. (%)	TOF (h⁻¹)	M_n (kg/mol)	Đ	Solvent
$2^{Me}(OR_b)$' (I)	*rac*-LA	50	-	RT	10 min	91	273	9.6	1.12	toluene
$2^{Me}(OR_a)$' (I)	CL	50	-	RT	24	80	1.7	30.6	2.22	toluene
$2^{Me}(OR_b)$' (I)	CL	2 000	-	RT	10 min	99	11 880	390.0	1.21	toluene
70 (III)	*rac*-LA	1 000	-	70	77 min	88	686	39.5	1.88	toluene
70 (III)	CL	200	-	25	4.25	100	47	23.1	1.82	toluene
71 (II)	*rac*-LA	100	-	25	20 min	94	282	37.5	1.12	toluene
71 (II)	CL				5 min	95	1 140	86.2	1.38	toluene
72 (II)	*rac*-LA	500	-	70	24	78	16.2	18 (M_v)	-	toluene
73a (III)[a]	*rac*-LA	100	PO	60	24	90	3.8	19.4	1.58	PO
73b (III)[a]	*rac*-LA	100	PO	60	24	91	3.8	18.1	1.46	PO
73c (III)[a]	*rac*-LA	100	PO	60	4	91	22.8	24.5	1.54	PO
73g (III)[a]	*rac*-LA	100	PO	100	5.1	94	18.4	3.3	3.46	PO
73c (III)	CL	100	PO	25	15	95	6.3	25.6	1.47	PO
73h (III)	CL	100	PO	60	1.6	96	60	15.2	2.07	PO
74 (II)[b]	*rac*-LA	200	-	20	45 min	83	221	112.5	1.32	toluene
74 (II)[b]	*rac*-LA	200	^{i}PrOH (1)	20	20 min	82	492	24.8	1.04	toluene
74 (II)[c]	*rac*-LA	200	^{i}PrOH (1)	-10	3	43	14	6.7	1.16	toluene
75 (II)[d]	*rac*-LA	200	^{i}PrOH (1)	20	1 min	75	9 000	16.7	1.20	toluene
76 (II)[e]	*rac*-LA	800	^{i}PrOH (1)	20	1 min	67	32 160	51.9	1.14	toluene

[a]Tacticty: $P_m = 0.78$ (73a), $P_m = 0.77$ (73b), $P_m = 0.68$ (73c), $P_r = 0.63$ (73a), [b]$P_m = 0.84$; [c]$P_m = 0.92$; [d]$P_m = 0.79$; [e]$P_m = 0.82$

1.2. Conclusion

As can be seen in this bibliographic survey, the field of well-defined iron-catalyzed coordination-insertion polymerization has given rise to considerable applications in a wide range of monomers including ethylene, 1,3-dienes and polar cyclic esters. This clearly demonstrates the flourish and versatile nature of this area of research.

Throughout this chapter, we often encounter a recurrent catalytic structure based on the bis(imino)pyridyl skeleton, which has been extensively used for the coordination-insertion polymerization of both polar and non-polar monomers. Thanks to the discovery by the Gibson and Brookhart groups of an extremely active system for the polymerization of ethylene, based on the iron-BIP/MAO catalytic system, this finding has attracted a lot of interest and motivation for many research groups to exploit its potential. One can advance that this is mainly related to the modularity of the BIP ligand skeleton, which can be easily adjusted in term of electronic and steric properties according to the type of chemistry envisioned. In parallel, the ability of the BIP ligand to act, in some cases, as electron-reservoir (redox non-innocent ligand,[113] has enabled the development of novel synthesis methodologies in "*iron-catalyzed reactions in organic chemistry*"[64,114]

Since the review of Olivier-Bourbigou and coworkers in 2015,[18c] the field of iron-catalyzed 1,3-dienes polymerization has progressed steadily (section 1.1.2). Overall, these catalysts are still moderately active compared to the industrial systems based on other transition metals (*e.g.* Ti, Co, Ni) or rare earths (*e.g.* Nd) and the stereo-/regio-selectivity remains an issue that needs to be further improved for iron-based systems. From this point of view, much remains to be done for understanding the structure-properties relationships of iron-catalyzed 1,3-dienes polymerization. This is particularly evidenced by the works described in section 1.1.2.3, where the same iron-based complexes gave rise to significantly different results depending on the activation mode of the pre-catalysts (complexes **17** and **21**), the experimental conditions and the nature of the cocatalysts. Nevertheless, some trends can be cautiously drawn from this survey. All truly active iron catalytic systems for the polymerization of 1,3-dienes are supported by nitrogen-based bidentate or tridentate ligands. Overall, we conclude that the iron-based complexes bearing bidentate ligands are apparently more active than the related pre-catalysts supported by tridentate ligands. Moreover, in the case of iron complexes bearing *N*-alkyl iminopyridine ligands, the combination of borate co-reagent with alkyl-aluminum or MAO cocatalysts may be beneficial for the formation of 1,4-

trans units, whereas in the absence of borate, there is a tendency to favor 1,4-*cis* selectivity. In contrast, no obvious pattern regarding the activation mode of the iron complexes supported by *N*-aryl iminopyridine ligand can be identified: as such i) the use of the dual alkyl aluminum/borate or MAO alone as cocatalysts leads to a slight selectivity for 1,4-*cis* content, while ii) the combination of MAO/borate cocatalysts exhibits a high 1,4-*trans* stereo-selectivity with complexes bearing fluorinated *N*-aryl iminopyridine ligands. Advances in the area of butadiene polymerization seem to be emerging with respect to the thermal stability of the catalytic system, with the formation of highly regular syndiotactic 1,2-polybutadiene resulting from the combination of an iron precursor with phosphorous additives (section 1.1.2.1).

With respect to the ROP of cyclic esters, the best iron catalysts in terms of activity reach a good level of performance, which is approaching that of the most active metal-based complexes.[75] To the extent that the complex is well-defined and bears an alkoxy(aryloxy) group, which may also result from *in situ* reaction of a pre-catalyst with an alcohol/phenol, the reaction can proceed under mild experimental conditions (in solution and at low temperature). This strategy affords a process that can display good activity and control over the molecular weights, even being competitive with efficient catalytic systems based on other metals conventionally used in ROP.

As it also results from the ROP section, a number of neutral and ionic bulky ligands allow the preparation and isolation of iron complexes with several oxidation state (from 0 to +III herein), which makes it possible to highlight the impact of the oxidation state on ROP. To summarize on that point, the best performances were obtained with the lowest oxidation states, even if it is prudent not to deduce a general rule from it. Moreover, the recently proposed concept of redox triggering of a polymerization with complexes based on group 3 and 4,[115] with on-off switch control, could be successfully applied in the field of iron-based ROP of cyclic esters, through the elaboration of well-defined iron (II)/iron (III) couples of catalysts. Regarding the ROP mechanism, with iron salts, it is accepted as of AMM type. In absence of alcohol as co-reagent, protic impurities were suspected to account for the initiation reaction. However, a CM pathway was alternatively proposed when the catalytic species contains an alkoxide moiety, which can also alternatively be formed *in situ*. Noteworthy, higher reactivity towards LA than CL was noticed for a number of iron catalysts (**65**, **68** and **70**). This is quite unusual when compared to other metal complexes where the homopolymerization of CL is much faster than LA for a given complex. This allows us to see opportunities for the controlled statistical copolymerization of LA and CL, one of the major

challenges to improve the mechanical and physical properties of biodegradable polymers.[106] Finally, one aspect that is still to improve is the control of the stereo-selectivity with iron, which has just emerged very recently with the work described by the group of Byers, to be able to withstand comparison with the performances of the best catalysts in this area.[101,116]

In summary, the field of iron-catalyzed coordination-insertion polymerization has been widely investigated in recent years and, despite significant advances from an academic point of view, the industrial application of such systems based on this abundant and low toxic metal is still limited. To our knowledge, there is to date one example of iron-based catalyst that has been successfully applied on a 500 tons pilot plant for the preparation of short chain α-olefins.[17e] The search for efficient iron-based catalysts for industrial applications therefore remains a major challenge. Therefore, in this context, we look forward to answer all these questions by the studies we conduct throughout this thesis in search of highly efficient iron-based catalytic systems specifically for the polymerization of isoprene, styrene, lactide and ε-caprolactone.

References

(1)   (a) Ziegler, K.; Holzkamp, E.; Breil, H.; Martin, H. *Angew. Chem.* **1955**, 67 426;
        (b) Natta, G.; Pino, P; Corradini, P.; Danusso, F.; Mantica, E.; Mazzanti, G.; Moraglio, G. *J. Am. Chem. Soc.* **1955**, 77, 1708.

(2)   (a) Nakatani, H.; Miyazaki, K.; Terano M. Ziegler-Natta Polymerization. In: *Kobayashi S., Müllen K. (eds) Encyclopedia of Polymeric Nanomaterials*. Springer, Berlin, Heidelberg 2013;
        (b) Eisch, J. J. *Organometallics* **2012**, 31, 4917;
        (c) Shamiri, A.; Chakrabarti, M. H.; Jahan, S.; Hussain, M. A.; Kaminsky, W.; Aravind, P. V.; Yehye, W. A.*M aterials* **2014**, 7, 5069;
        (d) Huang, J.; Rempel, G. L. *Prog. Polym. Sci.* **1995**, 20, 459.

(3)   Kuran W. *Principles of Coordination Polymerisation*, ISBN 0-470-84141-9. Wiley-VCH. 2001, pp. 544.

(4)   (a) Böhm, L. L. *Angew. Chem. Int. Ed.* **2003**, 42, 5010;
        (b) Chen, E. Y.-X.; Marks, T. J. *Chem. Rev.* **2000**, 100, 1391;
        (c) Bochmann, M. *J. Chem. Soc., Dalton Trans.* **1996**, 255.

(5)   (a) Coates, G.W. *J. Chem. Soc., Dalton Trans*. **2002**, 467;
        (b) Breuil, P.-A.; Magna, L.; Olivier-Bourbigou, H. *Catal. Lett.* **2015**,145, 173.

(6)   (a) Britovsek, G. J. P.; Gibson, V.C.; Wass, D.F. *Angew. Chem. Int. Ed.* **1999**, 38, 428;
        (b) Alt, H. G.; Köppl, A. *Chem. Rev.* **2000**, 100, 1205;
        (c) Kaminsky, W.; Laban, A. *Appl. Catal. A* **2001**, 222, 47.

(7)   (a) Brintzinger, H. H.; Fischer, D.; Mulhaupt, R.; Rieger, B.; Waymouth, R. M. *Angew. Chem. Int. Ed. Engl.* **1995**, 34,1143;
        (b) McKnight, A. L.; Waymouth, R. M. *Chem. Rev.* **1998**, 98, 2587;
        (c) Resconi, L.; Cavallo, L.; Fait, A.; Piemontesi, F. *Chem. Rev.* **2000,** 100,1253;
        (d) Coates, G. W. *Chem. Rev.* **2000**, 100,1223;
        (e) Coates, G. W. *J. Chem. Soc., Dalton Trans*. **2002**, 467;
        (f) Gibson, V. C.; Spitzmesser, S. K. *Chem. Rev.* **2003**, 103, 283;
        (g) Domski, G. J.; Rose, J. M.; Coates, G. W.; Bolig, A. D.; M. Brookhart, *Prog. Polym. Sci*. **2007**, 32, 30.

(8)   Coates, G. W.; Hustad, P. D.; S. Reinartz, *Angew. Chem. Int. Ed.* **2002**, 41, 2236.

(9)   (a) Ittel, S. D.; Johnson, L. K.; Brookhart, M. *Chem. Rev*. **2000**, 100, 1169;
        (b) Mecking, S. *Angew. Chem., Int. Ed.* **2001**, 40, 534;
        (c) Guan, Z.; Popeney, C. S. *Top. Organomet. Chem.* **2009**, 26, 179;
        (d) Camacho, D. H.; Guan, Z. *Chem. Commun*. **2010**, 46, 7879.

(10)   (a) Boffa, L.S.; Novak, B. M. *Chem. Rev*. **2000**, 100, 1479;
        (b) Berkefeld, A.; Mecking, S. *Angew. Chem. Int. Ed.* **2008**, 47, 2;
        (c) Goodall, B. L. *Top. Organomet. Chem.* **2009**, 26, 159;
        (d) Nakamura, A.; Ito, S.; Nozaki, K. *Chem. Rev.* **2009**, 109, 5215.

(11)   (a) Cossee, P. J. *J. Catal.* **1964**, 3, 80;
        (b) Arlman, E. J.; Cossee, P. *J. Catal.* **1964**, 3, 99

(12)   Stridsberg, K. M.; Ryner, M.; Albertsson A.-C. Controlled Ring-Opening Polymerization: Polymers with designed Macromolecular Architecture. In: Degradable Aliphatic Polyesters. *Advances in Polymer Science,* 2002; vol 157. Springer, Berlin, Heidelberg.

(13)   Dechy-Cabaret, O.; Martin-Vaca, B.; Bourissou, D. *Chem. Rev.* **2004,** 104, 6147.

(14)   (a) Britovsek, G. J. P.; Gibson, V. C.; McTavish, S. J.; Solan, G. A.; White, A. J. P.; Williams, D. J.; Kimberley, B. S.; Maddox, P.J. *Chem. Commun*. **1998**, 849;
        (b) Bennet A.M. A. (DuPont) WO 98/27124, 1998;
        (c) Small, B. L.; Brookhart, M.; Bennett, A. M. A. *J. Am. Chem. Soc.* **1998**, 120, 4049;
        (d) Britovsek, G. J. P.; Dorer, B.; Gibson, V. C.; Kimberley, B. S.; Solan G. A. (BP Chemicals) WO 9912981 A1 19990318, 1999.

(15) Britovsek, G. J. P.; Bruce, M.; Gibson, V. C.; Kimberley, B. S.; Maddox, P. J.; Mastroianni, S.; McTavish, S.J.; Redshaw, C.; Solan, G. A.; Strömberg, S.; White, A. J. P.; Williams, D. J. *J. Am. Chem. Soc.* **1999**, 121, 8728.

(16) Britovsek, G. J. P.; Mastroianni, S.; Solan, G. A.; Baugh, S. P. D.; Redshaw, C.; Gibson, V. C.; White, A. J. P.; Williams, D. J.; Elsegood, M. R. J. *Chem. Eur. J.* **2000**, 6, 2221.

(17) (a) Bianchini, C.; Giambastiani, G.; Rios, I.G.; Mantovani, G.; Meli, A.; Segarra, A.M. *Coord.   Chem. Rev.* **2006,** 250, 1391;
(b) Gibson, V. C.; Redshaw, C.; Solan, G. A. *Chem. Rev.* **2007,** 107, 1745;
(c) Sun, W.-H.; Zhang, S.; Zuo W., *C. R. Chimie* **2008,** 11, 307;
(d) Xiao, T. ; Zhang, W. ; Lai, J.; Sun, W.-H. *C. R. Chimie* **2011**, 14, 851;
(e) Zhang, W.; Sun, W.-H.; Redshaw, C. *Dalton Trans.* **2013,** 42, 8988;
(f) Ma, J.; Feng, C.; Wang, S.; Zhao, K.-Q.; Sun, W.-H.; Redshaw, C.; Solan, G. A. *Inorg. Chem. Front.* **2014**, 1, 14;
(g) Boudier, A. ; Breuil, P.-A.R.; Magna, L.; Olivier-Bourbigou, H.; Braunstein, P. *Chem. Commun.* **2014**, 50, 1398;
(h) Small, B. L. *Acc. Chem. Res.* **2015,** 48, 2599;
(i) Flisak, Z.; Sun, W.-H. *ACS Catalysis* **2015**, 5, 4713;
(j) Wang, Z.; Solan, G.A.; Zhang, W.; Sun, W.-H. *Coord. Chem. Rev.* **2018,** 363, 92;
(k) Suo, H.; Solan, G. A.; Ma, Y.; Sun, W.-H. *Coord. Chem. Rev.* **2018,** 372, 101;
(l) Chen, Q.; Zhang, W.; Solan, G. A.; Zhang, R.; Guo, L.; Hao, X.; Sun, W.-H. *Organometallics* **2018,** 37, 4002.

(18) (a) Gibson, V. C.; Solan, G. A. *Top. Organomet. Chem.* **2009,** 26, 107;
(b) Li, L.; Gomes P. T. in: Bianchini, C. and Cole-Hamilton, D. J. P. W. N. M. van Leeuwen (Ed.), Olefin upgrading catalysis by nitrogen-based metal complexes II, *Catalysis by metal complexes. Springer*, Dordrecht, 2012, vol 36, pp. 77;
(c) Burcher, B.; Breuil, P.-A. R.; Magna, L.; Olivier-Bourbigou, H. *Top. Organomet. Chem.* **2015**, 50, 217;
(d) Gibson, V. C.; Solan, G. A. in Catalysis Without Precious Metals (Ed.: R. M. Bullock), Wiley-VCH, Weinheim, 2010, pp. 111.

(19) Champouret, Y.; Hashmi, O. H.; Visseaux, M. *Coord. Chem. Rev.* **2019**, *390*, 127–170.

(20) Patel, R. H.; Hodgson, L. M.; Williams, C. K. *Polym. Rev.* **2008**, 48, 11.

(21) (a) Thiele, S. K.-H.; Wilson, D. R. *J. Macromol. Sci., Polym. Rev.* **2003,** 43,58;
(b) Porri, L.; Giarrusso, A.; Ricci, G. *Prog. Polym. Sci.* **1991,** 16, 405;

(22) (a) Gridnev, A. A.; Ittel, S. D. *Chem. Rev.* **2001,** 101, 3611;
(b) Hawker, C. J.; Bosman, A. W.; Harth, E. *Chem. Rev.* **2001,** 101, 3661;
(c) Jitchum, V.; Perrier, S. *Macromolecules* **2007,** 40,1408;
(d) Ajellal, N.; Thomas, C. M.; Carpentier, J.-F. *Polymer* **2008,** 49, 4344;
(e) Harrisson, S.; Couvreur, P.; Nicolas, J. *Macromolecules* **2011,** 44, 9230;
(f) Harrisson, S.; Couvreur, P.; Nicolas, J. *Macromol. Rapid Commun.* **2012,** 33, 805;
(g) Zhu, Y.-F. Jiang, F.-J.; Zhang, P.-P.; Luo, J.; Tang, H.-D. *Chin. Chem. Lett.* **2016,** 27, 910;
(h) Moad, G. *Polymer International* **2017,** 66, 26;
(i) Vasu, V; Kim, J.-S.; Yu, H.-S.; Bannerman, W. I.; Johnson, M. E.; Asandei, A. D. *Polym. Chem.* **2018,** 9, 2389.

(23) Ouardad, S.; Deffieux, A.; Peruch, F. *Pure Appl. Chem.* **2012,** 84, 2065–2080.

(24) (a) Bywater, S. *Prog. Polym. Sci.* **1994,** 19, 287;
(b) Jérôme, R. J. Tong, Curr. Opin. *Solid State Mater. Sci.* **1998,** 3, 573.

(25) Raynaud, J.; Wu, J. Y.; Ritter, T. *Angew. Chem. Int. Ed.* **2012,** 51, 11805.

(26) Jing, C.; Wang, L.; Zhu, G.; Hou, H.; Zhou, L.; Wang, Q. *Organometallics* **2020**, *39* (22), 4019–4026.

(27) (a) Ciesielski, A. 2000 *An introduction to rubber technology*, (Shawbury, Shrewsbury, Shropshire,UK: RPRA Publishing) and references cited therein;

(b) Stern, H. J. *History in rubber technology and manufacture*, CM Blow (ed) (London:Newnes-Butterworths) 1977 and references cited therein;

(c) Hofmann, W. *Rubber technology handbook* (Munich: Hanser Publishers) 1989 and references cited therein;

(d) Bhowmick, A. K.; Stephens, H. L. *Handbook of Elastomers*, 2nd Ed. Revised and Expanded, (USA: Marcel Dekker Inc.) 2001 and references cited therein;

(e) White, J. R.; De, S. K. *Rubber technologist's handbook*, (RPRA Publishing) 2001 and references cited therein;

(f) Whitby, G. S.; Davis, C. C.; Dunbrook, R.F. *Synthetic rubber* (John-Wiley & Sons Inc.). 1954.

(28) (a) *Rubber Statistical News*, May 2012;
(b) Dutia, P. *Chemical Weekly* October 13, 2009; 213

(29) (a) Cooper, W. *The stereo rubbers* W M Saltman (ed.) (New York: John Wiley & Sons, Inc.) 1977; p. 21;
(b) Teyssie, P.; Hadjiandreou, P.; Julemont, M.; Warin, R. *Transition metal catalysed polymerizations Ziegler–Natta and metathesis polymerization* R P Quirk (ed.) (Cambridge: Cambridge University Press) 1988; p. 639.

(30) Wang, B.; Cui, D.; Lv, K. *Macromolecules* **2008,** 41, 1983.

(31) Thiele, S. K. H. and Wilson, D. R. *J. Macromol. Sci. C Polym.* Rev. **2003**, 43, 581–628.

(32) (a) Huang, J.; Liu, Z.; Cui, D.; Liu, X. *ChemCatChem* **2018,** 10, 42;
(b) Friebe, L.; Nuyken, O; Obrecht, W. *Adv. Polym. Sci.* **2006,** 204, 1;
(c) Jothieswaran, J.; Fadlallah, S.; Bonnet, F.; Visseaux, M. *Catalysts* **2017,** 7, 378;
(d) Zhang, Z.; Cui, D.; Wang, B.; Liu, B.; Yang, Y. *Struct. Bond.* **2010,** 137, 49.

(33) (a) Ricci, G.; Sommazzi, A.; Masi, F.; Ricci, M.; Boglia, A.; Leone, G. *Coord. Chem. Rev.* **2010,** 254, 661;
(b) Porri, L.; Giarrusso, A.; Ricci, G. *Prog. Polym. Sci.* **1991,** 16, 405–441.

(34) Srivastava, V.K.; Maiti, M.; Basak, G.C.; Jasra, R.V. *J. Chem. Sci.* **2014**, 126, 415–427.

(35) (a) Von Dohlen W, 1967 *U.S. Pat. 3297667*;
(b) Throckmorton, M. C.; Saltman, W. M. 1972 *U.S. Pat. 3676411*;
(c) Throckmorton, M. C.; Mournighan, R. E. 1974 *U.S. Pat. 3794604*;
(d) Sylvester, G.; Witte, J.; Marwede, G. 1980 *U.S. Pat. 4242232* and 1981 *U.S. Pat. 4260707*;
(e) Gordini, S.; Carbonaro, A.; Spina, S. 1987 *U.S. Pat. 4699960*;
(f) Carbonaro, A.; Ferraro, D.; Bruzzone, M; 1984 *U.S. Pat. 4444903*;
(g) Witte J. *Angew. Makromol. Chem.* **1981**, 94, 119;
(h) Yu G, Li Y, Qu Y,Li X *Macromolecules* **1993,** 26**,** 6702

(36) (a) Zinck, P.; Terrier, M.; Mortreux, A.; Valente, A.; Visseaux, M. *Macromol Chem. Phys.* **2007,** 208, 973;
(b) Bonnet, F.; Visseaux, M.; Pereira, A. *Macromol. Rapid Commun.* **2004,** 25, 873.

(37) Lasky, J. S.; Garner, H. K.; Ewart, E. H. *Ind. Eng. Chem. Prod. Res. Dev.* 1962; 1 82

(38) Tobisch S. *Can. J. Chem.* **2009,** 87, 1392.

(39) Ricci, G.; Sommazzi, A.; Masi, F.; Ricci, M.; Boglia, A. Leone, A. *Coord. Chem. Rev.* **2010,** 254, 661.

(40) Ricci, G.; Leone, G. *Polyolefins J.* **2014,** 1, 43.

(41) Noguchi, H.; Kambara, S. *J. Polym. Sci. Part B: Polym. Lett.* **1964,** 2, 593.

(42) Swift, H. E.; Bozik, J. E.; Wu, C.Y. *J. Catal.* **1970,** 17,331.

(43) Lu, J.; Hu, Y.; Zhang, X.; Bi, J.; Dong, W.; Jiang, L. and Huang, B. *Journal of Applied Polymer Science* **2006,** 100, 4265.

(44) Gong, D.; Dong, W.; Hu, J.; Zhang, X.; Jiang, L. *Polymer* **2009,** 50, 2826.

(45) Zheng, W.; Wang, F.; Bi, J.; Zhang, H.; Zhang, C.; Hu, Y; Bai, C.; Zhang, X. *J. Polym. Sc. A: Polym. Chem.* **2015,** 53, 1182.

(46) Nakayama, Y.; Baba, Y.; Yasuda,H.; Kawakita, K; Ueyama, N. *Macromolecules* **2003,** 36, 7953

(47) Gong, D.; Wang, B; Bai, C; Bi, J.; Wang, F.; Dong, W.; Zhang, X.; Jiang, L. *Polymer* **2009,** 50,

6259.

(48)   Chen, Y. F.; Qian, C. T.; Sun, J. *Organometallics* **2009,** 22, 1231.

(49)   Gong, D.; Jia, X.; Wang, B.; Wang, F.; Zhang, C.; Zhang, X.; Jiang, L.; Dong, W. *Inorg. Chim. Acta* **2011,** 373, 47.

(50)   Nobbs, J. D.; Tomov, A. K.; Cariou, R.; Gibson, V. C.; White, A. J. P.; Britovsek, G. J. P. *Dalton Trans.* **2012,** 41,5949.

(51)   Gong, D.; Jia, X.; Wang, B.; Zhang, X.; Jiang, L. *J. Organomet. Chem.* **2012,** 702, 10

(52)   Wang, B.; Bi, J.; Zhang, C.; Dai, Q.; Bai, C.; Zhang, X.; Hu, Y.; Jiang, L. *Polymer* **2013,** 54, 5174.

(53)   Zhang, J.; Gao, W.; Lang, X.; Wu, Q.; Zhang, L.; Mu, Y. *Dalton Trans*. **2012,** 41, 9639.

(54)   Jiang, X.; Wen, X.; Sun, W.-H.; He, A. *J. Polym. Sci. Part A Polym. Chem.* **2014,** 52, 2395.

(55)   Gong, D.; Liu, W.; Pan, W.; Chen, T.; Jia, X.; Huang, K.-W.; Zhang, X. *J. Mol. Catal. A: Chem.* **2015,** 406, 78.

(56)   Zhang, Z. Y.; Zhang, H. J.; Ma, H. M.; Wu, Y. *J. Mol. Catal.* **1982,** 17, 65.

(57)   (a) Xie, D.; Sun, Q. *Acta Polym. Sinica* **1987,** 1, 1.
         (b) Sun, Q.; Wang, F. *Acta Polym. Sinica* **1988,** 2, 145.

(58)   Hsu, W. L.; Halasa, A. F. *Rubber Chem. Technol*. **1994,** 67, 865.

(59)   Ricci, G.; Morganti, D. ; Sommazzi, A.; Santi, R.; Masi, F. *J. Mol. Cat. A Chem*. **2003,** 204-205, 287.

(60)   (a) Bazzini, C.; Giarrusso, A.; Porri, L. *Macromol. Rapid Commun*. **2002,** 23, 922.
         (b) Bazzini, C.; Giarrusso, A.; Porri, L.; Pirozzi, B; Napolitano, R. *Polymer* **2004,** 45, 2871.

(61)   De Rosa, C.; Malafronte, A.; Scoti, M.; Auriemma, F.; Pierro, I.; Leone, G. ; Ricci, G. *Macromolecules* **2018,** 51,8574.

(62)   (a) Ricci, G.; Bertini, F; Boccia, A. C.; Zetta, L.; Alberti, E.; Pirozzi, B.; Giarrusso, A.; Porri, L. *Macromolecules* **2007,** 40, 7238;
         (b) Pirozzi, B.; Napolitano, R.; Giusto, G.; Esposito, S.; Ricci, G. *Macromolecules* **2007,** 40, 8962.

(63)   Luo, L.; Kang, X.; Zhou, G.; Chen, S.; Luo, G.; Qu, J.; Luo, Y. *Int. J. Quantum Chem*. **2016,** 116, 1274.

(64)   Blanchard, S.; Derat, E.; Desage-El Murr, M; Fensterbank, L. Malacria, M.; Mouriès-Mansuy, V. *Eur. J. Inorg. Chem.* **2012,** 2012, 376.

(65)   Guo, L.; Jing, X.; Xiong, S.; Liu, W.; Liu, Y.; Liu, Z.; Chen, C. *Polymers* **2016,** 8, 389.

(66)   Zhu, G.; Zhang, G.; Zhao, M.; Wang, L.; Jing, C.; Wang, P.; Wang, X.; Wang, Q. *Polymers* **2018,** 10, 934.

(67)   Wang, X.-B.; Zhang, M.; Luo, L.; Hussain, M.; Luo, Y. *Chemical Physics Letters* **2020**, *755*, 137811.

(68)   Lin, W.; Zhang, L.; Suo, H.; Vignesh, A.; Yousuf, N.; Hao, X.; Sun, W.-H. *New J. Chem.* **2020**, *44* (19), 8076–8084.

(69)   Liu, H.; Wang, F.; Jia, X.-Y.; Liu, L.; Bi, J.-F.; Zhang, C.-Y.; Zhao, L.-P.; Bai, C.-X.; Hu, Y.-M.; Zhang, X.-Q. *J. Mol. Cat. A: Chem*. **2014,** 391, 25.

(70)   Zhao, M.; Wang, L.; Mahmood, Q.; Jing, C.; Zhu, G.; Zhang, X.; Wang, X.; Wang*,* Q. *Appl. Organomet. Chem.* **2019**

(71)   Zhang, X.; Zhu, G.; Mahmood, Q.; Zhao, M.; Wang, L.; Jing, C.; Wang, X.; Wang, Q. *J. Polym. Sci., Part A: Polym. Chem*. **2019,** 57, 767.

(72)   Li, X.; Zhang, L.; Tan, R. P.; Fazzini, P.-F.; Hungria, T.; Durand, J.; Lachaize, S.; Sun, W.-H.; Respaud, M.; Soulantica, K.; Serp, P. *Chem. Eur. J*. **2015,** 21,17437.

(73)   Jing, C.; Wang, L.; Mahmood, Q.; Zhao, M.; Zhu, G.; Zhang, X.; Wang, X.; Wang, Q. *Dalton Trans.* **2019**,*48* (22), 7862–7874.

(74)   Wang, L.; Wang, X.; Hou, H.; Zhu, G.; Han, Z.; Yang, W.; Chen, X.; Wang, Q. *Chem Commun.* **2020**, *56* (62), 8846–8849.

(75)   (a) O'Keefe, B. J.; Hillmyer, M. A.; Tolman, W. B. *J. Chem. Soc., Dalton Trans.* **2001**, 2215.
         (b) Sauer, A.; Kapelski, A.; Fliedel, C.; Dagorne, S.; Kol M.; Okuda, J. *Dalton Trans*. **2013,** 42, 9007.
         (c) Dagorne, S.; Normand, M.; Kirillov E.; Carpentier, J. F. *Coord. Chem. Rev*. **2013,** 257, 1869;
         (d) Buchard, A.; Bakewell, C. M.; Weiner, J.; Williams, C. K. *Top. Organomet. Chem*. **2012,** 39,175;

(e) Thomas, C. M. *Chem. Soc. Rev*. **2010,** 39, 165.

(76) (a) Okamoto, Y. *Makromol. Chem., Macromol. Symp*. **1991,** 42/43, 117;
      (b) Nomura, N.; Taira, A.; Tomioka, T.; Okada, T. *Macromolecules* **2000,** 33, 1497.

(77) (a) Lecomte, P.; Jerome, R. Ring Opening Polymerization, Vol 11, in *Encyclopedia of Polymer Science and Technology*, Wiley. 2004, pp. 547-565;
      (b) Dechy-Cabaret, O.; Martin-Vaca, B.; Bourissou, D. *Chem. Rev*. **2004,** 104, 6147 and references therein.

(78) (a) Di Lorenzo, M. L.; Androsch, R.; Synthesis, Structure and Properties of Poly(Lactic Acid); Eds.; *Advances in Polymer Science*; Springer International Publishing: Cham, 2018; Vol. 279.
      (b) Arbaoui, A.; Redshaw, C. *Polym. Chem.* **2010**, *1* (6), 801.

(79) (a) Albertsson, A.-C.; Varma, I. K. *Biomacromolecules* **2003**, *4* (6), 1466–1486.
      (b) Ikada, Y.; Tsuji, H. Biodegradable Polyesters for Medical and Ecological Applications. 16.

(80) (a) Wang, S.; Urban, M. W. *Nat. Rev. Mater.* **2020**, *5* (8), 562–583.
      (b) Burattini, S.; Greenland, B. W.; Chappell, D.; Colquhoun, H. M.; Hayes, W. *Chem. Soc. Rev.* **2010**, *39* (6), 1973.

(81) (a) Hu, Y.; Daoud, W.; Cheuk, K.; Lin, C. *Materials* **2016**, *9* (3), 133.
      (b) Li, G.; Zhao, M.; Xu, F.; Yang, B.; Li, X.; Meng, X.; Teng, L.; Sun, F.; Li, Y. *Molecules* **2020**, *25* (21), 5023.
      (c) Moon, S.-I.; Lee, C.-W.; Taniguchi, I.; Miyamoto, M.; Kimura, Y. *Polymer* **2001**, *42* (11), 5059–5062.
      (d) Kim, K. W.; Woo, S. I. Synthesis of High-Molecular-Weight Poly(L-lactic Acid) by Direct Polycondensation. 6.

(82) Ajioka Masanobu, Enomoto Katashi, Suzuki Kazuhiko, Yamaguchi Akihiro. *Bull. Chem. Soc. Jpn.* **1995,** *68*, 2125–2131.

(83) (a) Xavier, M. V.; Macedo, M. F.; Benatti, A. C. B.; Jardini, A. L.; Rodrigues, A. A.; Lopes, M. S.; Lambert, C. S.; Filho, R. M.; Kharmandayan, P. *Procedia CIRP* **2016**, *49*, 213–221.
      (b) Gupta, A. P.; Kumar, V. *Eur. Polym. J.* **2007**, *43* (10), 4053–4074.

(84) Thomas, C. M. *Chem Soc Rev* **2010**, *39* (1), 165–173.

(85) Vink, E. T. H.; Rábago, K. R.; Glassner, D. A.; Gruber, P. R. *Polym. Degrad. Stab.* **2003**, *80* (3), 403–419.

(86) Wang, X.; Liao, K.; Quan, D.; Wu, Q. *Macromolecules* **2005**, *38* (11), 4611–4617.

(87) Shang, X.-J.; Zhang, W.-H.; Lang, J.-P. *RSC Adv.* **2016**, *6* (14), 11400–11406.

(88) (a) Kricheldorf, H. R.; Damrau, D.-O. *Macromol. Chem. Phys.* **1997**, *198* (6), 1767–1774.
      (b) Stolt, M.; Södergård, A. *Macromolecules* **1999**, *32* (20), 6412–6417.
      (c) Södergård, A.; Stolt, M. *Macromol. Symp.* **1998**, *130* (1), 393–402.
      (d) Naolou, T.; Lendlein, A.; Neffe, A. T. *Front. Chem.* **2019**, *7*, 346.

(89) (a) Delle Chiaie, K. R.; Biernesser, A. B.; Ortuño, M. A.; Dereli, B.; Iovan, D. A.; Wilding, M. J. T.; Li, B.; Cramer, C. J.; Byers, J. A. *Dalton Trans.* **2017**, *46* (38), 12971–12980.
      (b) Gibson, V. C.; Marshall, E. L.; Navarro-Llobet, D.; White, A. J. P.; Williams, D. J. A *J. Chem. Soc. Dalton Trans.* **2002**, No. 23, 4321–4322.
      (c) O'Keefe, B. J.; Breyfogle, L. E.; Hillmyer, M. A.; Tolman, W. B. *J. Am. Chem. Soc.* **2002**, *124* (16), 4384–4393.

(90) Duan, R.; Hu, C.; Li, X.; Pang, X.; Sun, Z.; Chen, X.; Wang, X. *Macromolecules* **2017**, *50* (23), 9188-9195.

(91) (a) Gorczynski, J. L.; Chen, J.; Fraser, C. L. *J. Am. Chem. Soc.* **2005**, *127* (43), 14956–14957.
      (b) Chen, J.; Gorczynski, J. L.; Fraser, C. L. *Macromol. Chem. Phys.* **2010**, *211* (11), 1272 1279.

(92) (a) Dobrzyski, P.; Kasperczyk, J.; Janeczek, H.; Bero, M.; *Polymer* **2002,** 43, 2595
      (b) Dobrzynski, P.; Pastusiak, M.; Bero, M. *J. Pol. Sci. Part A: Polym. Chem.* **2005,** 43, 1913.
      (c) Helou, M.; Miserque, O.; Brusson, J.-M. ; Carpentier, J.-F.; Guillaume, S. M.; *ChemCatChem.* **2010,** 2, 306

(93)   Kang, Y. Y.; Park, H.-R.; Hyung Lee, M.; An, J.; Kim, Y.; Lee, J. *Polyhedron* **2015,** 95, 24.

(94)   Gorczynski, J. L.; Chen, J.; Fraser, C. L. *J. Am. Chem. Soc*. **2005,** 127, 14956.

(95)   Chen, J.; Gorczynski, J. L.; Zhang, G.; Fraser, C. L. *Macromolecules* **2010,** 43, 4909.

(96)   Chen, J.; Gorczynski, J. L.; Fraser, C. L. *Macromol. Chem. Phys*. **2010,** 211, 1272.

(97)   O'Keefe, B. J.; Monnier, S. M.; Hillmyer, M. A.; Tolman, W. B. *J. Am. Chem. Soc*. **2001,** 123, 339.

(98)   O'Keefe, B. J.; Breyfogle, L. E.; Hillmyer, M. A.; Tolman, W. B. *J. Am. Chem. Soc.* **2002,** 124, 4384.

(99)   Biernesser, A. B.; Li, B and Byers, J. A. *J. Am. Chem. Soc.*, **2013,** 135, 16553.

(100) Delle Chiaie, K. R.; Biernesser, A. B.; Ortuño, M. A.; Dereli, B.; Iovan, D. A.; Wilding, M. J. T.;
Li, B.; Cramer, C. J.; Byers, J. A. *Dalton Trans.* **2017,** 46, 12971.

(101) Sarazin, Y.; Carpentier, J. F. *Chem. Rev.* **2015,** 115, 3564.

(102) Ortuño, M. A.; Dereli, B.; Chiaie, K. R. D.; Biernesser, A. B.; Qi, M.; Byers, J. A. and Cramer, C. J.
Inorg. Chem. **2018,** 57, 2064.

(103) Biernesser, A. B.; Delle Chiaie, K. R.; Curley, J. B.; Byers, J. A. *Angew. Chem. Int. Ed*. **2016,** 55, 5251.

(104) Delle Chiaie, K. R.; Yablon, L. M.; Biernesser, A. B.; Michalowski, G. R.; Sudyn, A. W.; Byers, J.
A. *Polym. Chem.* **2016,** 7, 4675.

(105) Manna, C. M.; Kaur, A.; Yablon, L. M.; Haeffner, F.; Li, B.; Byers, J. A. *J. Am. Chem. Soc*. **2015,** 137, 14232.

(106) Stirling, E.; Champouret, Y.; Visseaux, M. *Polym. Chem*. **2018,** 9, 2517.

(107) O'Keefe, B. J.; Breyfogle, L. E.; Hillmyer, M. A.; Tolman, W. B. *J. Am. Chem. Soc.* **2002,** 124, 4384.

(108) Smith, J. M.; Lachicotte, R. J.; Holland, P. L. *Chem. Commun.* **2001,** 1, 1542.

(109) Gibson, V. C.; Marshall, E. L.; Navarro-Llobet, D.; White, A. J. P.; Williams, D. J. *J. Chem. Soc.*
Dalton Trans. **2002**, 4321.

(110) Li, Y.; Wu, Q. and Gao, M. *Adv. Mat. Res*. **2012,** 393, 1346.

(111) Duan, R.; Hu, C.; Li, X.; Pang, X.; Sun, Z.; Chen, X.; Wang, X. *Macromolecules* **2017,** 50, 9188.

(112)   Marin, P.; Tschan, M. J. -L.; Isnard, F.; Robert, C.; Haquette, P.; Trivelli, X.; Chamoreau, L.; Guérineau,
 V.; del Rosal, I.; Maron, L.; Venditto, V.; Thomas, C. M. *Angew. Chem.* **2019**, *131* (36), 12715–12719.

(113) (a) Chirik, P. J.; Wieghardt, K. *Science* **2010,** 327, 794;
          (b) Lyaskovskyy, V.; de Bruin, B. *ACS Catal*. **2012,** 2, 270.

(114) (a) Bolm, C.; Legros, J.; Le Paih, J.; Zani, L. *Chem. Rev.* **2004,** 104, 6217;
          (b) Bauer, I.; Knölker, H. J. *Chem. Rev*. **2015,** 115, 3170;
          (c) Wei, D.; Darcel, C. *Chem. Rev*. **2019,** 119, 2550.

(115) (a) Broderick, E. M.; Guo, N.; Vogel, C. S.; Xu, C.; Sutter, J.; Miller, J. T.; Meyer, K.; Mehrkhodavandi,
          P.; Diaconescu, P. L. *J. Am. Chem. Soc.* **2011,** 133, 9278;
           (b) Broderick, E. M.; Guo, N.; Wu, T.; Vogel, C. S.; Xu, C.; Sutter, J.; Miller, J. T.; Cantat, T.; Diaconescu
          P. L. *Chem. Commun.* **2011,** 47, 9897;
          (c) Broderick, E. M.; Thuy-Boun, P. S.; Guo, N.; Vogel, C. S.; Sutter, J.; Miller, J. T.; Meyer, K.;
          Diaconescu, P. L. *Inorg. Chem.* **2011,** 50, 2870.

(116) Cao, T.-P.-A.; Buchard, A.; Le Goff, X. F. ; Auffrant, A.; Williams, C. K. *Inorg. Chem*. **2012,** 51, 2157.

CHAPTER 2.

SYNTHESIS AND APPLICATIONS OF ALKYLATED *N*-ARYL SUBSTITUTED IMINOPYRIDINE IRON BASED CATALYSTS FOR THE COORDINATIVE POLYMERIZATION

2.1. Introduction

Since the initial report twenty years ago on the high catalytic activity of the (BIP)iron/MAO system for the polymerization of ethylene (BIP = bis(imino)pyridine),[1,2] the field of iron-catalyzed polymerization reactions has seen a substantial surge of interest for the preparation of a variety of polymeric materials.[3,4] Particular attention has been paid to the development of homogeneous single-site polymerization catalysts, as these systems have, to some extent, provided precise control over molecular weights, molecular weight distribution and stereo-regularity of the polymer chains in comparison with heterogeneous catalysts.[5–7] In this context, the research community has been motivated to ingeniously design discrete iron-based pre-catalysts for the coordination-insertion polymerization of not only olefins and related monomers, but also vinyl and cyclic polar monomers.[8]

Among the family of synthetic polymers, polydienes and especially polyisoprene are currently receiving special attention for their use in a wide range of applications in the rubber industry, e.g. tire manufacturing, medical science and others.[9–15] The coordination-insertion polymerization of isoprene produces four types of unit distributions such as 1,4-*cis*, 1,4-*trans*, 3,4 and 1,2-vinyl arrangements (Scheme 2.1), the amount and type of sequences dictating the resulting thermal, mechanical and physical properties of the polymer. To date, single-site catalysts for the polymerization of 1,3-dienes are mainly based on transition (Ti, Co, Ni) and rare earth (Nd) metal-based systems, producing concomitantly, to a certain degree, high molecular weight polymers with controlled microstructures.[16–21] On the other hand, single-site iron-based catalysis for the polymerization of isoprene has received less attention, whereas this metal is easily accessible, inexpensive and essentially non-toxic compared to its counterparts.[22]
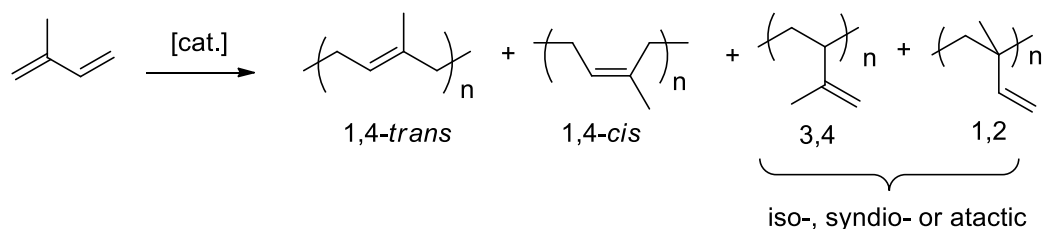
Scheme 2.1. Possible microstructures of polyisoprene

Most iron-active systems are mainly supported by bidentate and tridentate aromatic nitrogen ligands,[3,20] the former system displaying the most promising performances in terms of activity and

selectivity as it offers an additional coordination site to accommodate the isoprene monomer when compared to the latter.[8] As previously discussed in the last chapter, there have been various contributions to the field of coordinative polymerization of isoprene with iron based catalytic systems. From the highly active bipyridine system to the systems comprising specifically the iminopyridine skeleton – the modification of which by varying the *N*-aryl substituents and/or reducing the imine has resulted in a wide variety of iron (II) iminopyridine/aminopyridine complexes whose catalytic applications in the polymerization of isoprene have been observed in the literature**.** A short descriptive summary of some of these works by different research groups including those of Ricci,[23] Ritter,[24] Chen[25] and Wang[26–28] is presented in Chart 2.1. Overall, these results highlight the importance of the structure/properties of the iron pre-catalyst systems bearing bipyridine, iminopyridine and aminopyridine ligand as well as their mode of activation for controlling the polymerization of isoprene. At this stage, it is difficult to draw any rational conclusions regarding the influence of the electronic and steric properties of the ancillary ligand along with the nature of the cocatalyst on the selectivity and activity of the polymerization process.

Herein, we wish to contribute to this field by reporting the polymerization of isoprene with iron complexes supported by various iminopyridine ligands with a methyl substituent on the carbon of the imino group (Chart 2.1, bottom). To our knowledge, the use of ketiminopyridine-iron pre-catalysts for the polymerization of isoprene was only studied for the embedment of iron nanoparticles in polyisoprene within the cavity of carbon nanotubes.[29] In any case, no details on the selectivity and activity of the polymerization were described.

In the present chapter, the iron-catalyzed polymerization of isoprene will be investigated through the modification of the iminopyridine ligand framework using the complexes bearing *N*-aryl substituted ketiminopyridine, which will be compared with their aldiminopyridine counterparts. We look forward to gain control over the polymerization of isoprene using these complexes under different experimental conditions, in particular by changing the nature of the co-catalyst, the temperature of polymerization and the isoprene/catalyst ratio.[30]
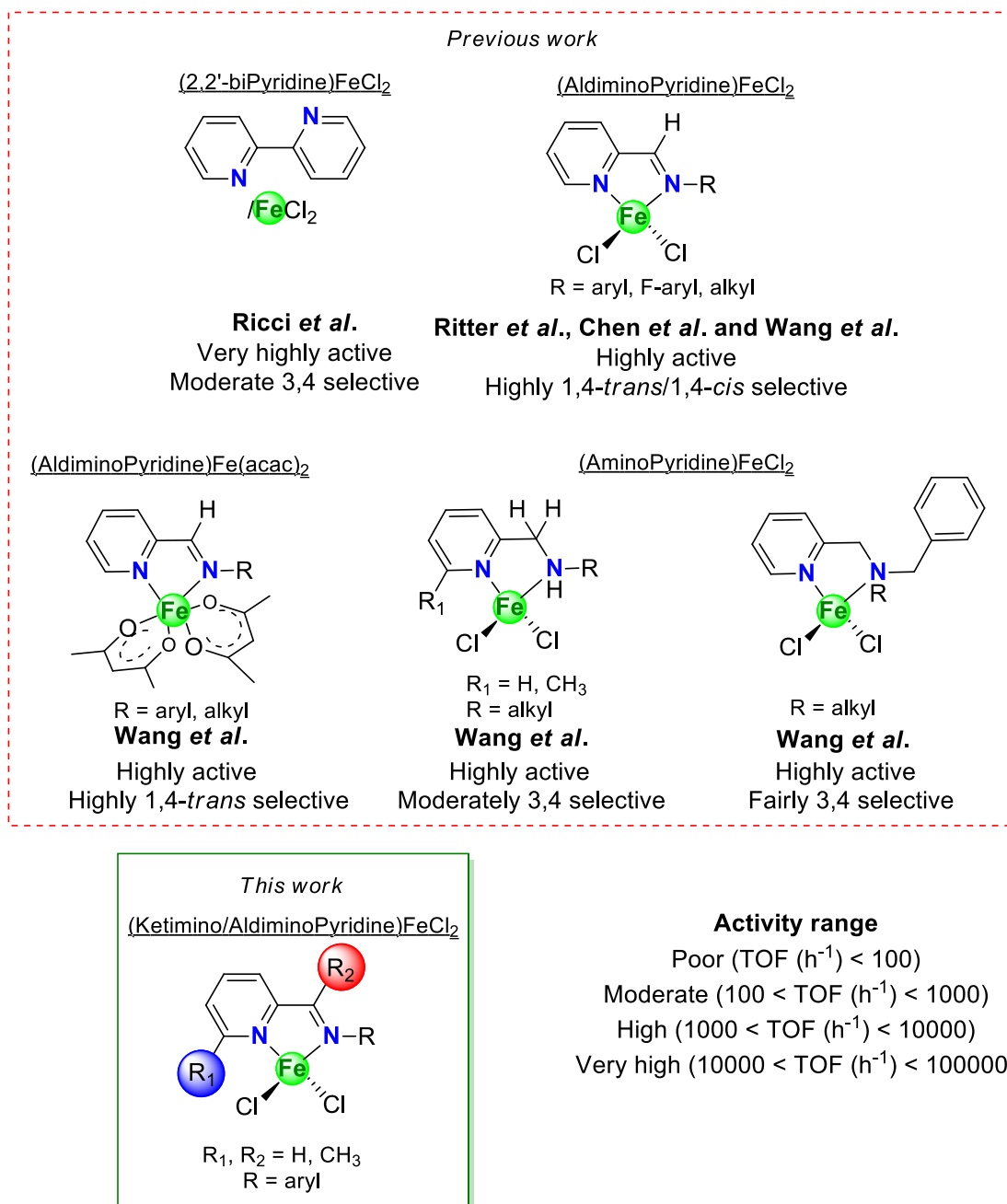
Chart 2.1. Iron-based complexes bearing bidentate pyridine-based ligands for the polymerization of isoprene

2.2 Results and Discussion

2.2.1. Synthesis of iminopyridine ligands L1–L5

All the iminopyridine ligands have been prepared following the synthetic strategy as shown in Scheme 2.2. The family of known ligands **L1–L5**, bearing *N*-aryl substituents with alkyl groups on the *ortho* positions of the phenyl ring, were synthesized *via* acid-catalyzed condensation reaction between 2-pyridinecarboxaldehyde or 2-acetylpyridine or 6-methyl-2-acetylpyridine with 2,6-dimethylaniline or 2,6-diisopropyaniline in methanol at high temperatures (see experimental part for details).[31–37] The reactions were monitored through ^{1}H NMR spectroscopy to determine the conversions as the formation of imine is reversible and typically driven to completion by the precipitation of imine or removal of water, or both. Due to this reason, the byproduct water was removed from the reaction mixture by adsorption on sodium sulfate or by azeotropic removal through Dean-Stark apparatus to prevent the reversible process, thereby, avoiding the reaction to proceed backwards.
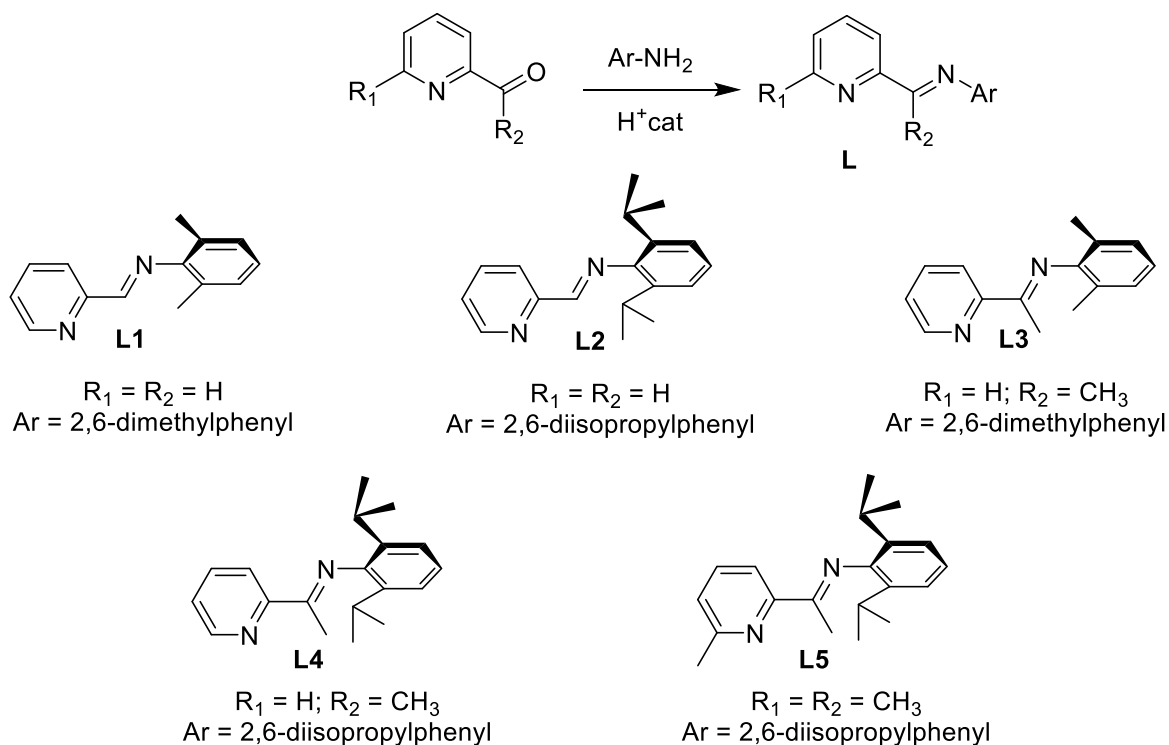
**Scheme 2.2.** Synthesis of the ligands **L1–L5**

All the ligands, which were afforded in poor to high yields (15–89%), were further characterized by ^{1}H NMR & IR spectroscopy, High Resolution Mass Spectrometry (HRMS) and elemental analysis. The ^{1}H NMR spectra of these ligands were consistent with the reported data.[31–]

[37] The huge differences in the obtained yield of the ligands corresponds to the outcome of a normal condensation that depends on the substituent on the carbonyl group. For instance, the difference between the carbonyl groups between aldehydes and ketones can be an important factor, which determines the outcome of a condensation reaction, aldehydes being more reactive towards the nucleophilic additions of substituted anilines than ketones because of both steric and electronic effects.[38] Therefore, depending on the reactivity of aldehydes, some condensations can principally proceed on their own at room temperature unlike the condensation of ketones which requires some external energy (*eg*. heating) to proceed.[39] For example, the condensation reaction of 2-acetylpyridine with 2,4,4-trimethylpentane-2-amine did not proceed even when the reaction parameters were modified from moderate to harsh conditions (120 °C).

Analyses of the IR spectra of all ligands revealed the characteristic vibration band of the C=N bond in the range of 1633 – 1643 cm^{-1}, showing the negligible effect on the stretching frequency caused due to the variation of *N*-aryl substituents. Elemental analysis were performed and confirmed the molecular formula of ligands (See experimental section).

2.2.2. Synthesis of iminopyridine iron-based complexes (1–5)

Thereafter, the complexation of ligands **L1**–**L5** with one equivalent of anhydrous FeCl$_2$ in CH$_2$Cl$_2$ was carried out as shown in Scheme 2.3.
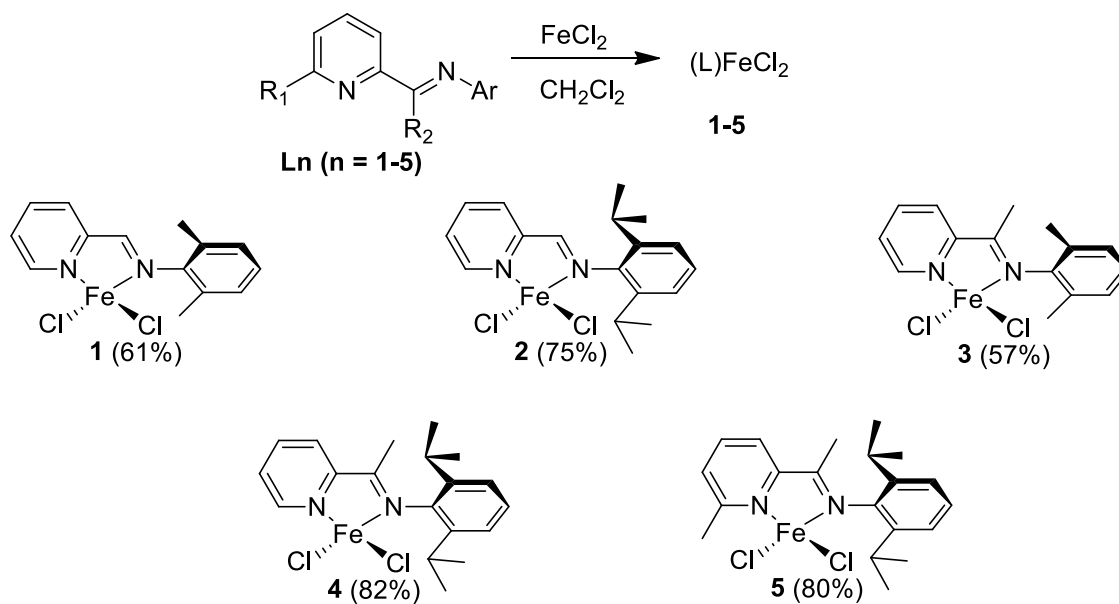
Scheme 2.3. Synthesis of iron (ii) based complexes **1–5** from their related ligands (**L**)

The crude product was washed with dry pentane to remove any unreacted ligand in the solution, affording the related iminopyridine-based iron complexes **1–5** in moderate to good yields (57 – 83%) as previously described in the literature.[33,34,36,40–42] Elemental analyses were performed and confirmed the molecular formula of the resulting iron complexes **1–5** (experimental section). The IR spectra of the resulting complexes displayed a stretching frequency of the C=N bond between 1589 – 1593 cm^{-1}; values lower than those identified for their related free ligand due to the coordination of the N atom of the imino group on the metal center ($\Delta \upsilon_{(C=N)} = 40$–46 cm^{-1}). The complexes **1–5** were also characterized by ^{1}H NMR spectroscopy as they have not been characterized yet by this technique. For a better comparison, the stacked ^{1}H NMR spectra of the complexes are shown below in Figure 2.1.
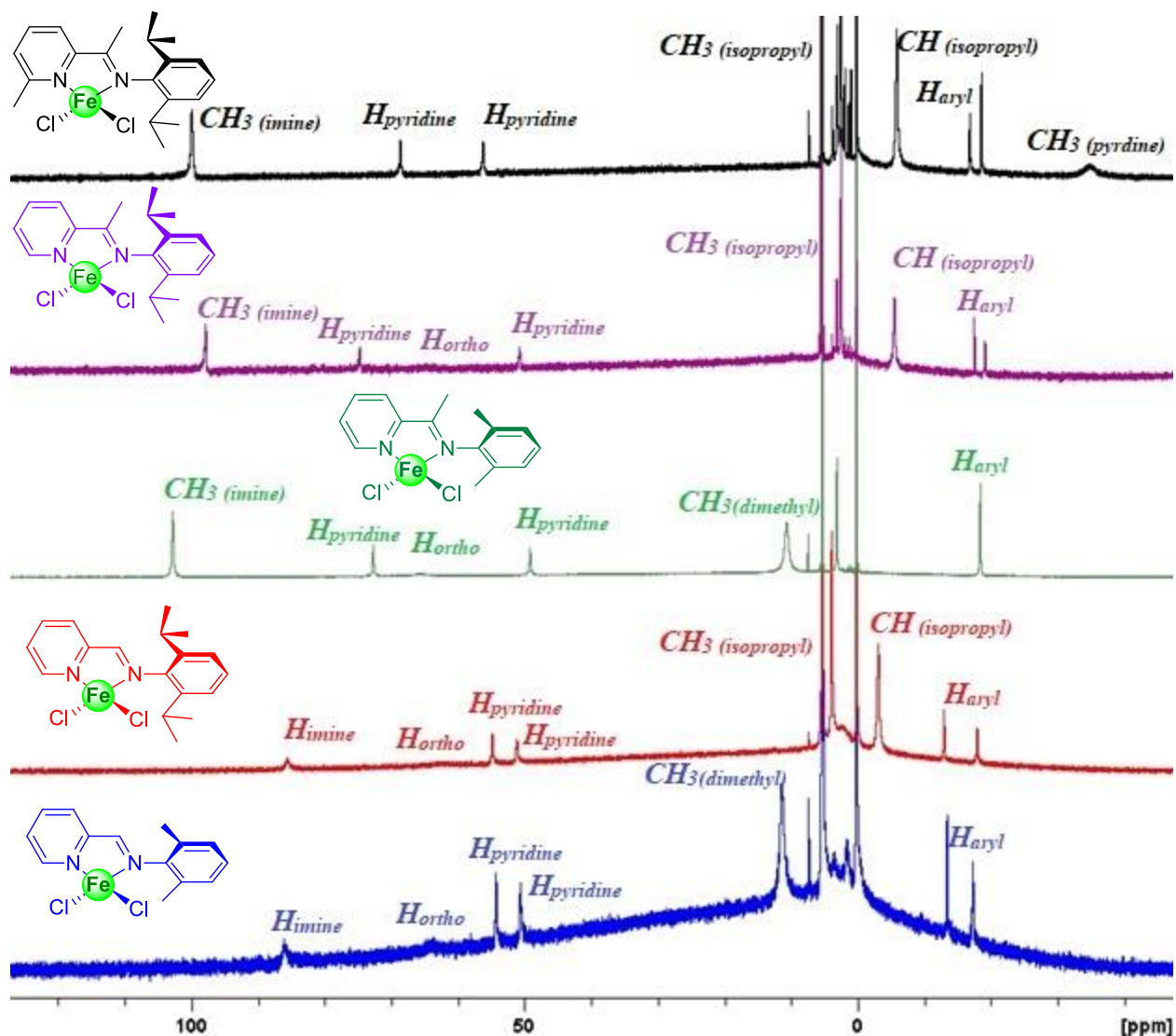

Figure 2.1. ^{1}H NMR spectrum of complexes **1–5** stacked (300 MHz, CD$_2$Cl$_2$, 25 °C)

74

All the complexes were sparingly soluble in $CDCl_3$ and benzene-d_6, so their spectra were recorded in dichloromethane-d_2. It is clearly evident from the spectra that the coordination of ligands to the iron (II) center has occurred as the characteristic signals corresponding to each proton are located from -19 to 102 ppm due to the presence of the paramagnetic Fe (II) metal that results in wider chemical shift window when compared to the spectra of ligands alone. The same trend in the shift window can be observed with Ritter's complexes bearing trimethylpentyl/triphenylbenzyl groups as their *N*-aryl substituents.[24] The tentative assignments of these broad singlets could be proposed based on integration and proximity to the metal center, although in most of the cases, the integrations did not correspond exactly as their expected value, probably due to the broadening of some signals. As expected, the dramatic differences in chemical shifts were observed for some protons between the ligand and the paramagnetic metal. Also, the signals corresponding to the ligand were absent implying the absence of any unreacted ligand or starting material.

From the stacked ^{1}H NMR spectra of complexes, we can observe that the signal of *ortho*-pyridyl proton (H_{ortho}) of the coordinated ligand, nearest to the paramagnetic iron center, is likely to be found as a very broad singlet shifted downfield at 60 ppm for **1** and **2**, whereas for **3-5**, it almost gets disappeared in the baseline due to the increased broadening. The remaining pyridyl protons ($H_{pyridine}$) which are comparatively far from the iron center are visibly shifted downfield around 50 ppm. Comparing the spectra of complex **1** and it's related ketimine **3**, we observe a singlet around 10 ppm which might correspond to the methyls of 2,6-dimethyl substituent whereas in a similar way, for the complexes **2**, **4** and **5**, we can observe the resonance of methyl groups of 2,6-diisopropyl substituent upfield in the range of 2-5 ppm. In addition, the backbone methyls on imino carbon and the isopropyl C*H* should be largely unaffected as most of them are further removed from the iron center, appearing downfield nearly at 100 ppm and upfield at -5 ppm, respectively. Lastly, the methyl group on the pyridine in complex **5**, which is very near to the paramagnetic iron center appears as a broad singlet upfield at -35 ppm. For instance, a hypothetical assignment of the resonances for complex **4** could be suggested, as indicated in the Figure 2.2.

It is worthy to notice that the presence of various electron donating groups within this family of ligands/complexes impacts the electron density around the paramagnetic iron (II) center which can be clearly observed from the ^{1}H NMR spectra of complexes. For instance, the complexes **1** and **2** bearing hydrogen as the imino substituent exhibit lesser splitting of their

characteristic signals (-17.9 to 86.2 ppm) when compared to the complexes **3–5** (-34.8 to 102.7 ppm) bearing methyl group at the imine position which imparts more electron density at the iron center (aldimine *vs* ketimine). In addition, beyond the nature of the substituents, it is also the geometry of the complex in solution (which is different from the solid state), following an induced magnetic field (depending on this geometry), will impact the spectral width and the position of signals.
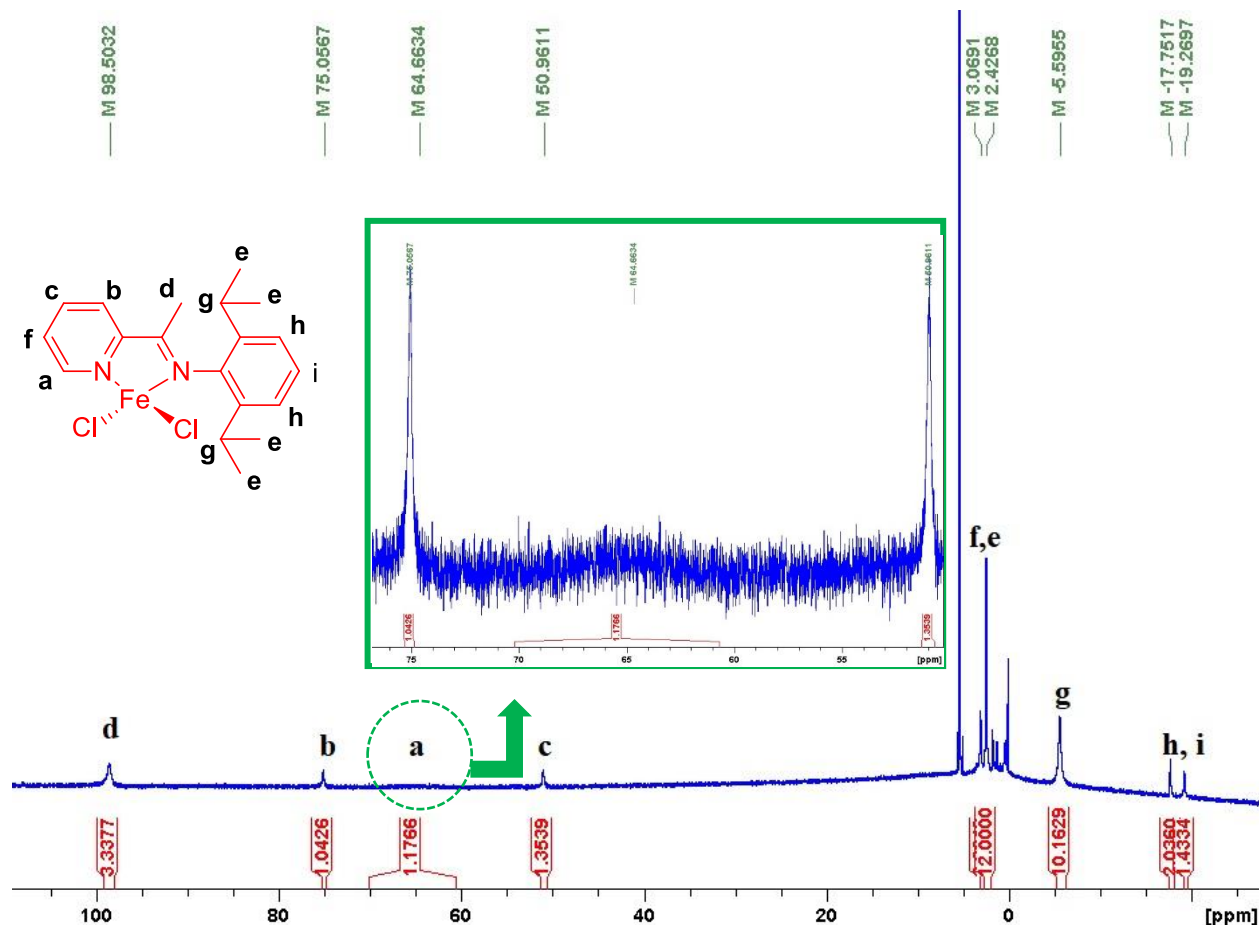
Figure 2.2. ^{1}H NMR spectrum of complex **4** (300 MHz, CD$_2$Cl$_2$, 25 °C)

2.2.3. Polymerization studies with iron-based complexes

*2.2.3.1. Polymerization of Isoprene with Iron-based Complexes **1–5***

2.2.3.1.1. Screening various combinations of complex and co-catalyst

The polymerization of isoprene was assessed at room temperature using pre-catalysts **1–5** under different modes of activation. Various reagents such as MAO in excess and triisobutylaluminium (Al^{i}Bu$_3$) or triethylaluminium (AlEt$_3$), the two latter ones being combined with trityl tetrakis(pentafluorophenyl)borate [Ph$_3$C][B(C$_6$F$_5$)$_4$], were employed as co-catalysts. The results of the polymerization of isoprene using the binary **1–5**/MAO catalytic systems are presented in Table 2.1 below.

Table 2.1. Polymerization of isoprene using **1–5**/MAO catalytic systems [a]

Entry [a]	Complex	Conv. (%)	$M_{n(exp)}$ [b] (g/mol)	$Đ$ [b]	Microstructure [c] (%) 1,4 (*trans/cis*)	3,4
1	**1**	>99	33 500	1.9	89 (32/57)	11
2	**2**	>99	29 000[d]	1.4	76 (30/46)	24
3	**3**	>99	21 000	2.2	81 (50/31)	19
4	**4**	>99	13 000[d]	1.3	91 (77/14)	9
5	**5**	<1	-	-	-	-

[a] Polymerization conditions: 10 µmol of Fe (II) complex; isoprene/Fe/MAO = 500/1/500; toluene = 5 mL; [C]$_{isoprene}$ = 1 mol/L; time = 1 h; temperature = room temperature (RT); [b] determined by size exclusion chromatography (SEC) analysis in THF using polystyrene standards; [c] determined by ^{1}H NMR and ^{13}C NMR; $M_{n(th)}$ = 33 700 g/mol (considering one growing chain per metal center); Activity = 34 kg$_{(PI)}$.mol$_{(cat)}^{-1}$.h^{-1} or Turn Over Frequency (TOF) = 500 h^{-1} for all; [d] contribution of a low amount (< 5 %) of a second fraction displaying high M_n.

From the Table 2.1, we can clearly see that the catalytic **1–4**/MAO combinations were highly active for the polymerization of isoprene, with complete conversion of 500 eqs of monomer per iron catalyst within 1 h (TOF = 500 h^{-1}). The analysis of the polyisoprenes (PIs) obtained from the **1**/MAO system by size-exclusion chromatography (SEC) revealed that the M_n value was quite close to the theoretical M_n, considering one polymer chain per metal center ($M_{n(th)}$ = 33 700 g/mol), which indicates a fairly controlled process (Table 2.1, Entry 1). For the systems **2–4**/MAO, the molar masses of the obtained polyisoprenes turned out to be lower to those expected, most likely

due, in some extent, to the occurrence of reversible chain transfer of the growing chain with aluminum because of the presence of free AlMe$_3$ (Table 2.1, Entries 2–4).[43] This effect of obtaining low M_n while using MAO (including free AlMe$_3$) in excess has already been observed in the literature with related iron iminopyridine systems.[26] Moreover, a small amount of polyisoprene displaying high M_n was found for polymerization reactions conducted with complexes **2** and **4**. The dispersities were broader for **1** and **3**, whereas they were quite narrower for **2** and **4**. Lastly, the **5**/MAO catalytic system proved to be inactive for the isoprene polymerization, owing to the increased steric hindrance around the iron center caused by the presence of the methyl group on the pyridine skeleton, which probably leads to a very poor coordination of the monomer on the metal propagation center and/or results in a very poor propagation.

All the polyisoprenes were analyzed *via* NMR spectroscopy studies to determine their microstructure content *via* integration of the characteristic signal of protons of 1,4- and 3,4-motifs in the ^{1}H NMR spectrum and 1,4-*trans,* 1,4-*cis* and 3,4-vinyl in the ^{13}C NMR spectrum, respectively. The resulting microstructure content of all the polyisoprenes prepared from Table 2.1 (Entries 1 to 4) are presented in Figure 2.3. The corresponding ^{1}H and ^{13}C NMR spectra for the polyisoprene obtained for entry 4 in Table 2.1 are displayed in Figure 2.4 as an example.

Figure 2.3. Microstructure content of the polyisoprene obtained from **1**–**4**/MAO catalytic systems

a) **^{1}H NMR spectrum**

1,4-units

3,4-units

b) **^{13}C NMR spectrum**

3,4-units

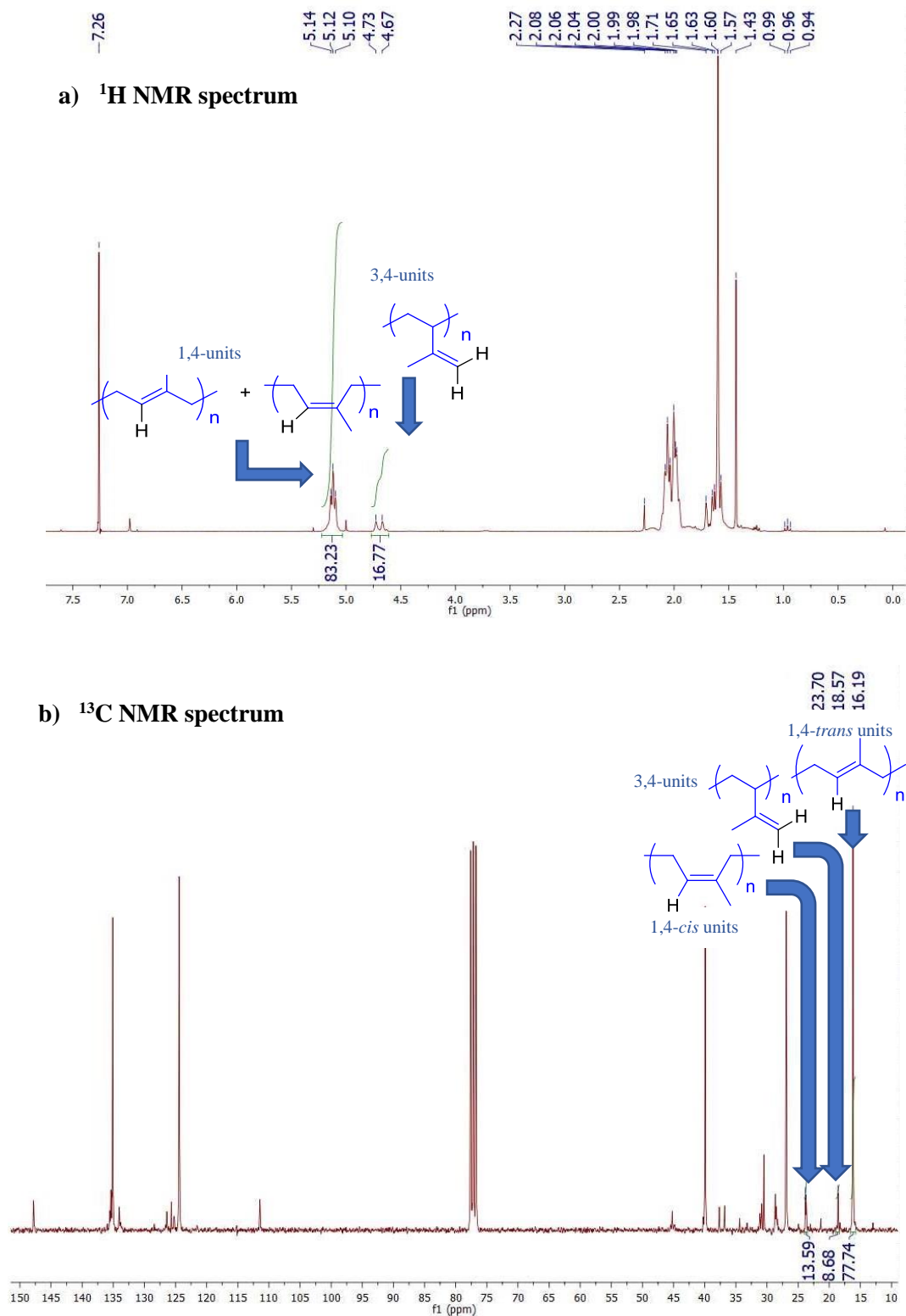1,4-*trans* units

1,4-*cis* units

Figure 2.4. NMR spectra (in CDCl$_3$) of the PI obtained from **4**/MAO (Table 2.1, Entry 4) showing the characteristic resonances of 1,4- and 3,4-units (a, ^{1}H NMR) and *trans*/*cis* configuration (b, ^{13}C NMR).[44,45]

The polyisoprene acquired from the binary **1-2**/MAO catalytic system (aldimino-pyridine iron complexes) consisted mainly of 1,4 motifs (>76%), which predominantly exhibited *cis* configuration (> 45%) along with a significant contribution of 1,4-*trans* and 3,4 motifs (Table 2.1, Entries 1 and 2).

The modification of complexes **1** and **2**, by changing the substituent on the carbon of the imino group of the ligand from H to CH_3 (aldimino-pyridine, *H*C=N *vs* ketimino-pyridine, C*H₃*C=N), resulted in similar selectivity for the pre-catalyst **3** but, interestingly, an improvement of the 1,4 selectivity (90 %), along with a small amount of 3,4 content (10 %), was observed for the pre-catalyst **4** (Table 2.1, Entries 3 and 4, Figure 2.2). On the contrary, both catalytic systems showed moderate selectivity for 1,4-*trans*, with the **4**/MAO system exhibiting the highest percentage of 1,4-*trans* (77%). From these data, it appears that the ketimino-pyridine-based iron pre-catalysts **3** and **4**, in comparison with the aldimino-pyridine-based iron complexes counterparts **1** and **2**, preferentially favor the 1,4-*trans* stereoregularity, which is also enhanced by the presence of sterically hindered *N*-aryl group (**4**). This 1,4-*trans* selectivity could be due to an increase in electron density at the iron center, as previously observed with a related electron-rich iron complex bearing an octyl-substituted aldimino-pyridine ligand.[24,26]

It is noteworthy to remind that the polymerization of isoprene using **2**/MAO catalytic systems has already been studied by Chen and coworkers (isoprene/**2**/MAO = 2 500/1/500),[25] which has led to the formation of polyisoprenes in good yield (83% in 2 hours at 25 °C) with a slight preference for 1,4-*cis*-stereoregularity (1,4-*trans*/1,4-*cis*/3,4 contents = 5/70/25). In our case, for isoprene/**2**/MAO = 500/1/500, the percentage of 1,4-*trans* units in the obtained polyisoprene proved to be higher than that reported previously, whereas the proportion of 1,4-*cis* contents was lower with identical amount of 3,4-motifs (1,4-*trans*/1,4-*cis*/3,4 = 30/46/24; Table 2.1, Entry 2). In order to compare these different results, we performed the polymerization of isoprene using the same experimental conditions as those described by Chen, *i.e.* dissolution of the pre-catalyst **2** (8 µmol) in 2 mL of dichloromethane followed by the addition of 7 mL of toluene with isoprene/**2**/MAO = 2 500/1/500. Again, a significant amount of polyisoprene containing 1,4-*trans* units was isolated (1,4-*trans*/1,4-*cis*/3,4 = 21/52/27, Figure 2.5). The reason for this difference in result is unknown at this stage, but we can confirm that it does not originate from the use of a chlorinated solvent to dissolve the pre-catalyst but might arrive from the quality of MAO which was not specified in Chen's article.
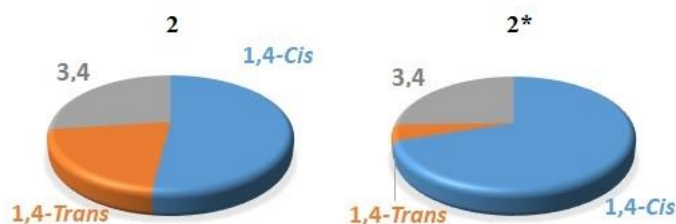
Figure 2.5. Microstructure content of the PIs obtained using Isoprene/**2**/MAO (2 500/1/500) catalytic systems (our study (left) *vs*. *Chen *et* al.*[25] (right))

Substitution of the co-catalyst activator MAO by AlEt$_3$/[Ph$_3$C][B(C$_6$F$_5$)$_4$], which has been scarcely used in iron-based polymerization catalysis of conjugated dienes,[24] had little effect on the results of the polymerization. These studies are displayed below in Table 2.2.

Table 2.2. Polymerization of isoprene using **1**–**5**/AlEt$_3$/[Ph$_3$C][B(C$_6$F$_5$)$_4$] catalytic systems[a]

Entry [a]	Complex	Conv. (%)	$M_{n(exp)}$ [b] (g/mol)	Đ [b]	Microstructure [c] (%) 1,4 (*trans/cis*)	3,4
1	**1**	>99	45 000	1.9	79 (25/54)	21
2	**2**	>99	47 000	1.5	75 (32/43)	25
3	**3**	>99	63 000	1.6	90 (57/33)	10
4	**4**	>99	19 000[d]	1.5	91 (79/12)	9
5	**5**	<1	-	-	-	-

[a] Polymerization conditions: 10 µmol of Fe (II) complex; isoprene/Fe/AlEt$_3$/[Ph$_3$C][B(C$_6$F$_5$)$_4$] = 500/1/10/1; toluene = 5 mL; [C]$_{isoprene}$ = 1 mol/L; time = 1 h; temperature = RT; [b] determined by SEC analysis in THF using polystyrene standards; [c] determined by ^{1}H NMR and ^{13}C NMR; $M_{n(th)}$ = 33 700 g/mol (considering one growing chain per metal center); Activity = 34 kg$_{(PI)}$.mol$_{(cat)}^{-1}$.h^{-1} or TOF = 500 h^{-1} for all; [d] contribution of a low amount (< 5 %) of a second fraction displaying high M_n

In contrast to the results obtained with **1-2**/MAO systems, the ternary **1**/AlEt$_3$/[Ph$_3$C][B(C$_6$F$_5$)$_4$] and **2**/AlEt$_3$/[Ph$_3$C][B(C$_6$F$_5$)$_4$] catalytic systems resulted in a better control of the polymerization, affording M_n slightly higher than the theoretical value and with almost similar Đ. (Table 2.2, Entries 1 and 2). On the other hand, the polymerizations were less

controlled in terms of molar masses for **3** with the presence of a very small amount of polyisoprene displaying high M_n (Table 2.2, Entry 3), although it is worth mentioning that low M_n value was obtained again with complex **4,** probably due to some chain transfer reactions with $AlEt_3$ present in excess, which indicates a potential for chain transfer reactions (Table 2.2, Entry 4). As observed previously with MAO, the catalytic system **5**/$AlEt_3$/[Ph_3C][$B(C_6F_5)_4$] was also found to be inactive for the isoprene polymerization (Table 2.2, Entry 5). These results compare well with related iron-based catalysts available in the literature.[8] However, no significant changes were noticed regarding the selectivity of the polymerization with all complexes by comparison with the results obtained with MAO as co-catalyst (Table 2.1).

The same polymerization reactions were studied by replacing the alkylating agent $AlEt_3$ by more sterically hindered Al^iBu_3, which has been previously employed in iron-based polymerization catalysis of conjugated dienes.[24,46,47] The results of the polymerization are displayed below in Table 2.3.

Table 2.3. Polymerization of isoprene using **1**–**5**/Al^iBu_3/[Ph_3C][$B(C_6F_5)_4$] catalytic systems [a]

Entry [a]	Complex	Conv. (%)	$M_{n(exp)}$ [b] (g/mol)	Đ [b]	Microstructure [c] (%)	
					1,4 (*trans*/*cis*)	3,4
1	**1**	>99	101 000	2.7	79 (24/55)	21
2	**2**	>99	84 000	1.5	76 (30/46)	24
3	**3**	>99	44 000	1.5	90 (67/22)	11
4	**4**	>99	44 000	1.7	90 (74/16)	10
5	**5**	<1	-	-	-	-

[a] Polymerization conditions: 10 µmol of Fe (II) complex; Isoprene/Fe/Al^iBu_3/[Ph_3C][$B(C_6F_5)_4$] = 500/1/10/1; toluene = 5 mL; [C]$_{isoprene}$ = 1 mol/L; time = 1 h; temperature = RT; [b] determined SEC analysis in THF using polystyrene standards; [c] determined by ^1H NMR and ^{13}C NMR; $M_{n(th)}$ = 33 700 g/mol (considering one growing chain per metal center); Activity = 34 kg$_{(PI)}$.mol$_{(cat)}^{-1}$.h^{-1} or TOF = 500 h^{-1} for all.

Unlike $AlEt_3$, the catalysts resulting from activation of **1** and **2** with Al^iBu_3/[Ph_3C][$B(C_6F_5)_4$] afforded polyisoprene with M_n values up to three times higher than expected, which speaks in favor of a slow initiation process under these conditions (Table 2.3, Entries 1 and 2). It was also observed that the catalytic systems **3**–**4**/Al^iBu_3/[Ph_3C][$B(C_6F_5)_4$] (ratio of 1/10/1) gave M_n slightly higher

than the theoretical value with monomodal curves displaying narrow dispersity, which argues in support of better control over the polymerization when compared to catalysts generated from **1** and **2** (Table 2.3, Entries 3 and 4). Lastly, as expected, the catalytic system **5**/Al^{i}Bu$_3$/[Ph$_3$C][B(C$_6$F$_5$)$_4$] was again found to be inactive for the isoprene polymerization as previously observed with AlEt$_3$ and MAO (Table 2.3, Entry 5). Nevertheless, all the SEC plots of the polyisoprenes obtained from **1**–**4**/Al^{i}Bu$_3$/[Ph$_3$C][B(C$_6$F$_5$)$_4$] exhibited a monomodal molar mass distribution, in line with the presence, in each case, of a single-site catalyst. It is worthy to mention that the replacement of alkylating agent MAO by Al^{i}Bu$_3$ had no significant change on the selectivity of the polymerization, as previously observed with AlEt$_3$ (Table 2.2). In fact, after assessing these three co-catalysts {Al^{i}Bu$_3$/[Ph$_3$C][B(C$_6$F$_5$)$_4$], AlEt$_3$/[Ph$_3$C][B(C$_6$F$_5$)$_4$] and MAO}, we did not observe any significant difference in the selectivity of all the catalytic systems arising from complexes **1** to **4**.

2.2.3.1.2. *Optimization of polymerization through variation in the amount of co-catalyst Al^{i}Bu$_3$*

After conducting the polymerization with various co-catalysts in the previous section, we can conclude that the activation of precatalysts **1**–**4** with the combination of AlR$_3$/[Ph$_3$C][B(C$_6$F$_5$)$_4$] is more appropriate than MAO, which leads to (slightly) more uncontrolled transfer reactions in most of the cases. While the alkylating agent AlEt$_3$ seems to be more suitable for complexes **1** and **2**, the polymerizations are rather better controlled with the most stereo-/regioselective catalytic systems generated from **3**–**4**/Al^{i}Bu$_3$/[Ph$_3$C][B(C$_6$F$_5$)$_4$] as the resulting M_n in each case is close to the expected value with a narrower molecular weight distribution. It is also worth mentioning that for the most stereoselective precatalyst **4**, the alkylation with the more sterically hindered reagent Al^{i}Bu$_3$ minimizes the rate of reversible transfer reactions that are present with MAO (AlMe$_3$) and AlEt$_3$ (Tables 2.1–2.3, Entry 4). From these results, not only we can observe the substantial influence of co-catalysts but also argue that it is the appropriate combination of precatalyst/ co-catalyst, which induce a better control over the polymerization. Therefore, keeping all these observations in mind, we preferred the combination Al^{i}Bu$_3$/[Ph$_3$C][B(C$_6$F$_5$)$_4$] for the activation of all complexes in the following chapters. We have further tried to optimize the polymerization conditions by choosing one pre-catalyst (**4**) and varying the amount of alkylating agent Al^{i}Bu$_3$ (from 1 to 10 eq./**4**) in order to obtain the optimum quantity that is most suitable for controlling the polymerization process. The results of this optimization are displayed below in Table 2.4.

Table 2.4. Polymerization of isoprene using **4**/Al^{i}Bu$_3$/[Ph$_3$C][B(C$_6$F$_5$)$_4$] catalytic system under optimized conditions [a]

Entry [a]	[Al]/[4]	Conv. (%)	$M_{n(exp)}$ [b] (g/mol)	Đ [b]	Microstructure [c] (%) 1,4 (*trans/cis*)	3,4
1	**1/1**	>99	130 000*	2.9	87 (68/19)	13
2	**2/1**	>99	76 000	1.6	90 (77/13)	10
3	**3/1**	>99	41 000	1.2	92 (76/16)	8
4[d]	**10/1**	>99	44 000	1.7	90 (74/16)	10

[a] Polymerization conditions: 10 µmol of Fe (II) complex; Isoprene/Fe/[Ph$_3$C][B(C$_6$F$_5$)$_4$] = 500/1/1; toluene = 5 mL; [C]$_{isoprene}$ = 1 mol/L; time = 1 h; temperature = RT; [b] determined by SEC analysis in THF using polystyrene standards; [c] determined by ^{1}H NMR and ^{13}C NMR; $M_{n(th)}$ = 33 700 g/mol (considering one growing chain per metal center); Activity = 34 kg$_{(PI)}$.mol$_{(cat)}^{-1}$.h^{-1} or TOF = 500 h^{-1} for all; [d] recalled from Table 2.3, entry 4; *Secondary contribution observed

Activation with 1 eq. of Al^{i}Bu$_3$ results in a catalytic system that produces high molecular weight polyisoprene (nearly four times higher than the theoretical value) with a broad molecular weight distribution (Đ = 2.9). This result indicates that the polymerization is poorly controlled with a maximum of only 25 % of active species during the polymerization (Table 2.4, Entry 1). In terms of microstructure content of the resulting polyisoprene, it can be definitely seen that the selectivity for 1,4 and 3,4 motifs is maintained whereas the proportion of 1,4-*trans* units is slightly reduced to 68% when compared to the previous results obtained with 10 eq. of Al^{i}Bu$_3$ (74%, Table 2.3, Entry 4). Increasing the Al/**4** feed ratio to 2/1 resulted in a system producing polyisoprene with a M_n two times higher than expected, with 50% of active species catalyzing the polymerization and speaking in favor of slow initiation. Although, a slight improvement in the 1,4-*trans* stereo-regularity (77%) along with narrow molecular weight distribution was observed, it was nevertheless found to be less controlled compared to the use of a Al/**4** = 10/1 (Table 2.4, Entry 2) ratio. Further, increasing the Al/**4** feed ratio to 3/1 (*i.e.* using 3 eq. of Al^{i}Bu$_3$ for the alkylation of **4**), resulted in a catalytic system that gave polyisoprene with M_n value slightly higher than expected (M_n = 41 000 g/mol, Table 2.4, Entry 3). As described in the previous section, when a Al/**4** feed ratio was increased to 10/1, polyisoprene with a comparatively much higher M_n than expected (M_n = 44 000 g/mol, Table 2.4, Entry 4) was produced. To summarize among all the four

entries, the fine control over the molecular weight with the narrowest dispersity ($Đ$ = 1.2) is observed only with entry 4, indicating that the polymerization is more controlled when the complex is activated with 3 eqs. of Al^{i}Bu$_3$.

In addition, it is noteworthy to mention that a decrease in the Al^{i}Bu$_3$/Fe ratio from 10 to 3 did not affect the stereo- and regio-selectivity of the catalyst, affording polymers with yields and microstructural properties identical to those observed in Table 2.3. We have therefore chosen the Al^{i}Bu$_3$/[Ph$_3$C][B(C$_6$F$_5$)$_4$] (3/1) combination as the preferred activation mode for all pre-catalysts **1–4.**

Table 2.5. Polymerization of isoprene using **1–4**/Al^{i}Bu$_3$/[Ph$_3$C][B(C$_6$F$_5$)$_4$] catalytic systems[a]

Entry	Complex	Conv. (%)	Microstructure [b] (%)	
			1,4 (*trans/cis*)	3,4
1	**1**	>99	78 (28/50)	22
2	**2**	>99	75 (26/49)	25
3	**3**	>99	91 (76/15)	9
4	**4**	>99	92 (76/16)	8

[a] Polymerization conditions: 10 µmol of Fe (II) complex; isoprene/Fe/Al^{i}Bu$_3$/[Ph$_3$C][B(C$_6$F$_5$)$_4$] = 500/1/3/1; toluene = 5 mL; [C]$_{isoprene}$ = 1 mol/L; time = 1 h; temperature = RT; [b] determined by ^{1}H NMR and ^{13}C NMR; Activity = 34 kg$_{(PI)}$.mol$_{(cat)}$$^{-1}$.h^{-1} or TOF = 500 h^{-1} for all.

*2.2.3.1.3. Kinetic studies of the polymerization of isoprene with the iron-based complexes **1–4***

Thereafter, the kinetic parameters of the polymerization processes were assessed with **1**–**4**/Al^{i}Bu$_3$/Ph$_3$C[B(C$_6$F$_5$)$_4$] (1/3/1) catalytic combinations at room temperature. The studies were carried out with 5 000 eqs. isoprene to ensure better reliability, as the highly active systems prevented us from correctly evaluating the overall rates of the polymerization using 500, 1 000 and 2 000 eqs. of isoprene/Fe, due to very short reaction times. Aliquots were taken at different times during the course of the polymerization to determine the conversions *via* ^{1}H NMR spectroscopy as shown below in Figure 2.6. The molecular parameters of the last sample of polyisoprene for each polymerization run are presented in Table 2.6.
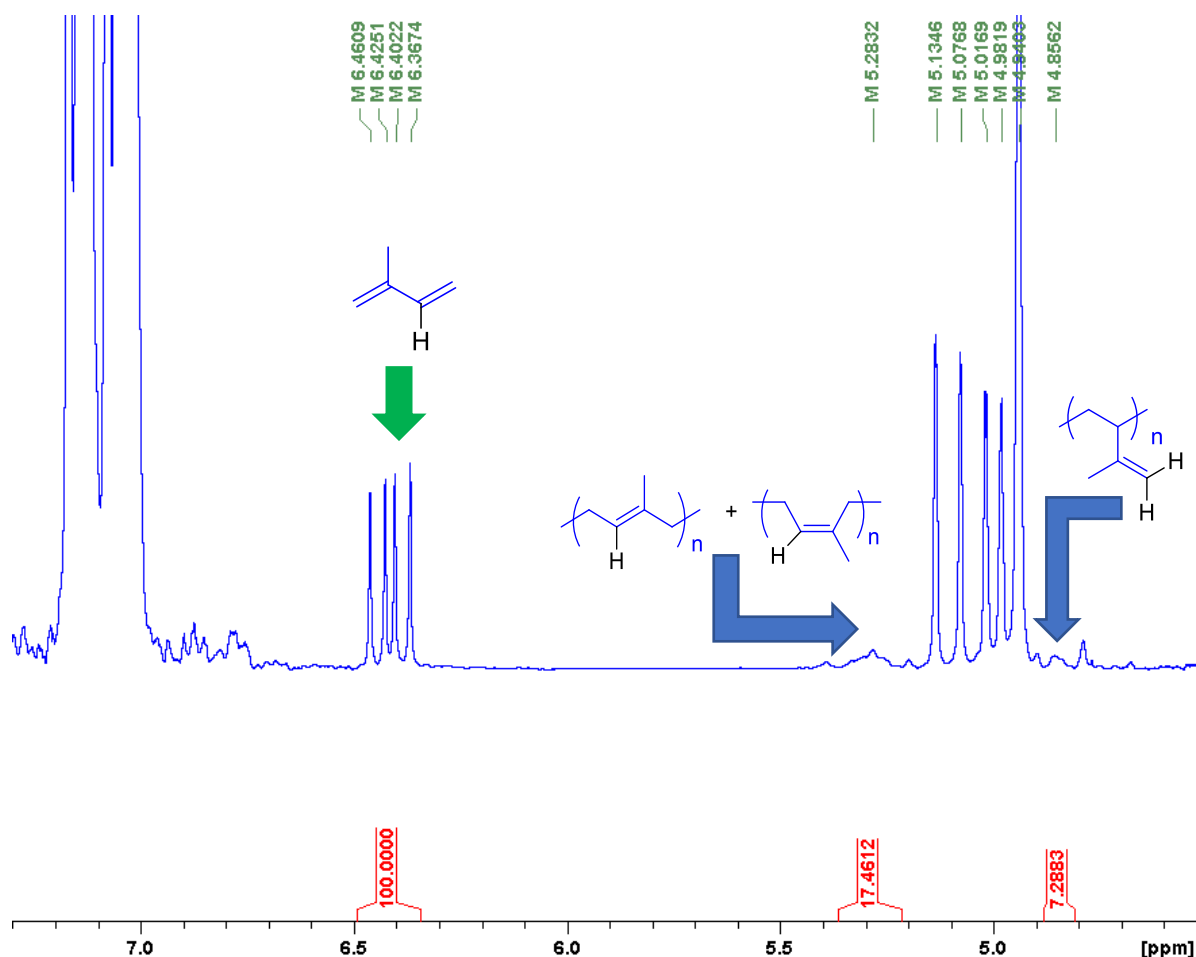

Figure 2.6. Determination of the conversion (17%) of isoprene (residual monomer signals in green, *vs.* polyisoprene signals in blue) by ^{1}H NMR of the crude aliquot

Table 2.6. Polymerization of 5 000 eqs. of isoprene/Fe using **1**–**4**/Al^{i}Bu$_3$/[Ph$_3$C][B(C$_6$F$_5$)$_4$] catalytic systems [a]

Entry	Complex	Conv. (%)	Time (min)	TOF (h^{-1})	$M_{n(exp)}$ [b] (g/mol)	Đ [b]	Microstructure [c] (%) 1,4 (*trans/cis*)	3,4
1	**1**	89	10	26 700	105 000	1.8	79 (25/54)	21
2	**2**	82	10	23 400	163 000	1.6	74 (26/48)	26
3	**3**	83	20	12 450	142 000	1.9	90 (60/30)	10
4	**4**	25	60	1 250	87 000	1.4	84 (69/18)	13

[a] Polymerization conditions: 5 µmol of Fe (II) complex; Isoprene/Al^{i}Bu$_3$/[Ph$_3$C][B(C$_6$F$_5$)$_4$]/Fe = 5 000/3/1/1; toluene = 25 mL; [C]$_{isoprene}$ = 1 mol/L; time = 1 h; temperature = RT; [b] determined by SEC analysis in THF using polystyrene standards; [c] determined by ^{1}H NMR and ^{13}C NMR

Figure 2.7a shows the plot of conversion *vs.* time for complexes **1**–**4** as pre-catalysts. From the profile of the curves, the activity of the complexes is in the order of **1** (TOF = 26 700 h^{-1}) > **2** (TOF = 23 400 h^{-1}) > **3** (TOF = 12 450 h^{-1}) > **4** (TOF = 1 250 h^{-1}). For pre-catalysts **1**–**3**, 80 % conversion was reached within less than 20 minutes. Thus, the various pre-catalysts when employed for isoprene polymerization were found to be highly active by comparison with data reported in the literature.[8] The catalyst based on complex **4** displayed the lowest activity, although showing the highest 1,4-*trans* selectivity amongst this series of complexes, possibly due to the relatively increased electron density and steric bulk at the iron center conferred by the simultaneous presence of bulky ^{i}Pr groups on *N*-aryl moiety and the methyl group on the imino carbon. These observations are in accordance with the literature where the authors suggested that the stereoselectivity is governed by the nature of substituents attached to the imino group.[24,48]

From Figure 2.7b, it appears that the polymerization is rather controlled for complexes **1**–**3**, and well controlled for complex **4**, displaying a *quasi*-first order kinetic profile for all, which speaks in favor of minimal loss of active species along the polymerization process. These results prompted us to study the living character of the polymerization, using pre-catalysts **3** and **4**, by sequential addition of isoprene (*vide infra*).
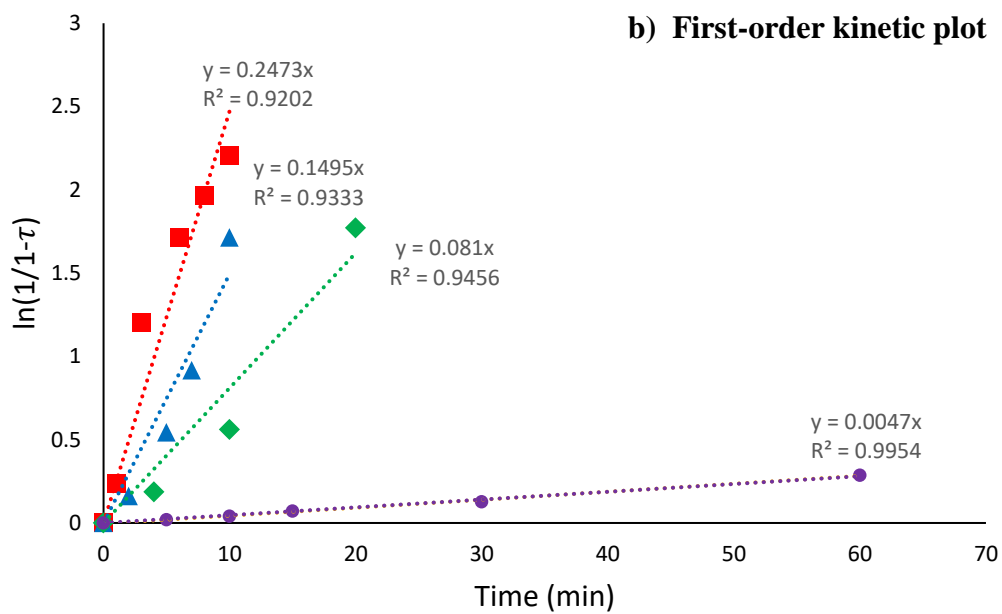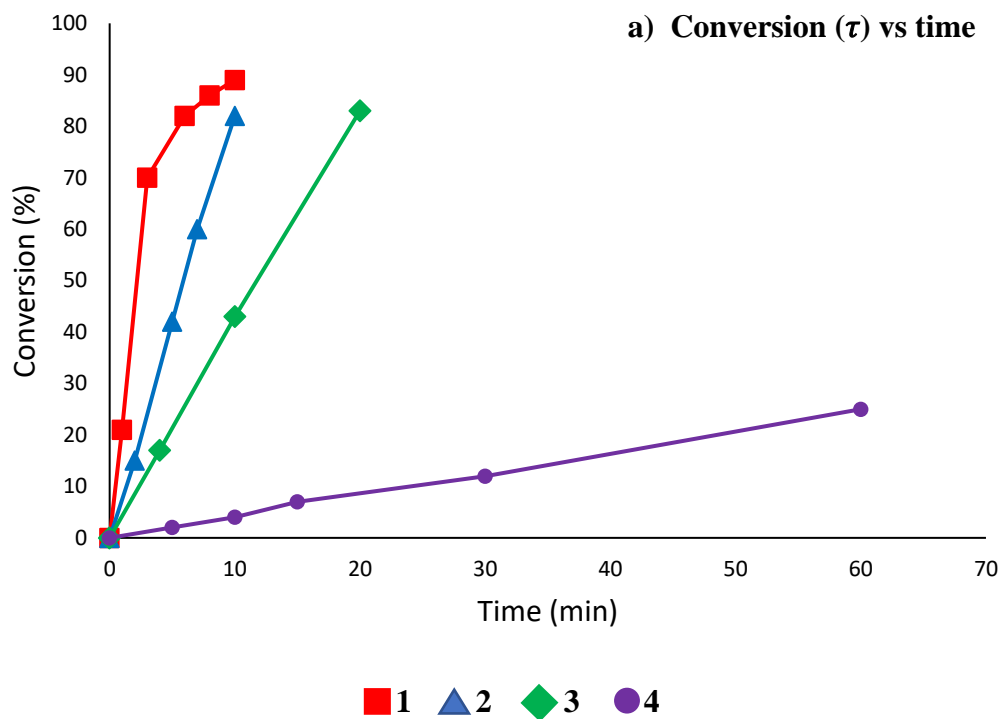
Figure 2.7. Monomer conversion (τ) in function of time (a) and first-order kinetic plot (b) for pre-catalysts **1**–**4** (isoprene/Al^{i}Bu$_3$/[Ph$_3$C][B(C$_6$F$_5$)$_4$]/Fe = 5 000/3/1/1).

*2.2.3.1.4. Sequential polymerization of isoprene with **3**–**4**/Al^{i}Bu$_3$/[Ph$_3$C][B(C$_6$F$_5$)$_4$]*

The living polymerization tests were carried out with the ternary **3**/Al^{i}Bu$_3$/[Ph$_3$C][B(C$_6$F$_5$)$_4$] and **4**/Al^{i}Bu$_3$/[Ph$_3$C][B(C$_6$F$_5$)$_4$] (1/3/1) catalytic systems by sequential addition of monomer in three steps. The polymerization was initially conducted with 500 eqs. of isoprene/Fe at room temperature. After completion of this first stage of the polymerization (15 min for **3** and 30 min for **4**), an aliquot was withdrawn from the reaction medium to determine the conversion and for SEC analysis, then an additional amount of isoprene (500 eqs./Fe) was added. The last step of the sequential polymerization was achieved by adding 1 000 eqs. of isoprene (after a total time of 30 min for **3** and 60 min for **4**) after withdrawing an aliquot for analysis; the results are displayed in Table 2.7, with the SEC traces obtained for each fraction of converted monomer illustrated in Figure 2.8.

Table 2.7. Sequential polymerization of isoprene using [Fe]/Al^{i}Bu$_3$/[Ph$_3$C][B(C$_6$F$_5$)$_4$] catalytic systems ([Fe] = **3** or **4**) [a]

Entry	Complex	Total monomer (intermediate addition of monomer) (equiv./Fe)	Time (min)	Conv. (%)	$M_{n(exp)}$ [b] (g/mol)	Đ [b]
		500 (500)	15	>99	36 500	1.6
1	**3**	1 000 (+ 500)	30	>99	69 000	1.5
		2 000 (+ 1 000)	60	>99	102 000	1.3
		500 (500)	30	>99	23 000	2.4
2	**4**	1 000 (+ 500)	60	>99	32 000	2.0
		2 000 (+ 1 000)	120	>99	62 000	1.3

[a] Polymerization conditions: 10 µmol of Fe (II) complex; Fe/Al^{i}Bu$_3$/[Ph$_3$C][B(C$_6$F$_5$)$_4$] = 1/3/1; [C]$_{isoprene}$ = 1 mol/L in toluene; temperature = RT; [b] determined by SEC analysis in THF using polystyrene standards; [c] determined by ^{1}H NMR and ^{13}C NMR; $M_{n(th)}$ = 135 000 g/mol for the last sample (considering one growing chain per metal center).
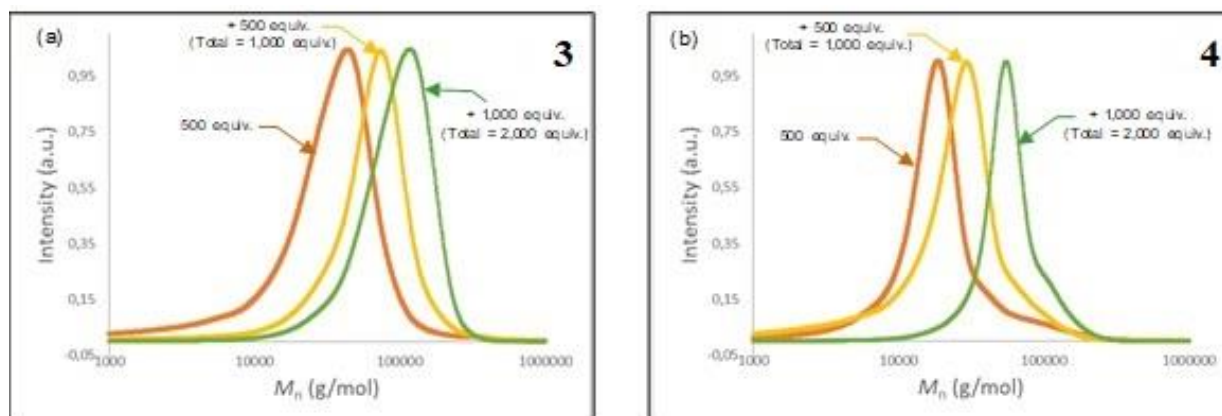
Figure 2.8. SEC traces of the sequential polymerization using pre-catalysts (a) **3** and (b) **4**.

Analyses of all withdrawn aliquots reveal a continuously increase in isoprene conversion with time for both pre-catalysts (Table 2.7, Entries 1 and 2). In addition, the SEC traces of the three fractions of the growing polyisoprene chains prepared from the ternary **3**/Al^{i}Bu$_3$/Ph$_3$C[B(C$_6$F$_5$)$_4$] and **4**/Al^{i}Bu$_3$/Ph$_3$C[B(C$_6$F$_5$)$_4$] catalytic systems show in each case a monomodal curve (Figures 2.8a and 2.8b, respectively) with a steady growth of M_n and an unexpected continuous decrease of the dispersity throughout the progression of the polymerization.

For both pre-catalysts, the M_n resulting from all the aliquots was lower than expected and indicates that the polymerization is not completely controlled.Nevertheless, for both runs, the gradual increment of M_n from the three-stage sequential addition of monomer suggests that the polymerization of isoprene with **3**/Al^{i}Bu$_3$/Ph$_3$C[B(C$_6$F$_5$)$_4$] and **4**/Al^{i}Bu$_3$/Ph$_3$C[B(C$_6$F$_5$)$_4$] display a *quasi*-living character.

*2.2.3.1.5. Temperature variation during the polymerization of Isoprene with complexes **1–4***

Up to this stage, we have observed the influence of the nature of ligands on the catalytic activities and microstructural properties of the acquired polyisoprenes. On the other hand, it is known that the reaction parameters, such as temperature, might also alter the selectivity of a catalyst, which primarily depends on the mode of coordination of the incoming monomer and its subsequent insertion between the Fe-alkyl (allyl) bond leading to the formation of *anti*-η^3 or *syn*-η^3 Fe-allyl intermediates, which are interchangeable (Scheme 2.4).[49,50]
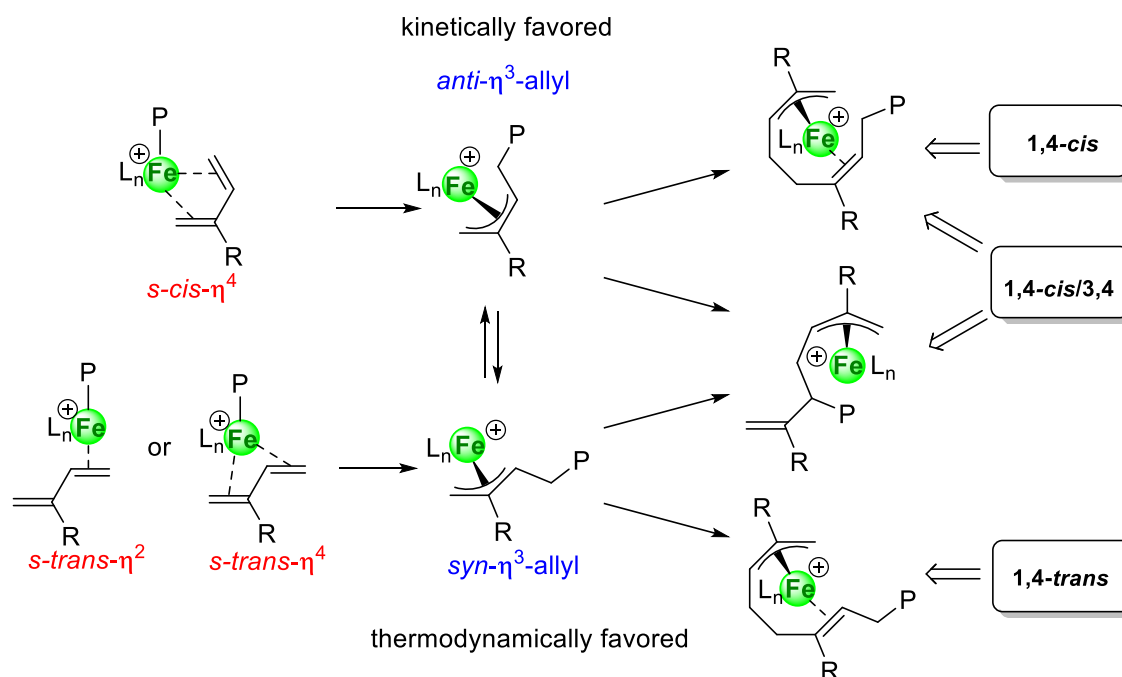
Scheme 2.4. Elementary steps, coordination-insertion, in isoprene polymerization

Therefore, the polymerization of isoprene was assessed at low temperature as well as high temperature using **1–4** in presence of Al^{i}Bu$_3$/[Ph$_3$C][B(C$_6$F$_5$)$_4$] to observe its influence on the selectivity of each catalytic system (*vide infra*).

i) At lower temperatures

The catalytic systems **1–3**/Al^{i}Bu$_3$/Ph$_3$C[B(C$_6$F$_5$)$_4$] were found active at temperatures as low as – 40 °C, while complex **4** was inactive under these conditions. The results of the polymerization carried out at – 40 °C are displayed below in Table 2.8.

Table 2.8. Polymerization of isoprene at lower temperatures (- 40 °C) with pre-catalysts **1–4** [a]

Entry	Fe	T (°C)	Time (h)	Conv. (%)	TOF (h^{-1})	$M_{n(exp)}$ [b] (g/mol)	*Đ* [b]	Microstructure [c] (%) 1,4 (*trans*/*cis*)	3,4
1	**1**	– 40	5	>99	100	169 000	1.3	89 (0/89)	11
2	**2**	– 40	5	>99	100	216 000	1.6	88 (0/88)	12
3	**3**	– 40	4	>99	125	106 000	2.0	90 (0/90)	10
4	**4**	-40	5	traces	-	-	-	-	-

[a] Polymerization conditions: 10 µmol of Fe (II) complex; isoprene/Al^{i}Bu$_3$/Ph$_3$C[B(C$_6$F$_5$)$_4$]/Fe = 500/3/1/1; toluene = 5 mL; [C]$_{isoprene}$ = 1 mol/L in toluene; [b] determined by SEC analysis in THF using polystyrene standards; [c] determined by ^{1}H NMR and ^{13}C NMR; the reaction times have not been optimized.

The ternary **1–3**/Al^{i}Bu$_3$/Ph$_3$C[B(C$_6$F$_5$)$_4$] catalytic systems exhibit moderate activity at – 40 °C (TOF = 100 – 125 h^{-1}), with the obtained polymers showing dispersity ranging from narrow (for **1** and **2**) to little broad (**3**) with very high M_n values compared to the expected M_n as found previously at room temperature, again speaking presumably in favor of a rate of propagation being higher than the initiation step even at low temperature (Table 2.8, Entries 1-3). In addition, a slight increase of 1,4-selectivity, at the expense of 3,4 selectivity, was observed at – 40 °C for **1** (1,4/3,4 = 89/11) and **2** (1,4/3,4 = 88/12) complexes when compared to those at RT (Table 2.5, 1,4/3,4 = 78/22 for **1** and 1,4/3,4 = 75/25 for **2**). More interestingly, the polyisoprenes obtained from the catalytic systems based on **1–3** at – 40 °C show a unique *cis* configuration for the 1,4-stereoregularity (*trans*/*cis* = 0/89 for **1**, 0/88 for **2** and 0/90 for **3**). We can suggest that the propagation takes place *via* an *anti* (kinetic) conformer that is not prone to isomerize into the *syn* (thermodynamic) conformer under these low temperature conditions (Scheme 2.4).[49,50] These observations are similar to the results obtained with Ritter's iron iminopyridine complex bearing supermesityl substituent where the moderate 1,4-*cis* selectivity of the catalyst could be improved to 85% at – 78 °C, implying that lower temperature preferentially favors the formation of 1,4-*cis* motif.[24] Lastly, only traces of polymer were obtained from the catalyst arising from **4**, implying that the activity is drastically reduced at – 40 °C (Table 2.8, Entry 4).

ii) At higher temperature

As observed in the last section, 1,4-*cis* content could be improved up to 90% by decreasing the temperature. Likewise, we intended to run polymerizations at higher temperature to observe its influence on 1,4-*trans* selectivity for each catalytic system. Therefore, the pre-catalysts, which were poorly 1,4-*trans* selective (**1** and **2)** and moderate 1,4-*trans* selective (**3** and **4)** at room temperature, were also assessed at 60 °C. The results of the polymerization at 60 °C are displayed below (Table 2.9).

Table 2.9. Polymerization of isoprene at high temperature (60 °C) with pre-catalysts **1–4** [a]

Entry	Complex	Conv. (%)	Time (h)	TOF (h^{-1})	$M_{n(exp)}$ [b] (g/mol)	Đ [b]	Microstructure [c] (%) 1,4 (*trans/cis*)	3,4
1	**1**	>99	0.5	1 000	82 000	2.7	76 (28/48)	24
2	**2**	>99	0.5	1 000	58 000	2.8	79 (26/53)	21
3	**3**	>99	1	500	40 000	2.0	90 (70/20)	10
4	**4**	>99	1	500	35 000	1.4	95 (87/8)	5

[a] Polymerization conditions: 10 µmol of Fe (II) complex; isoprene/Al^{i}Bu$_3$/Ph$_3$C[B(C$_6$F$_5$)$_4$]/Fe = 500/3/1/1; toluene = 5 mL; [C]$_{isoprene}$ = 1 mol/L in toluene; temperature = 60 °C; reaction times have not been optimized; [b] determined by SEC analysis in THF using polystyrene standards; [c] determined by ^{1}H NMR and ^{13}C NMR.

We can see that all the catalytic systems displayed in Table 2.9 were found active at 60 °C. The catalysts originating from **1** and **2** produced polyisoprenes of high molecular weight compared to the expected M_n, possibly due to the availability of a reduced number of active species while the rest decomposes at higher temperatures or the rate of propagation is much faster than initiation (Table 2.9, Entries 1 and 2). The high M_n values and the broader dispersities indicate that the polymerization is less controlled at high temperatures for **1** and **2**, whereas for the pre-catalysts **3** and **4**, the polymerizations were comparably more controlled as the catalytic system generated M_n very near to the expected value with a narrow dispersities (Table 2.9, Entries 3 and 4). The pre-catalysts **1–3** (Table 2.9, Entries 1–3) maintained the usual selectivity observed at room temperature (Table 2.4, 1,4/3,4 = 78/22 for **1**; 1,4/3,4 = 75/25 for **2;** 1,4/3,4 = 91/9 for **3**) whereas the selectivity for 1,4 motifs was improved for **4** at 60 °C (1,4/3,4 = 95/5, Table 2.9, Entry 4). The complexes **1** and **2** were again found to be fairly 1,4-*cis* selective whereas the complex **3**

maintained its moderate 1,4-*trans* selectivity even at 60 °C (Table 2.9, Entries 1–3). But interestingly for the pre-catalyst **4**, it is noticeable that increasing the temperature favored the increment of 1,4-*trans* content up to 87% (Table 2.9, Entry 4) formed *via* thermodynamic pathway (Scheme 2.4)[49,50] which is similar to the results obtained by Wang with iminopyridine iron (II) acetylacetonate complexes where 1,4-*trans* content could be improved to 86% at 50 °C.[27] A short summary describing the selectivity of pre-catalysts **1–4** is displayed in Figure 2.9 (*vide infra*).
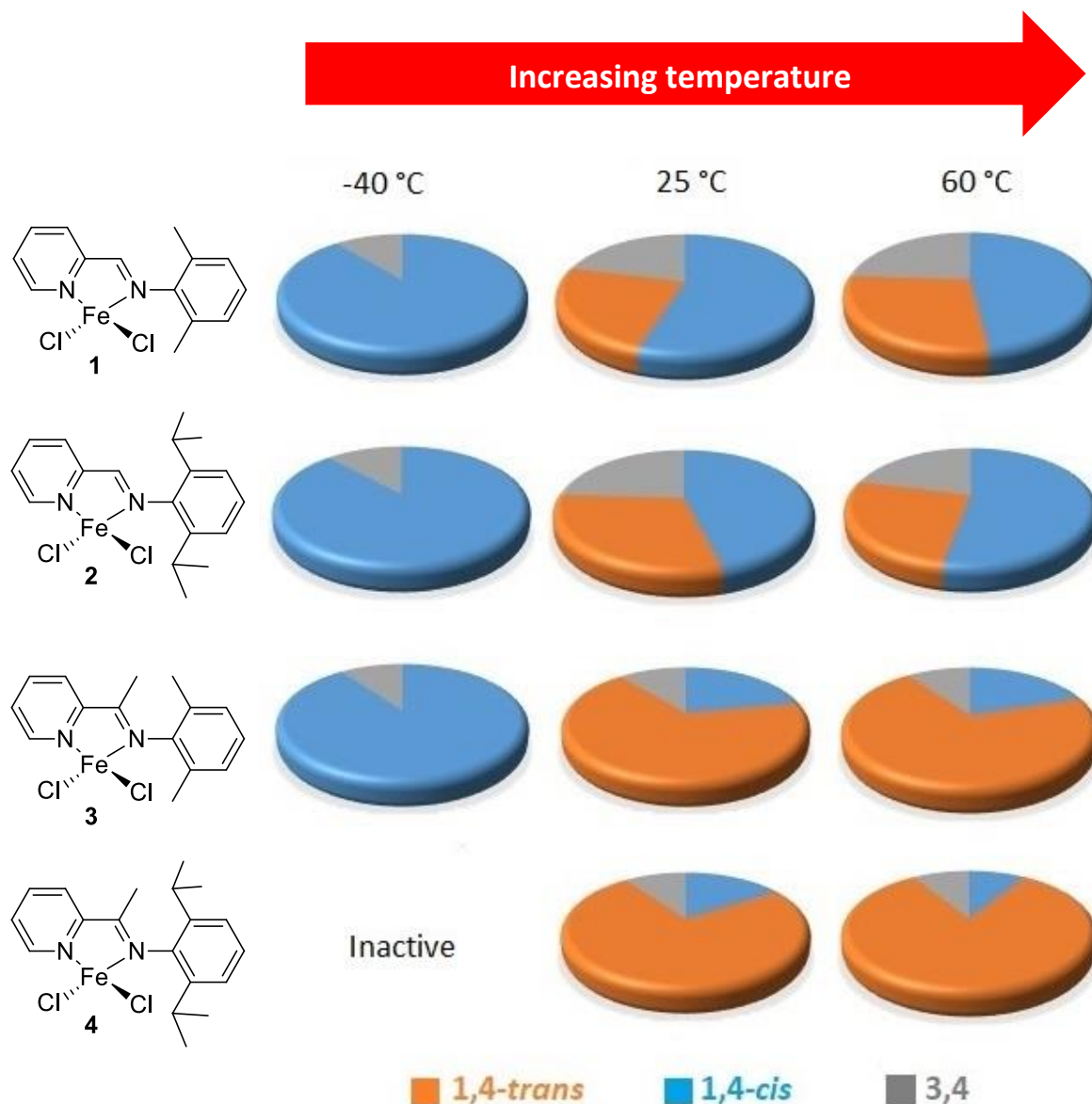
Figure 2.9. Temperature dependence on the selectivity of complexes **1–4**

2.2.3.2. Polymerization of Styrene with Iron-based Complexes 3–5

Polystyrene (PS) is a very important commodity polyolefin that constitutes 8% of the world polymer market. PS can be obtained by various pathways such as radical (which actually accounts for >99% of the production of *atactic* polystyrene), anionic, cationic and coordination-insertion polymerization. In the 1950s, the polymerization of styrene using Ziegler-Natta heterogeneous systems began to develop and was followed by the further developments of single-site" metallocene systems. At this point, coordination-insertion polymerization of styrene emerged as the method of choice and virtually so far, the only technique[51] for controlling precisely the stereoselectivity of the process and the resulting polystyrene tacticity. The coordination-insertion polymerization of styrene can result in the formation of polystyrenes possessing a variety of tacticity in their microstructure as shown below in Scheme 2.5.
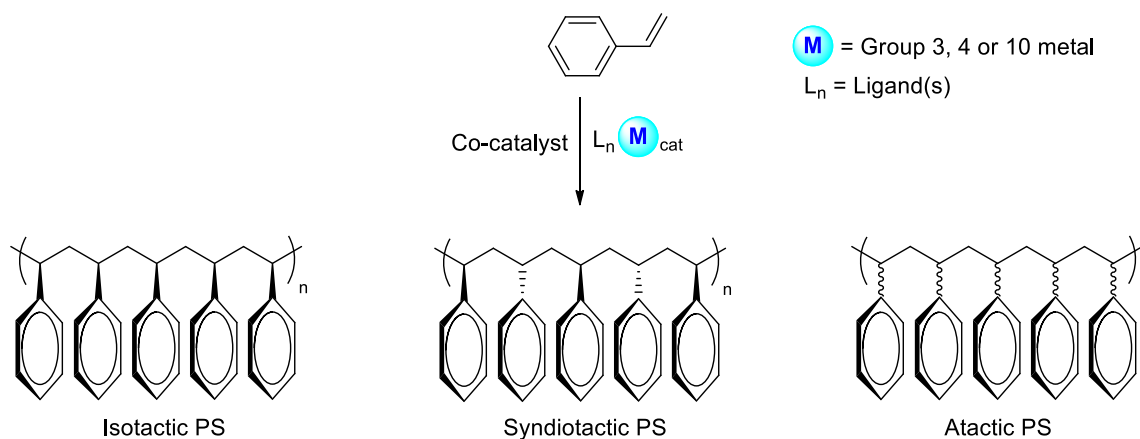
Scheme 2.5. Possible microstructures for polystyrene

The properties of the resulting polystyrenes are dependent on the tacticity they possess. For example, isotactic PS is semi-crystalline with melting temperature $T_m = 240\ °C$[52] whereas syndiotactic PS is highly crystalline with high melting temperature $T_m = 265\text{-}275\ °C$ and glass transition temperature $T_g = 100\ °C$.[53] On the other hand, atactic PS, which is the only commercially important form, is amorphous in nature ($T_g \sim 90\ °C$). Most of the systems used for the stereo-selective polymerization of styrene are based on group 3, 4 and rare-earth catalysts as well as few examples of complexes based on group 10.[16,54,55] However, to our knowledge, only two examples of coordination-insertion polymerization of styrene using iron-based catalytic systems have been described in the literature, one of which failed to promote the polymerization of styrene (Chart 2.2).[56]
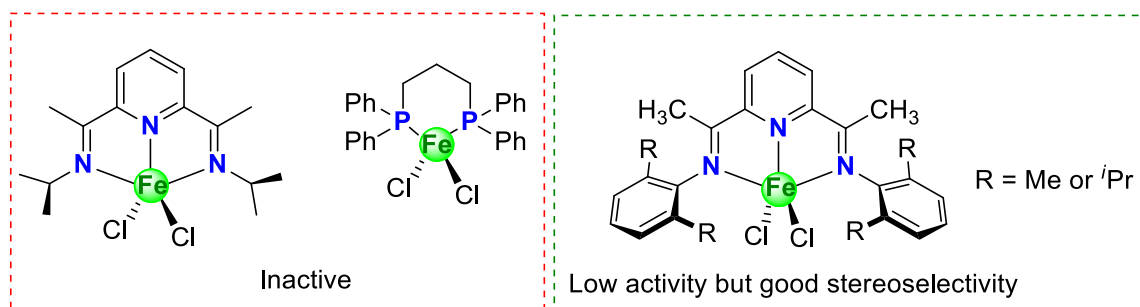
Chart 2.2. Iron-based complexes for the polymerization of styrene

In 2006, Schellenberg used the bisiminopyridine systems in the presence of 300 eqs. of MAO, to report the only active iron-based catalytic systems for the synthesis of syndiotactic polystyrenes but with very low yields (Chart 2.2, right).[57] Unexpectedly, the catalysts resulting from **1^{Me}(Cl)** and **2^{Me}(Cl)**/MAO produced low molecular weights (M_n = 26 000 – 32 000 g/mol) with broad dispersities (*Đ* = 11 – 28, trimodal distribution).

Therefore, in this context, we decided to investigate the polymerization of styrene with some of the complexes developed in this chapter. During isoprene polymerization, we observed that the ketiminopyridine complexes **3** and **4** exhibit much controlled polymerizations compared to their aldimine analogues. On the other hand, various catalytic systems derived from the precatalyst **5** were incapable to catalyze the polymerization of isoprene due to which we intended to further rationalize their activities by assessing them in the polymerization of a different monomer *i.e.* styrene. Therefore, the polymerization of styrene was assessed at room temperature using precatalysts **3–5** under different modes of co-catalyst activation.

We started with excess MAO as previous studies by Schellenberg show that the catalytic system (bisiminopyridine)FeCl$_2$/MAO is capable of producing syndiotactic polystyrenes in very low yields.[57] Apart from MAO and various cocatalysts such as triisobutylaluminium (Al^{i}Bu$_3$) or triethylaluminium (AlEt$_3$) or trimethylaluminium (AlMe$_3$) combined with trityl tetrakis(pentafluorophenyl)borate [Ph$_3$C][B(C$_6$F$_5$)$_4$], we also screened the MAO/[Ph$_3$C][B(C$_6$F$_5$)$_4$] combination as a potential co-catalyst because it is reported in the literature that the addition of a dealkylating agent to the catalytic (iminopyridine)FeCl$_2$/MAO system impacts the activity and the stereoselectivity of the resulting catalysts.[26] The different cocatalyst combinations for the polymerization of styrene were first evaluated in the presence of complex **5** to test their activities and observe whether they are different than those observed in isoprene polymerization. The

polymerization studies of styrene with various catalytic combinations generated from the precatalysts are presented below in Table 2.10.

Table 2.10. Polymerization of styrene using the pre-catalyst **5**[a]

Entry[a]	Activation	Time (h)	Yield (%)	$M_{n(exp)}$[b] (g/mol)	$Đ$[b]	Tacticity[c] (rr/mr/mm)(%)
1	MAO (500)	1	14	-	-	
2	MAO/[Ph$_3$C][B(C$_6$F$_5$)$_4$]	1	16	-	-	
3	Al(Et)$_3$/[Ph$_3$C][B(C$_6$F$_5$)$_4$]	6	<1	-	-	
4	Al(^{i}Bu)$_3$/[Ph$_3$C][B(C$_6$F$_5$)$_4$]	6	<1	-	-	
5	Al(Me)$_3$/[Ph$_3$C][B(C$_6$F$_5$)$_4$]	3	81	2 200	1.6	45/23/32
6[d]	Al(Me)$_3$/[Ph$_3$C][B(C$_6$F$_5$)$_4$]	3	87	2 100	1.7	53/25/32

[a] Polymerization conditions: 10 µmol of complex **5**; Styrene/Alkylaluminium/Ph$_3$C[B(C$_6$F$_5$)$_4$]/**5** = 500/10/1/1; toluene = 5 mL; temperature = RT; reaction times have not been optimized; [b] determined by size exclusion chromatography (SEC) analysis in THF using polystyrene standards; [c] determined by ^{13}C NMR; [d] Styrene/AlMe$_3$/Ph$_3$C[B(C$_6$F$_5$)$_4$]/**5** = 500/3/1/1

From entry 1 in Table 2.10, the activation of precatalyst **5** with 500 eqs. of MAO leads to a catalytic system that produces polystyrene in poor yields (14%), which is similar to the results obtained by Schellenberg.[57] Modifying the co-catalyst combination by adding 1 eq. of dealkylating agent [Ph$_3$C][B(C$_6$F$_5$)$_4$] with 10 eq. of MAO, again leads to a poorly efficient system for the polymerization of styrene, converting only 16% of monomer within 1 hour (Table 2.10, Entry 2). In a similar manner to the result obtained for the polymerization of isoprene (Tables 2.1–2.3, Entry 5), the catalyst resulting from complex **5** after activation with AlEt$_3$ or Al^{i}Bu$_3$/[Ph$_3$C][B(C$_6$F$_5$)$_4$] as cocatalysts, was found to be inactive for the polymerization of styrene (Table 2.10, Entries 3 and 4). From entries 1-4 in Table 2.10, one can conclude that the only active systems capable of catalyzing the polymerization of styrene comprises MAO as an activator. This result could be due to the fact that the presence of associated trimethylaluminum in certain sites of MAO might trigger its function as a co-catalyst.[58] Besides, there is a possibility that the chain propagation of styrene with respect to the active species generated from bulkier alkylating agents like AlEt$_3$ or Al^{i}Bu$_3$ is

not feasible due to steric factors.[59] We therefore went forward to assess the **5**/Al(Me)$_3$/[Ph$_3$C][B(C$_6$F$_5$)$_4$] catalytic system for styrene polymerization.

From entry 5 in Table 2.10, we can observe that the resulting catalyst is active for styrene polymerization as we achieved up to 81% of polystyrene within 3 h. To confirm that the initiation takes place *via* coordination-insertion mechanism, a polymerization was conducted only with AlMe$_3$ (3 eq.) which failed to produce polystyrene in 3 h. The resulting polystyrene was further analyzed by SEC to determine the molar mass, which turned out to display very low M_n (M_n = 2 200 g/mol) compared to the theoretical value ($M_{n(th)}$ = 42 000 g/mol), indicating the possibility of chain transfer of the growing polymer chain with the excess of AlMe$_3$ (10 eqs.). To confirm this, the amount of AlMe$_3$ was reduced from 10 to 3 eq. but, to our surprise, this again resulted in the formation of polystyrene with a similarly low M_n (Table 2.10, Entry 6). This indicates that the resulting catalyst, apart from being active for the polymerization of styrene, displays a non-living character due to the likely frequent occurrence of chain termination pathways such as possibly *β*-H elimination, leading to the formation of short chain oligomers with relatively low M_n values.

In addition, the polystyrenes were characterized by ^{1}H and ^{13}C NMR spectroscopy to determine their tacticity. The corresponding ^{1}H and ^{13}C NMR for the polystyrene in Entry 4, Table 2.10 are displayed in Figure 2.10. From the ^{1}H NMR depicted in Figure 2.10.a, one can clearly observe the typically broad signals in the region 1.70–2.27 ppm for the various triads (*rr*, *mr* and *mm*). To quantify the percentage of each triads, ^{13}C NMR was used to locate the typical broad signals of the phenyl carbon of atactic polystyrene in the 144.5–146.5 ppm region, where the signals at 145.3, 145.7 and 146.1 ppm were assigned to the syndiotactic (*rr*) triad, heterotactic (*mr*) triad and isotactic (*mm*) triad respectively.[60] The quantification of the corresponding signals in ^{13}C NMR indicates that the acquired PS from **5**/AlMe$_3$/[Ph$_3$C][B(C$_6$F$_5$)$_4$] catalytic system displays overall an atactic nature comprising mostly syndiotactic units (45%) in addition with heterotactic (23%) and isotactic (32%) units. Interestingly, by decreasing the amount of alkylating agent AlMe$_3$ from 10 to 3 eq. (Entry 5, Table 2.10), the PS obtained was comparatively more *syndio*-enriched (53%) than the one obtained in entry 4, indicating the slight effect of the co-catalyst towards the stereoregularity of the polymerization in this case, whereas the same co-catalyst had no impact on the M_n.
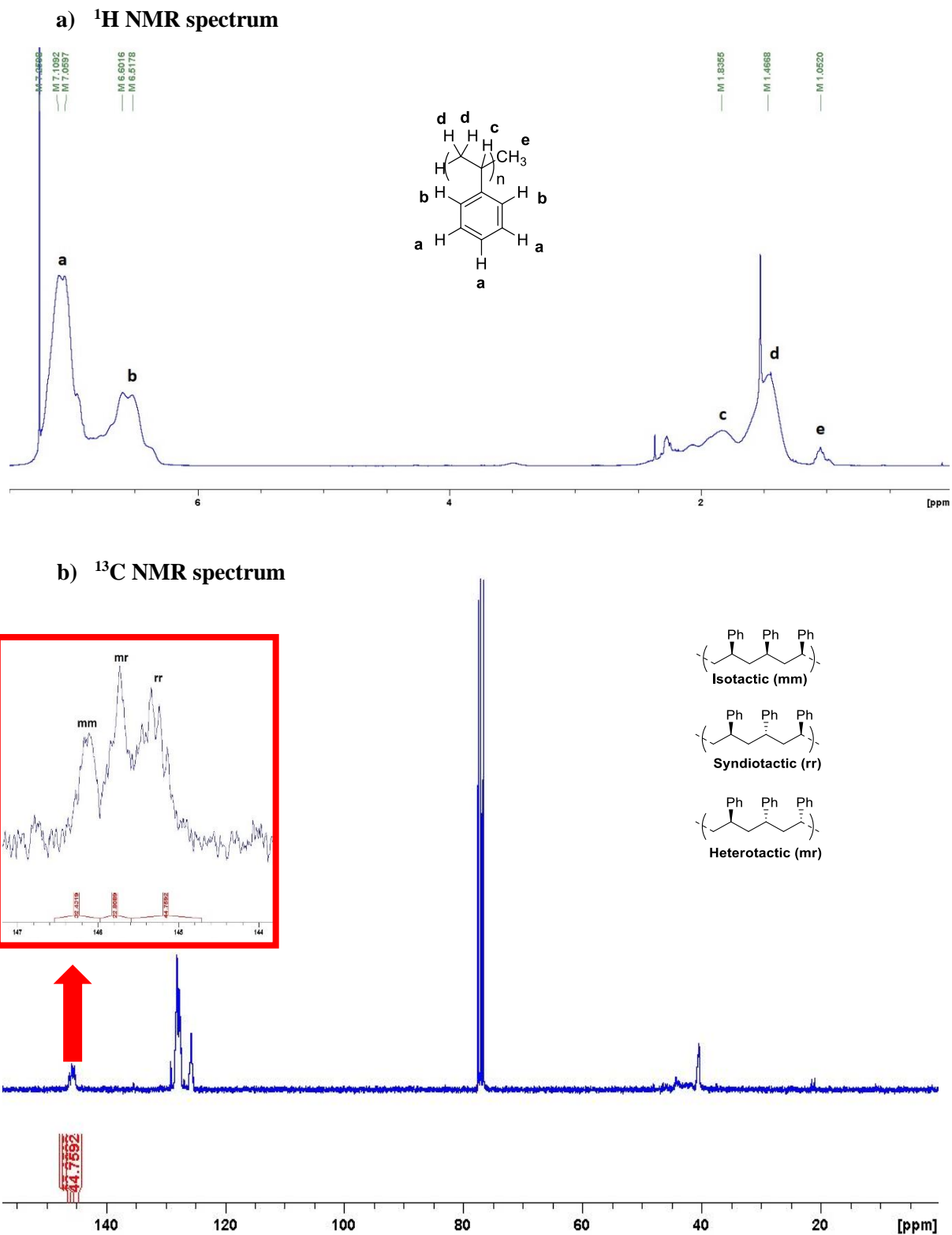
a) ¹H NMR spectrum

b) ¹³C NMR spectrum

Figure 2.10. NMR spectra (in CDCl₃) of the PS obtained from **5**/AlMe₃/[Ph₃C][B(C₆F₅)₄] (Table 2.10, Entry 4) showing the characteristic peaks (a, ¹H NMR) and tacticity (b, ¹³C NMR)

After screening various catalytic systems derived from the pre-catalyst **5,** some other complexes such as **3** and **4** were additionally employed as pre-catalysts to study their influence in styrene polymerization. The results of the polymerization of styrene using the various catalytic systems derived from the pre-catalysts **3** and **4** are presented in Table 2.11 below.

Table 2.11. Polymerization of styrene using the pre-catalysts **3** and **4**

Entry [a]	[Fe]	Activation	Time (h)	Yield (%)	$M_{n(exp)}$ [b] (g/mol)	$Đ$ [b]	Tacticity [c] (*rr/mr/mm*) (%)
1	**3**	Al(*i*Bu)$_3$/[Ph$_3$C][B(C$_6$F$_5$)$_4$]	1	65	3000	1.5	51/27/22
2		Al(Me)$_3$/[Ph$_3$C][B(C$_6$F$_5$)$_4$]	1	86	1600	2.5	40/24/36
3	**4**	Al(*i*Bu)$_3$/[Ph$_3$C][B(C$_6$F$_5$)$_4$]	24	5	-	-	-
4		Al(Me)$_3$/[Ph$_3$C][B(C$_6$F$_5$)$_4$]	6	85	2200	1.7	48/26/26

[a] Polymerization conditions: 10 µmol of Fe; styrene/alkylaluminium/Ph$_3$C[B(C$_6$F$_5$)$_4$]/Fe = 500/3/1/1; toluene = 5 mL; temperature = RT; [b]determined by SEC analysis in THF using polystyrene standards; [c]determined by ^{13}C NMR

For complex **3**, activation with Al(*i*Bu)$_3$/[Ph$_3$C][B(C$_6$F$_5$)$_4$] leads to the formation of an active catalytic system producing 65% of *syndio*-enriched PS within 1 h (Table 2.11, Entry 1), unlike the catalytic system **5**/Al(*i*Bu)$_3$/[Ph$_3$C][B(C$_6$F$_5$)$_4$] that failed to initiate the polymerization of styrene (Table 2.10, Entry 3) under the same conditions. The activity of the **3**/Al(*i*Bu)$_3$/[Ph$_3$C][B(C$_6$F$_5$)$_4$] catalytic system for styrene polymerization could be attributed to the lower steric hindrance around the iron center (see Scheme 2.3 for reminding the molecular structure of Fe complexes), resulting in easier monomer coordination. Replacing the Al(*i*Bu)$_3$ alkylating agent by AlMe$_3$ further decreased the steric hindrance around the metal center, accelerating potentially the chain initiation and consequently increasing the activity of the catalytic system which produces 86% PS within 1 h, although with similar stereo-/regioregularity (Table 2.11, Entry 2). This strong influence of co-catalyst on the activity of the resulting catalyst is already known in literature.[59] The same series of experiments were conducted with the pre-catalyst **4** bearing a bulkier ligand. The **4**/Al(*i*Bu)$_3$/[Ph$_3$C][B(C$_6$F$_5$)$_4$] catalytic system was found to be the least active, resulting in 5% yield after 24 h (Table 2.11, Entry 3), probably due to the steric hindrance around the metal center. On the other hand, the **4**/AlMe$_3$/[Ph$_3$C][B(C$_6$F$_5$)$_4$] catalytic system was comparatively more active,

producing 85% of *syndio*-enriched PS within 6 h (Table 2.11, Entry 4). Again we can clearly observe the influence of co-catalyst on the activity of polymerization which is particularly enhanced with the less bulky alkylaluminium.

Although, all the active catalytic systems gave narrower (Table 2.11, Entries 1 and 4) to broader (Table 2.11, Entry 2) dispersities, but unfortunately they could only produce short chain oligomers with very low M_n, most probably owing to the β-H elimination reactions that were supposed to be consistent throughout the experiments. Further analysis using efficient tools like MALDI-ToF-MS are needed in the future to confirm this hypothesis by identifying the chain ends of polystyrene, as the formation of vinyl chain-end produced by β-H elimination could not be found in the ^{1}H NMR spectra. Lastly, all the catalytic systems indicated in Table 2.11 were also assessed for the polymerization of styrene at higher temperature (40 °C) but, in all cases, neither the tacticity was influenced, nor did the rate of chain termination reactions, which highlights the fact that temperature has no influence at all on the reactivity of the catalytic systems with regard to styrene polymerization.

2.3 Conclusion

In this study, we observed that the activity of the catalytic system based on alkylated *N*-aryl substituted iminopyridine-iron complexes is clearly related to the electron density on iron and, to a lesser extent, to the environment of the coordination sphere at the metal center. Indeed, an increase in steric hindrance, conferred by the simultaneous presence of bulky *N*-aryl substituent as well as methyl group on the carbon of the imino group, results in a decrease of activity that could be attributed to the difficulty of the incoming monomer to coordinate with the active species. Thus, the presence of H on the carbon of the imino group in complexes **1** and **2** (aldimino series) leads to the formation of highly active catalysts, whereas the presence of a methyl group in complexes **3** and **4** (ketimino series) results in catalysts with a comparably lower activity. The influence of steric hindrance around the iron center can be easily observed in the case of catalysts resulting from **5**, which were found to be inactive for the isoprene polymerization, probably due to the inability of the incoming monomer to coordinate with the iron center. The ketiminopyridine complexes **3**/**4**, which comprise a more electron-rich metal center, were found to afford less active catalysts (Chart 2.3; TOF = 12 450 and 1 250 h^{-1}, respectively) than their homolog **1**/**2** aldiminopyridine complexes (Scheme 2.5; TOF = 26 700 and 23 400 h^{-1}, respectively). This might

be attributable to a decrease of the Lewis acidity of the iron center in **3** and **4** because of the inductive donor effect (+I) of the methyl group on the carbon of the imino substituent of the ligands **L3** and **L4**, when compared to **L1** and **L2**. Moreover, an increase of the steric hindrance around the iron metal center, for the same set of complexes with *N*-aryl group = 2,6-^{i}Pr$_2$ for **4** and **2** *vs* 2,6-Me$_2$ for **3** and **1**, resulted in a decrease of activity (in the order **4** > **3** and **2** > **1**), which could be connected to a restricted coordination of the isoprene to the metal center.
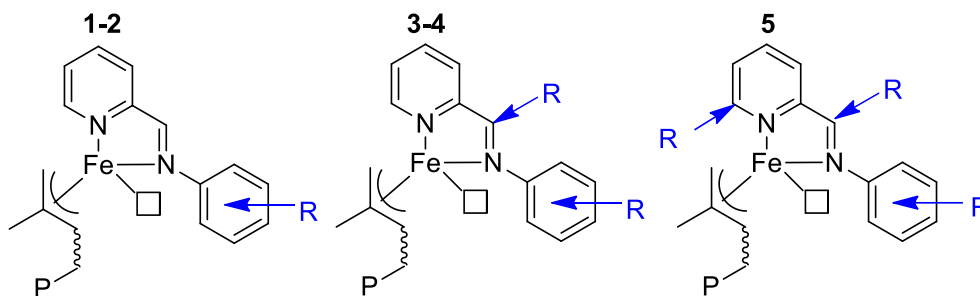
Activity	Very High	Moderate-High	Inactive
Selectivity	Fairly 1,4-*cis* (RT and High T) Highly 1,4-*cis* (low T)	Moderate to high 1,4-*trans* (RT and High T) Highly 1,4-*cis* (low T)	-

Chart 2.3. Structure-properties relationships in iminopyridine iron-based catalysts issued from **1–5**

Regarding the selectivity, the iron catalyst systems based on **1–4** are temperature dependent in terms of regio- and stereo-selectivity. The concomitant presence of a methyl group on the carbon of the imino substituent and a *N*-aryl group with alkyl substituent on the *ortho* position in **3**/**4** favor 1,4-*trans* selectivity (Figure 2.9) up to 76 % at room temperature, which could be improved to 87 % at higher temperatures. Regarding the high 1,4-*cis* rate (90 %) observed with **1–3** at low temperature, it reveals the importance of the *anti*/*syn* isomerization of the propagating species in the stereoselective iron-catalyzed 1,3-dienes polymerization (Scheme 2.4).

Some of the catalytic systems resulting from the complexes **3–5** when employed for styrene polymerization were also found to be active at room temperature. Ironically, the catalytic system **5**/AlMe$_3$/[Ph$_3$C][B(C$_6$F$_5$)$_4$] derived from the most sterically hindered complex **5** was found to be active for styrene polymerization, highlighting the role of steric hindrance imparted by the alkylating agents (Al(^{i}Bu)$_3$, AlEt$_3$) which might inhibit the monomer insertion between the Fe-R bond and consequently may lead to poor propagation as shown in Scheme 2.5
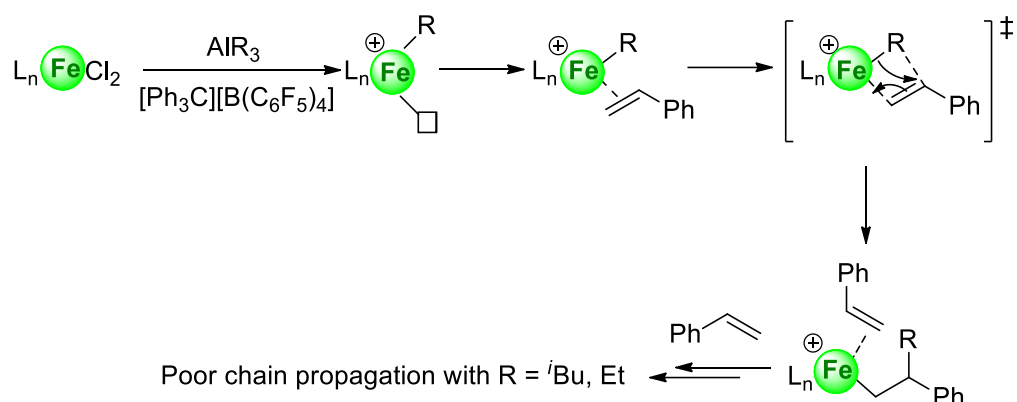
Scheme 2.5. Influence of alkylating agents on the chain propagation in styrene polymerization

The catalytic systems derived from the pre-catalysts **3–5** produced syndiotactic enriched polystyrenes with good conversions (up to 87%), albeit limiting the molecular weights to 2 100–3 000 g/mol owing to the likely occurrence of β-H elimination reactions which were consistent throughout the series of experiments (Scheme 2.6).[61] Further studies are needed in the future to optimize these catalytic systems by avoiding the chain termination pathways for their successful implementation in the controlled coordinative polymerization of styrene.
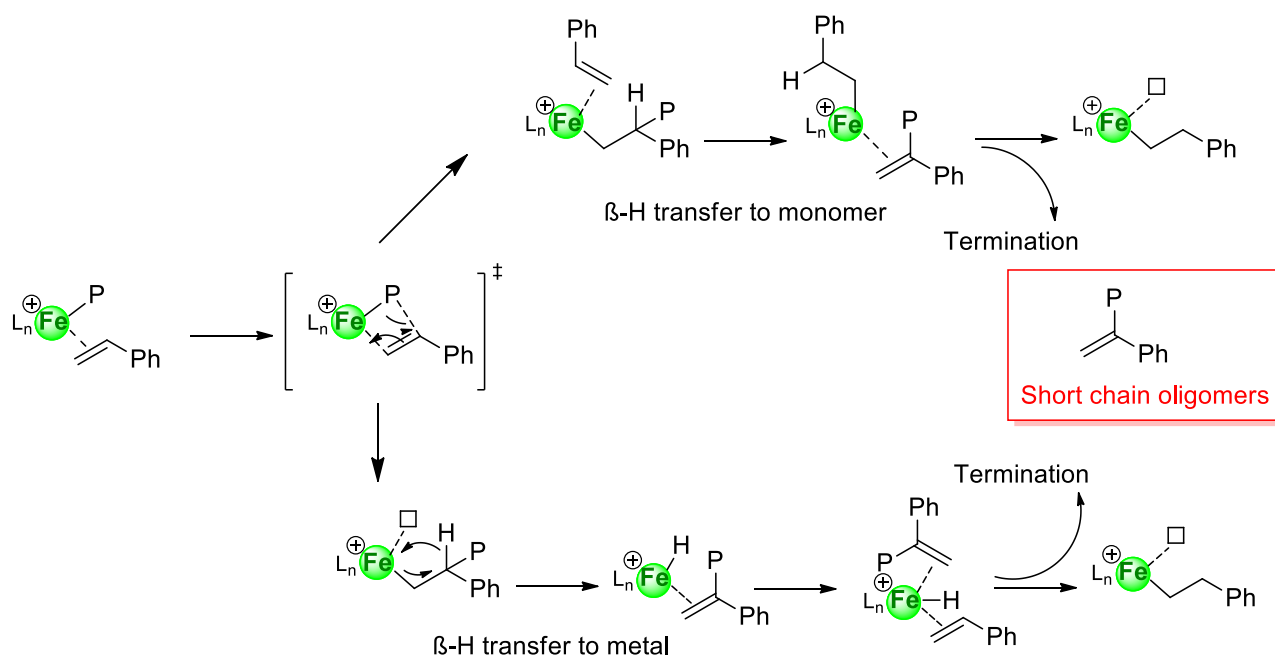
Scheme 2.6. Possible β-H elimination in styrene polymerization[61]

2.4 Experimental Section

2.4.1. General Considerations

All manipulations were performed under an inert atmosphere by using Schlenk techniques or in a dry solvent-free glovebox (Jacomex O_2<1 ppm, H_2O<1 ppm). Toluene was purified through an alumina column (Mbraun, Mérignac, France), stored, trap-to-trap distilled over sodium/benzophenone, and stored on 4 Å molecular sieves in a glove box before use. Isoprene (Sigma-Aldrich, St Quentin Fallavier, France) was dried over calcium hydride, distilled once over 4 Å molecular sieves, and stored at -20°C in a glove box before use. All the organic reagents (2-acetylpyridine, pyridine-2-carboxaldehyde, 2,6-diisopropylaniline and 2,6-dimethylaniline) were acquired from Sigma-Aldrich or Fischer Scientific S.A.S. (Illkirch, France), and used as received. Triisobutylaluminum [Al(^{i}Bu)$_3$, Sigma-Aldrich], triethylaluminum [Al(Et)$_3$, Sigma-Aldrich], trimethylaluminum [Al(Me)$_3$, Sigma-Aldrich], methylaluminoxane (MAO, 10 wt% in toluene, Sigma-Aldrich) and trityl tetrakis(pentaflurophenyl)borate {[Ph$_3$C][B(C$_6$F$_5$)$_4$]} (TCI Europe N.V., Zwijndrecht, Belgium) were stored in the glove box and used as received. ^{1}H and ^{13}C NMR spectra were recorded on a Bruker Avance 300 instrument at 300 K with at least 2000 scans and 5 sec relaxation time for ^{13}C. All ^{1}H chemical shifts (reported in [ppm]) were determined by using residual signals of the deuterated solvents. Elemental analyses and HRMS were performed by Céline Delabre on an Elementar Vario Micro Cube apparatus and SYNAPT G2-Si (Waters) equipment, respectively, at UCCS, University Lille Nord de France. In the case of polymers analyses, the conversion as well as the composition of the polymers and the microstructural magnitudes were determined as reported by means of ^{1}H and ^{13}C NMR spectroscopy by using the Topspin or MestreNova softwares. Size exclusion chromatography (SEC) analyses of the samples were performed in THF + 0.2 % toluene as an eluent at 40 °C (1 mL/min) with a SIS HPLC pump (Waters S.A.S, Saint-Quentin-en-Yvelines, France), a Waters 410 refractometer, and Waters Styragel columns (HR2, HR3, HR4, and HR5E) calibrated with polystyrene standards. The GPC profile was further retraced in MS excel with calibration equation and the data was verified. (Figure 2.11). FTIR analyses were performed on an ATR spectrometer (Shimadzu France, Marne-la-Vallée, France).
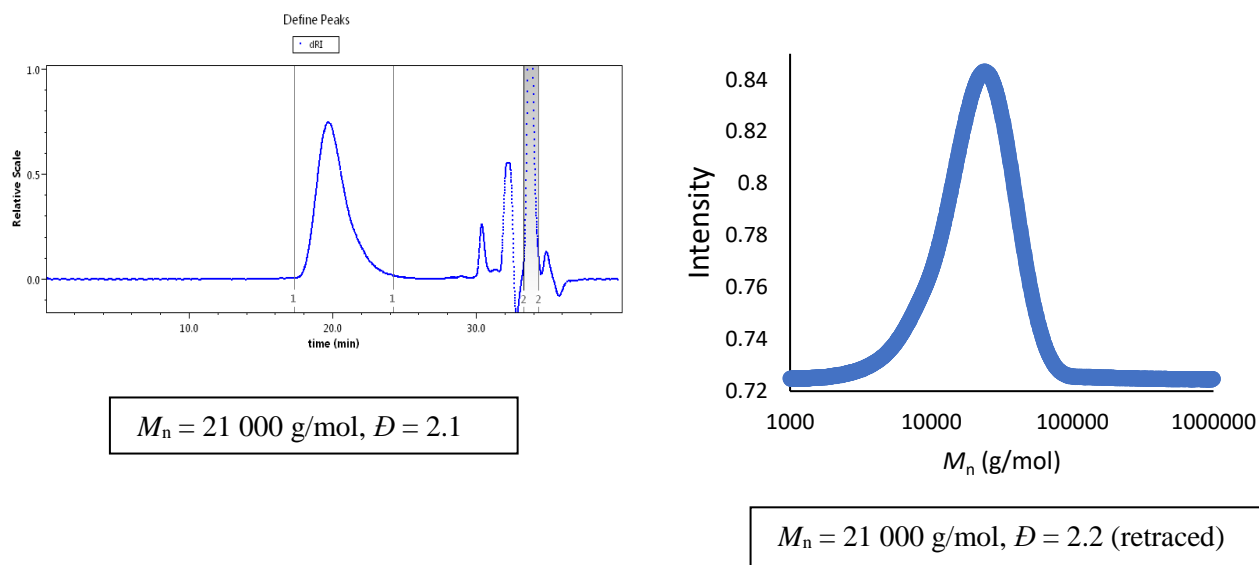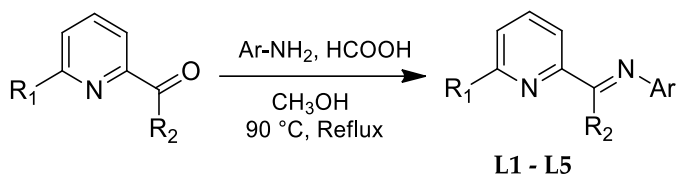
$M_n = 21\ 000$ g/mol, Đ = 2.1

$M_n = 21\ 000$ g/mol, Đ = 2.2 (retraced)

Figure 2.11. Results obtained by retracing SEC profiles of the polymer (Table 2.1, Entry 3)

2.4.2. General Procedure for the Synthesis of Ligands L1–L5

The solution of corresponding substituted aniline (8 mmol) and 2-pyridinecarboxaldehyde/2-acetyl pyridine (10 mmol) in methanol (15 mL) was prepared in a round-bottomed flask equipped with a magnetic stirrer. Catalytic amount of formic acid (3-4 drops) was added subsequently before the mixture was refluxed overnight at 90 °C (Scheme 2.7)

	L1	L2	L3	L4	L5
$R_1 =$	H	H	H	H	CH_3
$R_2 =$	H	H	CH_3	CH_3	CH_3
$R_3 =$	CH_3	$CH(CH_3)_2$	CH_3	$CH(CH_3)_2$	$CH(CH_3)_2$

Scheme 2.7. Synthetic strategy for ligands

N-(2,6-Dimethylphenyl)-1-(pyridin-2-yl)methanimine (**L1**): the reaction mixture was concentrated under reduced pressure which was further dissolved in pentane, dried over sodium sulfate and filtered. The mixture was concentrated again under reduced pressure to obtain a crude product as yellow-viscous oil which was further recrystallized in methanol at -20 °C to yield a yellow solid. Yield: 89%.^{1}H-NMR (300 MHz, CDCl$_3$, 25 °C) δ (ppm) = 8.76 (d, $^3J_{HH}$ = 4.7 Hz, 1H,H$_a$), 8.42 (s, 1H,H$_b$), 8.34 (d, $^3J_{HH}$ = 7.9 Hz, 1H, H$_c$), 7.85 (dd, $^3J_{HH}$ = 7.9, 7.9 Hz, 1H, H$_d$), 7.46–7.37 (m, 1H, H$_e$), 7.14–6.96 (m, 3H, H$_{f,g}$), 2.23 (s, 6H, H$_h$). (Figure A1). IR/cm^{-1} = 1637 ν(C=N). HRMS-ESI (m/z): [M + H]+ calcd for C$_{14}$H$_{14}$N$_2$, 211.1235; found, 211.1238. Anal. Calcd. for C$_{14}$H$_{14}$N$_2$: C 79.97, H 6.71, N 13.32; found C 79.42, H 6.63, N 13.53.The data are similar to those found in the literature.[32]

N-(2,6-Diisopropylphenyl)-1-(pyridin-2-yl)methanimine (**L2**): similar to **L1**. The crude product was recrystallized in ethanol at -20 °C to afford the product as yellow crystals. Yield: 29%. The synthesis protocol has not been optimized. ^{1}H-NMR (300 MHz, C$_6$D$_6$, 25 °C) δ (ppm) = 8.59 (s, 1H, H$_a$), 8.46 (dd, $^3J_{HH}$ = 4.8 Hz, $^4J_{HH}$ = 1.7 Hz, 1H, H$_b$), 8.27 (d, $^3J_{HH}$ = 7.9 Hz,1H, H$_c$), 7.13–7.04 (m, 3H, H$_{e,f,g}$), 6.65 (dd, $^3J_{HH}$ =7.5, 4.8 Hz, 1H, H$_d$), 3.15 (sept, $^3J_{HH}$ = 6.8 Hz, 2H, H$_h$), 1.15 (d, $^3J_{HH}$ = 6.8 Hz, 12H, H$_i$) (Figure A2). IR/cm^{-1} = 1633 ν(C=N). HRMS-ESI (m/z): [M + H]+ calcd for C$_{18}$H$_{22}$N$_2$, 267.1861; found, 267.1875. Anal. Calcd. for C$_{18}$H$_{22}$N$_2$: C 81.16, H 8.32, N 10.52; found C 80.96, H 8.41, N 10.34. The data are similar to those found in the literature.[32,34]

N-(2,6-Dimethylphenyl)-1-(pyridin-2-yl)ethan-1-imine (**L3**): similar to **L1**. The crude product obtained was purified over silica column with ethyl acetate/petroleum ether (1/10) as an eluent to yield a yellow oil. Yield: 15%.^{1}H-NMR (300 MHz, C$_6$D$_6$, 25 °C) δ (ppm) = 8.77 (ddd, $^3J_{HH}$ = 4.9 Hz, $^4J_{HH}$ = 1.7 Hz, $^5J_{HH}$ = 0.9 Hz, 1H, H$_a$), 8.48 (ddd, $^3J_{HH}$ = 7.8 Hz, $^4J_{HH}$ = 1.1 Hz, $^5J_{HH}$ = 0.9 Hz, 1H, H$_b$), 7.89 (td, $^3J_{HH}$ = 7.8, 7.8 Hz, $^4J_{HH}$ = 1.7 Hz,1H, H$_c$), 7.47 (ddd, $^3J_{HH}$ = 7.8, 4.9 Hz, $^4J_{HH}$ = 1.1 Hz, 1H, H$_d$), 7.18-7.01 (m, 3H, H$_{e,f}$), 2.29 (s, 3H, H$_g$), 2.14 (s, 6H, H$_h$). (Figure A3). IR/cm^{-1} = 1643 ν(C=N). HRMS-ESI (m/z): [M + H]+ calcd for C$_{15}$H$_{16}$N$_2$, 225.1392; found, 225.1392. The data are similar to those found in the literature.[32,33]
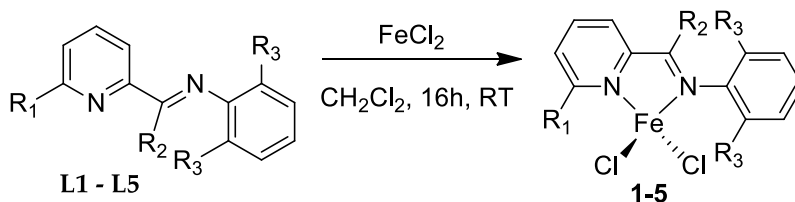
N-(2,6-Diisopropylphenyl)-1-(pyridin-2-yl)ethan-1-imine (**L4**): similar to **L1**. The crude was recrystallized in methanol at -20 °C to obtain light-yellow crystals. Yield: 46%. ^{1}H-NMR (300 MHz, CDCl$_3$, 25 °C) δ (ppm) = 8.70 (ddd, $^3J_{HH}$ = 4.8 Hz, $^4J_{HH}$ = 1.7 Hz, $^5J_{HH}$ = 0.8 Hz, 1H, H$_a$),

8.41 (d, $^3J_{HH}$ = 8.1 Hz, 1H, H$_b$), 7.85 (ddd, $^3J_{HH}$ = 8.1, 8.1 Hz, $^4J_{HH}$ = 1.7 Hz, 1H, H$_c$), 7.42 (ddd, $^3J_{HH}$ = 8.1 Hz, $^4J_{HH}$ = 4.8 Hz, $^5J_{HH}$ = 0.8 Hz, 1H, H$_d$), 7.21–7.03 (m, 3H, H$_{e,f}$), 2.74 (sept, $^3J_{HH}$ = 6.9 Hz, 2H, H$_g$), 2.24 (s, 3H, H$_h$), 1.15 (d, $^3J_{HH}$ = 6.9 Hz, 12H, H$_i$) (Figure A4). IR/cm^{-1} = 1637 ν(C=N). HRMS-ESI (m/z): [M + H]+ calcd for $C_{19}H_{24}N_2$, 281.2018; found, 281.2012. Anal. Calcd. for $C_{19}H_{24}N_2$: C 81.38, H 8.63, N 9.99; found C 81.52, H 8.85, N 9.87. The data are similar to those found in the literature.[31–33]

N-(2,6-Diisopropylphenyl)-1-(6-methylpyridin-2-yl)ethan-1-imine (**L5**): similar to **L4**. Yield = 45 %. ^{1}H NMR (300 MHz, CDCl$_3$, 25 °C) δ (ppm) = 8.17 (d, $^3J_{HH}$ = 7.8 Hz, 1H, H$_a$), 7.70 (dd, $^3J_{HH}$ = 7.8, 7.8 Hz, 1H, H$_b$), 7.25 (d, $^3J_{HH}$ = 7.8 Hz, 1H, H$_c$), 7.19-7.01 (m, 3H, H$_{d,e}$), 2.73 (sept, $^3J_{HH}$ = 6.9 Hz, 2H, H$_f$), 2.63 (s, 3H, H$_g$), 2.21 (s, 3H, H$_h$), 1.15 (d, $^3J_{HH}$ = 6.9 Hz, 12H, H$_i$) *(Figure A5)*. IR/cm^{-1} = 1637 ν(C=N). The ^{1}H NMR spectrum was consistent with the data displayed in the literature[33].

2.4.3. General Procedure for the Synthesis of Complexes C1–C5

The corresponding ligand (3.5 mmol), anhydrous FeCl$_2$ (3.5 mmol) and dry THF (32 mL) were added to a Schlenk inside the glove box (Scheme 2.8). The mixture was stirred overnight at room temperature under an argon atmosphere. The excess solvent was evaporated under reduced pressure and the product was washed with dry pentane (3 x 30 mL), further dried under high vacuum to obtain a powder from pink to purple.

	L1/1	L2/2	L3/3	L4/4	L5/5
R$_1$ =	H	H	H	H	CH$_3$
R$_2$ =	H	H	CH$_3$	CH$_3$	CH$_3$
R$_3$ =	CH$_3$	CH(CH$_3$)$_2$	CH$_3$	CH(CH$_3$)$_2$	CH(CH$_3$)$_2$

Scheme 2.8. Synthetic strategy for complexes **1-5**

[N-(2,6-dimethylphenyl)-1-(pyridin-2-yl)methanimine]FeCl$_2$ (**1**): violet powder. Yield: 61%. ^{1}H NMR (300 MHz, CD$_2$Cl$_2$, 25 °C, δ): 85.9 ($\Delta v_{1/2}$ = 183 Hz, 1H), 64.4 ($\Delta v_{1/2}$ = 1526 Hz 1H), 54.2 ($\Delta v_{1/2}$ = 62 Hz, 1H), 50.5 ($\Delta v_{1/2}$ = 77 Hz, 1H), 11.3 ($\Delta v_{1/2}$ = 228 Hz, 6H), 5.1 (1H), -13.5 ($\Delta v_{1/2}$ = 31 Hz, 2H), -17.3 ($\Delta v_{1/2}$ = 47 Hz, 1H) (Figure A6). IR/cm^{-1} = 1593 ν(C=N). Anal. Calcd. for C$_{14}$H$_{14}$Cl$_2$FeN$_2$: C 49.89, H 4.19, N 8.31; found C 48.16, H 4.03, N 7.97. The data are similar to those found in the literature.[33]

[N-(2,6-diisopropylphenyl)-1-(pyridin-2-yl)methanimine]FeCl$_2$ (**2**): violet powder. Yield: 75%. ^{1}H NMR (300 MHz, CD$_2$Cl$_2$, 25 °C, δ): 85.6 ($\Delta v_{1/2}$ = 156 Hz, 1H), 62.5 ($\Delta v_{1/2}$ = 2300 Hz, 1H), 54.8 ($\Delta v_{1/2}$ = 61 Hz, 1H), 51.1 ($\Delta v_{1/2}$ = 75 Hz, 1H), 3.8 ($\Delta v_{1/2}$ = 50 Hz, 12H), 2.2 ($\Delta v_{1/2}$ = 447 Hz, 1H), -3.1 ($\Delta v_{1/2}$ = 95 Hz, 2H), -13.0 ($\Delta v_{1/2}$ = 34 Hz, 2H), -18.0 ($\Delta v_{1/2}$ = 48 Hz, 1H) (Figure A7). IR/cm^{-1} = 1593 ν(C=N). Anal. Calcd. for C$_{18}$H$_{20}$Cl$_2$FeN$_2$: C 54.99, H 5.64, N 7.13; found C 53.05, H 5.48, N 6.91. The data are similar to those found in the literature.[41,42]

[N-(2,6-dimethylphenyl)-1-(pyridin-2-yl)ethane-1-imine]FeCl$_2$ (**3**): dark purple powder. Yield: 57%. ^{1}H NMR (300 MHz, CD$_2$Cl$_2$, 25 °C, δ): 102.7 ($\Delta v_{1/2}$ = 80 Hz, 3H), 72.6 ($\Delta v_{1/2}$ = 54 Hz, 1H), 65.5 ($\Delta v_{1/2}$ = 1089 Hz, 1H), 49.1 ($\Delta v_{1/2}$ = 61 Hz, 1H), 10.6 ($\Delta v_{1/2}$ = 194 Hz, 6H), 3.0 ($\Delta v_{1/2}$ = 28 Hz, 2H), -18.4 & -18.5 (2H) (Figure A8). IR/cm^{-1} = 1589 ν(C=N). Anal. Calcd. for C$_{15}$H$_{16}$Cl$_2$FeN$_2$: C 51.32, H 4.59, N 7.98; found C 49.84, H 4.43, N 7.76. The data are similar to those found in the literature.[33]

[N-(2,6-Diisopropylphenyl)-1-(pyridin-2-yl)ethan-1-imine]FeCl2 (**4**): purple solid. Yield: 82%. ^{1}H NMR (300 MHz, CD$_2$Cl$_2$, 25 °C, δ): 98.5 ($\Delta v_{1/2}$ = 134 Hz, 3H), 75.1 ($\Delta v_{1/2}$ = 55 Hz, 1H), 64.7 ($\Delta v_{1/2}$ = 2350 Hz, 1H), 51.0 ($\Delta v_{1/2}$ = 48 Hz, 1H), 3.1 ($\Delta v_{1/2}$ = 34 Hz, 1H), 2.4 ($\Delta v_{1/2}$ = 28 Hz, 12H), -5.6 ($\Delta v_{1/2}$ = 94 Hz, 2H), -17.8 ($\Delta v_{1/2}$ = 29 Hz, 2H), -19.3 ($\Delta v_{1/2}$ = 42 Hz, 1H) (Figure A9). IR/cm^{-1} = 1591 ν(C=N). Anal. Calcd. for C$_{19}$H$_{24}$Cl$_2$FeN$_2$: C 56.05, H 5.94, N 6.88; found C 55.32, H 5.84, N 6.74. The data are similar to those found in the literature.[33,40]

[N-(2,6-Diisopropylphenyl)-1-(6-methylpyridin-2-yl)ethan-1-imine]FeCl₂ (**5**): pink solid. Yield: 80%. ^{1}H NMR (300 MHz, CD$_2$Cl$_2$, 25 °C, δ): 99.9 (Δν$_{1/2}$ = 97 Hz, 3H), 68.5 (Δν$_{1/2}$ = 56 Hz, 1H), 62.4 (br, 1H), 56.1 (Δν$_{1/2}$ = 66 Hz, 1H), 2.9 (Δν$_{1/2}$ = 28 Hz, 1H), 2.4 (Δν$_{1/2}$ = 31 Hz, 12H), -5.9 (Δν$_{1/2}$ = 92 Hz, 2H), -16.9 (Δν$_{1/2}$ = 33 Hz, 1H), -18.6 (Δν$_{1/2}$ = 20 Hz, 1H), -34.9 (Δν$_{1/2}$ = 743 Hz, 3H) (Figure A10).IR/cm^{-1} = 1589 ν(C=N). Anal. Calcd. for C$_{20}$H$_{26}$Cl$_2$FeN$_2$: C 57.03, H 6.22, N 6.65; found C 56.32, H 5.83, N 6.05. The data are similar to those found in the literature.[33]

2.4.4. General Procedure for Isoprene Polymerization

In a typical polymerization experiment, a Schlenk reactor (20 mL) was heated, dried under vacuum and purged with argon three times before introducing it to the glove box. Iron (II) chloride complex (10 µmol, 1 eq.) and toluene (3 mL) were added to the reactor followed by the addition of the appropriate amount of aluminum co-catalyst at room temperature.

Activation with MAO (5 mmol, 500 eq.): the appropriate amount of MAO was added to the mixture under stirring for 2-3 mins and isoprene (0.346 g, 0.5 mL, 500 eq.) was introduced via a syringe. The reaction mixture was stirred for the desired time before being quenched with 5-6 drops of acidified toluene. The polymer was precipitated in ethanol (150 mL) containing the stabilizing agent BHT (*tert*-butylhydroxytoluene), isolated and dried in vacuum for at least 4 h to yield a gummy solid.

Activation with AlR₃ (100 µmol, 10 eq.)/Ph₃C[B(C₆F₅)₄] (10 µmol, 1 eq.): the reaction mixture was stirred for 2-3 mins and trityltetrakis(pentafluorophenyl)borate was added as a solution in 2 mL of toluene at room temperature. The mixture was stirred for 2 min and isoprene (0.346 g, 0.5 mL, 500 eq.) was added. The reaction mixture was stirred for the desired time before being quenched with 5-6 drops of acidified toluene. The polymer was precipitated in ethanol (150 mL) containing the stabilizing agent BHT, isolated and dried in vacuum for at least 4 h to yield a gummy solid.

For a given aliquot, the conversion was determined by ^{1}H NMR spectroscopy using the chemical shifts of the olefinic protons of polyisoprene (5.11 and 4-4.6 ppm) and isoprene (6.5-6.42 ppm). The aliquots which were taken at several intervals were quenched with isopropanol present inside the NMR tubes containing a benzene-d$_6$ capillary. The percentage conversion was calculated according to the equation:

$$[\% \ Conversion] = \frac{Area \ normalised \ for \ polymer}{Area \ normalised \ for \ polymer + Area \ normalised \ for \ monomer \ *}$$

$$= \frac{I(5.14 - 5.10 \ ppm) + \dfrac{I(4.72 - 4.67 \ ppm)}{2}}{I(5.14 - 5.10 \ ppm) + \dfrac{I(4.72 - 4.67 \ ppm)}{2} + (I \ (6.5 - 6.42 \ ppm) \ or \ I \ (5.22 - 5 \ ppm))}$$

*Can be chosen between the two olefinic regions of isoprene depending on the better resolution of peaks. (See kinetic profile section)

2.4.5 Calculation of Microstructure Contents

As previously known,[45] the characteristic signals of polyisoprene in a ^{1}H-NMR spectrum were found at 5.14-5.10 ppm and 4.72-4.67 ppm corresponding to 1,4 and 3,4 units respectively. The percentage content of 1,4 and 3,4 units was determined according to the equations:

$$[\%1,4 \ content] = \frac{I(5.14 - 5.10 \ ppm)}{I(5.14 - 5.10 \ ppm) + \dfrac{I(4.72 - 4.67 \ ppm)}{2}}$$

$$[\%3,4 \ content] = \frac{\dfrac{I(4.72 - 4.67 \ ppm)}{2}}{I(5.14 - 5.10 \ ppm) + \dfrac{I(4.72 - 4.67 \ ppm)}{2}}$$

The characteristic signals at 16.2 and 23.8 ppm in the ^{13}C NMR spectra correspond to the methyl carbon of *cis*-1,4 and *trans*-1,4 polyisoprene motifs respectively[44]. Therefore, the percentage *cis*-1,4 and *trans*-1,4 content is given by the equations:

$$[\%trans - 1,4 \ content] = \frac{I(16.2 \ ppm)}{I(16.2 \ ppm) + I \ (23.8 \ ppm)}$$

$$[\%cis - 1,4 \ content] = \frac{I(23.8 \ ppm)}{I(16.2 \ ppm) + I \ (23.8 \ ppm)}$$

References

(1)   Britovsek, G. J. P.; Gibson, V. C.; McTavish, S. J.; Solan, G. A.; White, A. J. P.; Williams, D. J.; Britovsek, G. J. P.; Kimberley, B. S.; Maddox, P. J. *Chem. Commun.* **1998**, No. 7, 849–850.

(2)   Small, B. L.; Brookhart, M.; Bennett, A. M. A. *J. Am. Chem. Soc.* **1998**, *120* (16), 4049–4050.

(3)   Burcher, B.; Breuil, P.-A. R.; Magna, L.; Olivier-Bourbigou, H. *Top. Organomet. Chem.* **2015**, *50*, 217

(4)   Li, L.; Gomes, P. T. Oligomerization and Polymerization of Olefins with Iron and Cobalt Catalysts Containing 2,6-Bis(Imino)Pyridine and Related Ligands. 121.

(5)   Coates, G. W. *Chem. Rev.* **2000**, *100* (4), 1223–1252.

(6)   Coates, G. W. *J. Chem. Soc. Dalton Trans.* **2002**, No. 4, 467–475.

(7)   Breuil, P.-A. R.; Magna, L.; Olivier-Bourbigou, H. *Catal. Lett.* **2015**, *145* (1), 173–192.

(8)   Champouret, Y.; Hashmi, O. H.; Visseaux,. *Coord. Chem. Rev.* **2019**, *390*, 127–170.

(9)   Thiele, S. K.-H.; Wilson, D. R. *J. Macromol. Sci. Part C Polym. Rev.* **2003**, *43* (4), 581–628.

(10)   Porri, L.; Giarrusso, A.; Ricci, G. *Prog. Polym. Sci.* **1991**, *16* (2–3), 405–441

(11)   Kwag, G.; Kim, P.; Han, S.; Choi, H. *Polymer* **2005**, *46* (11), 3782–3788.

(12)   Zhao, J.; Ghebremeskel, G. N. *Rubber Chem. Technol.* **2001**, *74* (3), 409–427.

(13)   Khodzhaeva, I. D.; Kislinovskaja, N. V.; Smurova, E. V. *Int. J. Polym. Mater. Polym. Biomater.* **1994**, *25* (1–2), 107–115.

(14)   Song, J.-S.; Huang, B.-C.; Yu, D.-S. *J. Appl. Polym. Sci.* **2001**, *82* (1), 81–89.

(15)   Zhang, J.; Xue, Z. *Polym. Test.* **2011**, *30* (7), 753–759.

(16)   Huang, J.; Liu, Z.; Cui, D.; Liu, X. *ChemCatChem* **2018**, *10* (1), 42–61.

(17)   Jothieswaran, J.; Fadlallah, S.; Bonnet, F.; Visseaux, M. Recent Advances in Rare Earth Complexes Bearing Allyl Ligands and Their Reactivity towards Conjugated Dienes and Styrene Polymerization. **2017**, 14.

(18)   Srivastava, V. K.; Maiti, M.; Basak, G. C.; Jasra, R. V. *J. Chem. Sci.* **2014**, *126*, 415–427.

(19)   Zhang, Z.; Cui, D.; Wang, B.; Liu, B.; Yang, Y. Polymerization of 1,3-Conjugated Dienes with Rare-Earth Metal Precursors In *Molecular Catalysis of Rare-Earth Elements*; Roesky, P. W., Ed.; Springer Berlin Heidelberg: Berlin, Heidelberg, 2010; pp 49–108.

(20)   Ricci, G.; Sommazzi, A.; Masi, F.; Ricci, M.; Boglia, A.; Leone, G. *Coord. Chem. Rev.* **2010**, 16.

(21)   Friebe, L.; Nuyken, O.; Obrecht, W. Neodymium-Based Ziegler/Natta Catalysts and Their Application in Diene Polymerization. In *Neodymium Based Ziegler Catalysts – Fundamental Chemistry*; Nuyken, O., Ed.; Advances in Polymer Science; Springer Berlin Heidelberg, 2006; Vol. 204, pp 1–154.

(22)   Egorova, K. S.; Ananikov, V. P. Toxicity of Metal Compounds: Knowledge and Myths. **2017**, 20.

(23)   Ricci, G.; Morganti, D.; Sommazzi, A.; Santi, R.; Masi, F. Polymerization of 1,3-Dienes with Iron Complexes Based Catalysts Influence of the Ligand on Catalyst Activity and Stereospecificity. **2003**, 7.

(24)   Raynaud, J.; Wu, J. Y.; Ritter, T. *Angew. Chem. Int. Ed.* **2012**, *51* (47), 11805–11808.

(25)   Guo, L.; Jing, X.; Xiong, S.; Liu, W.; Liu, Y.; Liu, Z.; Chen, C. *Polymers* **2016**, *8* (11), 389.

(26)   Zhu, G.; Zhang, X.; Zhao, M.; Wang, L.; Jing, C.; Wang, P.; Wang, X.; Wang, Q.. *Polymers* **2018**, *10* (9), 934.

(27)   Zhao, M.; Wang, L.; Mahmood, Q.; Jing, C.; Zhu, G.; Zhang, X.; Wang, X.; Wang, Q. *Appl. Organomet. Chem.* **2019**, *33* (4), e4836.

(28)   Jing, C.; Wang, L.; Zhu, G.; Hou, H.; Zhou, L.; Wang, Q. *Organometallics* **2020**, *39* (22), 4019–4026.

(29)   Li, X.; Zhang, L.; Tan, R. P.; Fazzini, P.-F.; Hungria, T.; Durand, Jø.; Lachaize, Sø.; Sun, W.-H.; Respaud, M.; Soulantica, K.; Serp, P. *Chem Eur J* **2015**, 8.

(30)   Hashmi, O. H.; Champouret, Y.; Visseaux, M. *Molecules* **2019**, *24* (17), 3024.

(31)   Laine, T. V.; Piironen, U.; Lappalainen, K.; Klinga, M.; Aitola, E.; Leskelä, M. *J. Organomet. Chem.* **2000**, *606* (2), 112–124.

(32) Bianchini, C.; Lee, H. M.; Mantovani, G.; Meli, A.; Oberhauser, W. *New J. Chem.* **2002**, *26* (4), 387–397.

(33) Cao, Y.; Zhang, Y.; Zhang, L.; Zhang, D.; Leng, X.; Huang, Z. *Org. Chem. Front.* **2014**, *1* (9), 1101–1106.

(34) Laine, T. V.; Klinga, M.; Leskelä, M. *Eur. J. Inorg. Chem.* **1999**, *1999* (6), 959–964.

(35) Zhou, Q.; Meng, W.; Yang, J.; Du, H. *Angew. Chem. Int. Ed.* **2018**, *57* (37), 12111–12115.

(36) Dai, Q.; Jia, X.; Yang, F.; Bai, C.; Hu, Y.; Zhang, X. *Polymers* **2016**, *8* (1).

(37) WO2012109343A2 - Iron complexes and methods for polymerization - Google Patents https://patents.google.com/patent/WO2012109343A2/en?oq=WO2012109343 (accessed Mar 25, 2020).

(38) Ahmed, B. M.; Rudell, N. A.; Soto, I.; Mezei, G. *J. Org. Chem.* **2017**, *82* (19), 10549–10562.

(39) Trotzki, R.; Hoffmann, M. M.; Ondruschka, B. *Green Chem.* **2008**, *10* (8), 873.

(40) Nienkemper, K.; Kotov, V. V.; Kehr, G.; Erker, G.; Fröhlich, R. *Eur. J. Inorg. Chem.* **2006**, *2006* (2), 366–379.

(41) Wu, J. Y.; Moreau, B.; Ritter, T. *J. Am. Chem. Soc.* **2009**, *131* (36), 12915–12917.

(42) Gibson, V. C.; O'Reilly, R. K.; Wass, D. F.; White, A. J. P.; Williams, D. J. *Dalton Trans.* **2003**, No. 14, 2824–2830.

(43) Busico, V.; Cipullo, R.; Cutillo, F.; Friederichs, N.; Ronca, S.; Wang, B. Improving the Performance of Methylalumoxane: A Facile and Efficient Method to Trap "Free" Trimethylaluminum. 2.

(44) Tanaka, Y.; Sato, H.; Seimiya, T. *Polym. J.* **1975**, *7* (2), 264–266.

(45) Beebe, D. H. *Polymer* **1978**, *19* (2), 231–233.

(46) Wang, B.; Bi, J.; Zhang, C.; Dai, Q.; Bai, C.; Zhang, X.; Hu, Y.; Jiang, L. *Polymer* **2013**, *54* (19), 5174–5181.

(47) Gong, D.; Jia, X.; Wang, B.; Wang, F.; Zhang, C.; Zhang, X.; Jiang, L.; Dong, W. *Inorganica Chim. Acta* **2011**, *373* (1), 47–53.

(48) Wang, X.-B.; Zhang, M.; Luo, L.; Hussain, M.; Luo, Y. *Chem. Phys. Lett.* **2020**, *755*, 137811.

(49) Tobisch, S. *J. Mol. Struct. THEOCHEM* **2006**, *771* (1), 171–179.

(50) Tobisch, S. *Can. J. Chem.* **2009**, *87* (10), 1392–1405.

(51) Maréchal, J.-M.; Carlotti, S.; Shcheglova, L.; Deffieux, A. *Polymer* **2004**, *45* (14), 4641–4646.

(52) Lemstra, P. J.; Kooistra, T.; Challa, G. *J. Polym. Sci. Part -2 Polym. Phys.* **1972**, *10* (5), 823–833.

(53) Pasztor, A. J.; Landes, B. G.; Karjala, P. J. *Thermochim. Acta* **1991**, *177*, 187–195.

(54) Schellenberg, J. *Prog. Polym. Sci.* **2009**, *34* (8), 688–718.

(55) Rodrigues, A.-S.; Kirillov, E.; Carpentier, J.-F. *Coord. Chem. Rev.* **2008**, *252* (18–20), 2115–2136.

(56) Castro, P. M.; Lankinen, M. P.; Uusitalo, A.-M.; Leskelä, M.; Repo, T. *Macromol. Symp.* **2004**, *213* (1), 199–208.

(57) Schellenberg, J. *Eur. Polym. J.* **2006**, *42* (3), 487–494.

(58) Linnolahti, M.; Collins, S. *ChemPhysChem* **2017**, *18* (23), 3369–3374.

(59) Zhang, J.; Gao, W.; Lang, X.; Wu, Q.; Zhang, L.; Mu, Y. *Dalton Trans.* **2012**, *41* (32), 9639.

(60) Ding, L.; Chu, Z.; Chen, L.; Lü, X.; Yan, B.; Song, J.; Fan, D.; Bao, F. *Inorg. Chem. Commun.* **2011**, *14* (4), 573–577.

(61) Britovsek, G. J. P.; Cohen, S. A.; Gibson, V. C.; van Meurs, M. *J Am Chem Soc* **2004**, *126*, 10701.

CHAPTER 3.

MOLECULAR STRUCTURES OF IRON(II) IMINOPYRIDINE/IMINOQUINOLINE SYSTEMS, ATTEMPTED SYNTHESIS AND REACTIVITY TOWARDS THE COORDINATIVE POLYMERIZATION OF ISOPRENE

3.1. Introduction

The pursuit of sustainable chemistry has indeed led to a rising focus on iron catalysis considering the natural abundance and relative non-toxicity of this metal, which offers a suitable alternative to other metal-based systems involved in the catalytic transformation of organic substrates. [1–7] Over the past decades, the development of well-defined single-site iron based catalysts has attracted extensive research in the coordination-insertion polymerization of ethylene more specifically,[8–11] and less attention has been paid to the conjugated dienes.[12–15] As seen earlier in the previous chapter, the materials applications of synthetic polyisoprenes make them a viable candidate for the rubber industry.[16] Within this framework, various research groups have focused their study on developing discrete iron-based complexes bearing an iminopyridine ligand for their application in coordinative polymerization of isoprene.[13–15,17,18] From these studies, the authors proposed that higher electron density at the iron center favor 1,4-*trans* selectivity of polyisoprene[13] whereas in terms of activity, it was found exactly opposite *i.e.* lower electron density on iron center increases the yield of the obtained polyisoprene.[14]

In the last chapter, we described the ability of a family of iron iminopyridine-supported complexes as precatalysts for the polymerization of isoprene, with the aim to highlight the relationships between their molecular structure and the catalytic performances.[19] When we started that study, the complexes available were limited mostly to iminopyridine having electron-donating substituents, which were found to be active when combined with $Al^iBu_3/[Ph_3C][BC_6F_5)_4]$ (Chart 3.1). There was only one example of ligands bearing electron withdrawing fluorinated substituents by Wang *et al.*, where the authors suggested that the iminopyridine complexes bearing fluorine substituents tend to enhance the catalytic activity of the resulting system, thereby, improving the yields of the obtained polyisoprenes.[15] Also, till now, there are not many studies for the polymerization of 1,3-dienes involving the catalytic systems bearing quinoline type framework except the one reported by Liu *et al.,* where the modification of iminopyridine skeleton was done by replacing the pyridine moiety with a quinoline ring and by substituting an additional chloride on the imino carbon rather than the conventional H or methyl.[20] The resulting complexes, when combined with MAO, were found to be very poorly active to catalyze the polymerization of butadiene with poor selectivities (Chart 3.1). Summarizing these studies from the literature and most importantly from our last work, we deduced that the nature of the substituents on the ligand

greatly impacted the activity and the stereoselectivity of the catalysts toward isoprene polymerization: aldiminopyridine complexes **1** and **2** bearing alkylated *N*-aryl groups were found highly active as well as stereoselective and the reaction was less controlled compared to their ketiminopyridine analogues **3** and **4,** which were found less active than aldiminopyridine complexes **1** and **2** but rather more stereoselective. Lastly, the ketiminopyridine complex **5** with an additional methyl group on the pyridine moiety proved to be inactive.

Our catalyst design was inspired by the previous studies in literature where the authors proposed that electron withdrawing substituents on the iminopyridine skeleton lead to better monomer coordination and faster chain propagation.[14] Therefore, in order to assess the impact of different substituents on the *N*-aryl moiety and also to extend the family of iron complexes, we will present our efforts to synthesize new fluorinated iminopyridine ligands and their related iron complexes (Chart 3.1) We also wish to replace the iminopyridine skeleton by iminoquinoline in order to assess the effect of extending π conjugated pyridine system on the catalytic performances of their related iron-based precatalysts and also to compare the structural features of two different skeletons. In addition, within the iminoquinoline system, we will compare the influence (if any) of a 5-membered chelate (2-substituted-quinolyl) *vs* a 6-membered chelate (8-substituted-quinolyl) on the catalytic activity of the resulting systems. This will ensure us to have a wide range of complexes available for their assessment in the coordinative polymerization of isoprene.
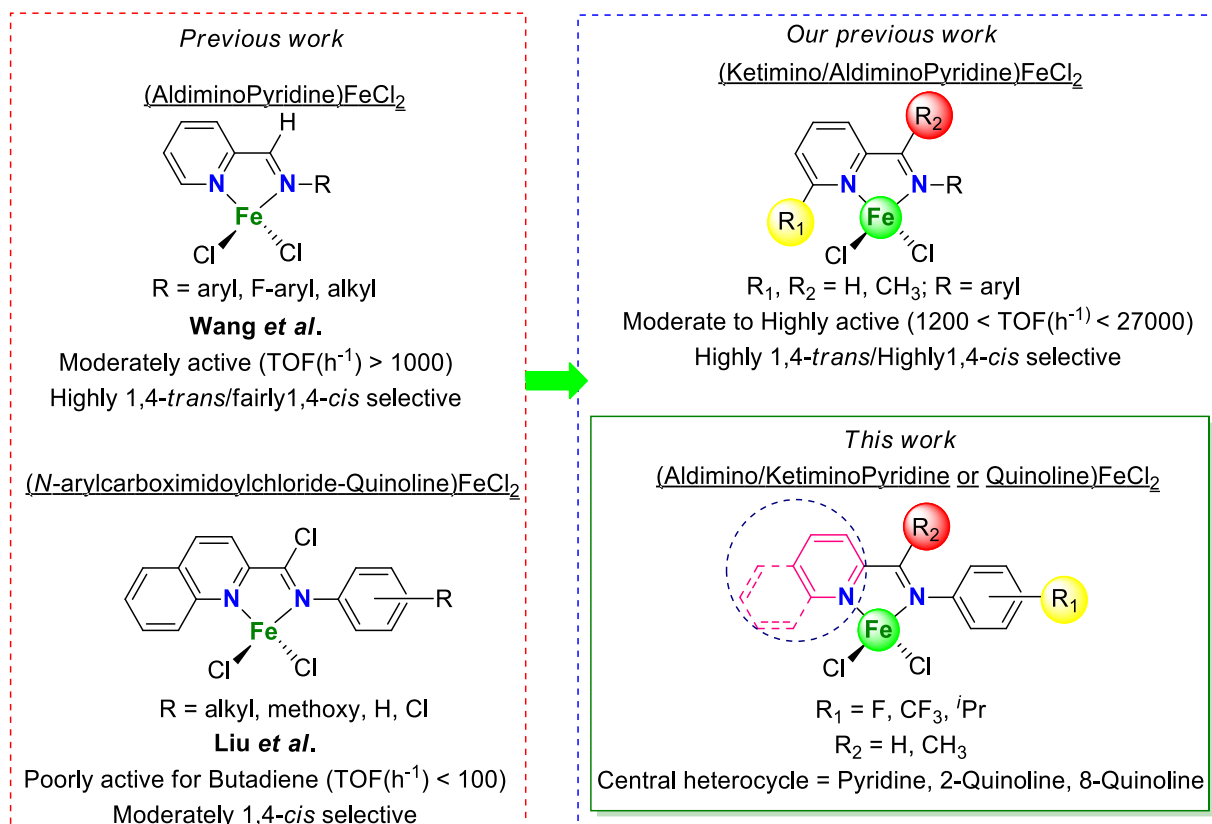
Chart 3.1. Structural evolution of [N, N] bidentate Iron-based precatalysts for the polymerization of isoprene

3.2 Results and Discussion:

3.2.1. Synthesis of iminopyridine/iminoquinoline ligands L6–L11

      The aldiminopyridine ligand **L6,** bearing two electron-withdrawing CF_3 groups on the *meta-* positions of the *N*-aryl substituent, was briefly disclosed in the patent literature, without further synthetic description/characterization**.**[21,22] To our knowledge, the aldiminopyridine **L7** ligand, containing a pentafluoro *N*-aryl substituent, has not been described but just mentioned once as potential ligand in a set of Pd and Pt complexes devoted to medical uses.[23] On the other hand, the ligand **L8** was recently reported as a starting material for its use in transfer hydrogenations with ammonia borane.[24] We therefore decided to synthesize **L6–L8** along with the new **L9–L10** to constitute a new family of ligands, possessing predominantly -CF_3 and -F electron-withdrawing groups on the *N*-aryl substituents.
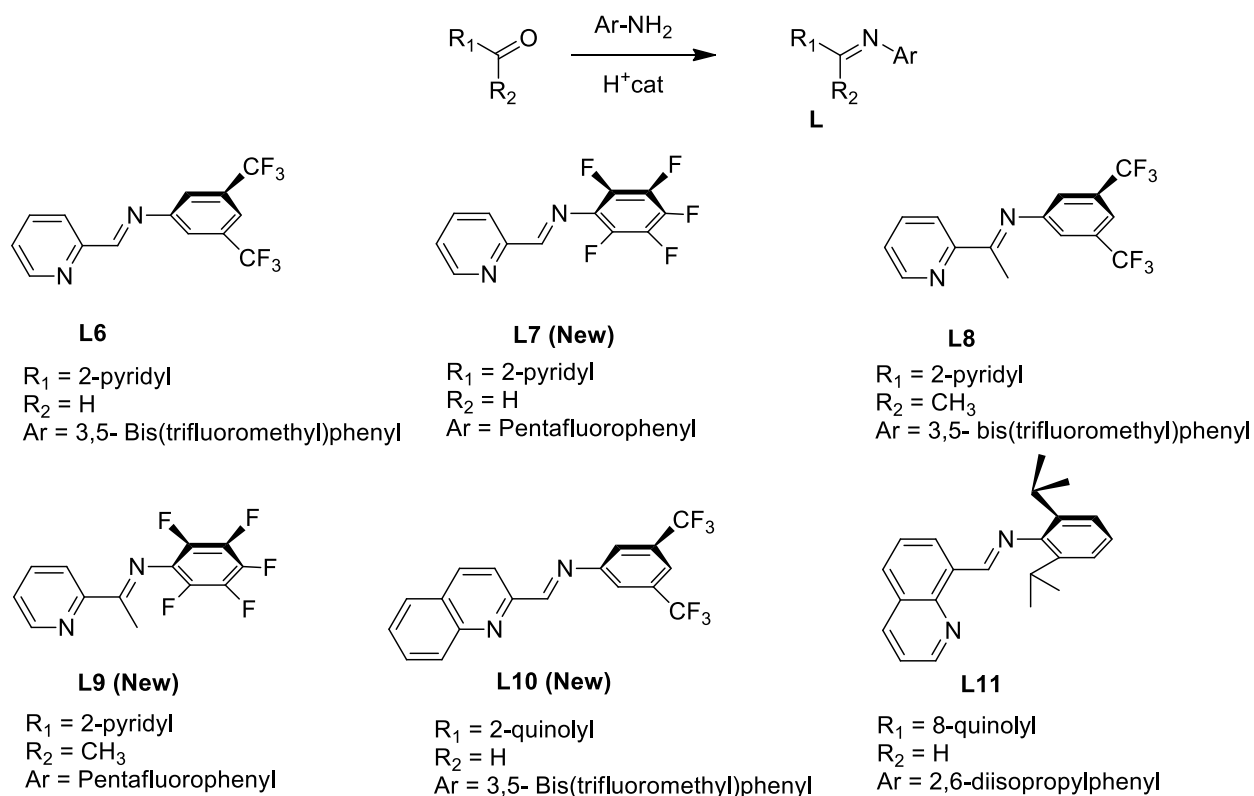
Scheme 3.1. Synthesis of the ligands **L6–L11**

      As seen earlier in chapter 2, a similar protocol (Scheme 3.1) was used to synthesize the new family of fluorinated ligands **L6–L10** and the previously known ligand **L11** comprising bulky *i*Pr groups on the *ortho* position of the *N*-aryl substituent along with a 8-quinoline skeleton instead

of pyridine.[25] The acid catalyzed condensation of the starting carbonyl pyridine/quinoline derivatives with their corresponding anilines in dichloromethane/methanol at high temperature afforded the ligands **L6–L11**. As done previously with the ligands **L1–L5,** the reactions were again monitored by ^{1}H NMR spectroscopy to determine the conversions as the formation of the final imine product is reversible and typically driven to completion by precipitation or/and removal of water. To prevent the hydrolysis of the ligand, the byproduct water was removed from the reaction mixture by adsorption on sodium sulfate or azeotropic removal through Dean-Stark apparatus.

All the ligands, which were afforded in moderate to high yields (43–94%), were further characterized by ^{1}H, ^{13}C, ^{19}F-NMR spectroscopies, HRMS spectrometry and elemental analysis (See experimental section). Apart from the difference in the reactivity of the carbonyl groups of aldehydes and ketones, which is an important factor governing the result of a condensation (as previously seen in chapter 2),[26] the nature of the substituents has also an impact on the outcome of the reaction. In this case, the experimental conditions were varied from moderate to harsh as some condensation reactions are quite difficult to perform due to the poor nucleophilic nature of anilines that bear fluorinated substituents. Indeed, the negative inductive (-I) effect arising from the fluorinated groups on the anilines leads, in some cases, to low yields as described previously in the literature.[15,27] This also indicates that the fluorinated *N*-aryl iminopyridines **L6–L10** would be more prone to hydrolyze compared to the alkylated *N*-aryl iminopyridines **L1–L5** and **L11**.[28] As we observed the hydrolysis of some of the imines due to traces of acid and/or water in the deuterated solvent CDCl$_3$, the NMR spectra were recorded in benzene-d$_6$. This time, in the case of fluorinated ligands **L6–L10**, we encountered the hydrolysis of the products even in benzene-d$_6$, which reveals the sensitivity of the fluorinated imines. Therefore, starting from the synthesis protocol, dry solvents were used for the synthesis and the NMR spectra were recorded every time in dry benzene-d$_6$.

Analyses of the IR spectra of all ligands revealed the characteristic C=N vibration band in the range of 1620 – 1649 cm^{-1}, showing the highest stretching frequency of the C=N bond bearing fluorinated *N*-aryl substituent, as expected, due to the negative inductive effect (-I) imparted by the -F or -CF$_3$ groups. The highest stretching (1649 cm^{-1}) was observed in the case of fluorinated ligands when compared to the alkyl substituted ligands (1643 cm^{-1}) in chapter 2.

Single crystals of the chelate ligands **L10** and **L11** were obtained by recrystallization from a concentrated acetonitrile and ethanol solutions containg the ligand **L10** or **L11**, respectively, which

were left to stand for 2 days at –20 °C. These crystals were further analyzed by X-ray diffraction studies to identify the structure and conformation of the ligands in the solid state. The ORTEP type view of the ligands **L10** and **L11** are shown below in Figure 3.1. Both ligands feature a close to planar central (iminoethyl)quinoline framework [Torsion angles: C9-C10-N2-C11 = 179.99(13)° for **L10**, C6-C10-N2-C11 = 179.62(13)° for **L11**] with a *transoid* conformation in which the nitrogen from the quinolyl and imino subunits are *s-trans* to each other, due to the repulsion of both nitrogen lone pairs. The C10-N2 bond length for **L10** (1.2771(19) Å) was found to be greater than observed for **L11** (1.2538(18) Å), probably due to the electron withdrawing effect of –CF$_3$ substituents on the *N*-aryl moiety. Nevertheless, they all were found in the typical C(sp^2)-N bond range. As expected, the C=N bond is *(E)*-configured *i.e.* the bulky quinolyl and 3,5-bis(trifluoromethyl)phenyl rings or 2,6-diisopropylphenyl rings favor *trans* orientation with respect to each other in the solid state. Lastly, the *N*-aryl substituent, 3,5-bis(trifluoromethyl)phenyl was inclined at 139.86(14)° [torsion C10-N2-C11-C12] with the quinoline plane whereas 2,6-diisopropylphenyl was found to be nearly orthogonal to the quinoline ring as evidenced from the torsion C10-N2-C11-C12 [100.15(17)°] angle. This observation highlights the effect of substituents on the *N*-aryl moiety, which alter the overall conformation of the ligand in solid state. The selected data for **L10** and **L11** is displayed below in Table 3.1.

Table 3.1. Selected bond distance (Å) and angles (°) for ligands **L10** and **L11**

Parameters	L10	L11
C10—N2	1.2771(19)	1.2538(18)
C9(C6)—C10—N2—C11	179.99(13)	179.62(13)
C10—N2—C11—C12	139.86(14)	100.15(17)
N1(C5)—C9(C6)—C10—CN2	176.61(14)	179.24(14)
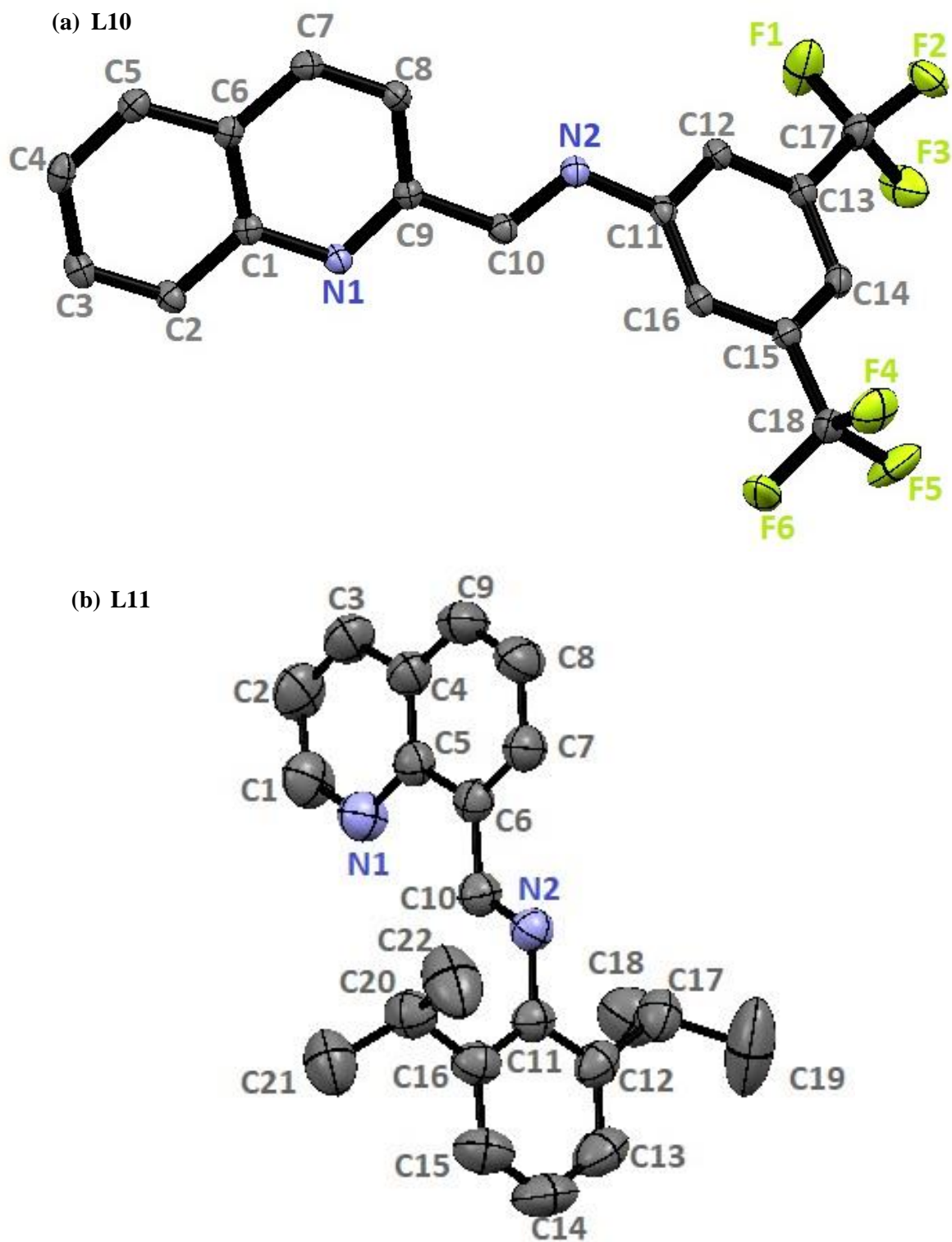
Figure 3.1. ORTEP-type view of ligands **L10 (a)** and **L11 (b)** with ellipsoids drawn at 50% probability level (hydrogen atoms have been omitted for clarity).

3.2.2. Synthesis of iminopyridine/iminoquinoline iron-based complexes 6–11

The new **6**–**11** iron complexes were synthesized in the same way as previously described for their congeners **1**-**5** in chapter two. The complexation of ligands **L6**–**L11** with one eq. of anhydrous FeCl$_2$ in THF was carried out as shown in Scheme 3.2. The obtained crude products were washed with dry pentane to remove any unreacted ligand in the solution, affording the related iminopyridine/iminoquinoline-based iron complexes **6**–**11** in moderate to excellent yields (58–93%).
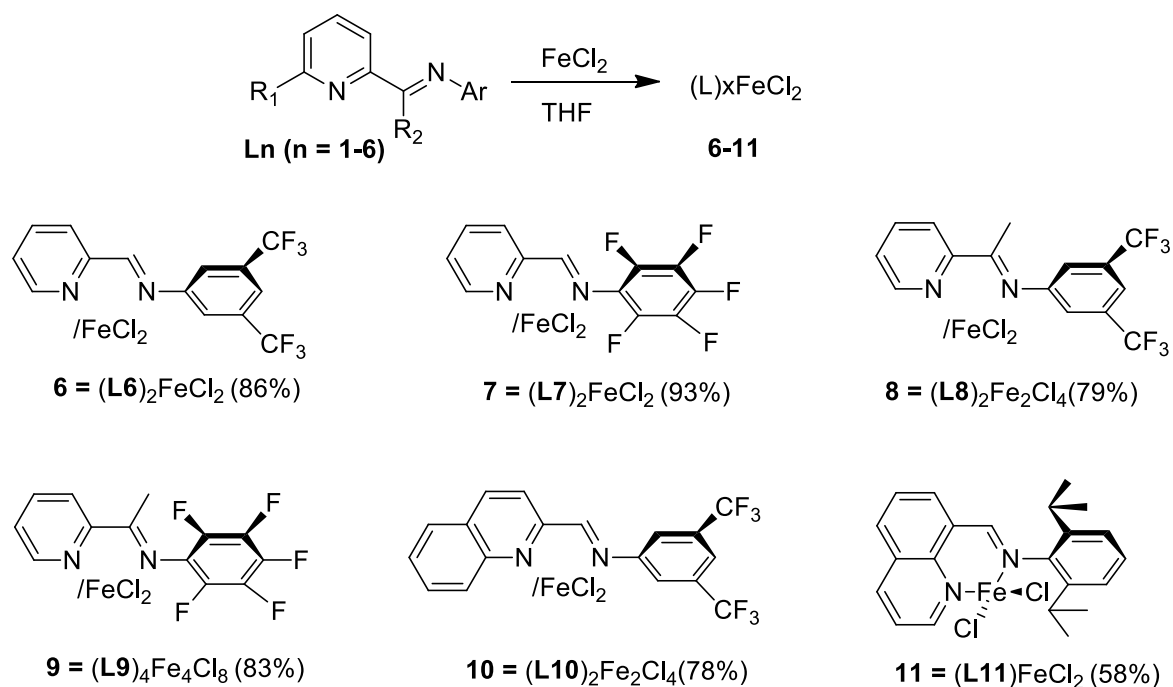
Scheme 3.2. Synthesis of iron (ii) based complexes **6–11** from their related ligands (**Ln**)

Elemental analyses were performed for the powders and were found to be in accordance with the molecular formula of the resulting iron complexes **6–11** (experimental section). The IR spectra of the resulting complexes displayed a C=N stretching frequency between 1595–1605 cm^{-1}; values lower than those identified for their related free ligand due to the coordination of the N atom of the imino group on the metal center. Furthermore, the highest wavenumber differences between ligands and complexes were predictably observed for these sets of complexes and ligands bearing electron-withdrawing fluorinated substituents (($\Delta\upsilon_{(C=N)} = 23 - 30$ cm^{-1} for **L6/6, L7/7** and **L10/10,** $\Delta\upsilon_{(C=N)} = 52$ cm^{-1} for **L8/8** and **L9/9** *vs* $\Delta\upsilon_{(C=N)} = 23$ cm^{-1} for **L11/11**), indicating, as expected, a more important decrease in electron density at the iron center for complexes **6**–**10** compared to **11**.

The newly developed series of iron complexes **6–11**, despite being paramagnetic in nature, was also characterized by ¹H NMR spectroscopy (details are given in the experimental section). For a better comparison, as previously done in chapter two, the stacked ¹H NMR spectra of the complexes are shown below in Figure 3.2. As seen earlier with the alkylated *N*-aryl iminopyridine iron complexes **1–5**, the complexes **6–11** were also sparingly soluble in CDCl₃ and benzene-D₆, so their spectra were recorded in dichloromethane-D₂.
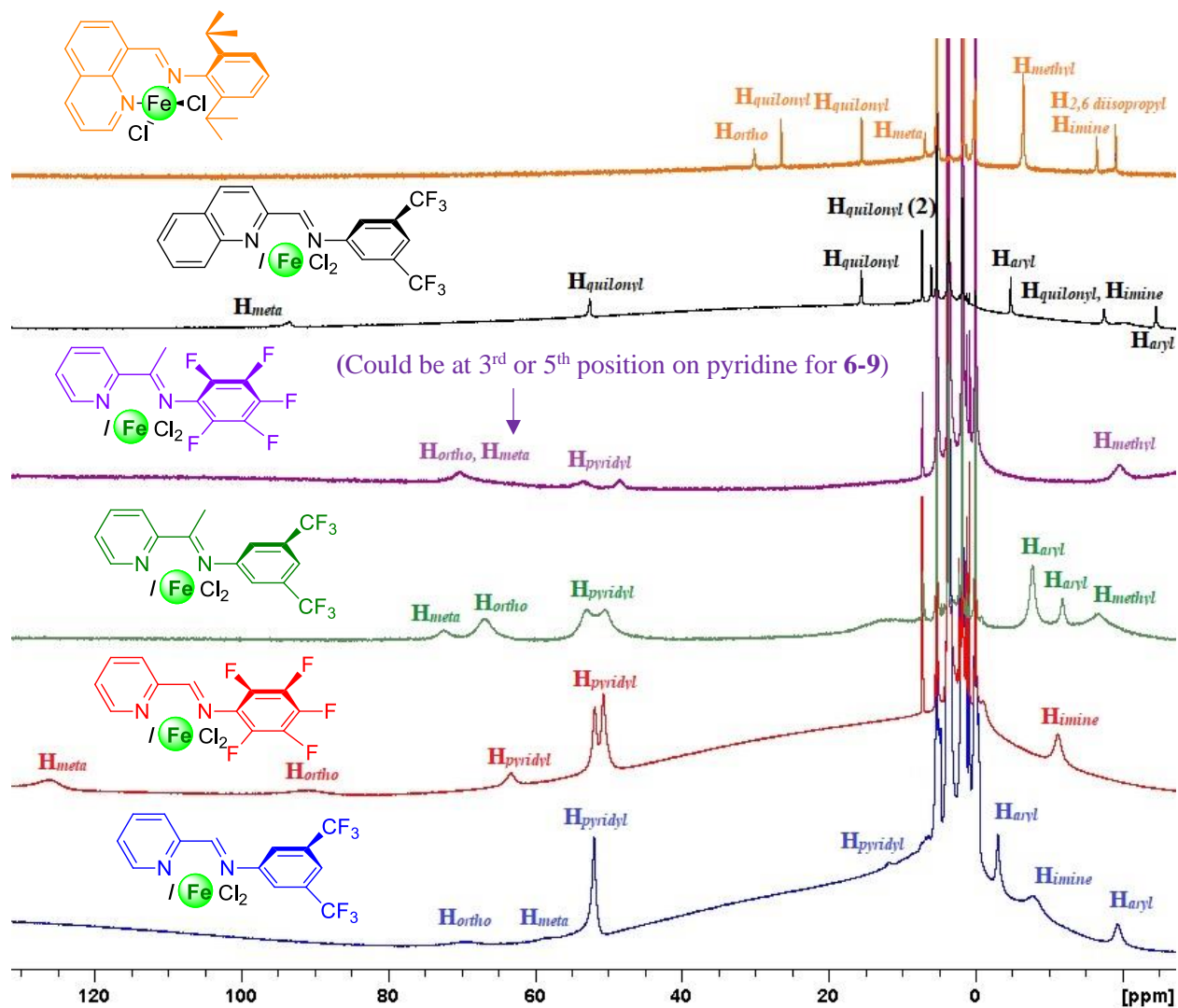
Figure 3.2. ¹H NMR spectrum of complexes **6–11** stacked (300 MHz, CD₂Cl₂, 25 °C)

The coordination of ligands to the paramagnetic iron (II) center gives rise to sharp to broad signals distributed over a wide frequency range and, for which, attempts at assignment can be made on the basis of i) integration, ii) proximity to the iron center and iii) by comparison with

similar complexes reported in the literature.[13] In some cases, not all the expected peaks were obtained due to the increased broadening of the signals resulting to the disappearance of some of them within the baseline, which has already been observed for the 2,6-bis(imino)pyridine iron chloride complex.[29] Within the complexes, the signals corresponding to each protons of the ligands are located between – 25 and + 126 ppm while the peaks of free ligands are absent in the diamagnetic region of the ^{1}H NMR spectra, implying that all ligands are coordinated to the metal center. From the stacked NMR spectra of complexes in Figure 3.2, it can be suggested that the *ortho*-pyridyl protons (H_{ortho}) of the coordinated ligand that are closest to the paramagnetic iron center, exhibit the broadest singlet downfield at δ (ppm) = 69 for **6**, 91 for **7**, 67 for **8**, 71 for **9** and 30 for **11**. Not very far from these peaks, we can see the potential singlets of *meta*-pyridyl protons (H_{meta}) downfield at δ (ppm) = 58 for **6**, 120 for **7**, 73 for **8**, 71 for **9** (very broad signal integrates for 2), 93 for **10** and 26 for **11**. The broad singlet found upfield at δ = – 7.8 ppm in the spectrum of **6** could be attributed to the imino hydrogen (H_{imine}), which can be further confirmed by the presence of similar signals arising in the spectra of similar complexes nearly in the same range (H_{imine} for **7** at – 11.7 ppm, for **10** at – 20.7 ppm and for **11** at – 16.4 ppm). In a similar way, the hydrogens of the backbone methyl group (H_{methyl}) present on the imino carbon could be attributed to broad singlets found at δ = – 16 ppm for **8** and – 19 ppm for **9**. The remaining pyridyl/quinolyl protons ($H_{pyridyl}$ or $H_{quinolyl}$) were found mostly downfield in the range of 11.8 – 53 ppm whereas the protons of the *N*-aryl group were found upfield between – 3 and – 24 ppm. Lastly for complex **11**, the sharp singlets at – 1.7 ppm and – 6.4 ppm would correspond to the diastereotopic methyl protons of the 2,6-diisopropryl group whereas the singlet at – 19 ppm could be attributed to – C*H*(Me)$_2$.

Overall, it can be observed that the presence of various electron donating and electron withdrawing groups within the family of ligands **L1** – **L11** clearly influenced the ^{1}H NMR spectra of the resulting complexes **1** – **11**. For instance, complexes **6–10**, bearing electron withdrawing CF$_3$ or F groups on the *N*-aryl substituent, present a higher number of broad singlets, whose chemical shifts are not easily identified, when compared to complexes **1–5** and **11** comprising electron donating CH$_3$ or ^{i}P$_r$ groups on the *N*-aryl moiety. As an example, the clear assignment of the characteristic resonances of complex **9** is shown below in Figure 3.3 whereas for the other complexes, it could be found in the experimental section.
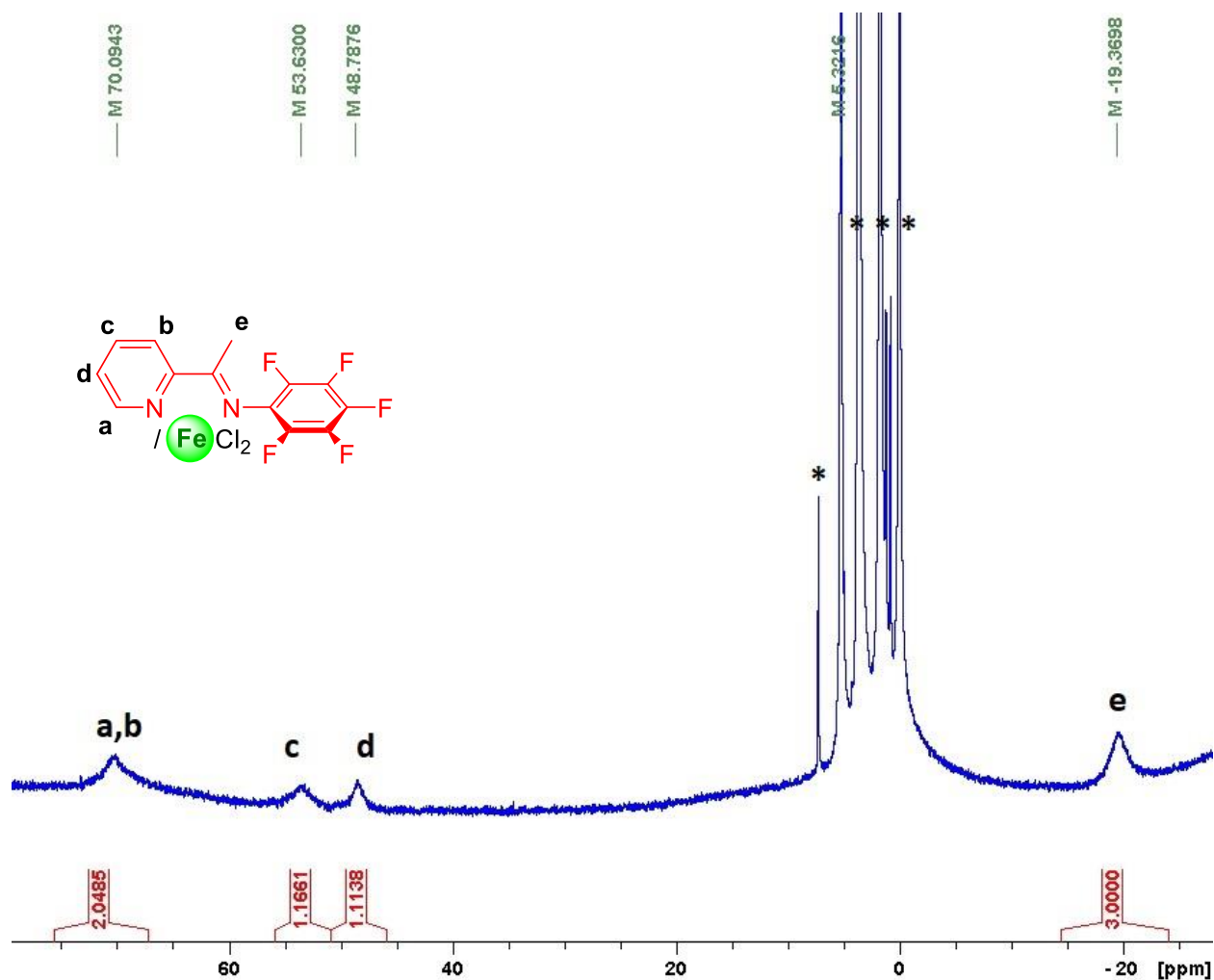
Figure 3.3. ^{1}H NMR spectrum of complex **9** (300 MHz, CD$_2$Cl$_2$, 25 °C) *Chloroform, THF and silicon grease

Apart from the minute traces of chloroform and silicon grease, the characteristic signals of protons of THF were also observed in the spectrum, resulting from the synthesis protocol. This was also confirmed through the elemental analysis of complex **9** (Found: C 42.10, H 3.12, N 5.78 for powder), which required one additional molecule of THF to obtain results corresponding to the molecular formula of the complex (calculated for C$_{13}$H$_7$N$_2$F$_5$FeCl$_2$ + one molecule of THF (C$_4$H$_8$O): C 42.09, H 3.06, N 5.72).

The newly developed series of iron complexes **6–11** was additionally characterized by X-ray diffraction studies. Single crystals of complexes **7–10** were obtained by recrystallization from a concentrated acetonitrile solution (along with the few drops of dichloromethane in some cases) of the respective complexes layered with diethyl ether (1/2) and left to stand for several days at –

20 °C under inert atmosphere. In contrast, after multiple attempts, single crystals of complex **6** were ultimately obtained by recrystallization from a concentrated acetonitrile/dichloromethane solution (5/1), which was left to stand at –20 °C inside the glove box for almost a month.

The molecular structure of complex **6'** is depicted in Figure 3.4a, selected bond lengths and angles are reported in Table 3.2.
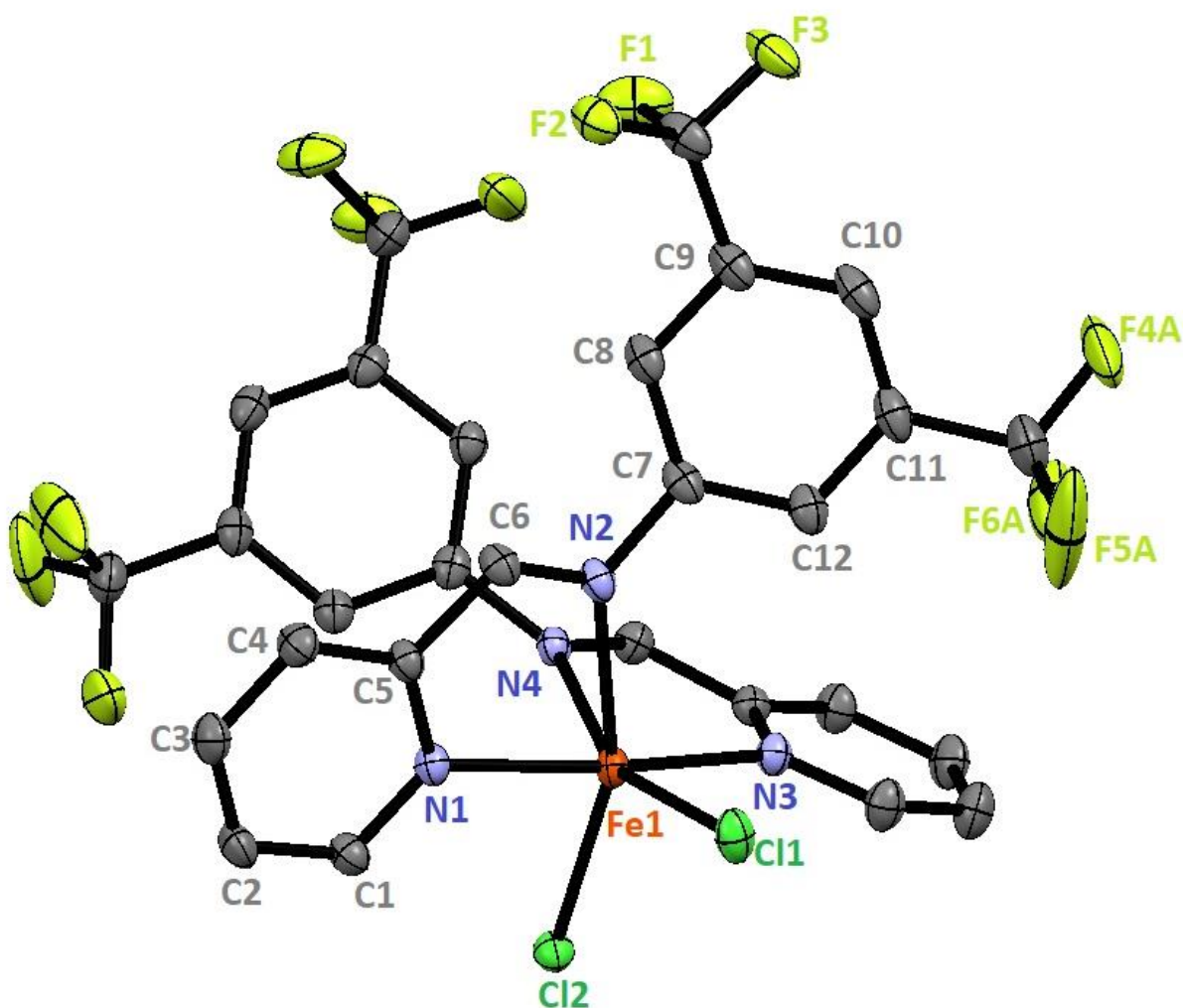
Figure 3.4a. ORTEP-type view of complex **6'** with ellipsoids drawn at 50% probability level (hydrogen atoms, secondary positions of F atoms and solvent molecules have been omitted for clarity and only specific atoms have been labelled)

From the ORTEP diagram, the geometry at the iron centre in complex **6'** can be best described as a distorted octahedron where the metal is surrounded by two bidentate iminopyridine ligands (**L6**), which act as bis-chelate with both N_{imine} and $N_{pyridine}$ atoms coordinated to the metal,

as well as two terminal chloride atoms (Cl1 and Cl2). The axial coordination sites are occupied by the Cl2 and the N2 imine nitrogen atoms (the axial sites are defined by taking the atom with the longest bonding distance to the iron centre and the atom in *trans* position), which subtends an angle of N2–Fe1–Cl2 = 160.03(5)° at the metal centre, deviating substantially from the expected linearity. The molecular formula of the bis-chelate structure **6'** was also confirmed through the elemental analysis (Found C 41.81, H 2.45, N 9.43) where the addition of one molecule of dichloromethane (used in crystallization) was essential to obtain the proper result (Calculated. for crystal $C_{32}H_{22}Cl_2F_{12}FeN_6$ + one molecule of CH_2Cl_2: C 42.61.50, H 2.60, N 9.03)

Regarding the arrangement of the two iminopyridine ligands in the neutral complex **6'**, the nitrogen atoms of the pyridine fragments are in *trans* position to each other while both *N* atoms of the imine moieties are oriented in *cis* position to one another, as the two chloride atoms. Similar coordination modes of related bidentate iminopyridine ligands with iron dichloride, such as 2,4,6-trifluoro-*N*-[(pyridine-2-yl)methylene]aniline,[15] *N*-[(pyridine-2-yl)methylene]aniline[30] and 3-nitro-*N*-[(pyridine-2-yl)methylene]aniline,[31] have been previously described in the literature. These analogous coordination patterns are likely due to the low steric hindrance of these ligand sets compared to complexes supported by more congested ligands such as *e.g.* 2,6-diisopropyl-*N*-[(pyridine-2-yl)methylene]aniline, where a centrosymmetric neutral dimeric complex of the type [2,6-diisopropyl-*N*-[(pyridine-2-yl)methylene]aniline]$_2$Fe$_2$Cl$_4$[32] or a penta-coordinated ionic species of the type {[2,6-diisopropyl-*N*-[(pyridine-2-yl)methylene]aniline]$_2$FeCl}$^+$FeCl$_4^{-}$[30] were formed. The distances between the two Fe–Cl bonds are inequivalent in complex **6'** [Fe1–Cl1: 2.3696(6) Å *vs* Fe1–Cl2: 2.4284(6) Å] and the Fe-N$_{imine}$ bond lengths [2.2727(19) – 2.2862(19) Å] are longer than the Fe-N$_{pyridine}$ bond ones [2.2217(19) – 2.2209(2) Å], all these bond distances being in the same range as those observed in the parent complexes [Fe-Cl: 2.33 – 2.44 Å; Fe-N$_{imine}$: 2.23 – 2.32 Å and Fe-N$_{pyridine}$: 2.15 – 2.22 Å].[15,30,31] The complex **6'** also features similar N1-Fe1-N2 bond angle of 73.69(7)°, N3-Fe1-N4 bond angle of 73.66(7)° and slightly larger Cl1-Fe1-Cl2 bond angle of 105.59(2)° than the ones observed in Wang's complex [N1-Fe1-N2 = 72.68(17)°, N3-Fe1-N4 = 72.58(17)° and Cl1-Fe1-Cl2 = 98.24(17)°], implying a more open space at the iron atom, which can overshadow an interesting reactivity in polymerization. In addition, it is noteworthy that the *N*-aryl substituents deviate significantly from the expected orthogonality relative to the imino group as evident from the torsion angles C6-N2-C7-C12 [146.8(2)°] and C20-N4-C21-C26 [136.1(3)°], which is probably attributable to the presence of CF$_3$ groups on the *meta*

position of the *N*-aryl substituent of the iminopyridine bis-chelate. From the crystal packing view depicted in Figure 3.4b, which contains an assembly of four complexes **6'**, the two pyridine rings are almost orthogonal to one another while the two *N*-aryl cycles are nearly parallel to each other in each complex. As described by Vener and coworkers,[33,34] the orientation of each complex within the crystal packing could potentially be due to the presence of weak non-bonding F···F contacts of 2.904(4) Å, which is slightly inferior than the sum of their van der Waals radii (*ca* 2.94 Å) along with the presence of weak H···F interactions of *ca* 2.46 Å (H...F interactions are considered for non-bonding distances less than *ca* 2.67 Å,[33] which represents the sum of their van der Waals radii[34] and taking into account that normalization of the C-H bond can lead to deviations of *ca* 0.15 Å). These observations could explain the coordination mode of **L6** with FeCl$_2$.
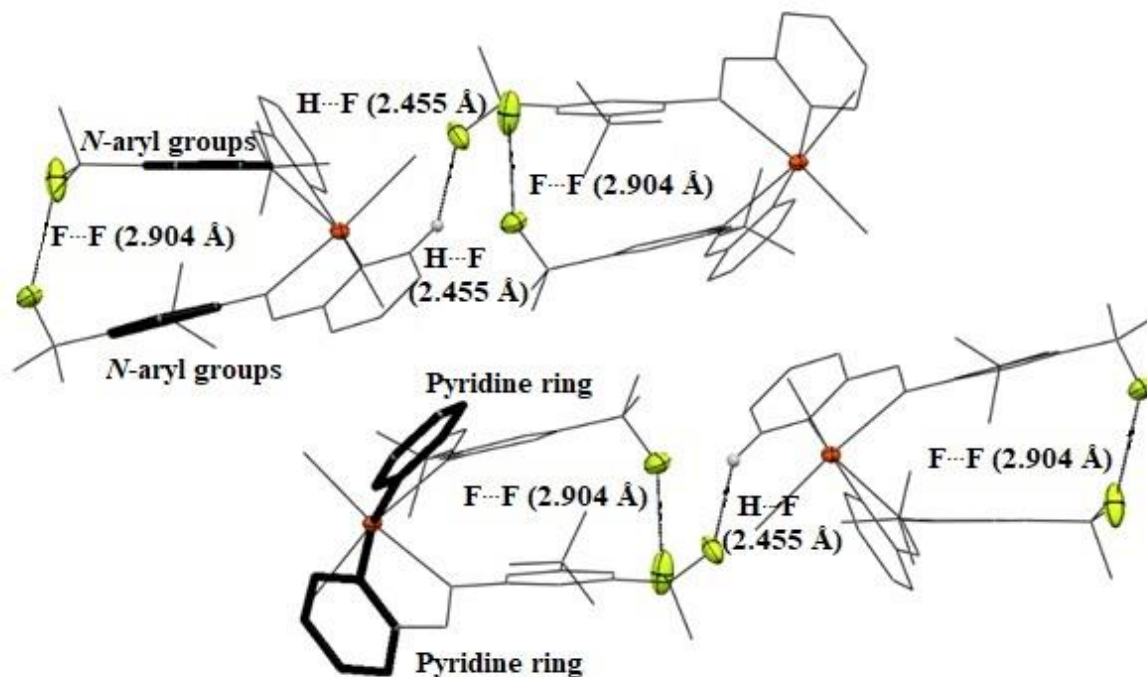
Figure 3.4b. Crystal packing of complex **6'** highlighting the pseudo-orthogonality of the two pyridine rings (in bold) and the nearly parallel orientation of the two *N*-aryl groups (in bold) with the weak non-bonding F···F (2.904 Å) and H···F (2.455 Å) contacts.

The aldiminopyridine complex **7** crystallizes in a similar fashion to complex **6** and adopts a comparable distorted octahedral geometry at the Fe center, with two **L7** iminopyridine chelates and two chloride ligands. The ORTEP type view of complex **7'** is shown below in Figure 3.5a, selected bond lengths and angles are depicted in Table 3.2. The Cl1 and the imine nitrogen N4

atoms occupy the axial coordination sites and form a marginally more open angle N4–Fe2–Cl1 of 162.53(3)° at the metal center than that observed in complex **6'**. Both iminopyridine ligands and the two chlorine atoms are similarly positioned around the metal center as in complex **6'**. The Fe-Cl bond distances [Fe1–Cl1: 2.4358(4) Å and Fe1–Cl2: 2.3430(4) Å] are even less equivalent than those found in complex **6'**, but still within the length range of related complexes [Fe-Cl: 2.33 – 2.44 Å].[15,30,31] In contrast to complex **6'**, the Fe–N$_{imine}$ bond distances are quite different [Fe1–N2: 2.2375(12) Å *vs* Fe1–N4: 2.3202(12) Å] and fall at the two extremes of the range reported in the literature [Fe-N$_{imine}$: 2.23 – 2.32 Å], the longest Fe1-N4 being in *trans* position to the longest Fe-Cl1 as both axial bonds (Fe-Cl1 and Fe1-N4) are elongated compared to their equatorial counterparts.
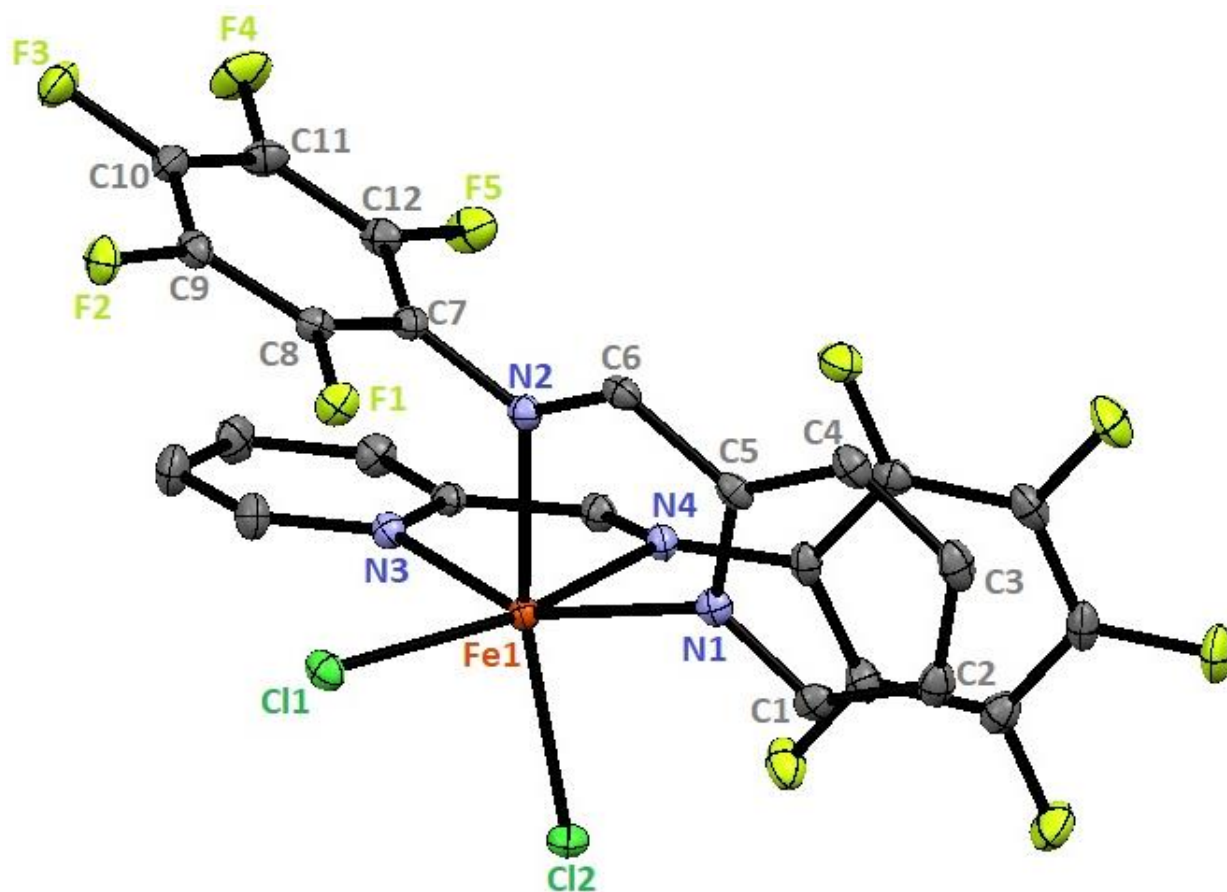
Figure 3.5a. ORTEP-type view of complex **7'** with ellipsoids drawn at 50% probability level (hydrogen atoms have been omitted for clarity and only specific atoms have been labelled)

Although, the Fe–N$_{pyridine}$ bond lengths [Fe1–N1: 2.2202(12) Å and Fe1–N3: 2.2295(12) Å] were found to be *quasi*-identical to those observed for the congener **6'** [Fe–N$_{pyridine}$: 2.2209(2)

– 2.2217(19) Å] and lie in the upper range of the parent complexes [Fe-N$_{pyridine}$: 2.15 – 2.22 Å],[15,30,31]. The order of Fe–N$_{pyridine}$ distances can be summarized as : 2,3,4,5,6-pentafluoro-*N*-aryl ≈ 3,5-trifluoromethyl-*N*-aryl (2.2295 - 2.2202 Å) > 2,4,6-trifluoro-*N*-aryl (2.215 - 2.204 Å)[15] > 3-nitro-*N*-aryl (2.20 - 2.19 Å)[31] > N-aryl (2.15 Å)[30] which can be potentially due to the comparatively increased (-I) inductive effect (2,3,4,5,6-F ≈ 3,5-CF$_3$ *vs* 2,4,6-F *vs* 3-NO$_2$) reducing the electron donating capability of N$_{pyridine}$ atoms, thereby increasing the Fe–N$_{pyridine}$ bond lengths. The *N*-aryl substituent is closer to the orthogonality to the imino group as evidenced from the torsion angles C6-N2-C7-C12 [115.60(16)°] and C18-N4-C19-C24 [116.83(16)°] when compared to complex **6'**.
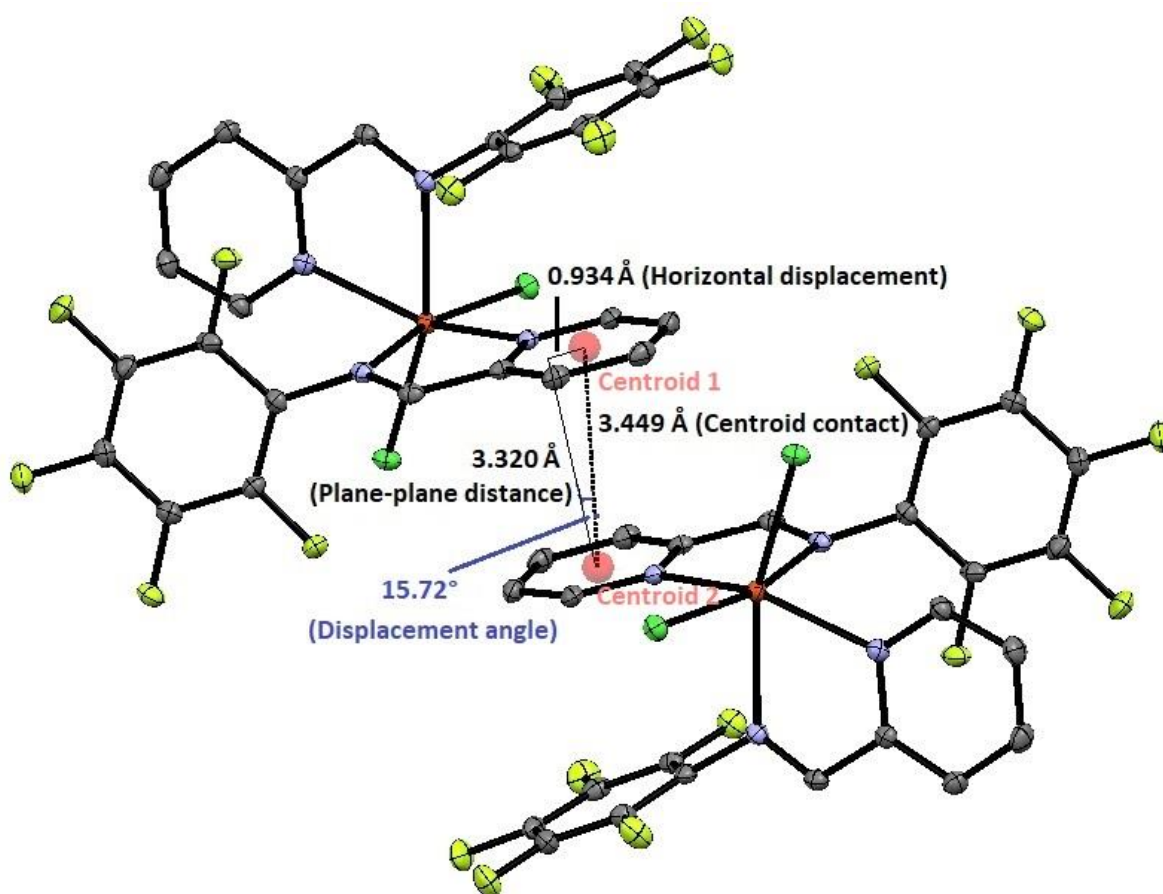
Figure 3.5b. Assembly of two complexes **7'**, extracted from a portion of the crystal packing diagram, showing the π – π stacking of pyridine rings represented by pseudo-centroid contact (Centroid1···Centroid2 = 3.449 Å).

From the crystal packing view of complex **7'** in Figure 3.5b, we can see that the two pyridines of the ligand **L7** from the two separate units of complex **7'** are nearly face-to-face aligned to each other. The interplane angle of the two pyridine rings is almost 0, which means that the two

pyridines are parallel (interplanar distance = 3.320Å), although they are parallelly displaced with respect to each other. The horizontal displacement is measured by the displacement angle formed between the ring-centroid vector (Centroid1Centroid2) and the normal to one of the pyridine planes. This arrangement results to a centroid contact (Centroid1···Centroid2) of 3.449 Å with a displacement angle of 15.72 °, which corresponds to a very small horizontal displacement of 0.934 Å. All these observations suggest a possible occurrence of $\pi - \pi$ interactions between the two pyridine rings which can play an important role in controlling the packing or assembly of compounds.[35]

Table 3.2. Selected bond distances (Å) and angles (°) for aldiminopyridine complexes **6'** and **7'**

Parameters	6'	7'
Fe1—Cl1	2.3696(6)	2.4358(4)
Fe1—Cl2	2.4284(6)	2.3430(4)
Fe1—N1	2.2217(19)	2.2202(12)
Fe1—N2	2.2727(19)	2.2375(12)
Fe1—N3	2.2209(2)	2.2295(12)
Fe1—N4	2.2862(19)	2.3202(12)
N2—Fe1—Cl2	160.03(5)	164.00(3)
N1—Fe1—N3	169.76(7)	151.35(4)
N4—Fe1—Cl1	157.90(5)	162.53(3)
N1—Fe1—Cl2	90.61(5)	91.76(3)
N4—Fe1—Cl2	90.95(5)	88.06(3)
N3—Fe1—Cl2	87.81(5)	104.38(3)
Cl1—Fe1—Cl2	105.59(2)	95.156(14)
N1—Fe1—N4	96.26(7)	85.58(4)
N1—Fe1—Cl1	98.08(5)	111.43(3)
N3—Fe1—Cl1	92.08(5)	90.84(3)
N3—Fe1—N4	73.66(7)	71.73(4)
C6—N2—C7—C12	146.8(2)°	115.60(16)°
C20—N4—C21—C26	136.1(3)°	-
C18—N4—C19—C24	-	116.83(16)°

The molecular structure of complex **8'** (Figure 3.6a, selected angle and bond distances are presented in Table 3.3) illustrates the effective coordination of the ligand on the metal center, which is depicted in the solid state as a neutral symmetrical binuclear coordination complex of the type **L8**$_2$Fe(µ-Cl)$_2$FeCl$_2$.(CH$_3$CN)$_2$, a structure containing two Fe centers with distinctive coordination environment, which is very rarely observed in the literature.[18,32,36] The molecular structure was also confirmed through elemental analysis accounting the presence of two non-coordinated acetonitrile molecules in the lattice (Calculated for crystal C$_{30}$H$_{20}$N$_2$F$_{12}$Fe$_2$Cl$_4$ + two molecules of CH$_3$CN: C 40.83.25, H 2.62, N 8.40; found C 41.17, H 2.77, N 8.72).
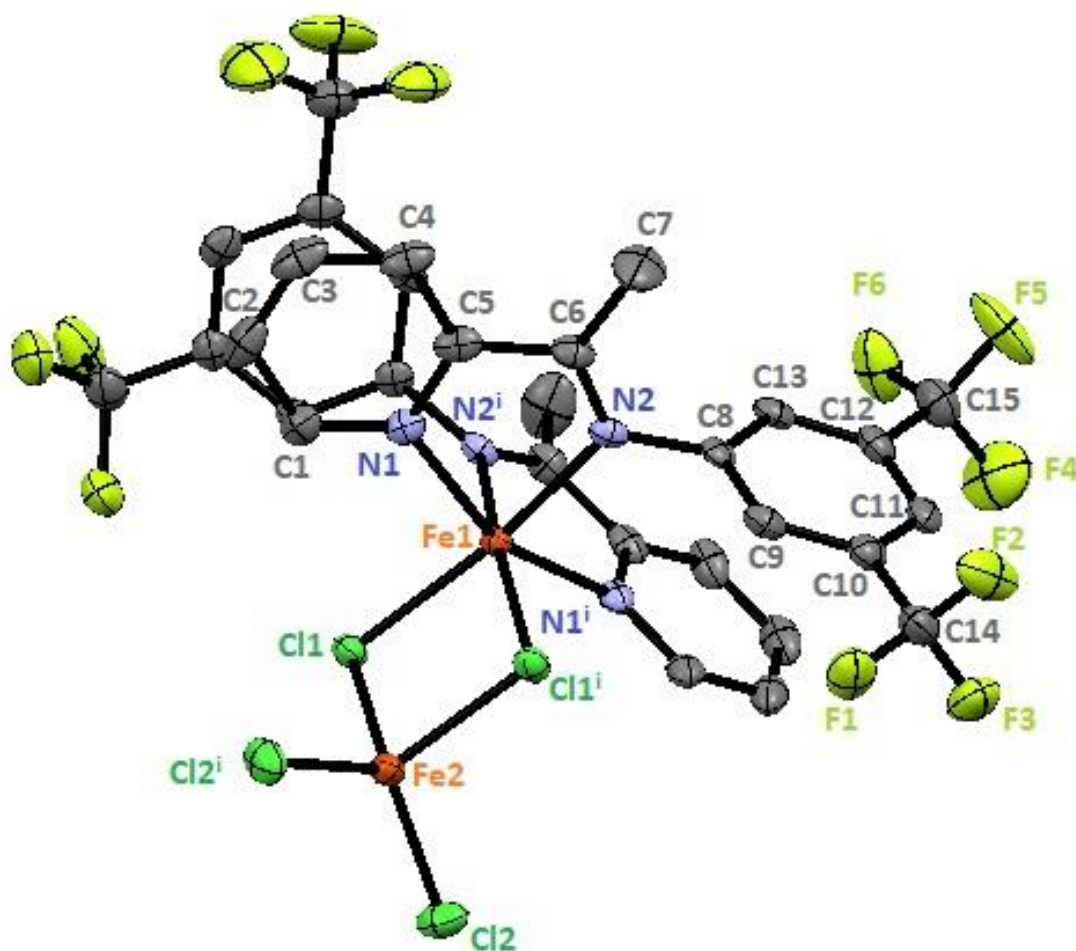
Figure 3.6a. ORTEP-type view of the crystallized complex **8'** with ellipsoids drawn at 50% probability level (hydrogen atoms and solvent molecules have been omitted for clarity and only specific atoms have been labelled)

The structure represents a monoclinic crystal system with space group $C2/c$ that corresponds to the point group C_{2h}. The symmetry in the structure can be observed by locating one of the major symmetry elements like a two-fold symmetry axis (in this case principal axis C_2) along the iron atoms Fe1 and Fe2, from which a rotation by 180 ° obtains the same molecule. Complex **8'** consists of two Fe centers in which the coordination sphere of Fe1 metal comprises two iminopyridine chelate ligands (**L8**) whereas the other metal Fe2 is surrounded by two terminal chlorides (Cl2 and Cl2^i), both Fe1 and Fe2 centers are ultimately connected via two bridging chloride atoms (Cl1 and Cl1^i). The bridging bond distances for Fe1 [Fe1–Cl1 = Fe1–Cl1^i = 2.4423(9) Å] were found to be higher than Fe2 [Fe2–Cl1 = Fe2–Cl1^i = 2.3927(10) Å] due to the higher coordination number of Fe1. In general, the Fe-Cl bridging bond distances were found to be a bit lower than observed for the reported values in literature for similar type of complexes [Fe-Cl: 2.409(2)–2.481(2) Å in (η^2-Ph$_2$P(O)Py)$_2$Fe(μ-Cl)$_2$FeCl$_2$) complex,[36] Fe-Cl: 2.414(2)–2.523(3) Å in (η^2-Ph$_2$C(N)Py)$_2$Fe(μ-Cl)$_2$FeCl$_2$)].[18] The arrangement of the two iminopyridine ligands **L8** in the neutral complex **8'** is similar to the one observed with the aldiminopyridine analogues **6'** and **7'**, where the nitrogen atoms of the pyridine fragments are in *trans* position to each other while both *N* atoms of the imine moieties are oriented in *cis* position to one another. The geometry around the Fe1 center can be described as distorted octahedral, in which one bridging chloride (Cl1) and the imine nitrogen (N2) occupy the axial sites due to the longer bond distances [Fe1–Cl1: 2.4423(9) Å; Fe1–N2: 2.188(3) Å], while the atoms Cl1^i, N1, N1^i and N2^i form the equatorial plane with the Fe-N$_{imine}$ distances [Fe1–N2^i: 2.188(3) Å] being greater than the Fe-N$_{pyridine}$ distance [Fe1–N1: 2.147(3) Å]. The axial angle N2–Fe2–Cl1 exhibits a moderate deviation from linearity [170.22(8)°] and the torsion N1-C5-C6-N2 was found to be 3.2(5)°, indicating that the imino group is almost planar to the pyridine ring.

As found in similar structures of (iminopyridine)MCl$_2$ [M = Ni, Pd, Fe] reported in the literature,[25,37] the *N*-aryl substituent is almost perpendicular to the imino group as evidenced from the torsion angle C6-N2-C8-C9 = 98.5(4)°. Regarding the other Fe2 metal center, the coordination geometry can be best described as distorted tetrahedron in which the Fe-Cl terminal bond distances [Fe2–Cl2: 2.2388(10) Å] were found in the similar range [2.234(2) Å–2.258(3) Å] for terminal chlorides in similar complexes from which we can suggest that the tetrahedral iron center is in +2 oxidation state.[18,36] It is also worthy to notice that the bridging arrangement of chloride ligands precludes the formation of metal-metal bond where the Fe-Fe interatomic distance (3.423 Å) was

found to be near to that observed for Wang's complex (3.508(2) Å)[18] but longer than Mak's complex (2.421(2) Å).[36] In addition, the presence of non-coordinated acetonitrile molecules in the lattice does not affect the geometry around each Fe center.

      The crystal packing of complex **8'** in Figure 3.6b shows a similar face-to-face arrangement of the two pyridines of the ligand **L8** as observed previously with complex **7.** This arrangement again suggests a possible occurrence of $\pi - \pi$ interactions between the two pyridine rings resulting from a pseudo-centroid contact (Centroid1···Centroid2) of 3.531 Å with a displacement angle of 11.42 ° and a small horizontal displacement of 0.699 Å.[35]
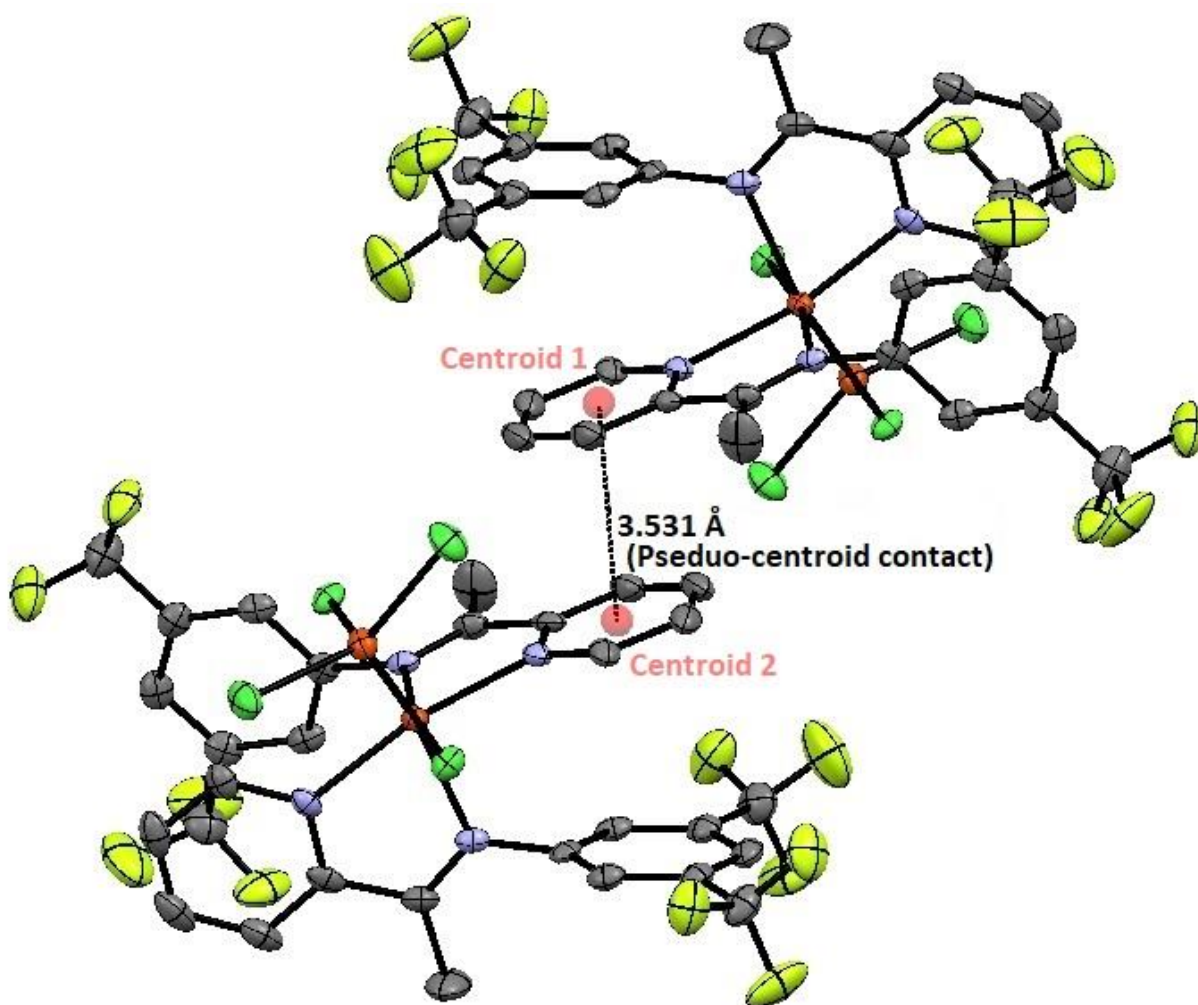
Figure 3.6b. Assembly of two complexes **8',** extracted from a portion of the crystal packing diagram, showing the $\pi - \pi$ stacking of pyridine rings represented by centroid contact (Centroid1···Centroid2 = 3.531 Å).

The solid state structure of complex **9'** shows a centrosymmetric tetranuclear coordination complex somewhat like **8'** but, interestingly, it exists as a dimer in the form of [(**L9**)$_2$Fe(μ-Cl)$_2$FeCl$_2$]$_2$.(CH$_3$CN)$_2$ (Figure 3.7a, selected angle and bond distances are presented in Table 3.3). Although, the powdery form (**9**) has already been characterized *via* elemental analysis (*vide supra*), the crystalline form (**9'**) was also verified through elemental analysis where the addition of one molecule of DCM (used for recrystallization) was necessary to obtain the reliable result. (Calculated for crystal C$_{56}$H$_{34}$N$_{10}$F$_{20}$Fe$_4$Cl$_8$ including two molecules of CH$_3$CN in lattice + one molecule of DCM (for recrystallization): C 37.64, H 1.99, N 7.70; found C 36.41, H 1.93, N 8.14).
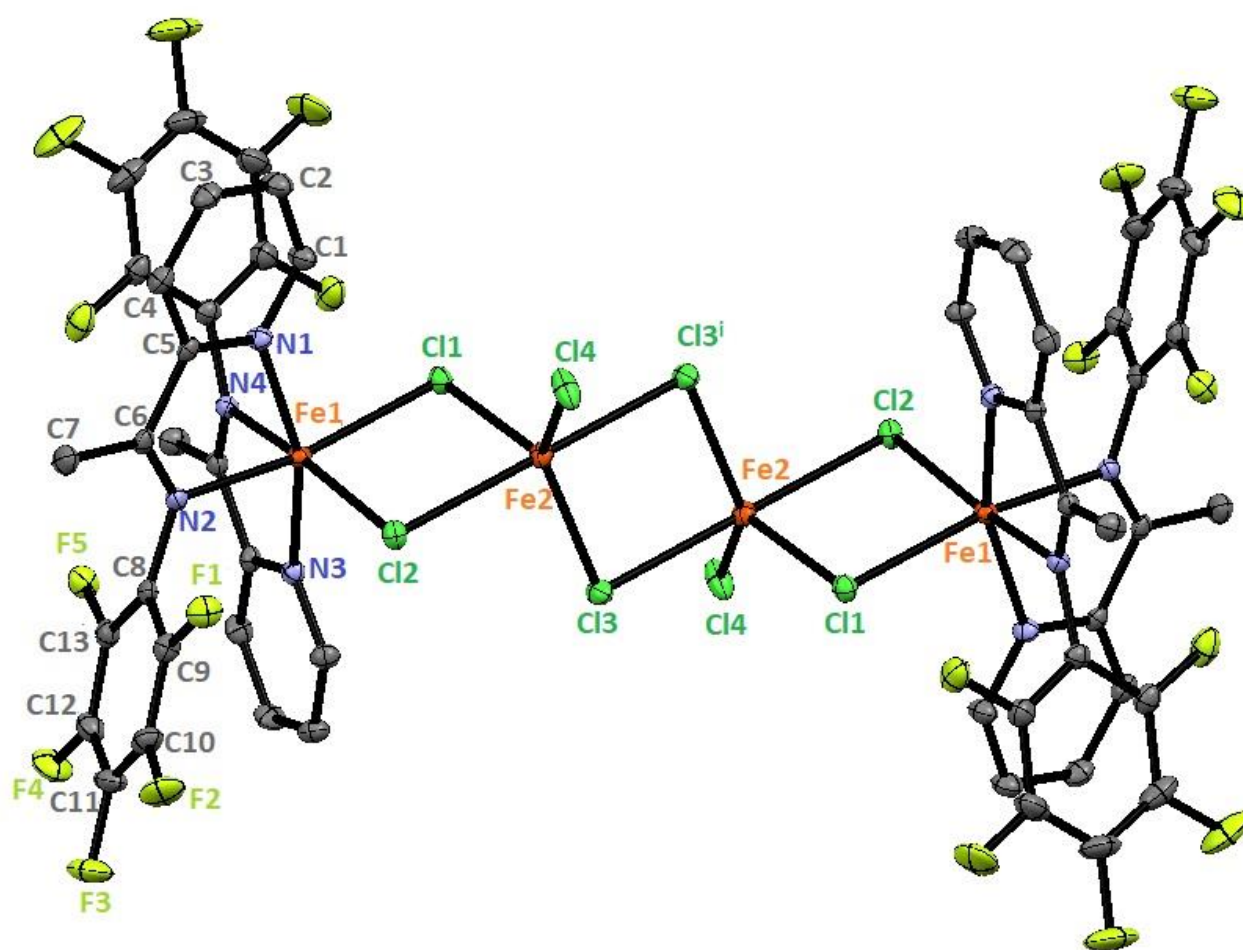
Figure 3.7a. ORTEP diagram of complex **9'** with ellipsoids drawn at 50% probability level (hydrogen atoms and solvent molecules have been omitted for clarity and only specific atoms have been labelled)

The structure represents an orthorhombic crystal system with space group *Pbca* that corresponds to the point group *D*$_{2h}$. At the centroid of the rhombus Fe2Cl3Fe2Cl3^i, lies an

inversion center of symmetry which generates the whole symmetric dimer from the asymmetric monomer unit [(**L9**)$_2$Fe(μ-Cl)$_2$FeCl$_2$] whose characteristics are similar to the unsymmetrical binuclear coordination complex (η^2-Ph$_2$P(O)Py)$_2$Fe(μ-Cl)$_2$FeCl$_2$) reported by Wang.[18] Complex **9'** consists of four iron centers of which the two Fe1 centers possess two iminopyridine ligands and share two bridging chloride (Cl1 and Cl2) ligands with both remaining Fe2 centers. In addition, the two Fe2 centers are linked by two bridging chloride atoms (Cl3), which are further bound to a terminal chloride (Cl4) to complete the coordination sphere. Like complex **8'**, this structure also consists of two different types of iron centers, Fe1 being in a distorted octahedral environment whereas the geometry at the Fe2 centers can be best described as distorted trigonal bipyramidal on the basis of τ_5 parameter (0.78) introduced by Addison and coworkers for five-coordinated arrrangement.[38] In the case of Fe1, we observe an environment around the metal center similar to that of complex **8**, the atoms Cl1 and N2 occupy the axial sites while the remaining atoms Cl2, N2, N3 and N4 constitute the equatorial plane. Due to its dimeric form in the solid state, the axial [Fe1–Cl1: 2.4796(6) Å; Fe1–N2: 2.2212(17) Å] and equatorial [Fe1–N1: 2.1644(16) Å; Fe1–N3: 2.1552(17) Å; Fe1–N4: 2.2114(17) Å; Fe1–Cl2: 2.3886(6) Å] bond distances for complex **9'** were found to be slightly longer than those observed for the complex **8'**.

Unlike its monomeric congener **8'**, the Fe-N$_{imine}$ bond distances [Fe1–N2: 2.2212(17) Å and Fe1–N4: 2.2114(17) Å] from the two sets of ligands are nearly equal. Similar trend can be observed for Fe-N$_{pyridine}$ bond distances [Fe1–N1: 2.1644(16) Å; Fe1–N3: 2.1552(17) Å], which is the reason why the monomeric unit is asymmetric in this case. The Fe-N$_{imine}$ distances were greater than Fe-N$_{pyridine}$ distances as seen previously with complexes **6'-8'**. The Cl1–Fe1–N2 bond angle [166(5)°] slightly deviates from linearity and the *N*-aryl group is also not orthogonal to the imino group, as evident from the torsions [C6-N2-C8-C9 = 63.4(3)° and C19-N4-C21-C22 = 70.9(3)°]. On the other hand, the trigonal bipyramidal Fe2 center is surrounded by four bridging chlorides (Cl1, Cl2, Cl3 and Cl3^i) and one terminal chloride (Cl4) in which the apical positions are occupied by Cl2 and Cl3^i whereas the remaining chlorides form the equatorial plane. The apical bond distances were found to be Fe2–Cl2: 2.5886(6) Å; Fe2– Cl3^i: 2.5901(6) Å and the equatorial distances were found to be Fe2–Cl1: 2.3881(6) Å; Fe2– Cl3: 2.3447(6) Å; Fe2– Cl4: 2.2746(6) Å. The apical bond angle Cl2–Fe2– Cl3^i was found to be *quasi*-linear [177.62(2)°] and the equatorial bonds measured nearly 120° (Table 3.3). The Fe-Fe interatomic distance (Fe1$^{...}$Fe2 = 3.578 Å) was found to be greater than that observed for complex **8'** and the values known in the

literature.[18,36] Also, as expected due to the dimeric nature, the terminal Fe-Cl bond distances [Fe2–Cl3: 2.3447(6) Å; Fe2– Cl4: 2.2746(6) Å] for the monomeric unit of complex **9'** were found longer than those observed for Wang's complex [2.234(2) Å–2.258(3) Å] with Fe^{2+} center.[18]

As seen previously with complex **6'**, the alignments of ligands within the crystal packing could also result from the presence of weak non-bonding F⋯F contacts of 2.94(2) Å and H⋯F interactions of *ca* 2.67 Å (Figure 3.7b). In addition, one can also observe a similar face-to-face arrangement of the two pyridines of the ligand **L9** as observed previously with complexes **7'** and **8'**, resulting to $\pi - \pi$ interactions between the two pyridine rings along the centroid pseudo-contact (Centroid1⋯Centroid2) of 3.988 Å (Figure 3.7c)
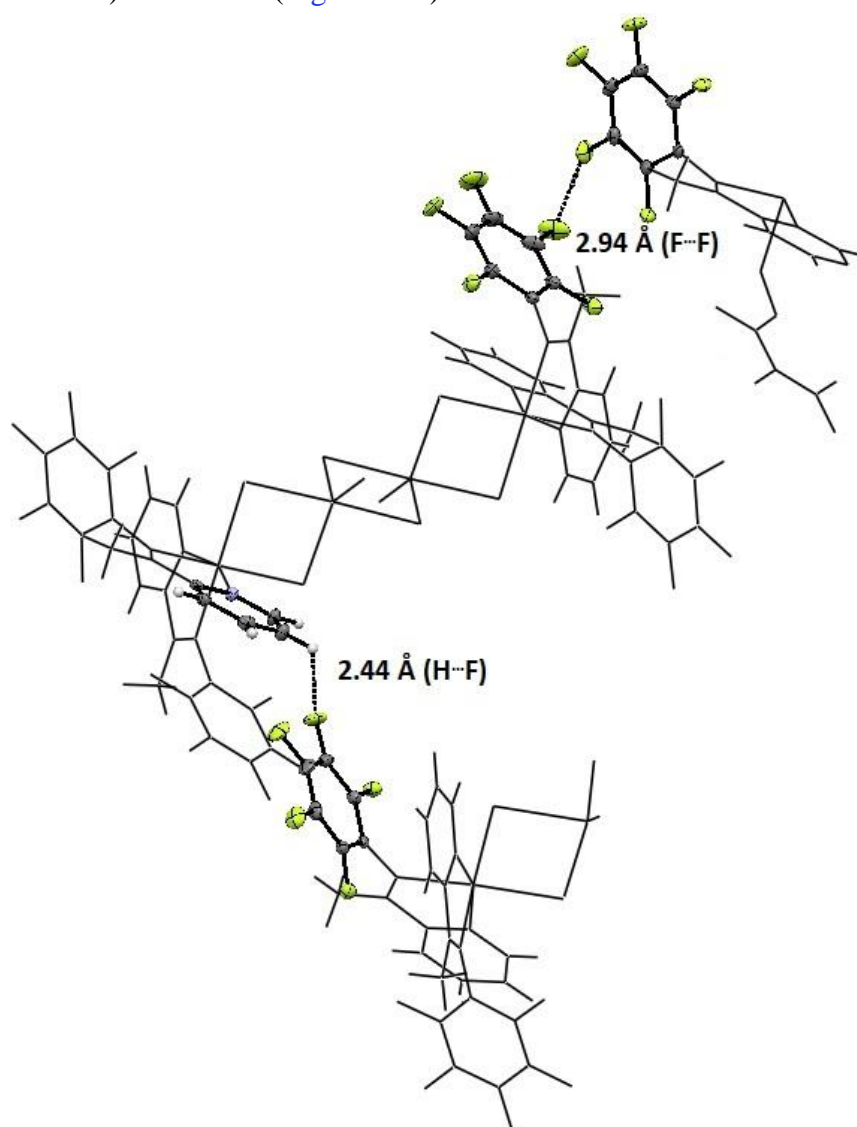
Figure 3.7b. Extract from the crystal packing of complex **9'** highlighting weak non-bonding F⋯F (2.94 Å) and H⋯F (2.44 Å) contacts.

137
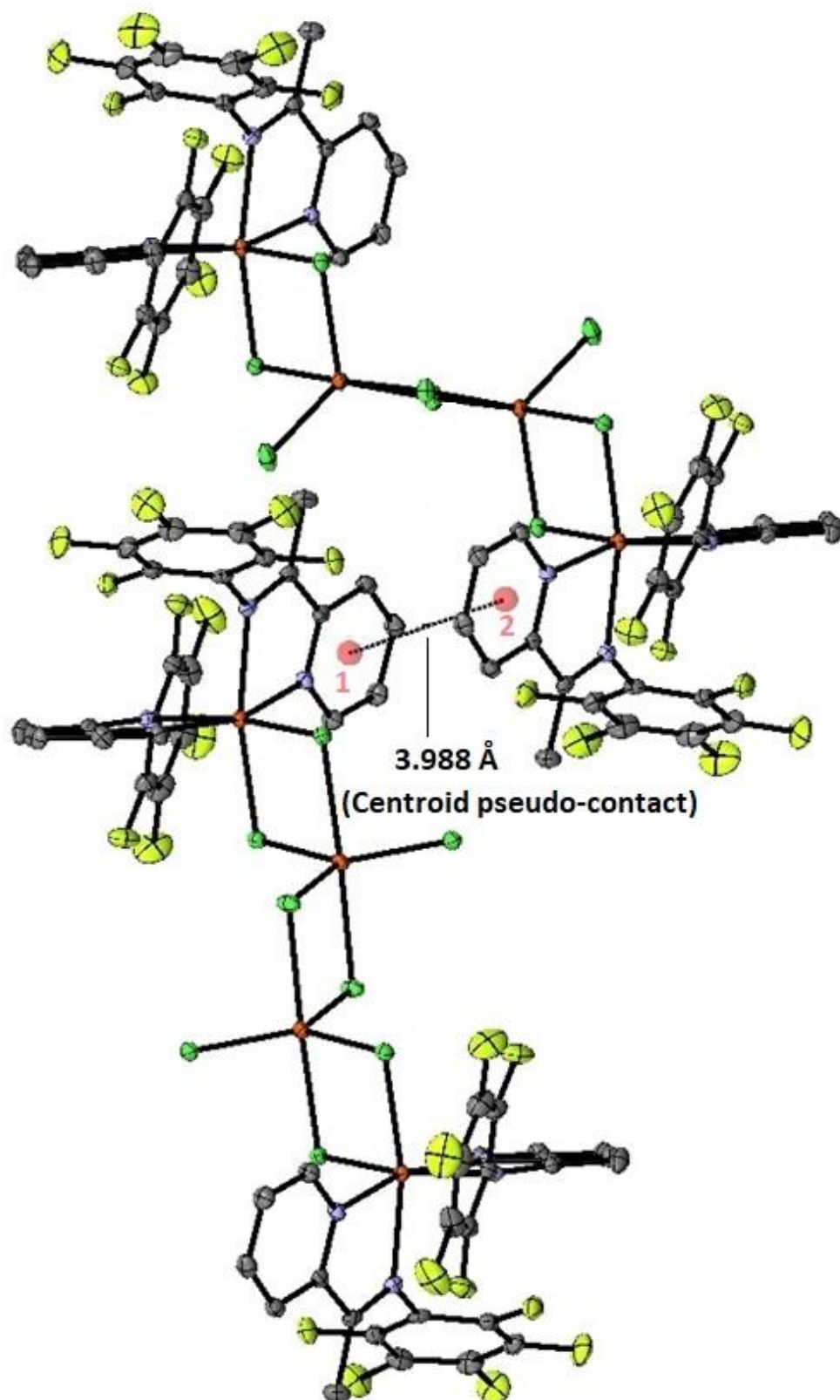
Figure 3.7c. Extract from the crystal packing of complex **9'** highlighting the $\pi - \pi$ stacking of pyridine rings represented by centroid pseudo-contact (Centroid1⋯Centroid2 = 3.988 Å)

Table 3.3. Selected bond distances (Å) and angles (°) for ketiminopyridine complexes **8'** and **9'**

Parameters	8'	Parameters	9'
Fe1—Cl1	2.4423(9)	Fe1—Cl1	2.4796(6)
Fe1—N1	2.147(3)	Fe1—N2	2.2212(17)
Fe1—N2	2.188(3)	Fe1—N1	2.1644(16)
Fe2—Cl1	2.3927(10)	Fe1—Cl2	2.3886(6)
Fe2—Cl2	2.2388(10)	Fe1—N3	2.1552(17)
Cl1—Fe1—N2	170.22(8)	Fe1—N4	2.2114(17)
Cl1—Fe1—N1	96.35(8)	Fe2—Cl1	2.3881(6)
Cl1—Fe1—N1^i	100.86(8)	Fe2—Cl2	2.5886(6)
Cl1—Fe1—Cl1^i	88.69(5)	Fe2—Cl3	2.3447(6)
Cl1—Fe1—N2^i	89.86(7)	Fe2—Cl3^i	2.5901(6)
Cl1^i—Fe1—N2^i	170.22(8)	Fe2—Cl4	2.2746(6)
N1—Fe1—N1^i	155.86(16)	Cl1—Fe1—N2	166.000(5)
N1^i—Fe1—C11^i	96.36(9)	Cl1—Fe1—N1	93.53(5)
N1^i—Fe1—N2^i	74.43(11)	Cl1—Fe1—N4	87.86(5)
N1—Fe1—Cl1^i	100.86(8)	Cl1—Fe1—Cl2	88.00(2)
N1—Fe1—N2^i	88.91(11)	Cl1—Fe1—N3	99.50(5)
Cl1—Fe2—Cl1^i	91.03(5)	Cl2—Fe1—N4	166.08(5)
Cl1^i—Fe2—Cl2^i	107.75(4)	N1—Fe1—N3	161.40(7)
Cl1^i—Fe2—Cl2	110.99(4)	N1—Fe1—N4	93.46(6)
Cl2^i—Fe2—Cl2	123.52(6)	N3—Fe1—Cl2	93.64(5)
C6—N2—C8—C9	98.5(4)°	N3—Fe1—N4	73.96(6)
		N1—Fe1—Cl2	100.06(5)
		Cl2—Fe2—Cl3^i	177.62(6)
		Cl2—Fe2—Cl4	90.33(2)
		Cl1—Fe2—Cl4	118.70(2)
		Cl1—Fe2—Cl3	110.96(2)
		Cl4—Fe2—Cl3	130.34(3)
		C6—N2—C8—C9	63.4(3)°
		C19—N4—C21—C22	70.9(3)°

Modifying the iminopyridine skeleton by extending the flat segments of the pyridine aromaticity gives a relatively bulkier iminoquinoline ligand, the corresponding iron complex (**10**) of which crystallizes in a manner similar to that observed for complex **8'**, although the two bounded ligands are not equivalent. The solid state structure of complex **10'** also shows a symmetrical binuclear coordination complex of the type (**L10**)$_2$Fe(μ-Cl)$_2$FeCl$_2$.(CH$_3$CN)$_2$, which exists as two different units in the crystal packing. The ORTEP type view of complex **10'** is shown in Figure 3.8a. The crystal structure was also confirmed *via* elemental analysis where again the addition of crystallizing solvent was needed to obtain the results (Calculated for C$_{36}$H$_{20}$N$_4$F$_{12}$Fe$_2$Cl$_4$ + four molecules of CH$_2$Cl$_2$: C 36.13, H 2.12, N 4.21; found C 37.12, H 2.07, N 4.03)
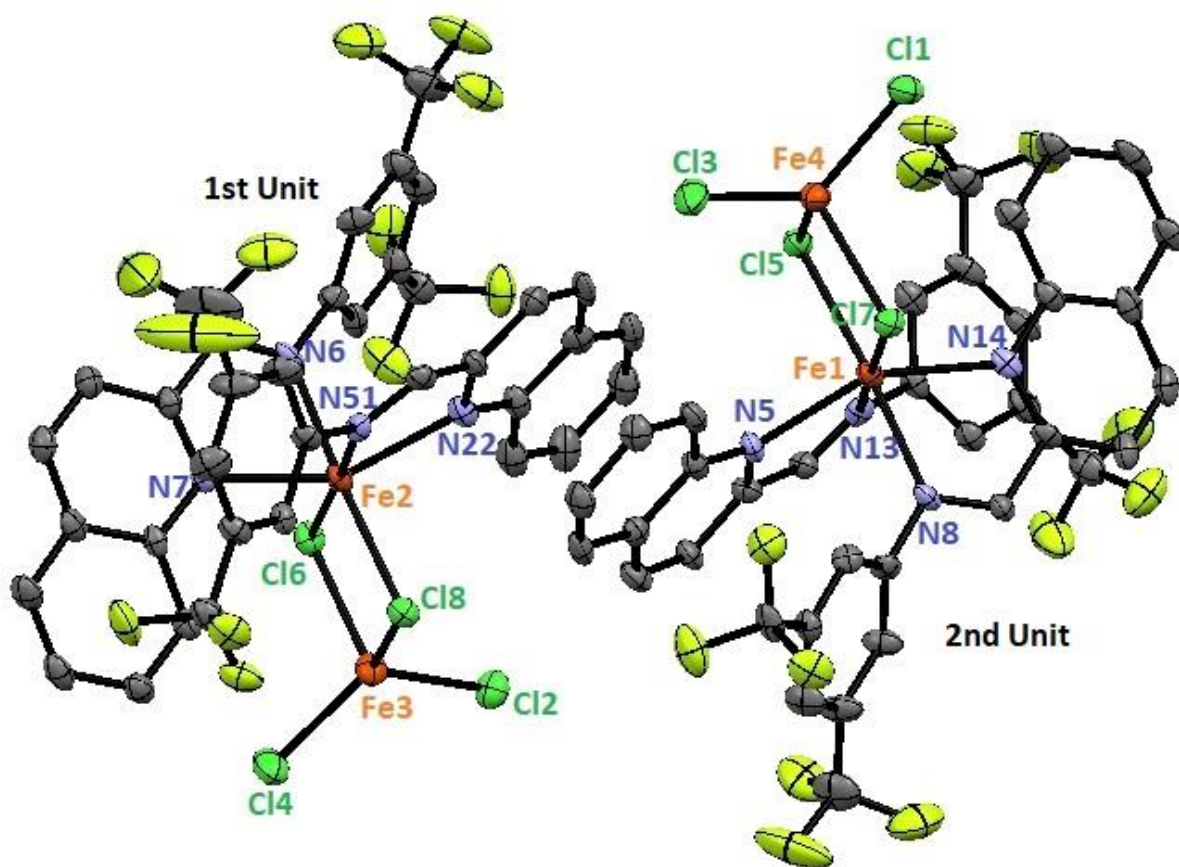
Figure 3.8a. ORTEP-type view of complex **10** with ellipsoid drawn at 50% probability level (hydrogen atoms have been omitted for clarity and only specific atoms have been labelled)

Unlike complex **9'**, which is dimeric in solid state, the complex **10'** does not tend to dimerize most likely due to the larger in-plane steric hindrance of this ligand as observed previously in the literature with iminoquinoline and α-diimine ligands,[25,39] although it attains similar geometry like complex **8'**, possibly due to the presence of CF_3 groups on the *N*-aryl moiety. Like complex **8'**, we could not find any possible H···F or F···F contacts in the crystal packing of **10'** but due to a similar face-to-face arrangement of the two quinolines of the ligand **L10**, we suggest the presence of intramolecular π – π interactions between the two quinoline rings which increase with the extended nature of the π systems leading to an increased overlap of the aromatic surface area.[35,40] Figure 3.8b shows the π – π interactions between the stacked quinoline rings along the centroid *pseudo*-contacts (Centroid1···Centroid2 = 3.679Å and Centroid3···Centroid4 = 3.726 Å).
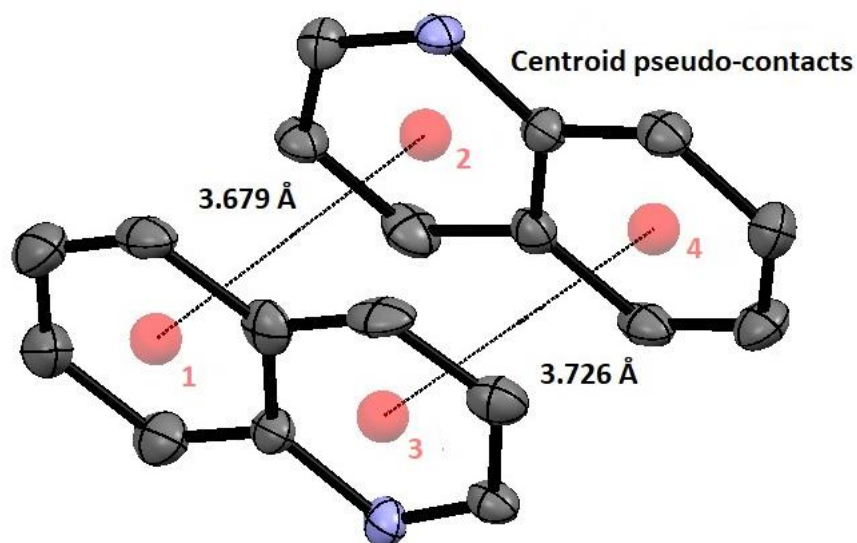
Figure 3.8b. Extract from the crystal packing of complex **10** highlighting the π – π stacking of quinoline rings represented by *pseudo* centroid contact (Centroid1···Centroid2 = 3.679 Å and Centroid3···Centroid4 = 3.726 Å)

For the sake of better understanding and comparison, we will focus only on one unit of complex **10'** (Figure 3.8c), whereas the data corresponding to the second unit will also be addressed in parallel because the two units are similar in terms of coordination mode (although the data corresponding to each unit are slightly different and do not lie within the error limits). Complex **10'** consists of two Fe centers in which the coordination sphere of Fe2 (Fe1 in 2nd unit) metal comprises of two iminoquinoline ligands (**L10**) whereas the other metal Fe3 (Fe4 in 2nd unit) is surrounded by two terminal chloride atoms (Cl2 and Cl4 for 1st; Cl1 and Cl3 for 2nd). The two

chloride atoms (Cl6 and Cl8 for 1st; Cl5 and Cl7 for 2nd) act as bridging ligands as evidenced from the longest Fe–Cl bond distances [Fe3–Cl6: 2.392(2) Å and Fe3–Cl8: 2.3734(19) Å for 1st; Fe4–Cl5: 2.3776(19) Å and Fe4–Cl7: 2.3911(19) Å for 2nd], which are close to those observed for complex **8** [Fe2–Cl1(Cl1i): 2.3927(10) Å].
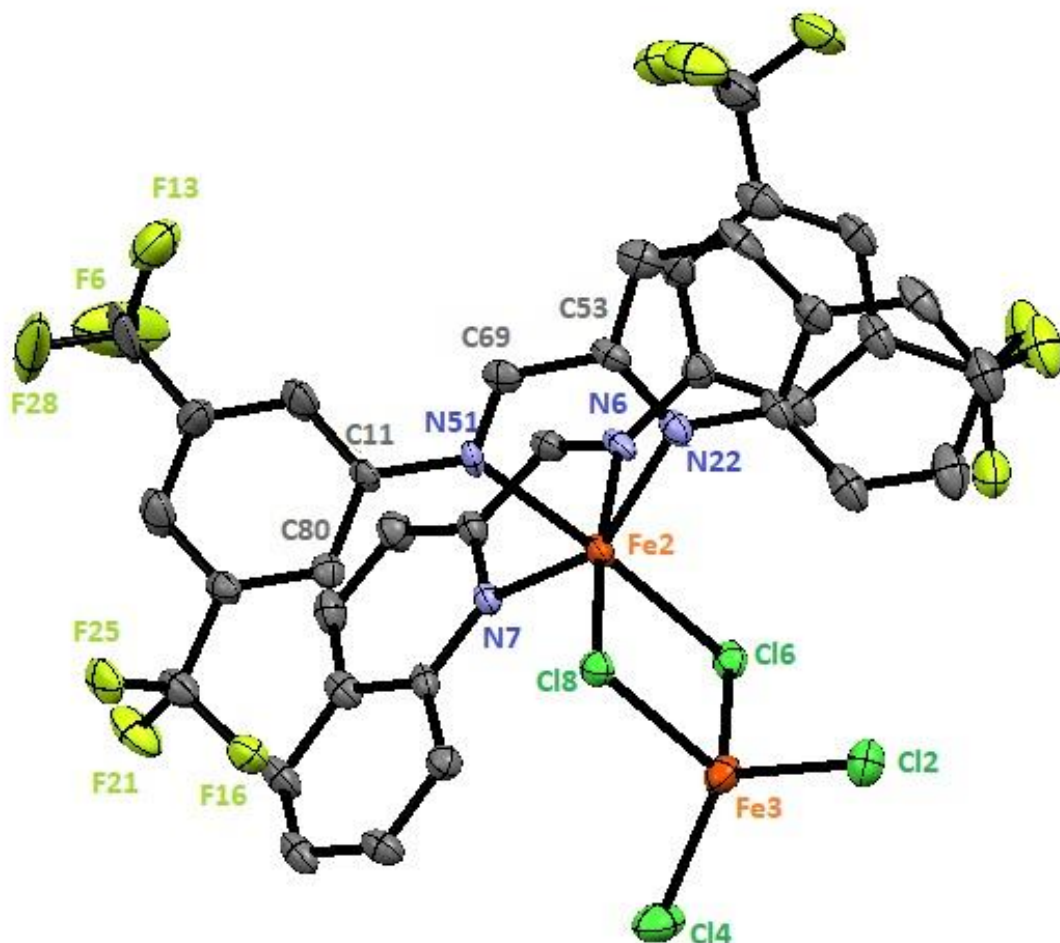

Figure 3.8c. ORTEP-type view of a single unit of complex **10'** with ellipsoid drawn at 50% probability level (hydrogen atoms and second unit have been omitted for clarity and only specific atoms

The geometry around the Fe2 (Fe1 for 2nd) center can be described as distorted octahedral, in which one bridging chloride Cl6 (Cl5 for 2nd) and the imine nitrogen N51 (N8 for 2nd) occupy the axial sites due to the longer bond distances [Fe2–Cl6: 2.4302(19) Å and Fe2–N51: 2.217(5) Å for 1st; Fe1–Cl5: 2.4506(19) Å and Fe1–N8: 2.223(5) Å for 2nd], while the atoms Cl8, N6, N7 and N22 form the equatorial plane (Cl7, N5, N13 and N14 for 2nd). The axial angle N51–Fe2–Cl6 exhibits a small non-linearity (176.06(14)°) and the torsion C69-N51-C11-C21 was found to be

42.8(9)° indicating that the replacement of pyridine moiety by quinoline affects the overall ligand conformation [For 2nd unit, N8-Fe1-Cl5 = 175.25(14)° and C46-N13-C24-C71 = 117.6(7)°]. This effect on dihedral angle is apparent with Ni and Co iminoquinoline complexes[41,42] whereas with a similar iron complex, the orthogonality of the *N*-aryl plane with the quinoline ring was maintained.[43]

The average Fe-N bond distances for both imine and pyridine [Fe-N = 2.196(6)-2.248(5) Å for 1st; Fe-N = 2.204(5)-2.246(5) Å for 2nd] were found to be longer than those observed for iminopyridine complex **8'** [Fe-N = 2.147(3)-2.188(3) Å], as expected, due to the relatively increased steric bulk around the iron center imparted by the quinoline skeleton. Unlike with the iminopyridine complexes where distances Fe-N$_{pyridine}$ < Fe-N$_{imine}$, the Fe-N$_{quinoline}$ [Fe2-N7 = 2.244(5) Å and Fe2-N22 = 2.248(5) Å for 1st; Fe1-N5 = 2.222(5) Å and Fe1-N14 = 2.246(5) Å for 2nd) bond distances were found to be greater than the Fe-N$_{imine}$ [Fe2-N6 = 2.196(6) Å and Fe2-N51 = 2.217(5) Å for 1st; Fe1-N8 = 2.223(5) Å and Fe1-N13 = 2.204(5) Å for 2nd) as seen previously in literature.[43] This is probably due to the less extent of nitrogen lone pair donation which degree of delocalization is much higher in quinoline than in pyridine. Interestingly, complex **10** features smaller bond angles [N6-Fe2-N51 = 90.62(19)°, N6-Fe2-N22 = 83.3(2)° and Cl6-Fe2-Cl8 = 86.06(6)° for 1st; N13-Fe1-N8 = 91.98(19)°, N13-Fe2-N14 = 83.46(19)° and Cl7-Fe2-Cl5 = 86.83(6)° for 2nd] subtended at the iron center than the ones observed for complex **8** [N2-Fe1-N2^{i} = 93.18(15)°, N1-Fe1-N2^{i} = 88.91(11)° and Cl1-Fe1-Cl1^{i} = 88.69(5)°]. These smaller bite angles associated with the chelating ligand implies congestion around the iron center resulting to a more compact environment when compared to other complexes. Regarding the other Fe (Fe3 in 1st and Fe4 in 2nd) metal centers, the coordination geometry can be best described as distorted tetrahedron in which the Fe-Cl terminal bond distances [Fe3–Cl2: 2.269(2) Å and Fe3–Cl4: 2.238(2) Å for 1st; Fe4–Cl1: 2.242(2) Å and Fe4–Cl3: 2.257(2) Å for 2nd] were found to be slightly higher than those observed for complex **8'** [2.2387(10) Å], although they were within the range of Wang's complex [2.234(2) Å–2.258(3) Å], which again suggests that iron is in +2 oxidation state. The selected bond lengths and angles concerning the two units of complex **10'** are displayed below in Table 3.4.

Table 3.4. Selected bond distances (Å) and angles (°) for complex **10'**

Parameters	1st unit	Parameters	2nd unit
Fe2—Cl6	2.4302(19)	Fe1—Cl5	2.4506(19)
Fe2—N51	2.217(5)	Fe1—N8	2.223(5)
Fe2—N6	2.196(6)	Fe1—N13	2.204(5)
Fe2—N7	2.244(5)	Fe1—N14	2.246(5)
Fe2—Cl8	2.400(19)	Fe1—Cl7	2.4194(19)
Fe2—N22	2.248(5)	Fe1—N5	2.222(5)
Fe3—Cl6	2.392(2)	Fe4—Cl5	2.3776(19)
Fe3—Cl8	2.3734(19)	Fe4—Cl7	2.3911(19)
Fe3—Cl2	2.269(2)	Fe4—Cl1	2.242(2)
Fe3—Cl4	2.238(2)	Fe4—Cl3	2.257(2)
Cl6—Fe2—N51	176.06(14)	Cl5—Fe1—N8	175.25(14)
Cl8—Fe2—N6	173.09(15)	Cl7—Fe1—N13	174.31(15)
N7—Fe2—N22	150.0(2)	N14—Fe1—N5	148.9(2)
Cl6—Fe2—Cl8	86.06(6)	Cl5—Fe1—Cl7	86.83(6)
Cl6—Fe2—N7	91.63(14)	Cl5—Fe1—N14	110.27(15)
Cl6—Fe2—N6	90.06(15)	Cl5—Fe1—N13	90.12(14)
Cl6—Fe2—N22	108.41(15)	Cl5—Fe1—N5	92.08(15)
Cl8—Fe2—N22	93.34(15)	Cl7—Fe1—N5	110.00(15)
N22—Fe2—N6	83.3(2)	N5—Fe1—N13	74.9(2)
N6—Fe2—N7	74.35(19)	N13—Fe1—N14	83.46(19)
Cl6—Fe3—Cl8	88.43(6)	Cl5—Fe4—Cl7	89.16(6)
Cl6—Fe3—Cl2	110.67(7)	Cl5—Fe4—Cl1	110.07(7)
Cl6—Fe3—Cl4	109.00(8)	Cl5—Fe4—Cl3	110.66(8)
Cl4—Fe3—Cl2	122.82(9)	Cl3—Fe4—Cl1	123.51(8)
C69—N51—C11—C21	42.8(9)	C46—N13—C24—C71	117.6(7)
C38—N6—C58—C50	61.5(9)	C57—N8—C49—C73	129.5(7)

Modifying the iminoquinoline skeleton by replacing the 2-quinoline moiety with 8-quinoline and *N*-aryl substituents from electron withdrawing to electron donating groups like ^{i}Pr, resulted to a previously known ligand (**L11**), the corresponding Fe (II) complex (**11**) of which crystallized in a totally different fashion with the major difference being the formation of 6-membered chelate with the iminoquinoline ligand **L11** when compared to the 5-membered chelate in complex **10'**. Single crystals of complex **11** were obtained by recrystallization from concentrated dichloromethane solution of compound layered with diethyl ether (1/1) and left to stand for several days at – 20 °C under an inert atmosphere. The ORTEP type view of complex **11** is shown in Figure 3.9a from which it can be seen that unlike other Fe (II) iminopyridine complexes possessing the similar *N*-aryl substituents and that exist as dimers in the solid state,[32,44] complex **11** exists as a monomer in the solid state with coordination environment similar to (6-[(2,6-^{i}Pr$_2$-C$_6$H$_3$)N=C(Me)]-8-C$_9$H$_5$N-2-Me)NiBr$_2$ used for ethylene oligomerization[41] and to complex **5** from the second chapter of this manuscript.[45]
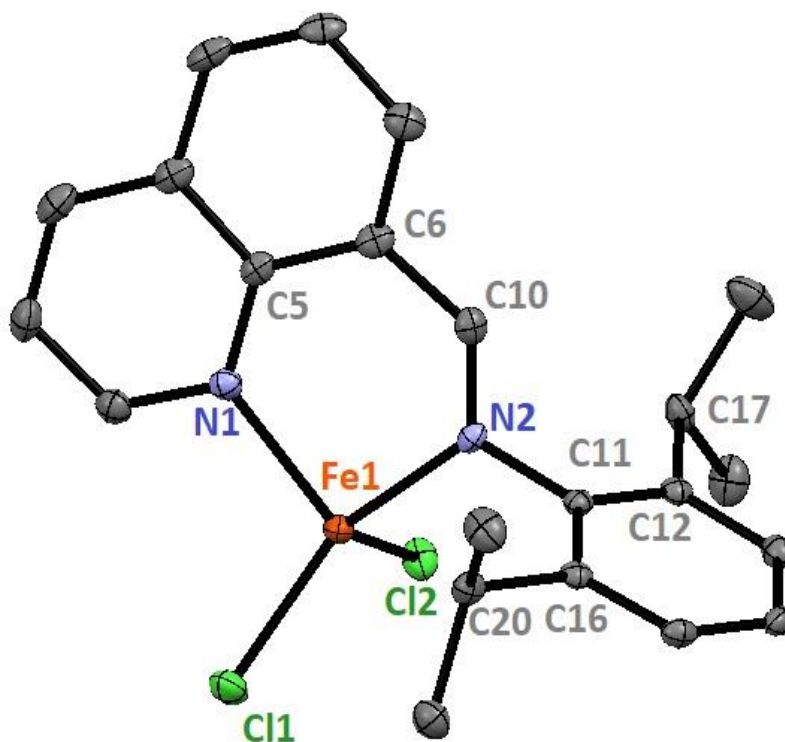
Figure 3.9a. ORTEP-type view of complex **11** with ellipsoids drawn at 50% probability level (hydrogen atoms have been omitted for clarity and only specific atoms have been labelled)

From Figure 3.9a, it can be observed that the monomeric four-coordinate complex **11** displays a distorted tetrahedral geometry around the iron center. The bond angles are ranging from 89.12(7)° to 131.94(6)° with the acute angle serving as the bite angle of chelating ligand **L11** (N2-Fe-N1 angle) and the obtuse angle is associated with N2 and Cl1 (N2-Fe-Cl1 angle). The complexation of free ligand **L11** with FeCl$_2$ changes its conformation from *transoid* to *cisoid* and also affects the C=N double bond length (C10-N2), which increased from 1.254(2) to 1.280(3) Å. The Fe-Cl bond distances [Fe1-Cl1 = 2.2519(7) Å and Fe1-Cl2 = 2.2523(6) Å] were found to be moderately longer than those observed for complex **5** [Fe1-Cl1 = 2.2309(7) Å and Fe1-Cl2 = 2.2289(7) Å] whereas the overall Fe-N bond distances [Fe1-N1 = 2.1138(19) and Fe1-N2 = 2.0823(19) Å] revealed to be almost similar [Fe1-N1 = 2.1111(16) Å and Fe1-N2 = 2.1160(17)Å for **5**]. As observed previously with the other iminoquinoline-supported congener **10'**, the Fe-N$_{quinoline}$ [Fe1-N1 = 2.1138(19) Å] distances were again found to be greater than the Fe-N$_{imine}$ [Fe1-N2 = 2.0823(19) Å] distances, in accordance with the literature.[43]

The complex **11** also features a similar face-to-face arrangement of the two quinoline rings from **L11** like its analogue complex **10'**, on the basis of which, we can also suggest the presence of intramolecular $\pi - \pi$ interactions along the centroid pseudo-contacts (C1$\cdots$C2 = C3$\cdots$C4 = 3.522 Å) as observed previously with higher N-heterocycles (Figure 3.9b).[40]
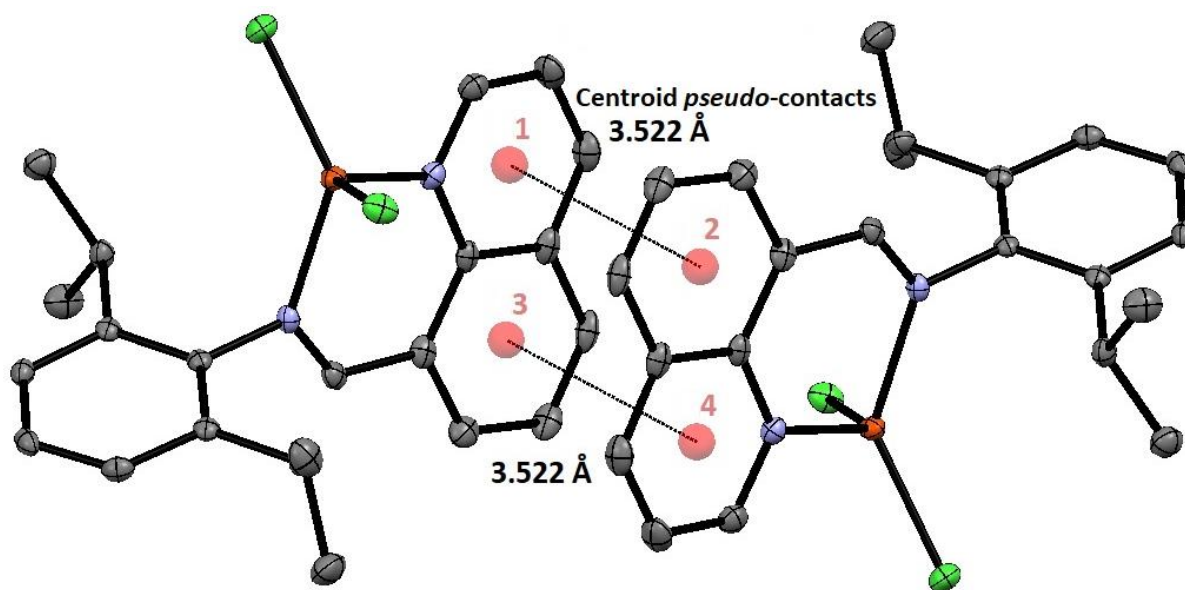
Figure 3.9b. Extract from the crystal packing of complex **11** highlighting the $\pi - \pi$ stacking of quinoline rings represented by centroid *pseudo*-contacts (Centroid1$\cdots$Centroid2 = Centroid3$\cdots$Centroid4 = 3.522 Å)

The incorporation of an 8-quinoline moiety does not significantly affect the ligand conformation (in the chelated state) where the dihedral C10-N2-C11-C16 angle of 101.8(2)° indicated that the 2,6-diiisopropyl phenyl ring is still approximately orthogonal to the N1-N2 chelate plane, as observed previously in the literature with complexes **5** and (6-[(2,6-^{i}Pr$_2$-C$_6$H$_3$)N=C(Me)]-8-C$_9$H$_5$N-2-Me)NiBr$_2$.[41,45] The associated bond angles in complex **11** [N1-Fe1-Cl1 = 101.16(6)°, N2-Fe1-Cl2 = 100.45(5)° and Cl1-Fe1-Cl2 = 111.35(3)°] were also found to be smaller than observed for complex **5** [N1-Fe1-Cl1 = 113.79(5)°, N2-Fe1-Cl2 = 119.45(5)° and Cl1-Fe1-Cl2 = 120.71(3)°], which implies congestion around the iron center as seen earlier with complex **10'** incorporating iminoquinoline skeleton. However, the bite angle N1-Fe1-N2 was found to be greater in **11** [89.12(7)°] than in **5** (77.32(6)°), due to the obvious formation of 6-membered chelate ring. The specific bond distances and angles of complex **11** are displayed below in Table 3.5.

Table 3.5. Selected bond distances (Å) and angles (°) for complex **11**

Parameters	11
Fe1—Cl1	2.2519(7)
Fe1—Cl2	2.2523(6)
Fe1—N1	2.1138(19)
Fe1—N2	2.0823(19)
N1—Fe1—Cl1	101.16(6)
N1—Fe1—Cl2	123.71(6)
N1—Fe1—N2	89.12(7)
Cl2—Fe1—Cl1	111.35(3)
N2—Fe1—Cl1	131.94(6)
N2—Fe1—Cl2	100.45(5)
C10—N2—C11—C16	101.8(2)

During the recrystallization process, there is always a possibility of degradation of a compound due to the presence of some impurities in the solvent such as traces of water, oxygen or others. In our case, we observed the oxidation of Fe (II) to Fe (III) during the recrystallization of one of the samples. Interestingly, single crystals of complex **9''** were obtained from the diffusion of diethyl ether in a concentrated solution of dichloromethane containing the complex **9** at room temperature, while taking careful precautions by performing all the operations under an inert atmosphere with degassed and distilled dry solvent. The Schlenk was brought outside the glove box and was left to stand for over 2-3 months. It seems that this time, the complex **9''** crystallized in a different fashion from **9'** and exists as $[\{(\mathbf{L9})_2Fe_{(\mu\text{-Cl})}\}_2][FeCl_4]_2$ in the solid state. The crystallographic data obtained in this case were not fully reliable in terms of quality ($R[F^2 > 2\sigma(F^2)$ = 0.095, see experimental section) due to which we can only suggest some of our results instead of claiming them unequivocally. However, the coordination chemistry can be compared to similar type of complexes known in the literature. The ball stick-type view (due to low quality crystals) of the complex **9''** is shown in Figure 3.10.
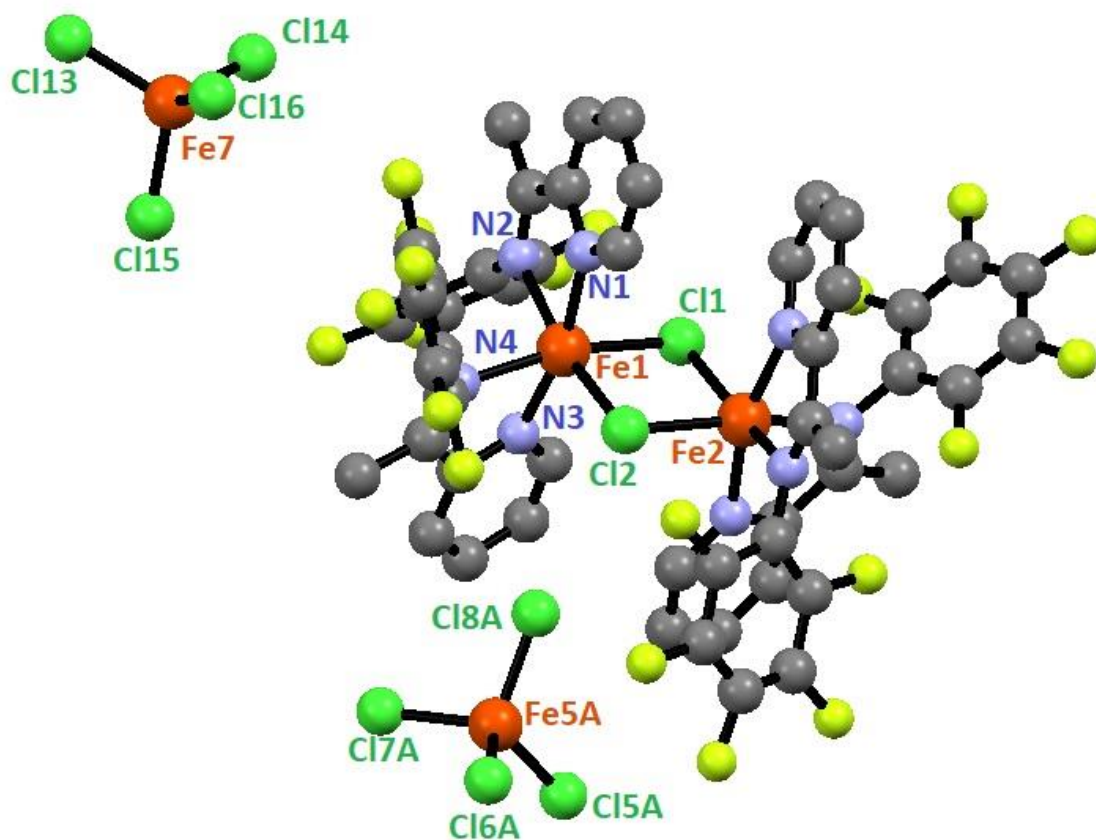
Figure 3.10. Ball stick-type view of complex **9''** (Hydrogen atoms and second units have been omitted for clarity and only specific atoms have been labelled)

Each unit consists of two independent iron centers exhibiting a distorted-octahedral coordination geometry comprising two bridging chloride anions and four N atoms from two **L9** ligands. The imine nitrogen atom (N4) and Cl1 occupy the axial coordination sites due to the larger bond lengths with the axial N4–Fe1–Cl1 angle exhibiting a slight non-linearity (167.2(3)°). The overall Fe–N bond distances [Fe1–N2: 2.17(1) Å, Fe1–N4: 2.213(9) Å, Fe1–N1: 2.17(1) Å, Fe1–N3: 2.14(1) Å] seem to be shorter than the corresponding Fe–N bond distances in complex **7** [Fe1–N1: 2.2202(12) Å; Fe1–N2: 2.2375(12) Å; Fe1–N3: 2.2295(12) Å; Fe1–N4: 2.3202(12) Å], which possibly shows a less spacious environment around the metal center (aldimine *vs* ketimine). On the other hand, the Fe–Cl bond lengths [Fe1–Cl1: 2.473(4) Å and Fe1–Cl2: 2.413(4) Å] were found in the similar range as observed with the corresponding aldimine **7** [Fe1–Cl1: 2.4358(4) Å; Fe1–Cl2: 2.3430(4) Å]. The torsion C6–N2–C8–C13 angle was found to be 75.09(2)°, indicating that the *N*-aryl group of the ligand is almost perpendicular to the pyridine ring. The structure also consists of two cationic iron centers and two counteranions $FeCl_4^-$ which exhibit tetrahedral coordination geometry. The bond distances of Fe–Cl in $FeCl_4^-$ [Fe7–Cl13: 2.183(6) Å, Fe7–Cl14: 2.189(4) Å, Fe7–Cl15: 2.184(5) Å, Fe7–Cl16: 2.191(5) Å] were found in the similar range of Fe–Cl bond distances [2.163(3)-2.218(3) Å] in Liu's complex where the authors reported that the counter anion $FeCl_4^-$ comprises of Fe^{3+} centers that exhibit tetrahedral geometry.[46] Therefore, it seems that, in our case too, the tetrahedral Fe centers exhibit +3 oxidation state due to the possible oxidation of Fe (II) to Fe (III) during the prolonged crystallization period whereas the octahedral Fe centers exhibit +2 oxidation state. The corresponding bond lengths and angles for complex **9''** are displayed in Table 3.6 below.

Table 3.6. Selected bond distances (Å) and angles (°) for ketiminopyridine complex **9''**

Parameters	9''	Parameters	9''
Fe1—Cl1	2.473(4)	Cl1—Fe1—N3	94.3(4)
Fe1—Cl2	2.413(4)	Cl1—Fe1—N1	93.8(3)
Fe1—N1	2.173(12)	Cl1—Fe1—N2	90.8(3)
Fe1—N2	2.172(12)	Cl2—Fe1—N1	93.2(3)
Fe1—N3	2.141(12)	Cl2—Fe1—N3	97.5(3)
Fe1—N4	2.212(11)	N1—Fe1—N2	73.8(5)
Fe7—Cl13	2.183(5)	N3—Fe1—N2	95.7(5)
Fe7—Cl14	2.189(5)	Cl15—Fe7—Cl13	110.10(18)
Fe7—Cl15	2.184(5)	Cl15—Fe7—Cl14	107.86(19)
Fe7—Cl16	2.191(5)	Cl15—Fe7—Cl16	110.00(19)
Cl1—Fe1—N4	167.2(3)	Cl13—Fe7—Cl14	110.9(2)
Cl2—Fe1—N2	166.8(4)	Cl14—Fe7—Cl16	110.85(18)
N1—Fe1—N3	166.8(4)	Cl16—Fe7—Cl13	107.1(2)
Cl1—Fe1—C12	87.95(13)	C6—N2—C8—C13	75.09(2)

To summarize, in this section, we observed a variety in the molecular structures of iminopyridine or iminoquinoline based iron complexes, which vary from being mononuclear to binuclear systems in solid state, depending on the type of ligand they possess. We propose that these arrangements of molecules could be related to the steric demands of the ligand skeleton as the addition of one methyl on the imino carbon (**8'** and **9'**) or the extension of flat heterocyclic pyridine segments to quinoline (**10'**) results to the attainment of this symmetrical binuclear arrangement (Scheme 3.3). Additionally, the presence of various electrostatic attractions such as H⋅F or F⋅F and $\pi - \pi$ stacking within the lattice might also be one of the determining factors for the attained geometry. These propositions are drawn from the rare studies in literature with similar type of iron complexes.[15,18] It is also worthy to notice that the simultaneous extension of central pyridine-type framework and the addition of bulkier ^{i}Pr groups as *N*-aryl substituents, no longer favors binuclear arrangement and exists as monomeric in solid state (**11**) displaying the geometry observed in the literature with similar types of iron complex.[41,45]
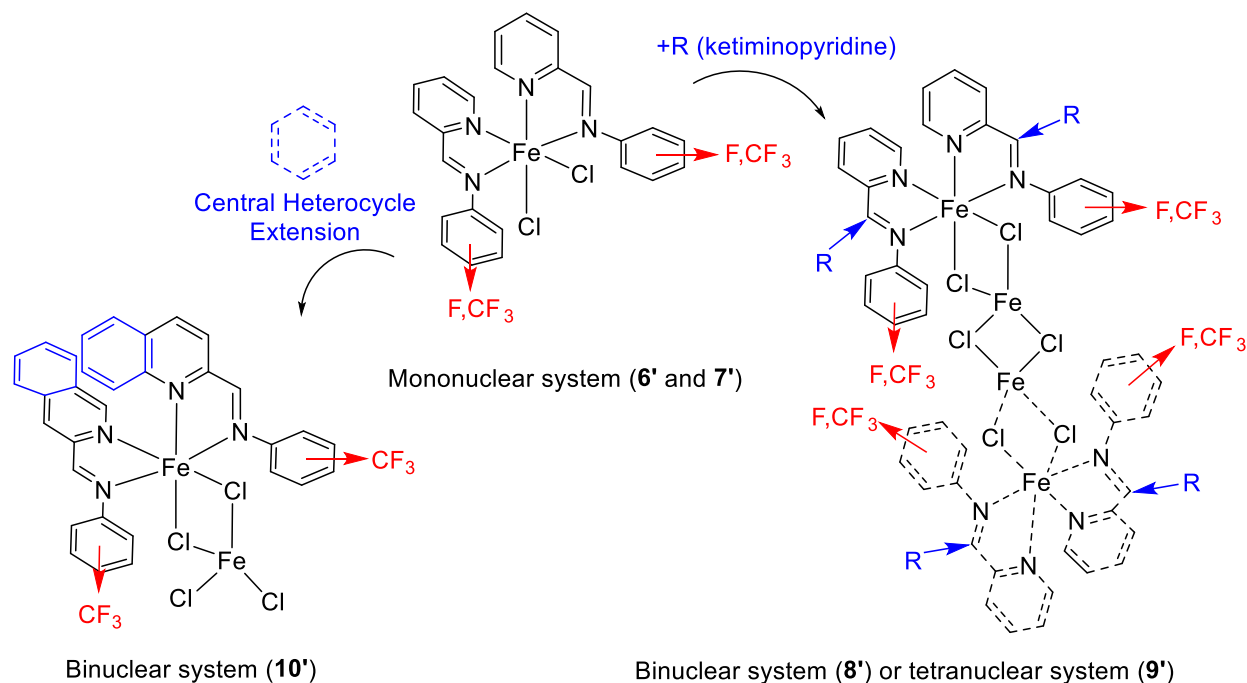
Scheme 3.3. Solid state structural evolution of complexes **6'-10'**

Ideally, the addition of 1 eq. of ligand to 1 eq. of $FeCl_2$ should result in the formation of mono-chelate as observed with complex **11** (Scheme 3.4). However, the huge difference among the substituents of *N*-aryl moiety (CF_3, F *vs* ^{i}Pr) in terms of steric as well as electronic, leads to a more electron deficient iron center, which can accommodate two ligands at once as observed for complexes **6'-10'.** This observation distinguishes the coordination ability of an electron-rich iron center *vs* an electron-deficient center.

Regarding the preferential formation of bis-chelate among the fluorinated series of complexes **6'-10',** we propose that, initially, the formation of mono-chelate (**6-10**) is most likely to happen. During the attempts of crystallization, the higher concentration of the complex solutions, might trigger a redistribution among the components of two mono-chelate units, resulting to the formation of a bis-chelated system. To confirm this hypothesis, X-ray powder diffraction (XRPD) experiments were performed to ascertain the powder phase purity of the crystalline materials **7'-9'**. A comparative study was performed between calculated patterns obtained through single-crystal Xray data and XRPD patterns of powdered samples (Appendix, Figure A37 and Figure A38). These comparisons display a difference in the number of peaks obtained for each pattern, from which we can confirm that the powder phase purity is different than the single-crystal data obtained. Additionally, this argument is also supported by the fact that

the elemental analysis of complexes **6-10** in the powdered state was consistent with the mono-chelated structure in each case, proving that the isolation of mono-chelate complex occurs initially.
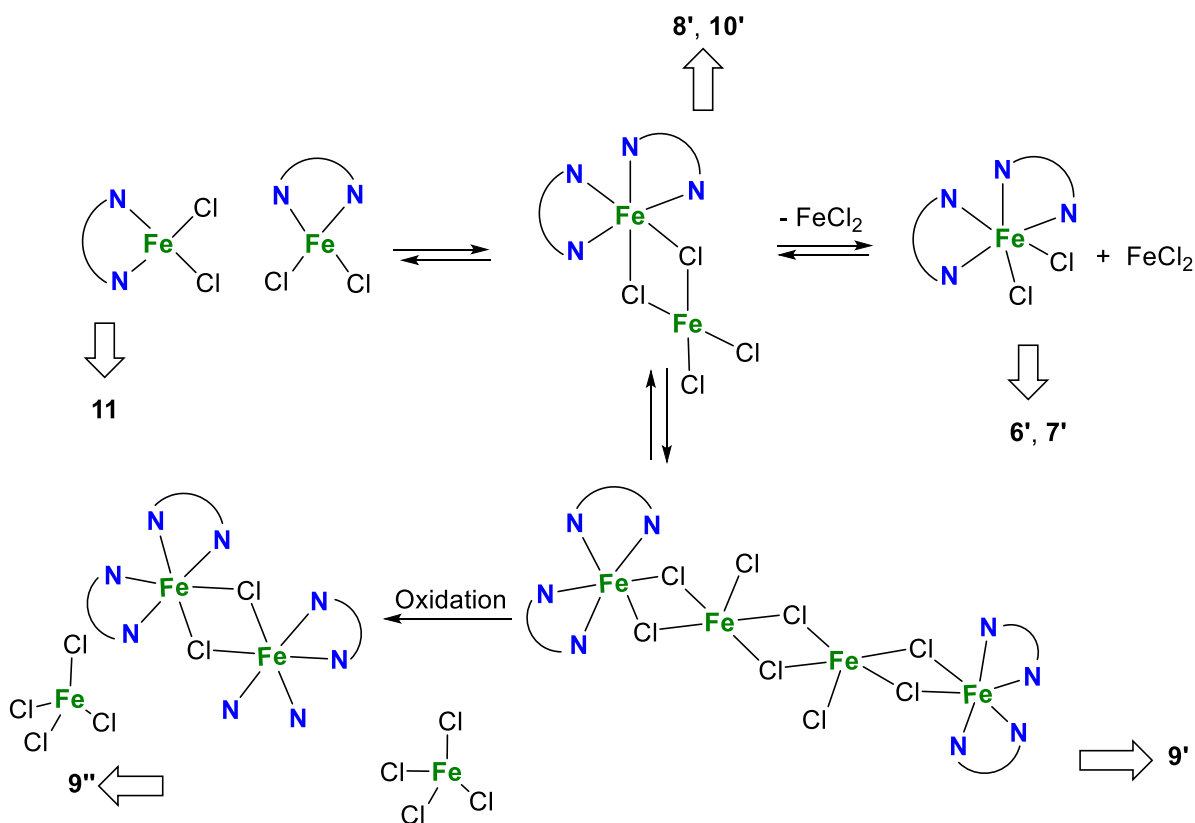
Scheme 3.4. Structural rearrangement of complexes **6'-10'** during the recrystallization

    With respect to the structural differences between complexes **6'**, **7'** and **8'-10'**, we can notice that complexes **6'** and **7'** were structurally derived from complexes **8'-10'** after a loss of one FeCl₂ unit as demonstrated in Scheme 3.4. The loss of free FeCl₂ was apparent during the recrystallization of **6** and **7,** where apart from the single crystals, one could also observe the appearance of yellow/grey salt in the reaction medium. Surprisingly, this also means that a slight addition of electron density on the iron center will favor the formation of binuclear system (**8'** and **10'**). Further, the binuclear structure can dimerize to form the tetranuclear system **9',** to rebalance the decreasing electron density on each iron center. The decrease in electron density occurs probably due to the relatively increased (-I) inductive effect conferred by the presence of 2,3,4,5,6-pentafluorophenyl group when compared to 3,5-bis(trifluoromethyl)phenyl group. Lastly, as observed earlier, the tetranuclear system **9'** can possibly rearrange further to form a mixed bivalent ion pair **9''** (a binuclear cation and a set of mononuclear anions) due to the oxidation of iron that

occurs most likely from the prolonged recrystallization period. At this stage, we could not draw any more rational conclusions but the calculation of electron density on the iron center *via* DFT studies could provide some insights regarding the structural evolution of this newly developed series of complexes.

3.2.2. Polymerization studies with iminopyridine/iminoquinoline iron-based complexes

3.2.2.1. Polymerization of isoprene with complexes 6–11

3.2.2.1.1 Assessment of 6–11/Al^{i}Bu$_3$/[Ph$_3$C][B(C$_6$F$_5$)$_4$] catalytic system

The newly developed series of iron (II) complexes **6-11** were assessed as pre-catalysts for the polymerization of isoprene. In the last chapter, we have already tested various combinations of pre-catalyst/co-catalyst systems such as Fe/MAO, Fe/AlEt$_3$/[Ph$_3$C][B(C$_6$F$_5$)$_4$] and Fe/Al^{i}Bu$_3$/[Ph$_3$C][B(C$_6$F$_5$)$_4$] and then concluded, through a detailed study, that the Al^{i}Bu$_3$/[Ph$_3$C][B(C$_6$F$_5$)$_4$] (3/1) combination was the preferred choice for activating the iron (II) pre-catalysts. Therefore, we conducted the polymerization of isoprene by using the catalytic system **6–11**/Al^{i}Bu$_3$/[Ph$_3$C][B(C$_6$F$_5$)$_4$] in a ratio of 1/3/1, respectively, the results of which are displayed in Table 3.7 below.

Table 3.7. Polymerization of isoprene using **6–11**/Al^{i}Bu$_3$/[Ph$_3$C][B(C$_6$F$_5$)$_4$] catalytic systems [a]

Entry [a]	Complex	Conv. (%)	$M_{n(exp)}$ [b] (g/mol)	Đ [b]	Microstructure [c] (%)	
					1,4 (*trans*/*cis*)	3,4
1	**6**	97	279 000	1.9	55 (0/55)	45
2	**7**	70	276 000	2.1	55 (0/55)	45
3	**8**	>99	217 800	1.8	59 (0/59)	41
4	**9**	>99	105 000	2.2	54 (0/54)	46
5	**10**	<1	-	-	-	-
6	**11**	<1	-	-	-	-

[a] Polymerization conditions: 10 µmol of Fe (II) complex; Isoprene/Fe/Al^{i}Bu$_3$/[Ph$_3$C][B(C$_6$F$_5$)$_4$] = 500/1/3/1; toluene = 5 mL; [C]isoprene = 1 mol/L; time = 1 h; temperature = 25 °C; [b] determined by SEC analysis in THF using polystyrene standards; [c] determined by ^{1}H NMR and ^{13}C NMR; $M_{n(th)}$ = 33 700 g/mol (considering one growing chain per metal center); TOF (h^{-1}) = 485 for **6**, 350 for **7** and >500 for **8-9**.

From the results in Table 3.7, the complexes **6–9** proved to be highly active for the polymerization of isoprene with total conversion of 500 eqs. of monomer per iron catalyst within

1 h (TOF > 350 h^{-1}). Analysis of the resulting (PIs) by SEC revealed that the ternary **6**–**7**/Al^{i}Bu$_3$/[Ph$_3$C][B(C$_6$F$_5$)$_4$] catalytic systems produced very high molecular weight PIs with M_n >276 kg/mol (Table 3.7, Entries 1 and 2). The polymerization was less controlled compared to the alkylated *N*-aryl iminopyridine iron catalysts **1**-**4** as the system displays broad dispersities ($Đ$ = 1.9-2.1) and the M_n obtained are nearly 8 times higher than expected ($M_{n,theo}$ = 33 700 g/mol), speaking in favor of a very high chain propagation rate than initiation step. This also means that only 12-13% (considering no chain transfer to Al) of the fluorinated aldiminopyridine catalyst **6**–**7**/Al^{i}Bu$_3$/[Ph$_3$C][B(C$_6$F$_5$)$_4$] is active for the polymerization. The polymerization of isoprene was comparably more controlled with the complexes **8** and **9** as the resulting systems produced 3 to 6 times higher M_n (>105 kg/mol) than expected, although displaying broad dispersity, like their aldiminopyridine analogues (Table 3.7, Entries 3 and 4). Regardless of the structural difference between aldimines *vs*. ketimines, one can say that faster chain propagation than initiation occurs with the fluorinated pre-catalysts **6**–**9.** It is also worthy to notice that the replacement of iminopyridine skeleton with an iminoquinoline skeleton directly affects the catalytic activity of the resulting systems generated from the complexes **10** and **11**. The systems **10**–**11**/Al^{i}Bu$_3$/[Ph$_3$C][B(C$_6$F$_5$)$_4$] were found to be inactive for the isoprene polymerization, probably owing to the increased steric hindrance around the iron center resulting in a very poor propagation. These results compare well with related iron-based catalysts available in the literature.[47]

The acquired polyisoprenes were also analysed *via* NMR spectroscopy studies to determine their microstructure content. The microstructure content of all the polyisoprenes prepared from Table 3.7 (Entries 1 to 4) are presented in Figure 3.11. As an example, the corresponding ^{1}H and ^{13}C NMR spectra for the polyisoprene obtained in entry 3, Table 3.7 are displayed in Figure 3.12.
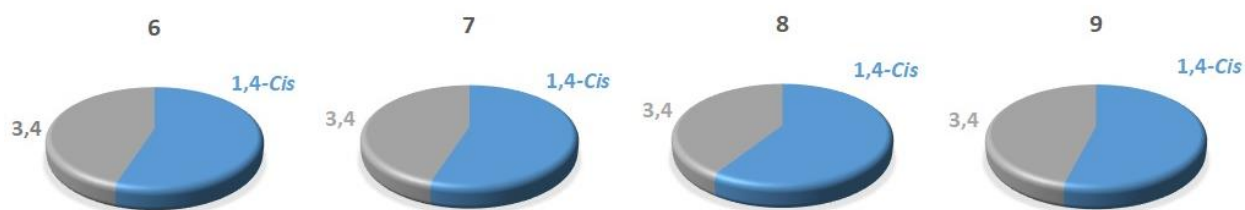
Figure 3.11. Microstructure content of the polyisoprene obtained from **6**–**9**/Al^{i}Bu$_3$/[Ph$_3$C][B(C$_6$F$_5$)$_4$]

a) **¹H NMR spectrum**
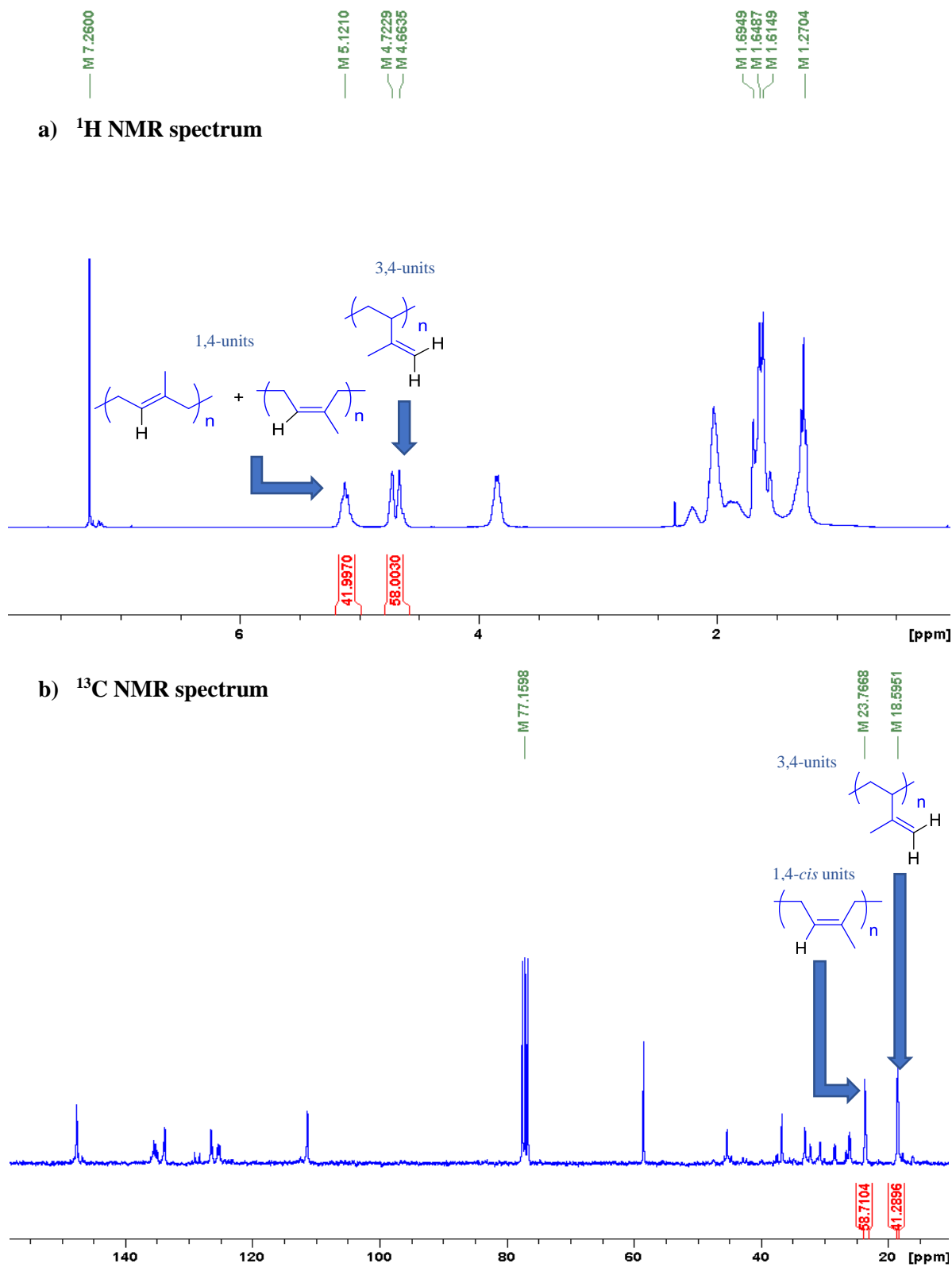
b) **¹³C NMR spectrum**

Figure 3.12. NMR spectra (in CDCl₃) of the PI obtained from **8**/Al^{i}Bu₃/[Ph₃C][B(C₆F₅)₄] (Table 3.7, Entry 3) showing the characteristic resonances of 1,4- and 3,4-units (a, ¹H NMR) and *trans*/*cis* configuration (b, ¹³C NMR)

The polyisoprene obtained from the ternary fluorinated aldimino-pyridine **6**–**7**/Al^{i}Bu$_3$/[Ph$_3$C][B(C$_6$F$_5$)$_4$] catalytic system contained a significant fraction of 3,4-motifs (45%) along with the higher percentage of 1,4 motifs (55%) (Table 3.7, Entries 1 and 2). Interestingly, the 1,4 units only exhibit a *cis* configuration. The modification of **6** and **7** by changing the imino substituent of the ligand from H to CH$_3$ (aldimino-pyridine, -*H*C=N- *vs* ketimino-pyridine, -C*H$_3$*C=N-) had no impact on the selectivity for the pre-catalysts **8** and **9** as they still exhibited a unique 1,4-*cis* configuration (Table 3.7, Entries 3 and 4)**.** These results are in contrast to the results obtained with the alkylated iminopyridine complexes **1–4** in chapter 2 where the ketimines were found to afford 1,4-*trans* selective catalysts at room temperature. This unique trend of selectivity for the fluorinated iminopyridine complexes **6**–**9** is clearly the result of a polymerization process that is governed by kinetic rather than thermodynamic parameters, as already reported with parent iron complexes supported by electron withdrawing fluorinated-aryl-substituted aldimino-pyridine ligands in combination with an excess of MAO**.**[15]

3.2.2.1.2. *Kinetic profile of the polymerization of isoprene with the iron-based complexes* **6**–**9**

After the successful assessment of **6**–**9**/Al^{i}Bu$_3$/[Ph$_3$C][B(C$_6$F$_5$)$_4$] catalytic system, the polymerization processes were further optimized by assessing the kinetic parameters of the polymerization with **6**–**9**/Al^{i}Bu$_3$/Ph$_3$C[B(C$_6$F$_5$)$_4$] (1/3/1) catalytic combinations at room temperature. As previously done in the last chapter, the studies were again carried out with 5000 eqs. of isoprene to ensure better reliability, as the highly active systems prevented us from correctly evaluating the kinetics at 500, 1000 and 2000 eqs. of isoprene/Fe. Aliquots were taken at different times during the course of the polymerization to determine the conversions *via* ^{1}H NMR as shown below in Figure 3.13. The molecular characteristics of the last sample of polyisoprene for each polymerization run are presented in Table 3.8.
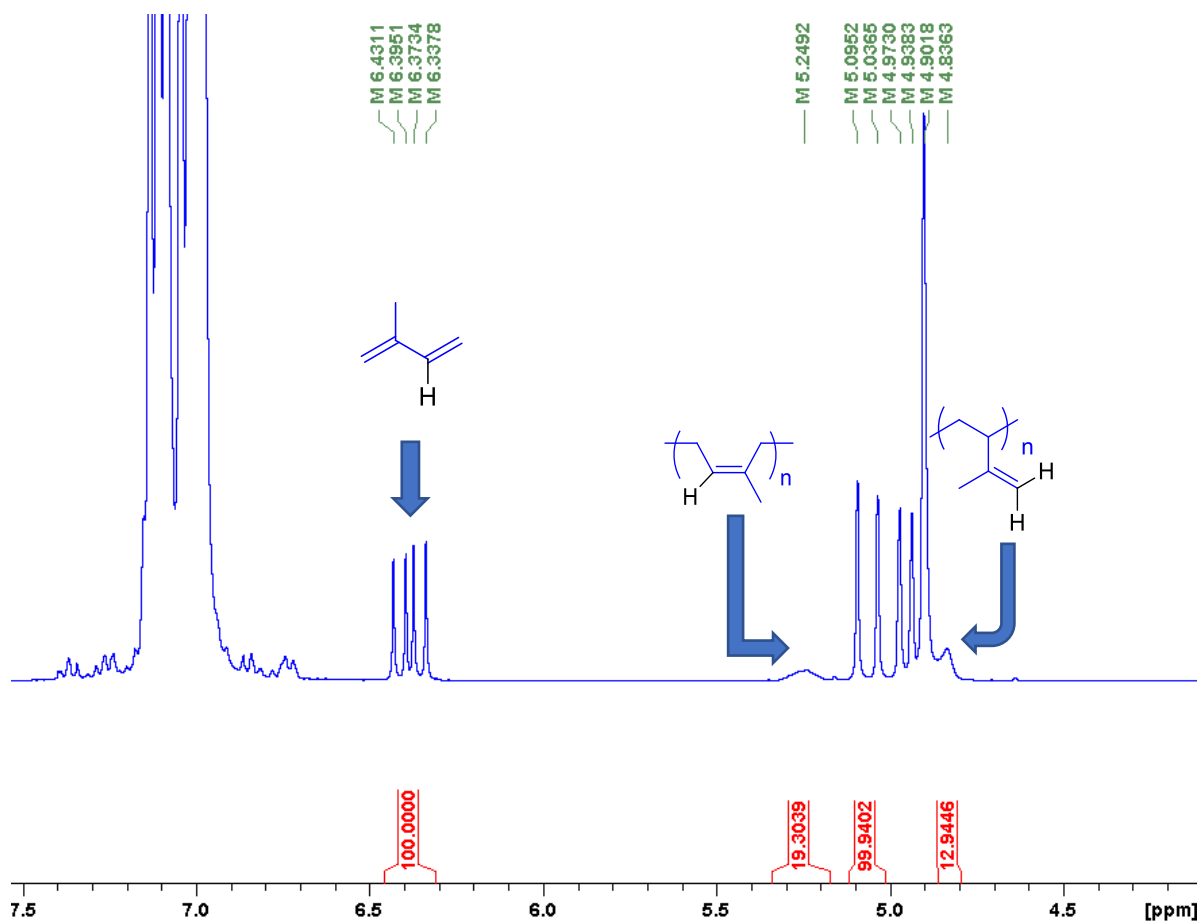
Figure 3.13. Determining the conversion (21%, Table 3.8, Entry 1) of isoprene by ^{1}H NMR of the aliquot

Table 3.8. Polymerization of 5000 eqs. of isoprene/Fe using **6–9**/Al^{i}Bu$_3$/[Ph$_3$C][B(C$_6$F$_5$)$_4$] catalytic systems [a]

Entry	Complex	Conv. (%)	Time (min)	TOF (h^{-1})	$M_{n(exp)}$ [b] (g/mol)	Đ [b]	Microstruc. [c] (%) 1,4 (*trans*/*cis*)	3,4
1	**6**	21	10	6 300	331 000	2.6	55 (0/55)	45
2	**7**	9	13	2 076	215 000	3.3	55 (0/55)	45
3	**8**	>99	<1	>300 000	323 000	1.7	58 (0/58)	42
4	**9**	>99	<1	>300 000	213 000	1.6	54 (0/56)	46

[a] Polymerization conditions: 5 µmol of Fe (II) complex; Isoprene/Al^{i}Bu$_3$/[Ph$_3$C][B(C$_6$F$_5$)$_4$]/Fe = 5000/3/1/1; toluene = 25 mL; [C]isoprene = 1 mol/L; time = 1 h; temperature = 25 °C; [b] determined by SEC analysis in THF using polystyrene standards; [c] determined by ^{1}H NMR and ^{13}C NMR

157
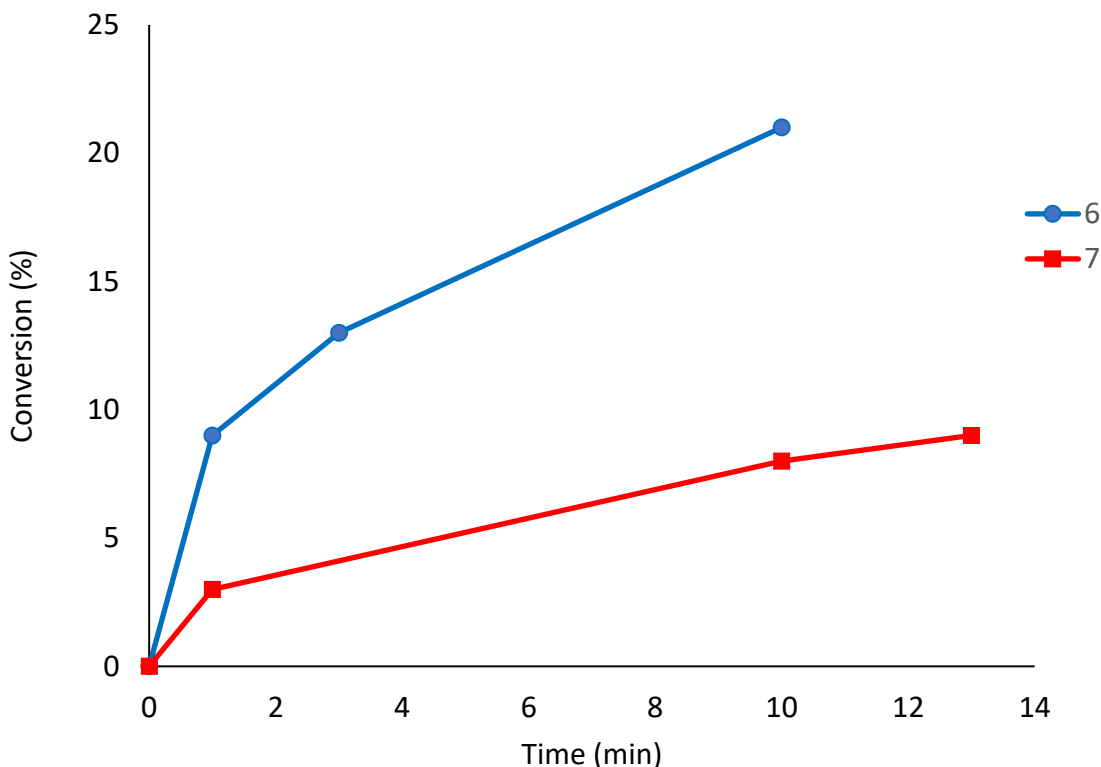
Figure 3.14. Monomer conversion (τ) in function of time for pre-catalysts **6** and **7**
($Isoprene/Al^iBu_3/[Ph_3C][B(C_6F_5)_4]/Fe = 5000/3/1/1$)

In comparison with the assessment of the kinetic profiles with complexes **1** to **4**, the addition of isoprene to a solution containing the catalyst (complexes **6-9**) instantly turned the polymerization mixture into a thick and viscous medium, followed by the formation of gel most likely due to the formation of PI with high M_n. Due to this reason, we could not take more aliquots to determine the conversion after a certain stage (formation of gel) for each catalyst (Figure 3.14). In particular, the kinetic assessments of complexes **8** and **9** could not be obtained because of their extremely high reactivity: full conversion was obtained in less than 1 min (even in 15 s, full conversion was observed), along with notable exothermicity for both pre-catalysts. In each case, the selectivity was maintained throughout as observed previously in the last section. In addition, as expected, the resulting catalysts produced very high molecular weight polyisoprenes (M_n >213 kg/mol) with broad dispersity for **6** & **7** indicating that the polymerization is not controlled (Table 3.8, Entries 1-4).

From the profile of the plot of conversion *vs* time (Figure 3.14), the activity of the complexes in the catalytic combinations is in the order of **8** ≈ **9** (TOF > 1 000 000 h^{-1}, considering that full conversion was obtained in less than 15 seconds) >> **6** (TOF = 6 300 h^{-1}) > **7** (TOF = 2 076 h^{-1}). Thus, the various pre-catalysts when employed for isoprene polymerization were found to be highly active by comparison with data from the literature.[47] The catalysts based on complex **6** and **7** displayed the lowest activity when compared to the alkylated iminopyridine complexes **1**–**3** (TOF > 12 450 h^{-1}) whereas the complexes **8** and **9** were found to be the most active within the developed series of pre-catalysts **1**–**8**.[19] These results could be attributed to the enhanced coordination of the monomer conferred by the presence of electron withdrawing group (-F, -CF$_3$) that reduces the electron density at the iron center. This, in turn, is followed by migratory-insertion of monomer in the growing polymer chain, which is favored by electron rich ketimine, thereby, leading to very high propagation and proving to be highly effective. Additionally, the fluorinated ketimine complexes **8** and **9**, to our knowledge, display the highest activities reported to date for an iron-catalyzed polymerization of isoprene.[47]

3.2.2.1.3. Temperature dependence of the polymerization of Isoprene with complexes **6**–**9**

As indicated in the last section, we observed an instantaneous increase in the viscosity of the reaction medium when conducting isoprene polymerization experiments at room temperature using the complexes **6**–**9**. We anticipated that the temperature might influence the high rate of propagation and exothermicity associated with these catalytic systems. As a result, the polymerization of isoprene was assessed at low temperatures using pre-catalysts **6**–**9** in presence of Al^{i}Bu$_3$/Ph$_3$C[B(C$_6$F$_5$)$_4$] for a sake of better control and improvement of the selectivity (*vide infra*).

Table 3.9. Polymerization of isoprene at lower temperatures with pre-catalysts **6–9** [a]

Entry	Fe	T (°C)	Time (min)	Conv. (%)	TOF (h⁻¹)	$M_{n(exp)}$ [b] (g/mol)	Đ [b]	Microstruc.[c] (%) 1,4 (*trans*/*cis*)	3,4
1		– 40	300	trace	-	-	-	-	-
2	**6**	0	300	trace	-	-	-	-	-
3		– 40	300	trace	-	-	-	-	-
4	**7**	0	300	trace	-	-	-	-	-
5		0	10	>99	3 000	294 000	1.2	58 (0/58)	42
6		– 20	10	>99	3 000	251 000	1.3	58 (0/58)	42
7	**8**	– 40	10	>99	3 000	173 000	1.3	58 (0/58)	42
8		– 78	480	trace	-	-	-	-	-
9		– 40	10	>99	3 000	274 500	1.2	54 (0/54)	46
10	**9**	– 78	180	traces	-	-	-	-	-

[a] Polymerization conditions: 10 µmol of Fe(II) complex; Isoprene/Al^{i}Bu$_3$/Ph$_3$C[B(C$_6$F$_5$)$_4$]/Fe = 500/3/1/1; toluene = 5 mL; [C]i$_{soprene}$ = 1 mol/L in toluene reaction times have not been optimized; [b] determined SEC analysis in THF using polystyrene standards; [c] determined by ^{1}H NMR and ^{13}C NMR.

The catalysts originating from complexes **6** and **7**, when assessed for polymerization at -40 °C, yielded traces of polymers (Table 3.9, Entries 1 and 3). Even when the temperature was increased to 0 °C, the system **6**–**7**/Al^{i}Bu$_3$ /[Ph$_3$C][B(C$_6$F$_5$)$_4$] was found inactive, reflecting a probable lack of initiation at low temperatures or chain propagation (Table 3.9, Entries 2 and 4). In contrast, the ternary **8** and **9**/Al^{i}Bu$_3$/Ph$_3$C[B(C$_6$F$_5$)$_4$] systems displayed high catalytic activity at low temperatures down to -40 °C (TOF = 3 000 h^{-1}); interestingly, the selectivity for 1,4 and 3,4 motifs was maintained throughout all the experiments (Table 3.9, Entries 5–7 and 9). The polymerization at low temperatures was found to be more controlled in terms of dispersities (Đ = 1.2-1.3 *vs* 1.8-2.2) which speaks in favor of slow initiation whereas the propagation was still high owing to the similar trend of obtaining high molecular weight polyisoprenes.. Reducing the polymerization temperature to -78 °C drastically decreases the high catalytic activity of the system **8**–**9**/Al^{i}Bu$_3$/[Ph$_3$C][B(C$_6$F$_5$)$_4$], as a result of which, traces of polymer were isolated from the polymerization (Table 3.9, Entries 8 and 10), reflecting again a probable lack of initiation at this temperature. These observations reflect the temperature dependence on the activity of each

catalyst, while the temperature does not influence the selectivity of the catalytic systems based on complexes **8**-**9**, reflecting the fact that the selectivity in this case is thermodynamically governed (Figure 3.15).
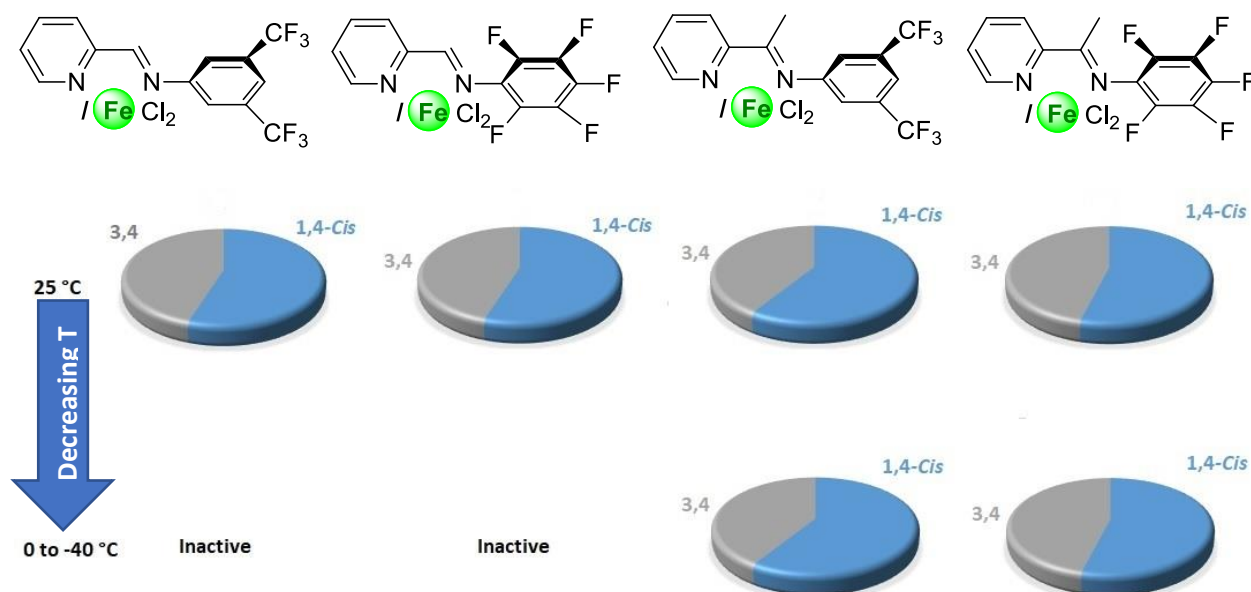
Figure 3.15. Temperature dependence on the selectivity of the complexes **6–9**

3.2.2.2. Polymerization of styrene with complexes 8, 9 and 11

In the last chapter, we assessed the alkylated *N*-aryl iminopyridine iron complexes **3–5** for the polymerization of styrene, where we observed that these complexes with a combination of $Al(^iBu)_3/[Ph_3C][B(C_6F_5)_4]$ or $AlMe_3/[Ph_3C][B(C_6F_5)_4]$ generated active albeit fairly stereoselective (53% $Al(^iBu)_3/[Ph_3C][B(C_6F_5)_4]$) catalytic systems for the polymerization of styrene. In a similar way, the newly developed series of complexes was also screened for the polymerization of styrene. The highly active catalytic systems **8-9**/$Al(^iBu)_3/[Ph_3C][B(C_6F_5)_4]$ and the inactive **11**/ $Al(^iBu)_3/[Ph_3C][B(C_6F_5)_4]$ catalytic system for isoprene polymerization were assessed as potential catalysts for the coordinative polymerization of styrene, the results of which are displayed in Table 3.10 below.

Table 3.10. Polymerization of styrene using the pre-catalysts **10** and **11**

Entry [a]	Fe	Activation	Time (h)	Yield (%)	$M_{n(exp)}$ [b] (g/mol)	*Đ* [b]	Tacticity [c] (rr/mr/mm) (%)
1	**8**	$Al(^iBu)_3/[Ph_3C][B(C_6F_5)_4]$	1	82	2 900	2.2	43/30/27
2	**9**	$Al(^iBu)_3/[Ph_3C][B(C_6F_5)_4]$	1	81	2 800	2.3	56/23/21
3	**11**	$Al(^iBu)_3/[Ph_3C][B(C_6F_5)_4]$	1	68	2 200	1.8	43/29/28
4		$Al(Me)_3/[Ph_3C][B(C_6F_5)_4]$	1	80	1 700	2.4	46/31/23

[a] Polymerization conditions: 10 µmol of Fe; Styrene/Alkylaluminium/$Ph_3C[B(C_6F_5)_4]$/Fe = 500/3/1/1; toluene = 5 mL; temperature = 23 °C; [b] determined by SEC analysis in THF using polystyrene standards; [c] determined by ^{13}C NMR.

All the resulting polystyrenes were characterized by ^1H and ^{13}C NMR spectroscopy to determine their tacticity as seen previously in the chapter 2 (Figure 2.9, Section 2.2.8). From the results displayed in Table 3.10, we can observe that the catalytic system resulting from **8**/$Al(^iBu)_3/[Ph_3C][B(C_6F_5)_4]$ was found to be active (TOF (h^{-1}) = 410) for styrene polymerization, producing syndiotactic enriched atactic polystyrene ($rr = 43\%$) with an excellent conversion (82%) within 1 h (Table 3.10, Entry 1). The related ketiminopyridine complex **9**, when employed for styrene polymerization, worked in a similar fashion as complex **8**, although improving the syndiotactic triad content up to $rr = 56\%$, which indicates the effect of pre-catalyst governing the stereoselectivity of the polymerization (Table 3.10, Entry 2). In contrast to isoprene polymerization, where the system **11**/$Al(^iBu)_3/[Ph_3C][B(C_6F_5)_4]$ was found to be inactive, the same

catalyst was found to be effective for styrene polymerization, producing syndiotactic enriched (*rr* = 43%) atactic polystyrene with a good conversion (68%) within 1 h (Table 3.10, Entry 3). The huge difference in the activities of the same catalytic system for different monomers arises probably due to the difference in their respective chain propagations, where the insertion of styrene between the Fe-^{i}Bu bond is much faster compared to the isoprene insertion. The same complex **11**, bearing bulky substituted iminoquinoline skeleton when activated with less bulkier co-catalyst Al(Me)$_3$/[Ph$_3$C][B(C$_6$F$_5$)$_4$], produced again syndiotactic enriched atactic polystyrene but this time with a slight improvement of the conversions to 80% (TOF (h^{-1}) = 400) in 1 hour (Table 3.10, Entry 4). From these results, we can see the influence of co-catalyst on the activity of the generated catalysts for the polymerization, however, no significant difference was observed within the selectivities of each catalytic system. It is also worthy to notice that no matter if the *N*-aryl substituents of the iminopyridine skeleton are electron donating (**1**–**5**) or electron withdrawing (**6**–**9**) groups, the resulting catalysts will generate every time a syndiotactic enriched atactic polystyrene which highlights the absence of selectivity dependence on the nature of substituents, unlike that observed in the case of polyisoprene where the selectivity was varying with the nature of the *N*-aryl substituents.

The acquired polystyrenes from complexes **8**, **9** and **11**, were also characterized by SEC analysis for the determination of their mass average molar masses. The dispersity varied from narrow to broad (Table 3.10, Entries 1-4) but, in each case, the M_n of the resulting polyisoprenes were still found in the range of 1700-2000 g/mol, which are below the expected M_n. This again implies that the resulting iron iminopyridine/iminoquinoline catalysts display a non-living character that might occur from the frequent occurrence of chain termination reactions such as *β*-H elimination, leading to the formation of short chain oligomers with relatively low M_n values.

3.3. Conclusion:

In this chapter, we synthesized a novel family of iron (II) iminopyridine/iminoquinoline complexes bearing electron withdrawing fluorinated substituents on the *N*-aryl position. All these new paramagnetic complexes were characterized by ^{1}H NMR, IR and elemental analysis for most of them. The molecular structures of these complexes were determined by single crystal X-ray diffraction studies where it was observed that the aldiminopyridine complexes **6** and **7** existed as bis-ligand mononuclear complexes in the solid state whereas their ketiminopyridine analogues **8** and **9** were found to exist as symmetrical binuclear coordinated complexes, moreover in the form of a tetranuclear bridged assembly for **9**. The modification of the iminopyridine skeleton to the bulkier iminoquinoline resulted to the attainment of similar type of geometry for the aldiminoquinoline system **10** from which we could see the steric influence of quinoline as well as the influence of CF_3 groups on *N*-aryl moiety governing the structure. Further modification to the iminoquinoline skeleton by replacing a 5-membered chelate to a 6-membered chelate comprising a bulkier *N*-aryl moiety no longer favored the attainment of binuclear geometry due to the increased steric bulk around the iron center which is already observed in the case of iminopyridines.[32] In a conclusive manner, we suggest that apart from the steric demands of the ligand skeleton, the presence of various electronic effects such as H···F, F···F contacts and $\pi - \pi$ stacking within the assembly of these complexes also govern the resulting geometry of these systems.

Regarding the catalytic application of the new series of iron complexes **6-11** in the polymerization of isoprene, we observed that the activity of the catalytic system based on iminopyridine-iron complexes is again related to the electron density on the iron center and, to a lesser extent, to the environment of the coordination sphere at the metal center. Indeed, the addition of fluorinated *N*-aryl substituents decreases the electron density on the iron center, resulting in better coordination of the incoming monomer that might enhance the chain initiation. In contrast to the alkylated *N*-aryl iminopyridine complexes **1-4**, where the presence of H on the imino carbon in **1** and **2** led to the formation of highly active catalysts compared to their ketiminopyridine analogues **3** and **4**, the activity in the case of fluorinated catalysts increased with the addition of methyl group on the imino carbon (**6**, **7** *vs* **8**, **9**) which favors the migratory-insertion and therefore increases the chain propagation. From this observation, it is proposed that the simultaneous

acceptor inductive effect (-I) of fluorinated *N*-aryl substituents and the donor inductive effect (+I) of methyl group on the imino substituent of the ligands **L8** and **L9** collectively enhances the activity of the resulting catalysts **8** and **9**, which are extremely active (TOF > 1 000 000 h^{-1}) as well as most effective among the families of iron-catalyzed polymerization of isoprene described to date.[19,47] On the other hand, increasing the steric hindrance by substitution of the iminopyridine skeleton with a bulkier iminoquinoline skeleton drastically decreases the activity of the resulting precatalysts (**10** and **11**), which could be attributed to the difficulty of the incoming monomer to coordinate with the active species or to insert itself within the polymer chain through propagation (Chart 3.2).
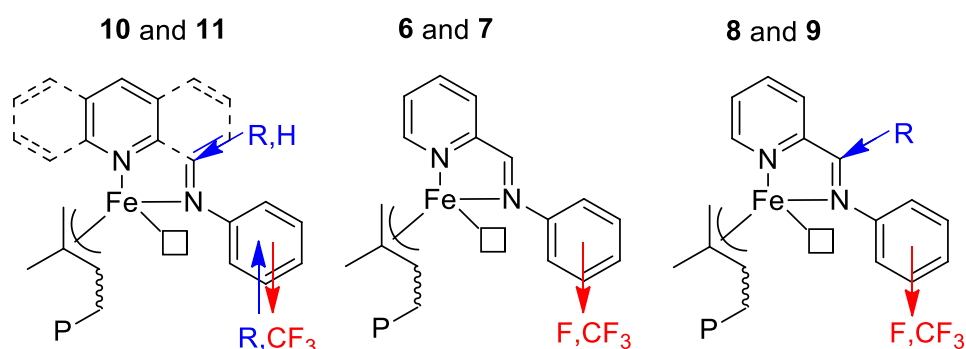
Activity	Inactive	Moderate at room temperature/Inactive at low temperatures	Extremely active at room and low temperatures
Selectivity	-	Fairly 1,4-*cis* (55%)	Fairly 1,4-*cis* (58%)

Chart 3.2. Structure-properties relationships in iminopyridine iron-based catalysts derived from **6-11**

In terms of selectivity, the electronic effect of fluorinated *N*-aryl substituent in **6-9** leads to a fair 1,4-*cis* selectivity (up to 58%) with a substantial amount of 3,4, presumably due to a preferential η^4-*cis* or η^2-*trans* coordination of the incoming monomer (Chapter 1, Scheme 1.5). These results are in line with previous experiments done by the group of Wang with fluorinated *N*-aryl substituted aldiminopyridine iron complexes activated with MAO.[15] Interestingly, the iron catalytic systems based on **6-9** are not temperature dependent in terms of regio- and stereo-selectivity, whereas a significant effect in terms of catalytic activity of these systems is observed (Chart 3.2).

As done previously in the last chapter with complexes **3–5**, the catalytic systems resulting from the newly developed iron complexes **8**, **9** and **11** were also employed for styrene polymerization, which were found to be active at room temperature. In contrast to isoprene polymerization, the various catalytic systems derived from complex **11** were found to be active for styrene polymerization highlighting the role of chain propagation between the Fe-^{i}Bu bond, which is probably poor in the case of isoprene with that complex. All the catalytic systems derived from the pre-catalysts **8**, **9** and **11** produced moderately syndiotactic-enriched (up to 56%) polystyrenes with good conversions (up to 82%) but, unfortunately, polystyrenes with low M_n (2100–3000 g/mol, chapter 2, Scheme 2.7) were obtained, presumably due to frequent occurrence of β-H elimination reactions. These results imply that there is no significant effect of electronic properties of the iminopyridine/iminoquinoline skeleton on the polymerization of styrene, which is rather uncontrolled in terms of dispersity. Further modifications/developments are needed in the future to avoid the recurring chain termination pathways in the iminopyridine-iron (II) catalyzed coordinative polymerization of styrene. Another advancement would be the attempt to copolymerize isoprene and styrene under statistical conditions.

3.4 Experimental Section:

3.4.1. General Considerations

Toluene, THF, dichloromethane, diethyl ether, pentane and acetonitrile were purified through an alumina column (Mbraun, Mérignac, France), stored, trap-to-trap distilled over sodium/benzophenone, and stored on 4 Å molecular sieves in a glove box before used. The organic reagents (Quinoline and aniline derivatives) were acquired from Sigma-Aldrich or Fischer Scientific S.A.S. (Illkrich, France), and used as received. Single-crystal X-ray measurements were performed at 100 K. The data were collected using an Apex II CCD 4K Bruker diffractometer (λ = 0.71073 Å). The structures were solved using SHELXT[48] and refined by least-squares procedures on F2 using SHELXL.[49] The remaining procedures are similar as described in section 2.4.1.

Table 3.11. Crystal and Refinement data for ligands **L10** and **L11**

Parameters	L10	L11
Chemical Formula	$C_{18}H_{10}F_6N_2$	$C_{22}H_{24}N_2$
Formula Weight	368.28	316.43
Crystal system	Monoclinic	Triclinic
Space group	$P2_1/c$	$P\overline{1}$
a	14.8818 (4)	8.7725 (16)
b	7.1089 (2)	9.0688 (16)
c	15.2136 (4)	13.816 (2)
α	90	71.726 (9)
β	103.120 (1)	72.429 (9)
γ	90	66.219 (8)
V(Å^3)	1567.48 (7)	935.4 (3)
Z	4	2
D$_{calc}$(g/cm^3)	-	-
μ (Mo-K_α) (mm^{-1})	0.14	0.07
$R_{int,} R[F^2 > 2\sigma(F^2)]$	0.043, 0.038	0.033, 0.050

Table 3.12. Crystal and Refinement data for complexes **6'** and **7'**

Parameters	6'	7'
Chemical Formula	$C_{28}H_{16}Cl_2F_{12}FeN_4 \cdot 2(C_2H_3N)$	$C_{24}H_{10}Cl_2F_{10}FeN_4$
Formula Weight	845.30	671.11
Crystal system	Monoclinic	Monoclinic
Space group	*P2$_1$/n*	*C2/c*
a	16.0481 (6)	22.3132 (9)
b	13.5780 (5)	15.8815 (7)
c	17.9533 (9)	14.0527 (6)
β *($\alpha= \gamma = 90°$)*	116.470 (2)	99.413 (2)
V(Å^3)	3501.9 (3)	4912.8 (4)
Z	4	8
D$_{calc}$(g/cm^3)	-	-
μ (Mo-K_α) (mm^{-1})	0.68	0.93
$R_{int}, R[F^2 > 2\sigma(F^2)]$	0.038, 0.044	0.040, 0.024

Table 3.13. Crystal and Refinement data for complexes **8'** and **9'**

Parameters	8'	9'
Chemical Formula	$C_{30}H_{20}Cl_4F_{12}Fe_2N_4 \cdot 2(C_2H_3N)$	$C_{52}H_{28}Cl_8F_{20}Fe_4N_8.4(C_2H_3N)$
Formula Weight	1006.13	1816.04
Crystal system	Monoclinic	Orthorhombic
Space group	*C2/c*	*Pbca*
a	19.4428 (17)	18.4331 (13)
b	15.3909 (13)	17.2242 (10)
c	16.9388 (15)	22.3241 (15)
β *($\alpha= \gamma = 90°$)*	123.558 (4)	-
V(Å^3)	4224.0 (7)	7087.8 (8)
Z	4	4
D$_{calc}$(g/cm^3)	1.582	1.702
μ (Mo-K_α) (mm^{-1})	1.03	1.21
$R_{int}, R[F^2 > 2\sigma(F^2)]$	0.049, 0.047	0.054, 0.036

Table 3.14. Crystal and Refinement data for complexes **9''**, **10'** and **11**

Parameters	9''	10'	11
Chemical Formula	$C_{52}H_{28}Cl_{10}F_{20}Fe_4N_8$	$C_{36}H_{20}Cl_4F_{12}Fe_2N_4$	$C_{22}H_{24}Cl_2FeN_2$
Formula Weight	1722.72	495.03	443.18
Crystal system	Triclinic	Monoclinic	Monoclinic
Space group	$P\bar{1}$	$P2_1/c$	$P2_1/n$
a	14.3901 (10)	17.4369 (10)	10.2153 (4)
b	16.7636 (12)	24.1888 (15)	16.2405 (7)
c	27.979 (2)	19.9519 (13)	12.4209 (4)
α	99.185 (3)	90	90
β	98.568 (3)	89.955 (4)	95.670 (2)
γ	94.162 (3)	90	90
$V(\text{Å}^3)$	6556.2 (8)	8415.3 (9)	2050.57 (14)
Z	4	17	4
$D_{calc}(g/cm^3)$	-	-	-
μ (Mo-K_α) (mm^{-1})	1.38	1.09	1.00
$R_{int}, R[F^2 > 2\sigma(F^2)]$	0.058, 0.095	0.086, 0.055	0.068, 0.039

3.4.2. General Procedure for the Synthesis of Ligands L6–L10

A solution of 3 5-bis(trifluoromethyl)aniline/2,3,4,5,6-pentafluoroaniline (8 mmol) and 2-pyridinecarboxaldehyde/2-acetylpyridine/2-quinolinecarboxaldehyde (10 mmol) in dry DCM (15 mL) was prepared in an ace pressure tube equipped with a magnetic stirrer. A catalytic amount of p‑toluenesulfonic acid (PTSA) and sodium sulphate (1g) was added subsequently before the mixture was refluxed overnight at 80 °C (Scheme 3.5). The reaction mixture was filtered over whatman paper, concentrated under reduced pressure to obtain a viscous crude which was further recrystallized in dry pentane at -40 °C.

Scheme 3.5. Synthetic strategy for ligands
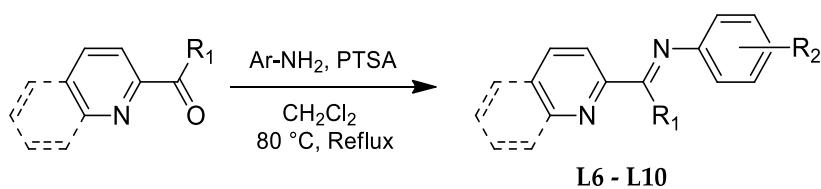
	L6	L7	L8	L9	L10
R$_1$ =	H	H	CH$_3$	CH$_3$	H
R$_2$ =	3,5-CF$_3$	2,3,4,5,6-F	3,5-CF$_3$	2,3,4,5,6-F	3,5-CF$_3$

N-(3,5-bis(trifluoromethyl)phenyl)-1-(pyridin-2-yl)methanimine (**L6**): orange crystals. Yield: 88%. ^{1}H NMR (300 MHz, C$_6$D$_6$, 25 °C) δ (ppm) = 8.47 (dd, $^3J_{HH}$ = 4.8 Hz, $^4J_{HH}$ = 1.7Hz, 1H, H_a), 8.27 (s, 1H, H_b), 8.08 (d, $^3J_{HH}$ = 7.8 Hz, 1H, H_c), 7.56 (s, 1H, H_d), 7.24 (s, 2H, H_e), 7.08 (ddd, $^3J_{HH}$ = 7.8, 7.8 Hz, $^4J_{HH}$ = 1.7Hz, 1H, H_f), 6.66 (dd, $^3J_{HH}$ = 7.8, 4.8 Hz, 1H, H_g) (Figure A11). ^{13}C NMR (75 MHz, C$_6$D$_6$, 25 °C) δ (ppm) = 164.3, 154.5, 152.8, 148.2, 136.8, 136.4, 136.3, 125.6, 123.5, 121.6, 121.4 (Figure A12). ^{19}F NMR (282 MHz, C$_6$D$_6$, 25 °C) δ (ppm) = -62.61 (s, 6F) (Figure A13). IR/cm^{-1} = 1620 ν(C=N). HRMS-ESI (m/z): [M + H]$^+$ calcd for C$_{14}$H$_8$F$_6$N$_2$, 319.0672; found, 319.0679

N-(Perfluorophenyl)-1-(pyridin-2-yl)methanimine (**L7**): brown crystals. Yield: 56% ^{1}H-NMR (300 MHz, C$_6$D$_6$, 25 °C, δ): 8.66 (s, 1H, H_a), 8.41 (dd, $^3J_{HH}$ = 4.8 Hz, $^4J_{HH}$ = 1.7Hz, 1H, H_b), 8.09 (d, $^3J_{HH}$ = 7.8 Hz, 1H, H_c), 6.97 (ddd, $^3J_{HH}$ = 7.8, 7.8 Hz, $^4J_{HH}$ = 1.7 Hz, 1H, H_d), 6.59 (dd, $^3J_{HH}$ = 7.8, 4.8 Hz, 1H, H_e) (Figure A14). ^{13}C NMR (75 MHz, C$_6$D$_6$, 25 °C) δ (ppm) = 170.1, 154.2,

150.1, 142.1, 140.1, 138.5, 136.3, 125.9, 121.6 (Figure A15).^{19}F NMR (282 MHz, C_6D_6, 25 °C) δ (ppm) = -153.4 (dd, J = 21.4, 6.4 Hz, 2F, F_{meta}), -160.3 (t, J = 21.4 Hz, 1F, F_{para}), -163.5 (dd, J = 21.4, 6.4 Hz, 2F, F_{ortho}) (Figure A16). IR/cm^{-1} = 1628 ν(C=N). HRMS-ESI (m/z): [M + H]$^+$ calcd for $C_{12}H_5N_2F_5$, 273.0451; found, 273.0453. Anal. Calcd. for $C_{12}H_5N_2F_5$: C 52.95, H 1.85, N 10.29; found C 53.42, H 2.01, N 10.14.

N-(3,5-bis(Trifluoromethyl)phenyl)-1-(pyridin-2-yl)ethan-1-imine (**L8**): dark yellow crystals Yield: 74%. ^{1}H NMR (300 MHz, CD_2Cl_2, 25 °C, δ): = 8.67 (dd, $^3J_{HH}$ = 4.8 Hz, $^4J_{HH}$ = 1.7 Hz, 1H, H_a), 8.25 (d, $^3J_{HH}$ = 7.8 Hz, 1H, H_c), 7.83 (dd, $^3J_{HH}$ = 7.8, 7.8 Hz, 1H, H_d), 7.65 (s, 1H, H_b), 7.42 (dd, $^3J_{HH}$ = 7.8, 4.8 Hz, 1H, H_e), 7.30 (s, 2H, H_f), 2.37 (s, 3H, H_g) (Figure A17). ^{19}F NMR (282 MHz, CD_2Cl_2, 25 °C, δ): -63.32 (s, 6F) (Figure A18). IR/cm^{-1} = 1649 ν(C=N). HRMS-ESI (m/z): [M + H]$^+$ calcd for $C_{15}H_{10}N_2F_6$, 333.0826; found, 333.0838.

N-(Perfluorophenyl)-1-(pyridin-2-yl)ethan-1-imine (**L9**): orange-brownish crystals. Yield: 44%. ^{1}H NMR (300 MHz, C_6D_6) δ (ppm) = 8.35 (dd, $^3J_{HH}$ = 4.8 Hz, $^4J_{HH}$ = 1.7 Hz, 1H, H_a), 8.25 (d, $^3J_{HH}$ = 7.8 Hz, 1H, H_b), 7.03 (ddd, $^3J_{HH}$ = 7.8, 7.8 Hz, $^4J_{HH}$ = 1.7 Hz, 1H, H_c), 6.63 (dd, $^3J_{HH}$ = 7.8 Hz, $^3J_{HH}$ = 4.8 Hz, 1H, H_d), 2.20 (s, 3H, H_e) (Figure A19). ^{13}C NMR (75 MHz, C_6D_6, 25 °C) δ (ppm) = 175.1, 154.9, 148.5, 139.7, 139.3, 139.1, 138.7, 135.9, 125.4, 121.8, 17.5 (Figure A20). ^{19}F NMR (282 MHz, C_6D_6, 25 °C) δ (ppm) = -152.5 (d, J = 23.8 Hz, 2F, F_{meta}), -163.1 (t, J = 21.7 Hz, 1F, F_{para}), -163.6 (dd, J = 23.8, 21.7 Hz, 2F, F_{ortho}) (Figure A21). IR/cm^{-1} = 1647 ν(C=N). HRMS-ESI (m/z): [M + H]$^+$ calcd for $C_{13}H_7N_2F_5$, 287.0608; found, 287.0617. Anal. Calcd. for $C_{13}H_7N_2F_5$: C 54.56, H 2.47, N 9.79; found C 54.57, H 2.48, N 9.72.

N-(3,5-bis(Trifluoromethyl)phenyl)-1-(quinolin-2-yl)methanimine (**L10**): red crystals. Yield: 95%. ^{1}H NMR (300 MHz, C_6D_6, 25 °C, δ): 8.43 (s,1H, H_a), 8.32 (d, $^3J_{HH}$ = 8.2 Hz, 1H, H_b), 8.26 (d, $^3J_{HH}$ = 8.6 Hz, 1H, H_c), 7.64 (d, $^3J_{HH}$ = 8.6 Hz, 1H, H_d), 7.57(s, 1H, H_e), 7.42-7.35 (m,2H, $H_{f,g}$), 7.29 (s, 2H, H_h), 7.20 (d, $^3J_{HH}$ = 8.2 Hz, 1H, H_i)) (Figure A22). ^{13}C NMR (75 MHz, C_6D_6, 25 °C) δ (ppm) = 164.5, 154.5, 152.7, 148.7, 136.7, 132.8, 132.4, 130.6, 130.3, 129.3, 125.5, 121.9, 121.5, 119.8, 118.6) (Figure A23).^{19}F NMR (282 MHz, C_6D_6, 25 °C, δ): -62.54 (s, 6F)) (Figure A24). IR/cm^{-1} = 1620 ν(C=N). HRMS-ESI (m/z): [M + H]$^+$ calcd for $C_{18}H_{10}N_2F_6$, 369.0826; found, 369.0845. Anal. Calcd. for $C_{18}H_{10}N_2F_6$: C 58.70, H 2.74, N 7.61; found C 58.23, H 2.46, N 7.30.

N-(2,6-Diisopropylphenyl-1-(quinolin-8-yl)methanimine (**L11**): a solution of 2,6-diisopropylaniline (8 mmol) and 2-pyridinecarboxaldehyde (10 mmol) in dichloromethane (15 mL) was prepared in a round-bottomed flask equipped with a magnetic stirrer. Catalytic amount of formic acid (3-4 drops) was added subsequently before the mixture was refluxed overnight at 90 °C. The reaction mixture was concentrated under reduced pressure which was further dissolved in pentane, dried over sodium sulfate and filtered. The mixture was concentrated again under reduced pressure to obtain a yellow powder which was further recrystallized in ethanol at -20 °C to yield yellow crystals. Yield: 65%. ^{1}H NMR (300 MHz, C_6D_6, 25 °C) δ (ppm) = 10.08 (s, 1H, H_a), 8.90 (dd, $^3J_{HH}$ = 8.2 Hz, $^4J_{HH}$ = 1.5 Hz, 1H, H_b), 8.64 (dd, $^3J_{HH}$ = 4.2 Hz , $^4J_{HH}$ = 1.5 Hz, 1H, H_c), 7.45 (dd, $^3J_{HH}$ = 8.4 Hz , $^4J_{HH}$ = 1.7 Hz, 1H, H_d), 7.38 (dd, $^3J_{HH}$ = 8.2 Hz , $^4J_{HH}$ = 1.7 Hz, 1H, H_e), 7.27-7.17 (m, 4H, $H_{f,g,h}$), 6.71 (dd, $^3J_{HH}$ = 8.2 Hz , 4.2 Hz, 1H, H_i), 3.35 (sept, $^3J_{HH}$ = 6.8 Hz, 2H, H_j), 1.24 (d, $^3J_{HH}$ = 6.8 Hz, 12H, H_k) (Figure A25). IR/cm^{-1} = 1628 ν(C=N). HRMS-ESI (m/z): [M + H]$^+$ calcd for $C_{22}H_{24}N_2$, 317.2018; found, 317.2009. Anal. Calcd. for $C_{22}H_{24}N_2$: C 83.50, H 7.64, N 8.85; found C 83.04, H 7.72, N 8.25. The data are similar to those found in the literature.[25]

3.4.3. General Procedure for the Synthesis of Complexes 6–11

The corresponding ligand (3.5 mmol), anhydrous $FeCl_2$ (3.5 mmol) and dry THF or CH_2Cl_2 (32 mL) were added to a Schlenk inside the glove box. The mixture was stirred overnight at room temperature under an argon atmosphere. The excess solvent was evaporated under reduced pressure and the product was washed with dry pentane (3 x 30 mL), further dried under high vacuum to obtain a powder.
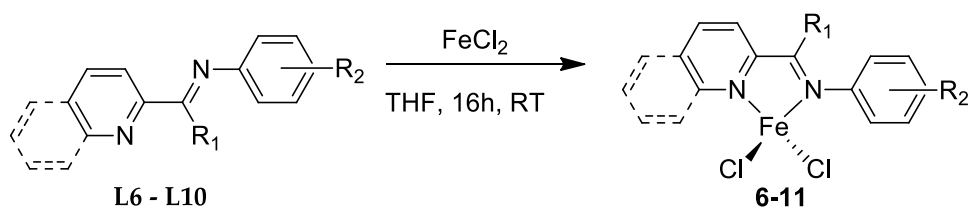
	L6/6	L7/7	L8/8	L9/9	L10/10	L11/11
R_1 =	H	H	CH_3	CH_3	H	H
R_2 =	3,5-CF$_3$	2,3,4,5,6-F	3,5-CF$_3$	2,3,4,5,6-F	3,5-CF$_3$	2,6-^{i}Pr

Scheme 3.6. Synthetic strategy for complexes

[N-(3,5-bis(Trifluoromethyl)phenyl)-1-(pyridin-2-yl)methanimine]FeCl$_2$ (**6**): dark purple powder. Yield: 86%. The title compound (**6**) was dissolved in minimum amount of acetonitrile (containing few drops of dichloromethane) and kept for a month at -20 °C inside the glove box to obtain the single crystals (**6'**). ^{1}H NMR (300 MHz, CD$_2$Cl$_2$, 25 °C, δ): 69.39 (Δν$_{1/2}$ = 1175 Hz, 1H), 58.55 (Δν$_{1/2}$ = 682 Hz, 1H), 52.03 (Δν$_{1/2}$ = 164 Hz, 1H), 11.88 (Δν$_{1/2}$ = 251 Hz, 1H), -2.99 (Δν$_{1/2}$ = 114 Hz, 2H), -7.82 (Δν$_{1/2}$ = 527 Hz, 1H), -19.36 (Δν$_{1/2}$ = 296 Hz, 1H) (Figure A26). IR/cm^{-1} = 1597 ν(C=N). Anal. Calcd. for powder (**6**) C$_{14}$H$_8$Cl$_2$F$_6$FeN$_2$: C 37.79, H 1.81, N 6.30; found C 37.46, H 1.93, N 5.92. Anal. Calcd. for crystal [**6'** bis(CH$_3$CN) solvate] C$_{32}$H$_{22}$Cl$_2$F$_{12}$FeN$_6$ + one molecule of CH$_2$Cl$_2$: C 42.61, H 2.60, N 9.03; found C 41.81, H 2.45, N 9.43.

[N-(Perfluorophenyl)-1-(pyridin-2-yl)methanimine]FeCl$_2$ (**7**): blue powder. Yield: 93%. Single crystals (**7'**) of the title compound were obtained by recrystallization from concentrated acetonitrile solution (containing few drops of dichloromethane) of complex **7** layered with diethyl ether (1/2) and left to stand for several days at -20°C inside the glove box. ^{1}H NMR (300 MHz, CD$_2$Cl$_2$, 25 °C, δ): 126.18 (Δν$_{1/2}$ = 802 Hz, 1H), 91.02 (Δν$_{1/2}$ = 1669 Hz, 1H), 63.37 (Δν$_{1/2}$ = 385 Hz, 1H), 51.92 & 50.78 (1H), -11.13 (Δν$_{1/2}$ = 313 Hz, 1H) (Figure A27). IR/cm^{-1} = 1597 ν(C=N). Anal. Calcd. for powder (**7**) C$_{12}$H$_5$Cl$_2$F$_5$FeN$_2$ + one molecule of C$_4$H$_8$O: C 40.80, H 2.78, N 5.95; found C 40.94, H 2.93, N 5.62. Anal. Calcd. for crystal **7'** C$_{24}$H$_{10}$Cl$_2$F$_{10}$FeN$_4$ + two molecules of CH$_2$Cl$_2$: C 37.13, H 1.68, N 6.66; found C 38.68, H 1.72, N 6.48.

[N-(3,5-bis(Trifluoromethyl)phenyl)-1-(pyridin-2-yl)ethan-1-imine]FeCl$_2$ (**8**): azure blue powder. Yield: 79%. Single crystals (**8'**) obtained in similar fashion as of **7** except only CH$_3$CN and Et$_2$O were used for recrystallization. ^{1}H NMR (300 MHz, CD$_2$Cl$_2$, 25 °C, δ): 72.7 (Δν$_{1/2}$ = 496 Hz, 1H), 67.1 (Δν$_{1/2}$ = 611 Hz, 1H), 53.2 & 50.65 (2H), -7.5 (Δν$_{1/2}$ = 215 Hz, 2H), -11.6 (Δν$_{1/2}$ = 162 Hz, 1H), -16.6 (Δν$_{1/2}$ = 1711 Hz, 3H) (Figure A28). IR/cm^{-1} = 1597 ν(C=N). Anal. Calcd. for powder (**8**) C$_{15}$H$_{10}$Cl$_2$F$_6$FeN$_2$: C 39.25, H 2.20, N 6.10; found C 41.10, H 2.43, N 6.07. Anal. Calcd. for crystal (**8'**) C$_{30}$H$_{20}$N$_2$F$_{12}$Fe$_2$Cl$_4$ + two molecules of CH$_3$CN: C 40.83.25, H 2.62, N 8.40; found C 41.17, H 2.77, N 8.72.

[N-(Perfluorophenyl)-1-(pyridin-2-yl)ethan-1-imine]FeCl$_2$ (**9**): navy blue powder. Yield: 83%. Single crystals (**9'**) obtained in similar fashion as of **7.** ^{1}H NMR (300 MHz, CD$_2$Cl$_2$, 25 °C, δ): 70.1 (Δν$_{1/2}$ = 809 Hz, 2H), 53.6 (Δν$_{1/2}$ = 555 Hz, 1H), 48.8 (Δν$_{1/2}$ = 304 Hz, 1H), -19.4 (Δν$_{1/2}$ = 487 Hz, 3H) (Figure A29). IR/cm^{-1} = 1595 ν(C=N). Anal. Calcd. for powder (**9**) C$_{13}$H$_7$N$_2$F$_5$FeCl$_2$ +

one molecule of THF (C_4H_8O): C 42.09, H 3.06, N 5.72; found C 42.10, H 3.12, N 5.78. Anal. Calcd. for crystal (**9'**) $C_{56}H_{34}N_{10}F_{20}Fe_4Cl_8$ including two molecules of CH_3CN in lattice + one molecule of CH_2Cl_2: C 37.64, H 1.99, N 7.70; found C 36.41, H 1.93, N 8.14.

[N-(3,5-bis(Trifluoromethyl)phenyl)-1-(quinolin-2-yl)methanimine]FeCl₂ (**10**): light green powder. Yield: 78%. Single crystals (**10'**) obtained in similar fashion as of **7.** ^{1}H NMR (300 MHz, CD_2Cl_2, 25 °C, δ): 93.53 ($\Delta v_{1/2} = 252$ Hz, 1H), 52.5 ($\Delta v_{1/2} = 71$ Hz, 1H), 15.6 ($\Delta v_{1/2} = 40$ Hz, 1H), 7.35 ($\Delta v_{1/2} = 15$ Hz, 1H), 6.11 ($\Delta v_{1/2} = 33$ Hz, 1H), -4.73 ($\Delta v_{1/2} = 33$ Hz, 2H), -17.41 ($\Delta v_{1/2} = 85$ Hz, 1H), -20.32 ($\Delta v_{1/2} = 840$ Hz, 1H), -24.49 ($\Delta v_{1/2} = 54$ Hz, 1H) (Figure A30). IR/cm[-1] = 1597 v(C=N). Anal. Calcd. for powder (**10**) $C_{18}H_{10}Cl_2F_6FeN_2$ + 1 molecule of CH_2Cl_2: C 39.35, H 2.09, N 4.83; found C 40.22, H 1.97, N 4.69. Anal. Calcd. for crystal (**10'**) $C_{36}H_{20}N_4F_{12}Fe_2Cl_4$ + four molecules of CH_2Cl_2: C 36.13, H 2.12, N 4.21; found C 37.12, H 2.07, N 4.03

[N-(2,6-Diisopropylphenyl-1-(quinolin-8-yl)methanimine]FeCl₂ (**11**): light red powder. Yield: 58%. Single crystals of the title compound were obtained by recrystallization from concentrated dichloromethane solution of complex **11** layered with diethyl ether (1/1) and left to stand for several days at -20°C inside the glove box. ^{1}H NMR (300 MHz, CD_2Cl_2, 25 °C, δ): 30.21 ($\Delta v_{1/2} = 47$Hz, 1H), 26.5 ($\Delta v_{1/2} = 17$ Hz, 1H), 15.5 ($\Delta v_{1/2} = 19$ Hz, 1H), 6.94 ($\Delta v_{1/2} = 42$ Hz, 1H), 3.46 ($\Delta v_{1/2} = 87$ Hz, 1H), -1.7 ($\Delta v_{1/2} = 27$ Hz, 2H), 0.35 & 0.17 (4H), -6.42 ($\Delta v_{1/2} = 57$ Hz, 3H), -16.4 ($\Delta v_{1/2} = 25$ Hz, 1H), -19.02 ($\Delta v_{1/2} = 18$ Hz, 12H) (Figure A31). IR/cm[-1] = 1605 v(C=N). Anal. Calcd. for $C_{22}H_{24}Cl_2FeN_2$: C 59.62, H 5.46, N 6.32; found C 59.01, H 5.18, N 6.06

3.4.4. General Procedure for Isoprene Polymerization

Similar as described in section 2.4.4, Chapter 2

3.4.5 Calculation of Microstructure Contents by NMR spectroscopy

Similar as described in section 2.4.5, Chapter 2

References

(1)   Bolm, C.; Legros, J.; Le Paih, J.; Zani, L. *Chem. Rev.* **2004**, *104* (12), 6217–6254.

(2)   Bauer, I.; Knölker, H.-J. *Chem. Rev.* **2015**, *115* (9), 3170–3387.

(3)   Fürstner, A. *ACS Cent. Sci.* **2016**, *2* (11), 778–789.

(4)   Ludwig, J. R.; Schindler, C. S. *Chem* **2017**, *2* (3), 313–316.

(5)   Piontek, A.; Bisz, E.; Szostak, M. *Angew. Chem. Int. Ed.* **2018**, *57* (35), 11116–11128.

(6)   Wei, D.; Darcel, C. *Chem. Rev.* **2019**, *119* (4), 2550–2610.

(7)   Guðmundsson, A.; Bäckvall, J.-E. *Molecules* **2020**, *25* (6), 1349.

(8)   Bianchini, C.; Giambastiani, G.; Rios, I. G.; Mantovani, G.; Meli, A.; Segarra, A. M. *Coord. Chem. Rev.* **2006**, 28.

(9)   Gibson, V. C.; Redshaw, C.; Solan, G. A. *Chem. Rev.* **2007**, *107* (5), 1745–1776.

(10)   Ma, J.; Feng, C.; Wang, S.; Zhao, K.-Q.; Sun, W.-H.; Redshaw, C.; Solan, G. A. *Inorg Chem Front* **2014**, *1* (1), 14–34.

(11)   Wang, Z.; Solan, G. A.; Zhang, W.; Sun, W.-H. *Coord. Chem. Rev.* **2018**, *363*, 92–108.

(12)   Ricci, G.; Morganti, D.; Sommazzi, A.; Santi, R.; Masi, F. *J. Mol. Catal. A: Chem.* **2003**, *204-205*, 287

(13)   Raynaud, J.; Wu, J. Y.; Ritter, T. *Angew. Chem. Int. Ed.* **2012**, *51* (47), 11805–11808.

(14)   Guo, L.; Jing, X.; Xiong, S.; Liu, W.; Liu, Y.; Liu, Z.; Chen, C. *Polymers* **2016**, *8* (11), 389.

(15)   Zhu, G.; Zhang, X.; Zhao, M.; Wang, L.; Jing, C.; Wang, P.; Wang, X.; Wang, Q. *Polymers* **2018**, *10* (9), 934.

(16)   Porri, L.; Giarrusso, A.; Ricci, G. *Prog. Polym. Sci.* **1991**, *16* (2–3), 405–441.

(17)   Lin, W.; Zhang, L.; Suo, H.; Vignesh, A.; Yousuf, N.; Hao, X.; Sun, W. H. *New J. Chem.* **2020**.

(18)   Wang, L.; Wang, X.; Hou, H.; Zhu, G.; Han, Z.; Yang, W.; Chen, X.; Wang, Q. *Chem. Commun.* **2020**, *56* (62), 8846–8849.

(19)   Hashmi, O. H.; Champouret, Y.; Visseaux, M. *Molecules* **2019**, *24* (17), 3024.

(20)   Liu, H.; Wang, F.; Jia, X.-Y.; Liu, L.; Bi, J.-F.; Zhang, C.-Y.; Zhao, L.-P.; Bai, C.-X.; Hu, Y.-M.; Zhang, X.-Q. *J. Mol. Catal. Chem.* **2014**, *391*, 25–35.

(21)   Raynaud, J.; Ritter, T.; Wu, J. Y. Iron complexes and methods for polymerization. WO2012109343A2, 2012.

(22)   Wang, Q.; Wang, X.; Wang, L.; Zhao, M.; Xian, M.; Zhang, X.; Zhu, G.; Jing, C.; Pyridine imine iron or cobalt metal complex catalyst. WO2019205309A1, 2019

(23)   Scales, S. J.; Zhang, H.; Chapman, P. A.; McRory, C. P.; Derrah, E. J.; Vogels, C. M.; Saleh, M. T.; Decken, A.; Westcott, S. A. *Polyhedron* **2004**, *23* (13), 2169–2176.

(24)   Zhou, Q.; Meng, W.; Yang, J.; Du, H. *Angew. Chem. Int. Ed.* **2018**, *57* (37), 12111–12115.

(25)   Britovsek, G. J. P.; Baugh, S. P. D.; Hoarau, O.; Gibson, V. C.; Wass, D. F.; White, A. J. P.; Williams, D. J. *Inorganica Chim. Acta* **2003**, *345*, 279–291.

(26)   Ahmed, B. M.; Rudell, N. A.; Soto, I.; Mezei, G. *J. Org. Chem.* **2017**, *82* (19), 10549–10562.

(27)   Sun, W.-H.; Jie, S.; Zhang, S.; Zhang, W.; Song, Y.; Ma, H.; Chen, J.; Wedeking, K.; Fröhlich, R. I *Organometallics* **2006**, *25* (3), 666–677.

(28)   Layer, R. W. *Chem. Rev.* **1963**, *63* (5), 489–510.

(29)   Britovsek, G. J. P.; Gibson, V. C.; Spitzmesser, S. K.; Tellmann, K. P.; White, A. J. P.; Williams, D. J. *J. Chem. Soc. Dalton Trans.* **2002**, No. 6, 1159.

(30)   Tsaulwayo, N.; Kumah, R. T.; Ojwach, S. O. *Polyhedron* **2021**, *197*, 115034.

(31)   Roy, A. S.; Biswas, M. K.; Weyhermüller, T.; Ghosh, P. *Dalton Trans* **2011**, *40* (1), 146–155.

(32)   Gibson, V. C.; O'Reilly, R. K.; Wass, D. F.; White, A. J. P.; Williams, D. J. *Dalton Trans.* **2003**, No. 14, 2824–2830.

(33)   Levina, E. O.; Chernyshov, I. Y.; Voronin, A. P.; Alekseiko, L. N.; Stash, A. I.; Vener, M. V. *RSC Adv.* **2019**, *9* (22), 12520–12537.

(34)   Bondi, A. *J. Phys. Chem.* **1964**, *68* (3), 441–451.

(35)   Janiak, C. *J. Chem. Soc. Dalton Trans.* **2000**, No. 21, 3885–3896.

(36) Kuang, S.-M.; Zhang, Z.-Z.; Xue, F.; Mak, T. C. W. *Polyhedron* **1999**, *18* (26), 3465–3468.

(37) Laine, T. V.; Piironen, U.; Lappalainen, K.; Klinga, M.; Aitola, E.; Leskelä, M. *J. Organomet. Chem.* **2000**, *606* (2), 112–124.

(38) Addison, A. W.; Rao, T. N.; Reedijk, J.; Rijn, J. van; Verschoor, G. C. *J. Chem. Soc. Dalton Trans.* **1984**, No. 7, 1349–1356.

(39) Gates, D. P.; Svejda, S. A.; On, E.; Johnson, L. K.; White, P. S.; Brookhart, M. Synthesis of Branched Polyethylene Using (R-Diimine)Nickel(II) Catalysts: Influence of Temperature, Ethylene Pressure, and Ligand Structure on Polymer Properties. **2000**, *33* (7), 15.

(40) Lopez, S.; Keller, S. W. *Inorg. Chem.* **1999**, *38* (8), 1883–1888.

(41) Song, S.; Xiao, T.; Liang, T.; Wang, F.; Redshaw, C.; Sun, W.-H. *Catal. Sci. Technol.* **2011**, *1* (1), 69.

(42) Song, S.; Xiao, T.; Redshaw, C.; Hao, X.; Wang, F.; Sun, W.-H. *J. Organomet. Chem.* **2011**, *696* (13), 2594–2599.

(43) Song, S.; Zhao, W.; Wang, L.; Redshaw, C.; Wang, F.; Sun, W.-H. *J. Organomet. Chem.* **2011**, *696* (18), 3029–3035.

(44) Nienkemper, K.; Kotov, V. V.; Kehr, G.; Erker, G.; Fröhlich, R. *Eur. J. Inorg. Chem.* **2006**, *2006* (2), 366–379.

(45) Cao, Y.; Zhang, Y.; Zhang, L.; Zhang, D.; Leng, X.; Huang, Z. *Org. Chem. Front.* **2014**, *1* (9), 1101–1106.

(46) Xia, H.; Liu, Y. *Acta Crystallogr. Sect. E Struct. Rep. Online* **2008**, *64* (12), m1504–m1504.

(47) Champouret, Y.; Hashmi, O. H.; Visseaux, M. *Coord. Chem. Rev.* **2019**, *390*, 127–170.

(48) Sheldrick, G. M. *Acta Crystallogr. Sect. Found. Adv.* **2015**, *71* (1), 3–8.

(49) Sheldrick, G. M. *Acta Crystallogr. Sect. C Struct. Chem.* **2015**, *71* (1), 3–8.

CHAPTER 4.

EXPLORING COORDINATIVE CHAIN TRANSFER IN IMINOPYRIDINE IRON MEDIATED ISOPRENE POLYMERIZATION

4.1. Introduction

4.1.1. General overview

The elaboration of a wide range of polymeric materials displaying unique characteristics and variety of physical, thermal and mechanical properties has been an important issue over the past few years.[1–3] The fine-tuning of the microstructure of polyolefins and polydienes is now possible, thanks to the development of homogeneous single-site catalysts.[4] These systems, up to some extent, are capable of producing polymers with a narrow molecular weight distribution and controlling the stereo-, regio- and chemo-selectivity depending on the steric and electronic properties of the ancillary ligand(s).[5–7] A critical issue for living coordinative polymerization is the limit of "one-chain-per-active-site" that restricts the ability to produce practical and scalable quantities of the final polymer due to the active site being derived from expensive transition metal-based catalysts which also require multistep synthesis (Scheme 4.1a). Therefore, in order to limit the consumption of highly exotic transition metal-based catalysts and to precisely control the molecular weight of the polymer, strategies like Coordinative Chain Transfer Polymerization (CCTP) have been developed.[8–13,1,14–17,3,18] This strategy involves the use of a single transition metal-based catalyst and a chain transfer agent (CTA) in the form of main group metal alkyl (Zn, Mg or Al). In this case, the growing polymer chain is reversibly transferred, by transmetalation, from the active metal center to the dormant chain transfer agent (CTA) metal center (Scheme 4.1b).[19]
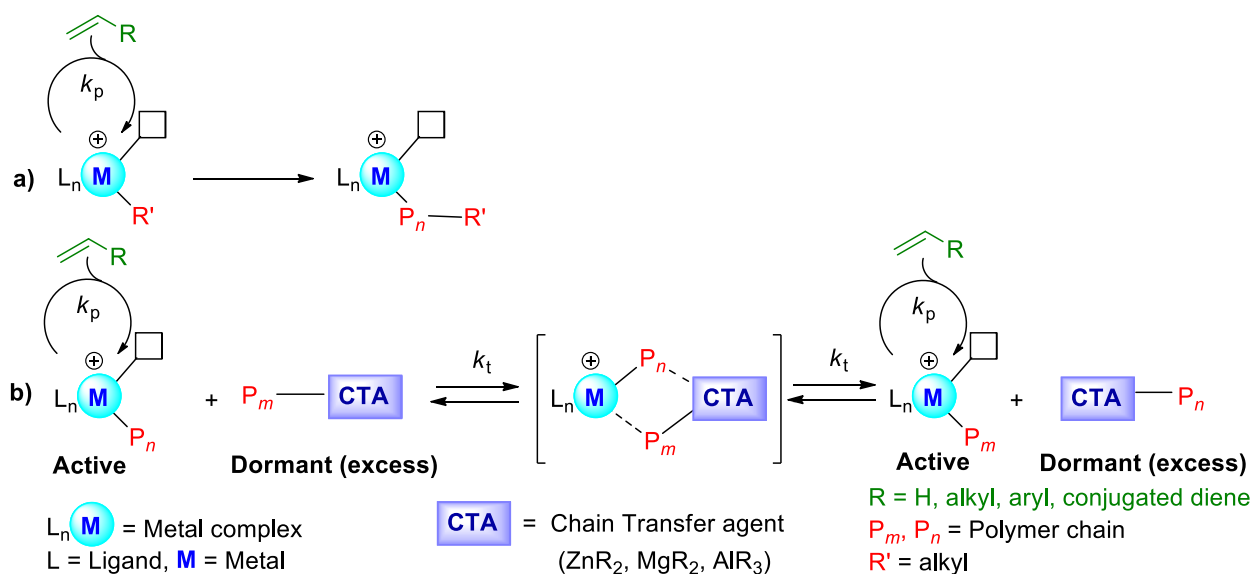
Scheme 4.1. Classical Coordinative Polymerization (a) *vs* Coordinative Chain Transfer Polymerization (b)

This process involves a dynamic equilibrium between propagating and dormant species. This methodology exhibits living characteristics and enables the control growth of several macromolecular chains per catalyst molecule since *i)* the chain transfer is fully reversible, *ii)* its rate is fast compared to the rate of propagation, *iii)* the formation of the heterobimetallic intermediate, resulting from the transmetalation, has a sufficient lifetime for the CCTP to be effective and *iv)* the chain transfer occurs in absence of any undesired irreversible transfer/termination pathway such as β-H abstraction.[20] All these requirements are highly dependent on the electronic and steric properties of the catalyst, in addition to the nature and adequacy of the CTA with the monomer used. In the end, narrow dispersities are obtained and the macromolecular chains are end-capped with the chain transfer metal, which enables further functionalization depending on the chemistry of main group metal. This can be viewed, as metal complex catalyzed Aufbaureaktion,[21] which was earlier proposed by Gibson[13] and Kempe.[16] If the transfer efficiency is high, i.e., most of the alkyl group are involved in the transmetalation, the polymer chain appears to grow on the main group metal alkyl. These latter reactions involving fast and reversible transfer along with the high transfer efficiencies and the non-occurrence of other chain termination pathways were defined as catalyzed chain growth (CCG),[13] which are different than catalytic chain growth involving metal catalyzed olefin insertion into a growing alkyl chain. CCG is interesting not only in terms of atom economy but also for the synthesis of block copolymers starting from the resulting polymer end-capped by the main group metal. In addition to the transfer efficiency, the ratio between the CTA and the catalyst is also an important parameter. The higher is this ratio and higher is the number of chains produced per expensive catalyst molecules, which can be considered overall as catalyst economy.

4.1.2. Iron-catalyzed CCTP

In the case of iron-based systems, CCTP processes are predominantly based on olefin monomers and only two proven examples are disclosed in the literature. Gibson and coworkers described the first CCG of ethylene using [BIP]FeCl$_2$/MAO in presence of 500 eqs. of ZnEt$_2$ as CTA (Scheme 4.2).[12,13] The polymerizations were conducted under much milder conditions than those using rare-earth precatalysts, i.e., 1.0 bar of ethylene pressure at room temperature, affording molecular weights up to 3 000 g/mol in transmetalation conditions. The authors proposed the key features for this process which could be responsible for the iron CCG: (i) less sterically hindered zinc center; (ii) the monomeric nature of ZnEt$_2$ in solution; (iii) the relatively weak Zn−C bond;

and (iv) a similar Zn−C and Fe−C bond strengths. Concerning (i), the size of the ligand on the main group metal and the extent of the observed chain transfer to the CTA were found to be correlated. Further, the data showed that the CTA having a monomeric nature in solution are more active. With respect to (iii) and (iv), a fine balance between these factors was needed to generate a catalyst latent state which is stable, yet highly reactive. A later study proved these findings to be relevant.[22]
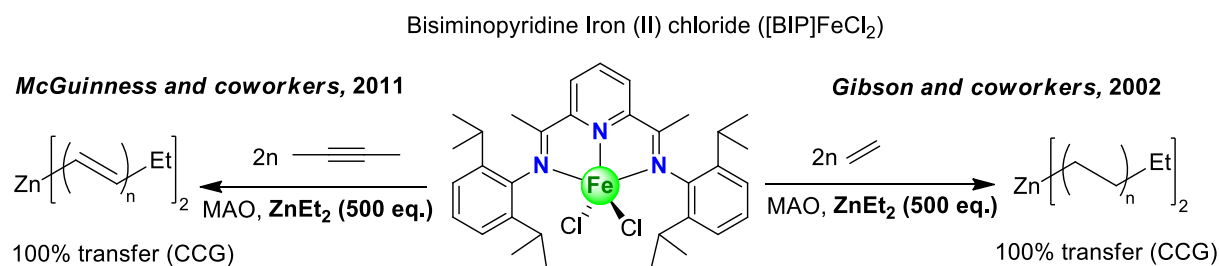
Scheme 4.2. [BIP]FeCl$_2$/MAO/ZnEt$_2$ catalyzed CCTP of ethylene and acetylene

Nearly, a decade later, after the inspiring work of Gibson *et al*, the second example of iron catalyzed CCG was reported by the group of McGuinness (Scheme 4.2) who firstly explored the polymerization of acetylene by combining pre-catalyst [BIP]FeCl$_2$ and 100 eqs. of MAO.[23] This system led to an extremely active catalyst (TOF up to 62 500 h^{-1}), with the formation of a polyacetylene/toluene gel in presence of [BIP]FeCl$_2$ = 100 µM, while the production of polyacetylene film was noted at lower catalyst concentration [BIP]FeCl$_2$ < 20 µM. The characterization of the polymers by IR spectroscopy revealed the presence of a mixture of *trans*/*cis* polyacetylene microstructure. Moreover, the same group performed the polymerization of acetylene with [BIP]FeCl$_2$/MAO (1/100) under reversible chain transfer condition by using 500 eqs. of ZnEt$_2$ as chain transfer agent (*vide supra*).[24] An even number of short-chain oligomers has been identified as the main product of the reaction. Furthermore, the absence of other irreversible chain termination has led to the quantitative production of oligomers with respect to zinc, which indicates the occurrence of a CCG process, similar to that found with ethylene. The presence of branched and cyclic oligomers has also been observed, suggesting a mechanism involving an intramolecular sigma-bond metathesis. Attempts to copolymerize ethylene and acetylene with [BIP]FeCl$_2$/MAO was unsuccessful and resulted in the formation of two disparate homopolymers. In addition, a striking variation in product selectivity was observed using the less congested pre-catalyst **4^{Me}** (Chart 1.1) in presence of MAO, which led to the formation of benzene *via* a metallacyclic mechanism, or 1,3-hexadiene when ZnEt$_2$ was used as chain transfer agent.[25]

To date, CCTP processes are predominantly based on olefin monomers and it is only recently that this process has been extended to conjugated dienes.[10,14,26–42] For the latter, the few examples disclosed in the literature focus exclusively on rare earth metal-based systems,[43–54] combined with Al or Mg alkyls as Chain Transfer Agent (CTA) and, to our knowledge, the successful implementation of transition metal-catalyzed reversible chain transfer polymerization of conjugated dienes, especially based on iron complexes, has yet to be proven.[55–57] Indeed, a delicate balance between the rates of propagation and transfer along with the stability of the transmetalation intermediate must be achieved for CCTP to be effective, this being highly dependent on the electronic and steric properties of the catalyst, the nature of the transfer agent and the monomer used.[19]

We, and others, have recently shown that iron-based complexes bearing an iminopyridine ligand are capable of efficiently catalyze the polymerization of isoprene after activation by an appropriate alkylating agent.[58–64] More specifically, the complexes **1-4** and **6-9** (Chart 4.1), which were previously described in Chapters 2 and 3 respectively, with the combination of Al^{i}Bu$_3$/[CPh$_3$][B(C$_6$F$_5$)$_4$] generated catalytic systems that are highly active for the isoprene polymerization whereas the catalytic systems resulting from complex **5** proved to be inactive for isoprene polymerization.
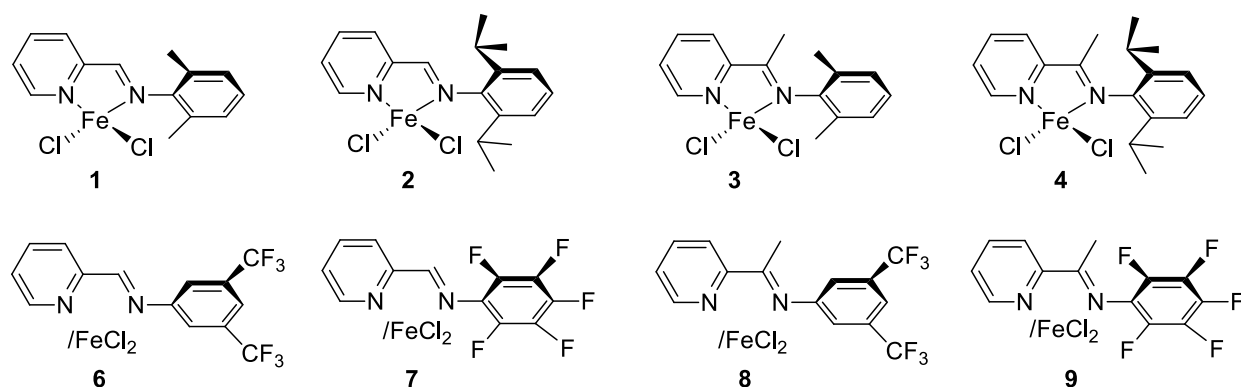
Chart 4.1. Iminopyridine iron (II) complexes studied in this work[61]

After the discovery of the 1st Aufbaureaktion for the chain growth of ethylene sixty eight years ago,[21] there have been various studies on the CCTP of ethylene and other monomers using transition metals and rare earths complexes associated with various CTAs such as alkyls of

aluminium,[21,27–30,65–73] zinc[12,13,22,74,26] and magnesium.[8–11,15,75] Therefore, in the present chapter, we will describe the studies we carried out in search of successful implementation of the CCTP of isoprene with the iminopyridine iron complexes **1-4** and **6-9** in combination with ZnEt$_2$ as CTA after activation. We have focused our study on the use of ZnEt$_2$ as CTA, since previous studies have shown that this CTA associates effectively with the bis(imino)pyridine iron dichloride [(BIP)FeCl$_2$]/MAO catalyst system for ethylene and acetylene polymerization (Scheme 4.3).[12,13,22,24] We also explored other combinations with alternative main-group metal CTAs, which may be of potential interest due to their previous ability in this field.[19,43,44,49,76,77] Starting from the preliminary screening of (Iminopyridine)FeCl$_2$ combined with different co-catalysts such as MAO, Al^{i}Bu$_3$/[CPh$_3$][B(C$_6$F$_5$)$_4$] etc., we intend to develop an efficient catalytic system combined with a potential CTA for a successful screening in CCTP of isoprene. We also look forward to optimize the chain transfer conditions and the detailed study under optimized conditions for a reversible CCTP will be addressed for these catalytic systems. The last part of this chapter will be devoted to the implementation of a Chain Shuttling Polymerization (CSP) stage where a brief discussion will be carried out regarding the selection of appropriate catalytic systems and the properties of the resulting polymers possessing different microstructure and architecture.
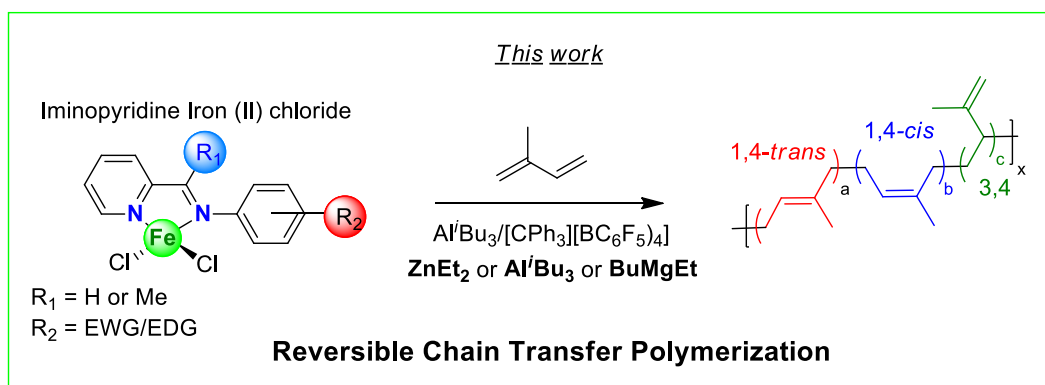
Scheme 4.3. Iron (II) catalyzed coordinative chain transfer polymerization

4.2. Results and Discussion

4.2.1. Screening 4/MAO/ZnEt₂ catalytic system for the reversible CCTP of isoprene

The group of Gibson demonstrated for the first time the use of $ZnEt_2$ as a CTA in the controlled coordinative chain transfer polymerization of ethylene (Scheme 4.2).[12,13] The highly efficient catalyst derived from the combination of $[BIP]FeCl_2/MAO/ZnEt_2$, in a ratio of 1/100/500, prompted us to attempt the similar system in the CCTP of isoprene using the *N*-aryl iminopyridine iron dichloride pre-catalysts precedently mentioned in chapter 2 and 3. Preliminary CCTP studies of isoprene were initially performed with precatalyst **4** using reaction conditions similar to those described by Gibson and coworkers, knowing that the complex **4** is most stereoselective among the series mentioned in Chart 4.1 and displays a *quasi*-living character with **4**/Al^{i}Bu₃/[Ph₃C][B(C₆F₅)₄] catalytic combination as described previously in chapter 2. Therefore, precatalyst **4** was activated with 100 eq. of MAO in the presence of various amounts of $ZnEt_2$ followed by the addition of isoprene, the results are shown below in Table 4.1.

Table 4.1. CCTP of isoprene using **4**/MAO catalytic system with different quantities of $ZnEt_2$[a]

Entry [a]	[ZnEt₂]/[4]	Yield (%)	$M_{n(exp)}$ [b] (g/mol)	$Đ$ [b]	N$_{chains}$[c]
1	0	>99	94 000	1.4	-
2	10	>99	34 600	1.4	2.7
3	50	>99	18 000	1.4	5.2

[a] Polymerization conditions: 10 µmol of iron complex; isoprene/Fe/MAO = 2000/1/100; toluene = 20 mL, [C]$_{isoprene}$ = 1 mol/L, temperature = 25 °C, time = 6h. [b] Determined by SEC analysis in THF using polystyrene standards. [c] N$_{chains}$ = $M_{n(exp)}$/$M_{n(exp) \, with \, CTA}$; $M_{n(th)}$ = 135 000 g/mol (considering one growing chain per metal center)

All the resulting PIs were analyzed by SEC to determine the number average molecular weight (M_n). From the results displayed in Table 4.1, we can observe that using the **4**/MAO system in absence of $ZnEt_2$ produced polyisoprene with an excellent conversion (>99%). However, the number average molecular weight of the resulting polyisoprene was found to be rather low compared to the theoretical value ($M_{n(exp)}$ = 94 000 g/mol *vs* $M_{n(th)}$ = 135 000 g/mol, respectively)

possibly due, to some extent, to the occurrence of unwanted transfer reactions with free $AlMe_3$ contained in MAO (Table 4.1, Entry 1).[60,78] Addition of 10 eqs. of $ZnEt_2$ to the reaction decreased the M_n of the resulting polyisoprene by a factor of 2.7, while adding 50 eq. of $ZnEt_2$ decreased the M_n by a factor of 5.2 (Table 4.1, Entries 2 and 3, respectively). This factor corresponds to the transfer efficiency of a system which is defined as the ratio of the number of chains obtained experimentally (*e.g.* Table 4.1, Entry 2, $N_{exp} = 2.7$ chains per 10eq./Fe of $ZnEt_2$) to the expected number of chains for a fully reversible transfer ($N_{th} = 21$ chains per 10eq./Fe of $ZnEt_2$ since the iron catalyst produces one polymer chain through activation with MAO cocatalyst and the two ethyl groups of $ZnEt_2$ can be transferred to the catalyst to theoretically initiate the propagation of 20 additional chains). The decrease in number average molecular weight together with the preservation of low dispersity upon increasing the amount of $ZnEt_2$ indicated that chain transfer did occur from Fe to Zn, as seen in Figure 4.1. Nevertheless, the catalytic system **4**/MAO/$ZnEt_2$ was found to exhibit low efficiency under transfer conditions as evidenced from the transfer efficiency of system (transfer efficiency (%) = 2.7/21 x 100 = 13 % for 10eqs./Fe of $ZnEt_2$).
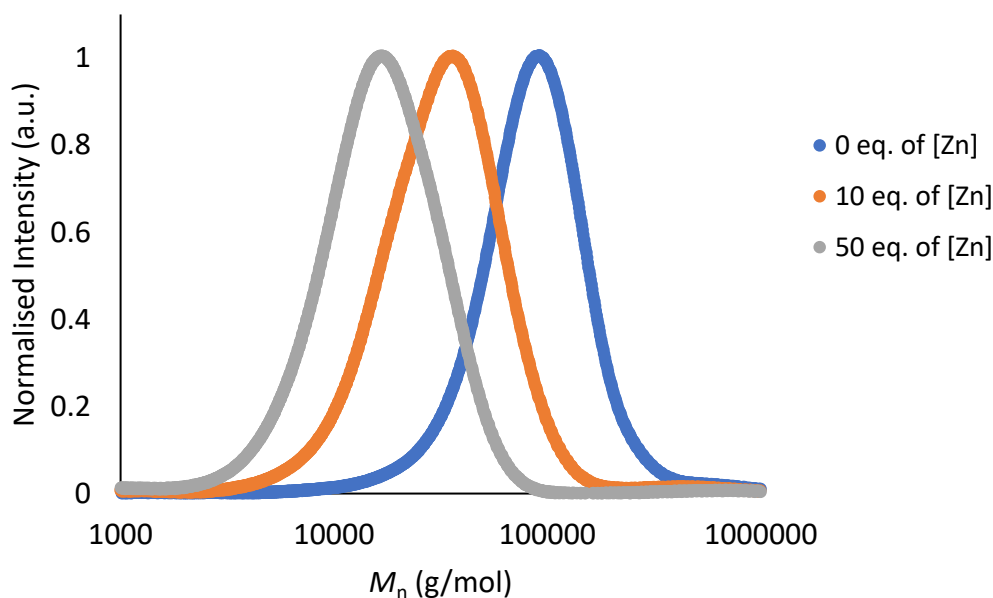
Figure 4.1. SEC traces showing the effect of the quantity of $ZnEt_2$ (0–50 eq./Fe) on the M_n of polyisoprene using **4**/MAO catalytic system (according to data displayed in Table 4.1)

4.2.2. Pre-liminary screening of various chain transfer agents for the CCTP of isoprene with complex 4

After screening **4**/MAO/ZnEt$_2$ system, we concluded that the transfer occurred between Fe and Zn but with poor efficiency. Therefore, we decided to opt for an alternative catalytic system based again on **4**, to assess the polymerization of isoprene under chain transfer conditions at room temperature in the presence of alkyls of aluminium, zinc and magnesium, which were deployed as CTAs. The results of this preliminary screening are presented below in Table 4.2.

Table 4.2. Polymerization of isoprene using **4**/Al^{i}Bu$_3$/[Ph$_3$C][B(C$_6$F$_5$)$_4$] catalytic system in the presence of various CTAs[a]

Entry [a]	CTA (eq./Fe)	Time (h)	Conv. (%)	$M_{n(exp)}$ (g/mol) [b]	$Đ$ [b]	N$_{chains}$ [c]	Microstructure [d] (%) 1,4 (*trans*/*cis*)	3,4
1	0	6	>99	155 000	1.3	-	90 (77/13)	10
2	ZnEt$_2$ (10)	6	>99	20 500	1.3	7.6	91 (79/12)	9
3	Al^{i}Bu$_3$ (7)	4	95	145 000	1.5	1.0	90 (82/8)	10
4	BuMgEt (10)	18	0	0	0	0	0	0

[a] Polymerization conditions: 10 µmol of Fe (II) complex; isoprene/Fe/Al^{i}Bu$_3$/[Ph$_3$C][B(C$_6$F$_5$)$_4$] = 2000/1/3/1; toluene = 20 mL, [C]$_{isoprene}$ = 1 mol/L, temperature = 25 °C. [b] Determined by SEC analysis in THF using polystyrene standards; $M_{n(th)}$ = 135 000 g/mol (considering one growing chain per metal center). [c] N$_{chains}$ = $M_{n(exp)}$/$M_{n(exp)\ CTA}$; [d] Determined by ^{1}H NMR and ^{13}C NMR.

In addition to SEC analysis for determining the M_n, the resulting PIs were also analyzed by NMR spectroscopy to identify their microstructure content. In the absence of any CTA, the polymerization was quite controlled as the experimental molar mass (Table 4.2, Entry 1, $M_{n(exp)}$ = 155 000 g/mol) was near to the expected value ($M_{n(th)}$ = 135 000 g/mol) with a narrow dispersity ($Đ$ = 1.3). Using 10 eqs. of ZnEt$_2$, the polymerization was also found to be well controlled ($Đ$ = 1.3) and the resulting PI gave a much lower M_n (Table 4.2, Entry 2, M_n = 20 000 g/mol) than the value without Zn alkyl (M_n = 155 000 g/mol), implying the occurrence of a moderate rate of reversible chain transfer reaction. In the presence of 10 eq./Fe of ZnEt$_2$, the number of chains is 7.75, indicating a transfer efficiency of 37% [transfer eff = (7.75/21) x 100]. In addition, the stereoselectivity of the **4**-based catalytic system was maintained in the presence of ZnEt$_2$ (1,4-

trans/1,4-*cis*/3,4 = 79/12/9 *vs* 77/13/10 without ZnEt$_2$). This observation reveals that the growth of the polymer chain is probably not influenced by the presence of the CTA, suggesting distinct mechanistic elementary steps of insertion (Fe catalyst) and transfer (Fe/Zn heterobimetallic species).

Changing Zn by other metal alkyls was much less exciting. Al^{i}Bu$_3$, which is known to alkylate iron center, can also act as a potential CTA.[21,27–30,65–73] Using seven eq. of Al^{i}Bu$_3$ in addition to the three eq. required for the proper alkylation of pre-catalyst **4** (chapter 2, section 2.2.3.1.2.) the experimental M_n was found to be slightly lower (Table 4.2, Entry 3, M_n = 145 000 g/mol) than the value obtained in the presence of three eq. of Al reagents (Table 4.2, Entry 1, M_n = 155 000 g/mol), indicating that the transfer is comparably less efficient between Al and Fe than between Zn and Fe, as evidenced by the number of chains obtained (N_{chains} = 1.0). Moreover, the broadening of the dispersity was noticeable ($Đ$ = 1.5 *vs*. 1.3), which was also apparent when using Al^{i}Bu$_3$ in excess for rare earth catalytic systems.[79] The resulting PI was acquired in good yields (95%), which consisted of 82% of 1,4-*trans* units along with the contribution of 3,4 (10%) and 1,4-*cis* sequences (8%) as previously observed for the selectivity of precatalyst **4** in our last study.[61]

Interestingly, in the presence of an excess of magnesium bis-alkyl, butylethylmagnesium (BuMgEt, BEM), the **4**-based system failed to produce polyisoprene (Table 4.2, Entry 4), which is similar to that found in the case of ethylene polymerization using (BIP)FeCl$_2$/MAO/Mg^{n}Bu$_2$ (1/100/500).[13] In addition to the question of the similarity of bonding strengths between the catalyst-polymer chain and CTA-polymer chain, it is clear that the monomeric nature of ZnEt$_2$ as compared to aggregated MgR$_2$ in non-polar solution[80] could be an explanation for a better CCTP efficiency when associated with the most sterically hindered precatalyst **4**. The highest transfer efficiency possessed by the catalytic system **4**/Al^{i}Bu$_3$/[Ph$_3$C][B(C$_6$F$_5$)$_4$]/ZnEt$_2$ may be attributed to a better adequation between bonds strength of the metal catalyst-growing polymer chain and of the metal CTA-dormant polymer chain. These observations have already been described for the catalyzed chain growth of ethylene and acetylene using [(BIP)FeCl$_2$]/MAO catalytic system in the presence of an excess of ZnEt$_2$,[12,13,22,24] where the authors proposed that an iron-based catalytic system is more efficient in the presence of Zn due to the almost similar Zn – C and Fe – C bond strengths and the relatively weak Zn – C bond.[12,13,22] As same, it is known that Mg and Al CTAs fit particularly well with rare earths and column 4 precatalysts, respectively.[16] Depending on these

impeccable findings in literature, a similar hypothesis can be drawn in our case from the **4**/Al^{i}Bu$_3$/[Ph$_3$C][B(C$_6$F$_5$)$_4$]/ZnEt$_2$ catalytic system with the assumption that metal-allyl bonds are involved in the polymerization of isoprene.[81]

4.2.3. Optimization of transfer conditions of 4/Al^{i}Bu$_3$/[Ph$_3$C][B(C$_6$F$_5$)$_4$]/ZnEt$_2$ catalytic system

The preliminary screening of various transfer agents revealed that the CCTP of isoprene is most efficient with ZnEt$_2$ as CTA while employing the **4**/Al^{i}Bu$_3$/[Ph$_3$C][B(C$_6$F$_5$)$_4$] catalytic system. We first decided to see if the concentration of monomer in the polymerization mixture could be a factor that would alter the transfer efficiency of the catalytic system employed in this study. After choosing ZnEt$_2$ as a suitable CTA, the CCTP of isoprene with **4**/Al^{i}Bu$_3$/[Ph$_3$C][B(C$_6$F$_5$)$_4$]/ZnEt$_2$ catalytic system was further optimized by conducting the polymerization under different concentrations of isoprene in absence and in the presence of 10 eq./Fe of ZnEt$_2$. The results are depicted below in Table 4.3.

Table 4.3. CCTP of isoprene using **4**/Al^{i}Bu$_3$/[Ph$_3$C][B(C$_6$F$_5$)$_4$]/ZnEt$_2$ catalytic system under different monomer concentrations[a]

Entry [a]	[4]/[Zn]	[Isoprene] (M)	Time (h)	Conv. (%)	$M_{n(exp)}$ (g/mol) [b]	$Đ$ [b]	N_{chains} [c]
1	1/0		6	>99	155 000	1.3	
2	1/10	1	6	>99	20 500	1.3	7.6
3	1/10		4	85	16 000	1.3	8.2
4	1/0	2	4	>99	270 000*	1.5	
5	1/10		4	75	11 500	1.4	17.6
6	1/0	4	3	>99	238 000*	1.5	
7	1/10		72	69	8 600	1.4	19.1
8	1/0	10	0.5	>99	90 000	1.4	
9	1/10		4	50	6 000	1.3	7.5
10	1/10		168	52	6 000	1.3	7.8

[a] Polymerization conditions: 10 µmol of Fe (II) complex; Isoprene/Fe/Al^{i}Bu$_3$/[Ph$_3$C][B(C$_6$F$_5$)$_4$] = 2000/1/3/1; temperature = 25 °C. [b] Determined by SEC analysis in THF using polystyrene standards; $M_{n(th)}$ = 135 000 g/mol (considering one growing chain per metal center); [c] N_{chains} = $M_{n(exp)}$/$M_{n(exp) CTA}$; *presence of a small amount of PI displaying high M_n

Under 1 M concentration of isoprene (Table 4.3, Entries 1-3), firstly we performed the reaction for the same duration of 6 h for both cases, without (entry 1) and with (entry 2) 10 eq. $ZnEt_2$. The conversion was found to be complete within this time, and the number of chains per Fe catalyst was calculated to 7.6 in the presence of the CTA (entry 2). In order to optimize the activity in the presence of 10 eq. of $ZnEt_2$, the reaction time was tentatively reduced from 6 h to 4 h. Unfortunately, in this case only incomplete conversion (85%) of the monomer was achieved (Table 4.3, Entry 3). However, it is worth to be noted that the number of chains obtained was found to be nearly eight, *i.e.* close to the value noted after 6 h reaction. For full conversion of isoprene (Table 4.3, Entry 2), the experiment under 1 M concentration of isoprene corresponded to a transfer efficiency equal to 36% (transfer eff = 7.6/21 x 100), as previously described. In the absence of CTA, M_n was 155 000 g/mol, which is not far from the theoretical value of 135 000 g/mol at full conversion (Table 4.3, Entry 1).

By doubling the concentration of isoprene to 2 M (Table 4.3, Entries 4 and 5), we observed a huge increase in the M_n of PI obtained in the absence of CTA. This was found to be nearly two times higher than the expected value ($M_{n(exp)}$ = 270 000 g/mol *vs* $M_{n(th)}$ = 135 000 g/mol), with an additional shoulder contribution (<5%), although the dispersity ($Đ$ = 1.5) was quite narrow (Table 4.3, Entry 4). The same polymerization, when performed under the presence of CTA, reduced the M_n to 11 500 g/mol and limited the conversion to 75% (Table 4.3, Entry 5).
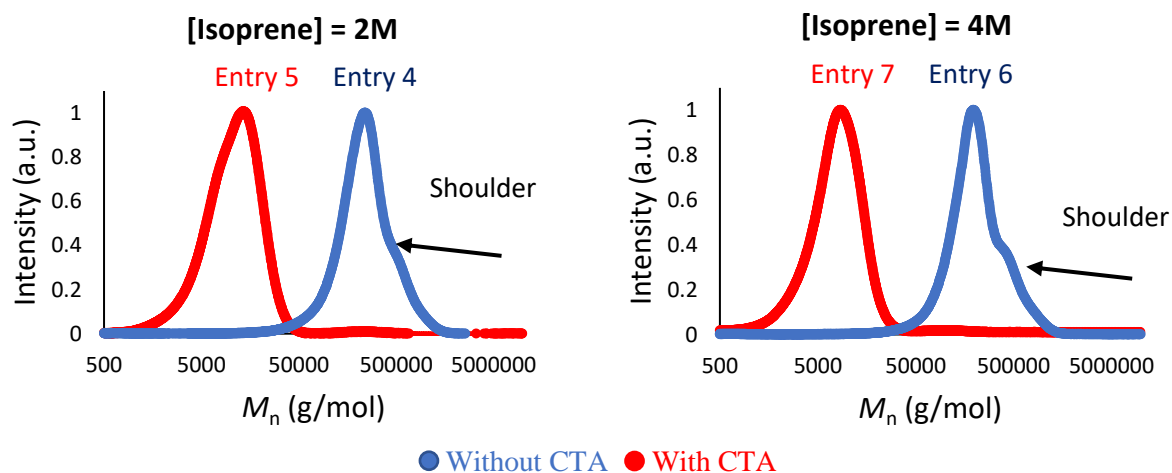
Figure 4.2. SEC traces comparison of entries (Table 4.3) under 2 M and 4 M concentration of isoprene

Repeating the same process of doubling the concentration of isoprene to 4 M (Table 4.3, Entries 6 and 7) again resulted to a very high molecular weight ($M_{n(exp)}$ = 238 000 g/mol) PI obtained in the absence of CTA, with an additional shoulder contribution (<5%) to the M_n (Table 4.3, Entry 6). This highlights that the initiation is very slow compared to chain propagation at concentrations 2 and 4M. In the presence of CTA, the M_n reduces to 8 600 g/mol but again, and much more significantly (72 h *vs.* 4 h) the conversion was limited to 69% even in 72 h (Table 4.3, Entry 7). The SEC traces of the entries under 2 M and 4 M concentration are displayed in Figure 4.2 below.

Lastly, at the highest concentration (Table 4.3, Entries 8-10), the resulting M_n of the experiment performed in the absence of CTA ($M_{n(exp)}$ = 90 000 g/mol) was comparatively lower than the expected value ($M_{n(th)}$ = 135 000 g/mol), although it comprised none of the secondary contributions unlike entries 4 and 6 (Table 4.3, Entry 8). Interestingly, under the CCTP conditions, very low molecular weights (M_n = 6 000 g/mol) and narrow dispersities ($Đ$ = 1.3-1.4) could be obtained without affecting the transfer efficiency (37%) like the previous system at 1 M (Table 4.3, Entries 9 and 10).

To our knowledge, such dependence of the decreasing molar masses, for a given conversion, with the increasing concentration of monomer could be due to the fact that the interaction of the incoming monomer with the metal center and, subsequently, the interaction of the growing macromolecular chains with Zn is particularly enhanced as a CTA. Unfortunately, full conversion of the monomer could not be achieved under 10 M concentration of isoprene, even after leaving the reaction for prolonged times (Table 4.3, Entries 9 and 10) indicating that at a certain stage, the transfer between Fe and Zn is blocked. A hypothesis would be that formation of a very stable Fe-Zn heterobimetallic species occur, allowing no further exchange of alkyl/allyl groups between Fe and Zn centers. This is likely to happen when the increasing concentration of monomer increases the rate of transfer, which enhances the transfer efficiency of the system by involving the exchange of all ethyl groups from one $ZnEt_2$ site upon transmetalation, to generate Et-Zn-polyisoprenyl species remaining with the second exchange site. This alkyl-Zn-allyl species could again interact with the active iron catalyst for the Et-polyisoprenyl chain exchange during the transmetalation step at which the transfer is probably blocked due to the formation of putative polyisoprenyl$_1$-Fe-Zn(Et)-polyisoprenyl$_2$ heterobimetallic species that are inactive for exchange,

as shown below in Scheme 4.3. The involvement of only one ethyl group from ZnEt$_2$ for chain transfer has already been demonstrated by the group of Landis using hafnium complex where the authors reported the formation of one polyoctene chain per ZnEt$_2$ molecule owing to steric barriers inhibiting the transfer of the Et group from Et-Zn-polymer.[82]
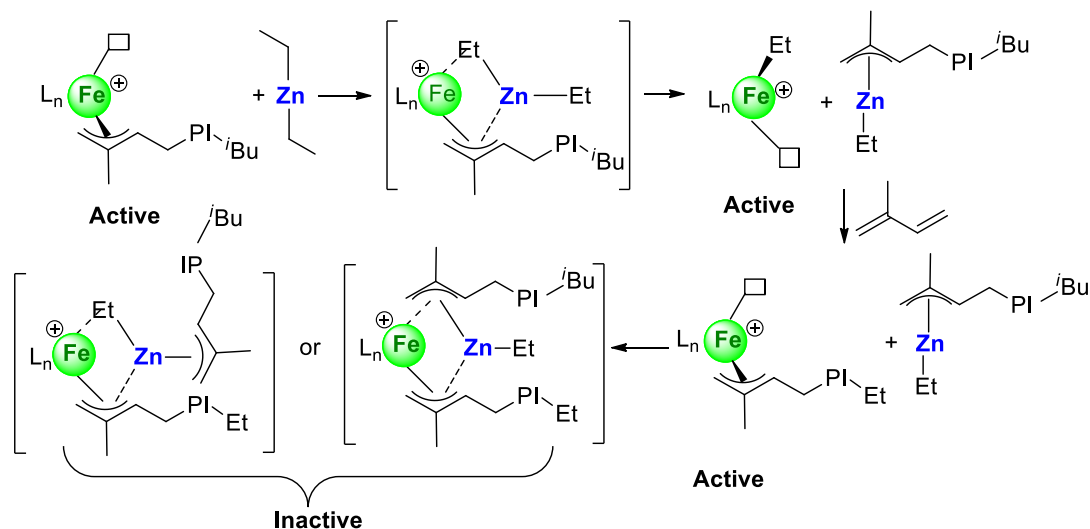
Scheme 4.3. Possible formation of putative heterobimetallic allyl species with ZnEt$_2$

Additionally, to confirm this hypothesis of transfer blockage at certain stage, we attempted a classical CCTP experiment with **4**/Al^{i}Bu$_3$/[Ph$_3$C][B(C$_6$F$_5$)$_4$] using bis-allylzinc as CTA. Prior to the addition of the monomer, the mixture of 10 eq. of bis-allylzinc with the **4**/Al^{i}Bu$_3$/[Ph$_3$C][B(C$_6$F$_5$)$_4$] catalytic system resulted in a color change from midnight green to brown, which is believed to be due to the formation of a heterobimetallic polyisoprenyl-Fe-Zn allyl complex (Scheme 4.4). The addition of isoprene after this stage did not afford any polymer, even after prolonged time. This could be related to the very high stability of the putative bimetallic allyl species, which precluded access to the iron catalyst.
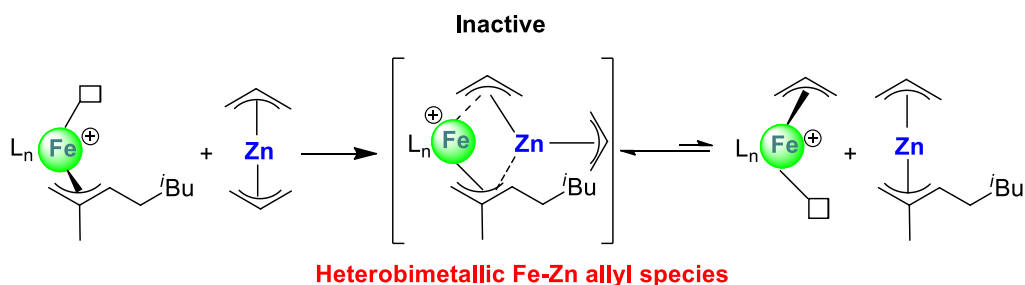
Scheme 4.4. Formation of putative heterobimetallic allyl species with bis-allylzinc

4.2.4. Assessment of the kinetic parameters of polymerization under CCTP

The chain transfer between the catalyst originating from complex **4** and $ZnEt_2$ was also studied through the kinetic profile of isoprene polymerization at 25 °C, in absence and in presence of 10 eq. of Zn per Fe (Figure 4.3). To ensure better reliability, the studies were conducted with 2000 eqs. isoprene (in chapter 2, 5 000 eq./Fe of isoprene) during which various aliquots were taken at different times of the polymerization to determine the conversions *via* ^{1}H NMR. The M_n of each sample of PI was determined through SEC analysis and the results are displayed below in Table 4.4.
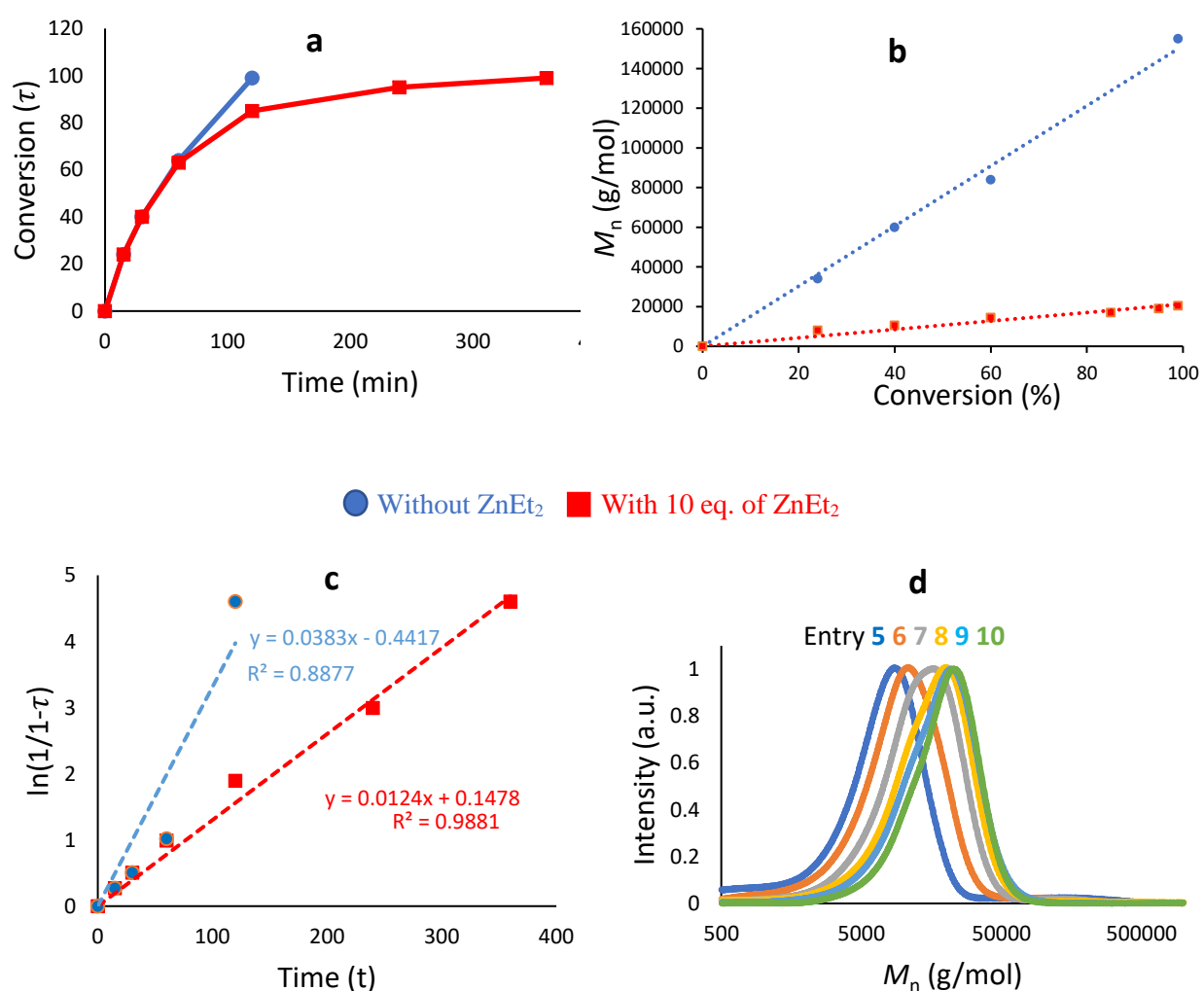
Figure 4.3 (a) Monomer conversion (τ) as function of time, (b) Dependence of M_n with isoprene conversion, (c) First order kinetics plot and (d) stacked SEC traces of the aliquots under CCTP for pre-catalyst **4** (Isoprene/Fe/Al^{i}Bu$_3$/[Ph$_3$C][B(C$_6$F$_5$)$_4$] = 2000/1/3/1)

From the kinetics plot in Figure 4.3a, it is clearly evident that the addition of 10 eqs. $ZnEt_2$ prolonged the polymerization time, indicating the possibility of transfer of the growing polymeric chain between complex **4** and Zn. As observed previously in chapter 2,[61] the *quasi*-living character of **4**/Al^{i}Bu$_3$/[Ph$_3$C][B(C$_6$F$_5$)$_4$] catalytic system is again displayed through the kinetic profile, where the *quasi* linear increase in M_n with conversion occurs in the absence of $ZnEt_2$ and also in the presence of 10 eq./Fe of $ZnEt_2$ (Figure 4.3b).

Table 4.4. Isoprene polymerization using **4**/Al^{i}Bu$_3$/[Ph$_3$C][B(C$_6$F$_5$)$_4$] catalytic system in the absence and presence of 10 eq./Fe of $ZnEt_2$[a]

Entry [a]	$ZnEt_2$ (eq/Fe)	Time (min)	Conv. (%)	$M_{n(exp)}$ [b] (g/mol)	$Đ$ [b]
1		15	24	34 000	1.5
2		30	40	60 000	1.7
3	0	60	64	84 000	1.9
4		120	99	155 000	1.3
5		15	24	8 000	1.3
6		30	40	10 600	1.3
7		60	63	14 500	1.3
8	10	120	85	17 000	1.3
9		240	95	19 000	1.3
10		360	99	20 500	1.2

[a] Polymerization conditions: 10 µmol of Fe (II) complex; isoprene/Fe/Al^{i}Bu$_3$/[Ph$_3$C][B(C$_6$F$_5$)$_4$] = 2000/1/3/1; toluene = 20 mL, [C]isoprene = 1 mol/L , temperature = 25 °C. [b] Determined by SEC analysis in THF using polystyrene standards; $M_{n(th)}$ = 135 000 g/mol for 100% conversion (considering one growing chain per metal center)

This trend was also confirmed through a significant drop in the M_n of the obtained polymer at each aliquot and is mostly visible at the end of the polymerization where the M_n value drops from 155 000 g/mol in the absence of CTA (Table 4.4, Entry 4) to 20 500 g/mol *via* CCTP of isoprene with 10 eq./Fe of $ZnEt_2$ (Table 4.4, Entry 10), with a transfer efficiency of 37%. It also appears that the polymerization is quite controlled with and without CTA, following nearly a first order kinetic profile for both cases, indicating minimal loss of active species during the polymerization (Figure 4.3c). The dispersities became narrower at the end for the experiments without $ZnEt_2$ (Đ decreases from 1.5 to 1.3), whereas they remained quite similar and narrow in the presence of $ZnEt_2$ (Đ = 1.3, Figure 4.3d).

4.2.5 Implementation of a reversible CCTP of isoprene with complexes 1-4 and 6-9

After conducting the preliminary screening of various CTAs and optimizing the chain transfer conditions for the precatalyst **4**, we implemented the reversible CCTP of isoprene with all the precatalysts **1-4** and **6-9** (Chart 4.1) that were active for the polymerization of isoprene. The results are displayed below in Table 4.5, under optimized experimental conditions, in absence and in presence of 10 eq./Fe of ZnEt$_2$, for an easier comparison.

Table 4.5. Screening **Fe**/Al^{i}Bu$_3$/[Ph$_3$C][B(C$_6$F$_5$)$_4$]/ZnEt$_2$ catalytic systems for the CCTP of isoprene[a]

Entry [a]	Fe	[Zn] /[Fe]	Time (min)	Conv. (%)	$M_{n(exp)}$ (g/mol) [b]	$Đ$ [b]	N$_{chains}$ [c]	Micro. [d] (%) 1,4 (*trans/cis*)	3,4
1	**1**	0	360	> 99	487 500*	1.6		79 (38/41)	21
2		10	360	>99	180 000	1.7	2.7	79 (33/46)	21
3	**2**	0	360	> 99	250 000	1.3		75 (35/40)	25
4		10	360	> 99	195 000	1.7	1.3	75 (32/43)	25
5	**3**	0	360	> 99	261 000	1.3		90 (69/21)	10
6		10	360	> 99	86 000	1.3	3.0	91 (69/22)	9
7	**4**	0	360	> 99	155 000	1.3		90 (77/13)	10
8		10	360	> 99	20 500	1.3	7.6	91 (79/12)	9
9	**6**	0	240	> 99	384 000	1.3	-	54 (0/54)	46
10		10	4320	< 1	-	-		-	-
11	**7**	0	240	49	448 000	1.4	-		
12		10	360	14	762 000	1.8		-	-
13	**8**	0	10	> 99	320 000	2.1		56 (0/56)	44
14		10	10	> 99	265 000	1.3	1.2	59 (0/59)	41
15	**9**	0	10	> 99	580 000	1.6		56 (0/56)	44
16		10	10	> 99	510 000	1.3	1.1	54 (0/54)	46

[a] Polymerization conditions: 10 µmol of Fe (II) complex; isoprene/Fe/Al^{i}Bu$_3$/[Ph$_3$C][B(C$_6$F$_5$)$_4$] = 2000/1/3/1; toluene = 20 mL, [C]isoprene = 1 mol/L , temperature = 25 °C. [b] Determined by size exclusion chromatography (SEC) analysis in THF using polystyrene standards (* minor contribution of high M_n, < 5%, observed); [c] N chains = $M_{n(exp)}/M_{n(exp)\ CTA}$; $M_{n(th)}$ = 135 000 g/mol (considering one growing chain per metal center). [d] Determined by ^{1}H NMR and ^{13}C NMR.

As mentioned previously, the expected effects of the CTA are i) decreasing the M_n values and ii) narrowing the dispersity (*Đ* value tending to 1). From the data given in Table 4.5, it can be observed that when comparing results from the experiments performed with and without excess of ZnEt$_2$, the first criteria is partially fulfilled by precatalysts **2**, **8** and **9**, where the number average molecular weight are getting reduced by a factor of 1.3 (**2**, Entries 3 and 4), 1.2 (**8**, Entries 13 and 14) and 1.1 (**9**, Entries 15 and 16) whereas for the precatalysts **1, 3** and **4**, the reduction in M_n is much significant as it is reduced by a factor of 2.7 (**1**, Entries 1 and 2), 3.0 (**3**, Entries 5 and 6) and 7.7 (**4**, Entries 7 and 8). Unexpectedly, the precatalyst **6** was found to be inactive in the presence of 10 eq./Fe of ZnEt$_2$ (< 1% conversion obtained after 72 h), whereas the formation of very high M_n PI was observed again in the case of **7**, indicating no effect of the presence of the CTA on the polymerization. The dispersity broadens with the precatalysts **1**, **2** and **7**, whereas it is almost similar for the complexes **3** and **4**. The polymerization is more controlled with the **8-9**/Al^{i}Bu$_3$/[Ph$_3$C][B(C$_6$F$_5$)$_4$]/ZnEt$_2$ catalytic systems(*Đ* decreases from 2.1 to 1.4 for complex **8** and 1.6 to 1.3 for complex **9**), despite the relative minor decrease in the M_n values. The results of CCTP are inconsistent with complex **7**, likely owing to its higher rate of propagation resulting in high molecular weight polyisoprenes, albeit limiting conversions to 14 % in 6 hours. The complexes **1-4** bearing alkyl groups on the *N*-aryl moiety were found to be more efficient under polymer chain transfer conditions, with the highest transfer efficiency (37%, transfer efficiency = {[155 000/(20 500]/21} x 100) exhibited by **4**/Al^{i}Bu$_3$/[Ph$_3$C][B(C$_6$F$_5$)$_4$]/ZnEt$_2$ catalytic system. Lastly, and remarkably, the selectivity of each catalytic system was maintained for all the complexes during the CCTP screening.

4.2.6. Varying the quantity of CTA during the CCTP of isoprene with complexes 1-4, 8 and 9

From the previous section, we concluded that the chain transfer was clearly observed with **1**, **3** and **4**/Al^{i}Bu$_3$/[Ph$_3$C][B(C$_6$F$_5$)$_4$]/ZnEt$_2$ catalytic systems, whereas a minor effect was noticed for the complexes **2**, **8** and **9**. On the other hand, for the precatalysts **6** and **7**, there was no effect of CTA on the polymerization. Therefore, at this stage, starting from the less efficient fluorinated catalytic systems **8-9**/Al^{i}Bu$_3$/[Ph$_3$C][B(C$_6$F$_5$)$_4$]/ZnEt$_2$ to more efficient catalytic systems **1-4**/Al^{i}Bu$_3$/[Ph$_3$C][B(C$_6$F$_5$)$_4$]/ZnEt$_2$, we conducted a detailed study through the variation in the amount of ZnEt$_2$ during the polymerization process. The quantity of ZnEt$_2$ (between 0-100 eq. of

Zn *vs.* Fe) was monitored and its impact on the M_n of the resulting polyisoprenes was observed, the results of which are displayed below in Table 4.6.

Table 4.6. CCTP of isoprene using **Fe**/Al^{i}Bu$_3$/[Ph$_3$C][B(C$_6$F$_5$)$_4$] catalytic system with different quantities of ZnEt$_2$[a]

Entry [a]	Fe	[Zn]/[Fe]	Time (min)	Yield (%)	$M_{n(exp)}$ [b] (g/mol)	$Đ$ [b]	N$_{chains}$[c]
1		0	10	> 99	320 000	2.1	-
2	**8**	10	10	> 99	265 000	1.4	1.2
3		50	10	>99	223 000	1.5	1.4
4		100	10	>99	179 000	1.6	1.8
5		0	10	> 99	580 000	1.6	-
6		10	10	> 99	510 000	1.3	1.1
7	**9**	50	10	>99	387 000	1.4	1.5
8		100	10	>99	276 000	1.5	2.1
9		0	360	> 99	487 500*	1.6	-
10	**1**	10	360	> 99	180 000	1.6	2.7
11		50	360	>99	59 000	1.6	8.3
12		100	360	60	20 000	1.4	14.6
13		0	360	> 99	250 000	1.3	-
14	**2**	10	360	> 99	195 000	1.8	1.3
15		50	360	>99	51 000	1.5	4.9
16		100	360	58	17 000	1.4	8.5
17		0	360	> 99	261 000	1.3	-
18	**3**	10	360	> 99	86 000	1.3	3.0
19		50	360	>99	31 000	1.4	8.4
20		100	360	79	13 000	1.4	15.9

[a] Polymerization conditions: 10 µmol of Fe (II) complex; isoprene/Fe/Al^{i}Bu$_3$/[Ph$_3$C][B(C$_6$F$_5$)$_4$] = 2000/1/3/1; toluene = 20 mL, [C]isoprene = 1 mol/L , temperature = 25 °C. [b] Determined by SEC analysis in THF using polystyrene standards. [c] N $_{chains}$ = $M_{n(exp)}$/$M_{n(exp)\,CTA}$; $M_{n(th)}$ = 135 000 g/mol (considering one growing chain per metal center)

From the results in Table 4.6, we can see that increasing the amount of $ZnEt_2$ from 0 to 100 eq./Fe, for the systems based on fluorinated precatalysts **8** and **9**, has a little impact on the resulting M_n of the polyisoprenes. For example, addition of 10 eq./complex **8** of $ZnEt_2$, reduces the M_n by a factor of 1.2 (Table 4.6, Entry 2), which is only reduced by a factor 1.4 as the amount of CTA is increased by 5-fold (50 eq./Fe of $ZnEt_2$) (Table 4.6, Entry 3). However, increasing the amount of CTA by 10-fold (100 eq./Fe of $ZnEt_2$) reduces the M_n by a factor of ~2 where the effect of CTA becomes much significant (Table 4.6, Entry 4). Similar observation can be made for the precatalyst **9**, where the M_n is marginally reduced by a factor of 1.1, 1.5 and 2.1 for the polymerization in the presence of 10, 50 eq. and 100 eq. of $ZnEt_2$, respectively (Table 4.6, Entries 6- 8). Although, the dispersities were somewhat improved for complex **8** ($Đ$ decreases from 2.1 to 1.6) and remained almost similar for complex **9** ($Đ = 1.6–1.5$) but in each case the resulting system produced high molecular weight polyisoprenes in less than 10 mins with excellent conversions (>99%), which again speaks in favor of the comparatively much higher rate of propagation than the rate of transfer.

On contrary, for the less active **1-3**/Al^iBu_3/$[Ph_3C][B(C_6F_5)_4]$ catalytic systems comprising alkylated *N*-aryl groups, varying the amount of $ZnEt_2$ during the course of the polymerization had a significant impact on the M_n of the resulting polyisoprenes. Unlike the catalytic systems issued from complexes **8** and **9**, a decreasing trend in the M_n values is observed for the polyisoprenes resulting from the precatalyst **1**. The addition of 10 eq./Fe of $ZnEt_2$ decreased the M_n by a factor of 2.7, which in turn is reduced by a factor of 8.3 for 50 eq./Fe of $ZnEt_2$ and is finally scaled down by a factor of 14.6 in the presence of 100 eq./Fe of $ZnEt_2$ (Table 4.6, Entries 10-12). Similar trend is observed for the complex **3**, where the M_n value of each entry starting from 10 eq. of $ZnEt_2$ is firstly reduced by a factor of 3, followed by a reducing factor of 8 for 50 eq./Fe of $ZnEt_2$ and finally scales down to a factor of approximately 16 for 100 eq./Fe of $ZnEt_2$ as the amount of CTA gets doubled (Table 4.6, Entries 18-20). On the other hand, unlike complexes **1** and **3**, the decreasing trend in M_n was less significant for complex **2** on the addition of 10 eq./Fe of $ZnEt_2$ where the reduction factor was only 1.3 (Table 4.6, Entry 10). However, a 5-fold increase in the amount of CTA (50 eq./Fe of $ZnEt_2$) reduces the M_n almost by a factor of 5 which further scales down to 8.5 on the addition of 100 eq./Fe of $ZnEt_2$ (Table 4.6, Entries 11 and 12). In addition, the dispersities were maintained with no significant change during the variation in the quantity of CTA. For better comparison, the stacked SEC traces of the obtained polymers are shown below in Figure 4.4.
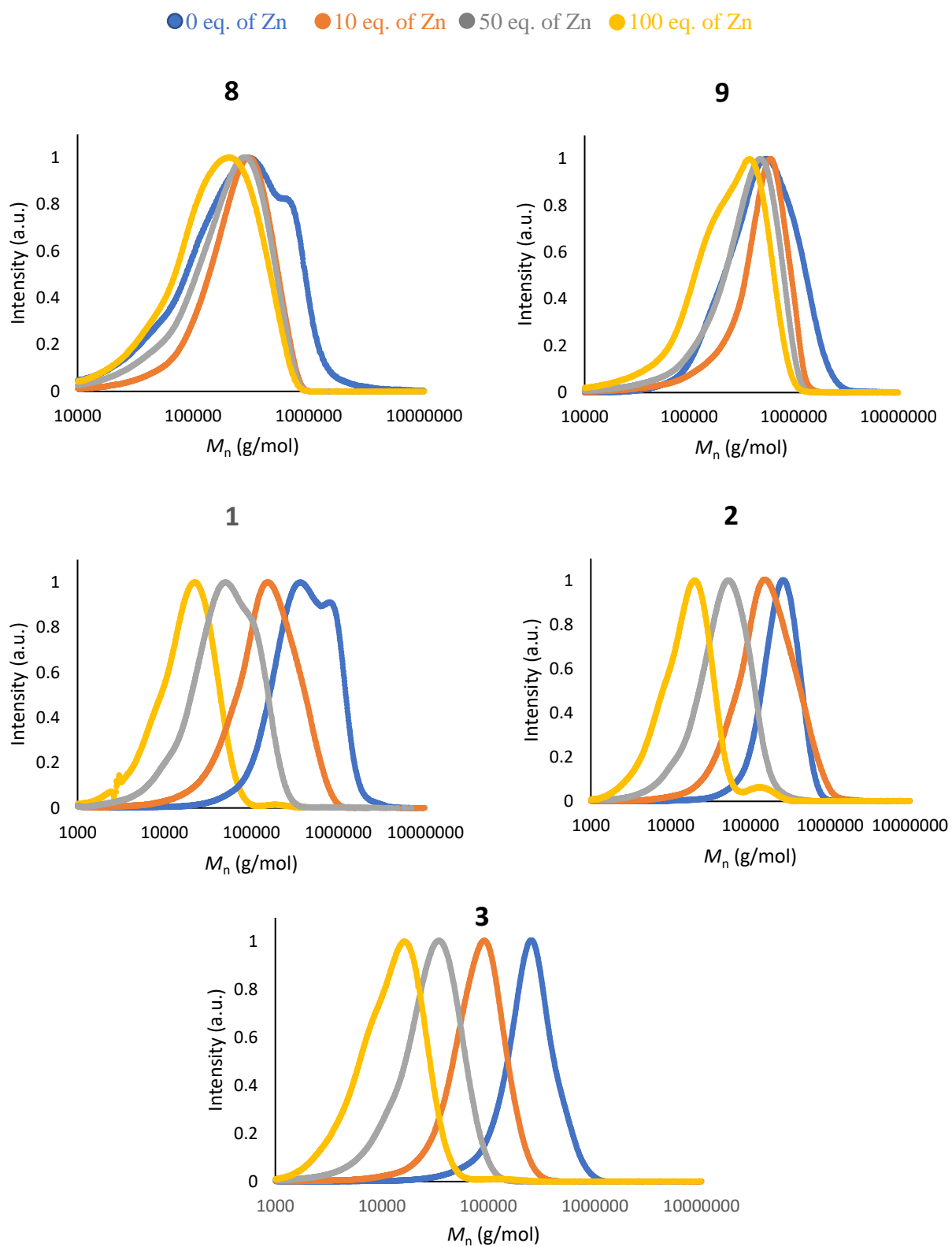
Figure 4.4. SEC traces of the polymers obtained under CCTP with the precatalysts **8, 9** and **1-3**

As we have seen earlier in the last section, the combination of **4**/Al^{i}Bu$_3$/[Ph$_3$C][B(C$_6$F$_5$)$_4$] is the most efficient catalytic system under transfer conditions. Therefore, we conducted a more detailed study of CCTP by increasing the concentration of ZnEt$_2$ with respect to complex **4**. The results of this detailed CCTP screening conducted with complex **4** are shown below in Table 4.7.

Table 4.7. CCTP of isoprene using **4**/Al^{i}Bu$_3$/[Ph$_3$C][B(C$_6$F$_5$)$_4$] catalytic system with different quantities of ZnEt$_2$[a]

Entry [a]	[Zn]/[4]	Time (h)	Yield (%)	$M_{n(exp)}$ [b] (g/mol)	$Đ$ [b]	N_{chains}[c]
1	0	6	>99	155 000	1.3	-
2	5	6	>99	33 000	1.5	4.7
3	10	6	>99	20 500	1.3	7.6
4	20	6	>99	15 000	1.2	10.3
5	30	6	>99	12 000	1.3	13.0
6	40	6	>99	10 000	1.3	15.5
7	50	6	>99	8 000	1.3	19.4
8	100	6	64	6 600	1.2	15.0

[a]Polymerization conditions: 10 µmol of Fe (II) complex; isoprene/Fe/Al^{i}Bu$_3$/[Ph$_3$C][B(C$_6$F$_5$)$_4$] = 2 000/1/3/1; toluene = 20 mL, [C]$_{isoprene}$ = 1 mol/L , temperature = 25 °C. [b] Determined SEC analysis in THF using polystyrene standards. [c] N chains = $M_{n(exp)}$/$M_{n(exp)\ CTA}$; $M_{n(th)}$ = 135 000 g/mol (considering one growing chain per metal center)

From the data in Table 4.7, we could certainly observe a unique and regular trend in the M_n values, which is consistent with the increasing quantities of CTA. By adding 5 eqs. of ZnEt$_2$, the M_n is reduced by a factor of 4.7 (Entry 2 *vs*. 1), which in turn is scaled down by a factor of *ca*. 8 (Entry 3 *vs*. 2) as the amount of CTA gets doubled (from 5 to 10 eq./Fe of ZnEt$_2$). This decreasing trend, which appears to be an exponential decay (Figure 4.5, bottom), is maintained throughout the series of experiments as we compare the M_n value of each entry with the value of the following entry where the quantity of CTA gets doubled. This can also be observed through SEC traces of the polymers obtained in each entry with the characteristic curve shifting to the left (lower masses) as the amount of CTA is increasing in the polymerization mixture (Figure 4.5, top).
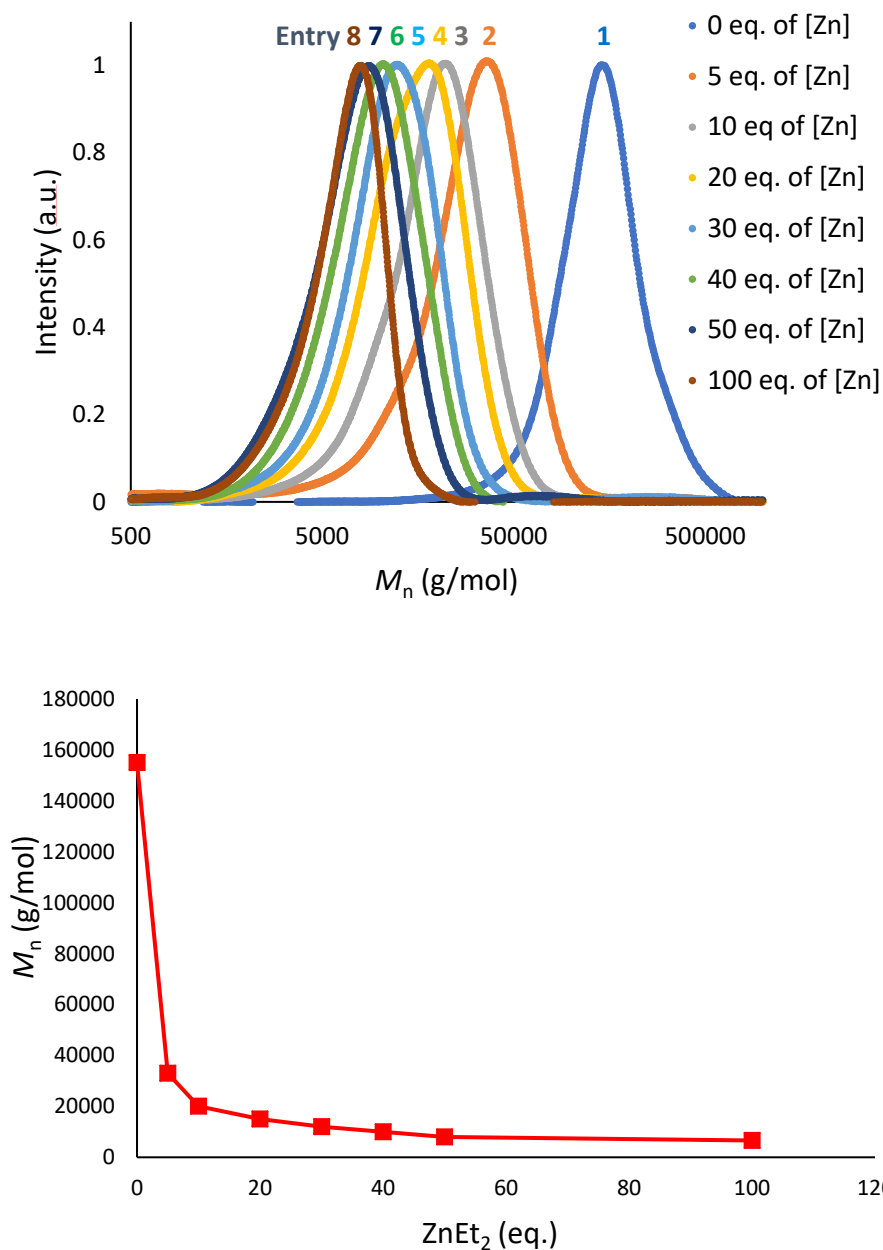
Figure 4.5. SEC traces of the polymers obtained under CCTP with precatalyst **4** (top) and variation in the molar masses with the concentration of ZnEt2 (bottom)

Regarding the selectivity of catalytic system obtained from complex **4**, we observed that it was maintained for the formation of 1,4 and 3,4 motifs, with 1,4-*trans* being the major product (> 77%) throughout the variation of the amount of ZnEt2. This revealed that the growth of the polymer chain is not influenced by the presence of a large amount of CTA, in agreement with what was observed in the previous section 4.2.2. Similarly, the selectivity is preserved for all the other

catalytic systems derived from the remaining complexes **1**-**3**, **8** and **9** as shown earlier in section 4.2.5. As an example, the comparison of selectivity of **4**/Al^{i}Bu$_3$/[Ph$_3$C][B(C$_6$F$_5$)$_4$]/ZnEt$_2$ catalytic system from Table 4.7 is shown in Figure 4.6.
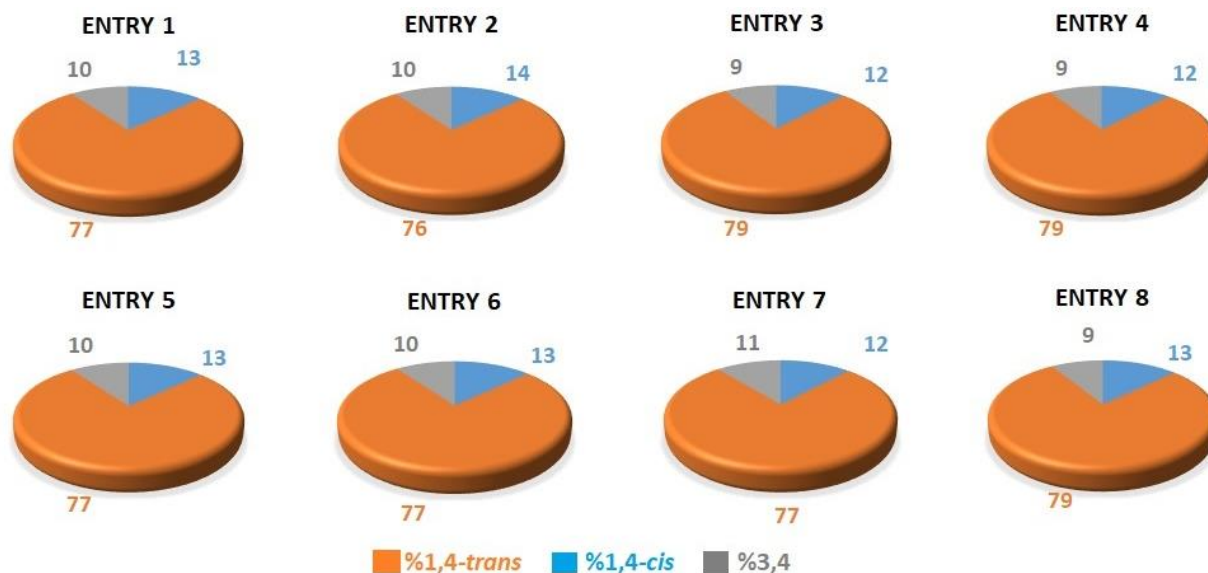
Figure 4.6. Microstructure content of the polyisoprenes obtained from **4**/Al^{i}Bu$_3$/[Ph$_3$C][B(C$_6$F$_5$)$_4$]/ZnEt$_2$

4.2.7. Implementation of Coordinative Chain Shuttling Polymerization using complexes 1-4

One of the remarkable extensions of CCTP concept is represented by Chain Shuttling Polymerization (CSP), where a dual-catalyst system in presence of CTA is used to generate distinct growing macromolecular chains, either from two comonomers or from a unique monomer that can lead to different chain regularities depending on the regio-, chemo- or stereo-selectivity of each catalyst. Thus, the two distinct growing chains are reversibly transferred from one catalyst to another by means of the CTA (here called the chain shuttling agent), giving rise to multiblock architectures that contain block segments with the microstructural signature of each catalyst (Scheme 4.4).

Concerning the CSP, some remarkable contributions have been made for the development of olefin block copolymers by the group of Arriola[1] and Sita.[83] In addition, Hou et al. also reported the CSP of isoprene-styrene using scandium-based catalysts.[84] In the context of dienes, CSP has been independently described by three research groups using either two regio-[85] or stereo-selective[86,87] rare-earth catalysts in the presence of CTA, producing poly(1,3-dienes) multiblock

containing alternated 3,4-/1,4-polyisoprene block or cis/trans-block of either polyisoprene or polybutadiene, respectively.
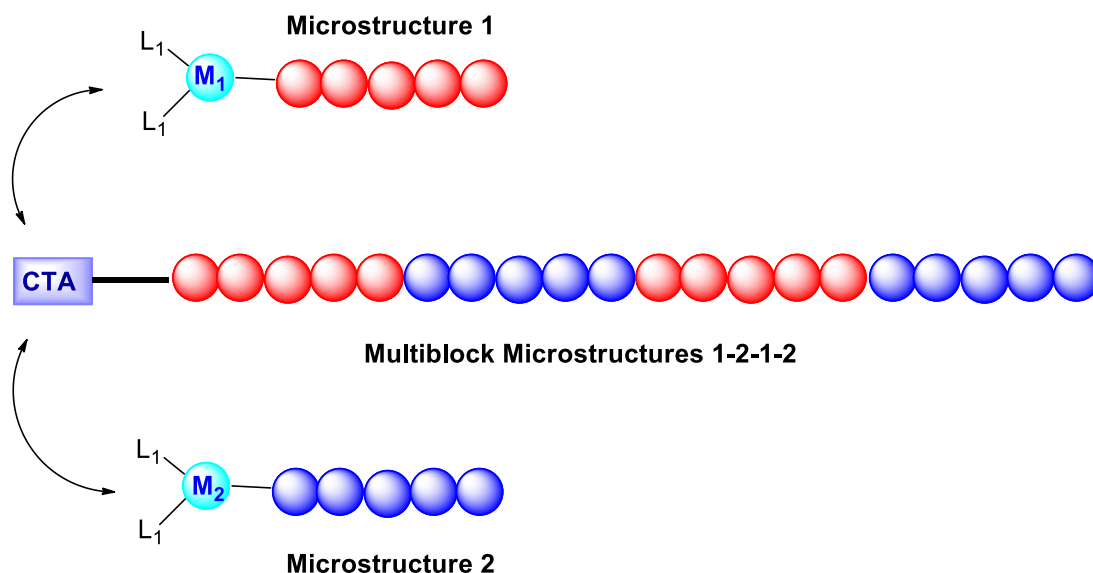
Scheme 4.4. Coordinative Chain Shuttling Polymerization

However, an iron-catalyzed CSP of dienes/olefins remains a challenge till this date. So, after the successful demonstration of a reversible CCTP of isoprene issued from the complexes **1-4**, **8** and **9**, we concluded that polyisoprenyl chain transfer is predominantly efficient with the **1-4**/Al^{i}Bu$_3$/[Ph$_3$C][B(C$_6$F$_5$)$_4$]/ZnEt$_2$ catalytic systems. Despite the moderate regio- and stereo-selectivity of these iron-based systems for the CCTP of isoprene, we still attempted to prepare multiblock polyisoprene by implementating a chain shuttling stage between two catalytic systems possessing different stereoselectivities.

*4.2.7.1. CSP of isoprene using complexes **2** and **4***

Once activated with Al^{i}Bu$_3$/[Ph$_3$C][B(C$_6$F$_5$)$_4$], the iron iminopyridine complexes **2** and **4**, bearing bulky 2,6-diisopropyl groups as their *N*-aryl substituents, generate two catalytic systems that possess a noticeable difference in terms of their respective selectivities; the former (complex **2**, aldiminopyridine) being fairly 1,4-*cis* selective whereas the latter (complex **4**, ketiminopyridine) is rather 1,4-*trans* selective at room temperature. Due to these reasons, we intended to establish a chain shuttling system by mixing the two individual catalysts derived from **2** and **4** in the presence of an excess of ZnEt$_2$, as shown in Scheme 4.5.
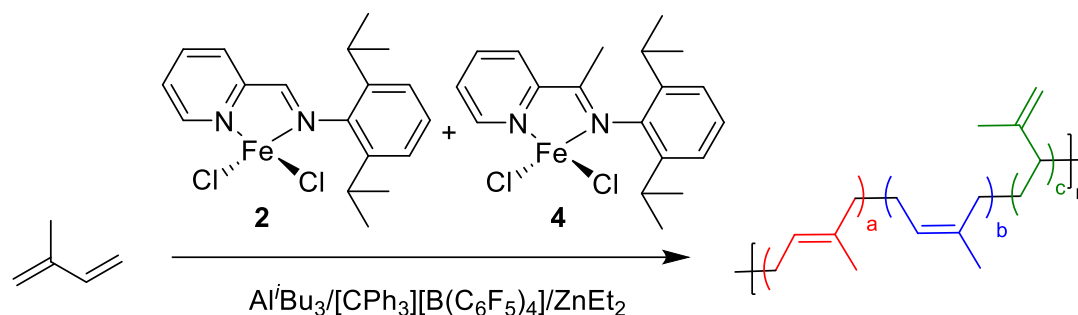
Scheme 4.5. CSP of isoprene using **2+4**/Al^{i}Bu$_3$/[Ph$_3$C][B(C$_6$F$_5$)$_4$]/ZnEt$_2$ catalytic system

The polymerizations were performed under the molar ratios of isoprene/Fe = 2000/1 (Fe = **2** + **4**) with ZnEt$_2$ (10 eqs./Fe) acting as a chain shuttling agent. The results of these chain shuttling experiments are depicted below in Table 4.8.

Table 4.8. Chain shuttling polymerization (CSP) of isoprene using **2+4**/Al^{i}Bu$_3$/[Ph$_3$C][B(C$_6$F$_5$)$_4$]/ZnEt$_2$ catalytic system[a]

Entry [a]	[4]/[2]	Yield (%)	$M_{n(exp)}$ (g/mol) [b]	Đ [b]	Microstructure [c] (%) 1,4 (*trans*/*cis*)	3,4
1	10/0	97	17 000	1.4	86 (66/20)	14
2	9/1	90	22 000	1.6	86 (60/26)	14
3	5/5	95	22 000	1.4	79 (41/38)	21
4	1/9	>99	61 000	1.5	72 (21/51)	28
5	0/10	>99	195 000	1.8	75 (32/43)	25
6 [d]	5/5	>99	234 000	1.4	78 (35/43)	22

[a] Polymerization conditions: 10 µmol of **[2+4]** complex; isoprene/**2+4**/Al^{i}Bu$_3$/[Ph$_3$C][B(C$_6$F$_5$)$_4$]/ZnEt$_2$ = 2000/1/3/1/10; toluene = 20 mL, [C]$_{isoprene}$ = 1 mol/L, temperature = 25 °C, time = 3h; [b] Determined by SEC analysis in THF using polystyrene standards; $M_{n(th)}$ = 135 000 g/mol (considering one growing chain per metal center). [c] Determined by ^{1}H NMR and ^{13}C NMR. [d] In absence of ZnEt$_2$

As discussed in the previous sections of this chapter, the **2**/Al^{i}Bu$_3$/[Ph$_3$C][B(C$_6$F$_5$)$_4$]/ZnEt$_2$ catalytic system produces PI containing a high percentage of 1,4 motifs (75%), with low 1,4-*cis* selectivity (43%), and 25% of 3,4-units (Table 4.8, Entry 5). On the other hand, the **4**/Al^{i}Bu$_3$/[Ph$_3$C][B(C$_6$F$_5$)$_4$]/ZnEt$_2$ catalytic system generates PI chains with 86% of 1,4-units, from which 66% are 1,4-*trans* units, together with a small amount of 3,4-unit (14%) (Table 4.8, Entry 1). The transfer between the growing polymer chain from complex **2** to the CTA occurs with low

effciency as evidenced by the poor reduction of M_n in the presence of 10eq./Fe of ZnEt$_2$ (M_n = 250 000 g/mol *vs.* 195 000 g/mol, Entry 13, Table 4.6 *vs.* Entry 5, Table 4.8, respectively). In contrast, the occurrence of a chain transfer process was clearly evident for the catalytic system issued from complex **4** since the resulting M_n was considerably lower than that of the polymer produced without the presence of ZnEt$_2$ (M_n = 155 000 g/mol *vs.* 17 000 g/mol, Entry 1, Table 4.7, *vs.* Entry 1, Table 4.8, respectively). By adding a small amount of the complex **2** in a solution containing the complex **4** (Table 4.8, Entry 2, **4/2** ratio = 9/1), a minor decrease in the *trans*-1,4 selectivity (60%) was observed with a modest increase of *cis*-1,4 units (26%) in the resulting PI chain, which also exhibits slightly higher M_n value (M_n = 17 000 *vs* 22 000 g/mol, Table 4.8, Entry 1 *vs* 2). Mixing equivalent amounts of complex **2** and **4** gave a catalytic system that produced PI with slightly lower 1,4 selectivity (79%) with an increase percentage of 3,4 motifs (21%). Interestingly, the resulting PI contained nearly equal amounts of 1,4-*trans* (41%) and 1,4-*cis* (38%) motifs, highlighting the individual contribution of each catalytic system (Table 4.8, Entry 3). However, in terms of number average molecular weight, the contribution of PI featuring a high M_n due to the addition of complex **2** was unexpectedly absent since the resulting polymer exhibited a low M_n as obtained earlier with the preceeding ratio **4/2** = 9/1. By comparison, the same polymerization was performed in the absence of ZnEt$_2$ (Table 4.8, Entry 6) and produced polyisoprene displaying stereo-, regio-regularity *quasi*-similar to that obtained in the presence of ZnEt$_2$, while the number average molecular weight (M_n = 234 000 g/mol) was found to be in the range of the M_n resulting from the individual catalysts in absence of ZnEt$_2$ (M_n = 250 000 g/mol for **2** and M_n = 155 000 g/mol for **4**). However, the resulting M_n of the polymer produced in presence of ZnEt$_2$ is nearly 11 times lower than that achieved without ZnEt$_2$ (M_n = 22 000 *vs* 234 000 g/mol, entry 3 *vs.* entry 6, respectively), which indicates the obvious presence of Fe/Zn polyisoprene chain transfer. An increase ratio of complex **2** to **4** (**4/2** = 1/9) has led to the PI displaying a microstructure content that tend to be closer to the polymer produced by complex **2** alone (Table 4.8, Entry 4 *vs* Entry 5: *trans*-1,4/*cis*-1,4/3,4 content = 21/51/28 *vs* 32/43/25, respectively), despite showing a PI with a lower M_n than expected (M_n = 61 000 g/mol).

In summary, the selectivity of the catalytic system varies from moderate 1,4-*trans* to fairly 1,4-*cis* depending on the amount of catalytic precursors, which appears as a good sign of CSP possibly operating. Increasing the ratio of complex **2** with respect to complex **4** enhances the 1,4-*cis* selectivity upto 51%. However, the inconsistency in the M_n values of the resulting

polyisoprenes from the catalytic system based on **2**+**4** prevents us from claiming the complete and successful establishment of a CSP stage between the precatalysts **2** and **4.** The unusual significant reduction in the M_n values could also be attributed to the high transfer efficiency possessed by the **2**+**4**/Al^{i}Bu$_3$/[Ph$_3$C][B(C$_6$F$_5$)$_4$]/ZnEt$_2$ catalytic combination which is somehow obvious for complex **4** but rather unusual for complex **2** when assessed individually under CCTP (Table 4.8, Entry 1 *vs* Entry 5).

4.2.7.2. CSP of isoprene using complexes 1 and 3

The anomalous CSP attempt with the catalytic precursors **2** and **4** prompted us to tentatively develop an alternative CSP system involving other catalytic precursors. As seen earlier, the system **1**/Al^{i}Bu$_3$/[Ph$_3$C][B(C$_6$F$_5$)$_4$] exhibits fair 1,4-*cis* selectivity, whereas the system **3**/Al^{i}Bu$_3$/[Ph$_3$C][B(C$_6$F$_5$)$_4$] exhibits moderate 1,4-*trans* selectivity at room temperature. Since the transfer efficiencies are quite similar between these two catalysts (N$_{chains}$ = 2.7 – 3 for complex **1** and **3**, Table 4.5, Entry 2 and 6) in addition to the least possible difference they possess in their respective activities (TOF (h^{-1}) = 26 700 for **1** and 12 450 for **3**, Section 2.2.3.1.3), we intended to establish a chain shuttling system by mixing the two individual catalysts derived from **1** and **3** as shown below in Scheme 4.6.
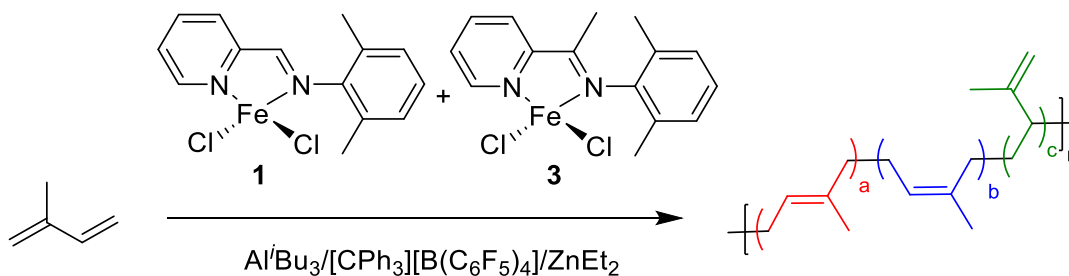
Scheme 4.6. CSP of isoprene using **1**+**3**/Al^{i}Bu$_3$/[Ph$_3$C][B(C$_6$F$_5$)$_4$]/ZnEt$_2$ catalytic system

The CSP of isoprene was carried out at room temperature for 6 hours using different ratios of a mixture of complexes **1** and **3** combined with Al^{i}Bu$_3$/[B(C$_6$F$_5$)$_4$][CPh$_3$] in the presence of 10 eq. of ZnEt$_2$/**1**+**3**. The results of these chain shuttling polymerization experiments are depicted below in Table 4.9.

Table 4.9. Chain shuttling polymerization of isoprene using $\mathbf{1+3}$/Al^{i}Bu$_3$/[Ph$_3$C][B(C$_6$F$_5$)$_4$]/ZnEt$_2$ catalytic system[a]

Entry [a]	[3]/[1]	Time (h)	Yield (%)	$M_{n(exp)}$ (g/mol) [b]	$\eth$ [b]	Microstructure [c] (%) 1,4 (*trans*/*cis*)	3,4	T_g (°C) [d]
1	10/0	6	>99	86 000	1.3	90 (69/21)	10	-61.7
2	9/1	6	>99	97 000	1.5	89 (66/23)	11	-60.3
3	5/5	6	>99	120 000	1.5	85 (40/45)	15	-56.8
4	1/9	6	>99	150 000	1.5	79 (38/41)	21	-51.2
5	0/10	6	>99	180 000	1.7	79 (33/46)	21	-51.6
6 [e]	5/5	6	>99	380 000	1.6	84 (43/41)	16	-55.5

[a] Polymerization conditions: 10 µmol of **[1+3]** complexes; isoprene/$\mathbf{1+3}$/Al^{i}Bu$_3$/[Ph$_3$C][B(C$_6$F$_5$)$_4$]/ZnEt$_2$ = 2000/1/3/1/10; toluene = 20 mL, [C]$_{isoprene}$ = 1 mol/L, temperature = 25 °C. [b] Determined by SEC analysis in THF using polystyrene standards; $M_{n(th)}$ = 1350 00 g/mol (considering one growing chain per metal center). [c] Determined by ^{1}H NMR and ^{13}C NMR. [d] Determined by DSC. [e] In absence of ZnEt$_2$

Firstly, the catalytic system **3**/Al^{i}Bu$_3$/[B(C$_6$F$_5$)$_4$][CPh$_3$]/ZnEt$_2$ produced polyisoprene (M_n = 86 000 g/mol, $\eth$ = 1.3) whose microstructure contains 1,4-*trans*/1,4-*cis*/3,4 units = 69/22/9 with a T_g value of – 61.7 °C (Table 4.9, Entry 1). In contrast, the catalytic system **1**/Al^{i}Bu$_3$/[Ph$_3$C][B(C$_6$F$_5$)$_4$]/ZnEt$_2$ generates polyisoprene (M_n = 180 000 g/mol, $\eth$ = 1.7) whose microstructure contains 1,4-*trans*/1,4-*cis*/3,4 units = 33/46/21 with a T_g value of – 51.6 °C (Table 4.9, Entry 5). By adding a small amount of complex **1** (**3/1** ratio = 9/1), a minor decrease in the 1,4-*trans* selectivity was observed with a modest increase of 3,4 units in the resulting polyisoprene (1,4-*trans*/3,4 = 66/11, Table 4.9, Entry 2), which also exhibits slightly higher values of T_g and M_n (T_g = – 60.3 *vs* – 61.7 °C and M_n = 97 000 *vs* 86 000 g/mol for **3/1** = 9/1 and 3 alone, respectively). Most interestingly, when a 1/1 ratio of complexes **3/1** was used in presence of 10 eq. of ZnEt$_2$, the resulting polyisoprene exhibits average values of microstructure contents, M_n and T_g values (1,4-*trans*/1,4-*cis*/3,4 = 40/45/15, M_n = 120 000 g/mol, T_g = – 56.8 °C, Table 4.9, Entry 3) of both individual catalytic systems under CCTP. The same polymerization was also carried out in the absence of ZnEt$_2$ and resulted in a polyisoprene presenting a stereo-, regio-regularity along with a T_g value *quasi* similar to that obtained in the presence of CTA (Table 4.9, Entry 3 *vs* 6). This can also be observed through the stacked NMR spectra (Figure 4.7) and DSC thermograms (Figure 4.8) of the obtained PIs produced with and without ZnEt$_2$.
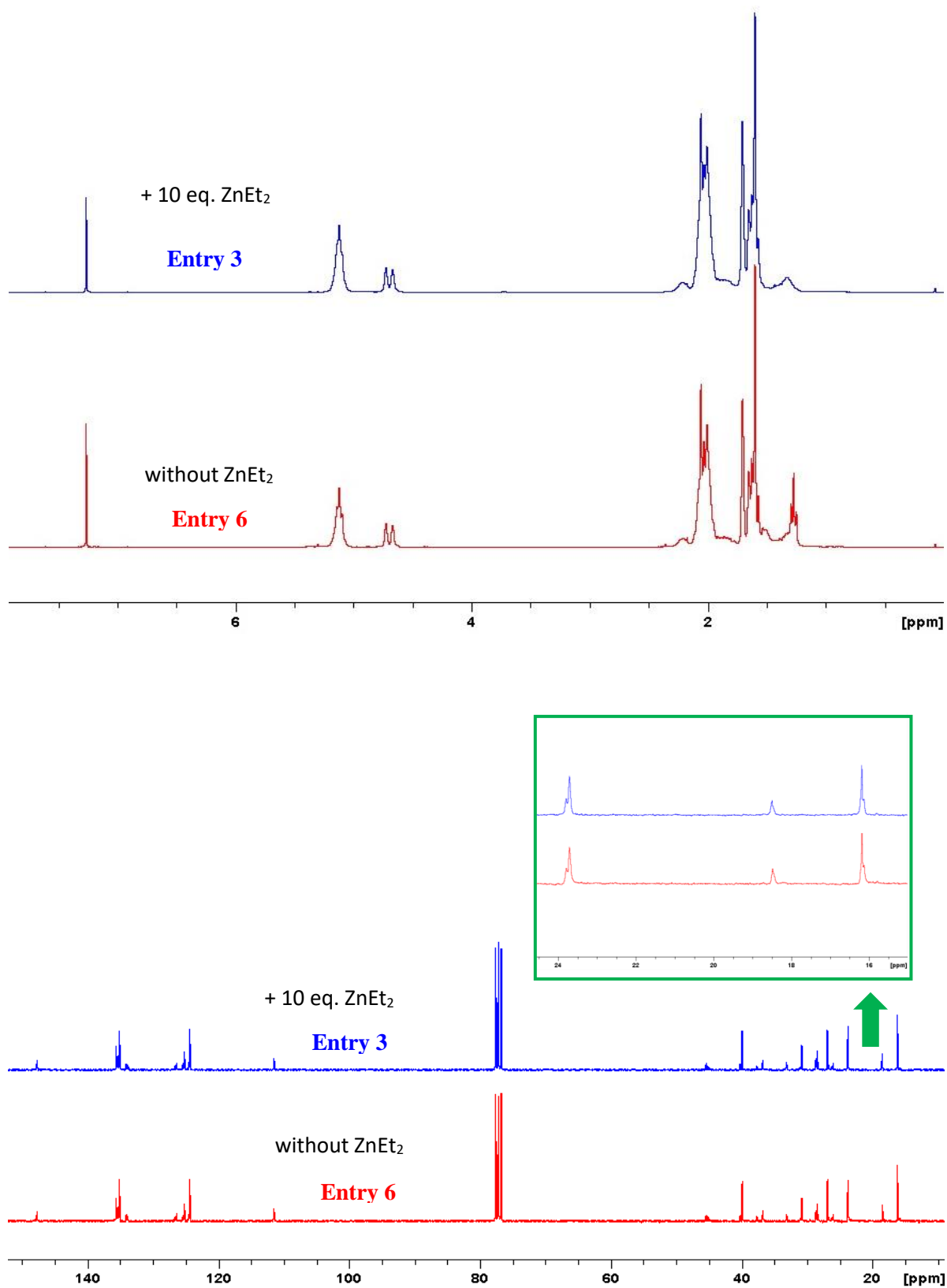
Figure 4.7. Stacked NMR spectra (¹H top and ¹³C bottom) of polyisoprene (Table 4.9, Entry 3 *vs* Entry 6)
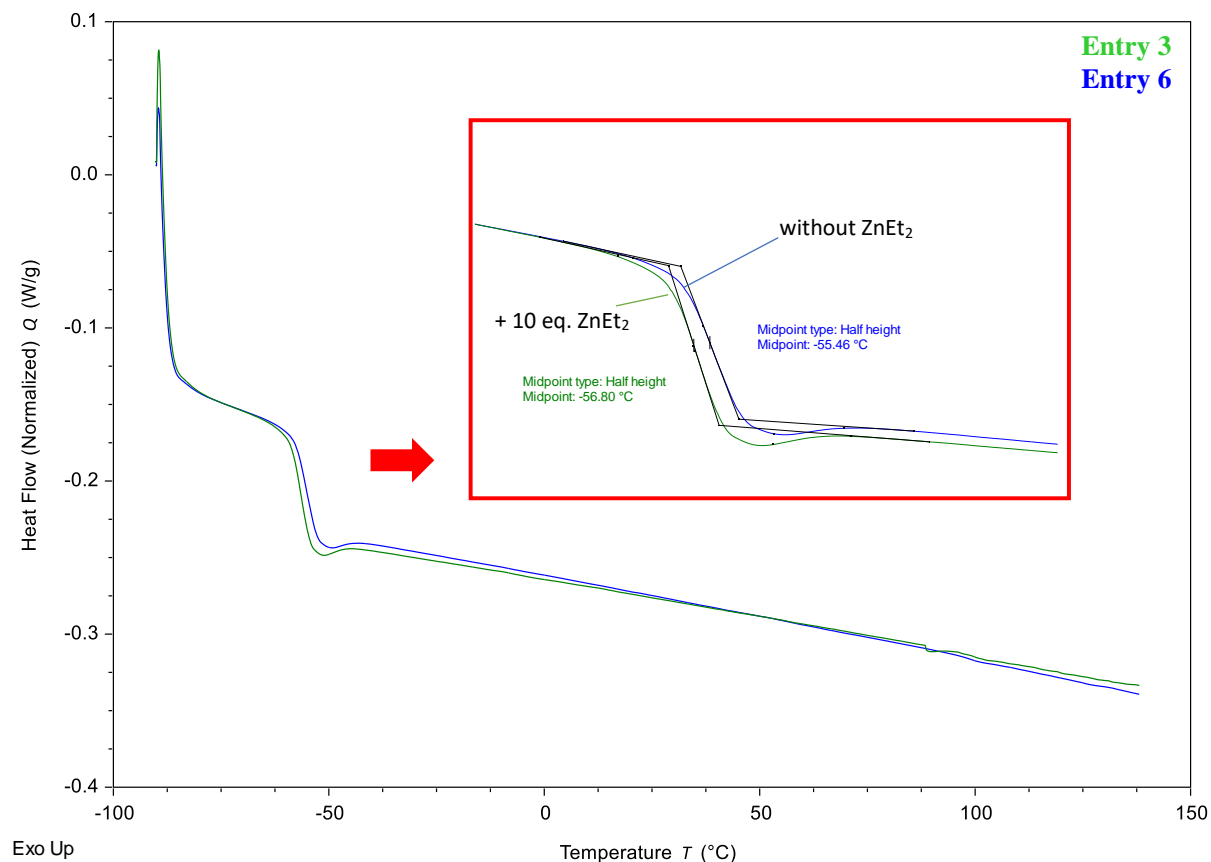
Figure 4.8. Stacked DSC thermograms (2nd Heating) of polyisoprenes (Table 4.9, Entry 3 *vs* Entry 6)

The unique glass transition found at $-55.5\ ^\circ\text{C}$ was expected given that the physical mixture of the two homopolymers, produced independently by CCTP, displays a single T_g of $-57.1\ ^\circ\text{C}$ due to the miscibility of the blend. However, the resulting M_n of the polymer produced under CSP was found to be 3 times lower than that achieved without $ZnEt_2$ ($M_\text{n} = 180000\ vs\ 380000$ g/mol, respectively, Figure 4.9), which is similar to the number of chains generated for each independent catalyst under CCTP conditions ($N_\text{chains} = 2.7 - 3$).
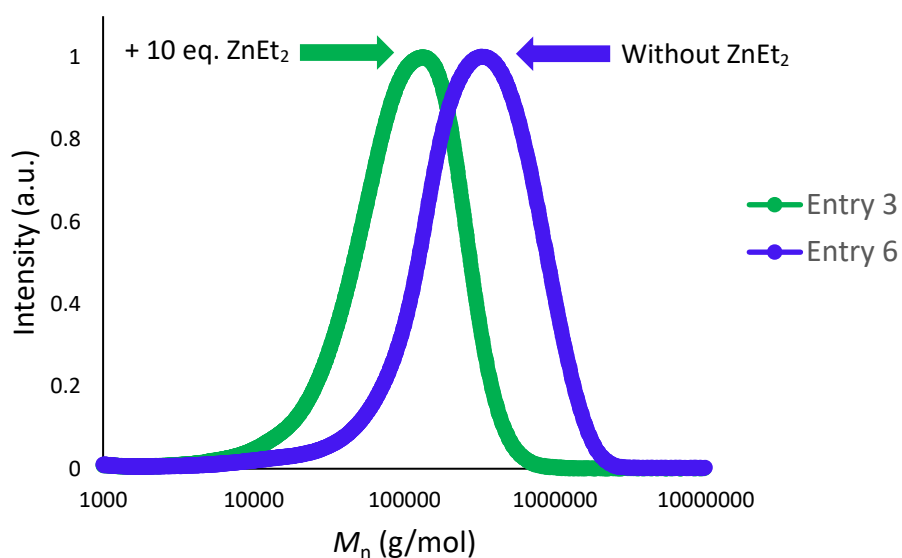
Figure 4.9. Stacked SEC traces of polyisoprene (Table 4.9, Entry 3 *vs* Entry 6)

An increased ratio of complex **1** to **3** (**3/1** = 1/9, Table 4.9, Entry 4) has led to the polyisoprene displaying a microstructure content (1,4-*trans*/1,4-*cis*/3,4 units = 38/41/21) along with M_n (150 000 g/mol) and T_g (− 51.2 °C) values that tend to be closer to the polymer produced by complex **1** alone (M_n = 180 000 g/mol, T_g = − 51.6 °C, Table 4.9, Entry 5). As expected, the dispersity broadens and the molar mass increases at each new step of complex **1** loading (Table 4.9, Entries 4 and 5).

In summary, despite the similarity of the DSC thermograms (Figure 4.8) and NMR spectra (Figure 4.7) of the polymers resulting from a 1/1 ratio of complexes **1** and **3** in the absence and the presence of ZnEt$_2$, these results prevent us from stating unequivocally that the cross-transfer process has actually taken place, however, the 3-fold reduction in the M_n of the polymer produced in the presence of ZnEt$_2$ compared to that without ZnEt$_2$ strongly suggests the occurrence of a CSP process. Moreover, it also proves that CSP process seems efficient here, as observed previously in similar fashion by the group of Cui with rare-earth catalysts.[85]

4.3. Conclusion

In this study, we have successfully reported the first CCTP of isoprene with an iron-based catalytic system. The preliminary screening of **4**/MAO catalytic system with different amounts of $ZnEt_2$ suggested that the transfer occurred, but it was found to be less efficient and inconsistent with increasing quantities of $ZnEt_2$, probably due to the occurrence of some cross-transfer reactions with free $AlMe_3$. The alternative system **4**/Al^{i}Bu$_3$/[Ph$_3$C][B(C$_6$F$_5$)$_4$] with a combination of various metal alkyls as potential CTAs (Al^{i}Bu$_3$, $ZnEt_2$ and BuMgEt) was screened during the CCTP of isoprene, amongst which it was observed that the transfer is only efficient with $ZnEt_2$, probably owing to its monomeric nature in solution and less steric bulk around Zn, as was already argued during the CCTP of ethylene by the group of Gibson.[12]

The transfer conditions were also optimized by varying the concentration of monomer in order to investigate its influence on the transfer efficiency of the **4**/Al^{i}Bu$_3$/[Ph$_3$C][B(C$_6$F$_5$)$_4$]/$ZnEt_2$ catalytic system. Varying the concentration of monomer from 1 M to 10 M resulted in the formation of low molecular weight PIs without altering the transfer efficiency, albeit limiting the conversions to 52% at highest concentration that could arise from the blockage of the transfer between Fe and Zn at a certain stage, according to our own hypothesis. We propose that due to the formation of a stable heterobimetallic Fe-Zn allyl species, the polymerization is impeded to proceed to full conversion. This was also supported by the screening of bis-allylzinc as a CTA, which failed to polymerize isoprene under transfer conditions.

Furthermore, under the optimized conditions, the catalytic systems involving the iron complexes **1-4** and **6-9**, with a combination **Fe**/Al^{i}Bu$_3$/[Ph$_3$C][B(C$_6$F$_5$)$_4$]/$ZnEt_2$, were assessed individually for the CCTP of isoprene and the order of transfer efficiency was found to be dependent on the molecular structure of the precatalysts, as described below in Chart 4.2. The complexes **6-9** bearing fluorinated substituents on their *N*-aryl moieties were found to be the least efficient under transfer conditions due to their high rate of propagation, which led to an extremely high activity towards the polymerization of isoprene.[61] The complexes **1-4** bearing alkyl groups on the *N*-aryl substituents were found to be more efficient under CCTP conditions, with the **4**/Al^{i}Bu$_3$/[Ph$_3$C][B(C$_6$F$_5$)$_4$]/$ZnEt_2$ catalytic system exhibiting the highest transfer efficiency (37%),

which was also confirmed through a detailed study. This combination is to our knowledge the first one reported as efficient for the CCTP of isoprene in the case of an iron-based catalyst.
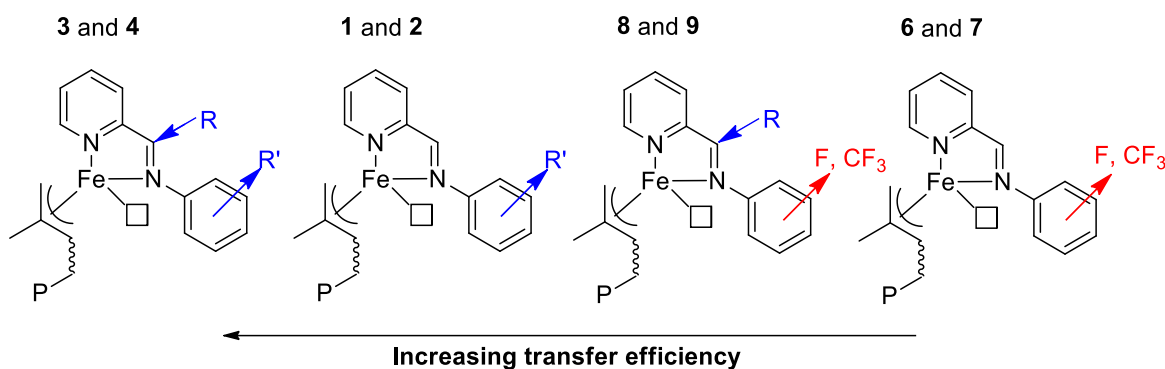
Chart 4.2. Order of transfer efficiency of pre-catalysts

Lastly, attempts of performing a polymerization of isoprene using a mixture of the complexes **2** and **4** combined with 10 eq. ZnEt$_2$, after cocatalyst activation, resulted to a dual catalytic system that was capable of producing polyisoprene with a variety of stereo- and regioregularity. However, due to the huge activity difference between the two individual catalytic systems and the resulting inconsistency in the M_n values, a successful establishment of CSP stage could not be claimed undoubtedly between the two catalytic precursors. On the other hand, using the other set of catalytic precursors **1** and **3** combined with 10 eq. ZnEt$_2$, after cocatalyst activation, suggested the occurrence of Chain Shuttling Polymerization process through which we observed a strong selectivity dependence on the ratio of the catalytic precursors. Further detailed studies can be carried out in the future for development of this topic.

4.4 Experimental Section

4.4.1. General Information

ZnEt$_2$ (Sigma-Aldrich) and MAO were used as received. Differential Scanning Calorimetry (DSC) experiments were carried out on a DSC 25TA (Thermal Analysis) instrument which was calibrated with a high purity indium sample according to standard procedures. The samples (≈ 4 mg) were put in sealed pans and analyzed in the temperature range from -90 to +140 °C at a

heating rate of 10 °C/min under nitrogen atmosphere. The T_g values corresponding to the second heating were calculated and reported. The remaining procedures are exactly similar as described in Section 2.4.1.

4.4.2. General Procedure for Chain transfer Polymerization of Isoprene and Calculation of Microstructure Contents

A Schlenk flask (100 mL) was heated, dried in a vacuum and purged with argon three times before introducing it to the glove box. Iron (II) chloride complex (10 µmol, 1 eq.) and toluene (17 mL) were added to the reactor followed by the addition of triisobutylaluminum (30 µmol, 3 eq.) at 23 °C. The reaction mixture was stirred for 2-3 mins and a solution of trityltetrakis(pentafluorophenyl)borate (10 µmol, 1 eq.) in toluene (3 mL) was added to the reaction mixture at 23 °C. The mixture was stirred for 2 min and $ZnEt_2$ (50-1000 µmol) was added under stirring conditions before adding isoprene (1.362 g, 2 mL, 2000 eq.). The reaction mixture was stirred for 6 hours before opening it to air and quenching it by 2-3 drops of diluted HCl (1 M) followed by its dilution with toluene. The polymer was precipitated in ethanol (150 mL) containing the stabilizing agent BHT (tert-butyl hydroxytoluene), isolated and dried in vacuum for 4 h to yield a gummy solid.

The remaining procedure is similar as previously described in Section 2.4.1.

4.4.3. General Procedure for Chain Shuttling Polymerization of Isoprene

A Schlenk flask (100 mL) was heated, dried in a vacuum and purged with argon three times before introducing it to the glove box. Iron (II) chloride complexes (5 µmol, 0.5 eq.) were weighed in separate vials and were further dissolved in toluene (1 mL). The activation of each complex at 23 °C was done by the addition of triisobutylaluminum (15 µmol, 1.5 eq.) to each vial containing the complex solutions. The mixtures were stirred for 2-3 mins and a solution of trityltetrakis(pentafluorophenyl)borate (5 µmol, 0.5 eq.) in toluene (1 mL) was added to the vials containing reaction mixture at 23 °C. The resulting mixtures were stirred for 2 mins before being mixed in a Schlenk flask and diluted with toluene (16 mL) for the chain shuttling experiments. Further, $ZnEt_2$ (100 µmol, 10 eq.) was added under stirring conditions before adding isoprene (1.362 g, 2 mL, 2000 eq.) to initiate the polymerization.

The remaining procedure is similar as previously described in Section 4.4.2.

References

(1)   Arriola, D. J.; Carnahan, E. M.; Hustad, P. D.; Kuhlman, R. L.; Wenzel, T. T. *Science* **2006**, *312*, 714.

(2)   Chenal, T.; Visseaux, M. *Macromolecules* **2012**, *45* (14), 5718–5727.

(3)   Amin, S. B.; Marks, T. J. *Angew Chem* **2008**, *47*, 2006.

(4)   *Metal Catalysts in Olefin Polymerization*; Guan, Z., Ed.; Topics in Organometallic Chemistry; Springer Berlin Heidelberg: Berlin, Heidelberg, 2009; Vol. 26.

(5)   Coates, G. W. *J. Chem. Soc. Dalton Trans.* **2002**, No. 4, 467–475.

(6)   Breuil, P.-A. R.; Magna, L.; Olivier-Bourbigou, H. *Catal. Lett.* **2015**, *145* (1), 173–192.

(7)   Coates, G. W. *Chem. Rev.* **2000**, *100* (4), 1223–1252.

(8)   Olonde, X.; Mortreux, A.; Petit, F. *J Mol Catal* **1993**, *82*, 75.

(9)   Pelletier, J. F.; Mortreux, A.; Petit, F.; Olonde, X.; Bujadoux, K.; Soga, K.; Terano, M. *Catalyst Design for Tailor Made Polyolefins*; 1994.

(10)   Pelletier, J. F.; Mortreux, A.; Olonde, X.; Bujadoux, K. *Angew Chem* **1996**, *35*, 1854.

(11)   Bujadoux, K.; Chenal, T.; Fouga, C.; Olonde, X.; Pelletier, J. F.; Mortreux, A.; Kaminsky, W. *Metalorganic Catalysts for Synthesis and Polymerization*; 1999.

(12)   Britovsek, G. J. P.; Cohen, S. A.; Gibson, V. C.; Maddox, P. J.; van Meurs, M. *Angew Chem Int Ed* **2002**, *41*, 489.

(13)   Britovsek, G. J. P.; Cohen, S. A.; Gibson, V. C.; van Meurs, M. *J Am Chem Soc* **2004**, *126*, 10701.

(14)   Zinck, P.; Valente, A.; Mortreux, A.; Visseaux, M. *Polymer* **2007**, *48*, 4609.

(15)   Chenal, T.; Olonde, X.; Pelletier, J. F.; Bujadoux, K.; Mortreux, A. *Polymer* **2007**, *48*, 1844.

(16)   Kempe, R. *Chem Eur J* **2007**, *13*, 2764.

(17)   Sita, L. R. *Angew Chem Int Ed* **2009**, *48*, 2464.

(18)   Heurtefeu, B.; Vaultier, F.; Leino, R.; Boisson, C.; Cramail, H. *Encyclopedia of Polymer Science and Technology*; 4, Ed.; 2012.

(19)   Valente, A.; Mortreux, A.; Visseaux, M.; Zinck, P. *Chem. Rev.* **2013**, *113* (5), 3836–3857.

(20)   Liu, H.; Wang, F.; Liu, L.; Dong, B.; Zhang, H.; Bai, C.; Hu, Y.; Zhang, X. *Inorganica Chim. Acta* **2014**, *421*, 284–291.

(21)   Aluminium-organische Synthese im Bereich olefinischer Kohlenwasserstoffe - Ziegler - 1952 - Angewandte Chemie - Wiley Online Library https://onlinelibrary.wiley.com/doi/abs/10.1002/ange.19520641202 (accessed Mar 25, 2020).

(22)   van Meurs, M.; Britovsek, G. J. P.; Gibson, V. C.; Cohen, S. A. *J Am Chem Soc* **2005**, *127*, 9913.

(23)   Karpiniec, S. S.; McGuinness, D. S.; Britovsek, G. J. P.; Wierenga, T. S.; Patel, J. *Chem. Commun.* **2011**, *47* (24), 6945–6947.

(24)   Karpiniec, S. S.; McGuinness, D. S.; Britovsek, G. J. P.; Davies, N. W.; Patel, J. *Catal. Today* **2011**, *178* (1), 64–71.

(25)   Karpiniec, S. S.; McGuinness, D. S.; Britovsek, G. J. P.; Patel, J. *Organometallics* **2012**, *31* (8), 3439–3442.

(26)   Zhang, W.; Wei, J.; Sita, L. R. *Macromolecules* **2008**, *41*, 7829.

(27)   Rogers, J. S.; Bazan, G. C. *Chem Commun* **2000**, 1209.

(28)   Mani, G.; Gabbai, F. P. *Angew Chem* **2004**, *116*, 2313.

(29)   Kretschmer, W. P.; Meetsma, A.; Hessen, B.; Schmalz, T.; Qayyum, S.; Kempe, R. *Chem—Eur J* **2006**, *12*, 8969.

(30)   Kuhlman, R. L.; Wenzel, T. T. *Macromolecules* **2008**, *41*, 4090.

(31)   Zhang, W.; Sita, L. R. *J Am Chem Soc* **2008**, *130*, 442.

(32)   Bogaert, S.; Chenal, T.; Mortreux, A.; Nowogrocki, G.; Lehmann, C. W.; Carpentier, J.-F. *Organometallics* **2001**, *20*, 199.

(33)   Zinck, P.; Visseaux, M.; A. Mortreux, Z. *Anorg Allg Chem* **2006**, *632*, 1943.

(34)   Zinck, P.; Valente, A.; Bonnet, F.; Violante, A.; Mortreux, A.; Visseaux, M.; Ilinca, S.; Duchateau, R.; Roussel, P. *J Polym Sci Part Polym Chem* **2010**, *48*, 802.

(35) Wei, J.; Duman, L. M.; Redman, D. W.; Yonke, B. L.; Zavalij, P. Y.; Sita, L. R. *Organometallics* **2017**, *36* (21), 4202–4207.

(36) Belaid, I.; Poradowski, M.-N.; Bouaouli, S.; Thuilliez, J.; Perrin, L.; D'Agosto, F.; Boisson, C. *Organometallics* **2018**, *37* (10), 1546–1554.

(37) Minyaev, M. E.; Komarov, P. D.; Roitershtein, D. M.; Lyssenko, K. A.; Nifant'ev, I. E.; Puntus, L. N.; Varaksina, E. A.; Borisov, R. S.; Dyadchenko, V. P.; Ivchenko, P. V. *Organometallics* **2019**, *38* (15), 2892–2901.

(38) Lee, H. J.; Baek, J. W.; Kim, T. J.; Park, H. S.; Moon, S. H.; Park, K. L.; Bae, S. M.; Park, J.; Lee, B. Y. *Macromolecules* **2019**, *52* (23), 9311–9320.

(39) Hanifpour, A.; Bahri-Laleh, N.; Nekoomanesh-Haghighi, M.; Poater, A. *Green Chem.* **2020**, *22* (14), 4617–4626.

(40) Maddah, Y.; Ahmadjo, S.; Mortazavi, S. M. M.; Sharif, F.; Hassanian-Moghaddam, D.; Ahmadi, M. *Macromolecules* **2020**, *53* (11), 4312–4322.

(41) Cueny, E. S.; Sita, L. R.; Landis, C. R. *Macromolecules* **2020**, *53* (14), 5816–5825.

(42) Park, K. L.; Baek, J. W.; Moon, S. H.; Bae, S. M.; Lee, J. C.; Lee, J.; Jeong, M. S.; Lee, B. Y. *Polymers* **2020**, *12* (5), 1100.

(43) Friebe, L.; Nuyken, O.; Windish, H.; Obrecht, W. *Macromol Chem Phys* **2002**, *203*, 1055.

(44) Friebe, L.; Windish, H.; Nuyken, O.; Obrecht, W. *J Macromol Sci* **2004**, *A41* (3), 245.

(45) Fan, C.; Bai, C.; Cai, H.; Dai, Q.; Zhang, X.; Wang, F. *J Polym Sci Part Polym Chem* **2010**, *48*, 4768.

(46) Taniguchi, Y.; Dong, W.; Katsumata, T.; Shiotsuki, M.; Masuda, T. *Polym Bull* **2005**, *54*, 173.

(47) Vitorino, M. J.; Zinck, P.; Visseaux, M. *Eur Polym J* **2012**, *48*, 1289.

(48) Valente, A.; Zinck, P.; Vitorino, M. J.; Mortreux, A.; Visseaux, M. *J Polym Sci Part Polym Chem* **2010**, *48*, 4640.

(49) Visseaux, M.; Mainil, M.; Terrier, M.; Mortreux, A.; Roussel, P.; Mathivet, T.; Destarac, M. *Dalton Trans* **2008**, 4558.

(50) Jian, Z.; Cui, D.; Hou, Z.; Li, X. *Chem Commun* **2010**, *46*, 3022.

(51) Li, S.; Miao, W.; Tang, T.; Dong, W.; Zhang, X.; Cui, D. *Organometallics* **2008**, *27*, 718.

(52) Annunziata, L.; Duc, M.; Carpentier, J. F. *Macromolecules* **2011**, *44*, 7158.

(53) Tang, Z.; Liang, A.; Liang, H.; Zhao, J.; Xu, L.; Zhang, J. *Macromol. Res.* **2019**, *27* (8), 789–794.

(54) Göttker-Schnetmann, I.; Kenyon, P.; Mecking, S. *Angew. Chem. Int. Ed.* **2019**, *58* (49), 17777–17781.

(55) Zheng, W.; Yan, N.; Zhu, Y.; Zhao, W.; Zhang, C.; Zhang, H.; Bai, C.; Hu, Y.; Zhang, X. *Polym. Chem.* **2015**, *6* (33), 6088–6095.

(56) Champouret, Y.; Hashmi, O. H.; Visseaux, M. *Coord. Chem. Rev.* **2019**, *390*, 127–170.

(57) Jing, C.; Wang, L.; Zhu, G.; Hou, H.; Zhou, L.; Wang, Q. *Organometallics* **2020**, *39* (22), 4019–4026.

(58) Raynaud, J.; Wu, J. Y.; Ritter, T. *Angew. Chem. Int. Ed.* **2012**, *51* (47), 11805–11808.

(59) Guo, L.; Jing, X.; Xiong, S.; Liu, W.; Liu, Y.; Liu, Z.; Chen, C. *Polymers* **2016**, *8* (11), 389.

(60) Zhu, G.; Zhang, X.; Zhao, M.; Wang, L.; Jing, C.; Wang, P.; Wang, X.; Wang, Q. *Polymers* **2018**, *10* (9), 934.

(61) Hashmi, O. H.; Champouret, Y.; Visseaux, M. *Molecules* **2019**, *24* (17), 3024.

(62) Zhao, M.; Wang, L.; Mahmood, Q.; Jing, C.; Zhu, G.; Zhang, X.; Wang, X.; Wang, Q. *Appl. Organomet. Chem.* **2019**, *33* (4), e4836.

(63) Lin, W.; Zhang, L.; Suo, H.; Vignesh, A.; Yousuf, N.; Hao, X.; Sun, W.-H. *New J. Chem.* **2020**, *44* (19), 8076–8084.

(64) Wang, L.; Wang, X.; Hou, H.; Zhu, G.; Han, Z.; Yang, W.; Chen, X.; Wang, Q. *Chem. Commun.* **2020**, *56* (62), 8846–8849.

(65) Samsel, E. G. Catalyzed chain growth process. EP0539876A2, 1993.

(66) Samsel, E. G.; Eisenberg, D. C. Actinide catalyzed chain growth process. EP0574854A3, 1993.

(67) Bazan, G. C.; Rogers, J. S.; Fang, C. C. *Organometallics* **2001**, *20*, 2059.

(68) G. Mani, F.; Gabbai, P. *J Organomet Chem* **2005**, *690*, 5145.

(69) Hustad, P. D.; Kuhlman, R. L.; Carnahan, E. M.; Wenzel, T. T.; Arriola, D. J. *Macromolecules* **2008**, *41*, 4081.

(70) Kretschmer, W. P.; Bauer, T.; Heessen, B.; Kempe, R. *Dalton Trans* **2010**, *39*, 6847.

(71) Haas, I.; Kretschmer, W. P.; Kempe, R. *Organometallics* **2011**, *30*, 4854.

(72) Boisson, C.; Monteil, V.; Ribour, D.; Spitz, R.; Barbotin, F. *Macromol Chem Phys* **2003**, *204*, 5145.

(73) Rouholahnejad, F.; Mathis, D.; Chen, P. *Organometallics* **2010**, *29*, 294.

(74) Hustad, P. D.; Kuhlman, R. L.; Arriola, D. J.; Carnahan, E. M.; Wenzel, T. T. *Macromolecules* **2007**, *40* (20), 7061.

(75) US6063882A - Long-chain dialkylmagnesium, its preparation process and applications - Google Patents https://patents.google.com/patent/US6063882 (accessed Mar 25, 2020).

(76) Valente, A.; Zinck, P.; Mortreux, A.; Visseaux, M. *Macromol Rapid Commun* **2009**, *30*, 528.

(77) Friebe, L.; Müeller, J. M.; Nuyken, O.; Obrecht, W. *J Macromol Sci* **2006**, *204*, 1.

(78) Busico, V.; Cipullo, R.; Cutillo, F.; Friederichs, N.; Ronca, S.; Wang, B. Improving the Performance of Methylalumoxane: A Facile and Efficient Method to Trap "Free" Trimethylaluminum. 2.

(79) Kaita, S.; Yamanaka, M.; Horiuchi, A. C.; Wakatsuki, Y. *Macromolecules* **2006**, *39*, 1359.

(80) Jean Ducom. Études physiochimiques des organomagnésiens. *Bull. Société Chim. Fr.* **1971**, *10*, 3518–3523.

(81) Wang, X.-B.; Zhang, M.; Luo, L.; Hussain, M.; Luo, Y. *Chem. Phys. Lett.* **2020**, *755*, 137811.

(82) Johnson, H. C.; Cueny, E. S.; Landis, C. R. *ACS Catal.* **2018**, *8* (5), 4178–4188.

(83) Wei, J.; Zhang, W.; Sita, L. R. *Angew Chem Int Ed* **2010**, *49*, 1768.

(84) Zhang, H.; Luo, Y.; Hou, Z. *Macromolecules* **2008**, *41*, 1064.

(85) Liu, B.; Cui, D. *Macromolecules* **2016**, *49* (17), 6226–6231.

(86) Phuphuak, Y.; Bonnet, F.; Stoclet, G.; Bria, M.; Zinck, P. *Chem Commun* **2017**, *53* (38), 5330–5333.

(87) Dai, Q.; Zhang, X.; Hu, Y.; He, J.; Shi, C.; Li, Y.; Bai, C. *Macromolecules* **2017**, *50* (20), 7887–7894.

CHAPTER 5.

SYNTHESIS AND DEVELOPMENT OF AMIDO-PYRIDINE IRON (II) BIS(TRIMETHYL)AMIDE COMPLEXES FOR THE RING-OPENING (CO)POLYMERIZATION OF CYCLIC ESTERS

5.1. Introduction

Over the past few decades, environmental problems arising from the exploitation of petroleum resources and the accruement of plastic waste have led the research communities to develop sustainable and eco-compatible alternatives.[1–3] In this context, synthetic aliphatic polyesters have generated considerable interest as biodegradable, biocompatible and eco-friendly substitutes of oil-based materials.[4,5] Within this family, polylactide (PLA) and polycaprolactone (PCL) are among the most widely used biodegradable polyester materials since they can be applied in a broad range of applications, from food packaging to medicine.[6–12] PLA is produced from lactide (LA), a cyclic dimer of lactic acid present in the form of three different stereoisomers (*L*-LA, *D*-LA and *meso*-LA) and is obtained from abundant renewable supplies (details in section 5.2.3.1).[13] On the other hand, PCL is prepared from ε-caprolactone (ε-CL) which is mainly derived from petroleum derivatives, although strategies to generate this monomer from biomass resources are currently in progress.[14] It is now generally assumed that the most effective method for obtaining high molar masses polyesters in a controlled fashion is the Ring-Opening Polymerization (ROP) of their related cyclic esters monomers, which proceeds mainly through a coordination-insertion mechanism process when well-defined metal-based or organic catalysts bearing an active ligand/initiator are used.[15–19]

To date, one of the main challenges in this area is to improve the overall properties of these biodegradable polyesters. PLA apart from possessing good mechanical strength also displays brittleness, poor elasticity and low thermal stability under melting conditions.[20–23] It also possesses a very high T_g (>55°C), which limits the biodegradability of PLA in natural conditions. On the other hand, PCL presents good elasticity but low toughness.[11] Hence, taking into account that PLA and PCL have substantially opposite properties, special attention has also been paid to the statistical copolymerization of LA and ε-CL in order to enhance the overall properties of these polyesters.[24]

A various plethora of organocatalytic systems[17] and metal based complexes have been used for the ROP of LA and ε-CL but, surprisingly, little attention has been paid to the development of iron catalysts in this field, and even less to their copolymerization (ROCoP),[25] yet this metal has low toxicity and is readily available, making it a good candidate for sustainable uses.[26,27] Former studies that are relevant for the ROP of cyclic esters, specially LA and ε-CL, have been based on

FeX$_2$ or FeX$_3$ (X = Cl, Br, ClO$_4$),[28] Fe powder,[29] carboxylates[30–33] homo- or hetero-metallic alkoxides/phenoxides,[34–36] salen-iron based systems,[37] iron amides[38] and β-diketonate complexes,[39,40] which are in the form of a discrete compound or *in situ* generated from metal/reagent combination and amido derivatives (Chart 5.1).
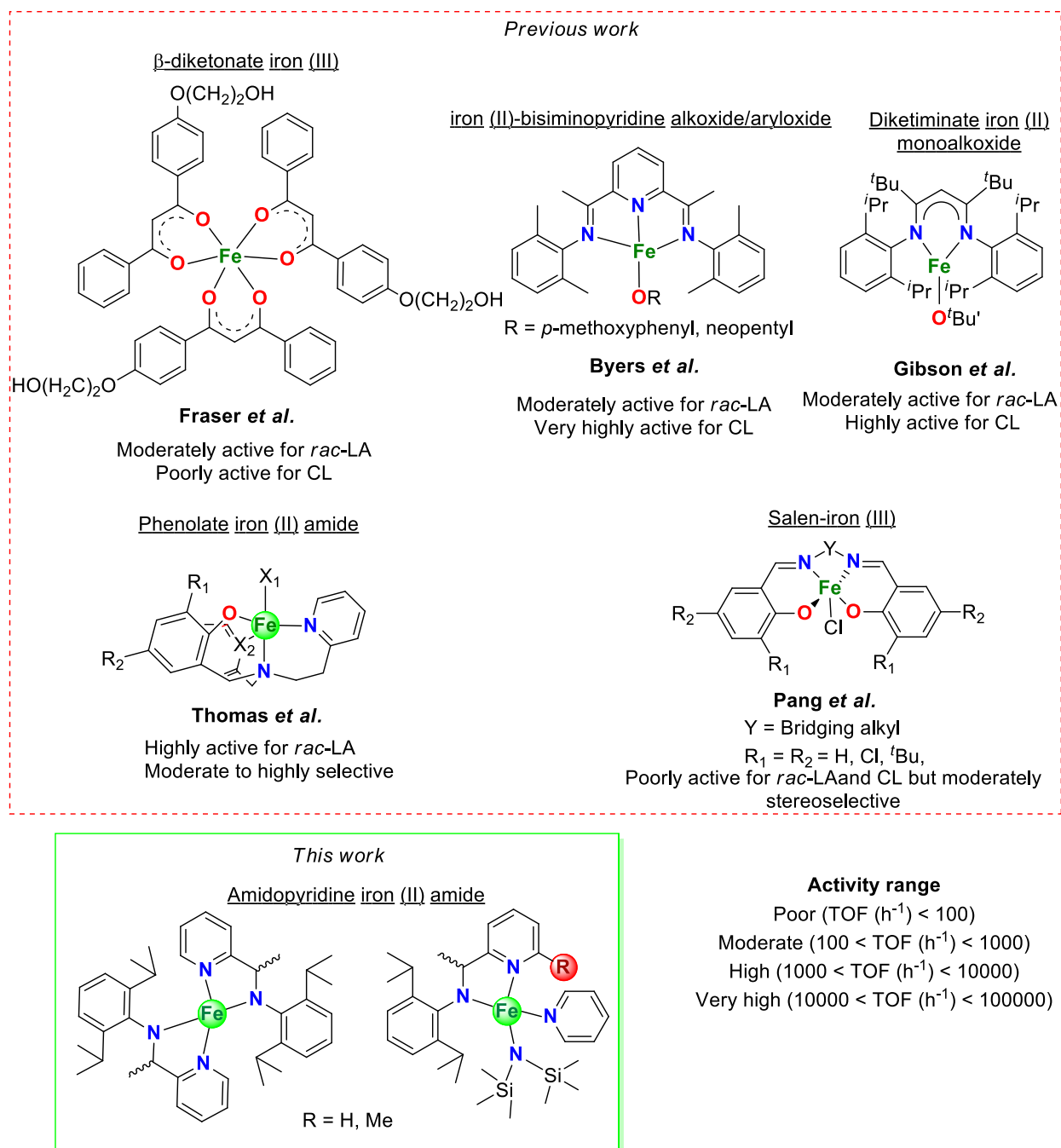
Chart 5.1. Iron-based complexes for the ROP/ROCoP of lactide and ε-caprolactone

One of the major drawbacks of some of these systems described in these studies is the assessment under bulk polymerization conditions, which are usually conducted at high temperatures that may lead to broad molecular weight distributions, gel effect as well as high molecular weight polymers. The catalytic activities of these systems in the ROP of LA and CL range from very low to high activities as summarized in Chart 5.1 above. Therefore, in this context, knowing that alkoxide, alkyl or amido group can initiate the coordinative polymerization, we look forward to synthesize a set of heteroleptic amidopyridine iron (II) amide complexes as new and hopefully efficient initiators for the ROP/ROCoP of *L*-LA and ε-CL. We will also focus to optimize the polymerization conditions for each catalytic system and confirm the mechanism/initiating group by identifying the chain-ends.

5.2. Results and Discussion

5.2.1. Synthesis of amino-pyridine pro-ligands *rac*-**L¹H** and *rac*-**L²H**

The preparation of the two racemic amino-pyridine pro-ligands (***rac*-L¹H** – ***rac*-L²H**), each comprising a 2,6-diisopropylphenyl substituent on the *N*-aryl group, was carried out by adapting procedures that have been previously described in the literature (Scheme 5.1).

R = H, CH₃

L¹ (R = H), **L²** (R = CH₃)
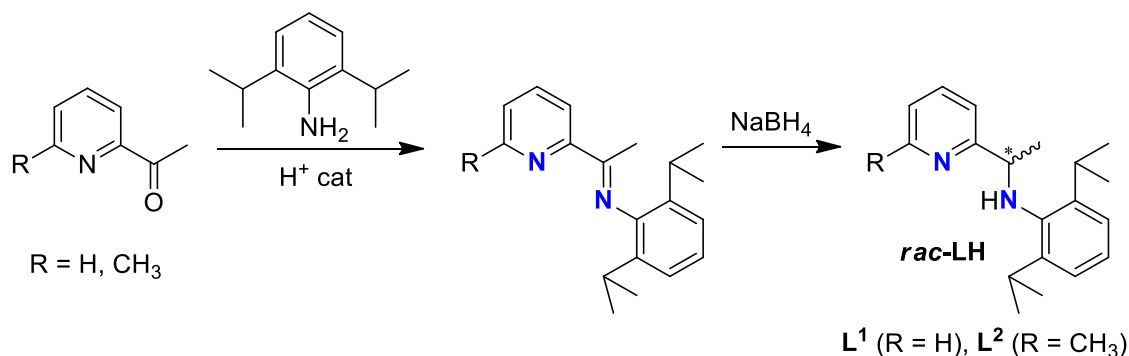
Scheme 5.1. Synthesis of amido-pyridine pro-ligands *rac*-**LH**

The known pro-ligand ***rac*-L¹H** was synthesized in two steps starting from acid-catalyzed condensation reaction of 2-acetylpyridine with 2,6-diisopropylaniline in absolute ethanol under reflux conditions to obtain the iminopyridine precursor as seen earlier in Chapter 2. The iminopyridine was then subjected to reduction of the imine group with an excess of NaBH₄ in methanol at room temperature to yield the pro-ligand ***rac*-L¹H** (Scheme 5.1).[41,42] Following a similar protocol, the preparation of the new pro-ligand ***rac*-L²H** initially started by the synthesis of 2-acetyl-6-methylpyridine from methylation of 2-bromo-6-methylpyridine in diethyl ether at low temperature using dimethylacetamide (Experimental Section), followed, respectively, by a condensation reaction[43] and a reduction step as outlined above for ***rac*-L¹H** (Scheme 5.1). All the pro-ligands were obtained in good yields (75-80%). The ¹H NMR spectra of the know amino-pyridine compound ***rac*-L¹H** was similar to that found in the literature. The new 2,6-diisopropyl-*N*-(1-(6-methylpyridin-2-yl)ethyl)aniline pro-ligand ***rac*-L²H** was characterized by ¹H, ¹³C NMR spectroscopies. The ¹H NMR spectrum of ***rac*-L²H** is shown below in Figure 5.1, which features a 1H intensity quartet signal at $\delta = 4.29$ ppm and a broad singlet corresponding to the N-H amino moiety at $\delta = 4.56$ ppm. In addition, the doublet signal corresponding to the methyl group on the amino substituent shifts further upfield at $\delta = 1.58$ ppm when compared to the shift ($\delta = 2.21$ ppm)

of methyl found in the related iminopyridine substrate **L5,** due to the decreased electronegativity of amine owing to the reduced percentage s character (sp^3 amine *vs* sp^2 imine). Furthermore, the spectrum also features two doublets corresponding to a pair of diastereotopic isopropyl methyls at $\delta = 1.26$, 1.13 ppm, each of 6H intensity, along with a single corresponding –CH(Me)$_2$ septet at $\delta = 3.55$ ppm (2H). These observations highlight the differences between the aminopyridine and the related iminopyridine counterpart.
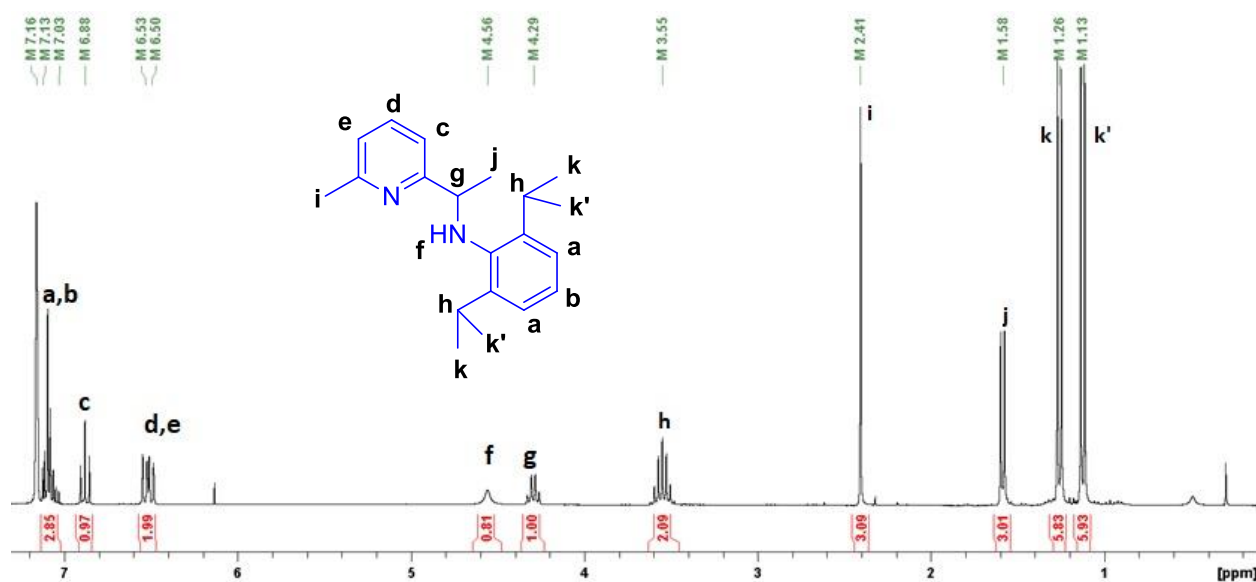
Figure 5.1. ^{1}H NMR of *rac*-**L^{2}H** (300 MHz, C$_6$D$_6$, 25 °C)

The newly developed pro-ligand *rac*-**L^{2}H** was also characterized by ^{13}C DEPT 135 NMR spectroscopy (Experimental section). The shifts corresponding to the aromatic carbons (pyridine/N-aryl) were found ranging downfield from 163–118 ppm, followed by the doublets ($\delta = 61$ and 28 ppm) associated to the carbon of amino group and 2,6-diisopropyl substituent, respectively. Lastly, the signals associated to the methyl carbons were found upfield in the range 24–22 ppm (δ(ppm) = 24.02 for CH_3(Py), 23.99 for ((CH_3)$_2$CH) and 22.1 for CH(CH_3)NH).

5.2.2. *Preparation of heteroleptic/homoleptic iron amide complexes 12-14*

The attempted synthesis of the $\mathbf{L^1}$-supported heteroleptic iron amide complex was carried out by the dropwise addition of a colorless THF solution containing the amino-pyridine ligand *rac-*$\mathbf{L^1H}$ (1 eq.) to a green THF solution of 1 eq. of $Fe[N(SiMe_3)_2]_2$, which immediately produced a deep red mixture (Scheme 5.2).
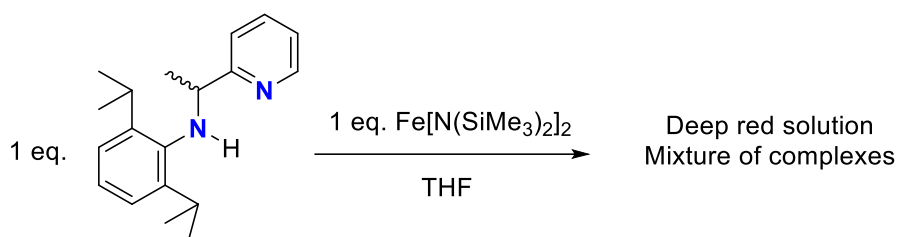
Scheme 5.2. Attempted synthesis in THF of heteroleptic amidopyridine iron (II) amide complex

The mixture was concentrated under vacuum to obtain a red crude product which was further subjected to ^{1}H NMR characterization studies. The ^{1}H NMR spectrum of the crude in C_6D_6 is shown below in Figure 5.2, which reveals several broad resonances ranging from δ = -121 to +128 (δ in ppm) in the paramagnetic region as observed previously with other paramagnetic iron complexes **1-11** in the last chapters. The spectrum displays twenty-two peaks (nearly twice than expected) that probably arise due to the formation of homoleptic complex $(\mathbf{L^1})_2$Fe as well as the targeted heteroleptic counterpart $\mathbf{L^1}$Fe[N(SiMe_3)_2], owing to the high intensity broad signal at δ = 34 ppm, which should correspond to the methyl groups of –N(Si(CH_3)_3)_2.
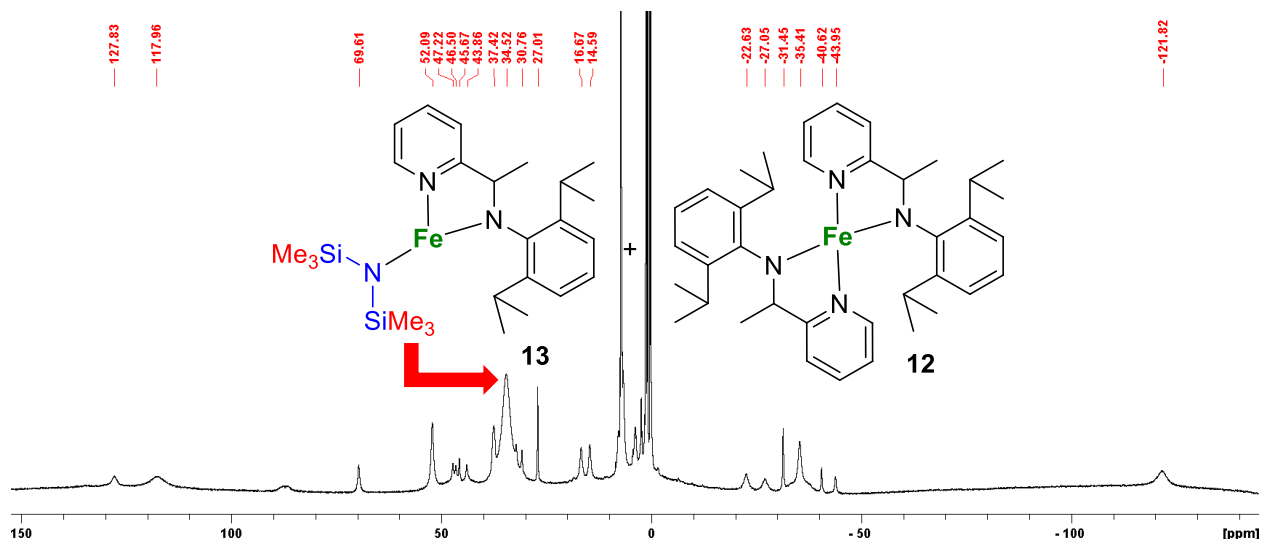
Figure 5.2. ^{1}H NMR spectrum of the crude obtained in the attempted synthesis of heteroleptic iron amide $\mathbf{L1}$Fe[N(SiMe_3)_2] (300 MHz, C_6D_6, 25 °C)

The primary attempt to synthesize the heteroleptic iron amide complex **L¹**Fe[N(SiMe₃)₂] by reacting 1 eq. of ***rac*-L¹H** with 1 eq. of Fe[N(SiMe₃)₂]₂ in THF resulted probably in the formation of a mixture of heteroleptic/homoleptic complexes. Therefore, in order to synthesize and isolate one major counterpart, we repeated the last synthetic protocol but this time with 2 eqs. of ***rac*-L¹H** to target preferentially the homoleptic iron amide complex (**L¹**)₂Fe as shown below in Scheme 5.3.
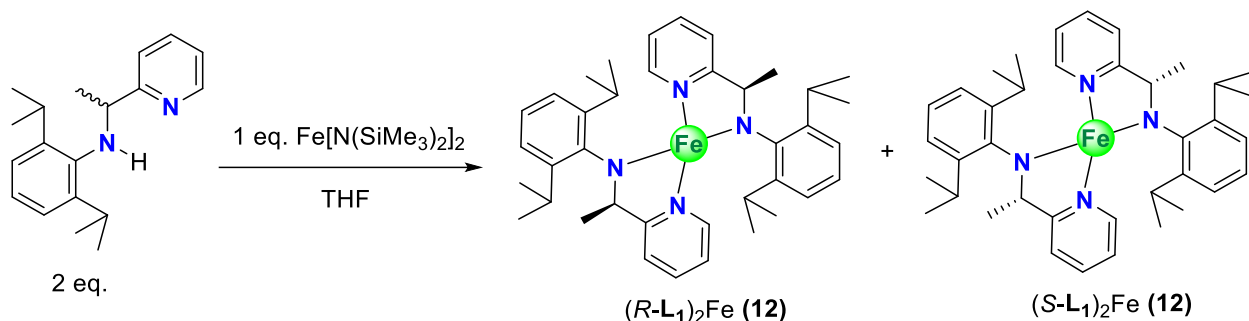
Scheme 5.3. Attempted synthesis of homoleptic amidopyridine iron (II) amide complex **12**

The solvent THF was evaporated and the resulting crude was subjected to recrystallization in pentane at -20 °C to yield dark pink-purple crystals, corresponding possibly to the homoleptic counterpart. The crystals were subjected to elemental analyses to confirm the molecular formula in which the result was consistent with the formation of homoleptic iron amide complex **12** of formula (**L¹**)₂Fe (calculated for $C_{38}H_{50}FeN_4$: C 73.77, H 8.15, N 9.06; Found: C 73.23, H 8.55, N 9.00). The newly developed homoleptic complex **12** was also characterized by ¹H NMR, which again displayed a typical paramagnetically-shifted spectrum, revealing this time eleven broad resonances ranging from δ = -43 to +134 (δ in ppm) as observed previously in Figure 5.2. The absence of a high intensity broad peak at δ = 34 ppm which should integrate to 18H of –N(Si(CH₃)₃)₂, also confirms that these eleven broad singlets correspond to the formation of a homoleptic complex **12** of (**L¹**)**₂Fe** type (Figure 5.3). The assignments of these resonances could be done based on integration and proximity to the metal center, although, in our case, the integrations did not correspond exactly as their expected value, probably due to the broadening or merging of some signals but we still proceeded with a tentative assignment.
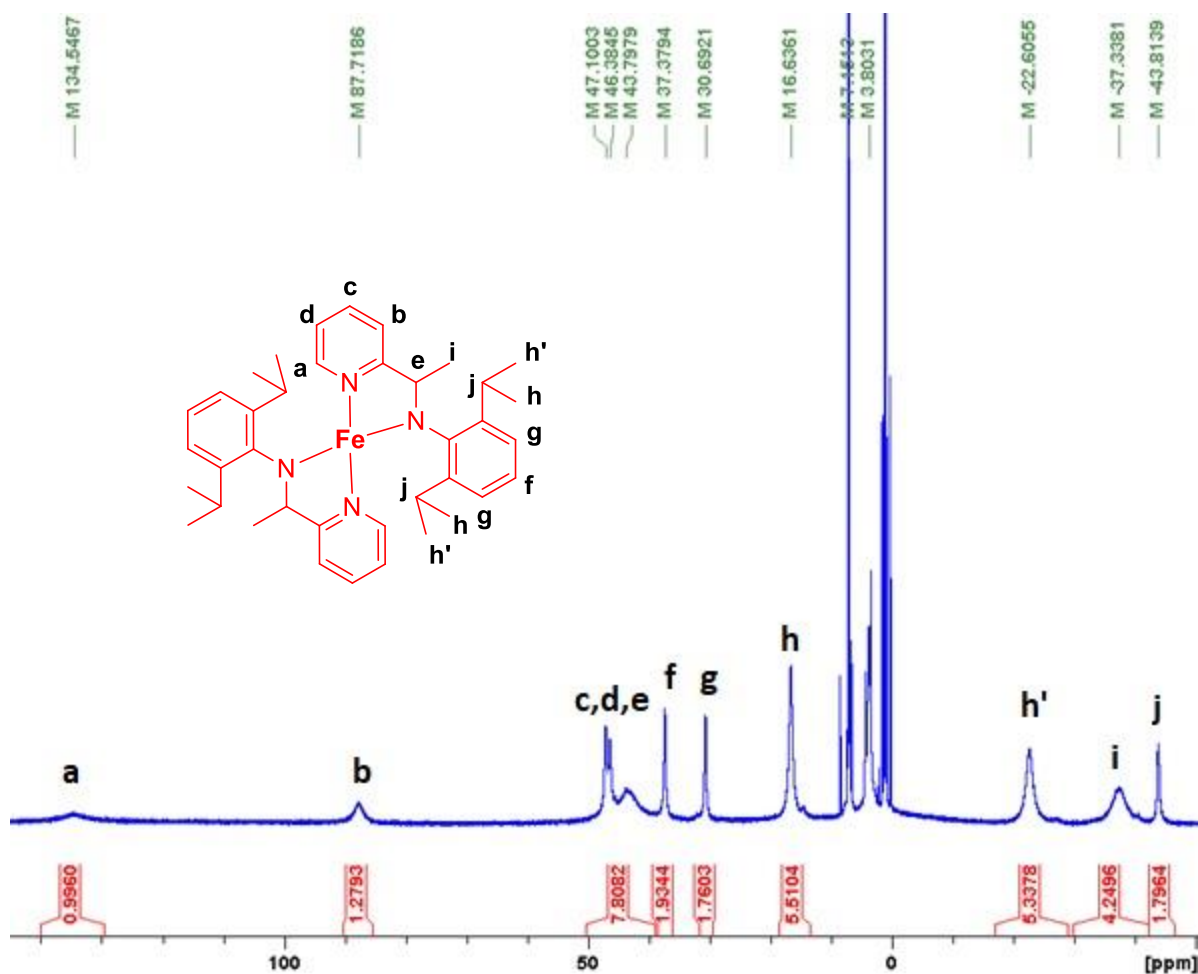
Figure 5.3. ¹H NMR spectrum of homoleptic complex **12** (300 MHz, C₆D₆, 25 °C)

From the ^{1}H NMR spectrum of complex **12**, it can be seen that the *ortho*-pyridyl protons (H$_a$) of the coordinated ligand, which are nearest to the paramagnetic iron center, were found to constitute a broadest singlet downfield at 134 ppm. These were followed by *meta*-pyridyl protons (H$_b$) at 87 ppm and a very broad signal at 44 ppm constituting sharp singlets, which might correspond to the hydrogens of the amine carbon (H$_e$) and the remaining pyridyl protons (H$_{c,d}$). The following singlets at 37 and 30 ppm could be attributed to the hydrogens (H$_{f,g}$) of *N*-aryl substituent and the remaining sharp singlets will correspond to the pair of diastereotopic isopropyl methyl of 2,6-diisopropyl group (H$_{h,h'}$), amine carbon (H$_i$) and H$_j$ of 2,6-diisopropyl group due to their proximity from the iron center.

The obtained single crystals of the homoleptic complex **12** were further analyzed by X-ray diffraction studies to determine their structure in the solid state. The solid-state structural determination of complex **12** reveals a four-coordinated geometry at the metal center. The Fe

center is bound to two monoanionic amido-pyridine unit, after deprotonation of the amino group, with the two nitrogen atoms of both ligand L^{1-} acting as chelate (Figure 5.4). It is important to notice that the complexation leads to stereospecific binding of the same enantiomeric pair (*R, R* or *S, S*) to the iron center in the unit cell of the molecular structure of complex **12.** The geometry at the iron center is very rarely observed in the literature.[44] Depending on the τ_4 value (0.67) defined by Houser,[45] the geometry can be best described as an intermediate between distorted see-saw or trigonal pyramidal.
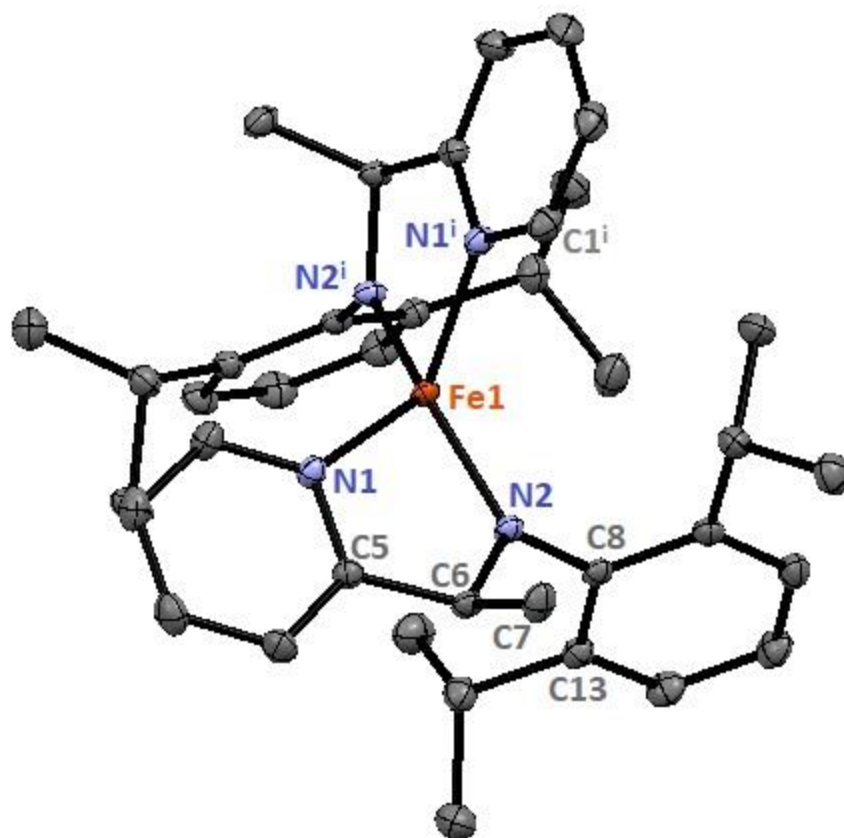
Figure 5.4. ORTEP-type view of the crystallized homoleptic complex **12** with ellipsoid drawn at 50% probability level (hydrogen atoms have been omitted for clarity and only specific atoms have been labelled)

The homoleptic iron amide complex **12** can be best compared to the homoleptic iron complex supported by two 2-(2-pyridyl)-1-aza(2,6-^{i}Pr$_2$C$_6$H$_3$)propene (PyEA-2,6-^{i}Pr$_2$C$_6$H$_3$) ligands reported by the group of Wolczanski, where the Fe center exhibits a distorted tetrahedral arrangement.[46] The Fe-N bond distances [1.9323(9)–2.1205(9) Å] were found in the similar range as observed in Wolczanski's complex [1.9427(15)–2.1221(17) Å], whereas the bite angles [N1-

Fe1-N2 = 81.61(4) °] of the N-N chelate were found to be slightly higher than the ones obtained in (PyEA-Ar^{i}Pr$_2$)$_2$Fe complex [N1-Fe1-N2 = 79.66(7) °; N3-Fe1-N4 = 79.37(6) °].

Unlike the iminopyridine systems **6-9** where the Fe-N$_{pyridine}$ distances were found less than the Fe-N$_{imine}$, the amidopyridine system showcases the opposite relation where Fe-N$_{pyridine}$ [Fe1-N1 = 2.1205(9) Å] > Fe-N$_{amide}$ [Fe1-N2 = 1.9323(9) Å], due to the higher donating capability of amide compared to pyridine. Likewise, the N(sp^2)-C(sp^3) bond distance [N2-C6 = 1.452 (13) Å] in amidopyridine was found to be more than the N(sp^2)-C(sp^2) bond distances [N-C (*imine*) = 1.278–1.292 Å] in iminopyridine systems **6-9** and falls within the typical range of N(sp^2)-C(sp^3) bond distances.[47] The larger bite angles subtended by the amidopyridine chelate results in displacing the nitrogens of the bulky 2,6-diisopropylphenylamide moiety to be 144.59(6) ° [N2$_{amide}$-Fe1-N2$^i_{amide}$] apart and those of pyridine segments by 81.61(4) ° [N1$^i_{pyridine}$-Fe1-N1$_{pyridine}$] which are again greater than those observed for Wolczanski's complex [N2$_{amide}$-Fe1-N4$_{amide}$ = 136.70(7) °; N1$_{pyridine}$-Fe1-N3$_{pyridine}$ = 100.94(7) °]. These differences in bond angles arises possibly due to the simultaneous presence of methyl group on the amino carbon and bulkier 2,6-diisopropyl groups of the *N*-aryl substituent, imparting more steric repulsion as a result of which the amide and pyridine segments are widely displaced. This also leads to the orientation of methyl group on C6 position which is coplanar with the other pyridine as evidenced from the torsion C7-C6-N1^i-C1^i = 1.62(9) °. As already observed with iminopyridine complexes in the previous chapters, the *N*-aryl group in the case of amidopyridine chelate is also nearly orthogonal to the C6-N2 segment [C6-N2-C8-C13 = 77.1(1) °] and the amino group is almost planar to the pyridine ring [N2-C6-C5-N1 = -16.5(1) °].

As seen earlier, the synthesis of iron amide complexes in THF preferentially favors the formation of homoleptic counterpart **12** irrespective of the variations in stoichiometry. Therefore, in order to achieve the target heteroleptic molecule **L^1**Fe[N(SiMe$_3$)$_2$], we modified our synthetic protocol by changing the polar solvent THF by a non-polar solvent. Firstly, the reaction was carried out at the NMR scale in C$_6$D$_6$ by adding 1 eq. of ligand *rac*-**L^{1}H** in the presence of 1 eq. Fe[N(SiMe$_3$)$_2$]$_2$. In this case, the ^{1}H NMR spectrum of the crude in C$_6$D$_6$ again reveals the production of a mixture of complexes but, this time, the selectivity for the formation of the putative heteroleptic compound being higher than the homoleptic, in contrast to what was observed when the reaction was carried out in THF (Figure 5.5.a *vs* Figure 5.3). To this mixture, another 1 eq. of *rac*-**L^{1}H** ligand was added and the reaction was monitored through ^{1}H NMR spectroscopy. After

20 h, there was still no change in the reaction mixture as the presence of both species was observed in ^{1}H NMR (Figure 5.5.b), due to which the reaction was left for 3 days. The crude was again analyzed by ^{1}H NMR, which indicated the presence of only homoleptic complex **12** (Figure 5.5.c)
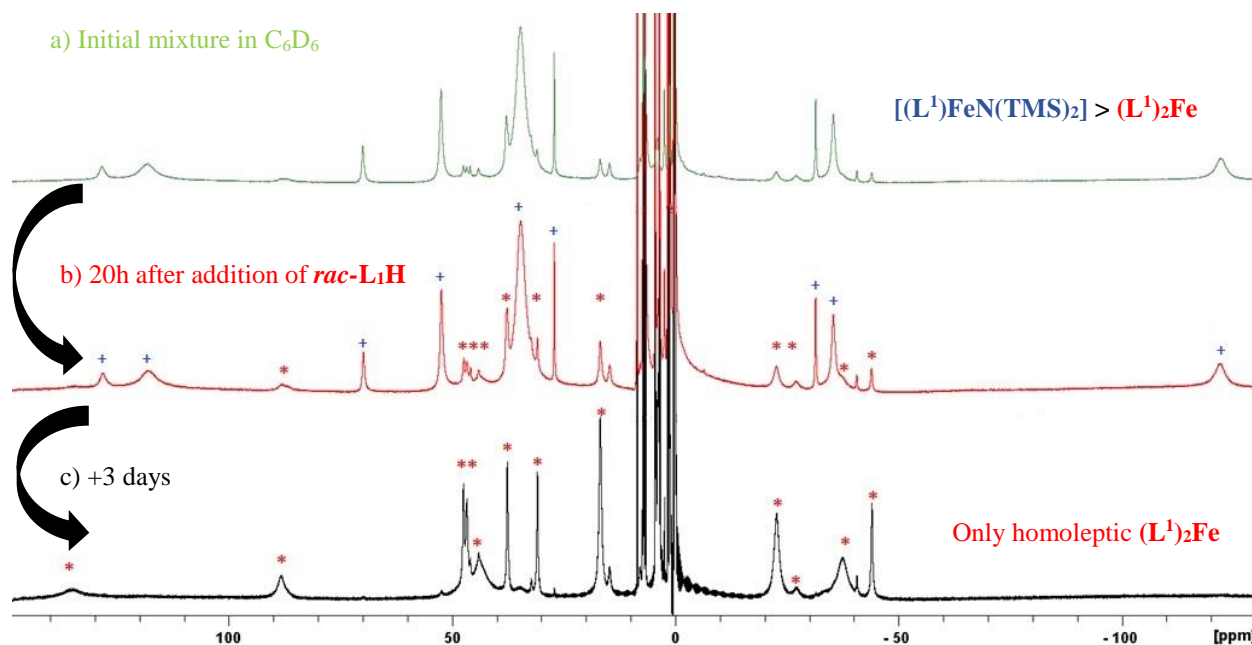
Figure 5.5. Evolution of homoleptic complex **12** in benzene-d$_6$

Consequently, a similar protocol was again followed to carry out the synthesis of the heteroleptic iron complex **L^{1}Fe[N(SiMe$_3$)$_2$]** in toluene and, as expected, the results were similar to those observed in benzene-d$_6$ (Figure 5.6) with a mixture of complexes.
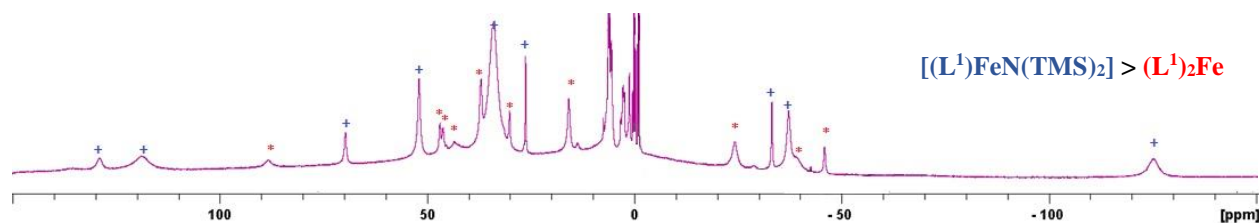
Figure 5.6. Synthesis of iron amide complexes in toluene- d$_8$

Lastly, to observe the influence of extremely reduced polarity, we changed the solvent to pentane and the synthesis of the heteroleptic iron amide complex was again carried out by the dropwise addition of a colorless pentane solution containing ***rac*-L^{1}H** ligand to a green pentane solution of Fe[N(SiMe$_3$)$_2$]$_2$]$_2$ (Scheme 5.4), producing a deep red solution. The solvent was evaporated and the crude was analyzed by ^{1}H NMR spectroscopy.(Figure 5.7.a).
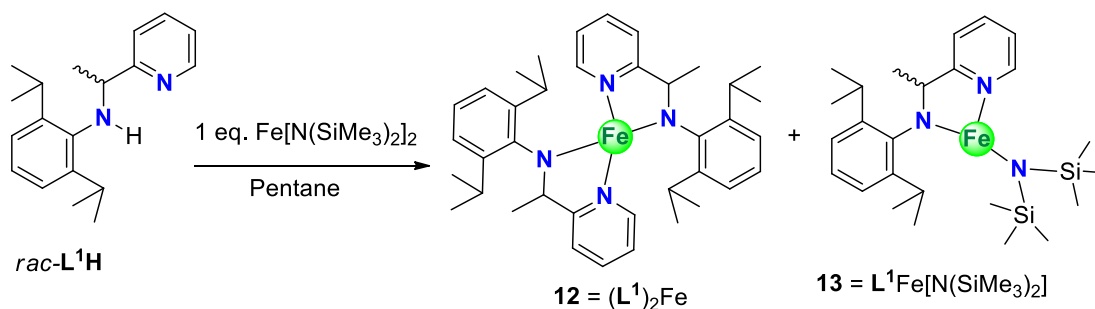
Scheme 5.4. Attempted synthesis in pentane of heteroleptic amidopyridine iron (II) amide complex
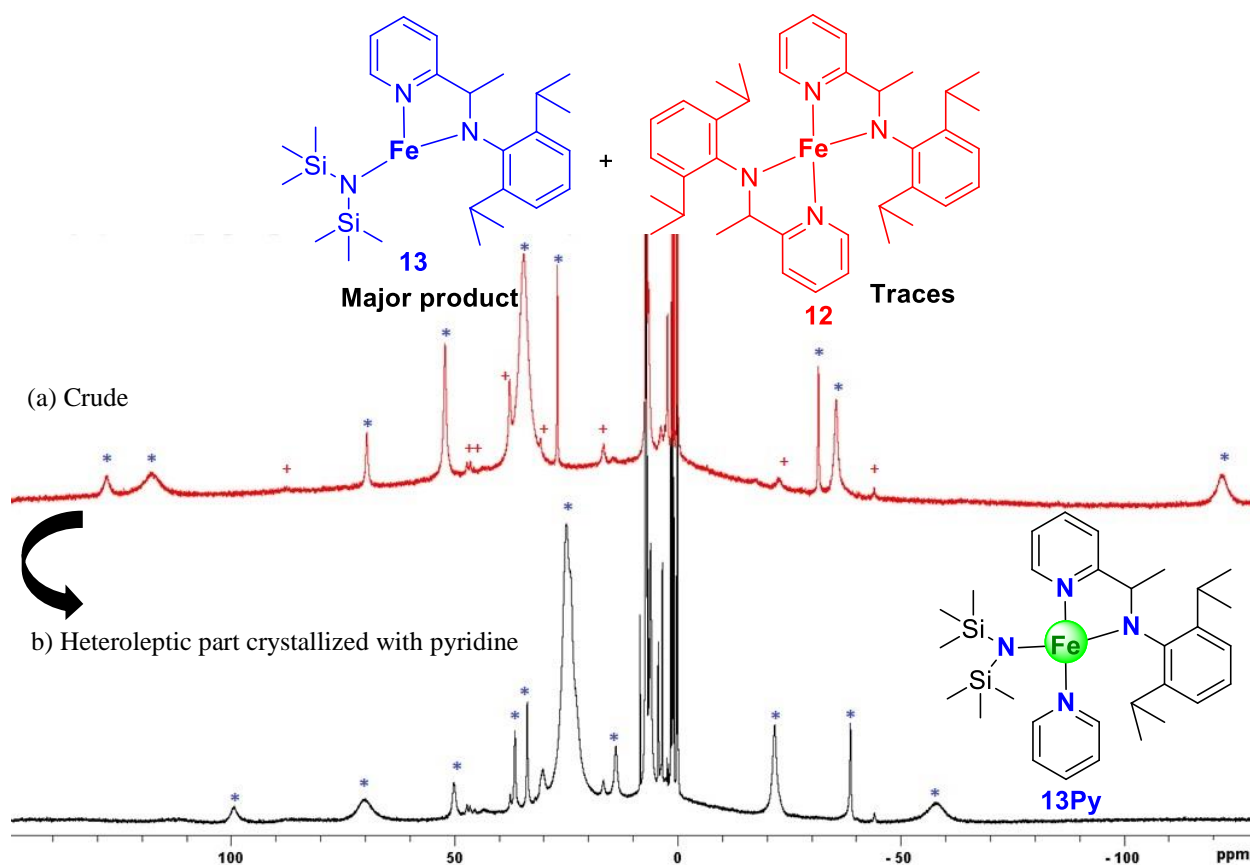
Figure 5.7. Evolution of heteroleptic complex $L_1Fe[N(SiMe_3)_2](Py)$ **(13Py)** in pentane

From the ^{1}H NMR of crude shown in Figure 5.7.a, we can see some broad singlets of high intensity (marked in blue) in the paramagnetic region with some additional peaks of very low intensity (marked in red) that correspond to the previously characterized homoleptic analogue **12.** Depending on the intensities of the first set of peaks, we can claim that the formation of targeted heteroleptic complex **13** in pentane has occurred in major amounts which is supported by the fact that these set of peaks also constitute a broad signal of –N(SiMe₃)₂ at $\delta = 34$ ppm. Attempts to

crystallize the resulting heteroleptic complex **13** in different solvents (THF, toluene and pentane) and at different temperatures unfortunately failed. On the other hand, treatment of the crude mixture in a pentane solution containing an excess of pyridine (4 eq./Fe complex, pyridine abbreviated as Py) resulted in the rapid formation of deep red single crystals of **L^{1}Fe[N(SiMe$_3$)$_2$](Py) (13Py)** (Figure 5.7.b, Scheme 5.5), with moderate yield (50%). The crystals were further analyzed *via* elemental analysis, which confirmed the molecular formula **L^{1}Fe[N(SiMe$_3$)$_2$](Py)** of the resulting complex **13Py** (Calculated for C$_{30}$H$_{48}$FeN$_4$Si$_2$: C 62.48, H 8.39, N 9.71; Found: C 62.03, H 8.49, N 9.50).

Before proceeding with the description of further characterization of complex **13Py**, which has been isolated, we will describe the synthesis of the analogue with ***rac*-L^{2}H** ligand, **L^{2}Fe[N(SiMe$_3$)$_2$] (14)** as these two complexes were found to have similar molecular characterization. This other heteroleptic analogue was obtained in a similar manner as of **13Py,** by following the same synthetic strategy, in presence of pyridine, as shown below in Scheme 5.5. Likewise, single crystals of the pyridine adduct **14Py** were also analyzed *via* elemental analysis to confirm the molecular formula **L^{2}Fe[N(SiMe$_3$)$_2$].Py** (Calculated for C$_{31}$H$_{50}$FeN$_4$Si$_2$: C 63.02, H 8.53, N 9.45; Found: C 62.62, H 8.78, N 9.09).

Isolated Crystals - major product

13Py = **L^1**Fe[N(SiMe$_3$)$_2$](Py) for R = H
14Py = **L^2**Fe[N(SiMe$_3$)$_2$](Py) for R = Me
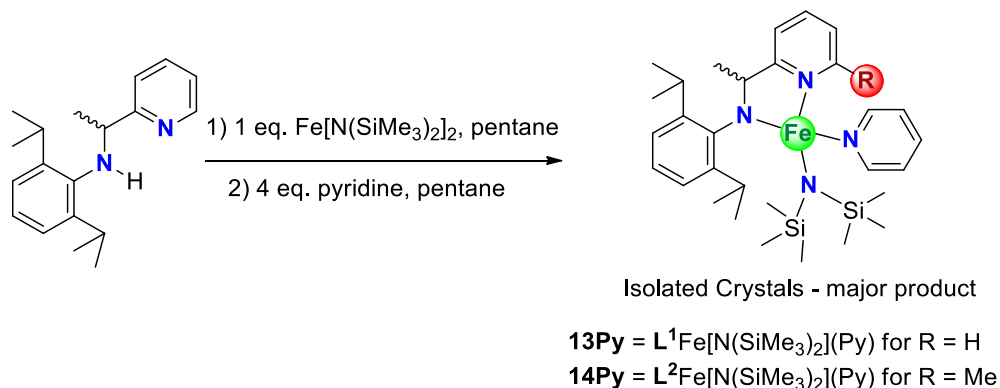
Scheme 5.5. Synthesis of heteroleptic iron amide complexes **13Py** and **14Py.**

Unfortunately, the homoleptic analogue of **12** could not be obtained even after prolonging the reaction time and increasing the temperatures up to 70 °C. The unsuccessful formation of homoleptic **(L^2)$_2$Fe** could be most likely due to the steric inhibition imparted by the presence of methyl group on the pyridine, which prevents the simultaneous coordination of the two deprotonated amido-pyridine chelate to the iron precursor. A summarized protocol for the

synthesis of homoleptic/heteroleptic amidopyridine iron (II) amide complexes is shown below in Scheme 5.6.
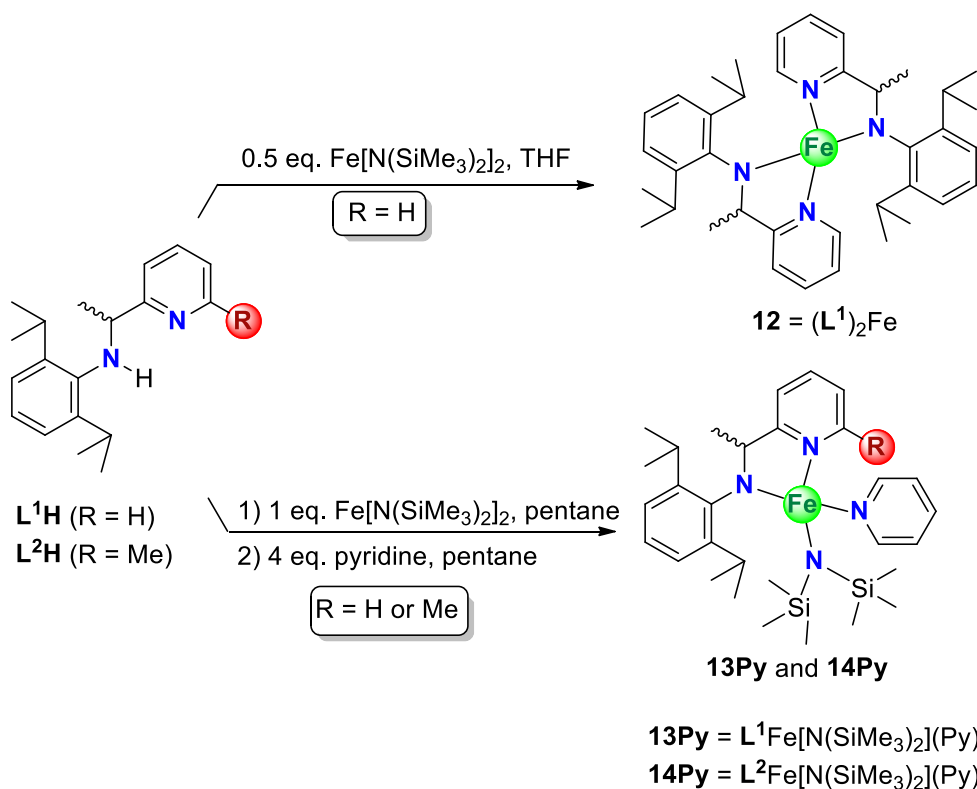
Scheme 5.6. Synthesis of heteroleptic/homoleptic amidopyridine iron (II) amide complexes **12, 13Py** and **14Py**

The newly developed heteroleptic amidopyridine iron (II) amide complexes **13py** and **14py** were further characterized by ^{1}H NMR spectroscopy studies in which their spectra were recorded in C_6D_6 owing to their high solubility. The ^{1}H NMR spectrum of the heteroleptic paramagnetic complexes revealed several broad resonances ranging from δ = -93 to +128 (δ in ppm) as already observed above with the homoleptic analogue **12**. For a better overview of each spectrum, the stacked ^{1}H NMR spectra of complexes **13Py** and **14Py** is shown in Figure 5.8. The tentative assignments of these broad singlets were done based on integration and mainly proximity to the metal center. One broad signal is observed in each spectrum at around 40–25 ppm that can be ascribed, relative to the integration of all peaks, to the protons of the bis(trimethylsilyl)amide group. Also, the broadest singlets arising in the spectra of heteroleptic iron amide complexes **13Py** and **14Py** in the range of 74 to 98 ppm and -93 to -64 ppm could be attributed to the *ortho*-pyridyl protons of the coordinated pyridine or the *ortho-/meta*-pyridyl protons of the ligand. Regarding

the integrals, it was not possible to obtain the expected values for each. For instance, we expected a total integration of 48 protons ideally for complex **13Py** but we ended up in obtaining only 39 protons. Similar observation could be drawn for the remaining complex **14Py** (Experimental
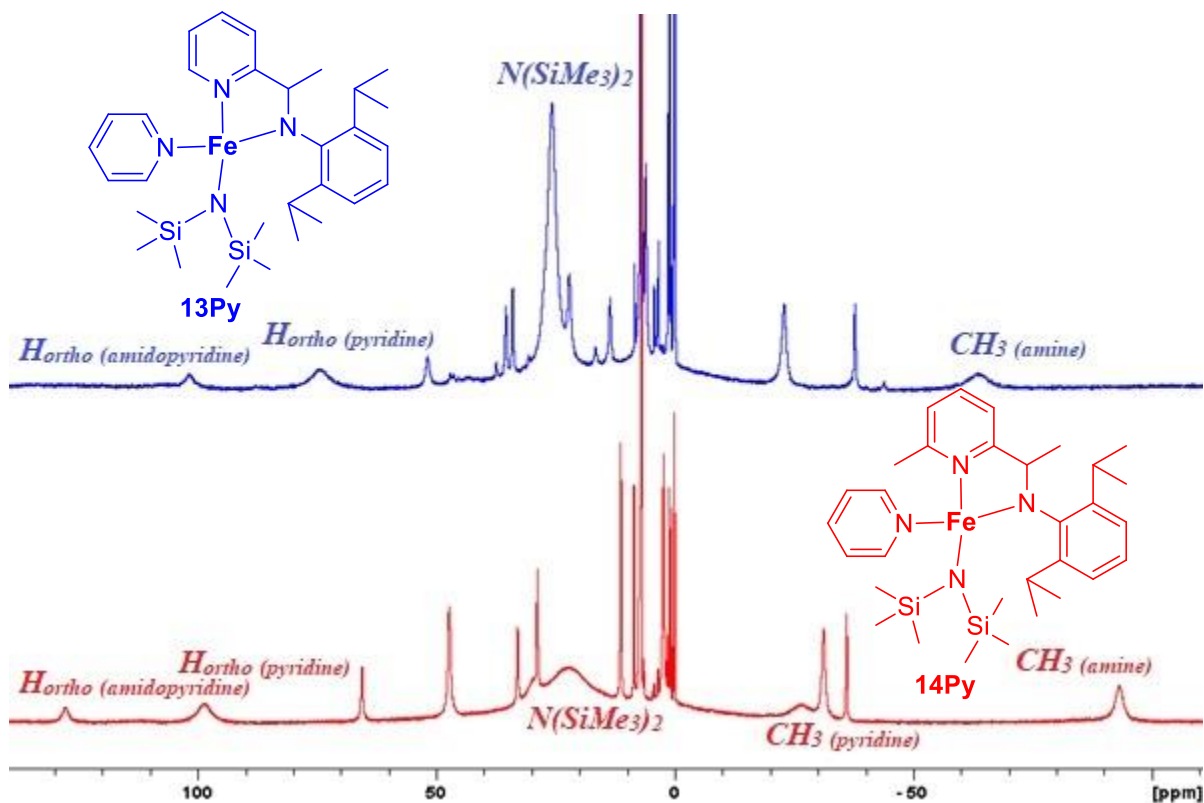
Section).

Figure 5.8. ^{1}H NMR spectrum of complexes **13Py** and **14Py** stacked (300 MHz, C$_6$D$_6$, 25 °C)

Lastly, the obtained single crystals of heteroleptic iron amide complexes **13Py** and **14py** were also analyzed by X-ray diffraction studies to determine their structure in solid state. The solid-state structural determination of complexes **13Py** and **14Py** revealed that these two neutral complexes have a closely related structure in the solid state, with the molecular structure revealing in each case a four-coordinated geometry at the metal. The Fe center is bound to a monoanionic amido-pyridine unit, after deprotonation of the amino group, with the two nitrogen atoms of the ligand **L**⁻ acting as chelate. The coordination sphere is then completed by one nitrogen atom from the pyridine and one monoanionic nitrogen atom from the $N(SiMe_3)_2$ fragment. Due to the presence of four distinct substituents on the metal, the iron turns into a stereogenic center. Furthermore, considering the additional chiral carbon (C13, C13A) on the amino-pyridine pro-ligand, we therefore expected the formation of four diastereoisomers. In fact, the complexation in presence of pyridine leads to a stereo-differentiation in the solid state,[48] producing two pair of enantiomers R_{C13},R_{Fe} and S_{C13},S_{Fe} in the unit cell of the molecular structure of the two complexes **12** and **14**.[49,50] Because of the steric repulsion induced by the bis(trimethylsilyl) amide and the isopropyl groups of the *N*-aryl substituent, the methyl C14(A) points in the same direction as the pyridine with respect to the amido-pyridine chelate N1-C13(A)-C15-N2, as already observed with complex **12** above. The geometry at the iron center again displays an intermediate geometry that can be best described as distorted from either trigonal pyramidal or see-saw, τ_4 value ranging from 0.69–0.72.[45] The amido-pyridine chelating framework is almost planar [N1-C13-C15-N2 ranging from 2.4(2)–12.1(3)°] while the *N*-aryl group slightly deviates from orthogonality to this plane [C13-N1-C1-C6 ranging from 103.6(2)–105.0(2)°]. The Fe1-N1 distance of the *N*-amido group [1.959(1)–1.961(1) Å] is shorter than the Fe1-N2 distance of the pyridine fragment of the binucleating ligand [2.144(1)–2.155(1) Å], the latter being quasi-identical to the Fe1-N3 distance of the pyridine ligand [2.155(1)–2.159(1) Å]. In addition, the Fe1-N4 bond length [1.979(1)–1.988(1) Å] is longer than the terminal Fe-N distances in $[Fe(N(SiMe_3)_2)_2]_2$ [*ca* 1.925(3) Å][51] and lies in the upper range of other four-coordinated bis(trimethylsilyl)amide iron complexes reported in the literature (1.95–1.99 Å).[44,52–57] The lengths of the C13-C15 [1.517(2)–1.520(2) Å] and C13-N1 [1.451(2)–1.461(4) Å] bonds fall within the typical intervals of $C(sp^3)$-$C(sp^3)$ and $C(sp^3)$-N bond distances, respectively.[47] The selected bond lengths and angles concerning the structures of complexes **12, 13Py and 14Py** are given below in Table 5.1. and the ORTEP type views of the complexes **13Py** and **14Py** are given in Figure 5.9.

Table 5.1. Selected bond distances (Å) and angles (°) for amidopyridine iron (II) amide complexes **12, 13Py** and **14Py**

Parameters	12	Parameters	13Py	14Py
τ_4	0.67	τ_4	0.73	0.69
Fe1—N1	2.1205(9)	Fe1—N1	1.9612(12)	1.9594(11)
Fe1—N2	1.9323(9)	Fe1—N2	2.1435(12)	2.1551(11)
C6—N2	1.4542(13)	Fe1—N3	2.1554(13)	2.1593(13)
C6—C5	1.5131(15)	Fe1—N4	1.9879(12)	1.9789(11)
N1—Fe1—N2	81.61(4)	C13(A)—N1	1.4514(18)	1.461(3)
N1—Fe1—N1^i	108.76(5)	C13(A)—C15	1.517(2)	1.520(3)
N2—Fe1—N2^i	144.59(6)	N1—Fe1—N2	79.21(5)	80.05(4)
N1—Fe1—N2^i	120.01(4)	N1—Fe1—N3	118.99(5)	113.95(5)
C7—C6—N1^i—C1^i	1.62(9)	N1—Fe1—N4	132.69(5)	130.93(5)
C6—N2—C8—C13	77.1(1)	N2—Fe1—N3	87.87(5)	89.11(4)
N1—C5—C6—N2	-16.5(1)	N2—Fe1—N4	124.45(5)	131.13(4)
		N3—Fe1—N4	103.56(5)	104.51(5)
		C13(A)—N1—C1—C6	105.0(2)	103.6(2)
		N2—C15—C13(A)—N1	2.4(2)	-12.1(3)
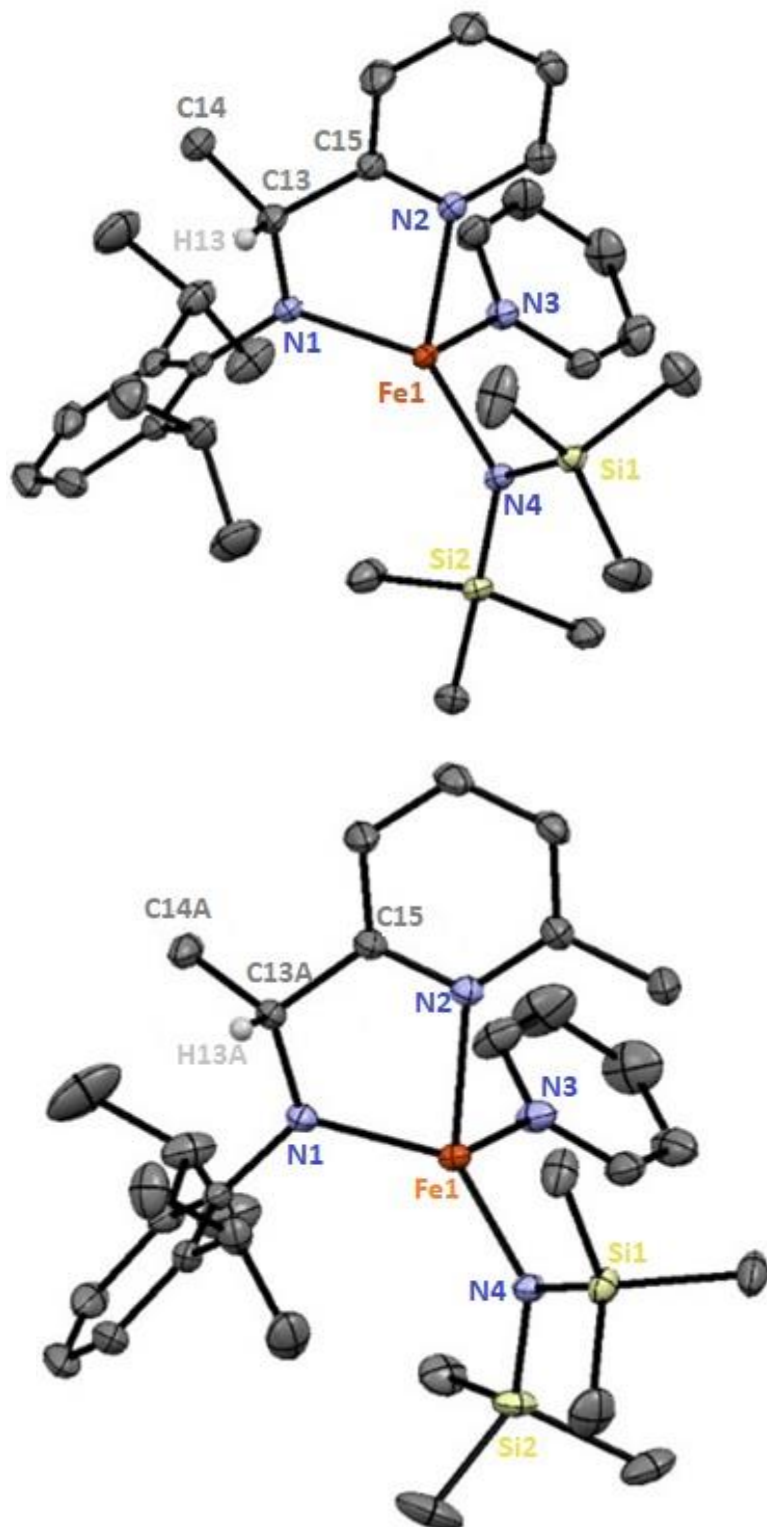
Figure 5.9. ORTEP-type view of the crystallized complexes **13Py** (top) and **14Py** (bottom) drawn at 50% probability level (Hydrogen atoms have been omitted for clarity with the exception of H13(A) on the chiral carbon C13(A))
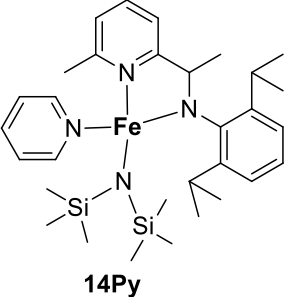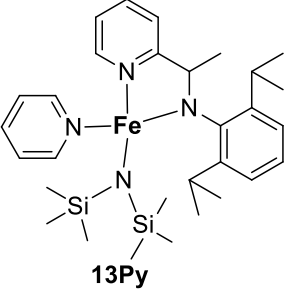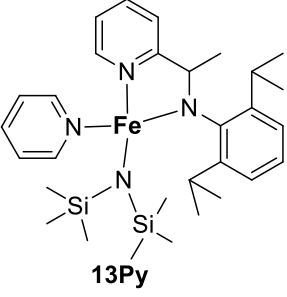
5.2.3. Ring Opening Polymerization of cyclic esters using complexes 13Py and 14Py

After the synthesis of targeted heteroleptic amidopyridine iron (II) amide/pyridine complexes (**13Py** and **14Py**), we intended to study their catalytic applications in the controlled ring-opening polymerization (ROP) of cyclic esters such as lactide (LA) and ε-caprolactone (CL).

5.2.3.1. Ring Opening Polymerization of L-lactide

The ROP of *L*-lactide was carried out using the initiators **13Py** and **14Py** at various temperatures, the results of which are displayed below in Table 5.2. The polymerizations (Scheme 5.7) were first conducted with the most sterically hindered initiator **14Py** and then **13Py**, to observe the influence of steric bulk on the activity of each catalytic system.

Table 5.2. Polymerization of *L*-lactide (*L*-LA) using initiators **13Py** and **14Py**[a]

Entry[a]	Fe	T (°C)	Time (h)	Conv.[b] (%)	$M_{n(exp)}$[c] (g/mol)	Đ[c]
1			64	89	94 000	1.36
2		23	16	89	94 000	1.36
3			6	73	89 000	1.27
4		50	16	>99	92 000	1.23
5	**14Py**		4	82	88 000	1.27
6			15	96	104 000	1.18
7		70	2	96	102 000	1.19
8			1	80	97 000	1.24
9		23	6	75	100 000	1.41
10		50	2	75	91 000	1.25
11			3	97	96 000	1.27
12	**13Py**		0.5	61	92 000	1.28
13		70	0.75	81	95 000	1.25
14			1	94	97 000	1.29

[a] Polymerization conditions: 2.5 µmol of Fe (II) complex; LA/Fe = 200/1; toluene = 0.5 mL; [*L*-LA] = 1.0 M in toluene; [b] determined by ^{1}H NMR; [c] determined by SEC analysis in chloroform using the correction $M_{nexp} = M_{nsec} \times 0.58$;[71] $M_{n(th)} = (LA/Fe) \times 144.13 = 28\,826$ g/mol, considering 100% conversion of monomer with one growing chain per metal center.
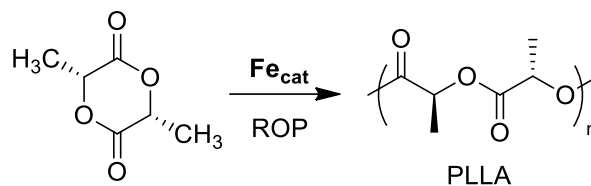
Scheme 5.7. ROP of *L*-LA using iron-based catalysts

The heteroleptic complex **14Py** was found active for the polymerization of *L*-LA at room temperature, as it successfully converts 200 eqs. of monomers with very good conversion in 64 hours (Table 5.2, Entry 1). The conversions of *L*-LA monomer in each case were determined by ¹H NMR spectroscopy of the aliquots in CDCl₃ by comparing the integrations of the quartet resonances of the methine protons of *L*-LA and PLLA in the region 5.0–5.2 ppm, as shown below in Figure 5.10.
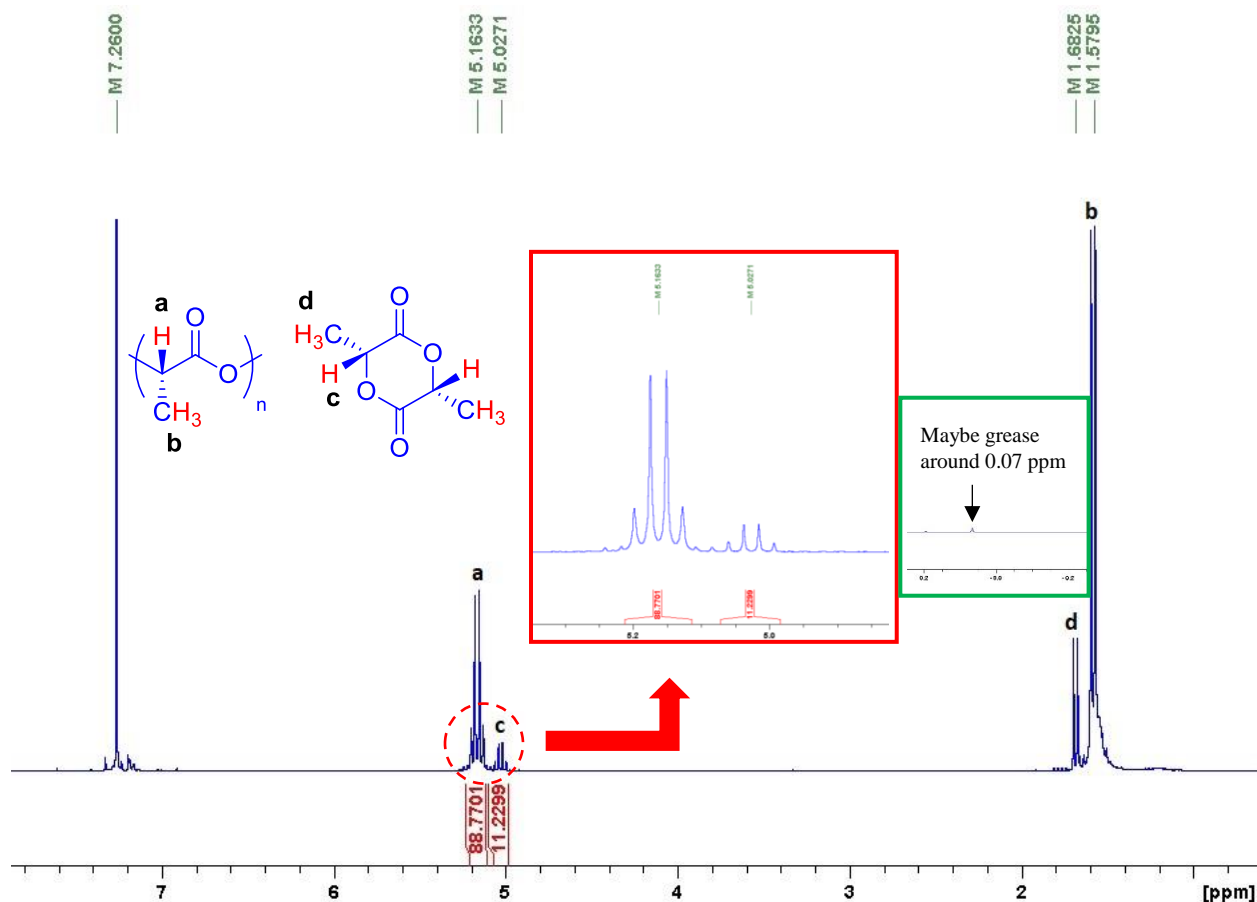
Figure 5.10. Determining conversion (89%) *via* ¹H NMR of the aliquot in CDCl₃ (Table 5.2, Entry 1)

To optimize the reaction at room temperature, we quenched the same reaction at 16 h and ended up with exactly the same conversion (Table 5.2, Entry 2). The reaction time was further optimized to 6 h in which 73% of *L*-LA monomers were converted to PLLA (Table 5.2, Entry 3). The resulting extracted PLLAs were further analyzed by ^{1}H and ^{13}C NMR spectroscopy, as shown below in Figure 5.11 from which we can observe the formation of isotactic PLLA indicating the absence of epimerization. The signal of probable chain-end –N(SiMe₃)₂ around 0.15 ppm could not be observed in this case whereas a residual peak probably corresponding to silicone grease was observed at 0.07 ppm.[72] The identification of end group will be specifically discussed later in the section 5.2.3.3.
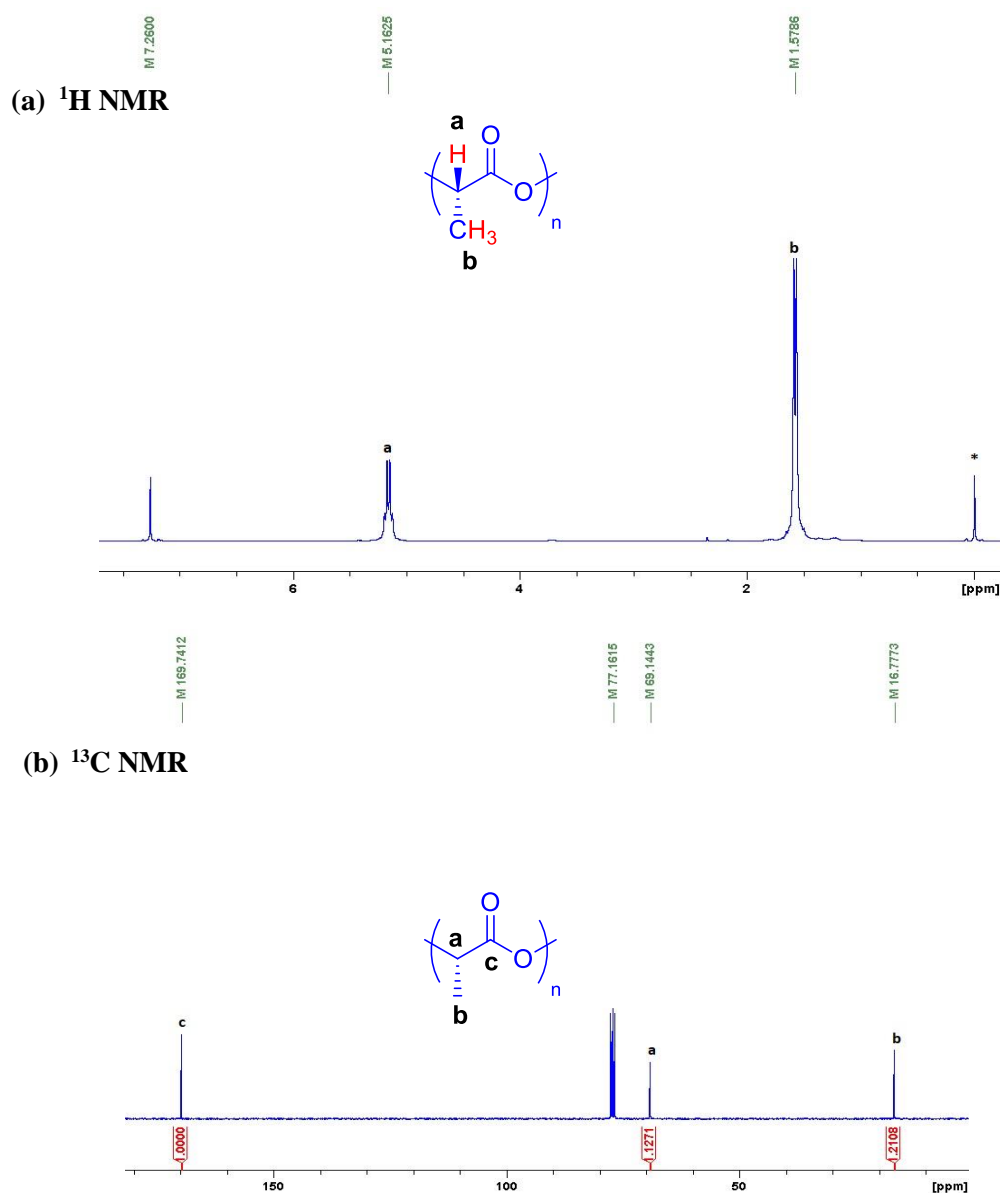
Figure 5.11. ^{1}H NMR (a) and ^{13}C NMR (b) of the polymer in CDCl₃ *trace of grease (Table 5.2, Entry 1)

SEC analysis of the PLLAs were performed to determine their molar masses. As usual, the analyses were initially performed in THF but due to the limited solubility of the polymers, the obtanied traces were not good enough to rely on the corresponding data (Figure 5.12). Therefore, in case of PLLA, the analyses were performed in chloroform and the molar masses were reported.
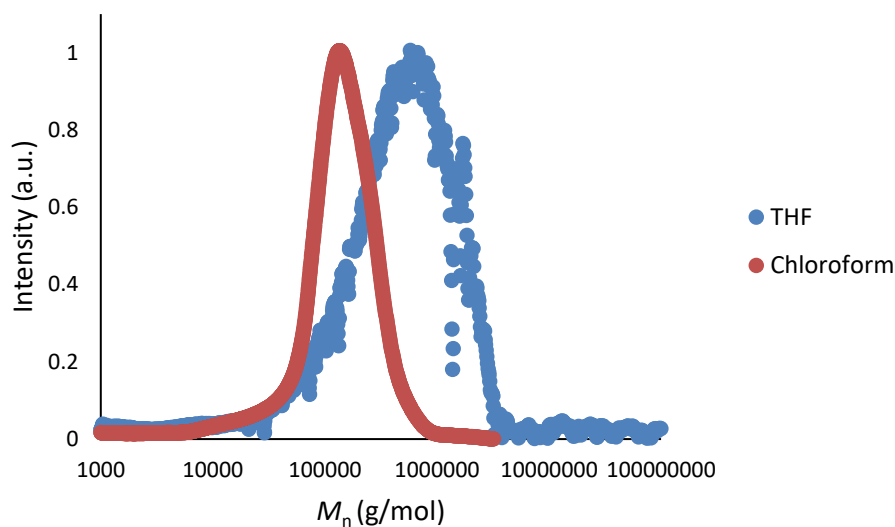
Figure 5.12. Comparison of SEC traces obtained in different solvents (Table 5.2, Entry 1)

The M_n values of the PLLAs were found to be same owing to the same conversion of the monomer and the obtained dispersities were quite narrow in accordance with a controlled process (Table 5.2, Entries 1 and 2). However, the obtained M_n (94 000 g/mol) was nearly 3 times higher than expected ($M_{n(th)}$ = 26 000 g/mol), speaking in favor of a faster chain propagation than rate of initiation. These high values could also imply that every molecule of **14Py** does not necessarily participate in the polymerization as previously observed with mono-/trihapto nitrogen-based lanthanide catalysts for the polymerization of ε-CL.[73] Decreasing the reaction time to 6 h provides no significant change in terms of control over polymerization, however, only limits the conversion to 73% (Table 5.2, Entry 3).

After optimizing the polymerization at room temperature, we intended to observe the influence of reaction parameters such as temperature on the polymerization activity. Therefore, the polymerizations were conducted at 50 °C and then eventually at 70 °C. At 50 °C, excellent conversion (>99%) of *L*-LA was obtained within 16 h (Table 5.2, Entry 4) and the reaction time was then reduced to 4 h where a conversion of 82% was obtained, indicating that the catalytic activity increases with temperature (Table 5.2, Entry 5 *vs* Entry 3). However, increasing the

temperature did not provide better control over the polymerization, as the resulting M_n were still 3-4 times higher than their expected value (Table 5.2, Entries 4 and 5).

In a similar manner, the polymerizations were conducted at 70 °C where up to 96% conversion of monomer was achieved within 15 h. The polymerizations were again optimized by quenching the reactions at 2 h and 1 h, corresponding to 96% and 80% conversions of *L*-LA, respectively (Table 5.2, Entries 6–8). These observations highlight the activity dependence on the reaction temperature where the activity of catalyst **14Py** increases with temperature. Narrow dispersities were obtained but the usual trend of obtaining high M_n values was still present.

Changing the initiator **14Py** to a less sterically hindered complex **13Py** had an impact on the activity of the polymerization. At room temperature, 75% conversion of *L*-LA was obtained within 6 h, which is almost similar to the result obtained with complex **14py** (Table 5.2, Entry 9 *vs* Entry 1). However, as the reaction temperature was increased to 50 °C, the same conversion level could be reached within 2 h (Table 5.2, Entry 10). The reaction was further optimized to 3 h for reaching 97% conversion of monomer, which implies that the catalyst **13Py** is slightly more active for the ROP of *L*-LA than the catalyst **14py**, probably due to less hindered iron center in **13Py** compared to **14Py** that could facilitate the coordination of the monomer.

The initiator **13Py** was further assessed at 70 °C where the reactions were stopped at various intervals of 30 min, 45 min and 1h corresponding to 61%, 81% and 94% conversion of *L*-LA, respectively, which again confirms that the activity of catalysts increases with temperature (Table 5.2, Entries 12–14 *vs* Entries 9–11). These values were plotted to obtain a conversion *vs* time plot and also the first-order kinetics plot where it appears that the polymerization is well controlled for catalyst **13**, displaying a *quasi*-first order kinetic profile, which speaks in favor of minimal loss of a small fraction of active species along the polymerization process (Figure 5.13).
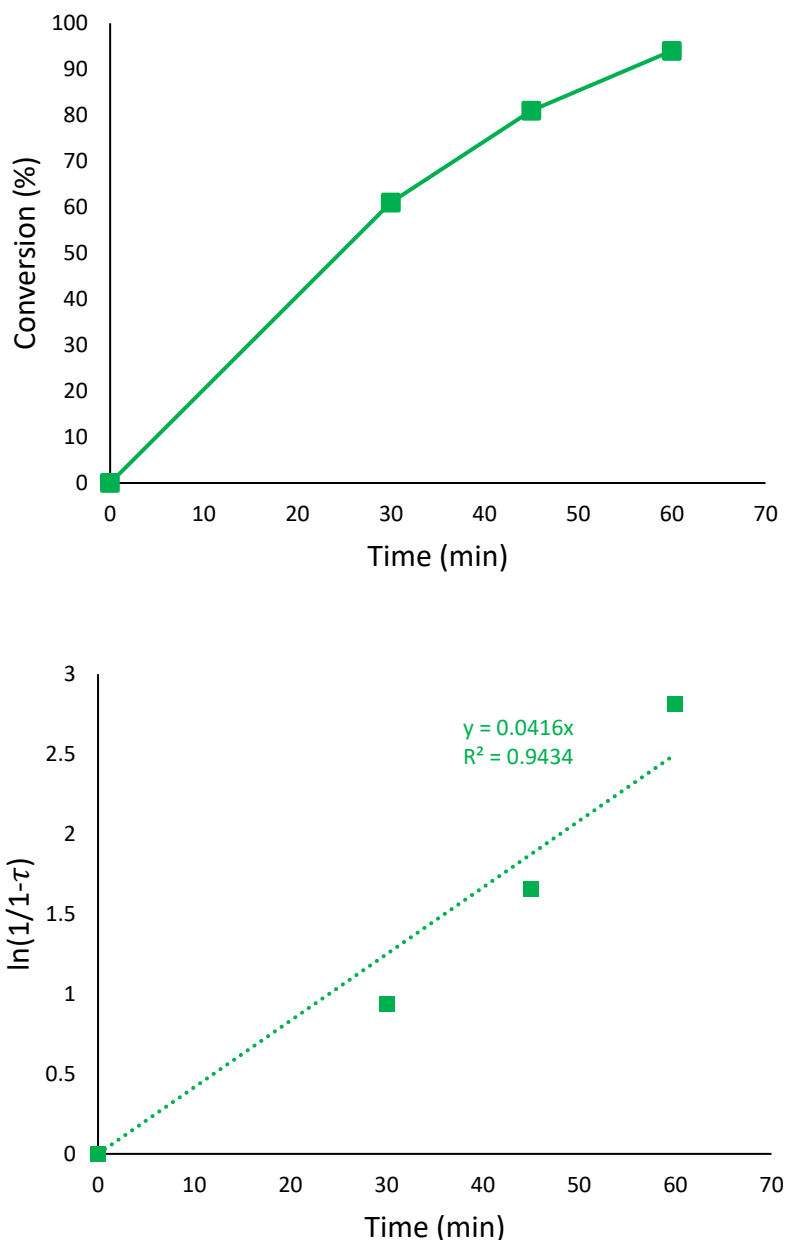
Figure 5.13. Monomer conversion (τ) as a function of time (left) and first-order kinetic plot (right) for initiator **13Py** at 70 °C (LA/Fe = 200/1)

Nevertheless, the M_n values of the PLLAs resulting from catalyst **13Py** were again found to be 3-4 times higher than their expected molar mass as seen previously with its congener **14Py**, speaking again in favor of faster chain propagation (Table 5.2, Entries 1–14). From these results, we can probably suggest that no matter if the iron center is sterically more or less hindered, faster

propagation than initiation occurs, producing polymers with high M_n along with narrow dispersities. It could also mean that within these systems, neither the steric bulk nor the temperature has an influence on the rate of propagation or it might be possible that only 25–30% of catalyst is active to catalyze the polymerization. Although, the difference in their respective catalytic activities is noticeable which arises only due to the addition of methyl group on the pyridine ring that hinders the access of monomer to the iron center.

5.2.3.2. Ring Opening Polymerization of L-lactide in the presence of Benzyl alcohol

In the previous section, we have seen that the heteroleptic amidopyridine iron (II) amide complexes **13Py** and **14Py** can efficiently catalyze the ROP of *L*-LA at different temperatures with the highest activity of each system observed at 70 °C but, in each case, we observed the formation of high molecular weight polymers deviating from the expected molar mass. Therefore, we conducted the polymerization with one of the initiators (**14py**) in the presence of benzyl alcohol, which is known to control the polymerization by substituting $-N(SiMe_3)_2$ with $-OBn$ which might act as a better initiating group.[74–76] The polymerizations were conducted under optimized conditions and the results are displayed in Table 5.3 below.

Table 5.3. Polymerization of *L*-lactide (*L*-LA) in the presence of BnOH using initiator **14**[a]

Entry[a]	LA/Fe/BnOH	Time (min)	Conv.[b] (%)	$M_{n(exp)}$[c] (g/mol)	Đ[c]
1	200/1/0.5	15	84	93 000	1.23
2	200/1/1	30	98	94 000	1.29

[a] Polymerization conditions: 2.5 µmol of Fe (II) complex; toluene = 0.5 mL, [*L*-LA] = 1.0 M in toluene, temperature = 70 °C ; [b] determined by ^{1}H NMR; [c] determined by SEC analysis in chloroform using the correction $M_{nexp} = M_{nsec} \times 0.58$;[71] $M_{n(th)} = (LA/Fe) \times 144.13 \times$ conversion, considering one growing chain per metal center.

The addition of 0.5 eq of BnOH increased the catalytic activity of the complex **14Py**, resulting in 84% conversion of the monomer within 15 min (Table 5.3, Entry 1), when compared to the same reaction in the absence of BnOH (Table 5.2, Entry 8). Increasing the ratio of Fe/BnOH to 1, afforded 98% of PLLA units in 30 min. However, despite the positive influence of the presence of BnOH on catalytic activity of the initiator **14Py**, the fine control over polymerization could not be gained even in the presence of BnOH, which failed to enhance the slow initiation compared to propagation as there was no significant reduction in the M_n values of the obtained

polymer in each case (Table 5.3, Entries 1 and 2). In fact, the dispersities and M_n values obtained in the presence of BnOH were found very close to the ones obtained in the absence of BnOH (Table 5.3, Entries 1 and 2 *vs* Table 5.2, Entries 6–8).

5.2.3.3. Chain-end group analysis of PLLA

After the successful implementation of heteroleptic iron complexes **13Py** and **14Py** in the ROP of *L*-LA, we anticipated the formation of PLLA chains bearing the amide –C(O)–N(SiMe₃)₂, providing that the polymerization proceeds *via* coordination-insertion mechanism. In this context, the determination of polymer chain-ends is of vital importance as it helps to identify the polymerization mechanism. Therefore, we used ¹H NMR spectroscopy, which is commonly used to identify the protons of the chain-ends as they have different chemical shifts with respect to the ones within the repeat units. In order to determine the chain-end structure of the PLLA produced using initiator **14Py**, we conducted a polymerization by reducing the LA/Fe ratio to 20 under optimized conditions to achieve 94% conversion of *L*-LA, as described in Scheme 5.8 below.
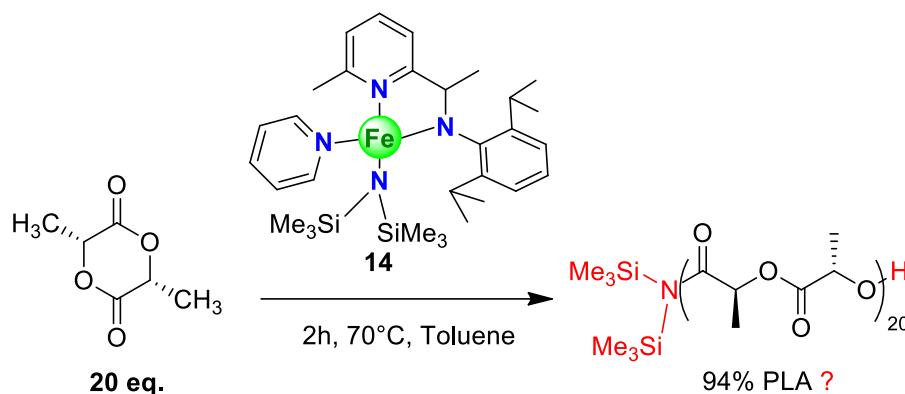
Scheme 5.8. Synthesis of short-chain PLA using initiator **14Py** to identify the chain-end

The ¹H NMR spectrum of the produced PLLA in Scheme 5.8 is shown below in Figure 5.14.a. Apart from the methine and methyl protons of PLLA, we can clearly observe some small additional signals arising at 0.07 and 0 ppm, which might correspond to the silicon grease or –N(SiMe₃)₂ chain end group, respectively. To differentiate between the signals in the region 0–0.1 ppm, we performed the hydrolysis of lithium trimethylsilylamide to generate NH(SiMe₃)₂, whose signal in ¹H NMR would lie in the range 0–0.2 ppm. In parallel, we also added a little bit of grease to the NMR tube containing the polymer sample and stacked all the three spectra for identification of peaks (Figure 5.14b)
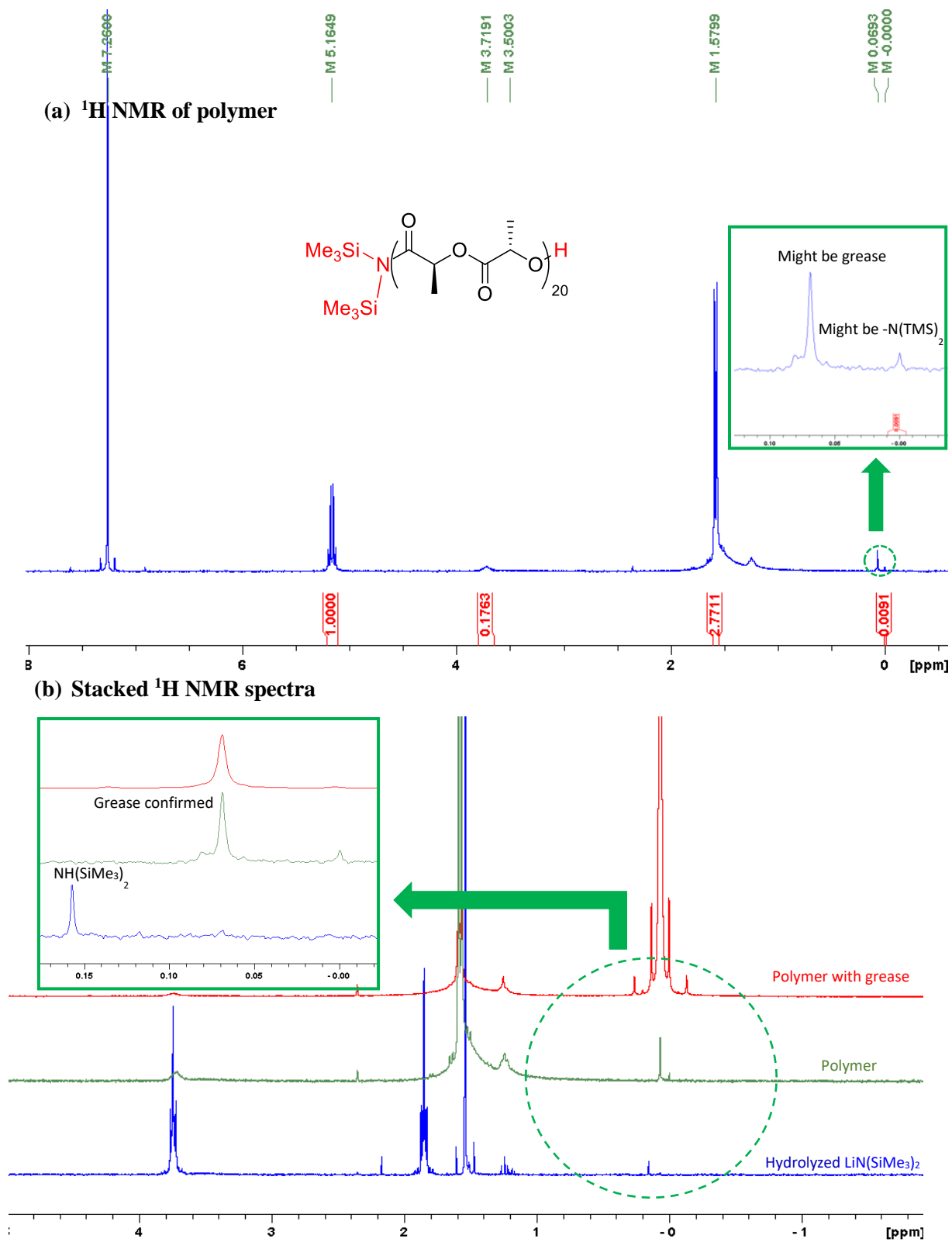
Figure 5.14. ¹H NMR of the polymer (a) obtained in Scheme 5.4 and stacked ¹H NMR spectra (b) of hydrolyzed LiN(SiMe₃)₂, polymer and polymer with grease (*ethanol trace)

From the stacked ^{1}H NMR spectra in Figure 5.14b, we can see the peak arising at 0.16 ppm that corresponds to the methyl protons of NH(SiMe3)2. Furthermore, the addition of a small amount of grease to the polymer increases the signal at 0.07 ppm which confirms that this peak represents the grease. Therefore, this leaves us only with one small peak approximately at 0 ppm, which cannot be the chain-end –N(SiMe3)2 as it contradicts the fact that this value corresponds to the reference tetramethylsilane (TMS).

Additionally, to confirm the chain-end, we also performed diffusion-ordered NMR spectroscopy (DOSY), which is a powerful method to deconvolute complicated 1D ^{1}H NMR spectra.[77] This method seeks to separate the NMR signals of different species according to their diffusion coefficient. A series of spin echo spectra is measured with different pulsed field gradient strengths, and the signal decays are analyzed to extract a set of diffusion coefficients with which to synthesize the diffusion domain of a DOSY spectrum. This technique was used to characterize aggregates, such as micelles[78] or coordination polymers,[79] but more recently, DOSY is widely used as a method to complement size exclusion chromatography for determining the molecular weight of polymers[80] and to distinguish copolymers from mixtures of homopolymers.[81–83]

The ^{1}H DOSY NMR spectrum of the PLLA obtained in Scheme 5.8 is shown below in Figure 5.15 from which we can observe that a total of 3 diffusion coefficients exists for the sample.
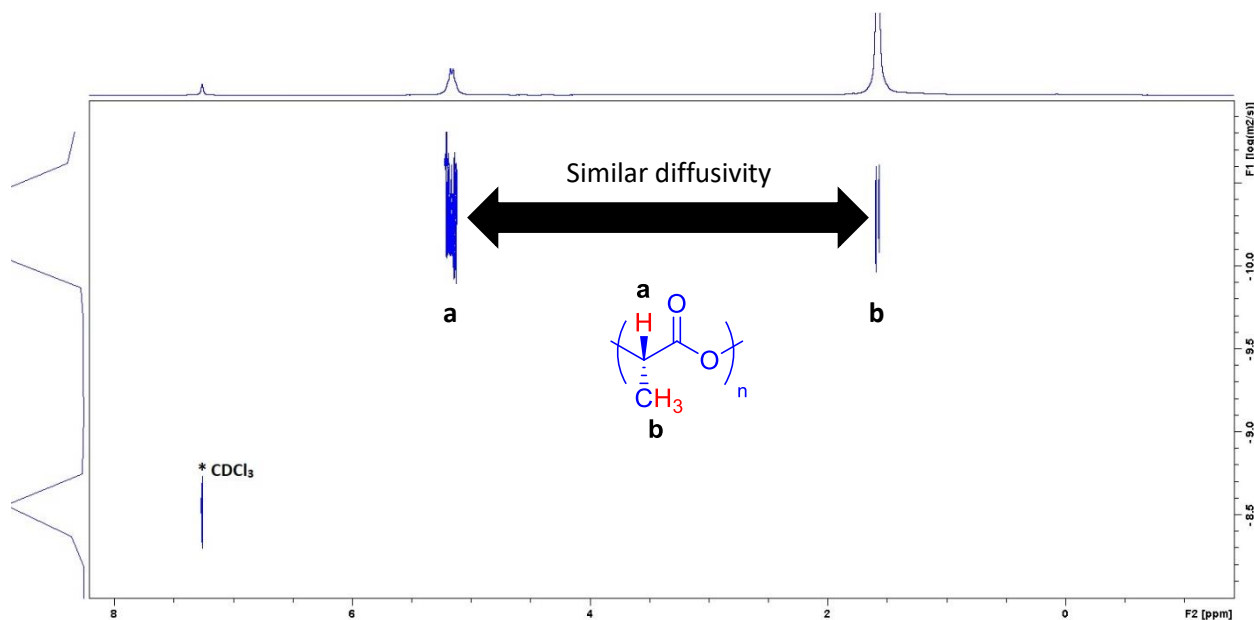
Figure 5.15. ^{1}H DOSY NMR spectrum of the PLLA obtained in Scheme 5.8

It is clear from the spectrum that the intensities of all the 3 coefficients observed are not similar implying that some of the species are different and are not part of the same PLLA chain. The first peak around 7.26 ppm corresponds to the NMR solvent (in this case $CDCl_3$) whose diffusivity is less than the second signal at 5.16 ppm which refers to the methine protons of the PLLA. The diffusivity of the second signal is almost similar to the third signal at 1.57 ppm corresponding to the protons of the methyl group in PLLA as they are in the same line. Lastly, we do not observe any signal or diffusivity near 0.07 ppm, which means either there is no end group or the diffusion coefficient corresponding to the end group is very small. This observation could be attributed to two possibilities: i) the high molecular weight of the resulting PLLAs or ii) the formation of macrocyclic PLLA with no chain-ends.

In the first case, to observe chain-ends in the ^{1}H NMR spectrum, it is essential to analyze low molecular weight polymers with a smaller number of repeat units as the resonances of each end group would be small in intensity when compared to the resonances of repeating units. So, for the PLLA obtained in Scheme 5.8 with 20 eqs. of *L*-LA, we expect theoretically a molar mass of 2700 g/mol whereas in reality according to the M_n values obtained in Table 5.2, we should be near 9400 g/mol which is relatively large for a PLLA with 20 repeat units. Therefore, we propose that due to this reason, the detection of end-groups in the ^{1}H NMR spectrum was unsuccessful.

Considering the second possibility, the formation of a macrocyclic PLLA can be suggested on the basis of intramolecular transesterification reactions or back-biting where the oxygen from one chain-end acts as a nucleophile to attack the carbonyl group attached to $-N(SiMe_3)_2$ (Scheme 5.9), which can lead to a huge difference between calculated and experimental M_n values in as observed in Table 5.2. This observation is already apparent in literature with rare-earth lanthanum homoleptic complex $La[N(SiMe_3)_2]_3$ for the polymerization of manOCA(O-carboxyanhydride from mandelic acid)[84] and lanthanide trisborohydrides $Ln(BH_4)_3(THF)_3$ complexes for bulk polymerization of *L*-LA.[85,86] The same transesterification could happen with the PLLA constituting $-OBn$ as a chain end owing to the high M_n values obtained in Table 5.3. Therefore, in order to confirm among the two possibilities of PLLA structure, we conducted a Matrix-assisted laser desorption ionization-time-of-flight mass spectrometry (MALDI-ToF-MS) study of PLLA sample.
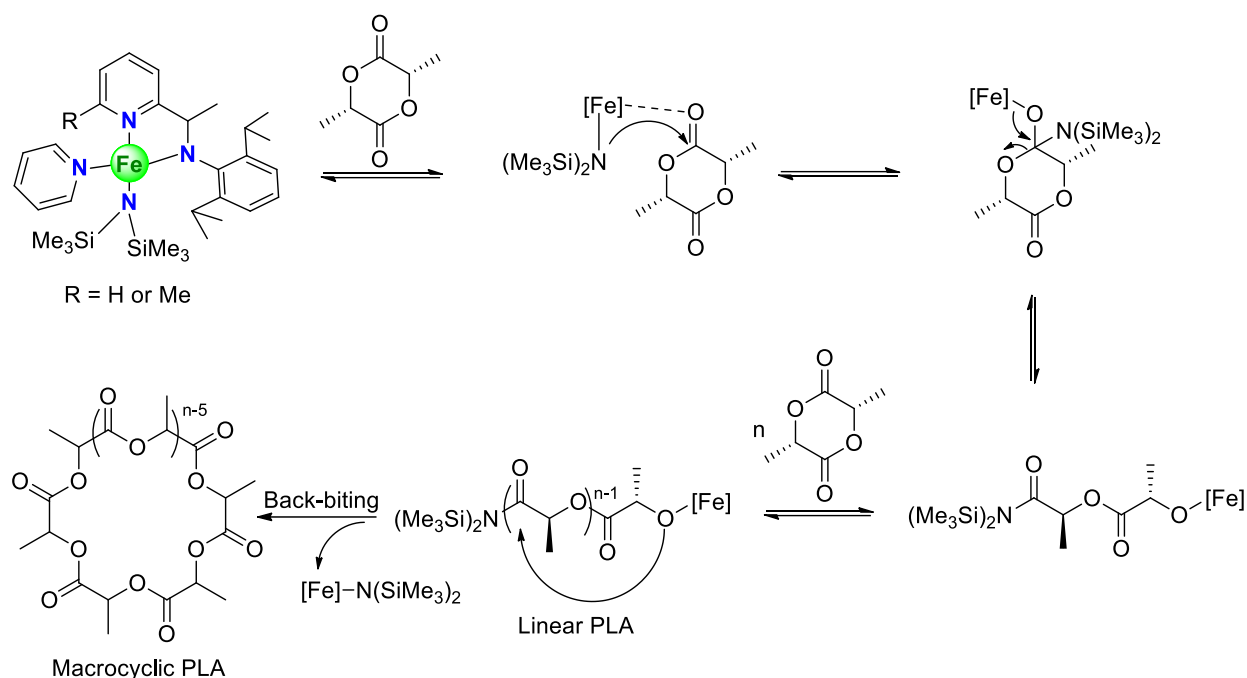
Scheme 5.9. Proposed mechanism of transesterification for the ROP of *L*-LA by complexes **13Py** and **14Py**

MALDI-ToF-MS was developed in late 1980s by Karas and Hillenkamp[87] and has become established as a technique for the analysis and accurate molecular weight determination of large macromolecules such as proteins, polysaccharides, nucleic acids, and synthetic polymers with high mass accuracy, extreme sensitivity, and an almost unlimited mass range and speed of analysis.[88] It is a "soft" ionization process which uses a pulsed laser beam to cause adsorption of a matrix from sample plate that includes ions of the analyte which in turn produces charged ions with minimum fragmentation. The type of ionizing salt (generally alkali metal salts) used partially depends on the type of polymer to analyze. MALDI-ToF-MS is highly sensitive and capable of detecting ions at high masses due to which it has been demonstrated as an important technique for analysis of a variety of synthetic polymers as it provides valuable structural information such as absolute molecular weight, repeat unit, and end group of synthetic polymers. This information, especially the end group information, affords deeper insight into polymers structures, reaction mechanisms, and side reactions including the occurrence or not of intra-/intermolecular transesterification reactions.[85,86,89–93]

As described above, the intramolecular transesterification or back-biting (Scheme 5.9) leads to the formation of PLA macrocycle and can be observed in MALDI spectra by the presence of

macrocyclic PLA (No chain ends). On the other hand, intermolecular transesterification occurs between two macromolecules which can be advanced in the case of lactide monomer when distributions containing both even-and odd-membered oligomers, with peaks separated by 72 Da (corresponding to lactyl or half monomer of lactide) are observed (Scheme 5.10).
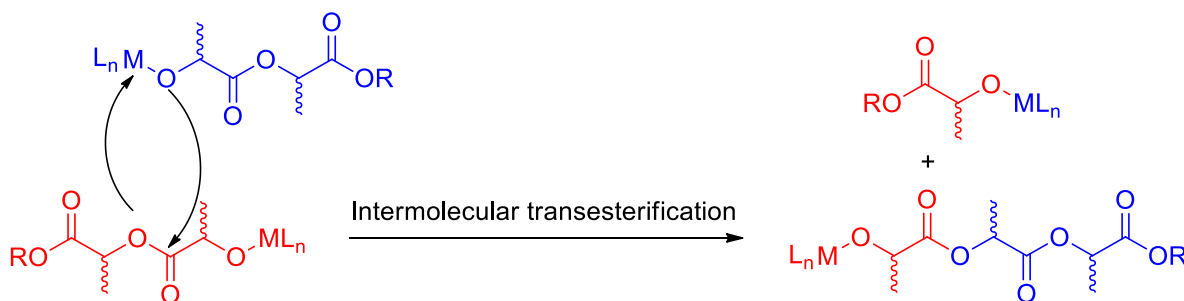
Scheme 5.10. Chain redistribution of PLA *via* intermolecular transesterification

The difference between peaks observed in the mass spectrum is the mass of the repeating unit. This peak-to-peak difference can be used to identify certain polymeric species but the difference between the experimental (m_{exp}) and calculated (m_{cal}) masses of a proposed polymer structure can give information about the structure and the related end groups using the equations (1) and (2) below.

$$m_{exp} - m_{cal} \leq 1 \quad (1)$$

$$m_{cal} = nM_w + E_1 + E_{11} + M^+ \quad (2)$$

E_1 and E_{11} are molar masses of chain ends at opposite side, n is the number of monomer units, M_w is the molar mass of the monomer and M^+ is the molar mass of the cation.

The PLLA acquired from Table 5.2, Entry 14 was analyzed by MALDI-ToF-MS and the mass spectrum is shown in Figure 5.16. From the spectrum, initially, we can observe the most intense peaks corresponding to 1291.912 Da, 1512.252 Da, 1733.005 Da, 1953.125 Da etc. These peaks are separated by almost 220 Da which speaks in favor of the absence of intermolecular transesterification reactions leading to linear PLAs with interpeak separation of about 72 Da corresponding to lactyl units. Each mass number peak turns out to be in good agreement with the calculated one assuming cyclic PLLA with no chain end. For instance, m/z (obs) = 1512.252 *vs* m/z (cal) = 1512.42 for M (n = 21, 21 × 72.02) with 21 repeat units in macrocycle. Likewise, the peak 1733.005 suggests that this fragment is more cyclic than the previous one (n = 1733.005

/72.02 = 24). Overall, each peak reveals the presence of cyclic PLLA [O–C(O)–CH(CH$_3$)]$_n$ with n (multiple of 3) = 18 – 33 (Major peak = Cationic M + Na$^+$, where M = 72.02 n). Further, if we look at the additional signals in each pattern, we could see that the difference between each signal is either 19 or 21 Da which could attribute to the presence of water or sodium (Figure 5.16). For instance, the second peak in the pattern almost corresponds to 1754.206 = 24 × 72.02 + 22.99 (Na$^+$). These results confirm that the PLLAs resulting from the polymerization of *L*-LA using iron (II) amide complexes **13Py** and **14Py** are cyclic in nature with no chain ends.
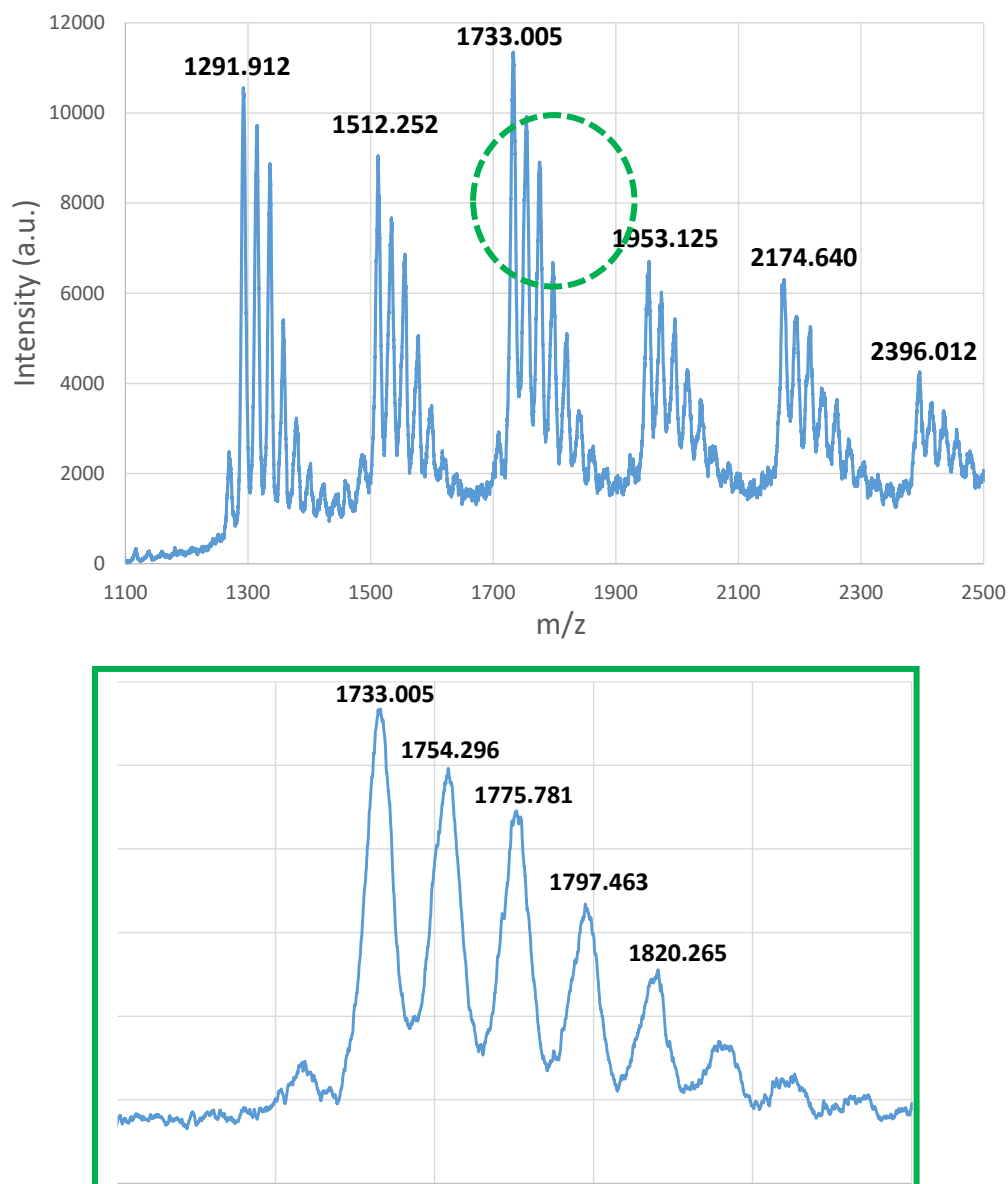
Figure 5.16. MALDI-ToF MS spectrum of PLLA obtained with **13Py** (Table 5.2, Entry 14)

This result also undermines the molecular weights obtained with the current SEC analysis, however, still a comparison between the M_n values can be drawn to rationalize the activity of each catalytic system. Further studies can be conducted in future to determine the accurate molecular weights using molecular weight sensitive detectors which are essential specially when complex polymers have to be analyzed or when the shape of polymer is unknown. Multi-angle LS is by far the most common LS detector for the measurement of dispersities and molecular weight averages. In an SEC-MALLS setup, the RI-detector is required to determine the concentration of the analyte. Being a universal detector, it recognizes every difference between the pure solvent and the sample solution. Through the specific refractive index *dn/dc*, it is possible to calculate the concentration of the sample. MALLS covers the full range of molecular weights and has earned strong acceptance in some industries, in particular, for protein measurements.

5.2.3.4. Ring Opening Polymerization of ε-caprolactone

The ring opening polymerization of ε-caprolactone (CL), a petro-sourced cyclic monomer (Scheme 5.11), produces polycaprolactone (PCL), which is also an attractive biodegradable polymer.[11,94]
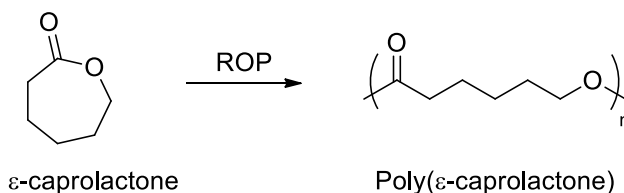
Scheme 5.11. ROP of ε-caprolactone

There have been various iron-based catalytic systems reported for the ROP of ε-CL including inorganic salts, coordination catalysts and well defined catalytic systems but their activities varied from moderate to low in most of the cases.[25] Therefore, we assessed the ROP of ε-CL initiated by complexes **13Py** and **14Py** under optimized conditions, the results of which are presented below in Table 5.4.

Table 5.4. Polymerization of ε-caprolactone (CL) using initiators **13Py** and **14Py**[a]

Entry[a]	Fe	Time (min)	Conv.[b] (%)	$M_{n(exp)}$[c] (g/mol)	Đ[c]
1	**13**	15	80	97 000	1.23
2		30	87	100 000	1.28
3	**14**	15	82	92 000	1.25
4		30	88	100 000	1.29

[a] Polymerization conditions: 2.5 µmol of Fe (II) complex, CL/Fe = 200/1, toluene = 0.5 mL, [ε-CL] = 1.0 M in toluene, temperature = 70 °C; [b] determined by ^{1}H NMR; [c] determined by (SEC) analysis in chloroform using the correction $M_{nexp} = M_{nsec} \times 0.56$;[71] $M_{n(th)} = (CL/Fe) \times 114.14 \times$ conversion, considering one growing chain per metal center.

From the results in Table 5.4, we can see that both complexes **13Py** and **14Py** were found to be active for the ROP of ε-CL. ^{1}H NMR spectroscopy was used to determine the conversion by withdrawing an aliquot from the polymerization mixture and analyzing the resulting PCL, as shown in Figure 5.17 at the end of this section.

Upon the addition of monomer to the catalyst solution, the solution slowly turns viscous in a range of minutes and forms a gel, implying the completion of reaction. The initiator **13py** converts 80% of the CL units within 15 min and doubling the reaction time to 30 min increases the conversion to 87% (Table 5.4, Entries 1 and 2). Changing the initiator to a bulkier complex **14Py** does not significantly impact the activity of the catalyst, converting 82% of monomer in 15 min and 88% in 30 min, which illustrates the negligible effect of steric bulk on the activity of these catalytic systems in the ROP of ε-CL (Table 5.4, Entries 3 and 4).

The resulting PCLs were also analyzed by SEC to determine their M_n values. Like PLLA, the analyses were performed in chloroform due to the better solubility of polymer and reliability of data. The M_n values of the obtained PCL ranged from 92 000 to 100 000 g/mol, which is again nearly 4-5 times higher than the theoretical value ($M_{n(th)} = 18\ 000 – 20\ 000$ g/mol), speaking again in favor of higher rate of propagation than initiation or due to uncontrolled back-biting/intramolecular transesterification reactions leading to the formation of cyclic PCL which can be confirmed by the absence of –N(SiMe$_3$)$_2$ signal around 0 ppm in ^{1}H NMR (Figure 5.17). Nevertheless, all the PCLs displayed monomodal SEC traces with narrow disperties that tend to 1.
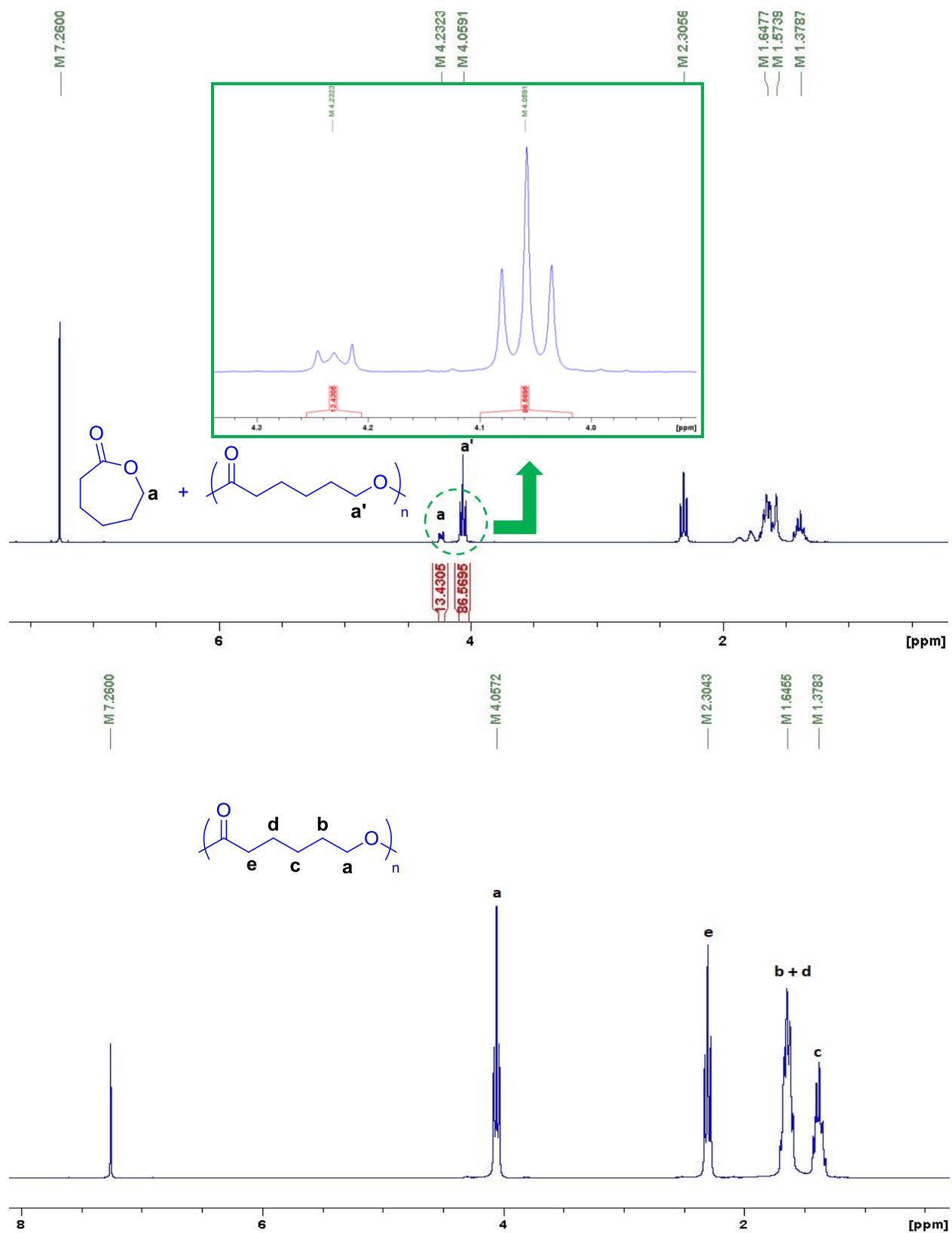
Figure 5.17. Determining conversion (87%) of CL *via* ^{1}H NMR of the aliquot (top) and ^{1}H NMR of the PCL (bottom) in CDCl$_3$ (Table 5.4, Entry 2)

5.2.3.5. Ring Opening Copolymerization of L-lactide and ε-caprolactone

PLA is one of the major biodegradables and biocompatible thermoplastics that could serve as an alternative to the widely used petroleum-based plastics. However, its limitations have restricted the commercialization of PLA to food packaging, pharmaceutical and biomedical fields.[6–9,95] As a matter of fact, PLA possesses several disadvantages such as (i) brittleness, (ii) poor elasticity, (iii) low thermal stability and (iv) poor gas/water permeability that limit its potential applications.[20–23] One of the major strategies that can suppress these drawbacks is the Ring-Opening copolymerization (ROCoP) of LA with another lactone, in particular ε-CL, which enables the inherent properties of each homopolymer to be incorporated into the resulting copolymer. The contrasting physical and thermal properties of the two homopolymers make them complementary to each other. For example, PCL ($T_g = -60$ °C) is more permeable to drugs than PLA ($T_g \approx 57$ °C) due to its less hydrophilicity, on the other hand, PLA has comparably shorter lifetime (weeks) than PCL (1 year) under similar conditions of degradability.[96–98] Therefore, the copolymerization of LA and ε-CL can produce biodegradable polymers with improved properties. The ROCoP of LA and ε-CL, results in the formation of block, poly(LA-*block*-CL) or gradient, poly(LA-*grad*-CL) or statistical, poly(LA-*stat*-CL) copolymers as shown in Scheme 5.12 below.[99,100]
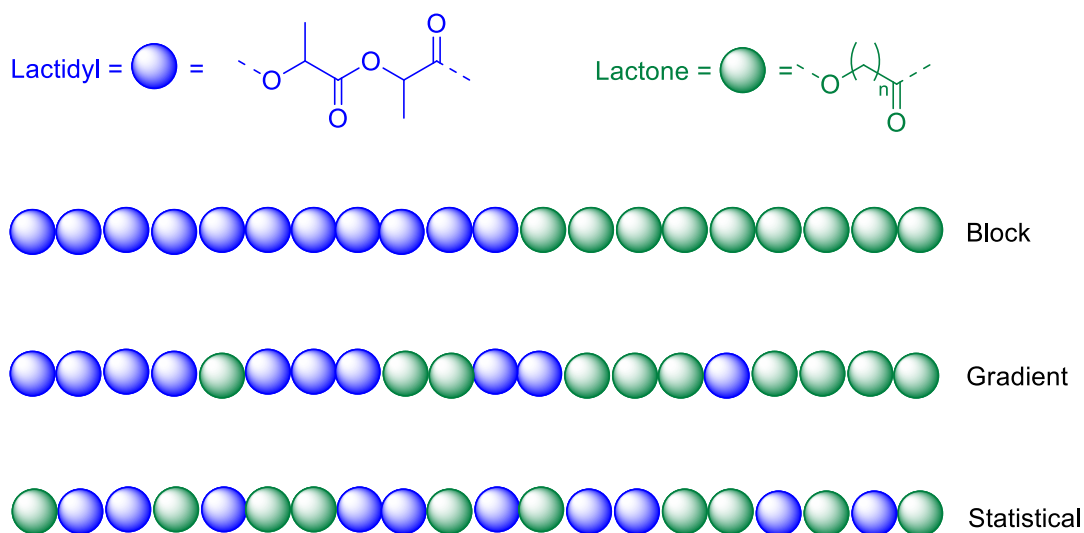
Scheme 5.12. Possible microstructures of lactide-lactone copolymers

A various plethora of organocatalytic systems and metal based complexes have been used for the ROCoP of LA and ε-CL,[24] but surprisingly, little attention has been paid to the development

of iron catalysts in this field.[25] Herein, we report the catalytic behavior of heteroleptic amidopyridine iron (II) amide complex **13Py** towards the statistical copolymerization of *L*-LA and CL. The copolymerization was conducted with an equimolar feed monomer ratio LA:CL = 100:100 and the reactions were carried out in toluene at 70 °C. The results of the copolymerization are presented below in Table 5.5.

Table 5.5. Copolymerization of *L*-lactide (*L*-LA) and ε-caprolactone (CL) using initiator **13**[a]

Entry[a]	Time (h)	Conversion[b]		Composition[b]		$M_{n(exp)}$[c] (g/mol)	$Đ$[c]
		%LA	%CL	%LA	%CL		
1	1	71	1.2	93	7	90 000	1.18
2	16	94	1.2	95	5	95 000	1.18

[a] Polymerization conditions: 2.5 µmol of Fe (II) complex, LA/CL/Fe = 100/100/1; toluene = 0.5 mL, [*L*-LA + CL] = 1.0 M in toluene, temperature = 70 °C; [b] determined by ^{1}H NMR; [c] determined by (SEC) analysis in chloroform using the correction $M_{nexp} = M_{nsec} \times 0.58$;[71] $M_{n(th)} = (LA/Fe) \times 144.13 \times$ conversion (LA) + (CL/Fe) $\times$ 114.14 $\times$ conversion (CL), considering one growing chain per metal center.

From the results in Table 5.5, we can see that the initiator **13Py** was found to be active for the ROCoP of *L*-LA and ε-CL. The conversions and compositions of each monomer were determined by ^{1}H NMR spectroscopy based on the methine signals of PLA and LA (incorporated in the copolymer) found at 5.15 and 5.05 ppm, respectively, and the signals of methylene protons of the PCL around 4.05, 4.13 ppm and CL (incorporated in the copolymer) at 4.23 ppm (Figure 5.18). In the presence of CL, the conversion of lactide units was limited to 71% in 1h whereas the conversion of CL was very poor in comparison. This resulted in copolymers containing mostly LA units (93%) whereas the percentage of CL (7%) incorporated was very low (Table 5.5, Entry 1). The polymerization time was increased to observe the influence of prolongation on the conversion of both monomers. After running the polymerization for 16h, the conversion of LA was improved to 94% whereas very poor conversion of CL (1%) was again obtained (Table 5.5, Entry 2). The compositions of both monomers hardly changed as obvious from their respective conversions. From these results, we can conclude that despite the rate of propagation of ε-CL is higher than that of *L*-LA in their respective homopolymerizations, the copolymerization of both monomers often leads to the preferential consumption of *L*-LA over ε-CL. These results are also in agreement with what is generally obtained in LA/CL copolymerization attempts under smooth experimental conditions where LA inhibits the incorporation of CL, preventing to enchain two CL units

successively.[24] One of the hypothesis would be the higher coordination of ability of LA than CL to the iron center, due to the presence of two ester groups. In this regard, the reduction of the coordination ability of LA can reduce the reactivity gap in ROCoP by altering the structure of the catalyst through the incorporation of bulkier ligands which might rebalance the reactivity ratios of both comonomers.
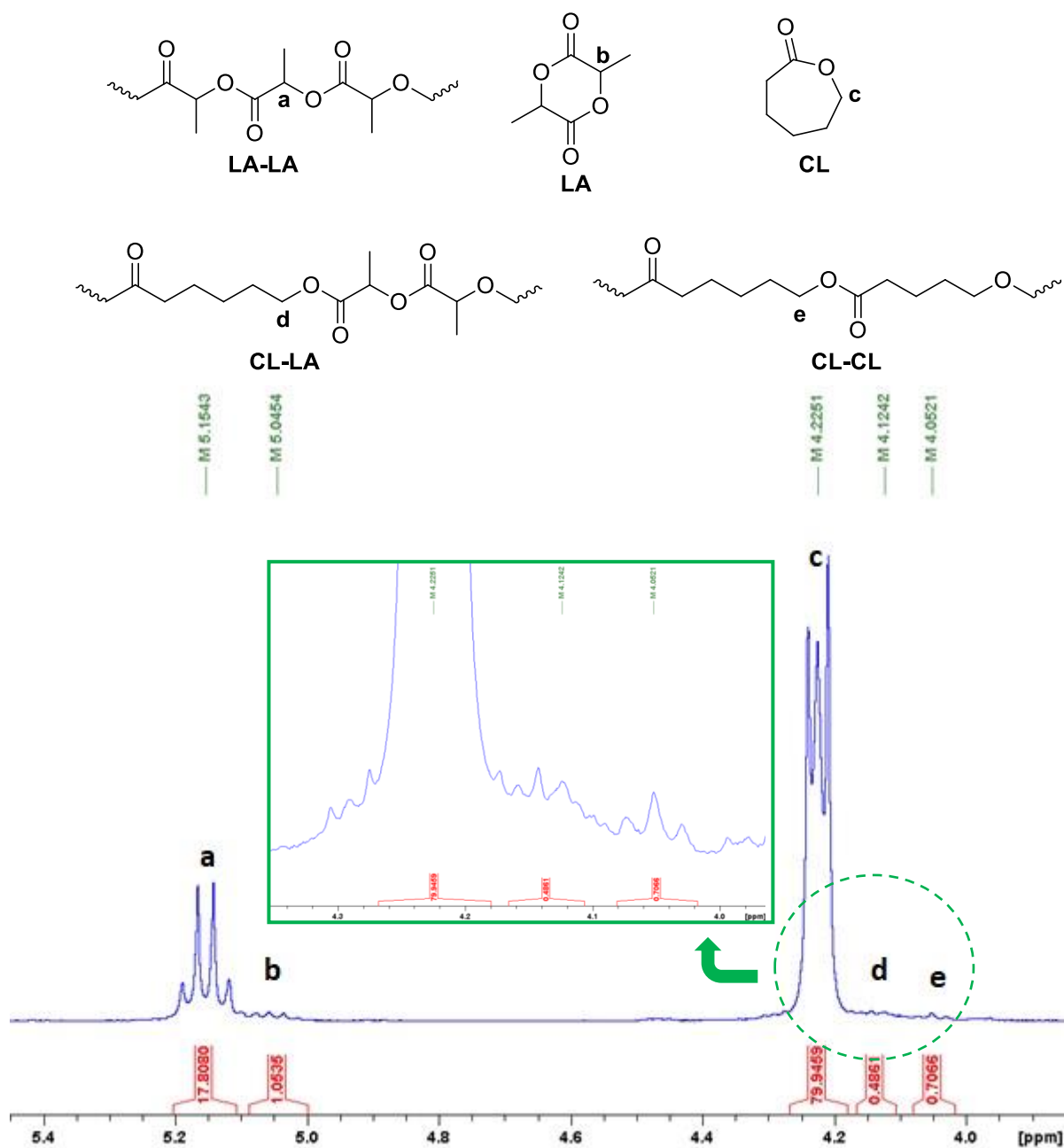
Figure 5.18. Determining conversions of LA (94%) and CL (1%) *via* ^{1}H NMR of the aliquot in CDCl$_3$ (Table 5.5, Entry 2)

The resulting copolymers were also analyzed by SEC where the GPC profile of each copolymer was found to be monomodal with very narrower dispersity (Table 5.5, Entries 1 and 2). However, the obtained M_n values were found to be nearly 9 times greater than the theoretical value ($M_{n(th)}$ = 10 000 – 14 000 g/mol), which again implies a high propagation rate compared to the initiation. It also means that the activity of the catalyst is reduced in ROCoP where only 10% of active species are catalyzing the reaction whereas the number of active species generated for the same complex was nearly 25% in the homopolymerization of *L*-LA and ε-CL.

5.3. Conclusion

In this chapter, we developed the targeted heteroleptic amidopyridine iron (II) amide complexes bearing bulky ^{i}P$_r$ groups as their *N*-aryl substituents. The synthesis of the complex **13Py** was performed in various solvents through which it was observed that the selectivity for the formation of homoleptic/heteroleptic complexes depends on the type of solvent used and especially its polarity. Performing the synthesis in THF, benzene and toluene, preferentially favors the formation of homoleptic complex **12** in major amount whereas the inversion of selectivity was observed in pentane, i.e. the major product being the heteroleptic analogue **13Py,** which was further recrystallized in pentane with excess of pyridine (Scheme 5.13). The implementation of the same synthetic strategy in pentane could yield the other heteroleptic analogue **14Py,** whereas the formation of its associated homoleptic analogue **(L^2)$_2$Fe** was unsuccessful due to the steric bulk imparted by relatively bulkier ligand ***rac*-L^{2}H** which forbids the coordination of the two deprotonated amido-pyridine chelate to the iron precursor, even after prolonging the reaction time and increasing the temperature. The newly developed homoleptic/heteroleptic iron (II) complexes were fully characterized by ^{1}H NMR, X-ray diffraction studies and their molecular formula were confirmed by elemental analysis.

The heteroleptic complexes **13Py** and **14Py** were assessed as initiators for their catalytic application in the ROP and ROCoP of *L*-LA and ε-CL. Both of these complexes were found efficient enough to catalyze the ROP of *L*-LA and ε-CL producing up to 99% of PLLA and 88% of PCL with moderate activities. The polymerization conditions were optimized by varying the temperature from 23 °C to 70 °C and we observed that the catalytic activity of these systems increased with the temperature, producing up to 94% PLLA in 1h and 88% of PCL in 15 min. To our surprise, the catalytic systems **13Py** and **14Py** produced high molecular weight PLLAs with

the M_n values being nearly four times than the expected, speaking in favor of a high rate of propagation with 25% of catalyst efficiency. The polymerizations seemed to be less controlled in terms of molecular weight despite the dispersities being quite narrow, which is a characteristic of a controlled process. Consequently, we attempted to control the polymerization by conducting it in the presence of BnOH, to enhance the initiation but unfortunately no influence of alcohol was observed on the molecular weights and dispersities of the resulting PLLAs, although, the catalytic performance of the system **14Py** was highly improved (up to 84% of PLLA in 15 mins).
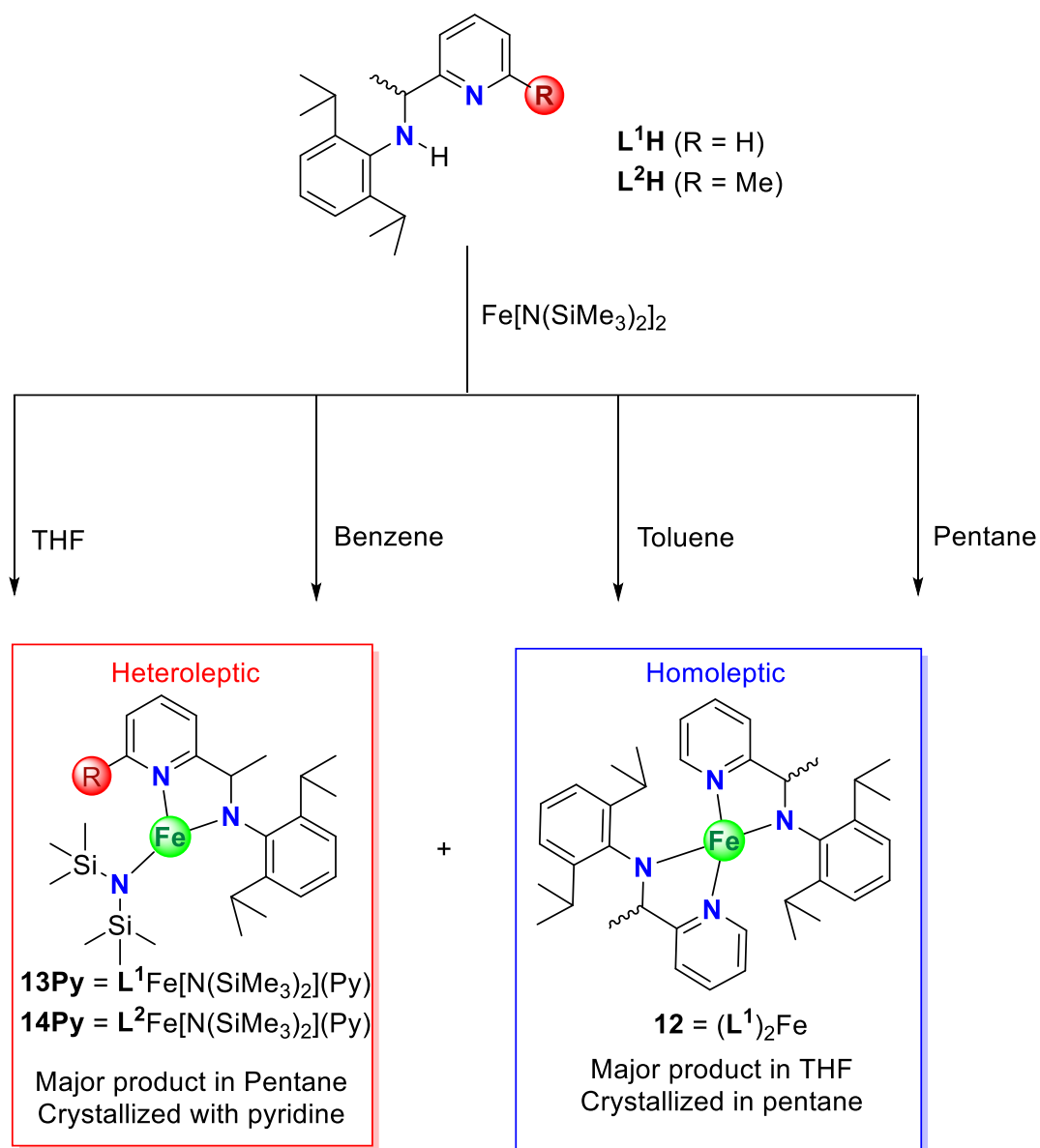
Scheme 5.13. Effect of solvent on the synthesis of heteroleptic/homoleptic amidopyridine iron (II) amide complexes **12, 13Py** and **14Py**

Furthermore, we also studied chain-end group analysis *via* ^{1}H NMR spectroscopy studies, to confirm the initiation by –N(SiMe$_3$)$_2$ group. The signals corresponding to the end group could not be confirmed by ^{1}H NMR spectroscopy due to which we performed a 2D DOSY NMR from where it was concluded that a total of two similar diffusion coefficients existed, each corresponding to the methine protons and methyl protons of the polymer chain. On the basis of this result, we can argue that the detection of chain-end was unsuccessful due to the relatively high molecular weight possessed by the PLLA chain or the possibility of the occurrence of uncontrolled transesterification reactions/back-biting that could lead to the formation of PLA macrocycle as described above in Scheme 5.9. This was later confirmed through MALDI-ToF-MS experiment where the obtained mass spectrum of PLA was consistent with the formation of cyclic PLLA with no chain ends due to which we could not observe any end group in NMR studies.

The high catalytic activity of the initiator **13Py** towards the ROP of ε-CL prompted us to conduct a statistical ROCoP of LA/CL for the synthesis of copolymers with improved properties than exhibited by that of PLA alone. The catalyst **13Py** was found to be active for the ROCoP of LA/CL but unfortunately the poor conversions of CL units could not be improved, even after prolonging the reaction hours that led to high conversion rate of *L*-LA units. Overall, these observations are in accordance with the fact that despite the propagation for ε-CL being higher than that of LA, preferential consumption of LA over ε-CL occurs in the ROcoP. This barrier could possibly be surpassed by utilizing complexes offering very high reactivity towards ε-CL such that the inhibition of CL does not occurs by LA. Further, the incorporation of different ligands might reduce the coordination ability of lactide, thereby reducing the reactivity gap in ROCoP and enabling a better incorporation of the typically less reactive lactone under copolymerization conditions.[24] Also, the variation of LA:CL feed ratio could also be an important factor which might improve the incorporation of CL units in the copolymer. Undeniably, further studies are needed in the future for the development of limited iron-based catalytic systems for the controlled statistical ROCoP of LA/CL or its extension to other bio-sourced comonomers such as epoxides or carbonates instead of petro-sourced ε-CL, for the development of new biodegradable polymeric materials.[25]

5.4. Experimental

5.4.1. General Considerations

Reagents [^{n}BuLi solution (2M in hexanes), $NaBH_4$, dry dimethylacetamide, $FeCl_2$ and $LiN(SiMe_3)_2$] were acquired from Sigma-Aldrich or Fisher SAS or TCI Europe N.V. and used as received. Deuterated solvent C_6D_6, pyridine, isopropanol, benzyl alcohol and ε-caprolactone were dried over CaH_2, distilled and degassed by freeze-pump-thaw before being stored over activated 4 Å molecular sieves in the glove box *L*-LA was recrystallized twice from hot toluene followed by sublimation under dynamic vacuum (0.01 mbar) at 70 °C. Size exclusion chromatography (SEC) analysis of the samples were performed in chloroform as an eluent at 40 °C (1 mL/min) with a SIS HPLC pump (Waters S.A.S, Saint-Quentin-en-Yvelines, France), a Waters 410 refractometer, and Waters Styragel columns (HR2, HR3, HR4, and HR5E) calibrated with polystyrene standards, with the correction $M_{n,SEC} = M_{n,PS}$ x 0.56 (PCL)[101] and $M_{n, SEC} = M_{n,PS}$ x 0.58 (PLA).[71] The remaining procedures are similar as described in previous chapters. The crystal and refinement data is presented below in Table 5.6.

Table 5.6. Crystal and Refinement data for complexes **12, 13Py** and **14Py**

Parameters	12	13Py	14Py
Chemical Formula	$C_{38}H_{50}FeN_4$	$C_{30}H_{48}FeN_4Si_2$	$C_{31}H_{50}FeN_4Si_2$
Formula Weight	618.67	576.75	590.78
Crystal system	Monoclinic	Monoclinic	Monoclinic
Space group	*C2/c*	*P2$_1$/c*	*P2$_1$/c*
a	20.2777 (10)	12.1488 (4)	11.9955 (4)
b	9.2534 (5)	15.9382 (6)	16.6908 (5)
c	19.4995 (8)	16.7038 (6)	17.9165 (5)
β (α= γ = 90°)	111.475 (3)	97.568 (2)	109.182 (2)
V(Å^3)	3404.8 (3)	3206.2 (2)	3387.98 (18)
Z	4	4	4
D$_{calc}$(g/cm^3)	-	-	
μ (Mo-K_α) (mm^{-1})	0.47	0.57	0.54
$R_{int,} R[F^2 > 2\sigma(F^2)]$	0.057, 0.036	0.033, 0.032	0.034, 0.038

5.4.2. General Procedure for the Synthesis of Ligands rac-L¹H and rac-L²H

N-(2,6-Diisopropylphenyl)-1-(pyridin-2-yl)ethylaniline (**rac-L¹H**): Synthesis of precursor is similar to **L4** in chapter 2. **L4** (1.79 g, 6.1 mmol) was dissolved in 20 mL of CH_2Cl_2 in round bottom flask equipped with a condenser followed by the addition of $NaBH_4$ (23 g, 0.608 mol, 100 eq.) to afford a white yellowish slurry. MeOH (100 mL) was added by portion to this mixture (caution exothermic reaction) and the solution was stirred at room temperature for 24 hours. The evolution of the reaction was monitored by TLC (eluent: petroleum ether/EtOAc = 20/1) and, if necessary, addition of $NaBH_4$ and MeOH was carried out until the starting material disappeared. The solvent was removed under vacuum and the resulting oil was further purified by column chromatography (SiO_2; petroleum ether/EtOAc = 30/1) to afford a colorless solid after the evaporation of eluent. Yield = 75 %, m = 1.36 g. ^{1}H NMR (300 MHz, CD_2Cl_2, 25 °C) δ (ppm) = 8.60 (ddd, $^3J_{HH}$ = 4.8 Hz, $^4J_{HH}$ = 1.8 Hz, $^5J_{HH}$ = 0.9 Hz, 1H, H_a), 7.55 (ddd, $^3J_{HH}$ = 7.8 Hz, $^3J_{HH}$ = 7.8 Hz, $^4J_{HH}$ = 1.8 Hz, 1H, H_b), 7.16 (ddd, $^3J_{HH}$ = 7.8 Hz, $^3J_{HH}$ = 4.8 Hz, $^4J_{HH}$ = 1.2 Hz, 1H, H_c), 7.04 – 6.93 (m, 4H, $H_{d,e,f}$), 4.16 (q, $^3J_{HH}$ = 6.9 Hz, 1H, H_g), 4.06 (br s, 1H, H_h), 3.23 (sept, $^3J_{HH}$ = 6.7 Hz, 2H, H_i), 1.47 (d, 3H, H_j), 1.20 (d, $^3J_{HH}$ = 6.7 Hz, 6H, H_k), 1.03 (d, $^3J_{HH}$ = 6.7 Hz, 6H, $H_{k'}$). The ^{1}H NMR data were consistent with those found in the literature (Figure A32).[42]

N-(2,6-Diisopropylphenyl)-1-(6-methylpyridin-2-yl)ethylaniline (**rac-L²H**): Synthesis of precursor is similar to **L5** in chapter 2. A procedure analogous to that described for **rac-L¹H**, employing L5 (588 mg, 2 mmol), $NaBH_4$ (7.57 g, n = 0.2 mol), CH_2Cl_2 (8 mL), MeOH (40 mL), produced **rac-L²H** as a colorless/yellow oil. Yield = 80 %, m = 474 mg. ^{1}H NMR (300 MHz, C_6D_6, 25 °C) δ (ppm): 7.13 – 7.03 (m, 3H, $H_{a,b}$), 6.88 (dd, $^3J_{HH}$ = 7.6 Hz, $^3J_{HH}$ = 7.6 Hz, 1H, H_c), 6.53 (d, $^3J_{HH}$ = 7.6 Hz, 2H, $H_{d,e}$), 4.56 (br s, 1H, H_f), 4.29 (q, $^3J_{HH}$ = 6.7 Hz, 1H, H_g), 3.23 (sept, $^3J_{HH}$ = 6.8 Hz, 2H, H_h), 2.41 (s, 1H, H_i), 1.58 (d, $^3J_{HH}$ = 6.7 Hz, 3H, H_j), 1.26 (d, $^3J_{HH}$ = 6.8 Hz, 6H, H_k), 1.13 (d, $^3J_{HH}$ = 6.8 Hz, 6H, $H_{k'}$). ^{13}C NMR (75 MHz, C_6D_6, 25 °C) δ (ppm): 162.8, 157.9, 142.4, 142.1, 136.0, 123.5, 123.3, 121.0, 118.5, 61.0, 27.7, 24.0, 24.0, 22.1 (Figure A33).

5.4.3. General Procedure for the Synthesis of Complexes 12, 13Py and 14Py

Iron bis(trimethylsilyl) amide Fe[N(SiCH₃)₂]₂: The iron precursor $Fe[N(SiCH_3)_2]_2$ was prepared according to a modified procedure described in the literature.[51,102,103] Typically, $FeCl_2$ (1 g, 7.9 mmol) was suspended in 30 mL of Et_2O and the solution was cooled to 0°C. A solution of

LiN(SiCH$_3$)$_2$ (2.64 g, n = 15.8 mmol, 2 eq., dissolved in 50 mL of Et$_2$O) was then added dropwise to the suspension and the mixture was stirred at room temperature for 18 h (Scheme 5.14). The solvent was removed under vacuum and the dark green product was extracted with pentane (3 x 20 mL). The dark green solution was dried under vacuum and the solid residue was distilled under reduced pressure (0.1 mbar) at 95 – 100 °C to give a green oil that was stored at – 20°C in the glove box. Yield = 68 %, m = 2.02 g. ^{1}H NMR (300 MHz, C$_6$D$_6$, 25 °C) δ (ppm) = 61.15 (br. s). The ^{1}H NMR spectrum was consistent with those found in the literature (Figure A35).
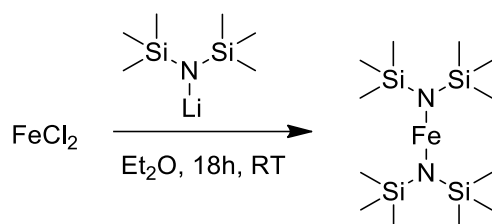
Scheme 5.14. Synthesis of Fe[N(SiCH$_3$)$_2$]$_2$

Further, the iron precursor Fe[N(SiCH$_3$)$_2$]$_2$ was used to synthesize the homoleptic/heteroleptic complexes as described in Scheme 5.15.
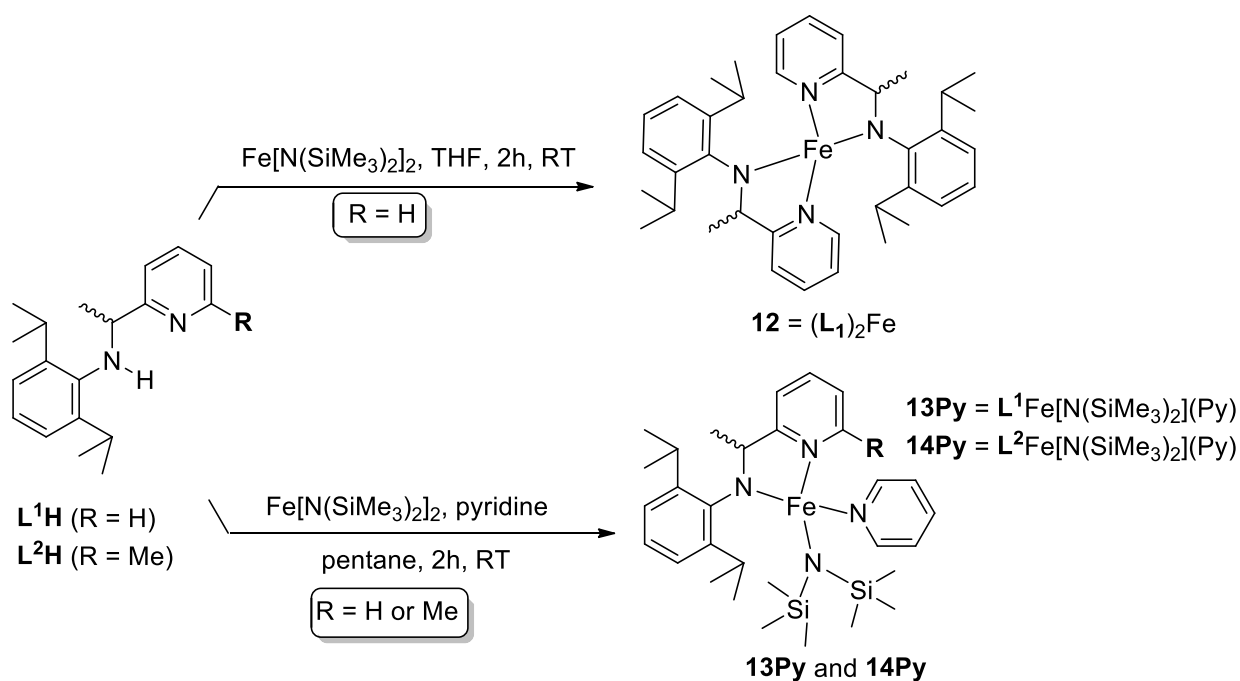
Scheme 5.15. Synthetic strategy for complexes **12-14**

Bis(N-(2,6-Diisopropylphenyl)-1-(pyridin-2-yl)ethyl) iron (II) amide (**12**)*:* The appropriate pro-ligand (1.06 mmol, 2 eq.) was placed in 5 mL of THF and this solution was added to a solution of 5 mL of THF (5 mL) containing $Fe[N(SiCH_3)_2]_2$ (0.53 mmol, 1 eq.). The solution turned from dark green to dark red instantly and was left to stir at room temperature for 2 hours. The solution was concentrated under vacuum and the dark red residue was placed in 6 mL of pentane. The mixture was stirred for 5 – 10 min and subsequently filtered through celite. The solvent was evaporated to obtain a dark red residue which was recrystallized in pentane at – 20°C. Yield: 65%. ^{1}H NMR (300 MHz, C_6D_6, 25 °C, δ): 134.5 ($\Delta v_{1/2} = 1415$ Hz, 1H), 87.7 ($\Delta v_{1/2} = 516$ Hz, 1H), 47.1, 46.3 and 43.7 (br, 3H), 37.4 ($\Delta v_{1/2} = 91$ Hz, 1H), 30.7 ($\Delta v_{1/2} = 96$ Hz, 2H), 16.6 ($\Delta v_{1/2} = 175$ Hz, 6H), -22.6 ($\Delta v_{1/2} = 394$ Hz, 6H), -37.3 ($\Delta v_{1/2} = 706$ Hz, 3H), -43.8 ($\Delta v_{1/2} = 120$ Hz, 2H). (Figure 5.3) Anal. Calc. for $C_{38}H_{50}FeN_4$: C 73.77, H 8.15, N 9.06; Found: C 73.23, H 8.55, N 9.00.

N-(2,6-Diisopropylphenyl)-1-(pyridin-2-yl)ethyl) iron (II) trimethylsilylamide (**13Py**)**:** The ***rac-L^{1}H*** pro-ligand (1.06 mmol) was placed in 5 mL of pentane and this solution was added to a solution of 5 mL of pentane (5 mL) containing $Fe[N(SiCH_3)_2]_2$ (400 mg, 1.06 mmol, 1 eq.). The solution turned from dark green to dark red after stirring at room temperature for 2 hours. The solution was concentrated under vacuum and the dark red residue was placed in 6 mL of pentane. The mixture was stirred for 5 – 10 min and was filtered through celite before being transferred to a pentane solution (2 mL) containing 4 eq. of pyridine (340 µl, 4.24 mmol, 4 eq.). After 30 min, red crystals of amidopyridine iron (trimethylsilyl) amide complexes were formed. In some cases, the solution had to be triturated in the glove box with a small spatula to induce crystallization. Yield: 47%, m = 290mg. ^{1}H NMR (300 MHz, C_6D_6, 25 °C) δ (ppm) = 101.9 ($\Delta v_{1/2} = 870$ Hz, 1H), 74.4 ($\Delta v_{1/2} = 1540$ Hz, 2H), 51.9 ($\Delta v_{1/2} = 386$ Hz, 1H), 35.5 ($\Delta v_{1/2} = 140$ Hz, 1H), 34.1 ($\Delta v_{1/2} = 106$ Hz, 1H), 25.8 ($\Delta v_{1/2} = 670$ Hz, 18H), 22.2 ($\Delta v_{1/2} = 323$ Hz, 3H), 13.6 ($\Delta v_{1/2} = 153$ Hz, 3H), 6.1 ($\Delta v_{1/2} = 120$ Hz, 2H), -22.8 ($\Delta v_{1/2} = 360$ Hz, 3H), -37.7 ($\Delta v_{1/2} = 82$ Hz, 1H), -63.6 ($\Delta v_{1/2} = 2218$ Hz, 3H) (Figure A36). Anal. Calc. for $C_{30}H_{48}FeN_4Si_2$: C 62.48, H 8.39, N 9.71; Found: C 62.03, H 8.49, N 9.50.

N-(2,6-Diisopropylphenyl)-1-(6-methylpyridin-2-yl)ethyl) iron (II) trimethylsilylamide (**14Py**)**:** Under argon, Fe[N(TMS)₂]₂ (m = 389 mg, 1.03 mmol) was placed in 5 mL of THF followed by the addition of the ***rac-L^{2}H*** pro-ligand (306 mg, 1.03 mmol) previously dissolved in 5 mL of THF. The solution turned dark yellow/red after stirring for 1h30 at room temperature. The solution was

reduced under vacuum to afford a red-yellow oil after 30 min. The oil was dissolved in 20 mL of pentane and filtered through celite and the oil was washed two times with 20 mL of pentane. The resulting solution was reduced to 10-20 mL and transferred by cannula to a solution of pentane (1 mL) containing pyridine (V = 330 µL, 4 eqs.) to afford a deep red solution. The mixture was placed at – 40 °C for 2 days to give red crystalline solid of $L_2Fe[N(TMS)_2](Py)$ (m = 388 mg, yield = 64 %). ^{1}H NMR (300 MHz, C_6D_6, 25 °C) δ (ppm) = 127.8 ($\Delta v_{1/2}$ = 985 Hz, 1H), 98.7 ($\Delta v_{1/2}$ = 952 Hz, 3H), 65.6 ($\Delta v_{1/2}$ = 137 Hz, 1H), 47.3 ($\Delta v_{1/2}$ = 182 Hz, 4H), 33.1, 28.8 and 22.4 (br, 18H), 11.4 ($\Delta v_{1/2}$ = 55 Hz, 3H), 8.6 ($\Delta v_{1/2}$ = 32 Hz, 1H), 2.4 ($\Delta v_{1/2}$ = 78 Hz, 3H), -26.4 and -31.1 (br, 6H), -35.9 ($\Delta v_{1/2}$ = 64 Hz, 1H), -93.2 ($\Delta v_{1/2}$ = 573 Hz, 3H) (Figure A37). Anal. Calc. $C_{31}H_{50}FeN_4Si_2$: C 63.02, H 8.53, N 9.45; Found: C 62.62, H 8.78, N 9.09.

5.4.4. General Procedure for L-Lactide Polymerization

An ace pressure tube was charged with an iron catalyst solution (250 µL, 2.5 µmol, 1 eq., 0.01M in toluene) *via* syringe and toluene (0.5 ml) was added subsequently to obtain a red solution. The solution was stirred for 1 min inside the glove box before adding purified *L*-LA (0.5 mmol, 200 eq.). The reactor was brought outside the glove box and the mixture was stirred at desired temperature (RT, 50 or 70 °C) for appropriate time. The reaction was quenched with acidifed toluene and the mixture was diluted with chloroform to homogenize the medium before withdrawing an aliquot. The aliquot was dried to evaporate the solvent and the conversion was determined by ^{1}H NMR spectroscopy in $CDCl_3$. The PLLA solution in chloroform was added dropwise to ethanol (150ml) to precipitate the gummy solid which was dried overnight under vacuum before being subjected to further characterization.

5.4.5. General Procedure for ε-caprolactone Polymerization

Similar to 5.4.4 except the addition of distilled ε-CL (0.5 mmol, 200 eq.) instead of *L*-LA.

5.4.5. General Procedure for L-Lactide/ ε-caprolactone copolymerization

L-LA (0.25 mmol, 100 eq.) and ε-CL (0.25 mmol, 100 eq.) were weighed inside the glove box and added to a typical reactor. Toluene was added to the reactor and the mixture was homogenized by stirring it for 1-2 mins. Further, iron catalyst solution (250 µL, 2.5 µmol, 1 eq., 0.01M in toluene) was added to the mixture to initiate the polymerization. Remaining procedure was similar to 5.4.4.

References

(1)   Yin, G.-Z.; Yang, X.-M. *J. Polym. Res.* **2020**, *27* (2), 38.

(2)   Haider, T. P.; Völker, C.; Kramm, J.; Landfester, K.; Wurm, F. R. *Angew. Chem. Int. Ed.* **2019**, *58* (1), 50–62.

(3)   Zhu, Y.; Romain, C.; Williams, C. K. *Nature* **2016**, *540* (7633), 354–362.

(4)   Satti, S. M.; Shah, A. A. *Lett. Appl. Microbiol.* **2020**, *70* (6), 413–430.

(5)   Rydz, J.; Sikorska, W.; Kyulavska, M.; Christova, D. *Int. J. Mol. Sci.* **2014**, *16* (1), 564–596.

(6)   Drumright, R. E.; Gruber, P. R.; Henton, D. E. Polylactic Acid Technology. 6.

(7)   Inkinen, S.; Hakkarainen, M.; Albertsson, A.-C.; Södergård, A. *Biomacromolecules* **2011**, *12* (3), 523–532.

(8)   Xiao, L.; Wang, B.; Yang, G.; Gauthier, M. Poly(Lactic Acid)-Based Biomaterials: Synthesis, Modification and Applications. In *Biomedical Science, Engineering and Technology*; Ghista, D. N., Ed.; InTech, 2012.

(9)   Tyler, B.; Gullotti, D.; Mangraviti, A.; Utsuki, T.; Brem, H. *Adv. Drug Deliv. Rev.* **2016**, *107*, 163–175.

(10)   *Synthesis, Structure and Properties of Poly(Lactic Acid)*; Di Lorenzo, M. L., Androsch, R., Eds.; Advances in Polymer Science; Springer International Publishing: Cham, 2018; Vol. 279.

(11)   Guarino, V.; Gentile, G.; Sorrentino, L.; Ambrosio, L. Polycaprolactone: Synthesis, Properties, and Applications: POLYCAPROLACTONE: SYNTHESIS, PROPERTIES, AND APPLICATIONS. In *Encyclopedia of Polymer Science and Technology*; John Wiley & Sons, Inc., Ed.; John Wiley & Sons, Inc.: Hoboken, NJ, USA, 2017; pp 1–36.

(12)   Labet, M.; Thielemans, W. *Chem. Soc. Rev.* **2009**, *38* (12), 3484–3504.

(13)   Choi, S.; Song, C. W.; Shin, J. H.; Lee, S. Y. *Metab. Eng.* **2015**, *28*, 223–239.

(14)   Buntara, T.; Noel, S.; Phua, P. H.; Melián-Cabrera, I.; de Vries, J. G.; Heeres, H. J. *Angew. Chem. Int. Ed.* **2011**, *50* (31), 7083–7087.

(15)   Byers, J. A.; Biernesser, A. B.; Delle Chiaie, K. R.; Kaur, A.; Kehl, J. A. Catalytic Systems for the Production of Poly(Lactic Acid). In *Synthesis, Structure and Properties of Poly(lactic acid)*; Di Lorenzo, M. L., Androsch, R., Eds.; Advances in Polymer Science; Springer International Publishing: Cham, 2018; pp 67–118.

(16)   Sauer, A.; Kapelski, A.; Fliedel, C.; Dagorne, S.; Kol, M.; Okuda, J. *Dalton Trans.* **2013**, *42* (25), 9007.

(17)   Dove, A. P. *ACS Macro Lett.* **2012**, *1* (12), 1409–1412.

(18)   Thomas, C. M. *Chem Soc Rev* **2010**, *39* (1), 165–173.

(19)   O'Keefe, B. J.; Hillmyer, M. A.; Tolman, W. B. *J. Chem. Soc. Dalton Trans.* **2001**, No. 15, 2215–2224.

(20)   Södergård, A.; Stolt, M. *Prog. Polym. Sci.* **2002**, *27* (6), 1123–1163.

(21)   Källrot, M.; Edlund, U.; Albertsson, A.-C. *Biomacromolecules* **2007**, *8* (8), 2492–2496.

(22)   Rasal, R. M.; Janorkar, A. V.; Hirt, D. E. *Prog. Polym. Sci.* **2010**, *35* (3), 338–356.

(23)   Auras, R.; Harte, B.; Selke, S. *Macromol. Biosci.* **2004**, *4* (9), 835–864.

(24)   Stirling, E.; Champouret, Y.; Visseaux, M. *Polym Chem* **2018**, *9* (19), 2517–2531.

(25)   Champouret, Y.; Hashmi, O. H.; Visseaux, M. *Coord. Chem. Rev.* **2019**, *390*, 127–170.

(26)   Egorova, K. S.; Ananikov, V. P. Toxicity of Metal Compounds: Knowledge and Myths. **2017**, 20.

(27)   Bauer, E. B. Iron Catalysis: Historic Overview and Current Trends. In *Iron Catalysis II*; Bauer, E., Ed.; Topics in Organometallic Chemistry; Springer International Publishing: Cham, 2015; Vol. 50, pp 1–18.

(28)   Wang, X.; Liao, K.; Quan, D.; Wu, Q. *Macromolecules* **2005**, *38* (11), 4611–4617.

(29)   Shang, X.-J.; Zhang, W.-H.; Lang, J.-P. *RSC Adv.* **2016**, *6* (14), 11400–11406.

(30)   Kricheldorf, H. R.; Damrau, D.-O. *Macromol. Chem. Phys.* **1997**, *198* (6), 1767–1774.

(31)   Stolt, M.; Södergård, A. *Macromolecules* **1999**, *32* (20), 6412–6417.

(32)   Södergård, A.; Stolt, M. *Macromol. Symp.* **1998**, *130* (1), 393–402.

(33) Naolou, T.; Lendlein, A.; Neffe, A. T. *Front. Chem.* **2019**, *7*, 346.

(34) Delle Chiaie, K. R.; Biernesser, A. B.; Ortuño, M. A.; Dereli, B.; Iovan, D. A.; Wilding, M. J. T.; Li, B.; Cramer, C. J.; Byers, J. A. *Dalton Trans.* **2017**, *46* (38), 12971–12980.

(35) Gibson, V. C.; Marshall, E. L.; Navarro-Llobet, D.; White, A. J. P.; Williams, D. J. *J. Chem. Soc. Dalton Trans.* **2002**, No. 23, 4321–4322.

(36) O'Keefe, B. J.; Breyfogle, L. E.; Hillmyer, M. A.; Tolman, W. B. *J. Am. Chem. Soc.* **2002**, *124* (16), 4384–4393.

(37) Duan, R.; Hu, C.; Li, X.; Pang, X.; Sun, Z.; Chen, X.; Wang, X. *Macromolecules* **2017**, *50* (23), 9188–9195.

(38) Marin, P.; Tschan, M. J. -L.; Isnard, F.; Robert, C.; Haquette, P.; Trivelli, X.; Chamoreau, L.; Guérineau, V.; del Rosal, I.; Maron, L.; Venditto, V.; Thomas, C. M. *Angew. Chem.* **2019**, *131* (36), 12715–12719.

(39) Gorczynski, J. L.; Chen, J.; Fraser, C. L. *J. Am. Chem. Soc.* **2005**, *127* (43), 14956–14957.

(40) Chen, J.; Gorczynski, J. L.; Fraser, C. L. *Macromol. Chem. Phys.* **2010**, *211* (11), 1272–1279.

(41) Meneghetti, S. P.; Lutz, P. J.; Kress, J. *Organometallics* **1999**, *18* (15), 2734–2737.

(42) Nienkemper, K.; Kehr, G.; Kehr, S.; Fröhlich, R.; Erker, G. *J. Organomet. Chem.* **2008**, *693* (8–9), 1572–1589.

(43) Cao, Y.; Zhang, Y.; Zhang, L.; Zhang, D.; Leng, X.; Huang, Z. *Org. Chem. Front.* **2014**, *1* (9), 1101–1106.

(44) Morris, W. D.; Wolczanski, P. T.; Sutter, J.; Meyer, K.; Cundari, T. R.; Lobkovsky, E. B. *Inorg. Chem.* **2014**, *53* (14), 7467–7484.

(45) Yang, L.; Powell, D. R.; Houser, R. P. *Dalton Trans* **2007**, No. 9, 955–964.

(46) Lindley, B. M.; Wolczanski, P. T.; Cundari, T. R.; Lobkovsky, E. B. *Organometallics* **2015**, *34* (19), 4656–4668.

(47) Allen, F. H.; Kennard, O.; Watson, D. G.; Brammer, L.; Orpen, A. G.; Taylor, R. *J CHEM SOC PERKIN TRANS* **1987**, 19.

(48) Bauer, E. B. *Chem. Soc. Rev.* **2012**, *41* (8), 3153.

(49) Cahn, R. S.; Ingold, C.; Prelog, V. *Angew. Chem. Int. Ed. Engl.* **1966**, *5* (4), 385–415.

(50) Prelog, V.; Helmchen, G. *Angew. Chem. Int. Ed. Engl.* **1982**, *21* (8), 567–583.

(51) Olmstead, M. M.; Power, P. P.; Shoner, S. C. *Inorg. Chem.* **1991**, *30* (11), 2547–2551.

(52) Lake, B. R. M.; Shaver, M. P. *Dalton Trans.* **2016**, *45* (40), 15840–15849.

(53) Jin, G.; Vendier, L.; Coppel, Y.; Sabo-Etienne, S.; Bontemps, S. *Dalton Trans.* **2015**, *44* (16), 7500–7505.

(54) Frazier, B. A.; Williams, V. A.; Wolczanski, P. T.; Bart, S. C.; Meyer, K.; Cundari, T. R.; Lobkovsky, E. B. *Inorg. Chem.* **2013**, *52* (6), 3295–3312.

(55) Sulway, S. A.; Collison, D.; McDouall, J. J. W.; Tuna, F.; Layfield, R. A. *Inorg. Chem.* **2011**, *50* (6), 2521–2526.

(56) Malassa, A.; Agthe, C.; Görls, H.; Podewitz, M.; Yu, L.; Herrmann, C.; Reiher, M.; Westerhausen, M. *Eur. J. Inorg. Chem.* **2010**, *2010* (12), 1777–1790.

(57) Frazier, B. A.; Wolczanski, P. T.; Lobkovsky, E. B.; Cundari, T. R. *J. Am. Chem. Soc.* **2009**, *131* (10), 3428–3429.

(58) Arbaoui, A.; Redshaw, C. *Polym. Chem.* **2010**, *1* (6), 801.

(59) Albertsson, A.-C.; Varma, I. K. *Biomacromolecules* **2003**, *4* (6), 1466–1486.

(60) Ikada, Y.; Tsuji, H. Biodegradable Polyesters for Medical and Ecological Applications. 16.

(61) Wang, S.; Urban, M. W. *Nat. Rev. Mater.* **2020**, *5* (8), 562–583.

(62) Burattini, S.; Greenland, B. W.; Chappell, D.; Colquhoun, H. M.; Hayes, W. *Chem. Soc. Rev.* **2010**, *39* (6), 1973.

(63) Hu, Y.; Daoud, W.; Cheuk, K.; Lin, C. *Materials* **2016**, *9* (3), 133.

(64) Li, G.; Zhao, M.; Xu, F.; Yang, B.; Li, X.; Meng, X.; Teng, L.; Sun, F.; Li, Y. *Molecules* **2020**, *25* (21), 5023.

(65) Moon, S.-I.; Lee, C.-W.; Taniguchi, I.; Miyamoto, M.; Kimura, Y. *Polymer* **2001**, *42* (11), 5059–5062.

(66) Kim, K. W.; Woo, S. I. Synthesis of High-Molecular-Weight Poly(L-lactic Acid) by Direct Polycondensation. 6.

(67) Ajioka Masanobu , Enomoto Katashi , Suzuki Kazuhiko, Yamaguchi Akihiro. *Bull. Chem. Soc. Jpn. 68* (1995), 2125–2131.

(68) Xavier, M. V.; Macedo, M. F.; Benatti, A. C. B.; Jardini, A. L.; Rodrigues, A. A.; Lopes, M. S.; Lambert, C. S.; Filho, R. M.; Kharmandayan, P. *Procedia CIRP* **2016**, *49*, 213–221.

(69) Gupta, A. P.; Kumar, V. *Eur. Polym. J.* **2007**, *43* (10), 4053–4074.

(70) Vink, E. T. H.; Rábago, K. R.; Glassner, D. A.; Gruber, P. R. *Polym. Degrad. Stab.* **2003**, *80* (3), 403–419.

(71) Kowalski, A.; Duda, A.; Penczek, S. *Macromolecules* **1998**, *31* (7), 2114–2122.

(72) Bonné, C.; Pahwa, A.; Picard, C.; Visseaux, M. *Inorganica Chim. Acta* **2017**, *455*, 521–527.

(73) Visseaux, M.; Brachais, C.-H.; Boisson, C.; Tortosa, K. Nitrogen-Containing Lanthanide Complexes: Initiators or Real Catalysts for the o-Caprolactone Polymerisation? **2000**, 8.

(74) Dobrzynski, P.; Kasperczyk, J.; Janeczek, H.; Bero, M. *Polymer* **2002**, *43* (9), 2595–2601.

(75) Dobrzynski, P.; Pastusiak, M.; Bero, M. *J. Polym. Sci. Part Polym. Chem.* **2005**, *43* (9), 1913–1922.

(76) Helou, M.; Miserque, O.; Brusson, J.-M.; Carpentier, J.-F.; Guillaume, S. M. *ChemCatChem* **2010**, *2* (3), 306–313.

(77) Morris, K. F.; Johnson, C. S. *J. Am. Chem. Soc.* **1992**, *114* (8), 3139–3141.

(78) Morris, K. F.; Johnson, C. S. *J. Am. Chem. Soc.* **1993**, *115* (10), 4291–4299.

(79) Fujita, D.; Ueda, Y.; Sato, S.; Mizuno, N.; Kumasaka, T.; Fujita, M. *Nature* **2016**, *540* (7634), 563–566.

(80) Viel, S.; Capitani, D.; Mannina, L.; Segre, A. *Biomacromolecules* **2003**, *4* (6), 1843–1847.

(81) Paul, S.; Romain, C.; Shaw, J.; Williams, C. K. *Macromolecules* **2015**, *48* (17), 6047–6056.

(82) Viel, S.; Mazarin, M.; Giordanengo, R.; Phan, T. N. T.; Charles, L.; Caldarelli, S.; Bertin, D. *Anal. Chim. Acta* **2009**, *654* (1), 45–48.

(83) Biernesser, A. B.; Delle Chiaie, K. R.; Curley, J. B.; Byers, J. A. *Angew. Chem. Int. Ed.* **2016**, *55* (17), 5251–5254.

(84) Wang, Y.; Xu, T.-Q. *Macromolecules* **2020**, *53* (20), 8829–8836.

(85) Hu, C.; Louisy, E.; Fontaine, G.; Bonnet, F. *J. Polym. Sci. Part Polym. Chem.* **2017**, *55* (19), 3175–3179.

(86) Bonnet, F.; Stoffelbach, F.; Fontaine, G.; Bourbigot, S. *RSC Adv.* **2015**, *5* (40), 31303–31310.

(87) Karas, M.; Hillenkamp, F. Laser Desorption Ionization of Proteins with Molecular Masses Exceeding 10,000 Daltons. 3.

(88) *Mass Spectrometry of Polymers*; Montaudo, G., Lattimer, R. P., Eds.; CRC Press: Boca Raton, Fla., 2002.

(89) Gies, A. P.; Nonidez, W. K.; Ellison, S. T.; Ji, H.; Mays, J. W. *Anal. Chem.* **2005**, *77* (3), 780–784.

(90) Gies, A. P.; Nonidez, W. K.; Anthamatten, M.; Cook, R. C. *Macromolecules* **2004**, *37* (16), 5923–5929.

(91) Chen, H.; He, M.; Pei, J.; He, H. Quantitative Analysis of Synthetic Polymers Using Matrix-Assisted Laser Desorption/Ionization Time-of-Flight Mass Spectrometry. 5.

(92) Chen, H.; He, M.; Pei, J.; Liu, B. *Anal. Chem.* **2002**, *74* (24), 6252–6258.

(93) Williams, J. B.; Chapman, T. M.; Hercules, D. M. *Anal. Chem.* **2003**, *75* (13), 3092–3100.

(94) Nair, N. R.; Sekhar, V. C.; Nampoothiri, K. M.; Pandey, A. Biodegradation of Biopolymers. In *Current Developments in Biotechnology and Bioengineering*; Elsevier, 2017; pp 739–755.

(95) *Industrial Applications of Poly(Lactic Acid)*; Di Lorenzo, M. L., Androsch, R., Eds.; Advances in Polymer Science; Springer International Publishing: Cham, 2018; Vol. 282.

(96) Shen, Y.; Zhu, K. J.; Shen, Z.; Yao, K.-M. *J. Polym. Sci. Part Polym. Chem.* **1996**, *34* (9), 1799–1805.

(97)   Schaefgen, J. R.; Pearce, E. M. Contemporary Topics in Polymer Science: Volume 2.

(98)   Van Butsele, K.; Jérôme, R.; Jérôme, C. *Polymer* **2007**, *48* (26), 7431–7443.

(99)   Vion, J. M.; Jerome, R.; Teyssie, P.; Aubin, M.; Prudhomme, R. E. *Macromolecules* **1986**, *19* (7), 1828–1838.

(100)   Vanhoorne, P.; Dubois, P.; Jerome, R.; Teyssie, P. Macromolecular Engineering of Polylactones and Polylactides. 7. Structural Analysis of Copolyesters of e-Caprolactone and l- or D,L-Lactide Initiated by Al(OiPr)3. **1992**, *25* (1), 8.

(101)   Save, M. Controlled Ring-Opening Polymerization of Lactones and Lactides Initiated by Lanthanum Isopropoxide, 1. General Aspects and Kinetics. 11.

(102)   Murray, B. D.; Power, P. P. *Inorg. Chem.* **1984**, *23* (26), 4584–4588.

(103)   Andersen, R. A.; Faegri, K.; Green, J. C.; Haaland, A.; Lappert, M. F.; Leung, W. P.; Rypdal, K. *Inorg. Chem.* **1988**, *27* (10), 1782–1786.

GENERAL CONCLUSION AND FUTURE PERSPECTIVES

General conclusion and future perspectives

The present study describes the synthesis of a family of iminopyridine and, to a lesser extent, iminoquinoline as well as aminopyridine ligands and their related iron-based complexes. All the complexes were fully characterized by ^{1}H NMR and IR spectroscopies, elemental analysis and, in the case of newly developed iron complexes, their molecular structures were also deduced *via* X-ray diffraction studies (Chart 1). These complexes have been deployed as precatalysts/catalysts for their application in the controlled coordinative polymerization of various monomers, affording (co)polymers with a wide range of potential applications.
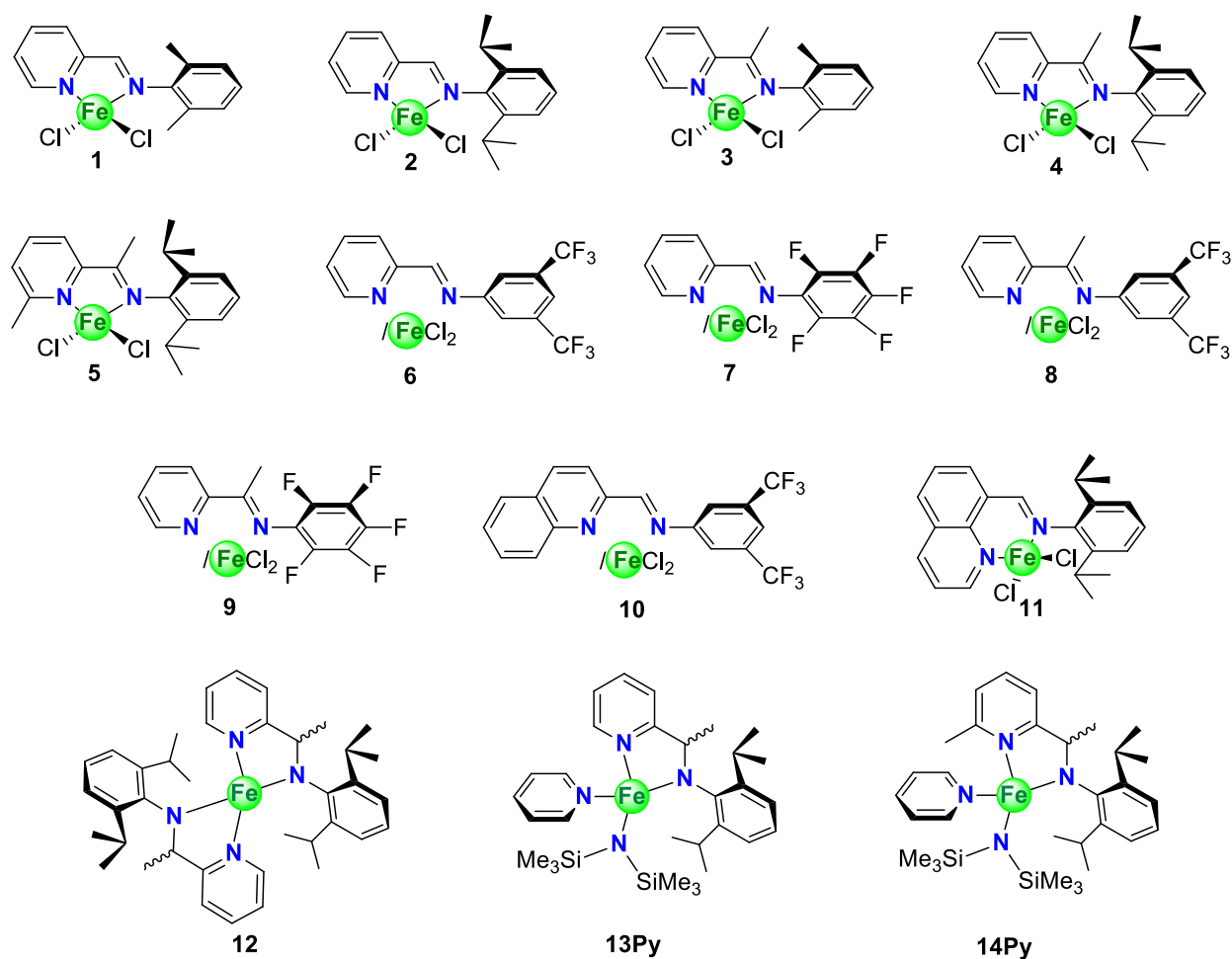
Chart 1. Family of complexes included in this thesis work

The iminopyridine/iminoquinoline ligands **L1-L11** were synthesized *via* acid-catalyzed condensation reactions of the carbonylated pyridine/quinoline substrates in the presence of 2,6-diisopropylaniline, whereas the same pathway followed by reduction of the imine moiety of **L4**

and **L5** yielded their related aminopyridine analogues ***rac*-L^{1}H** and ***rac*-L^{2}H** pro-ligands, respectively. Thereafter, the family of iron iminopyridine/iminoquinoline complexes **1-11** were obtained by reacting 1 eq. of ligand with 1 eq. of anhydrous FeCl$_2$ in DCM/THF. On the other hand, iron amide complexes **12, 13Py** and **14Py** were obtained by reacting Fe[N(SiMe$_3$)$_2$]$_2$ with 2 or 1 eqs. of aminopyridine ligands in THF or pentane. Additionally, the synthesis of heteroleptic complex **13Py** was performed in different solvents based on which it was observed that the formation of homoleptic/heteroleptic analogue was dependent on the polarity of the solvent used.

The determination of the molecular structures of the newly developed iminopyridine iron-based complexes **6-11** *via* X-ray diffraction studies illustrated different coordination modes of the ligands, which was found to be highly dependent on the nature of the substituents. The aldiminopyridine iron dichloride complexes **6** and **7** existed as bis-ligand mononuclear complexes in the solid state, whereas their ketiminopyridine analogues **8** and **9** turned out to exist as binuclear coordinated complexes, with complex **9** displaying a bridged tetranuclear assembly. The aldiminoquinoline system **10,** resulting from the modification of the iminopyridine skeleton, also attained a similar symmetrical binuclear type of geometry, whereas the other aldiminoquinoline counterpart **11** bearing bulky *^{i}*Pr groups as *N*-aryl substituents existed as mononuclear complex. These observations highlight the importance of the steric hindrance around the iron center as well as the presence of fluorinated groups on the *N*-aryl moiety, which collectively governs the structure through various electronic effects such as H$^{...}$F, F$^{...}$F contacts and $\pi - \pi$ stacking within the assembly of these complexes. On the contrary, the newly developed homoleptic/heteroleptic aminopyridine iron amide complexes displayed an unusual intermediate geometry between distorted see-saw and trigonal pyramidal, as highlighted by the τ_4 value that defined the geometry of tetracoordinated complexes.

Regarding the catalytic activity of complexes **1-11** in isoprene polymerization, we observed that the activity of the catalytic system based on iminopyridine-iron complexes is clearly related to the electron density on iron and, to a lesser extent, to the environment of the coordination sphere at the metal center. Indeed, an increase of the electrophilicity on the metal center leads to stronger monomer coordination and presumably faster chain propagation, while an increase in steric hindrance, conferred by the presence of bulky *N*-aryl substituent, results in a decrease of activity that could be attributed to the difficulty of the incoming monomer to coordinate with the

active species, which was observed in the case of complexes **5**, **10** and **11**. As such, the alkylated *N*-aryl substituted complexes were found to be less active than the complexes bearing fluorinated groups on the *N*-aryl moiety. However, the aldiminopyridine complexes **6** and **7** comprising the most electrophilic iron center turned out to be less active than the complexes **1-3** whereas their ketiminopyridine analogues **8** and **9** displayed exceptionally high catalytic activity for the isoprene polymerization that have been reported till now in the literature. These results suggested that the simultaneous acceptor inductive effect (-I) of fluorinated *N*-aryl substituents and the donor inductive effect (+I) of methyl group on the imino substituent of the ligands **L8** and **L9** collectively enhanced the activity of the resulting catalysts from complexes **8** and **9**.

In terms of selectivity, we could observe that the concomitant presence of methyl group on the carbon of the imino substituent and *N*-aryl group with alkyl substituent on the *ortho* position in complexes **3/4** favor 1,4-*trans* selectivity up to 76% at room temperature, which was later improved to 87% at higher temperatures. In contrast, the presence of electronic effects of fluorinated *N*-aryl substituent in complexes **6-9** leads to a fair 1,4-*cis* selectivity with a substantial amount of 3,4, presumably due to a preferential η^4-*cis* or η^2-*trans* coordination of the incoming monomer. Interestingly, these catalytic systems were not temperature dependent in terms of regio- and stereo-selectivity whereas the improvement of 1,4-*cis* rate (90%) or the inversion of selectivity for complexes **1–3** was observed at low temperature, revealing the importance of the *anti/syn* isomerization of the propagating species in the stereoselective iron-catalyzed 1,3-dienes polymerization.

In order to gain better control over the polymerization, we successfully and for the first time implemented a reversible CCTP of isoprene with the iron-based complexes **1-4** and **6-9** in combination with $ZnEt_2$ as CTA after activation. In search of the best Fe-CTA combination, we conducted a preliminary screening with various metal alkyls as potential CTAs (Al^iBu_3, $ZnEt_2$ and BuMgEt) through which we observed that the transfer is only efficient with $ZnEt_2$, probably owing to its i) monomeric nature in solution, ii) less steric bulk around Zn and iii) almost similar Fe-R and Zn-R bond energies. Also, in order to optimize the transfer conditions by varying the concentration of monomer from 1 M to 10 M resulted in the formation of low molecular weight polyisoprenes with fair conversions, which could be attributed to a transfer blockage at certain stage due to the possible formation of a stable heterobimetallic Fe-Zn allyl species.

Further, the catalytic systems involving the iron complexes **1-4** and **6-9**, under a combination **Fe**/Al^{i}Bu$_3$/[Ph$_3$C][B(C$_6$F$_5$)$_4$]/ZnEt$_2$ were individually screened for the CCTP of isoprene under optimized conditions, from which the order of transfer efficiency was deduced as **3-4 > 1-2 > 8-9 > 6-7**. The complexes **6-9** bearing fluorinated substituents on their *N*-aryl moieties were found to be the least efficient under transfer conditions due to their high rate of propagation. In contrast, the complexes **1-4** bearing alkyl groups on the *N*-aryl substituents were found to be more efficient under similar conditions, with the **4**/Al^{i}Bu$_3$/[Ph$_3$C][B(C$_6$F$_5$)$_4$]/ZnEt$_2$ catalytic system exhibiting the highest transfer efficiency (37%), which was also confirmed through a detailed study.

Finally, we also attempted to perform a polymerization of isoprene using a dual catalytic system **2** and **4** combined with 10 eq. ZnEt$_2$, after cocatalyst activation, which produced polyisoprene with a variety of stereo- and regioregularity. However, due to the resulting inconsistency in the M_n values in addition to the huge activity difference between the two individual catalytic systems, a successful establishment of CSP stage could not be claimed undoubtedly between the two catalytic precursors. On the bright side, using the other set of catalytic precursors **1** and **3** combined with 10 eq. ZnEt$_2$, after cocatalyst activation, suggested the occurrence of Chain Shuttling Polymerization process through which we observed a strong selectivity dependence on the ratio of the catalytic precursors.

Apart from isoprene polymerization, we also assessed some of the catalytic systems resulting from the complexes **3–5, 8, 9** and **11** in styrene polymerization, where most of them proved to be active at room temperature. Ironically, the catalytic systems derived from sterically hindered complexes **5** and **11,** which were inactive for isoprene, turned out to be active for styrene. These results again emphasize the crucial role of steric hindrance around the iron centre that might inhibit the monomer insertion between the Fe-(alkyl) bond and consequently may lead to poor chain propagation. Nevertheless, all the employed catalytic systems, led to the formation of syndiotactic enriched (52%) polystyrenes with good conversions (up to 87%), albeit limited the M_n values to 2 100–3 000 g/mol owing most likely to the consistent occurrence of *β*-H elimination reactions.

In the last phase of thesis, we studied the role of heteroleptic amidopyridine iron amide complexes **13Py** and **14Py** as potential initiators for the ROP and ROCoP of *L*-LA and ε-CL. These

catalysts were found to be moderately active for the homopolymerization of *L*-LA and ε-CL producing up to >99% of PLLA and 88% of PCL. Through a series of experiments, we concluded that the catalytic activity of these systems was proportional to the increase in temperature. However, the polymerizations were not controlled and led to the formation of high molecular weight polymers in all cases, speaking in favor of slow initiation compared to the faster chain propagation. Even, attempts to control the polymerization in the presence of BnOH failed, although, the presence of alcohol enhanced the catalytic activity of **14Py.**

End group analysis to determine the chain ends of the obtained PLLA *via* ^{1}H NMR and DOSY experiments could not provide the necessary information regarding the mechanism of polymerization and the structure of PLLA. In this aspect, MALDI-ToF-MS proved to be an efficient tool, which confirmed the absence of chain ends and as a result, the formation of cyclic PLLA which is yet to be known in the case of iron catalysts.

Knowing that the ROCoP of *L*-LA and ε-CL can be a promising way to yield copolymers with controlled microstructure and mechanical properties, we attempted the statistical copolymerization of *L*-LA and ε-CL using **13Py** as an initiator. The catalyst **13Py** turned out to be active for the ROCoP study, but sadly, in every case, poor conversions of CL units were obtained. In general, these results are in accordance with what is expected in the copolymerization of *L*-LA and ε-CL, where the preferential consumption of LA occurs over ε-CL.

Future research objectives will include the following:

- Development of new iminopyridine ligands and their related ketiminopyridine iron complexes by replacing the *N*-aryl substituent with more bulkier groups like *t*-Bu, –C(Me)$_2$CH$_2$*t*-Bu. Such complexes are expected to increase the 1,4-*trans* selectivity in isoprene polymerization, though they might decrease the activity of the resulting catalysts.

- Another modification could be the replacement of methyl group on the imino carbon by substituents like Et, ^{i}Pr, *t*-Bu etc. and observe the influence on the activity/selectivity of the systems. Last modification can be the simultaneous variation of electron donoting groups on the imino carbon as well electron withdrawing groups on the *N*-aryl moiety, which is expected to generate extremely active catalysts for isoprene polymerization.

- These new systems can also be assessed for styrene polymerization where the modification in ligand skeleton is a possible way to supress the frequent occurrence of *β*-H elimination reactions, which were consistent with our system.

- The reported catalysts in this study can be further assessed for the polymerization of other bio-sourced 1,3-diene monomers for e.g. *β*-myrcene. Further, an implementation of a CSP between isoprene/*β*-myrcene or isoprene/styrene for the development of copolymers with multiblock microstructures would be another advancement.

- Regarding the CCTP, studies can be targeted to improve the transfer efficiency of the iminopyridine iron-zinc diethyl system by deploying new complexes as suggested above or by utilizing another Zn-based CTA such as $ZnMe_2$ for the development of new catalytic system and comparing it with the existing one.

- Currently, work is still in progress for the ROP of *L*-LA and *rac*-LA to compare the activity and selectivity of existing iron amide catalytic systems for obtaining cyclic PLA with controlled microstructure. The idea would also be to study the influence of increasing the LA/Fe ratio on the molar masses of the resulting PLAs.

- Finally, the incorporation of bulkier ligands in the iron amide system can reduce the coordination ability of LA, which might rebalance the reactivity ratios of LA and ε-CL in the ROCoP of both monomers. In this aspect, some of the ligands have already been developed and are currently being assessed as a potential modification in the aminopyridine structure for the synthesis of new iron amide complexes.

On a conclusive basis, over the past two decades, a revival began in using iron as a catalytically active metal for homogeneous coordination-insertion polymerization catalysis and significant progress in this field has been achieved so far. Iron-based catalysts possess interesting features for multiple single-site catalysis giving access to new and unique polymers. A variety of highly intriguing specific iron-catalyzed transformations with an enormous potential for future polymerization catalysis were described in this work. Significant advances have been made in the characterization part from where we observed a very varied chemistry in structural point of view. Though, we encountered many challenges in this aspect with paramagnetic NMR and X-ray diffraction but once these hurdles are overcome, the rich iron chemistry will undoubtfully carry on changing the persona of polymerization catalysis. This will ensure a best alternative to precious

noble metals and will additionally pave the path for green catalytic combinations, which can also have a lot of potential for the development biodegradable polymers with controlled microstructure.

A

APPENDIX

Appendix

NMR spectra
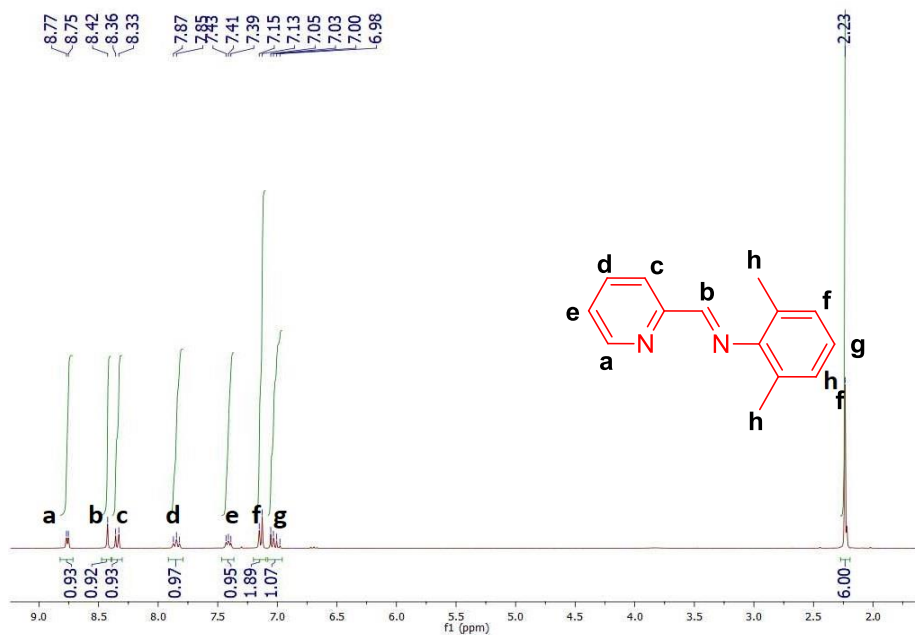
Figure A1. ^{1}H NMR of **L1** (300 MHz, CDCl$_3$, 25 °C)
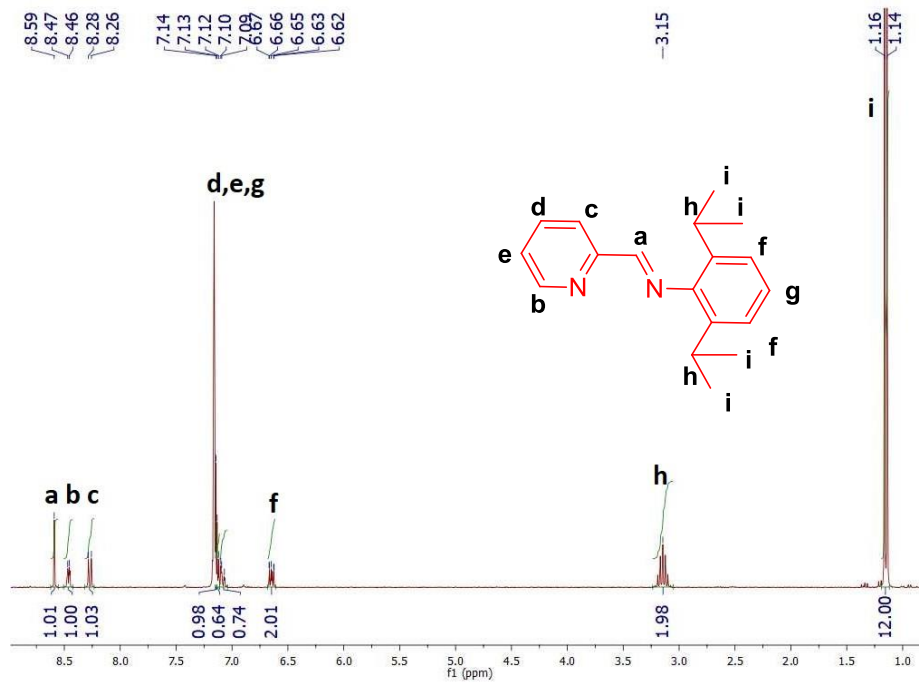
Figure A2. ^{1}H NMR of **L2** (300 MHz, C$_6$D$_6$, 25 °C)
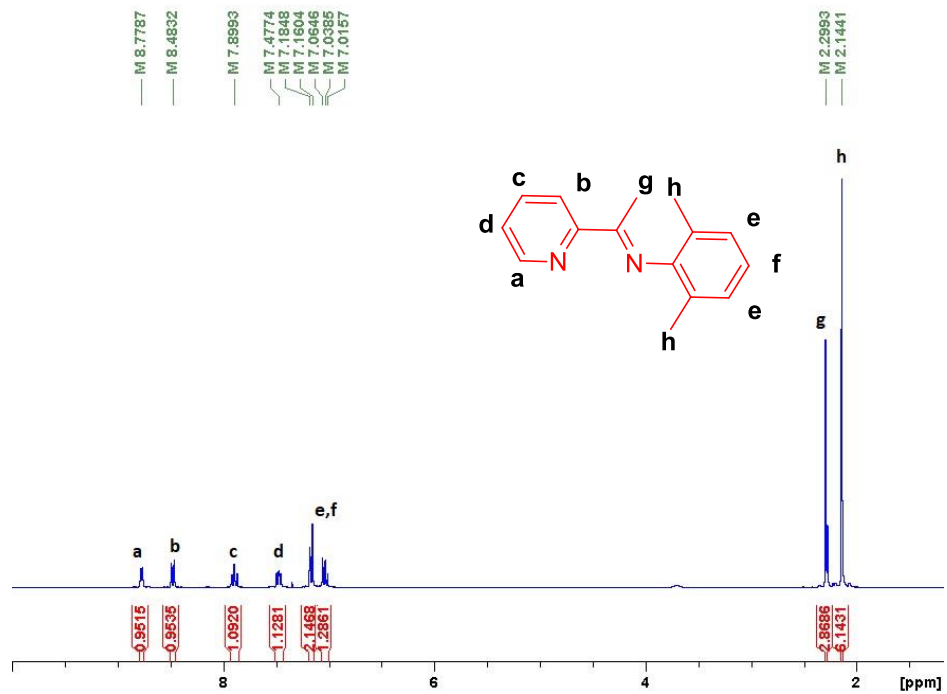
Figure A3. ^{1}H NMR of **L3** (300 MHz, C$_6$D$_6$, 25 °C)
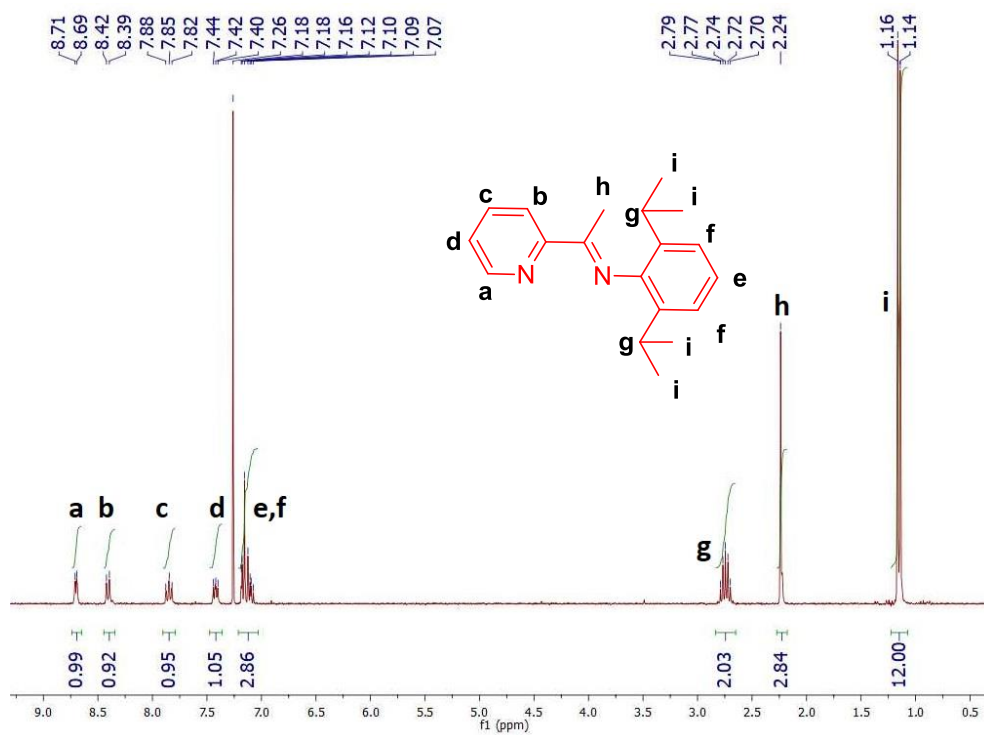
Figure A4. ^{1}H NMR of **L4** (300 MHz, CDCl$_3$, 25 °C)
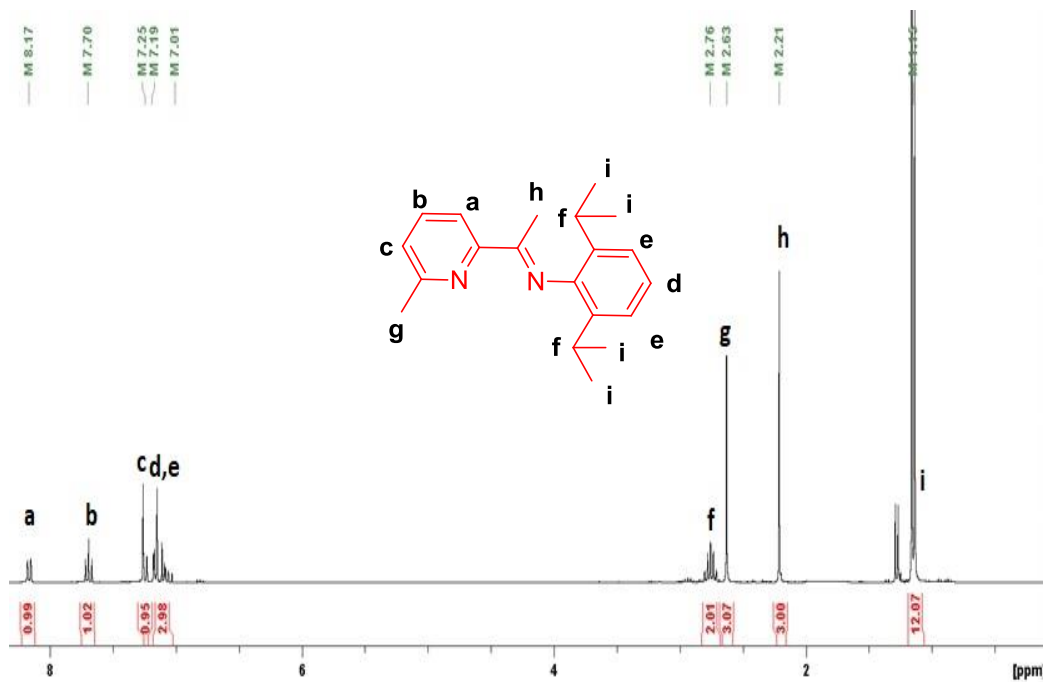
Figure A5. ^{1}H NMR of **L5** (300 MHz, CDCl$_3$, 25 °C)
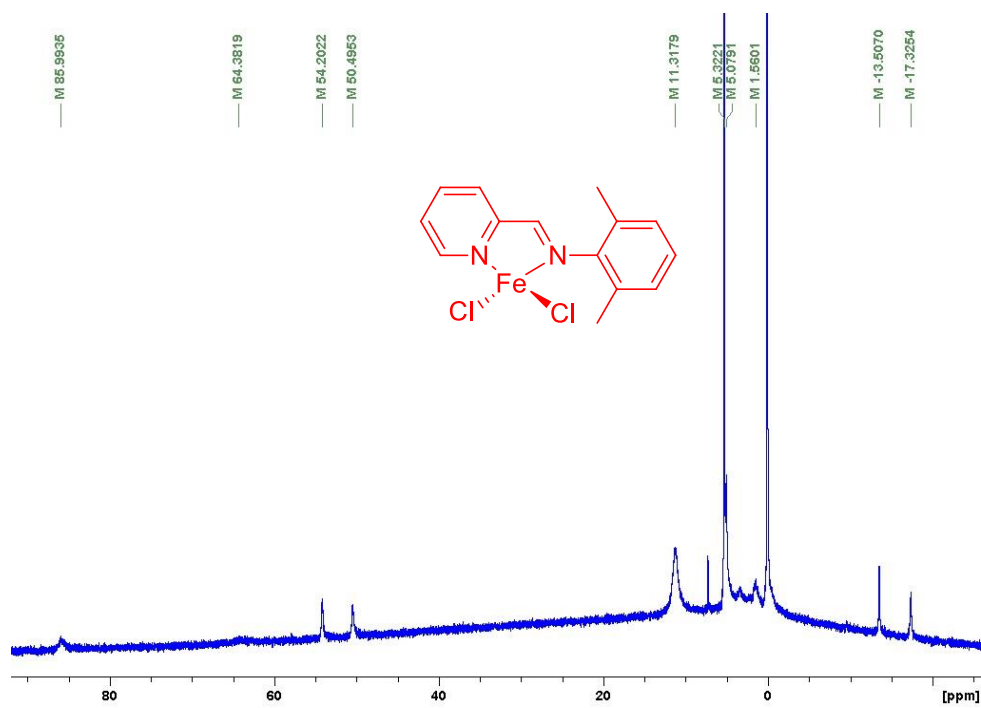
Figure A6. ^{1}H NMR spectrum of complex **1** (300 MHz, CD$_2$Cl$_2$, 25 °C)
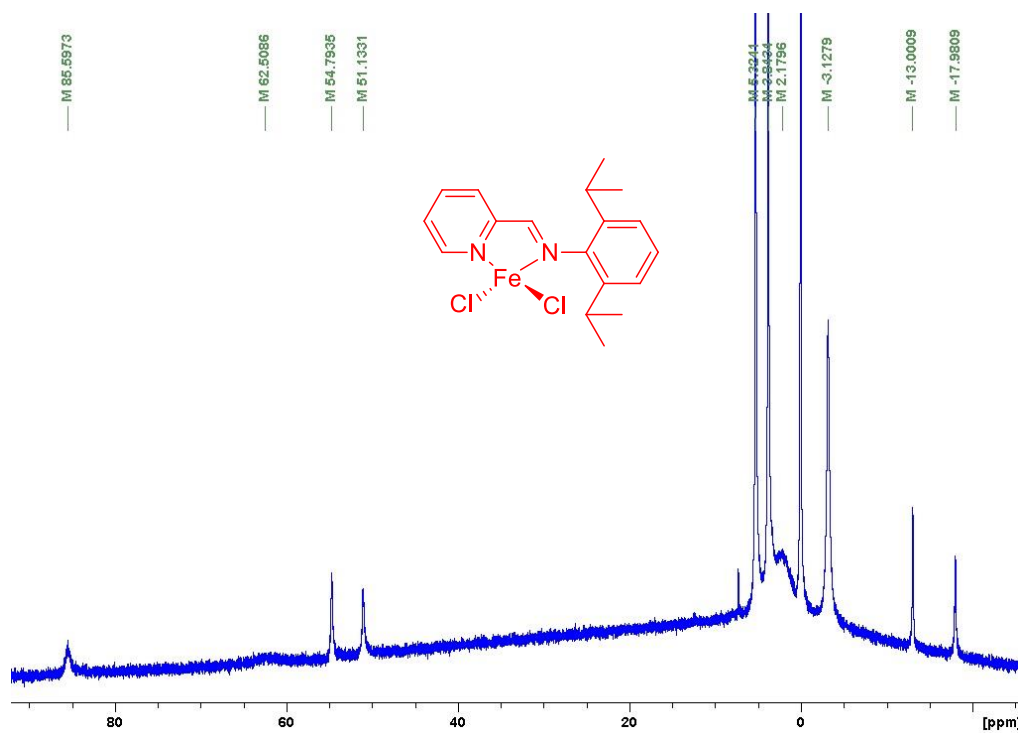
Figure A7. ^{1}H NMR spectrum of complex **2** (300 MHz, CD$_2$Cl$_2$, 25 °C)
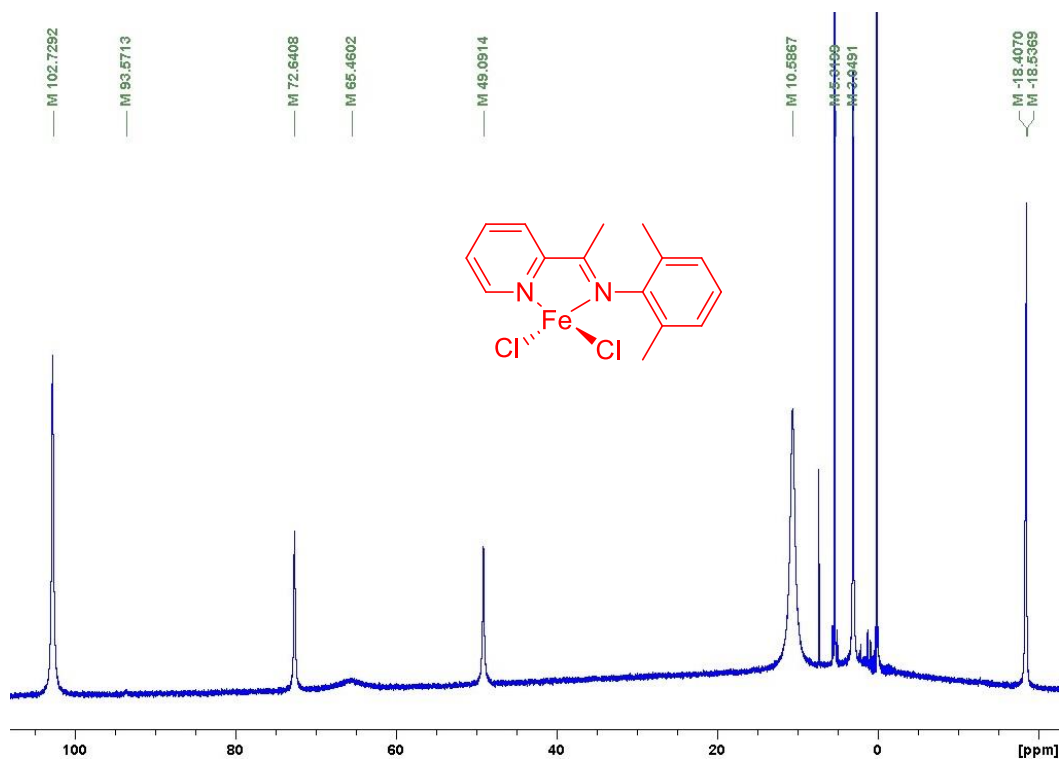
Figure A8. ^{1}H NMR spectrum of complex **3** (300 MHz, CD$_2$Cl$_2$, 25 °C)
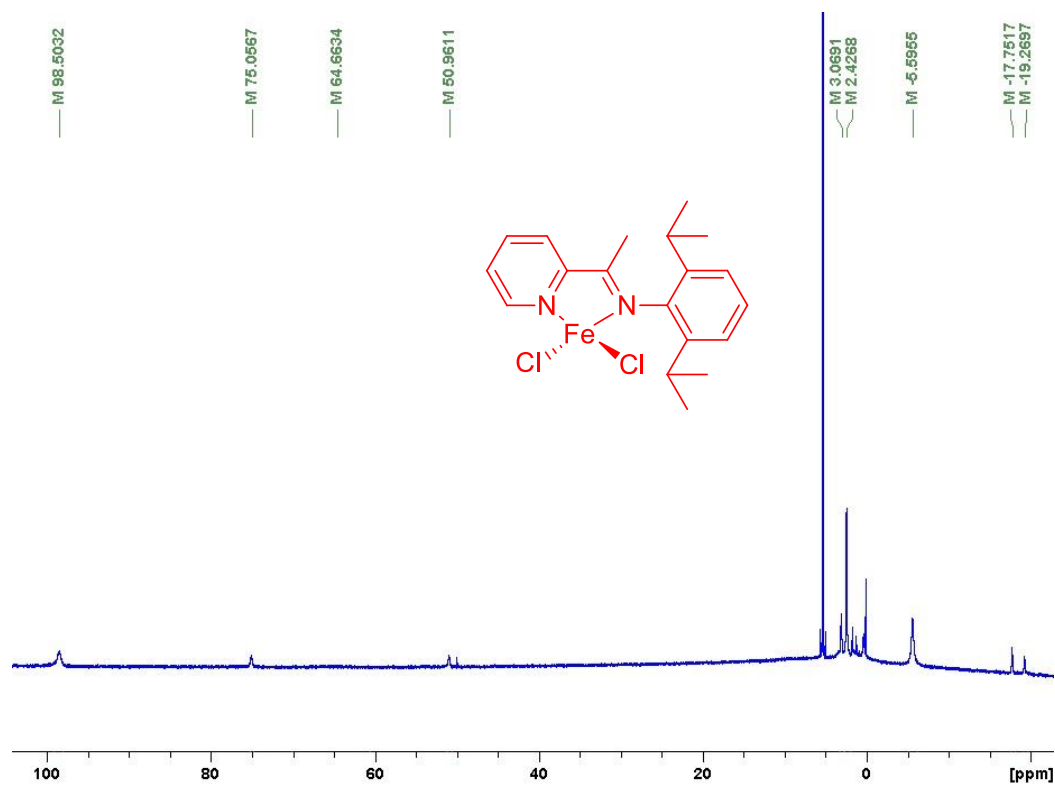
Figure A9. ^{1}H NMR spectrum of complex **4** (300 MHz, CD_2Cl_2, 25 °C)
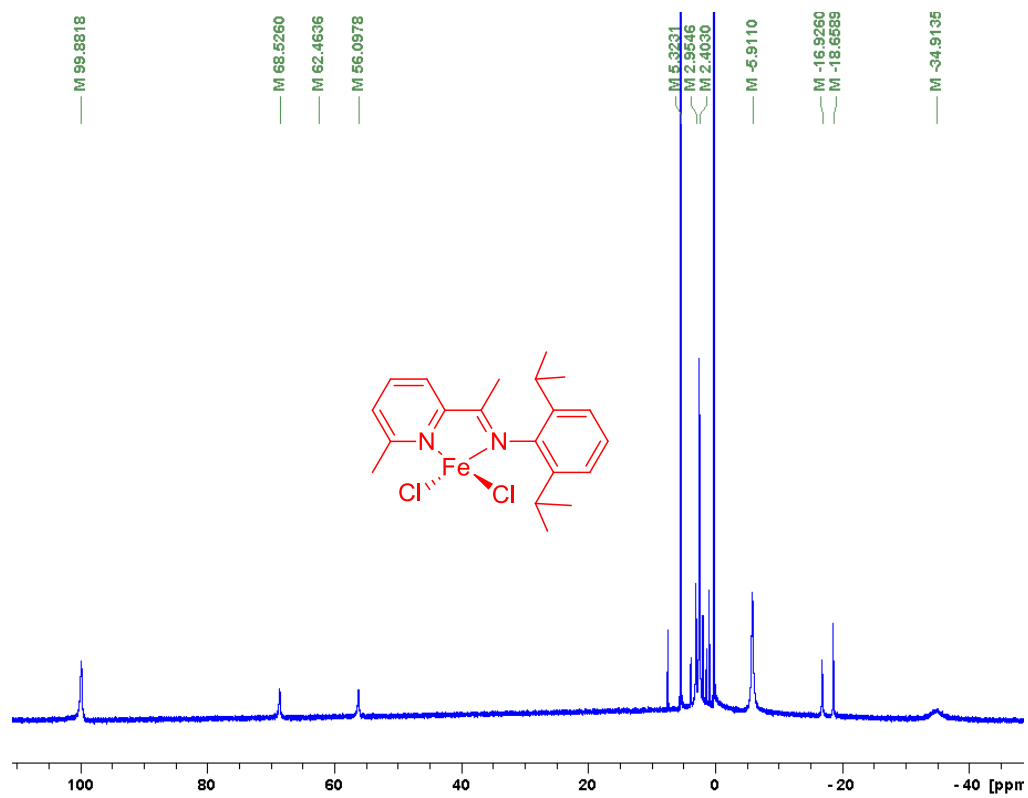
Figure A10. ^{1}H NMR spectrum of complex **5** (300 MHz, CD_2Cl_2, 25 °C)

283
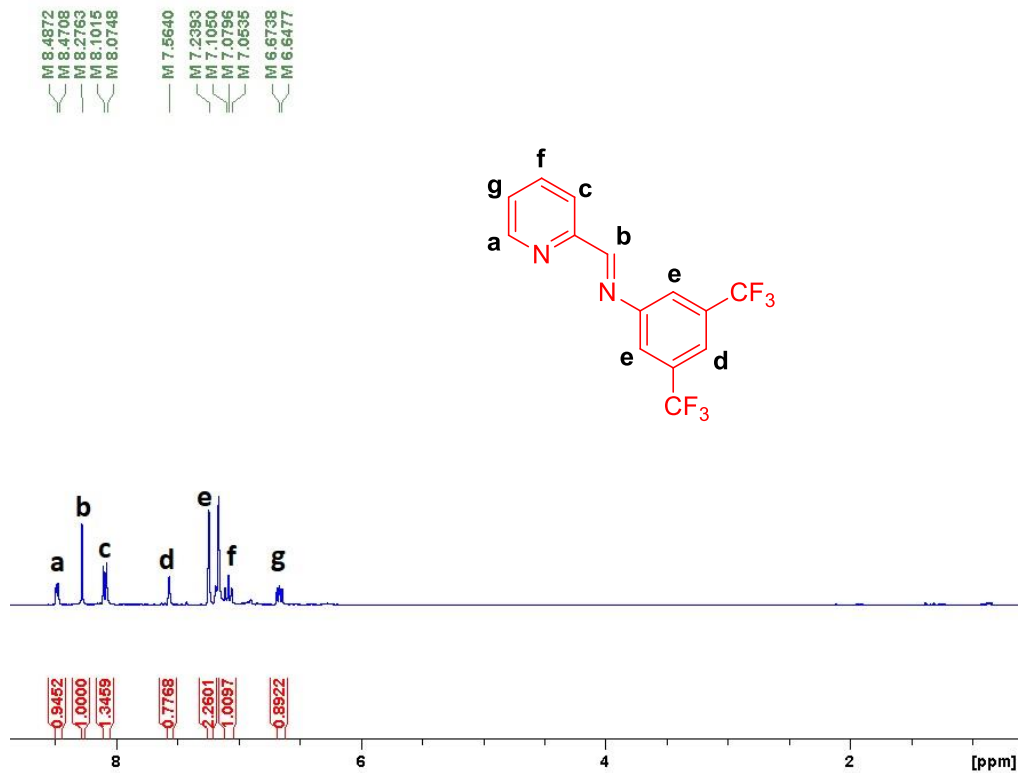
Figure A11. ^{1}H NMR of **L6** (300 MHz, C$_6$D$_6$, 25 °C)
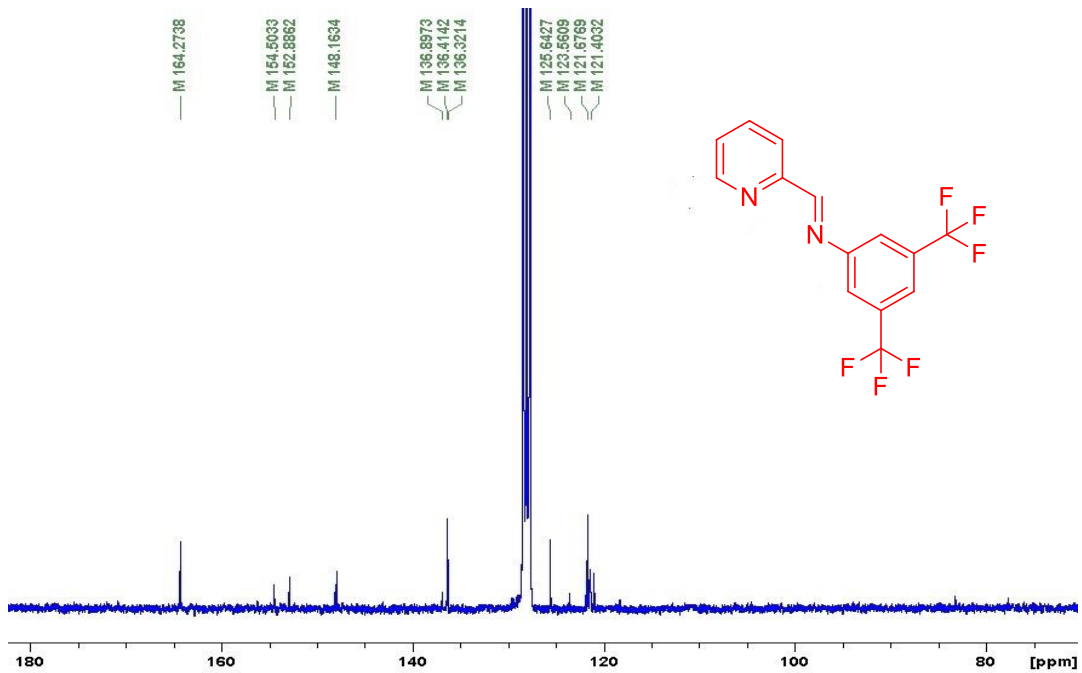
Figure A12. ^{13}C NMR of **L6** (75 MHz, C$_6$D$_6$, 25 °C)
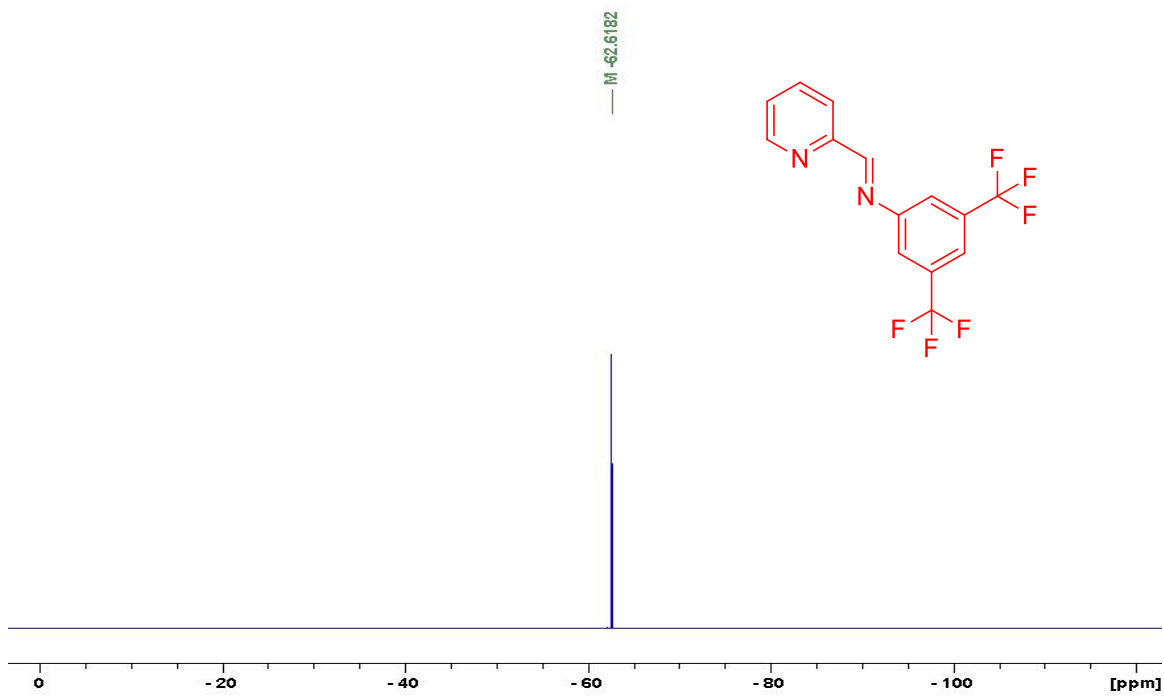
Figure A13. ^{19}F NMR of **L6** (282 MHz, C$_6$D$_6$, 25 °C)
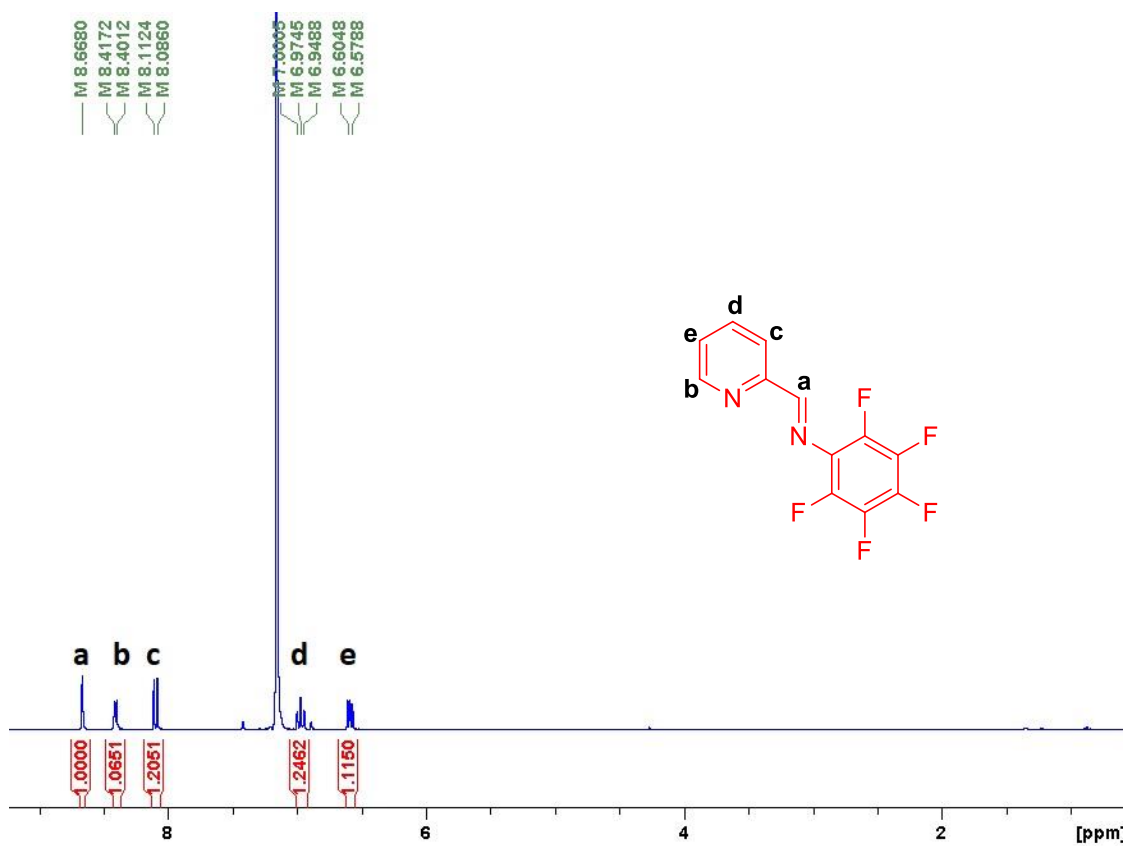
Figure A14. ^1H NMR of **L7** (300 MHz, C$_6$D$_6$, 25 °C)

285
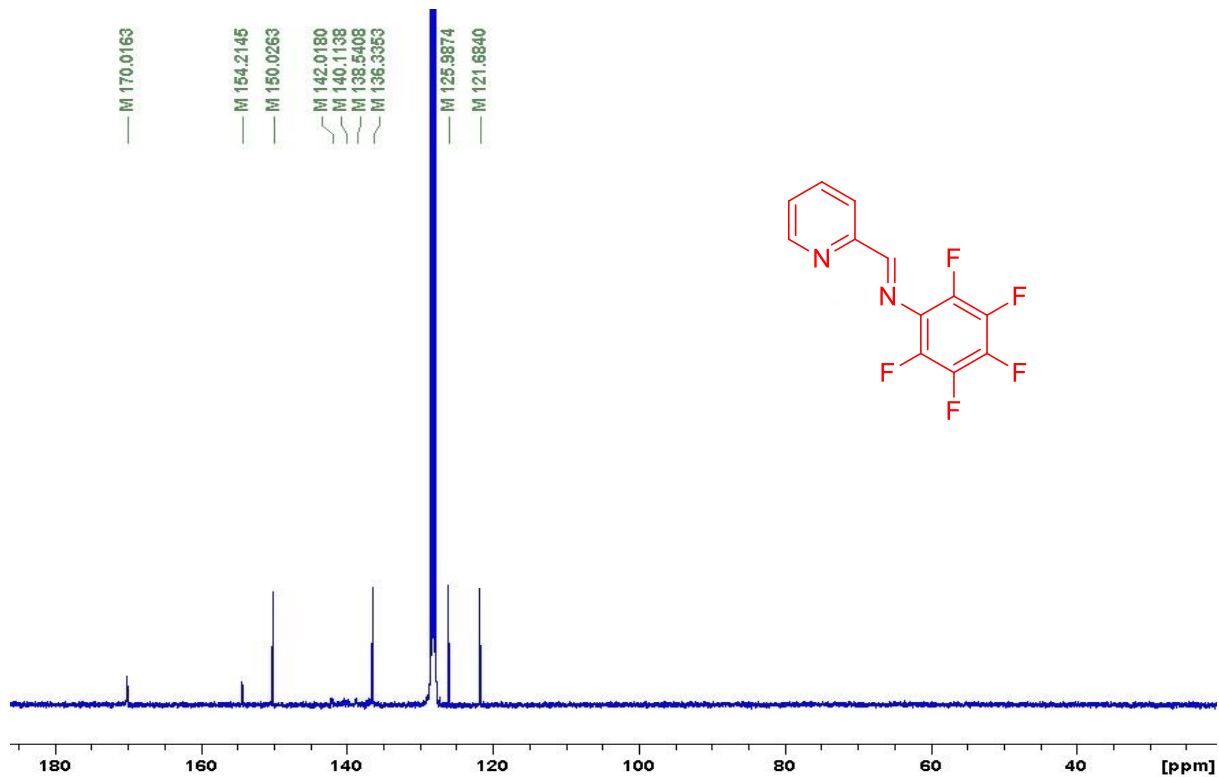
Figure A15. ^{13}C NMR of **L7** (75 MHz, C$_6$D$_6$, 25 °C)
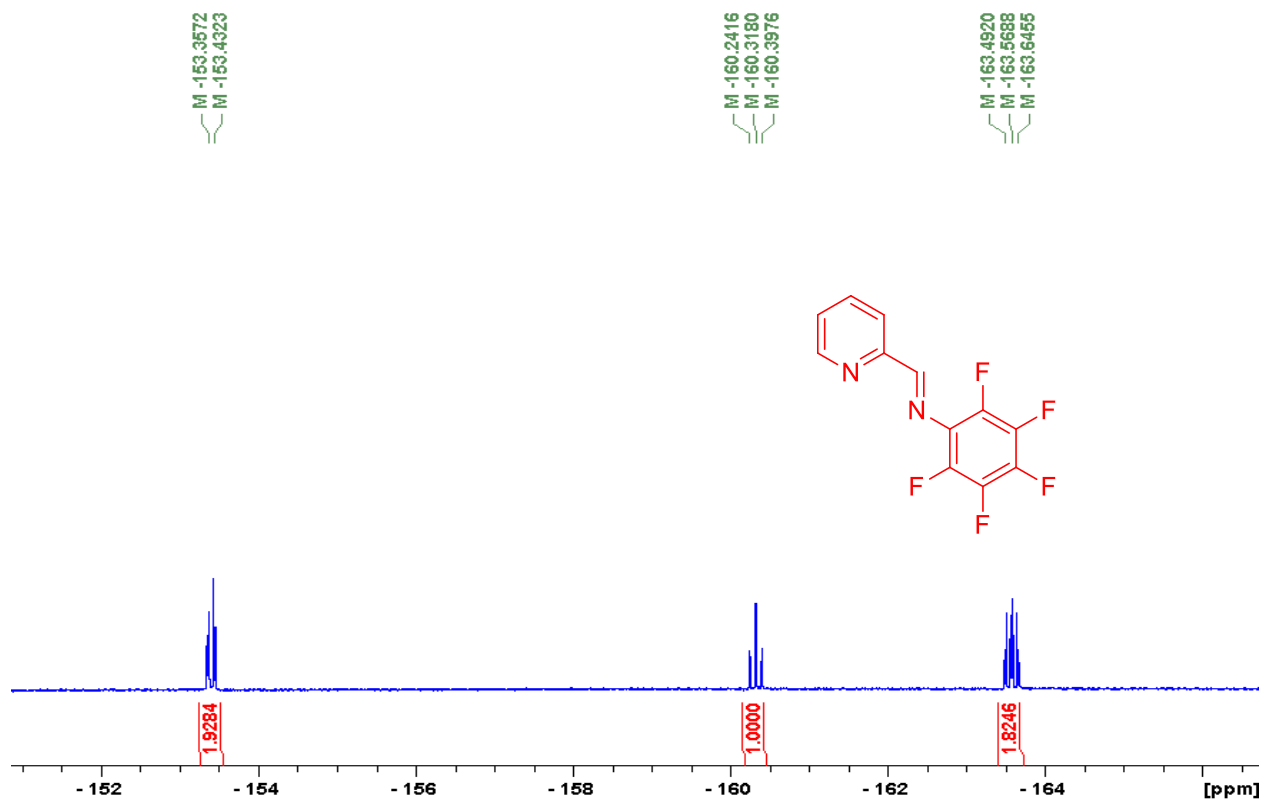
Figure A16. ^{19}F NMR of **L7** (282 MHz, C$_6$D$_6$, 25 °C)
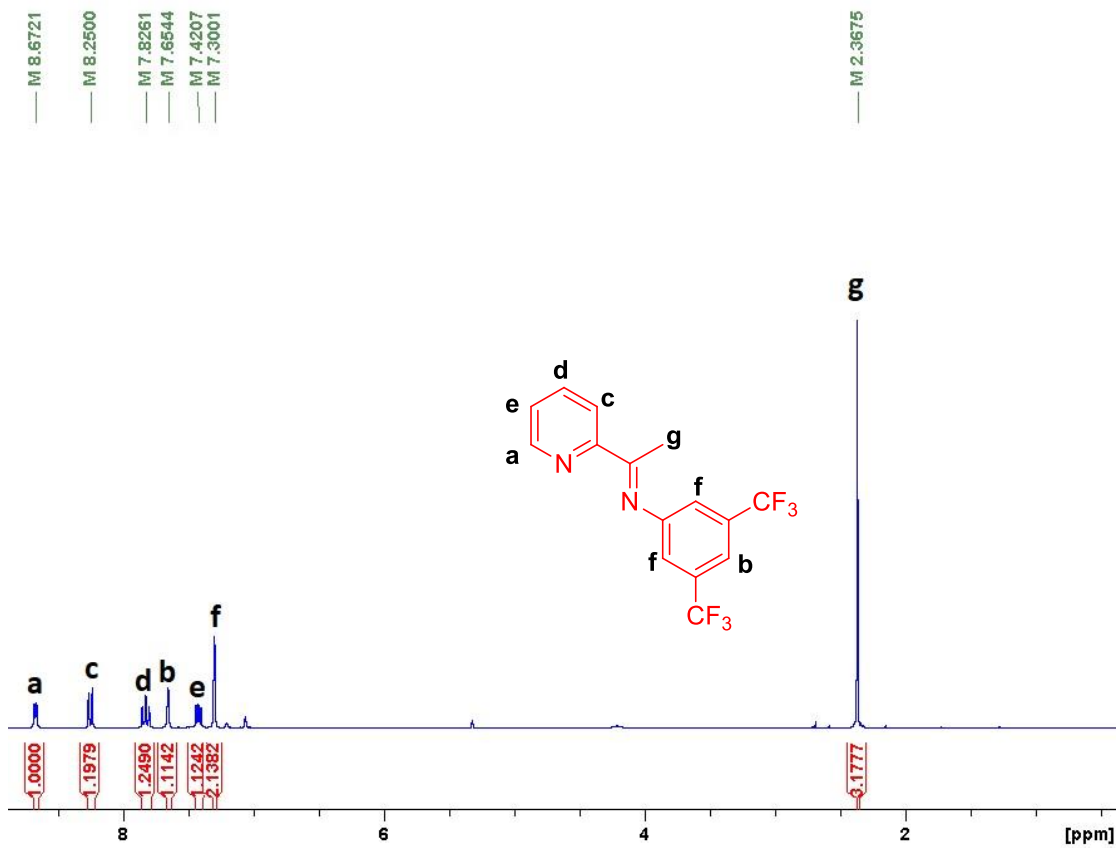
Figure A17. ^{1}H NMR of **L8** (300 MHz, CD$_2$Cl$_2$, 25 °C)
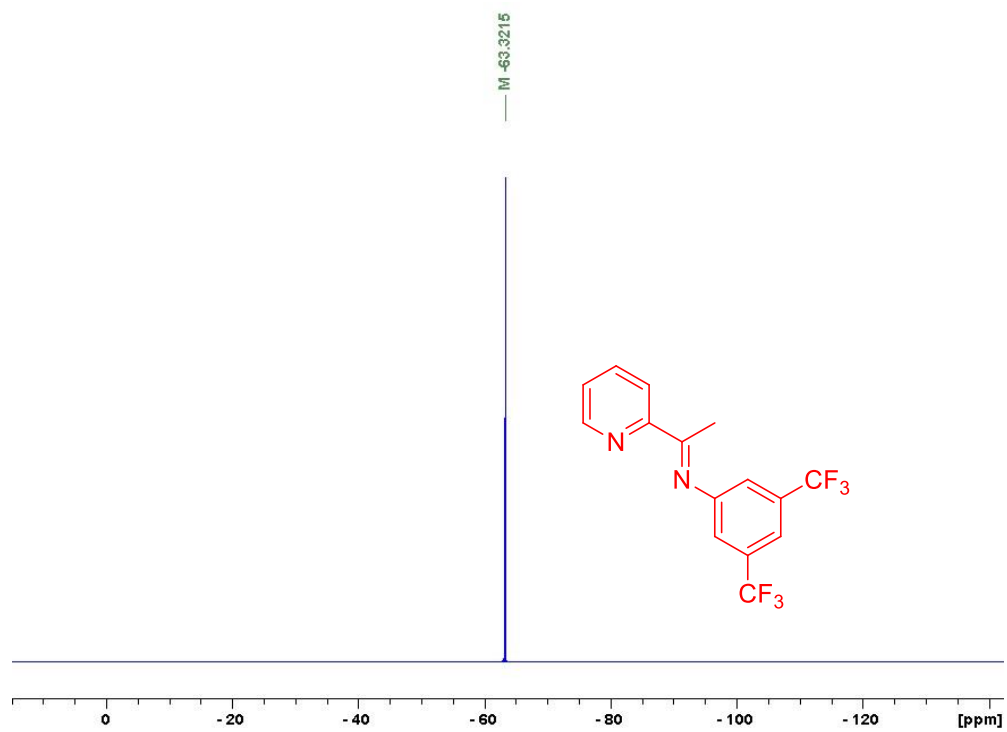
Figure A18. ^{19}F NMR of **L7** (282 MHz, CD$_2$Cl$_2$, 25 °C)

Figure A19. ^{1}H NMR of **L9** (300 MHz, C$_6$D$_6$, 25 °C)

Figure A20. ^{13}C NMR of **L9** (75 MHz, C$_6$D$_6$, 25 °C)
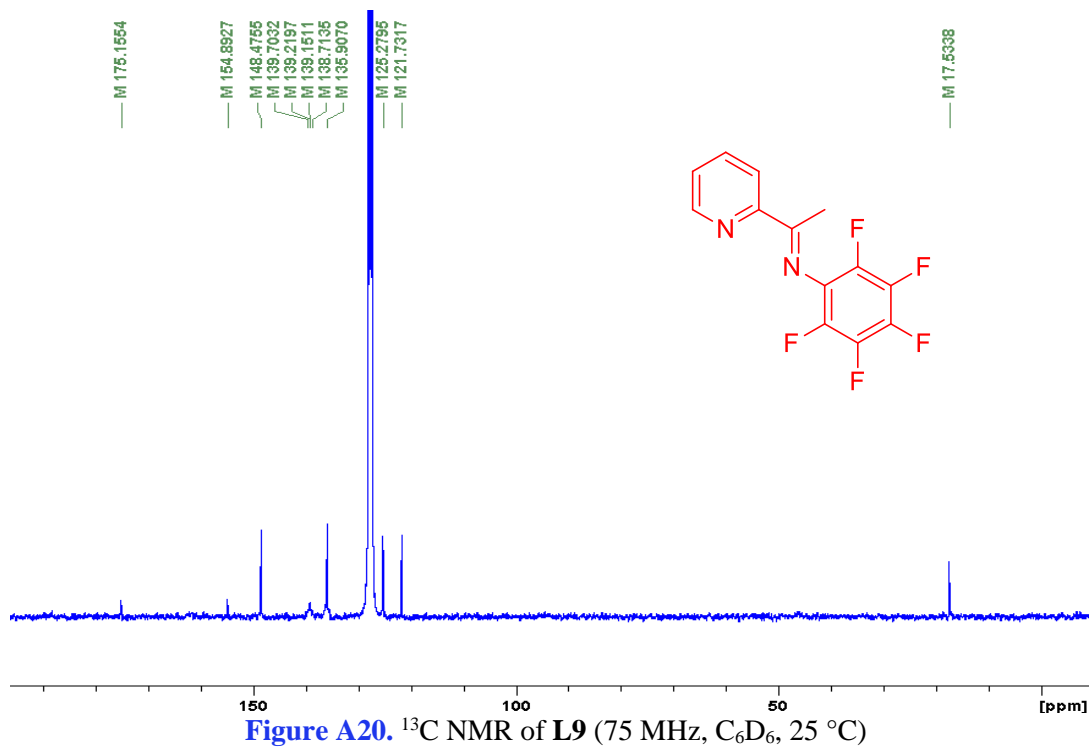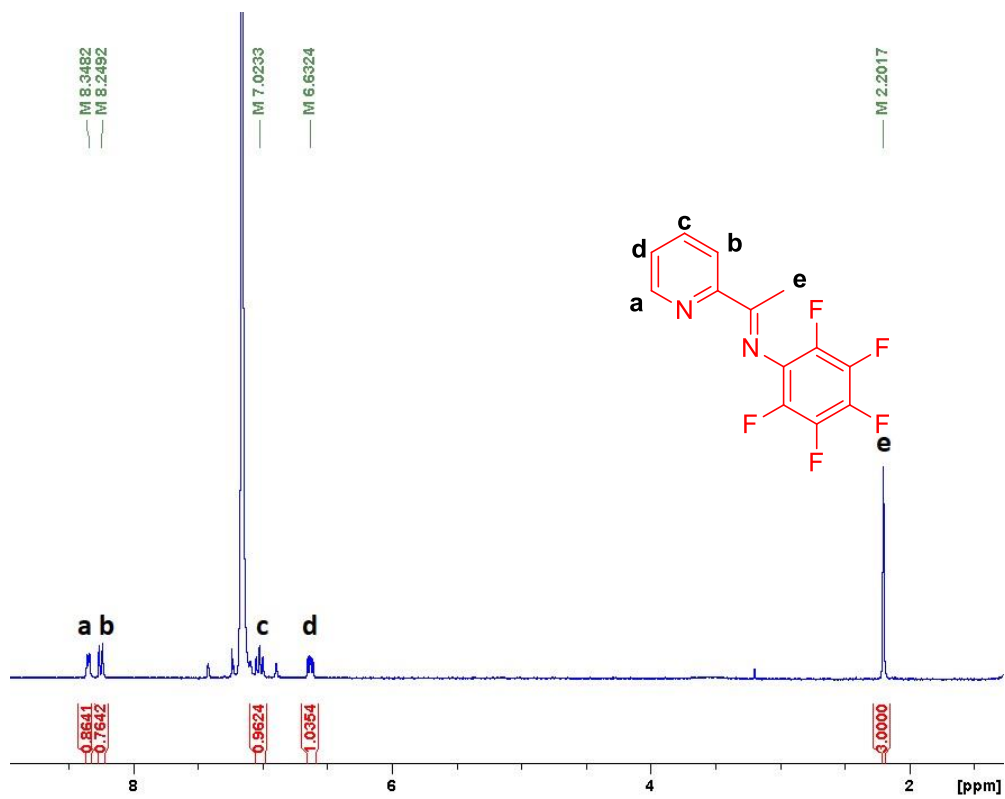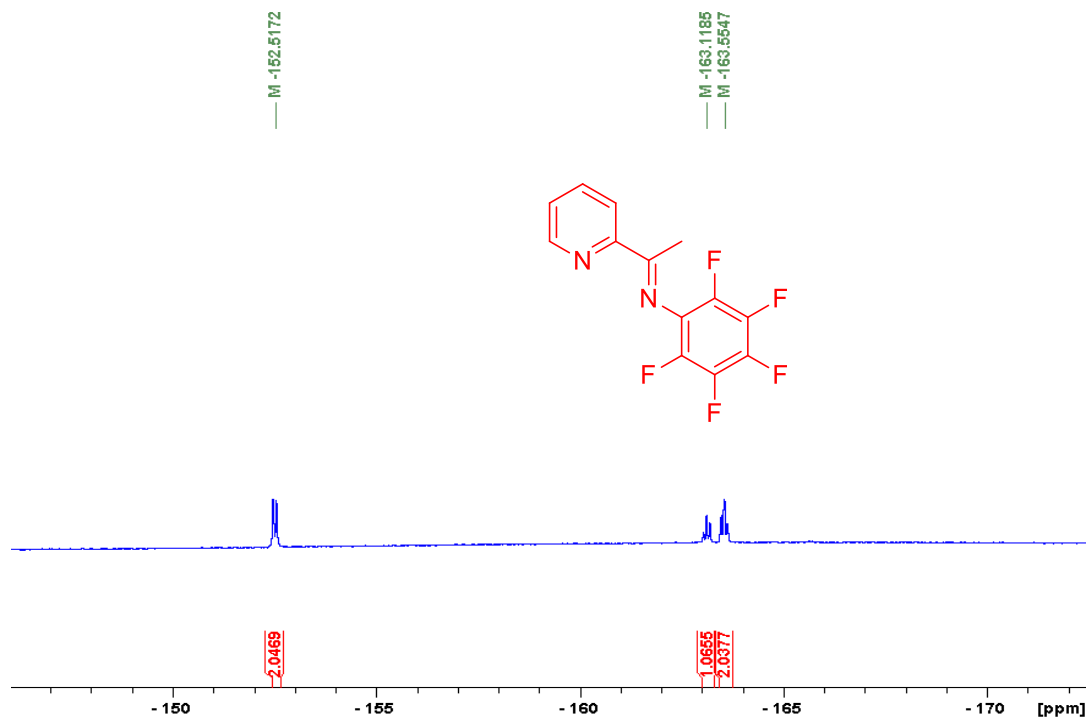
Figure A21. ^{19}F NMR of **L9** (282 MHz, C_6D_6, 25 °C)
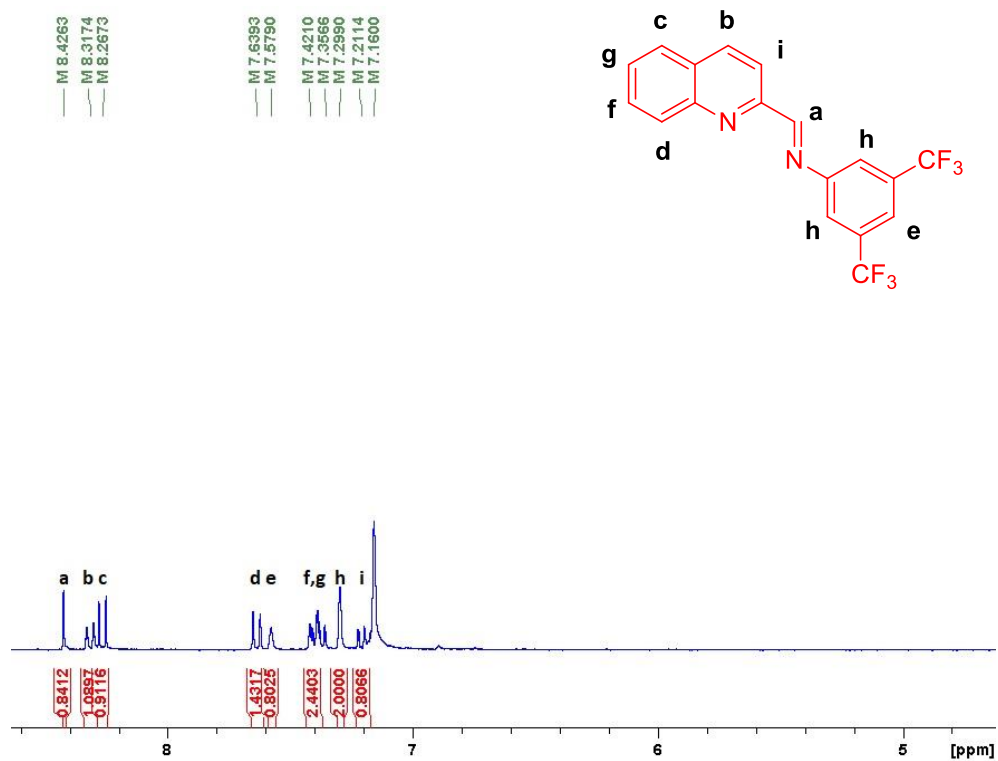
Figure A22. ^{1}H NMR of **L10** (300 MHz, C_6D_6, 25 °C)
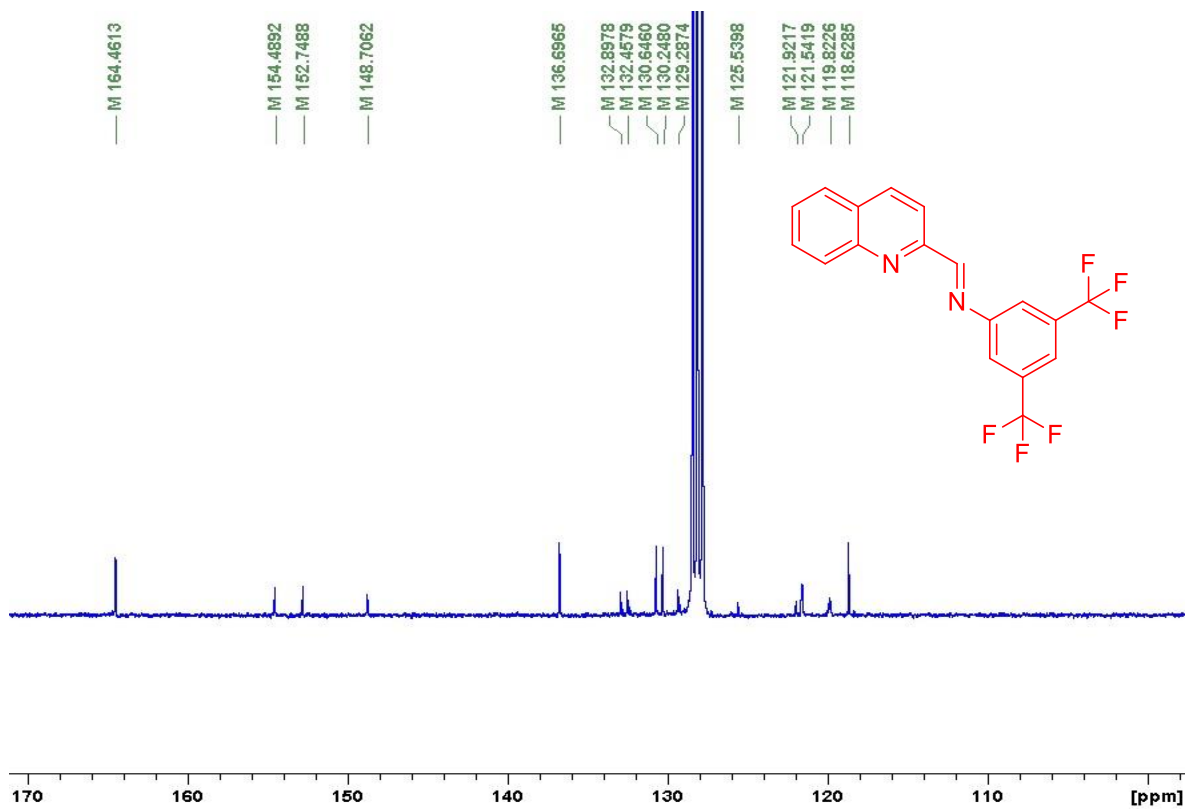
Figure A23. ^{13}C NMR of **L10** (75 MHz, C$_6$D$_6$, 25 °C).
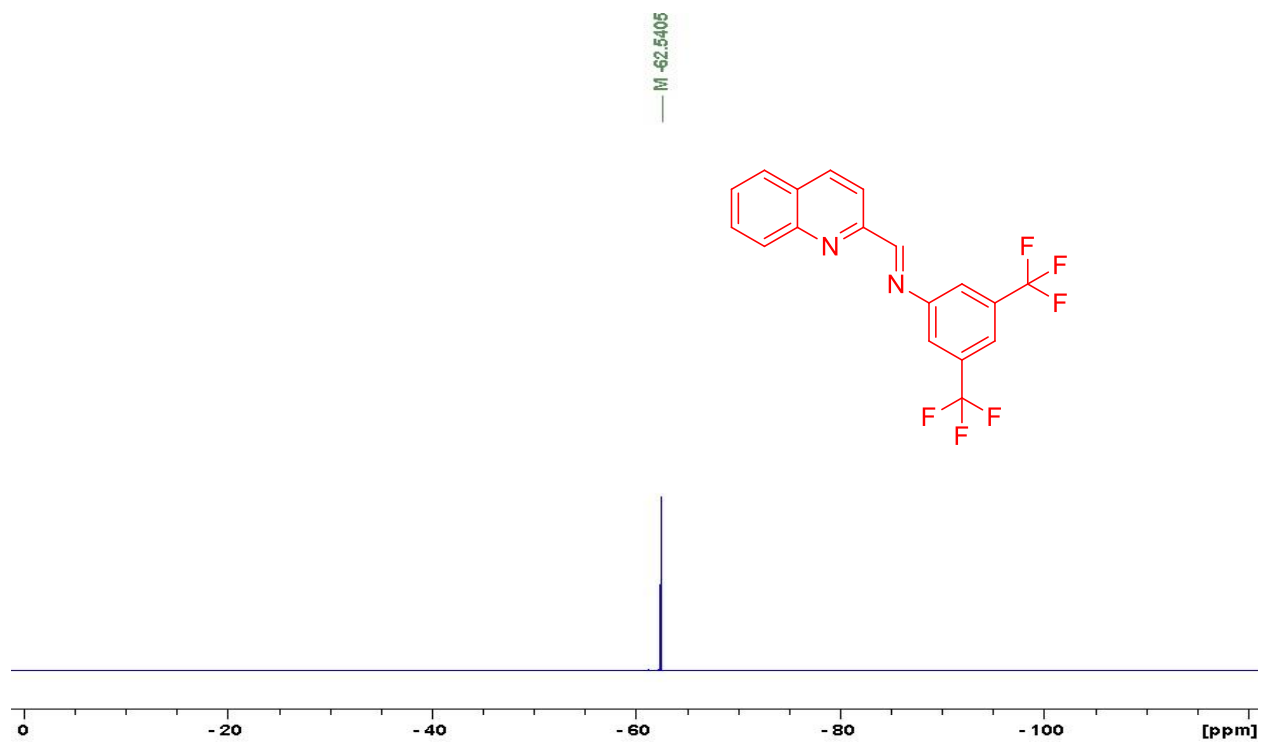
Figure A24. ^{19}F NMR of **L10** (282 MHz, C$_6$D$_6$, 25 °C)
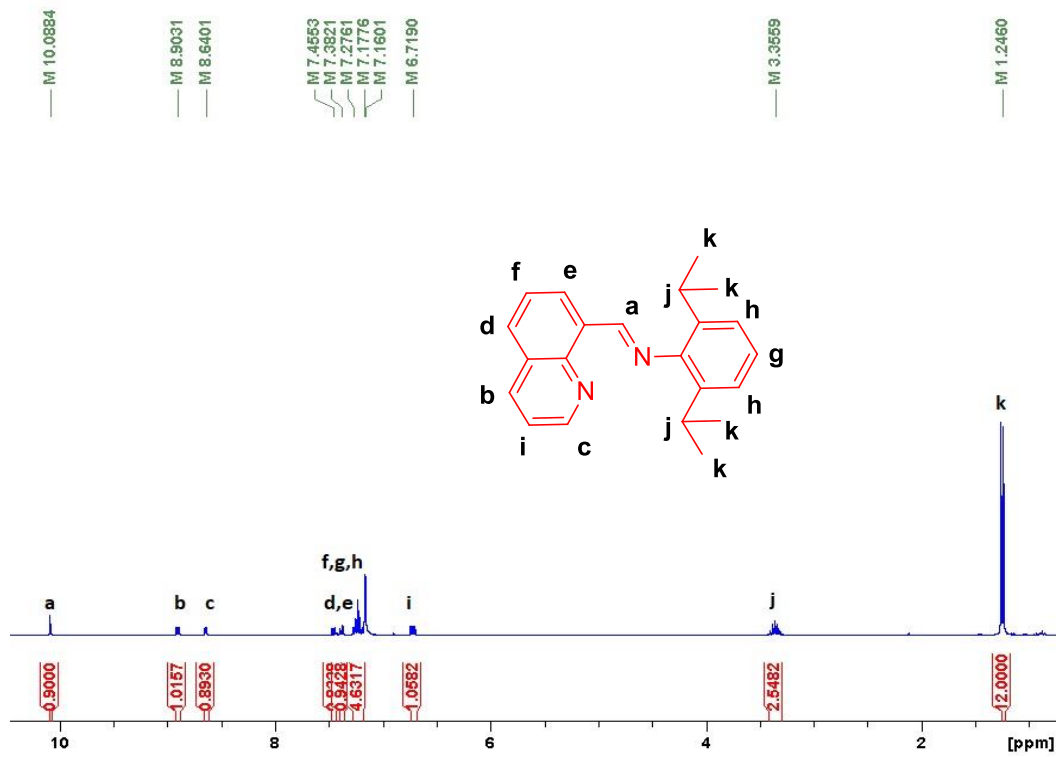
Figure A25. ^{1}H NMR of **L11** (300 MHz, C_6D_6, 25 °C)
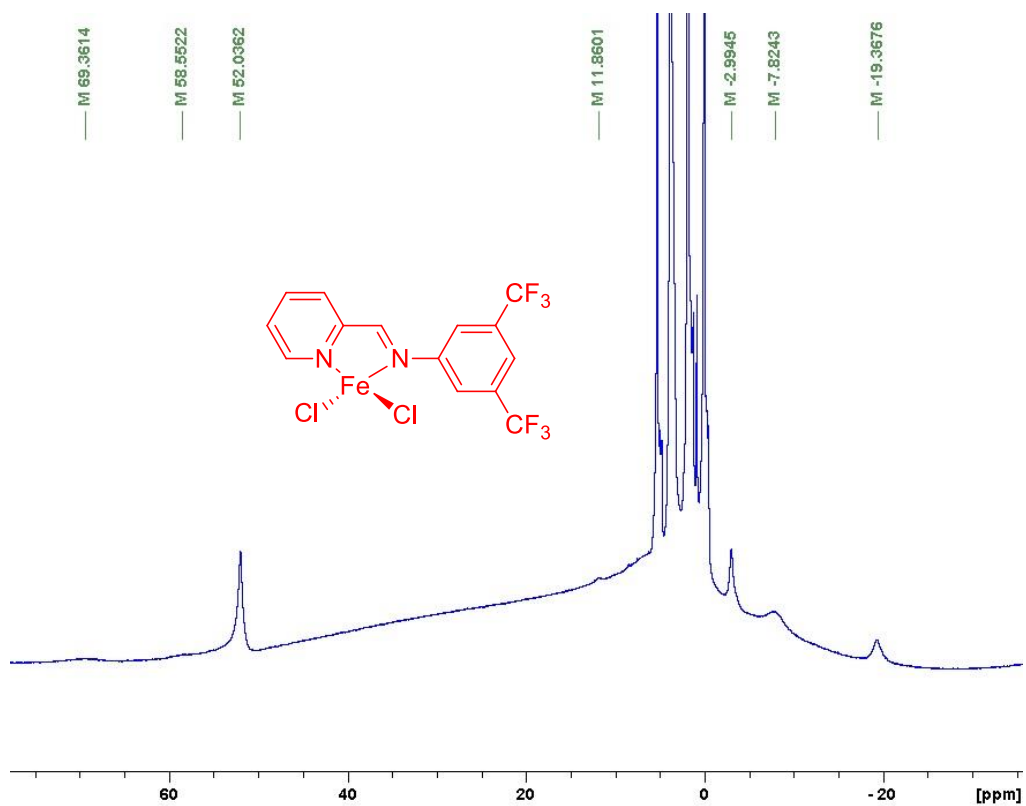
Figure A26. ^{1}H NMR of **6** (300 MHz, CD_2Cl_2, 25 °C)
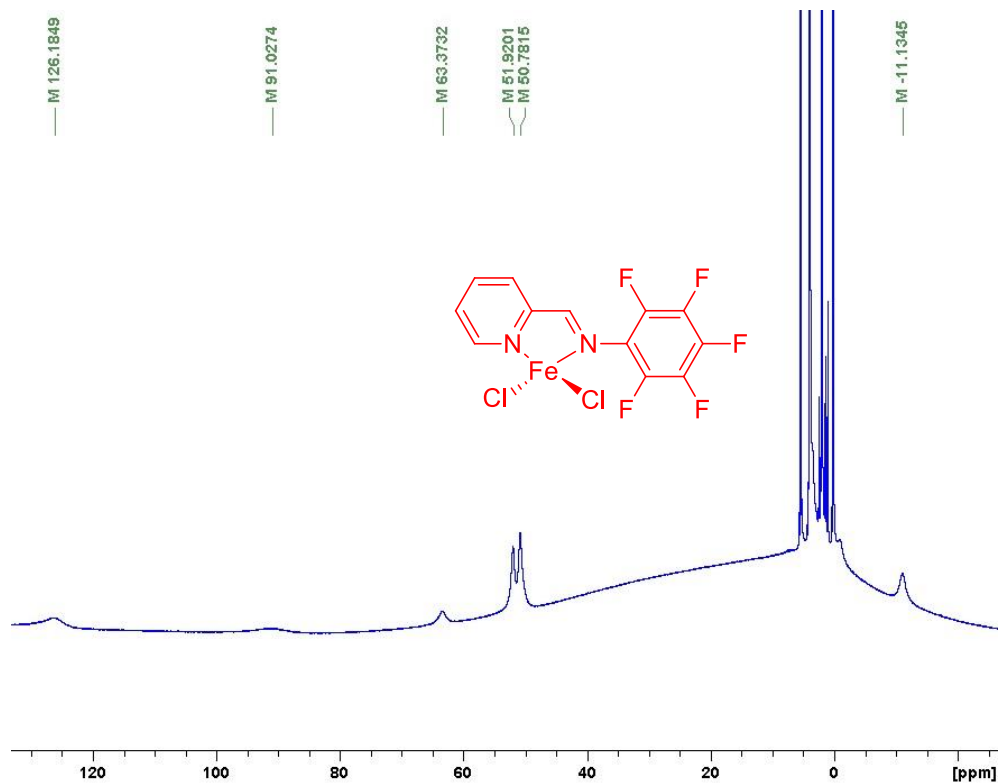
Figure A27. ^{1}H NMR of **7** (300 MHz, CD$_2$Cl$_2$, 25 °C)
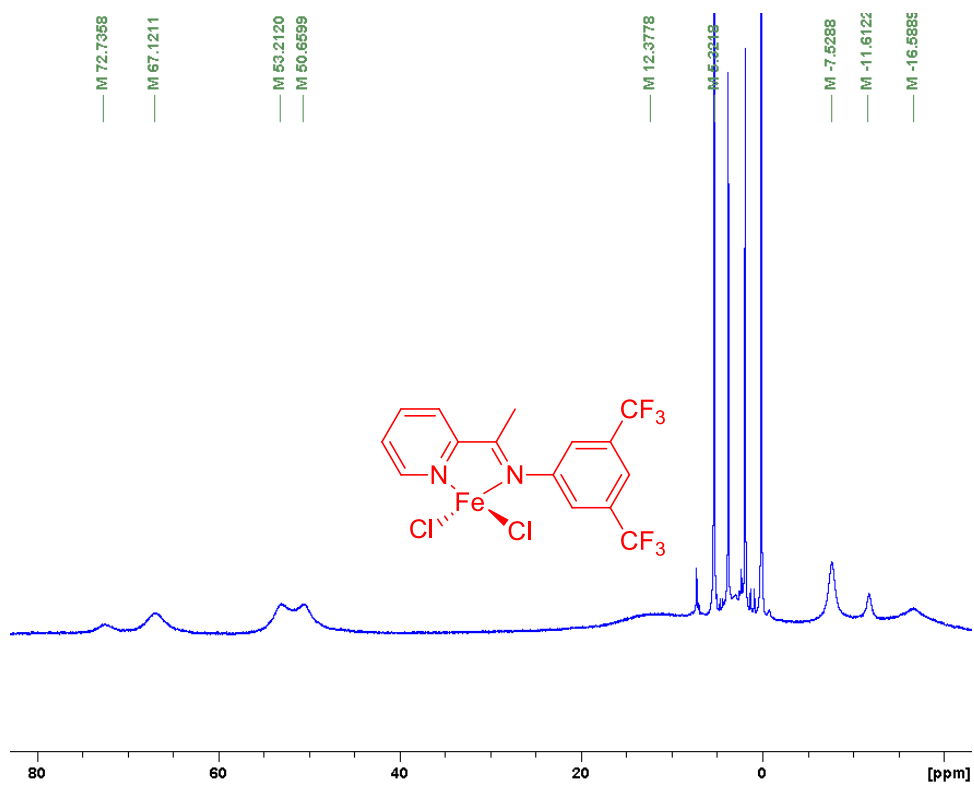
Figure A28. ^{1}H NMR of **8** (300 MHz, CD$_2$Cl$_2$, 25 °C)
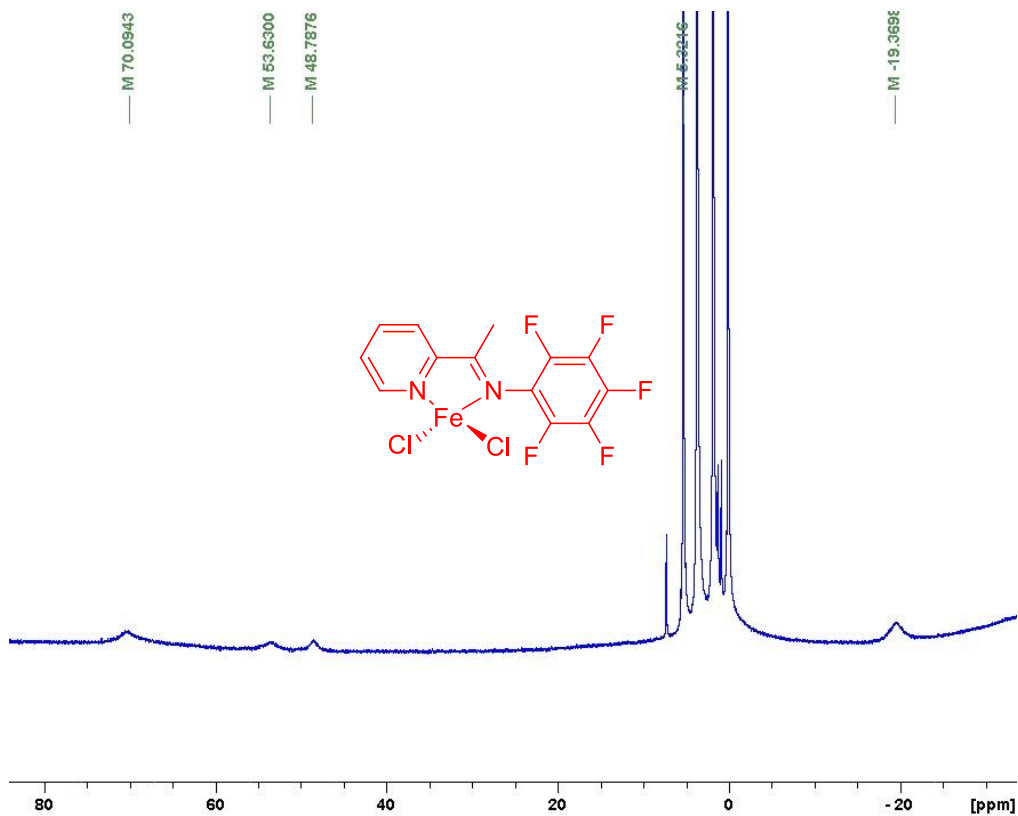
Figure A29. ^{1}H NMR of **9** (300 MHz, CD$_2$Cl$_2$, 25 °C)
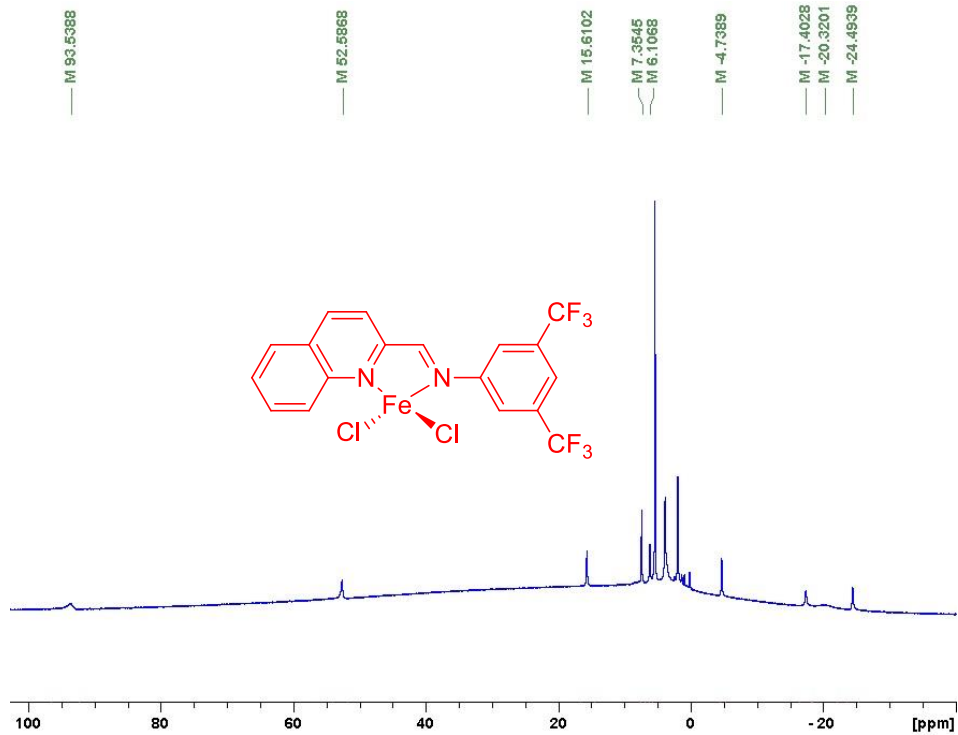
Figure A30. ^{1}H NMR of **10** (300 MHz, CD$_2$Cl$_2$, 25 °C)

293

Figure A31. ^{1}H NMR of **11** (300 MHz, CD$_2$Cl$_2$, 25 °C)

Figure A32. ^{1}H NMR of ***rac*-L^{1}H** (300 MHz, CD$_2$Cl$_2$, 25 °C)
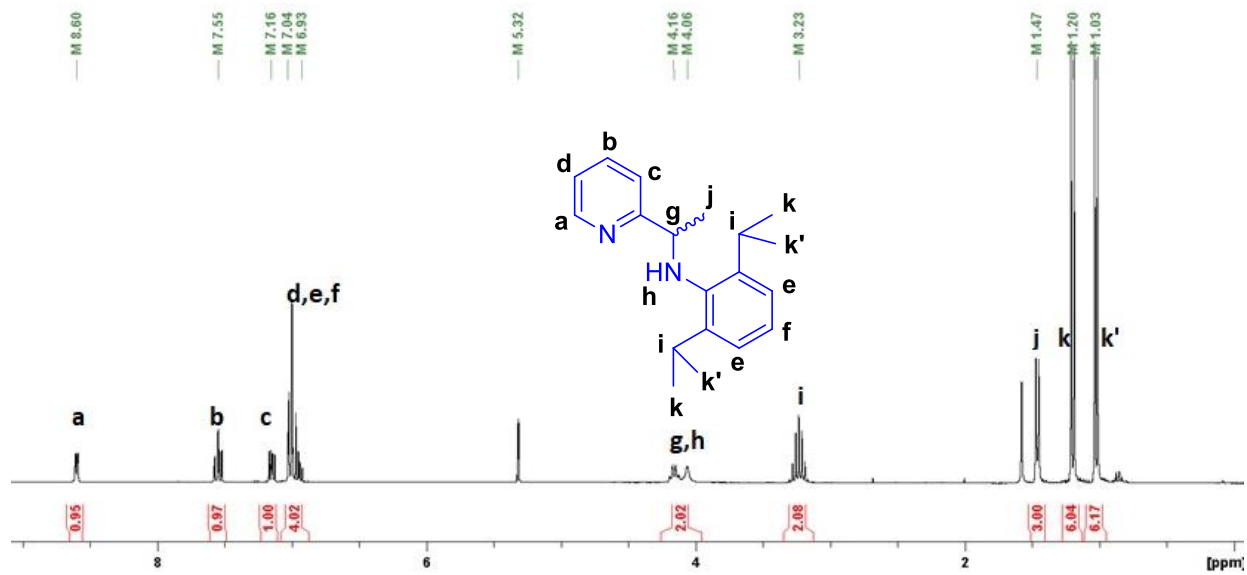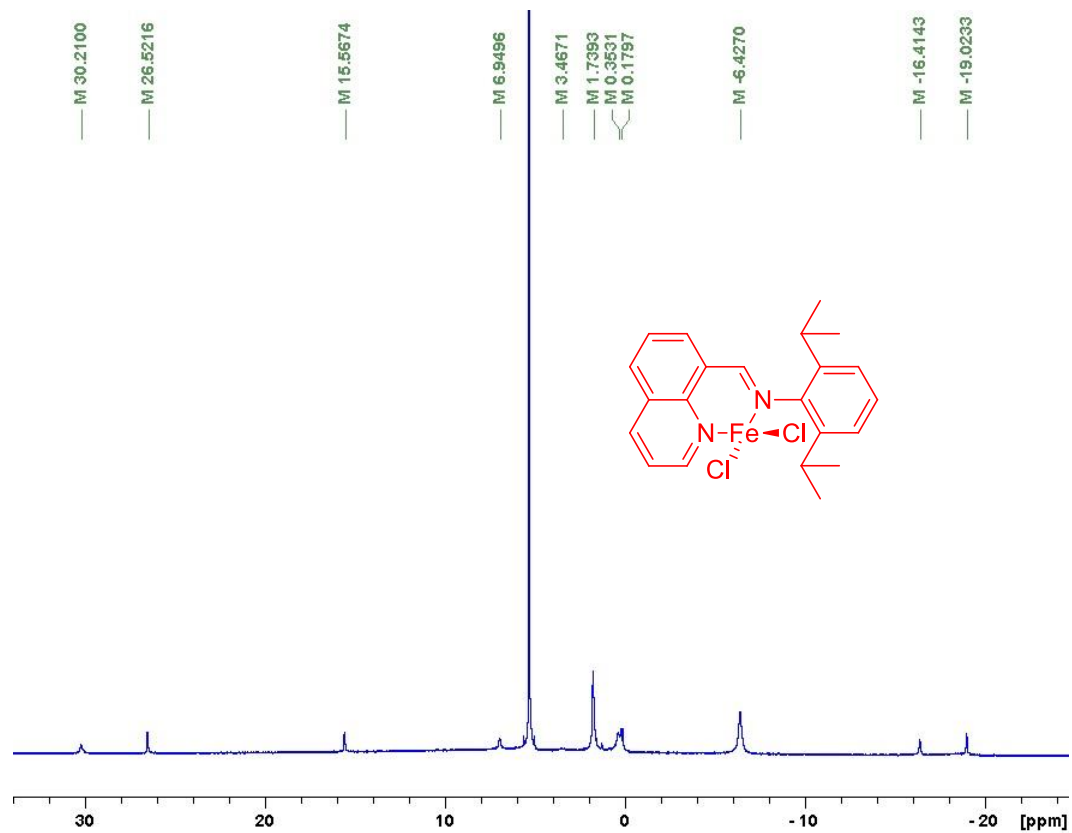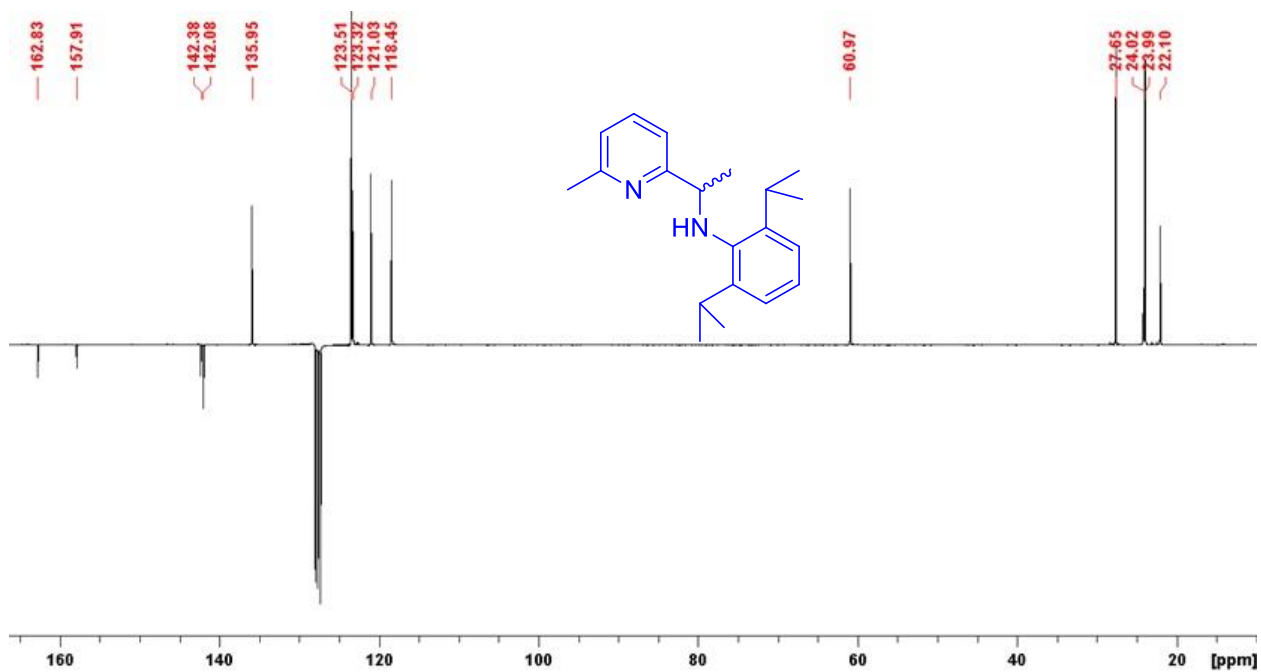
Figure A33. ^{13}C DEPT 135 NMR of *rac*-**L^{2}H** (75 MHz, C$_6$D$_6$, 25 °C)
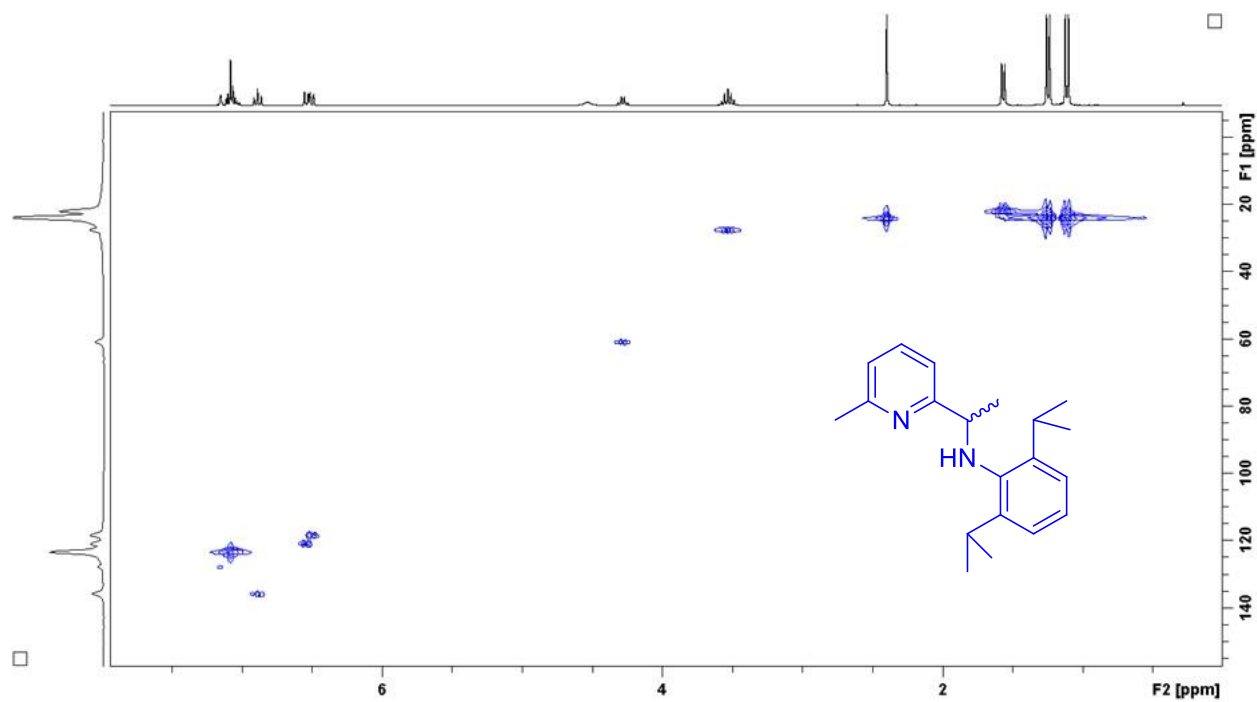
Figure A34. HMQC 2D NMR spectrum of *rac*-**L^{2}H**

Figure A35. ^{1}H NMR of Fe[N(SiCH$_3$)$_2$]$_2$ (300 MHz, C$_6$D$_6$, 25 °C)

Figure A36. ^{1}H NMR spectrum of heteroleptic complex **13Py** (300 MHz, C$_6$D$_6$, 25 °C)
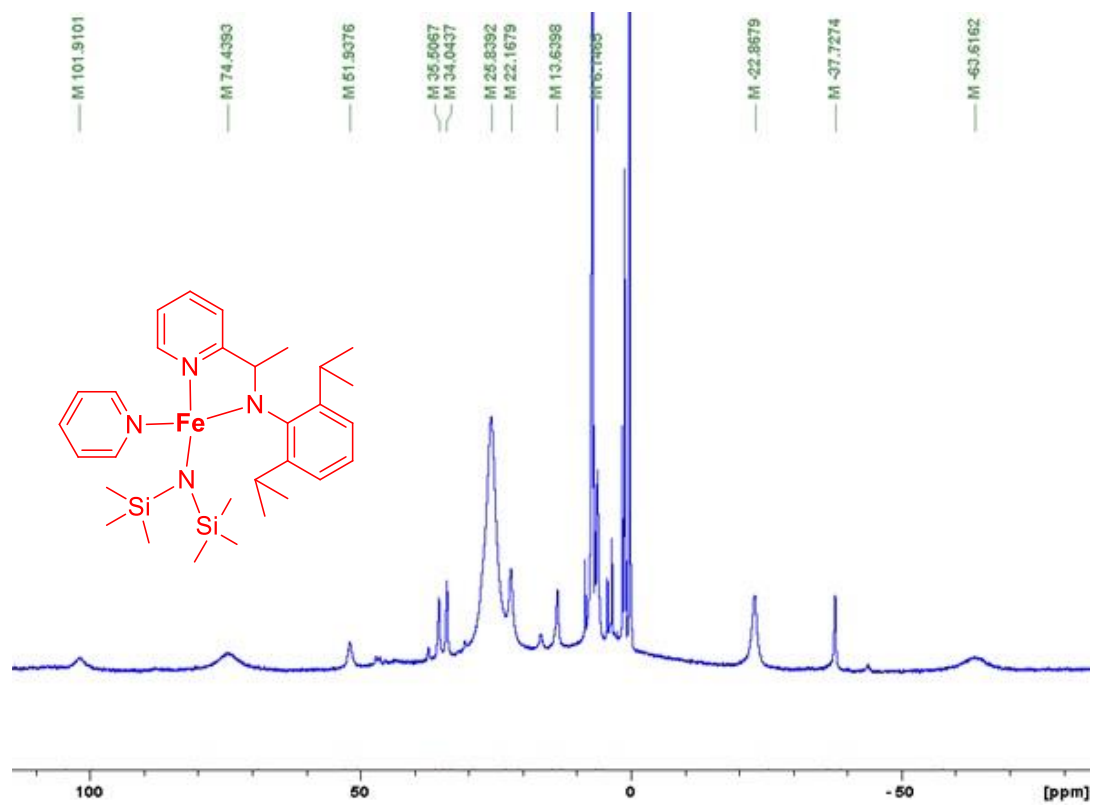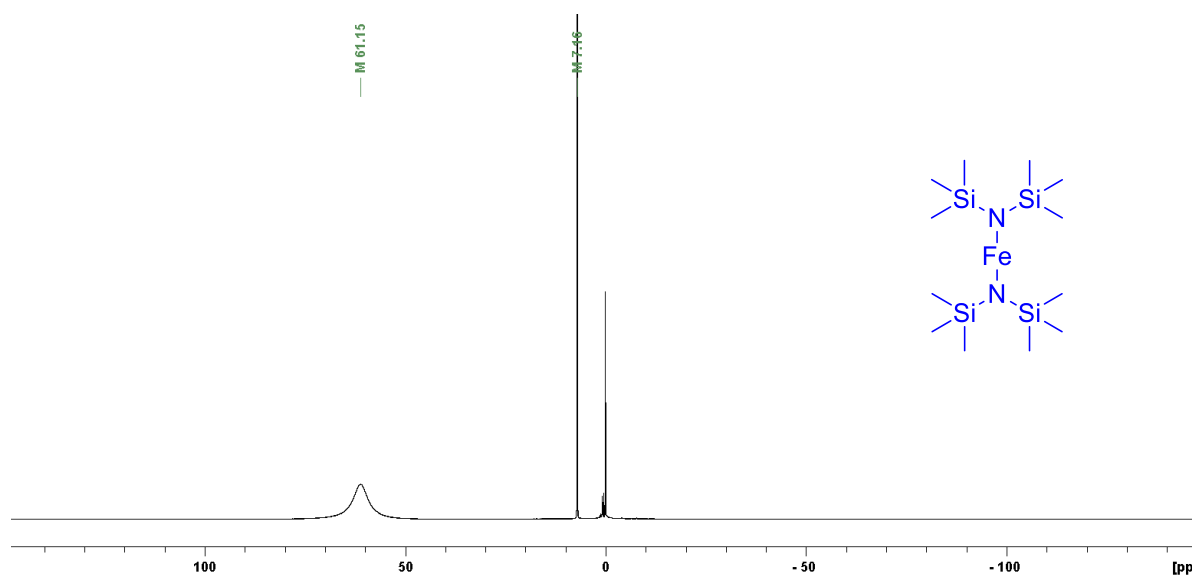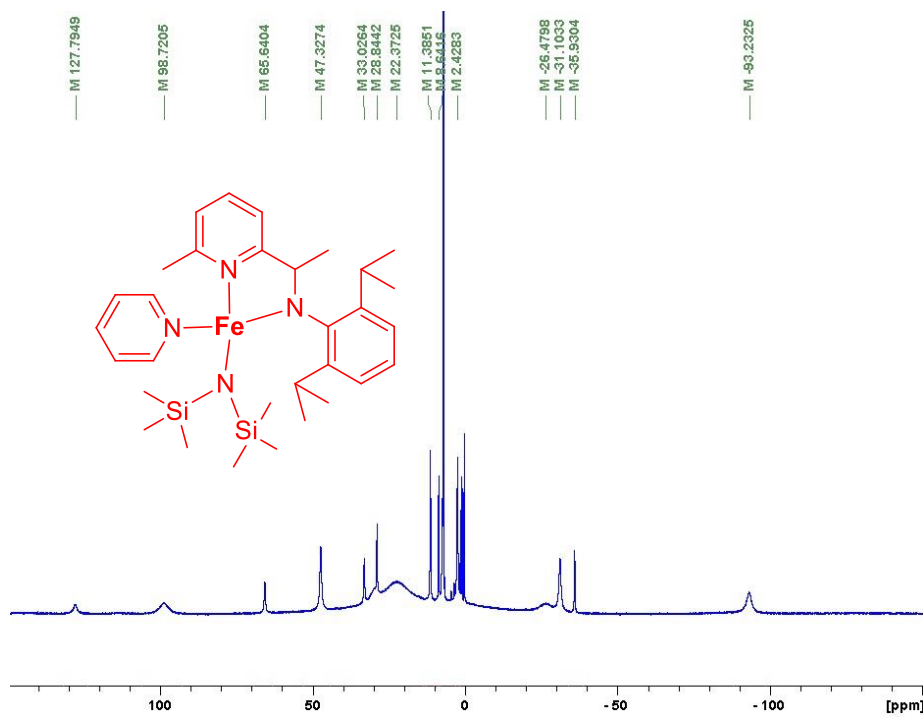
Figure A37. ^{1}H NMR spectrum of heteroleptic complex **14Py** (300 MHz, C_6D_6, 25 °C)
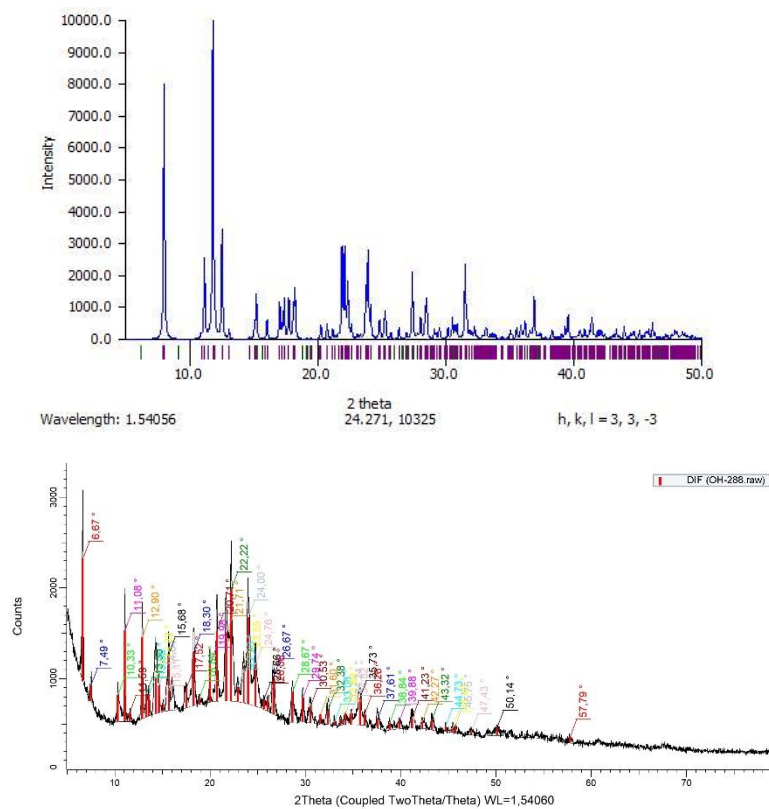

Figure A38. XRPD pattern of complex **8** for crystal (top) and powder (below).